STRUCTURE AND REACTIVITY OF DINUCLEAR AND POLYNUCLEAR METAL COMPLEXES

A thesis submitted in partial fulfilment of the requirement

for the degree of

Doctor of Philosophy in Chemistry

at the

University of Canterbury

by

Gurpreet Kaur

2014

ACKNOWLEDGEMENTS

It would not have been possible to write this doctoral thesis without the help and support of the kind people around me. Firstly, I would like to extend my sincere thanks to my supervisor, Associate Professor Richard Hartshorn, for his excellent and patient guidance both in the science of this thesis and in my development as a researcher. You were always there to listen and inspire me to keep going through the end. Besides my advisor, I would also like to thank my co-supervisor Dr. Jan Wikaira and committee members Prof. Bryce Williamson, Dr. Sally Gaw, Assoc. Prof. Owen Curnow, and Dr. Andy Pratt for their valuable advice and comments.

I would like to thank the staff in the Chemistry Department for all their help over the years. I would also like to take this opportunity to thank Dr. Matthew Polson for being always welcoming and approachable, for his valuable comments through this research and introducing me to the field of X-Ray crystallography. Special thanks to Dr. Marie Fitchett for NMR and mass spectrometric analysis, and Drs. Chris Fitchett, Jan Wikaira and Prof. Peter Steel for their assistance with X-ray crystallography. I would also like to thank all the technical staff, Wayne, Nick, Gill, Laurie, Rob and Danny, for many ways they contributed to this research.

My special thanks also go to the present and past members in Hartshorn group – especially Sally, Janadari and Fatemeh for your friendship, and benevolent support. I would also extend my thanks to present and past members of Kruger and Steel group – especially Chris Hawes and Rakesh for being exceptionally helpful when I started this research, and Dave and Rob for proofreading and Siji for always being there. I also wish to acknowledge Nathan Wain from Learning Skill Centre at University of Canterbury for his technical tips to handle the long documents.

I sincerely thank my employer Assoc. Prof. Gareth Rowlands at Massey University for his cooperation in completing this thesis. I also thank Dr. Alan Ferguson and my friend Dr. Ajaypal Pannu at Massey University for proofreading this thesis and other useful chemistry discussions.

Financial help from the Department of chemistry at University of Canterbury, Evan's Fund, Maslen Scholarship from Society of Crystallographers in Australia and New Zealand (SCANZ), and other funding from New Zealand Institute of Chemistry (NZIC) are gratefully acknowledged.

I would like to extend my thanks to all my family and friends for their support in many ways through this research.

Thank you big brother 'Dr. K.P.S. Dandiwal' to be a great source of motivation for me, I have no words to say my gratitude, love and respect for you; just know that I would not have been "Me" without you!

Last but not least, dear Mamma, Papa and Gulshan thank you for your support in my studies. I can never thank you enough for your unconditional love, financial and emotional support, and above all for your belief in me and my aspirations!!

TABLE OF CONTENTS

ABSTRACT

This thesis documents the successful syntheses of six novel 2,2':6',2''-terpyridine-amine based polydentate ligands and a range of mono-, di-, and polynuclear complexes derived from them. The ability of some dinuclear complexes to affect the rate of hydrolysis of the phosphate diester group in the DNA model compound, bis-*p*-nitrophenyl phosphate (BNPP) has also been explored. Owing to the presence of two potential ligating groups in each polydentate ligand, a number of dinuclear, tetranuclear and serendipitous supramolecular architectures have been produced and characterised during this research.

The polydentate ligands were synthesised by stepwise functionalisation of the progenitor ligand, 4'-(2'''-toluyl)-2,2':6',2''-terpyridine (**L2.1**), at its *ortho* methyl position *via* free radical bromination, and where various amine groups were appended by nucleophilic substitution reactions. The detailed ligand syntheses, and characterisation are discussed in Chapter 2, along with the crystal structures of some ligands.

Chapter 3 describes coordination chemistry of 4'-(2'''-toluyl)-2,2':6',2''-terpyridine with transition metal ions. Thirteen new complexes of Ni(II), Cu(II), Zn(II) and Ag(I) are reported, where Ag(I) produced a striking spiral shaped polymer with **L2.1** having unusual 'hyperdentate' nitrogen atoms.

Two polydentate ligands, 4'-[2'''-{(2-pyridylmethyl)aminomethyl}phenyl]-2,2':6',2''-terpyridine, **L2.3**, and 4'-[2'''-{bis(2-pyridylmethyl)aminomethyl}phenyl]-2,2':6',2''-terpyridine, **L2.4**, produced six different dinuclear and tetranuclear metal complexes (Chapter 4).

The Zn(II) dinuclear complexes were used to study kinetics of hydrolysis of BNPP, and the enhanced rates were reported compared to the analogous mononuclear complexes. The detailed experimental methodology and results are discussed in Chapter 5.

The most interesting outcome of this research was formation of the box and wheel shaped complexes, where the ligand **L2.3** binds with different metal ions *via* different coordination modes. The box shaped tetranuclear complexes were synthesised deliberately *via* structural control over the coordination chemistry of terpyridine-type site of **L2.3**, where

the coordination flexibility of the pendent picolylamine-type site of the ligand was used to bind with other metal ions.

The tetranuclear $[M^1_2M^2_2(\mathbf{L2.3})_4X_2]^{6+}$ box shaped complexes were formed *when* two divalent M^1 ions bridge between the ligands to produce octahedral bis-terpyridine type complex $M^1(\mathbf{L2.3})_2$, and then two divalent M^2 ions link two $M^1(\mathbf{L2.3})_2$ units together through picolylamine binding sites, where X = Cl^-, Br^-, CH_3COO^-; M^1 = Fe(II), Zn(II), Ni(II); M^2 = Zn(II), Cu(II).

The bis-bidentate bridging ligand terephthalate was also deliberately encapsulated in the middle of Fe_2Zn_2**L2.3** box to produce the complex where X_2 = terephthalate. These structures invite speculation that it may be possible to bind and react molecules within these boxes.

In a more fortuitous outcome, Ni(II) ions were found to bind to both sites of **L2.3** to give, exclusively, an unprecedented decanuclear wheel-shaped structure. A halide ion occupies the central position in the wheel, with Br^- being preferred over Cl^-. The detailed crystal structures, and properties of the wheels shaped $Ni_{10}(\mathbf{L2.3})_{10}$ complexes are discussed in Chapter 6.

ABBREVIATIONS

A	adenine
A *vs.* t	absorbance *versus* time
ACN	acetonitrile
BNPP	bis-*p*-nitrophenyl phosphate
BPO	benzoyl peroxide
C	cytosine
COSY	2D ^{1}H NMR correlation spectroscopy
DCM	dichloromethane
DMF	*N*,*N*-dimethylformamide
DMSO	dimethylsulfoxide
DNA	deoxyribonucleic acid
ESI-MS	electrospray ionisation mass spectrometry
EtOH	ethanol
G	guanine
HPNP	2-hydroxypropyl-*p*-nitrophenyl phosphate
HSQC	heteronuclear single quantum coherence spectroscopy
IR	infra-red frequency light
M	moles per litre
MeOH	methanol
ml	milli litre
m/z	mass/charge
NBS	N-bromosuccinimide
nm	nanometre

NMR	nuclear magnetic resonance
NOSEY	nuclear overhauser effect spectroscopy
NPD	non-positive definite atomic displacement
pa	picolylamine
pK_a	acid dissociation constant
R	refinement factor
RNA	ribonucleic acid
r.t	room temperature
T	thymine
THF	tetrahydrofuran
TPMS	3-(trimethylsilyl)-1-propane sulfonic acid
tpy	2,2':6',2''-Terpyridine
U	uracil
UV	ultra-violet frequency light
vis	visible light
λ_{max}	wavelength at maximum absorbance
ε_{max}	extinction coefficient at maximum absorbance

CHAPTER 1

INTRODUCTION

1.1. Preamble and Scope

The principle aim of this study was to investigate the catalytic properties of dinuclear complexes as model hydrolytic enzymes for the cleavage of phosphate diesters. We were interested in comparing the catalytic properties of the dinuclear complexes with their analogous mononuclear complexes. The model dinuclear complexes were synthesised from ligands containing two types of metal binding sites, with 2,2':6',2''-terpyridine being the common motif in all of them. Because these ligands can bind more than one metal ion there is always the possibility that metallosupramolecular assemblies may form under some conditions.

This introduction chapter is split into four sections: First, the model systems which comprise of basics of the model systems, structure of the nucleic acids – the phosphate diester group and their reactivity. Next, the role of the metal ions in biological systems and report on some related studies of hydrolysis of phosphate diesters using mononuclear and dinuclear complexes published by other groups in this area of chemistry will be outlined. Then the literature examples of terpyridine-containing complexes in catalysis will be discussed and at the last something of the scope of supramolecular chemistry in our proposed model compounds will be described.

1.2. Model Systems - Structural and Functional Models

Gaining understanding of biological systems using model compounds involves the design, synthesis, structural elucidation, physical measurements and reactions of simple coordination compounds. The study of model systems can: (i) provide structural information on biomolecules (e.g. enzymes), and (ii) prepare authentic reagents (catalysts) usable for chemical syntheses. Ultimately, model studies may lead to new catalysts for synthetic chemistry, new drugs in medicinal chemistry, and new nutrients in agrochemistry and at least may lead to new tools for biological studies. The applications of model studies are not only limited to biological systems but may also inspire new approaches to non-related areas of science such as organic synthesis.

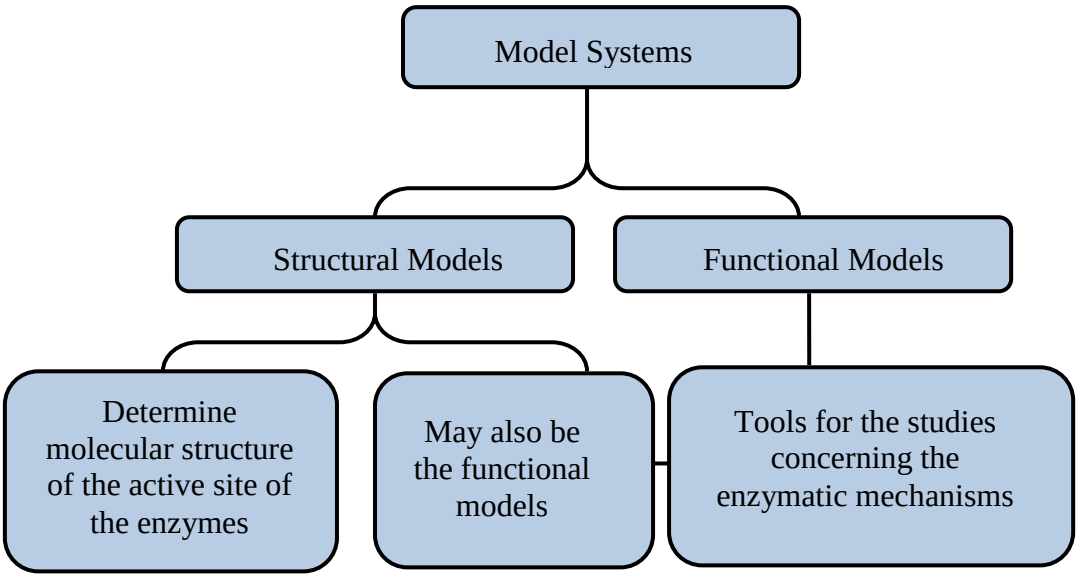

The chart above outlines the two classes of model systems for the active sites in metalloenzymes– structural models and functional models. Structural models for the active sites in metalloenzymes can help in understanding the molecular structure of the active site. The design of the structural models starts from partial spectroscopic data related to the enzyme itself and from the ensuing hypothesis for the molecular formula for the active site. By comparing the spectroscopic data from the model with the enzyme may confirm or invalidate the hypothesis, which in turn leads to the iterative improvement of the proposed active site structure. Many structures established by this method have been later confirmed by crystallographic structural analysis. Functional models try to mimic the reactivity of the active site and can exhibit the catalytic function of the enzyme. These models may be the potential catalysts for synthetic chemistry and may also be the tools for understanding the mechanism of the enzyme catalysed transformations.

However, models can straddle both classes and replicate both the structural models and functional models. This project focuses on functional models that contain a dinuclear complex that mimic active sites that hydrolyse phosphate diester bonds in nucleic acids. The design of functional models for metalloenzymes can start from the known, partially known, or unknown active sites of the enzyme. To design the functional models the only properties that have to be known are the stoichiometry of the catalysed reaction and the product of the reaction.

1.3. Nucleic Acids – an Overview

Often DNA is referred to as the 'building block of life'; because it carries the blueprint for cell growth, division and function.[1] DNA encodes the genetic information which determines how an organism will develop. DNA, deoxyribonucleic acid, is a double strand nucleic acid that is present mainly in the nucleus of the cells of most living organisms. In some organisms, DNA is also present in the cytoplasm and mitochondria of the cell. Small fractions of total DNA may also be found in chloroplasts if they are present in the cell (for example in plant cells). In comparison, RNA, ribonucleic acid is generally single stranded (although it is double stranded in some viruses). This nucleic acid is found in the nucleus and also in the cytoplasm of the cell. In some viruses, RNA carries the genetic information, but for most organisms RNA plays a vital role in gene regulation, protein synthesis and DNA replication. The most important function of RNA is to transfer information from DNA to the protein synthesis system of the cell (in the form of messenger RNA, mRNA).

1.3.1. Structure of DNA & RNA

From a structural point of view, usually DNA is a linear polymeric structure that exists as a double stranded helix. This double helix is made of two polynucleotide chains that are coiled around each other about same axis. RNA is not restricted to any such helical structure. RNA exists as a single strand but is often a highly complex three dimensional structure.

Both DNA and RNA contain chains of nucleotides. Nucleotides are phosphate esters of a five-carbon sugar (pentose), in which a nitrogenous base is covalently linked to C1' of the sugar residue.[1] In deoxyribonucleotides, **Figure 1.1(a)**, the monomeric units of DNA, the pentose is 2'-deoxy-D-ribose. In ribonucleotides, **Figure 1.1(b)**, the monomeric units of RNA, the pentose is D-ribose. The phosphate group may be attached to C5' of the pentose to form a 5'-nucleotide, **Figure 1.1**, or to its C3' to form a 3'-nucleotide.

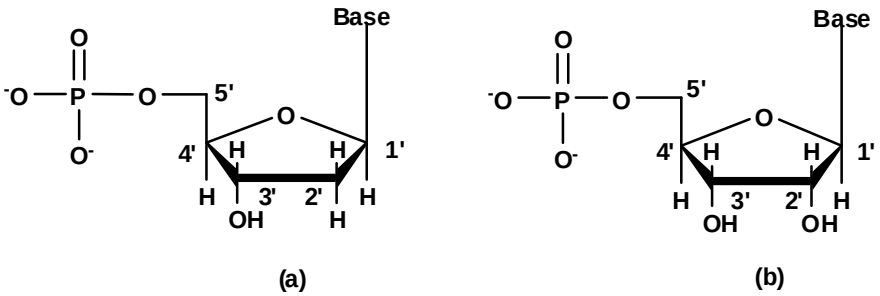

Figure 1.1. Chemical structures of a) 5'-deoxyribonucleotides and b) 5'-ribonuclotides

The nitrogenous bases display the characteristics of planarity, aromaticity, and heterocyclicity in their structures. The structures of these nitrogenous bases are based on either purine or pyrimidine skeletons. The major purine components of nucleic acids are adenine, A, and guanine, G, residues whereas the major pyrimidine residues are those of cytocine, C, uracil, U, (mainly occurs in RNA) and thymine, T, (5'-methyluracil, occurs in DNA).

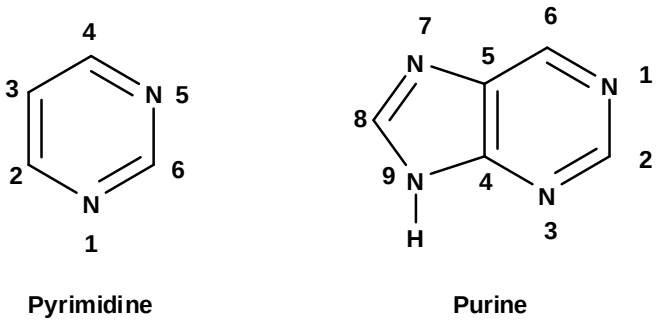

Figure 1.2. Basic structures of pyrimidine and purine

The purines are linked to ribose through their N9 atoms, whereas pyrimidines do so through their N1 atoms. The basic structures of pyrimidine and purine are shown in **Figure 1.2**.

In DNA, the hydrogen bonding of A with T, and, G with C means that the amount of adenine residues is equal to thymine residues and the amount of guanine residues is equal to cytosine residues (Chargaff's rule).[1] The main structural differences for RNA in comparison to DNA are that uracil (in RNA) is replaced with thymine (5-methyluracil in DNA) and the 2'-OH groups are present in RNA. Two strands of polynucleotide (sugar-phosphate backbone) associate through complementary base pairing and form stable helical structure.

1.3.2. The Phosphate Diester Group

In a nucleic acid chain, two nucleotides are linked by a phosphate diester group, which may be formed by a condensation reaction similar to the formation of the peptide bond. In cells, phosphate diester groups can be formed by ligation between two nucleic acid fragments; however, the whole nucleic acid chain is usually synthesised by RNA polymerase or DNA polymerase.

The phosphate diester bonds that link nucleosides are almost perfect to maintain the integrity of living organisms.[2] Phosphate diester groups are more resistant to hydrolysis than many other functional groups, such as phosphate triesters[3] and arsenates[4]. At pH 7 and 25^{o}C, phosphate diesters are very stable, with the half-life time for hydrolysis of 100 years for RNA[5] and around 16-200 million years for DNA[6]. This resistance to hydrolysis is due to repulsion between the negatively charged phosphate diester group and potential nucleophiles.[2] While the high stability of nucleotide chains is important, it is vital that DNA can be hydrolysed in order to allow mutations to be removed.

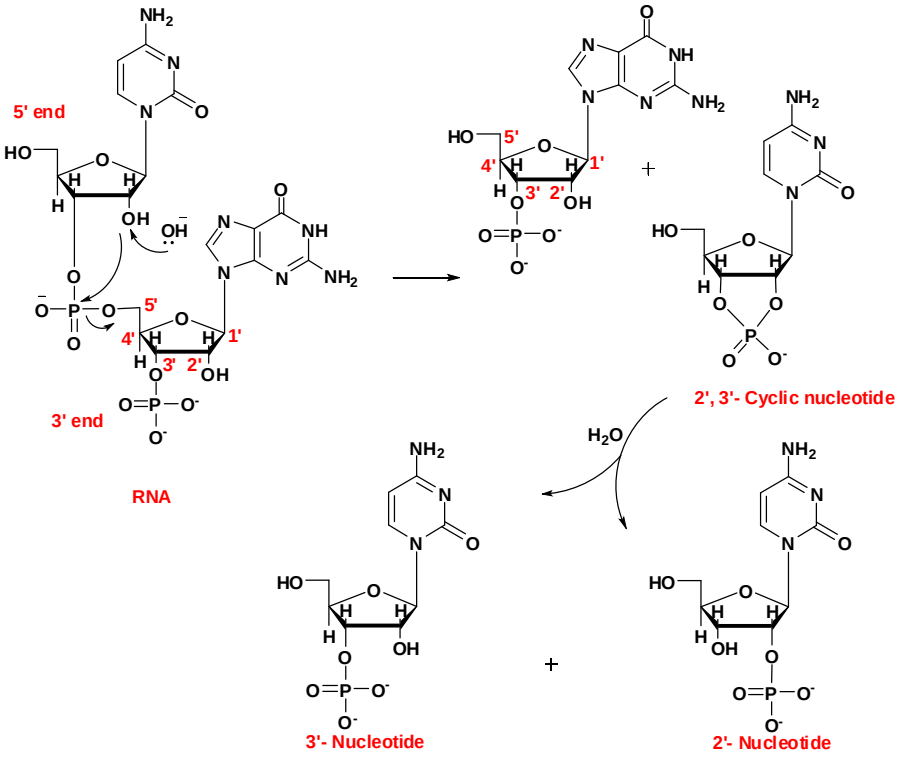

Figure 1.3. Mechanism of base-catalysed RNA hydrolysis

Compared to DNA, the RNA polymer is much more susceptible to hydrolysis due to presence of the hydroxyl group at 2' position. This hydroxyl group acts as an intramolecular nucleophile for base induced hydrolysis of RNA. The reaction mechanism is shown in **Figure 1.3**.

The uncatalysed hydrolysis of a DNA phosphate diester group is thermodynamically favourable ($\Delta G^{o'}$= -2217 kJ/mol) but kinetically it is very slow due to negatively charged oxygen atoms of the phosphate diester group.[7, 8] Nature has, therefore, produced a class of enzymes called nucleases with the purpose of hydrolysing DNA.

1.3.3. Enzymes for Nucleic Acid Hydrolysis – Nucleases

In the literature, there is a large variation in the estimated half-lives of hydrolytic cleavage for the DNA backbone ranging from about 16 million to 200 million years.[9-13] In order to catalyse the hydrolysis of nucleic acids, nature utilizes a class of enzymes called nucleases. Nucleases are able to hydrolyse DNA with a rate enhancement over the uncatalysed reaction exceeding 10^{16} under physiological conditions.[14] In living organisms, all cells contain nucleases that help in nucleic acid metabolism. Nucleases are also known as phosphate diesterases.

Depending upon the site of cleavage, nucleases can be divided into two categories: endonucleases and exonucleases. Endonucleases cleave bonds within the polymer chain of nucleic acid whereas exonucleases remove terminal nucleotides.

In many nucleases the active sites contains both the metal ions and reactive amino acid side chains that act in a synergistic manner. Such nucleases called metallonucleases, and are focus of this project.

In all the metallonucleases, metal ions act as cofactors that can do one or more of the following:

- Provide metal-bound nucleophile that can attack on the phosphorus atom of the diesters at neutral pH.

– Act as Lewis acids that move the negative charge away from phosphorus atom and facilitate nucleophilic attack and stabilise charge formed in transition state.

– Help in stabilization of leaving group.

– Provide metal-hydroxide that acts as a general base.

1.4. The Role of Metal Ions in Enzymes

Metal ions play an important role in biological systems. Approximately one third of enzymes contain metal ions in their active sites. Many enzymes contain one or more metal ions to achieve substrate activation. These are known as metalloenzymes. Metal ions in the active sites of enzymes can be tightly bound with strong covalent bonds or can be loosely associated. Most metal ions of the third and fourth period of the periodic table play a significant role of some kind in enzyme function. The tightly bound metal ions such as Fe(II), Cu(II), Zn(II), Mn(II), Co(III), Ni(III) and Mo(VI) are important for catalytic action of the metalloenzymes, but some other metal ions such as K(I), Na(II), Mg(II) and Ca(II) also help in catalysis where metal ions are not strongly bound to the metalloenzymes.

The metal ions can act as Lewis acid catalysts due to their high oxidation states, and activate the phosphoryl group by increasing the polarity of P=O bond. Another important role of metal ions is to provide a powerful nucleophile at neutral pH. The metal coordinated water will have increased reactivity but still less than a hydroxide ion.

$$M + HOH \rightleftharpoons M\text{----}OH_2 \rightleftharpoons M\text{----}OH^- + H^+$$

In nature, there are many enzymes that are involved in catalysing the hydrolysis of phosphate esters. Many of the enzymes are activated by two or more metal ions. These metal ions can accelerate the rate of phosphate ester hydrolysis in several ways as represented in **Figure 1.4**.

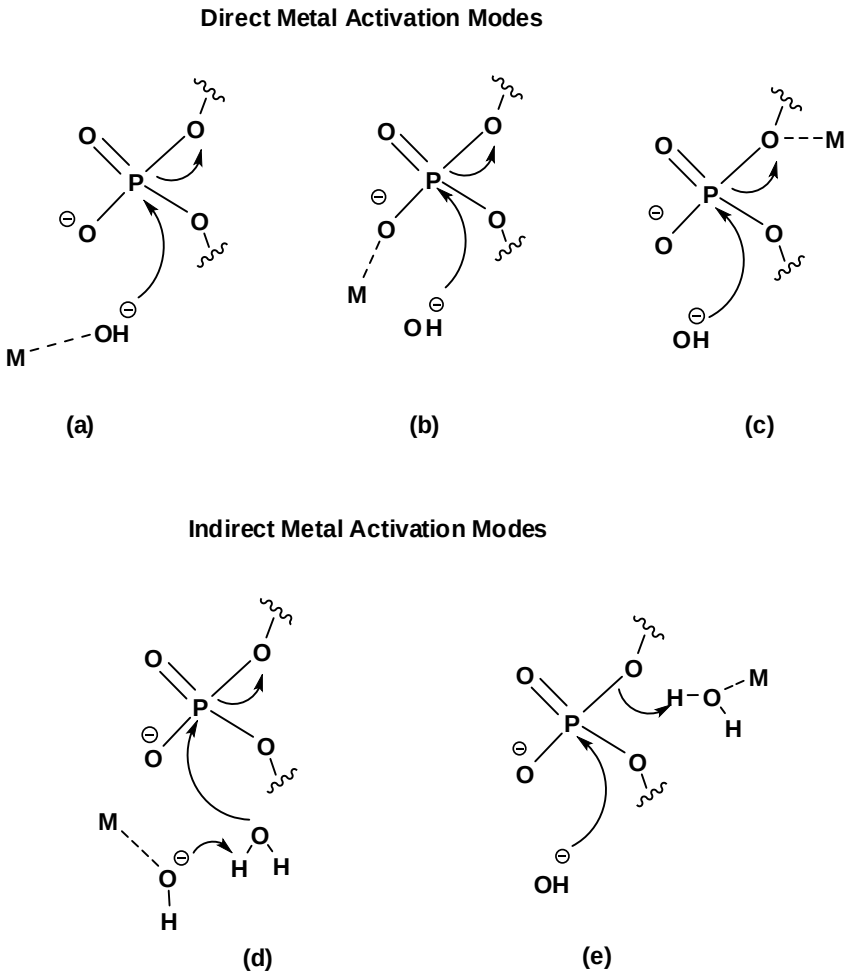

Figure 1.4. Various modes of activation by the metal ion for phosphate diester hydrolysis.[15]

Three direct modes of activation by metal ions for phosphate diester hydrolysis are:

Nucleophilic activation – Coordination of a nucleophile such as hydroxide to the metal, **Figure 1.4**(**a**).

Lewis acid activation – Electrophilic catalysis by a metal ion through coordination of one or both of the non-bridging phosphoryl oxygen atoms, **Figure 1.4**(**b**).

Leaving group activation – Coordination of the leaving group oxygen atom to the metal, **Figure 1.4**(**c**).

Two indirect modes of activation by metal ions for phosphate ester hydrolysis are:

General base catalyst – A metal coordinated hydroxide acts as a general base catalyst, **Figure 1.4**(**d**). The metal-bound hydroxide deprotonates a water molecule, and generate a nucleophilic hydroxide ion which attacks the phosphorus atom.

General acid catalyst- A metal-coordinated water molecule acts as a general acid catalyst, **Figure 1.4(e)**. The metal-bound water produces H^+ ion, which then acts as an electrophile that attaches to O and makes P atom more susceptible for nucleophilic attack. The H^+ formed can also attach to an oxygen atom of the leaving group.

Some of these possibilities are not mutually exclusive. This means the same metal ion may act as a source of hydroxide and Lewis acid catalyst, or Lewis catalyst and activate the leaving group, because all these activation processes occur on the same side of the phosphate diester unit. However, one metal ion cannot fulfil the role of nucleophile or general base, and leaving group activation or general acid. This is because the process of formation of metal coordinated nucleophile and general base catalysis occurs at same side of the phosphate diester group, whereas both leaving group activation and general acid catalysis occurs at the other end of phosphate diester. Clearly, one metal ion cannot activate the phosphate diester group from opposite sides at the same time. Hence, two or more metal ions could help in such cases. More than one metal ion means more than one mode of activation may operate simultaneously.[15]

Naturally occurring enzymes that contain two or more metal ions include phosphate monoesterases (enzymes that cleave phosphate monoester group). For example, alkaline phosphatase, which contain two Zn(II) and one Mg(II) ion in its active site[16], purple acid phosphatase contains two Fe ions in the active site.[17] Inositol monophosphatase shows an absolute requirement for a divalent metal ion and activity is supported by Mg(II), Mn(II) and Zn(II) ions[18, 19] and D-fructose 1,6-biphosphate1-phosphatase is also activated by divalent metal cations such as Mn(II) and Zn(II) and one Mg(II). [20]

Two examples of phosphate diesterases, which contain two or more metal ions, are RNaseH (from HIV reverse transcriptase) and the 3'-5' exonuclease domain (from the Klenow fragment). Mechanistic studies of the 3'-5'exonuclease propose that one metal ion acts as a source of nucleophilic hydroxide while second metal ion activates the leaving group and acts as an electrophilic catalyst.[21]

1.4.1. Mononuclear and Dinuclear Model Enzyme Systems – Literature Examples

Studies of the enzyme models can provide valuable information to understand the mechanisms, reaction rates and other important aspects of the chemistry involved in the action of the metalloenzymes. For many years, scientists have been using model compounds to study enzymes for two main reasons: First, it is easier to understand the relation between structure and reactivity of simple model compounds. Second, model compounds can be valuable tools in their own right for studying nucleic acids or can be helpful in designing some therapeutic agents in challenging medicinal areas such as for cancer treatment and other viral diseases.

The effectiveness of model systems in promoting hydrolysis of phosphate diesters is a function of many factors, including the nature of metal atoms, the attached ligands, the distance between reactive centres, positioning of the ligands, the phosphate species, and the compositions and structures of the intermediate complexes formed between them.[22-24] There are a number of reviews published about the role of metal ions in artificial phosphate diesterases and nucleases.[14, 23, 25-37] Artificial nucleases have been studied that contain different metal ions such as Zn(II), Cu(II), Co(II), Ni(II), Co(III), Fe(III), and lanthanides La(III), Eu(III), Er(III), Ho(III) and Ce(IV). Most of such metal ions are good for hydrolysis studies due to their abundant coordination geometries, high charge density and strong Lewis acidity. This section will discuss previous studies on mononuclear and/or dinuclear complexes act as catalysts to promote hydrolysis of phosphate diesterases, and how these studies can illuminate various mechanisms and other structural factors involved for activity of the models.

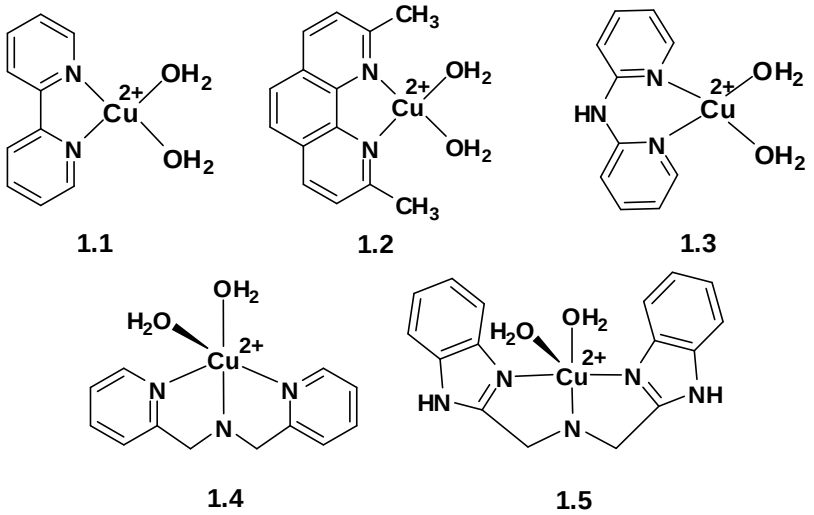

Figure 1.5. Mononuclear Cu(II) cis-diaqua complexes studied by Chin et al.

Chin *et al*. studied a number of mononuclear complexes including *cis*-diaqua Cu(II) complexes **1.1** – **1.5** in two studies, **Figure 1.5**. These complexes show different rates of cleavage of phosphate diesters due to the ligand effect. The complex **1.1** and **1.2** promoted the cleavage of phosphate diester by pseudo-first order rate constants of 1.9×10^{-5} s^{-1} and 3.9×10^{-3} s^{-1}. They observed that at neutral pH **1.1** dimerizes[38] with an equilibrium constant of 1×10^{5} M^{-1} as shown in **Figure 1.6**, and the dimer is inactive for hydrolyzing phosphate diester and at higher pH 7.8, only about 8% of **1.1** is in the monomeric form.

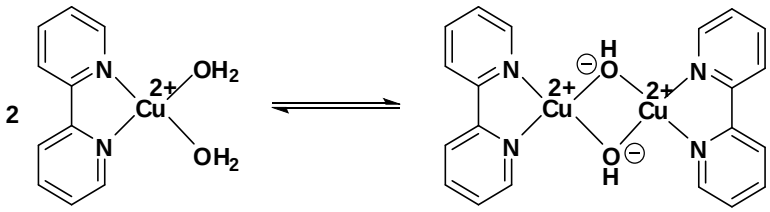

*Figure 1.6. Dimerization of complex **1.1** at neutral pH.*

The higher reactivity of **1.2** compared to **1.1** was justified by proposing a mechanism that involved double Lewis acid activation, where the developing negative charge on phosphorus was stabilised by the metal centre. In **1.2** the methyl groups of the neocuproine ligand should decrease the O-Cu-O bond angle, which should facilitate the chelation of the phosphate diesters. In phosphate chelated Co(III) complex $[Co(en)_2PO_4]$, en = ethylene diamine, studied by Sargeson *et al*. the O-Co-O bond angles are significantly smaller than the 90° angles found in regular octahedral complexes shown in **Figure 1.7**.[39]

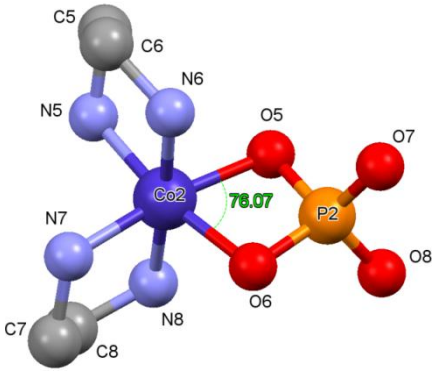

Figure 1.7. A ball-stick model of the crystal structure of [Co(en)$_2$PO$_4$] showing geometry of the Co(III) chelate ring and O-Co-O bond angle.[39]

Of the remaining complexes **1.3-1.5,** the complex **1.5** was the most reactive. It was observed that **1.5** becomes more reactive with increasing concentration whereas **1.3** and **1.4** becomes less reactive (pseudo-first order kinetics). It was particularly interesting that **1.5** was more reactive than **1.4**, considering that both complexes were closely related electronically, and their pK_a values are also comparable (5.2 for pyridinium and 5.4 for benzimidazolium). However, the solid state structure of **1.5** with coordinating ligands revealed that one chloride ion was in a highly hindered environment. So it was proposed that dihydroxy bridged dimerization of **1.5** would be difficult and it might dimerise to a highly reactive mono-hydroxy bridging complex.

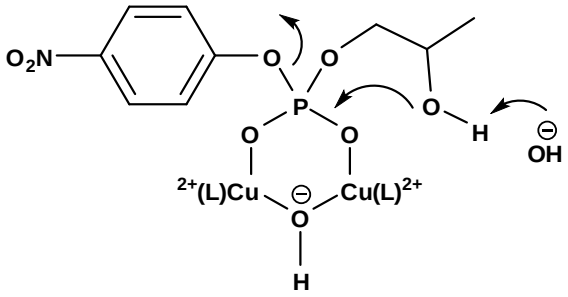

*Figure 1.8. Proposed intermediate during transesterification HPNP by complex **1.5***

The transesterification reaction of 2-hydroxypropyl-*p*-nitrophenyl phosphate (HPNP) was proposed to result in formation of a trigonal-bipyramidal intermediate, where the O-P-O bond angle in the six membered ring, **Figure 1.8**, was supposed to increase to about 120°. Complex **1.5** hydrolyses the phosphate diesters with second-order kinetics, where rate increases with increase in pH and levels off at the solution pH near to the pK_a of **1.5**. This means reaction was base-catalysed and maximum mono-hydroxy species are available at pH slightly above the pK_a of the solution of **1.5**.

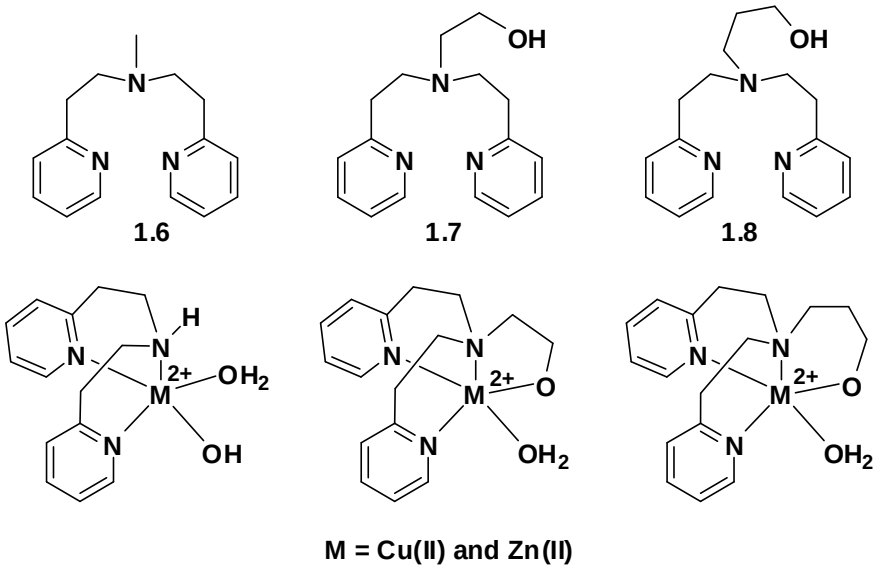

Figure 1.9. Tridentate and tetradentate ligands and their corresponding metal complexes.

Laing *et al.* studied that a small change in the coordination sphere of a complex can have a profound effect on their reactivity.[40] Three different nitrogen donor pyridyl-amine ligands (**Figure 1.9**) bis-(2-pyridine-2-yl-ethyl)amine (**1.6**), 2-[bis-(2-pyridine-2-yl-ethyl)amino]-ethanol (**1.7**), and 3-[bis-(2-pyridine-2-yl-ethyl)amino]-propanol (**1.8**) were synthesised and their Cu(II) and Zn(II) complexes were studied to investigate their ability to promote the hydrolysis of an activated phosphate diester bis(*p*-nitrophenyl)phosphate (BNPP).

The much higher reactivity of complexes of **1.8** compared to **1.7** and **1.6** was explained by the higher flexibility of the alkoxide tether in **1.8**, which was proposed to allow the nucleophilic alkoxide O atom in **1.8** a better access to attack a metal-bound BNPP substrate. Complex **1.7** has a shorter alkoxide tether which hydrolysed BNPP with metal-bound hydroxide instead of using its alkoxide unit because of constraints in the ligand tether. The higher reactivity of Cu(II) complex of **1.8** was also attributed to the long alcohol pendant being better oriented to serve as a proton acceptor from a Cu(II) bound aqua ligand which facilitates its deprotonation and subsequent nucleophilic attack of the Cu(II)-hydroxide moiety towards BNPP. The Cu(II) complexes of these ligands were more reactive than analogous Zn(II) complexes consistent with the higher Lewis acidity of Cu(II).[41]

Gultneh *et al*. studied the Zn(II) complexes of the chelating pyridyl donor ligands $[Zn(bpa)(H_2O)_2](ClO_4)_2$, (**1.9**), $[Zn_2(bpea)_2(\mu\text{-}OH)](ClO_4)_3$, (**1.10**), $[Zn_2(\mu\text{-}OH)(m\text{-}xylbpea)](ClO_4)_3$ (**1.11**) shown in **Figure 1.10**.[42, 43] A variation in pK_a, and catalytic

properties was observed with changing nuclearity and chelate ring size of Zn(II) complexes. For these complexes the second order rate constants of the order of 10^{-3}–10^{-2} $M^{-1}s^{-1}$ for hydrolysis of BNPP were measured, and the rate of reaction was dependent upon the concentrations of the active complex species and of the metal-coordinated hydroxide (the reactive nucleophile).

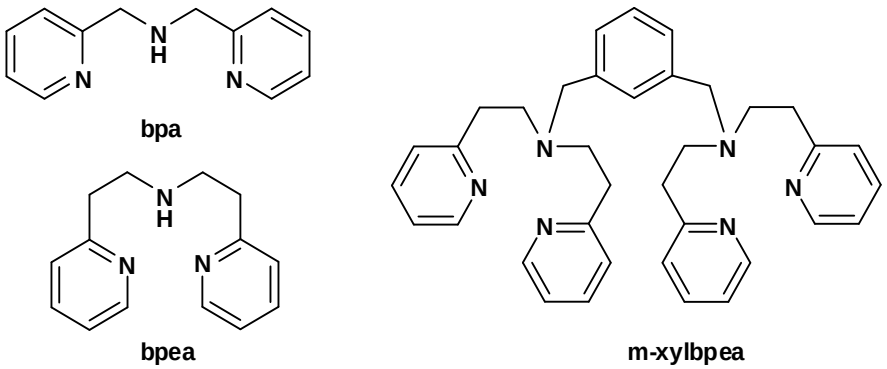

Figure 1.10. Chelating pyridyl donor ligands studied by Gultneh et al.

The pK_a value of the dinuclear hydroxo-bridged Zn(II) complex **1.10** was measured to be 8.35 and that of **1.11** was 7.55. The lower pK_a for the latter complex is accounted for by the entropic advantage gained by having the two Zn(II) ions held together by the dinucleating ligand. However, in the hydrolysis of BNPP catalysed by Zn(II) complexes, the observed rate constant above pH 8 for complex **1.10** is significantly higher than that shown by the analogous complex **1.11** formed by the dinucleating ligand. This difference for complex **1.10** was proposed to be due to the formation of a catalytically less active species, possibly a double hydroxy-bridged compound. The rate constants were observed to increase and pass through a maximum at or around the pK_a values of all the zinc complexes reported here. This observation was consistent with the widely accepted mechanism in many hydrolytic reactions catalysed by metal complexes in which the metal coordinated hydroxide is the reactive nucleophile.

Piovezan *et al*. reported the activity of three Fe(III) complexes, **Figure 1.11**, Fe_2(bbppnol)(μ-AcO)-$(H_2O)_2$]$(ClO_4)_2$, (**1.12**), [Fe_2(bbppnol)(μ-AcO)$_2$](PF_6), (**1.13**), and[Fe_2(bbppnol)(μ-OH)$(Cl)_2$]·$6H_2O$, (**1.14**), (where H_3bbppnol = N,N'-bis(2-hydroxybenzyl)-N,N'-bis(2-methylpyridyl)–1,3-propanediamine-2-ol) in hydrolysis of bis-*p*-nitrophenyl phosphate (BNPP).[44] They investigated accessibility of the substrate to the reaction site is the key steps to determinate the hydrolysis efficiency.

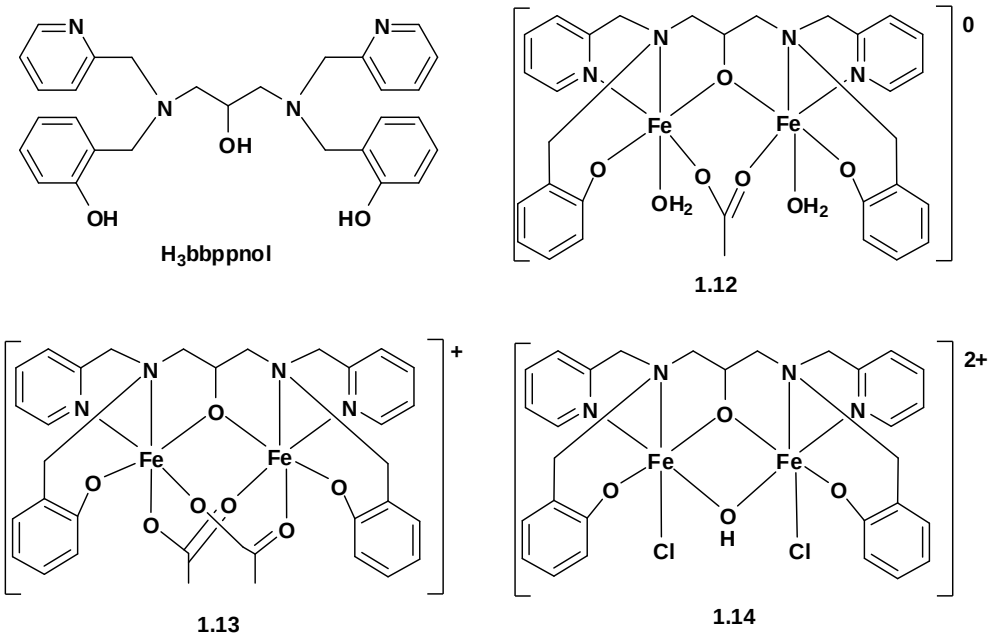

Figure 1.11. Dinuclear Fe(III) complexes with variable access to the substrate in the solution state.

Initially a similar complex was studied in weakly acidic media and hydrolysis of the phosphate diester BNPP was observed.[45] The maximum rate was observed at pH 5.6 and the metal coordinated hydroxide, $[Fe_2(OH)(OH_2)]$, was the reactive component. This is because the potentiometric titration of the complex demonstrates two titratable protons, at the pK_a values 4.88 and 6.33 corresponding to formation and dissociation of the hydroxide species $[Fe_2(OH)(OH_2)]$, as shown in the equation below. These species has its maximum concentration at pH 5.6.

$$Fe_2(OH_2)_2 \underset{-H^+}{\overset{K_{a1}}{\rightleftharpoons}} Fe_2(OH)(OH_2) \underset{-H^+}{\overset{K_{a2}}{\rightleftharpoons}} Fe_2(OH)_2$$

The hydrolysis studies were also performed in basic medium (pH 7-9) using **1.12**-**1.14** complexes to investigate if the presence of more than one deprotonated species bound to the binuclear structure would increase the reaction rate. It was reported that complex **1.13** shows highest reactivity, although spectrophotometric results suggest formation of the same species, [(OH)Fe(μ-AcO)Fe(OH)], in both **1.12** and **1.13**. This indicated that for **1.12** the additional acetate group remain in the structure to the iron centre, which might have hindered the hydroxyl attack to the phosphate. Similarly for **1.14** the inert chloride ligands may not be easily replaced by the substrate molecules. The

reactivity difference observed for these complexes confirms that the accessibility of the substrate to the reaction site is one of the key steps to determine the hydrolysis efficiency.

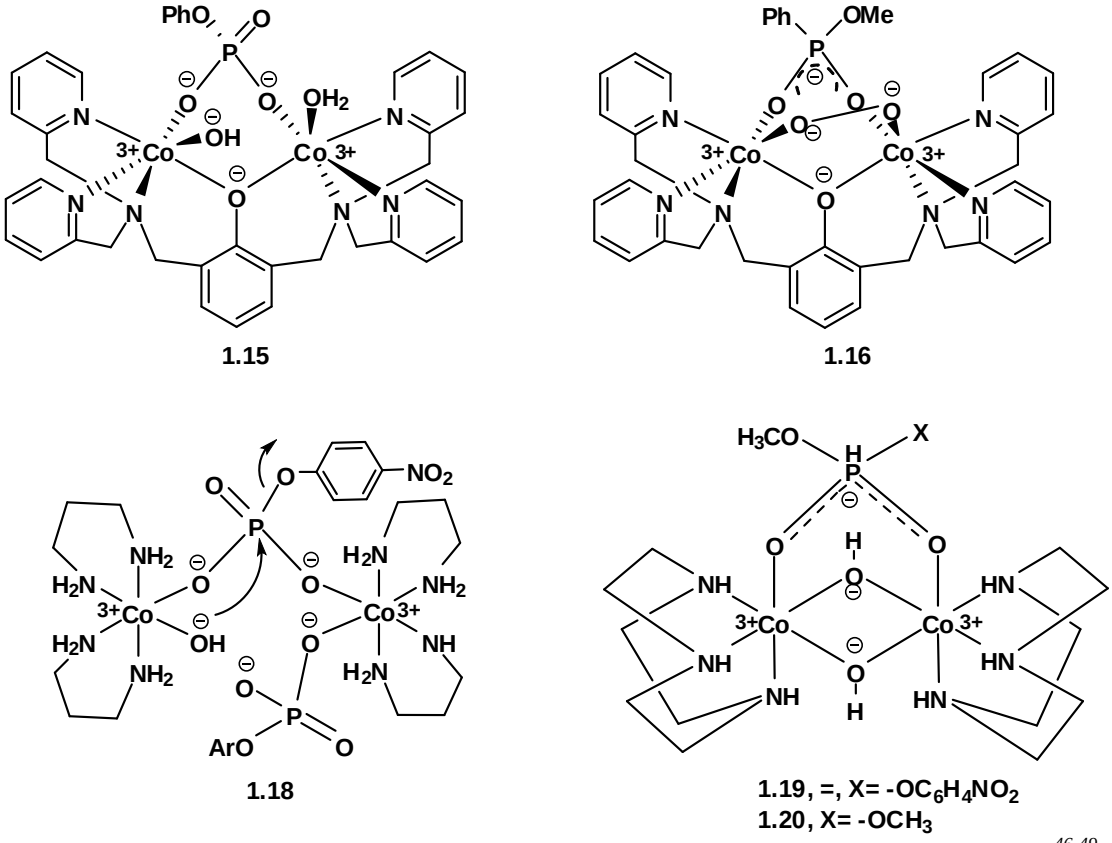

Figure 1.12. Some of the Dinuclear complexes studied by Chin et al. and Sargeson et al.[46-49]

Sargeson *et al*. and Chin *et al.* also studied a number of mononuclear and dinuclear complexes for metal-bound phosphate esters *via* intramolecular metal-coordinated hydroxide mechanism.[46-53] They also investigated higher reactivity of the dinuclear complexes, **1.15** – **1.20** in **Figure 1.12**, for cleavage of phosphate esters in comparison to mononuclear Co(III) analogues. The effect of the nature of the leaving groups was also studied during these experiments.

Hydrolysis of the bridging phosphate monoester in **1.15** was monitored by ^{1}H NMR and ^{13}C NMR.[49] In aqueous solutions, the ^{31}P NMR signal due to **1.15** gradually decreased with concomitant increase in the signal at 28 ppm. Over the same period, the ^{1}H NMR signal due to the methyl group in **1.15-H** was converted to that of **1.17**, **Figure 1.13**. The pH-rate profile for the hydrolysis reaction presented an increase in rate of hydrolysis with increase in pH but levels off at pH 10 (pK_a of the metal-bound water in

1.15 was calculated as 9.8). The simplest mechanism that fits these observations was the deprotonation of the metal-bound water in **1.15** to form **1.15-H** followed by intramolecular nucleophilic attack of the metal hydroxide on the bridging phosphate monoester to form **1.17** and phenol, **Figure 1.13**. There was only one signal in ^{31}P NMR for **1.17** and was about 28 ppm downfield shifted relative to the corresponding signal of the unbound phosphate, which is a characteristic of a phosphate with three of its oxygen atoms coordinated to Co(III).[54]

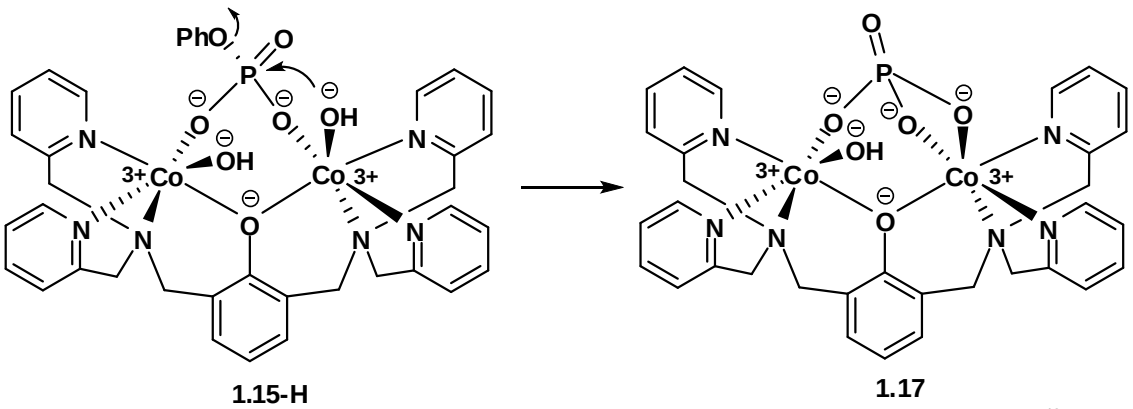

Figure 1.13. Intramolecular hydroxide attack on phosphorus studied by Chin et al.[49]

The X-ray crystal structure of a complex[49] very similar to that of **1.15** shows that the one of the coordinated water/hydroxide molecule is much closer to the phosphorus center (3.06 Å) than the other coordinated water/hydroxide molecule (3.67 Å). So Chin *et al*. proposed that only one product was formed because the coordinated water/hydroxide closer to the phosphorus centre was the nucleophile. The rate of hydrolysis of uncomplexed dianionic phenylphosphate is approximately 4×10^{-13} s^{-1}, and the estimated rate of hydrolysis of bridging monoester in **1.15-H** was about 4×10^{-1} s^{-1}, which indicated about 11 orders rate acceleration in dinuclear complexes.

Sargeson *et al*. proposed similar mechanism for the hydrolysis of *p*-nitrophenyl phosphate bridging two Co(III) ions as in **1.18**[47, 48, 52], **Figure 1.13**.[48] The estimated rate of hydrolysis of monoester in **1.18** was about 4×10^{-1} s^{-1}, and the rate of hydrolysis of uncomplexed dianionic *p*-nitrophenyl phosphate is approximately 2×10^{-9} s^{-1} at 25 °C. That means the dinuclear complex **1.18** provides about 8 orders of magnitude rate acceleration for the hydrolysis reactions. The greater rate of acceleration in hydrolysis of the monoester in **1.15-H** was proposed to be due to more rigid structure in **1.15-H** in comparison to **1.18**.

A study[55] of complexes **1.19** and **1.20** shows that **1.19**, which has a good leaving group, hydrolyses about 10^{11} times more rapidly than the metal-free diester while the phosphate diester in **1.20**, with a poor leaving group, dissociates from the Co(III) centre without any noticeable hydrolysis of the diester bond. This means that a catalyst which provides large rate acceleration for hydrolysis of the activated phosphates (those with good leaving groups) does not hydrolyse the unactivated phosphate with a comparable rate. Complexes **1.15**, **1.19** and **1.20** mimic dinuclear phosphate diesterases such as fructose-1,6-biphosphatases and purple acid phosphatases found in nature.[20, 56]

In 1999, Kim *et al*. compared Zn(II) and Cu(II) complexes of the dinucleating ligand **1.21** and the analogous mononucleating unit **1.22** towards hydrolysis of BNPP and NPP in aqueous solutions.[57]

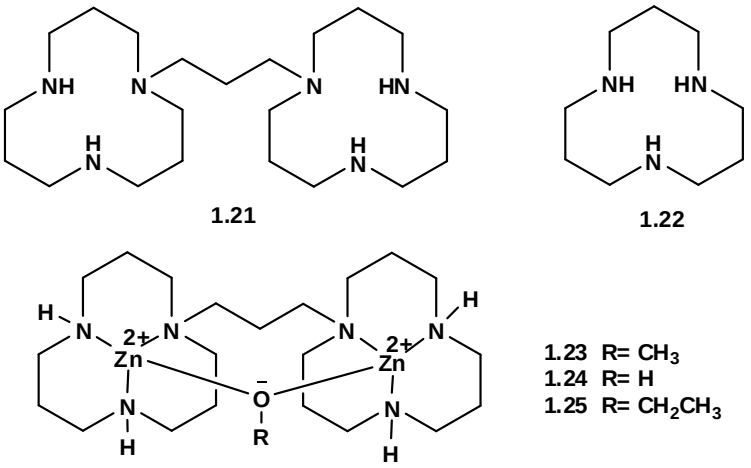

*Figure 1.14. 1,5,9,-Triazacyclododecane, **1.22**, analogous alkyl-bridged dinucleating ligand **1.21** and its Zn complexes*

The first order rate constant for BNPP hydrolysis by the dinuclear Zn complex **1.24** was only slightly higher than that by the mononuclear Zn complex of **1.22**. The low reactivity of **1.24** was considered to be due to dimerization or pK_a changes of the Zn-bound water molecules (this will be discussed in Chapter 5 of this thesis that describes the kinetic studies of hydrolysis conducted during this research). No cooperation was observed between two metal ions.

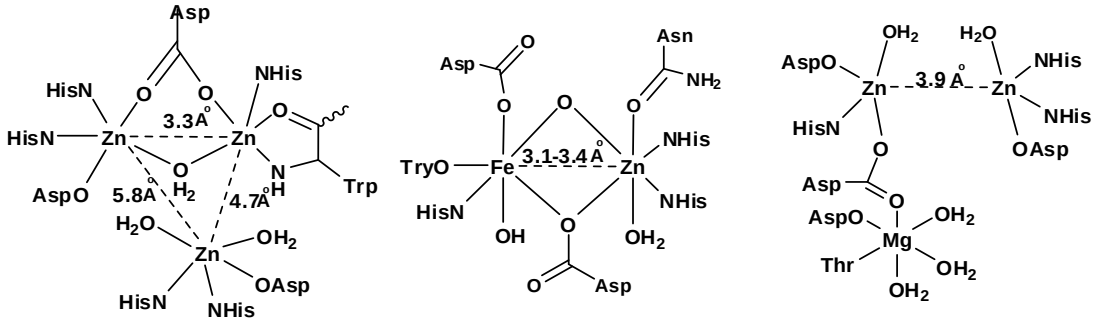

Figure 1.15. Some natural phosphate diesterases featuring bridging carboxyl units, the metal-metal distances are given.[58]

Many natural phosphate diesterases contain two or three zinc ions, bridged by a carboxylate group from an aspartate residue and a water molecule, in their catalytic sites, as shown in **Figure 1.15**.[29, 59-61] These zinc enzymes often use external water molecules or internal alcoholic hydroxyl residues as nucleophiles to react with electrophilic substrates.[62] The role of zinc centres in these enzymes is to orient and activate the substrate and this largely depends upon the metal-metal distance in the enzymes.[29, 59, 63-65]An example of a model system that was studied in order to understand the role of metal ions in such systems is shown in **Figure 1.16**.[58]

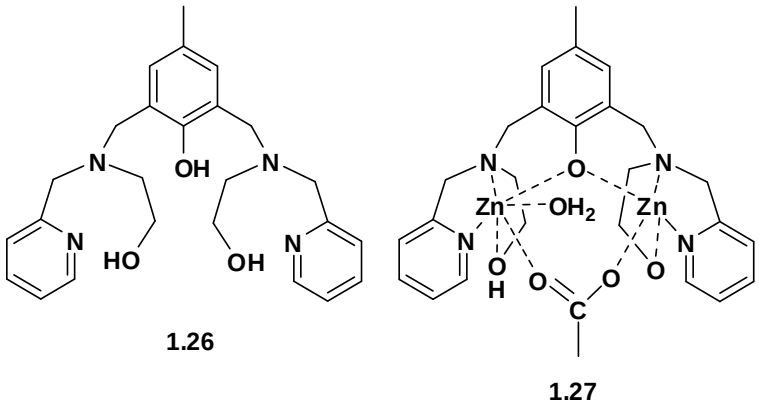

*Figure 1.16. Alcoholic hydroxyl containing phenolate-based ligand **1.26**, and its dinuclear Zn complex **1.27**.*[58]

Similar to a previous study done by Chin *et al.*[49] a double Lewis acid activation mechanism was proposed for the **1.27** catalysed BNPP cleavage. The cleavage of BNPP promoted by **1.27** may be triggered by the phosphate diester coordination to two zinc centers in a bidentate bridging mode, followed by an attack of the deprotonated alcoholic hydroxyl to the phosphorus center, and finally leading to cleavage of the P-O bond. The

Zn-Zn inter-metallic distance in **1.27** was 3.421 Å which facilitated the cooperative action for the phosphate bridging, and BNPP was activated by the zinc centres.

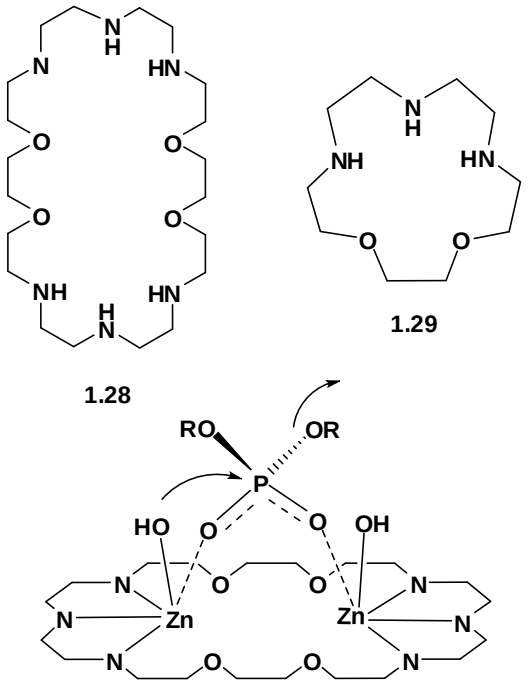

Figure 1.17. Macrocyclic ligands studied for hydrolysis of BNPP and proposed mechanism for hydrolysis of BNPP by the dinuclear Zn(II) complex of 1.28.[66]

Usually, in most of the dinuclear complexes, metal ions show cooperative action for phosphate diester hydrolysis when they lie less than 4 Å apart. However there are flexible dinuclear Zn(II) complexes of the macrocyclic ligands shown in **Figure 1.17**, where metal ions work cooperatively at a distance of greater than 5 Å.[66] The dinuclear complex $[Zn_2(\mathbf{1.28})(OH)_2]^{2+}$ complex was almost 10 times more active than the mononuclear $[Zn(\mathbf{1.29})(OH)]^{+}$ complex. The hydrolysis mechanism was proposed as shown in **Figure 1.17** where the phosphate ester interacts with two electrophilic Zn(II) centres, and at the same time one Zn-OH acts as a nucleophile to attack to phosphorus atom. This means, two Zn(II) ions play a cooperative role. This mechanism was supported by the crystal structure of a proposed intermediate compound $[Zn_2(\mathbf{1.28})(\mu\text{-PP})_2\text{-}(MeOH)_2]^{2+}$where the phosphate unit bridges both metal ions (μ-PP denotes bridging phosphate). In this complex the flexibility of the macrocycle allows two metal centres to lie at a large distance of 5.34 Å.

A series of Zn(II) complexes of a series of polyamine ligands shown in **Figure 1.18** have been investigated for their catalytic effect for hydrolysis of the activated phosphate

diester BNPP.[67] It was suggested that not only the number of coordinating atoms on the ligands but also a favoured geometry is an important parameter.

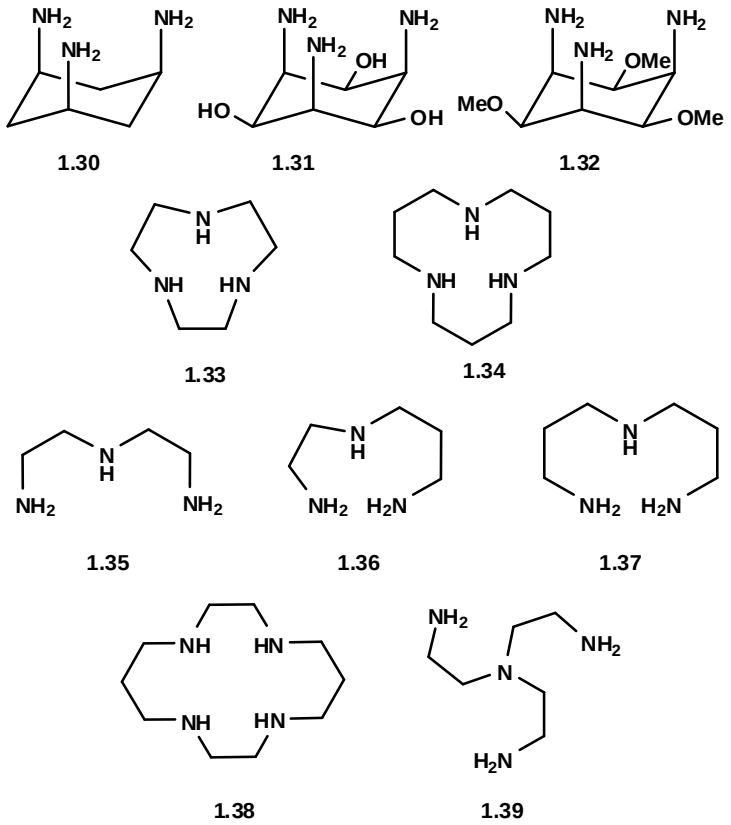

Figure 1.18. Tridentate and tetradentate polyamine ligand used to study their Zn(II) complexes for phosphate diester hydrolysis.[67]

The hydrolysis of BNPP promoted by the Zn(II) complexes of the ligands (**1.30-1.39**) was investigated in water at 25 °C. The kinetic studies were carried out by following the increase in absorption due to formation of the *p*-nitrophenolate ion, using the initial rate method. The metal-bound hydroxide was found to be the active nucleophile in the cleavage of BNPP. A plot of pK_a values with log *k* values showed a reactivity difference between different classes of ligands. The Zn(II) complexes of **1.30-1.35** showed an increase in rate with increasing Lewis acidity of the metal ion and lower pK_a. The Zn(II) complexes of **1.38** and **1.39** showed a very low reactivity, and the linear tridentate ligands **1.35-1.37** showed an intermediate efficiency without any clear trend. The triamino ligands with a facial or tripodal coordination mode were most reactive due to better access of the substrate for metal binding compared to tetradentate ligands, and similar coordination geometries are adopted by nature in the reactive site of Zn(II) based hydrolytic sites. These studies indicate that a good model should be the one with greater

Lewis acidity of the metal ions, lower pK_a values for the metal-bound nucleophile, and more importantly which allows the substrate to bind with metal ions.

1.4.2. 2,2':6',2''-Terpyridine Metal Complexes as Models for Enzyme Active Sites

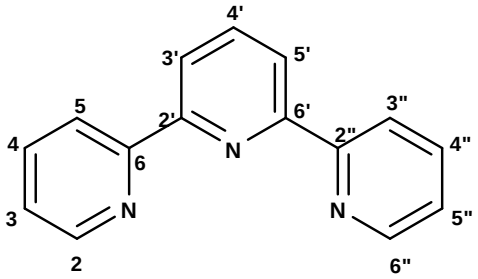

2,2':6',2"-Terpyridine (tpy)

2,2':6',2"-Terpyridine (tpy) is a planar, tridentate ligand which results in formation of stable complexes with different metal ions. There is a huge literature available on its complexes that discuss its coordination chemistry and its applications.[68-90] Literature studies where tpy or its derivatives have been used for hydrolysis studies are discussed in this section.

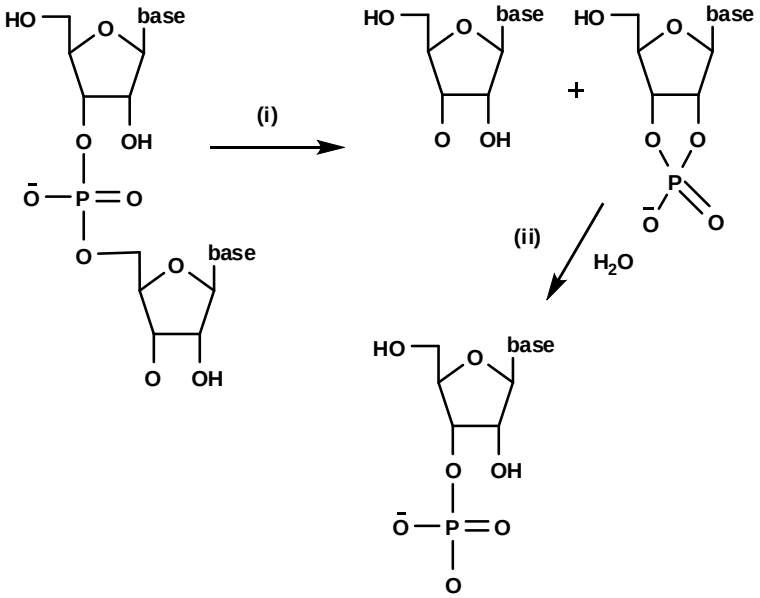

Figure 1.19. Two step hydrolytic cleavage of 2',3'-cAMP, (i) transesterificaton and (ii) hydrolysis

The Cu(II) and Zn(II) complexes of 2,2':6',2"-terpyridine have been the most studied complexes for cleavage of phosphate esters and RNA.[91-101] In 1993, Bashkin *et al.* studied $[Cu(tpy)H_2O]^{2+}$ (**1.40**) for hydrolysis of a model phosphate diester bis-*p*-

nitrophenyl phosphate (BNPP) and 2',3',-cyclic adenosine monophosphate (2',3'-cAMP).[92] The results showed that **1.40** can catalyse the hydrolysis of 2',3'-cAMP but does not hydrolyse the activated substrate BNPP. In 1991, Morrow *et al.* also suggested that Cu-tpy complexes are not good catalysts for hydrolysis of phosphate diesters.[100, 101]

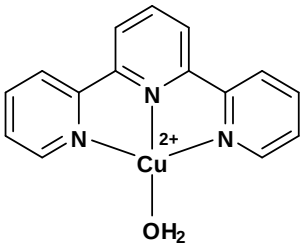

1.40

Figure 1.20. The Cu-tpy complex studied by Baskin et al. and Morrwo et al.

In case of 2',3'-cAMP the hydrolytic cleavage is a two step process, the first step is transesterification that employs the 2'-OH of RNA as an intramolecular nucleophile, while the second step is hydrolysis, **Figure 1.19**. The reaction is first order with respect to **1.40.** It was suggested that **1.40** and its analogues are inorganic analogues of imidazole, with the additional property that complex **1.40** can undergo direct coordination. This property leads to enhanced cleavage rate of 2',3'-cAMP to 800 fold in comparison to imidazole.[102]

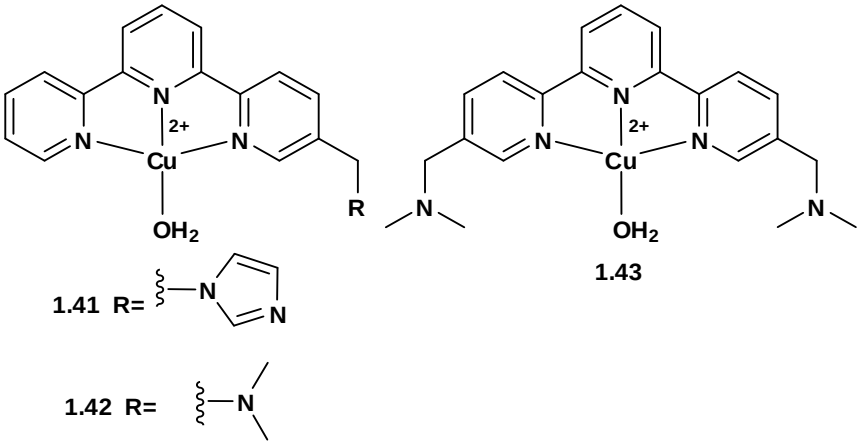

Figure 1.21. Cu(II) complexes of the terpyridine derivatives studied for catalysis of transesterification reaction of model RNA.

Complex **1.40** was found to be among the most active transition metal complexes that catalyse the hydrolysis of RNA,[103, 104] and it was well established that general base catalysis is required for transesterification of RNA and other model compounds.[105] Therefore, Liu and Hamilton developed some terpyridine derivatives and their corresponding Cu(II) complexes, which contain base groups on the periphery of the

ligands (**Figure 1.21**).[96] The idea was to see if activity of the complexes increases in the presence of base functionality by providing general base catalysis for transesterification of 2-hydroxypropyl-4-nitrophenyl phosphate (HPNPP), a RNA model compound.

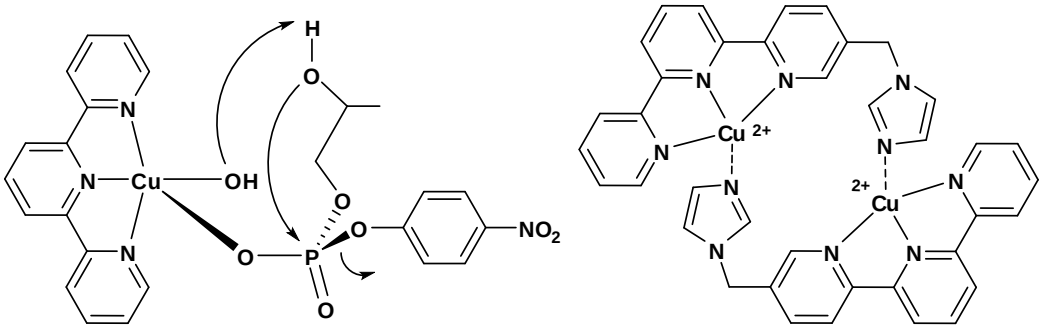

*Figure 1.22. (a) Proposed mechanism for catalysis of transesterification of HPNP by **1.40**, (b) Dimerization of Cu(II) complex of **1.41** due to intermolecular coordination of the peripheral imidazole group.*

It was observed that peripheral tertiary amines **1.42** & **1.43** lead to an increase in the activities of complex compared to **1.40**. However, the imidazole substituent decreased the activity of **1.41** by more than 8 times relative to **1.40**. This was possibly the result of the pendent imidazole group promoting dimerization as shown in **Figure 1.22(b)**. The imidazole group in the dimer would presumably occupy the coordination site of the Cu(II) ion that is used by water or the substrate for catalytic activation **Figure 1.22(a)**. Such binding does not occur in **1.42** and **1.43**, probably due to steric hindrance caused by the bulkier tertiary amines.

The pH-rate profiles for **1.40**, **1.42** and **1.43** demonstrates that Cu(II)-bound hydroxide group is essential for the ribonuclease activity of the Cu(II)-terpyridine complex **1.40**. The reactivity of **1.40** is, however, limited due to its protonation in near neutral media. Therefore, at low pH values, complexes **1.42** and **1.43** work better than **1.40** because of the presence of the peripheral tertiary amine groups. These amine groups help in general base catalysis when Cu(II)-bound hydroxide groups get protonated.

In another study, Baskin *et al.* also demonstrated that the Cu(II)-bound hydroxide group acts as nucleophile in hydrolysis of 2',3'-cAMP.[91] They observed that the presence of chloride ions in the reaction mixture inhibited the reaction because chloride and phosphate bind to the copper and prevent nucleophile coordination to Cu(II). Similar chloride inhibition was also observed by Jurek and Martell when they studied the hydrolysis of BNPP and DPP (di-phenyl phosphate) in the presence of Cu-tpy complex

1.40.[93] Crystal structures of the [Cu(tpy)(BNPP)Cl] and [Cu(tpy)(DPP)Cl] were obtained during these studies, which show that Cl and phosphate binds to Cu(II). Finally, hydrolysis reactions were studied in $NaClO_4$ containing solutions, on the assumption that ClO_4^- is a non-coordinating ligand relative to Cl^-. The rate of hydrolysis of DPP in the presence of Cu-tpy complex was immeasurably slow whereas BNPP was hydrolysed to 1% in a period of 2-3 days.

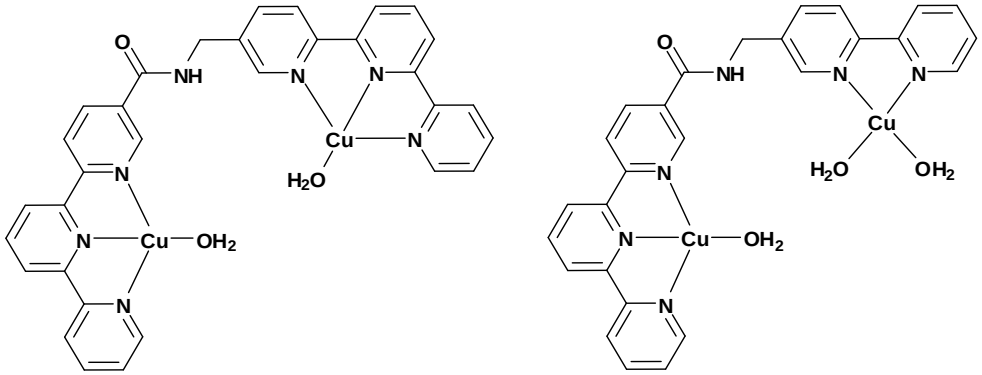

1.44 **1.45**

Figure 1.23. Dinuclear Cu(II) complexes studied for transesterification of HPNPP by Liu and Hamilton.[106]

Inspired by phosphate diesterases that contain two or more metal ions, Liu and Hamilton joined the complexes **1.1** and **1.40** together with simple amide spacers to make dinuclear Cu(II) complexes **1.44** and **1.45** shown in **Figure 1.23**.[94, 106] It was observed that **1.44** and **1.45** were more active than any of the closely related mononuclear complexes **1.1** and **1.40**-**1.43** in catalyzing transesterification of RNA model compound HPNP.

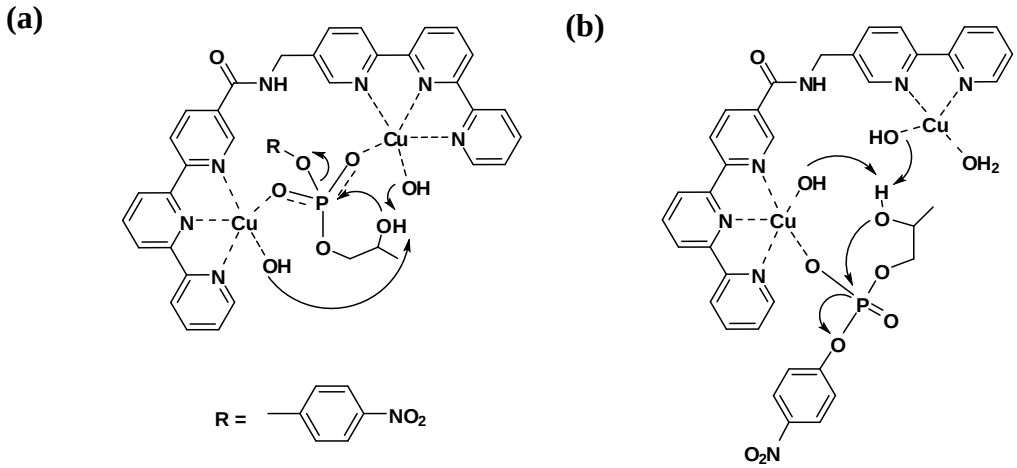

*Figure 1.24. The proposed mechanism for transesterification of HPNPP using (a) **1.44**, and (b) **1.45**. (Figure reproduced from reference).*[106]

Both **1.44** and **1.45** complexes were found to operate by different mechanisms. For bis-terpyridine complex **1.44**, the hydrolysis mechanism was consistent with a high degree of cooperativity between the two Cu(II) ions which supports a double Lewis acid activation mechanism as shown in **Figure 1.24(a)**. The bell-shaped pH rate profile indicates both general base and general acid catalysis. The terpyridine-bipyridine complex **1.45** is thought to catalyse the reaction by single Lewis acid activation (moderate degree of cooperativity between two Cu(II) ions) and double general base catalysis, shown in **Figure 1.24(b)**.

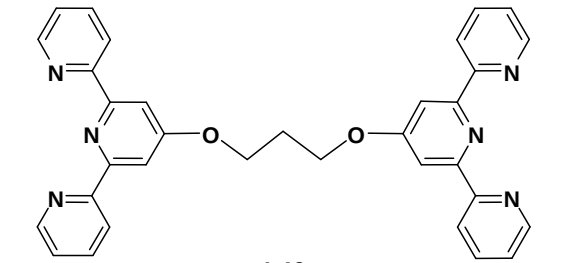

1.46

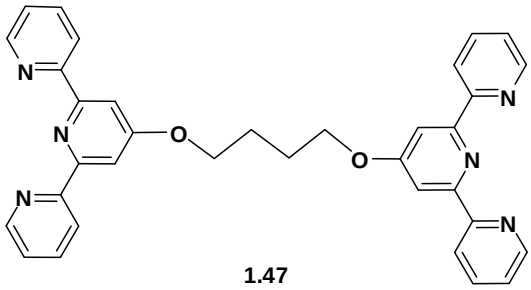

1.47

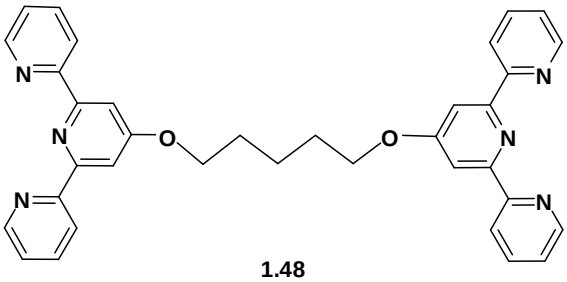

1.48

Figure 1.25. Alkyl-linked bis-terpyridine ligands. (Dinuclear Cu(II) complexes of these ligands were studied for the cleavage triphosphate bridge of different dinucleoside triphoshate substrates).

In 2009, Maanpää *et al.* synthesised ligands **1.46 – 1.48**, where two terpyridine unit link *via* an alkyl chain of three to five methylene units, **Figure 1.25**.[95] Their dinuclear Cu(II) complexes were found to be 600 times more efficient catalyst than mononuclear Cu(II)-tpy **1.40**, and up to 5×10^5-fold rate enhancement was achieved in comparison to the uncatalysed reaction. It was found that the catalytic activity of the bis-terpyridine complexes strongly depends on the length of the linkers. When the tpy ligands were

joined with a propyl linker, the Cu(II) complex **1.46** was only marginally better catalyst than mononuclear **1.40**. However, the butyl and pentyl linkers made the complexes **1.47** and **1.48** more efficient compared Cu(II)-tpy **1.40**. This rate enhancement clearly possible with the complexes of the ligands with butyl and pentyl linkers, and the propyl linker was too short to allow the simultaneous interaction of the two metals with the phosphate group. The differences were attributed to interactions between the Cu(II)-tpy and nucleic acid base moieties as well as steric factors that may hinder the productive interaction between the substrate and the catalyst.

1.5. The proposed Model Systems

A range of model enzyme systems containing 2,2':6',2''-terpyridine and other ligands have been introduced in **sections 1.4.1** and **1.4.2** of this chapter. These literature studies show that a change in ligand structure, the nature of the metal, the metal-metal distance, the solvents, and pH etc. are the factors that result in a change in efficiency of the metal complexes in hydrolysing phosphate esters. Natural enzymes usually contain more than one metal ion in their active site for high catalytic activity. To understand the role of metal ion and the hydrolysis mechanism a number of dinuclear complexes have been studied, and most of the dinuclear complexes are more efficient than their mononuclear analogues in hydrolysing phosphate esters. In dinuclear complexes, the two metal ions work synergetically. Greater cooperation and accessibility of the substrate to the metal-bound nucleophile may result in a higher rate enhancement for hydrolysis of the phosphate esters.

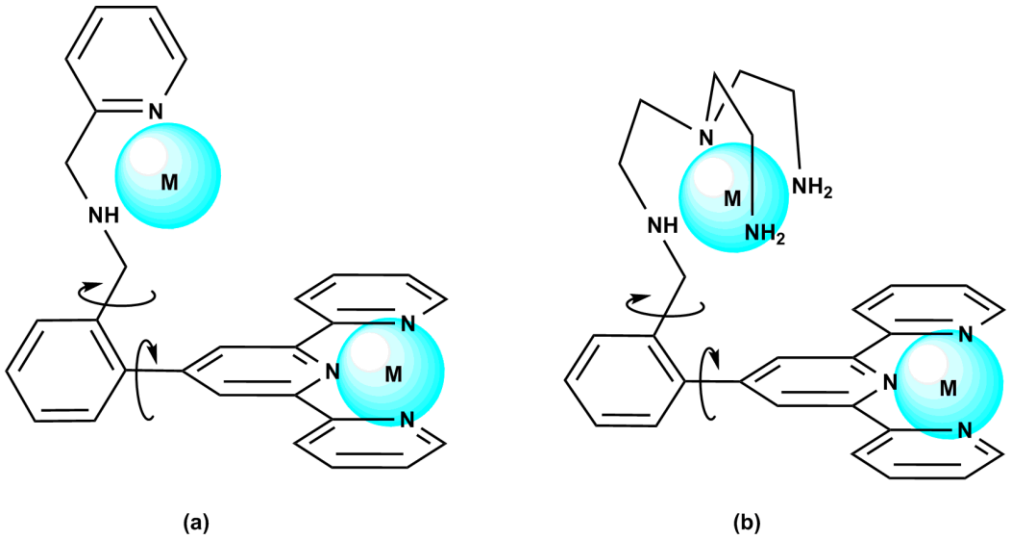

Figure 1.26. The proposed metal complexes, blue spheres representing a metal in the potential binding sites. Flexible bonds in the complexes are shown with curved arrows.

In most of the dinuclear complexes studied for hydrolysis in past, both of the metal binding sites were identical. We propose to synthesise polydentate ligands, where two metal binding sites are completely different from each other in terms of their geometry and metal binding properties. We also proposed to provide some flexibility to the system for better cooperation between two metal ions. Some examples of the proposed metal complexes are given in **Figure 1.26**. Detailed ligand design and synthesis strategies are discussed in Chapter 2 of this thesis.

1.6. Possible Supramolecular Chemistry – Some Literature Examples

As shown in **Figure 1.26**, our proposed ligands contain two potential metal binding sites – the tridentate terpyridine site (Head or H) and the other bidentate, tridentate or tetradentate amine binding sites (Tail or T). Each of these sites can coordinate with different metal ions in a different geometry. Due to the presence of multiple potential binding sites on both ends of the proposed ligands, these ligands can act as bridging ligands between two metal ions.

There is a possibility that these ligands could form oligomers, polymers or supramolecular assemblies when coordinating with metal ions. In the simplest complexes of these ligands, at least two metal ions can bind to one ligand – one in head binding site and other in tail, resulting in the formation of dinuclear complexes as illustrated in **Figure 1.26**.

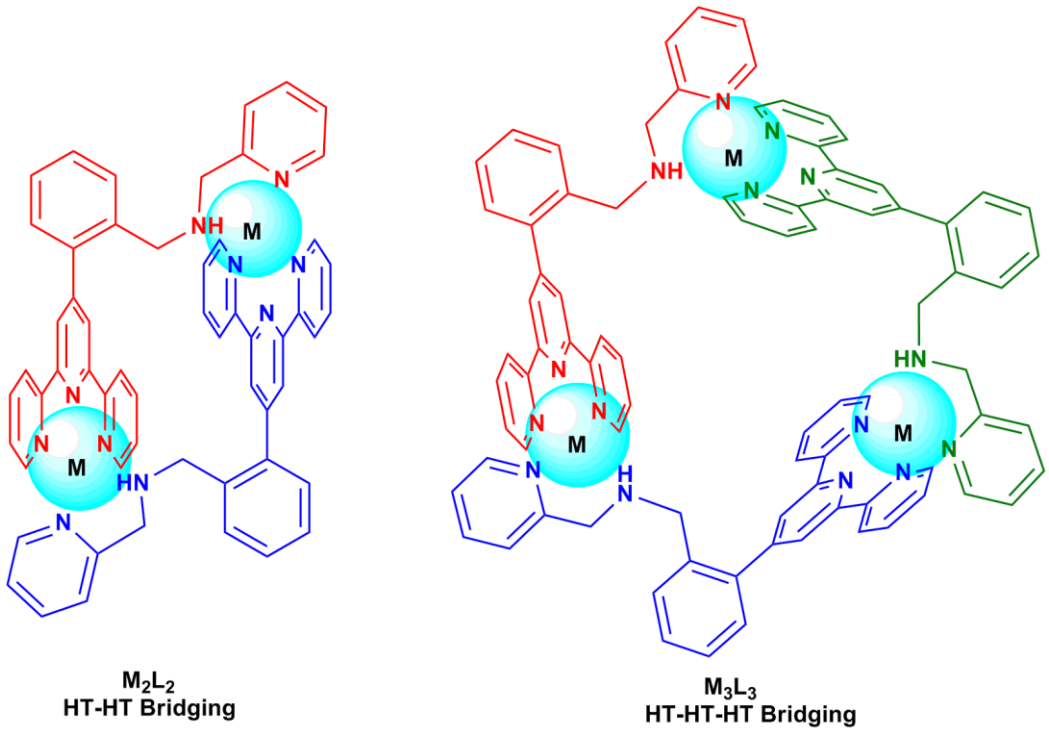

Figure 1.27. Diagram of possible dinuclear and trinuclear cyclic complexes.

The smallest cyclic oligomers that could form from the proposed ligands would be dinuclear with two ligands. M_2L_2 complexes could form by HT-HT bridging, M_3L_3 cyclic complex can form by HT-HT-HT bridging and so on, as shown in **Figure 1.27**. It is

unlikely to form dinuclear or trinuclear cycles of HH or TT bridging due to rigidity and planarity of the aromatic terpyridine and phenyl groups. Suppose if a ML_2 complex forms with terpyridine-terpyridine type (HH bridging) or picolylamine-picolylamine type binding (TT bridging) as shown in **Figure 1.28**, there is no way for the resulting ML_2 units to bend and connect from the free ends to make any dinuclear cycles.

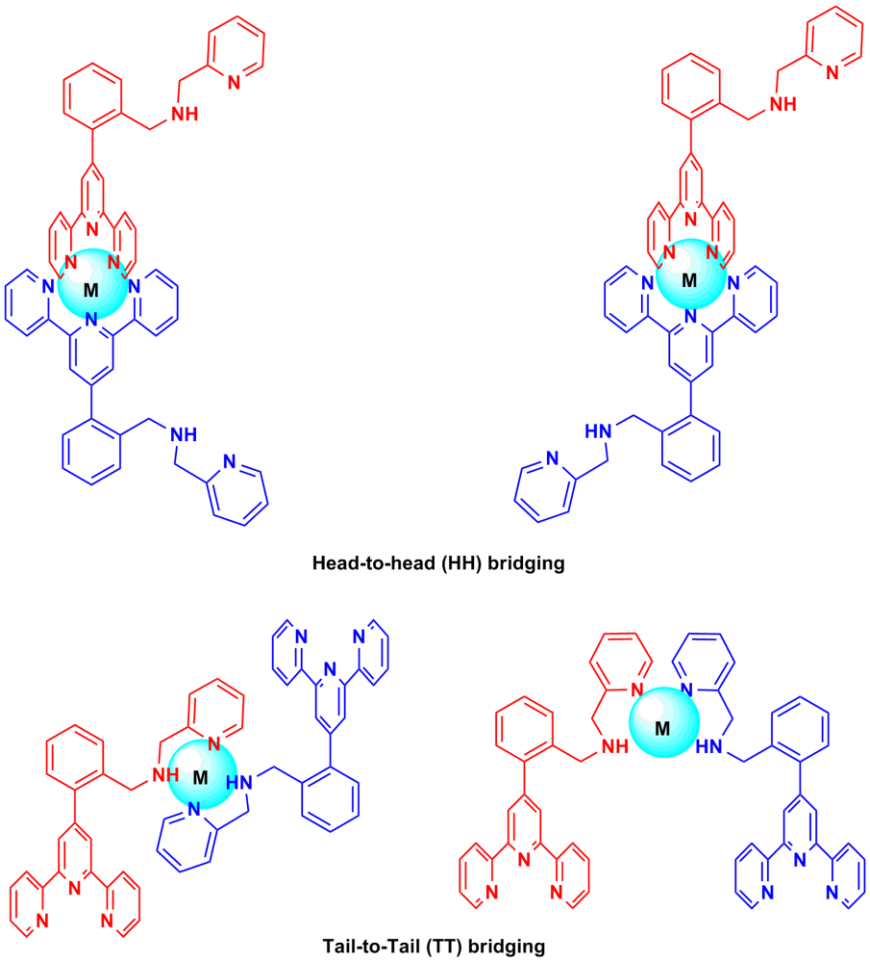

Figure 1.28. Diagram showing possible HH and TT bridging between two ligands, which also illustrates impossibility of formation of the M_2L_2 cyclic complexes by HH-TT bridging.

The ligand shown in **Figure 1.26 (a)** consists of two metal binding sites – tridentate terpyridine-type and bidentate picolylamine-type. Interestingly, the 2,2':6',2''-terpyridine metal binding site forms stable complexes with almost every metal in the periodic table.[107] Complexes of the type $[M(tpy)_2]$ are the most commonly synthesised and most of them are thermodynamically stable.[108] Owing to the stability of the $[M(tpy)_2]$ complexes it is possible to have a structural control over the synthesis of various supramolecular assemblies. A number of remarkable complexes synthesised will be discussed in Chapter 4 and Chapter 6 in this thesis.

There are no literature examples for the complexes where terpyridine- and picolylamine- type ligands are linked together, the closest analogues are the molecules containing both terpyridine- and bipyridine- units (bpy). The supramolecular chemistry of $[M(tpy)_2]$- and [M(tpy)(bpy)]- type complexes has been extensively studied and a *Cambridge Crystallographic Database* search for such complexes shows about 700 and 500 complexes, respectively. Here in this introduction only a few examples will be discussed where some related boxes or other self-assembled complexes were formed by terpyridine-terpyridine or terpyridine-bipyridine, or bipyridine-bipyridine type binding. A brief review of literature on wheel shaped complexes will also be given.

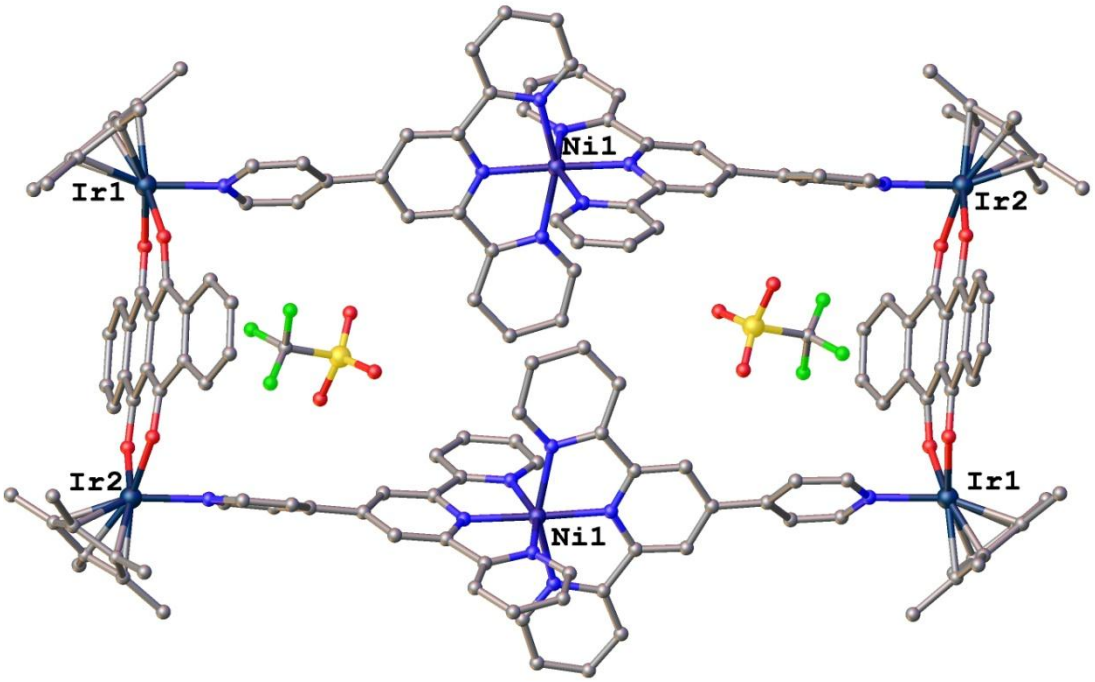

Figure 1.29. The crystal structure of the hexanuclear heterometallic box-shaped complexes.[109] *The hydrogen atoms and other solvent have been omitted for clarity.*

Liu *et al.* synthesised a number of hexanuclear box-shaped complexes as shown in **Figure 1.29**. In these heterometallic macrocycles, the $[M(pyterpy)_2]^{2+}$ complexes of Zn(II), Cu(II) and Ni(II) were used as building blocks for the box assemblies through the pendent pyridine rings, phterpy = 4'-(4-pyridyl)-2,2':6',2''-terpyridine.[109] These box shaped complexes have the ability to encapsulate guest molecules in their cavity.

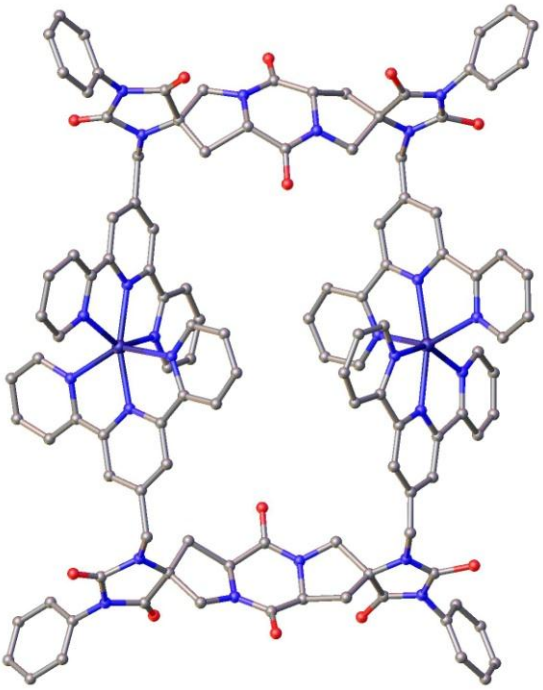

Figure 1.30. Binuclear box shaped spiroligomeric complex, M= Zn(II) and Mn(II)[110]

Some more box shaped $[M_2L_2]^{4+}$ complexes of Mn(II) and Zn(II) shown in **Figure 1.30** were reported by Schafmeister *et al.*[110] Two polydentate ligands with terpyridine side chains were treated with different metal ions and binuclear dimers in the shape of box were crystallised. These were the first metal-templated supramolecular complexes of such polydentate ligands.

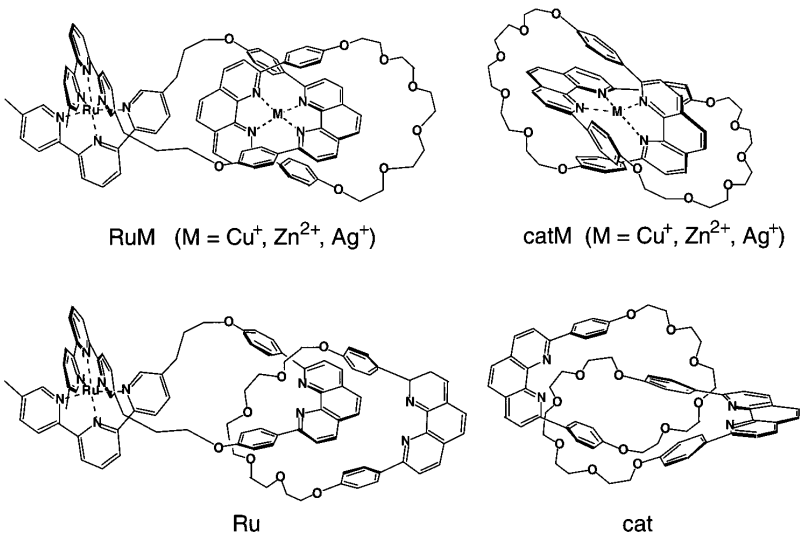

Figure 1.31. Diagrams of some catenane-type moieties, showing terpyridine-terpyridine and bipyridine-bipyridine type binding. Figure reproduced from references.[111]

Some multicomponent species consisting of [2]-catenates incorporating the $[Ru(tpy)_2]^{2+}$ moiety within their framework were prepared, and their electrochemical and

photophysical properties were studied by Cárdenas *et al.*[111, 112] They consist of two interconnected moieties, an octahedral $[Ru(tpy)_2]^{2+}$-type and a tetrahedral $[M(phenanthroline)_2]^{n+}$-type species. In the latter M can be Cu(II), Zn(II), or Ag(I), but such a moiety can also be metal free as shown in **Figure 1.31**. There are many other groups working towards synthesis of [2]-catenates currently to enhance their properties for various applications by modifying the ligands and spacers.[111 , 112-118]

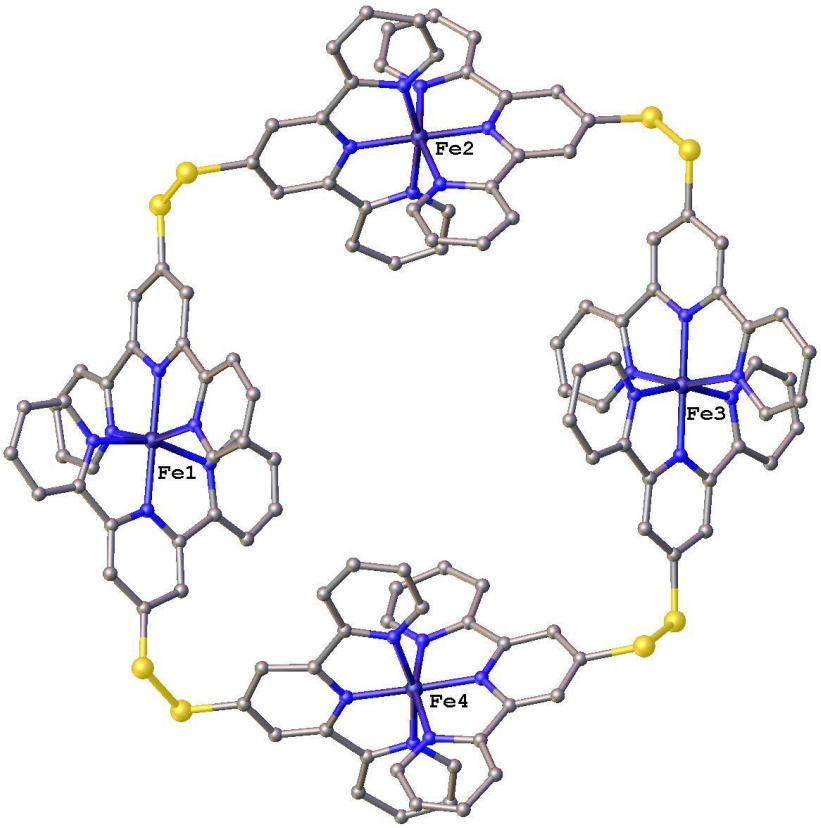

Figure 1.32. The box shaped tetranuclear Fe(II) complex, $[Fe_4(L)_4]^{8+}$, where L = bis(2,2':6',2''-terpyridin-4'-yl)disulfide ligand.[119]

A tetranuclear metallosupramolecular cyclic molecule was synthesised by Constable *et al*. using a bis-terpyridine ligand, bis(2,2':6',2''-terpyridin-4'-yl)disulfide, in the presence of Fe(II) and tetrafluoridoborate ions, **Figure 1.32**. In this metallocycle, the ligands are bridged between four Fe(II) ions *via* common terpyridine-terpyridine type binding.[108, 119]

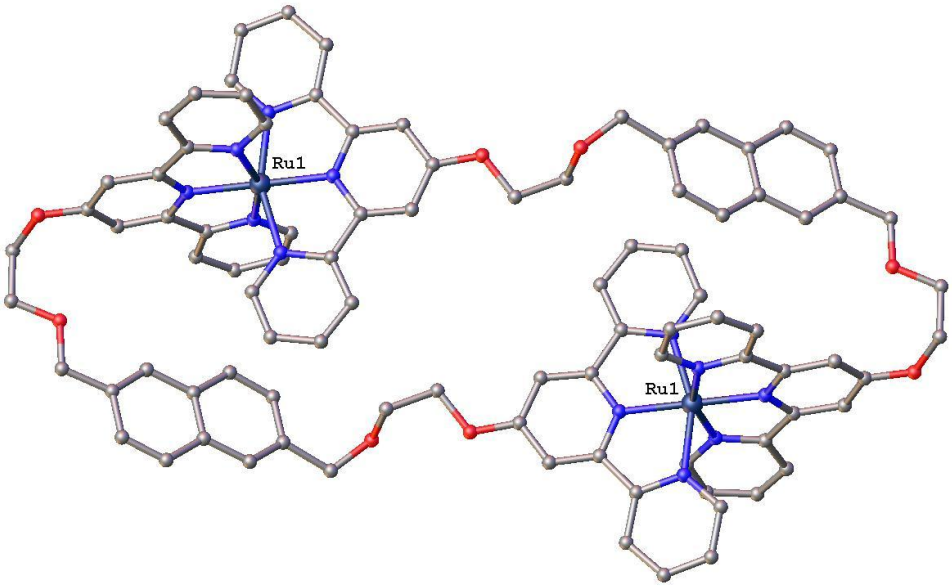

Figure 1.33. Molecular structure of $[Ru_2(L)_2]^{4+}$, L = 2,6-[Bis(2,2':6',2''-terpyridin-4'-yl)-1,4-dioxapentyl]naphthalene.

Many other ditopic ligands which contain polyethyleneoxy-substituted naphthalene spacers connecting two 2,2':6',2''-terpyridine metal binding sites were synthesised by Constable *et al.*[120] These ligands were used to prepare two series of ruthenium(II) complexes: linear complexes of type $[(tpy)Ru(L)Ru(tpy)]^{4+}$ as models for polymeric species, and metallomacrocyclic species $[Ru_nL_n]^{2n+}$ (n = 2 or 3), **Figure 1.33**.

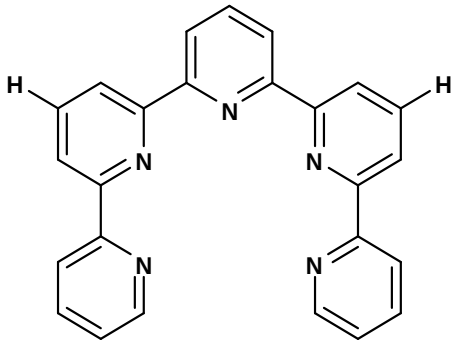

1.51

Many other cyclic complexes with terpyridine-terpyridine type binding were synthesised by Constable *et al.* and other groups.[111, 118-127] Many supramolecular assemblies have been synthesised where terpyridine-bipyridine type binding takes place.[128-130] In ligand **1.51**, a metal ion with a preference for octahedral coordination connects two ligands as an ML_2 unit and the remaining two pyridine type sites of each

ligand bind with another metal ion in bipyridine-bipyridine type binding. Double helical M_2L_2 complex $[(Co)(Ag)(\mathbf{1.51})_2]^{3+}$, was crystallised.[128]

Similar terpyridine-bipyridine (head-to-tail) type binding was also seen in ligand **1.52** which results in the formation of a dinuclear double helicate, $[Cu_2(\mathbf{1.52})][PF_6]_3$, with Cu(II).[119]

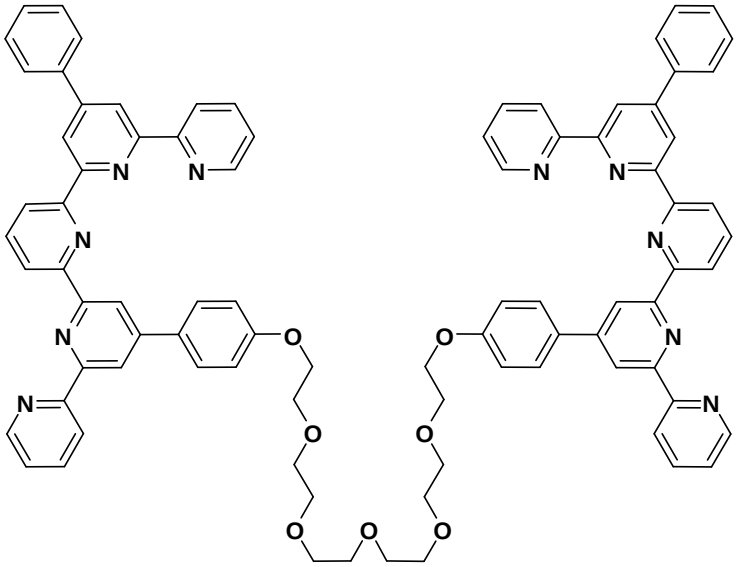

1.52

During this project, spectacular decanuclear wheel shaped complexes were synthesised using terpyridine-picolylamine based ligands. Detailed structure and discussion of the group of wheel shaped complexes is given in Chapter 6. These wheel shaped complexes were the accidental self-assembled supramolecular species crystallised from the reaction mixture. In the literature there are many examples of the similar wheel shaped complexes reported.[131-158] The largest reported wheels are the $\{Mo_{368}\}$ 'lemon' clusters containing 368 molybdenum ions, some more similar ones reported are the $\{Mo_{154}\}$,[158] and $\{Mo_{256}Eu_8\}$ known as ultra large polyoxomolybdate clusters.[133, 140] There are various other wheels such as alkoxy iron(III) Fe_6 wheels with a alkali metal in the middle with host-interactions,[131] octanuclear Fe(III) cluster $[CsFe_8\{N(CH_2CH_2O)_3\}_8]Cl$ where Cs is incorporated in the cavity,[132] dodecanuclear Zn(II) self-assembled bicycle-like wheels,[134] Fe_{10} and Fe_{12} ferric wheels,[136] Ga_{10}, Ga_{12} and Ga_{20} "Gallic wheels",[137, 138] Mn_{12},[142] Mn_{16},[143] and M_{84} giant 'torus' single molecule magnets,[139] and many more.[144-149, 154, 155, 157, 159]

Also there are a number of wheels formed from the terpyridine- or bipyridine-based ligands.[134, 140, 144-148, 152, 153] Many wheel shaped clusters incorporate several types of transition metal ions as well as lanthanides. Some of the wheels encapsulate anions in the middle of the ring held there with supramolecular forces. Since there is a vast literature associated with the wheel shaped complexes, here we will include only a few examples of the supramolecular wheel shaped complexes which have terpyridine or bipyridine type binding ligands as their main components.

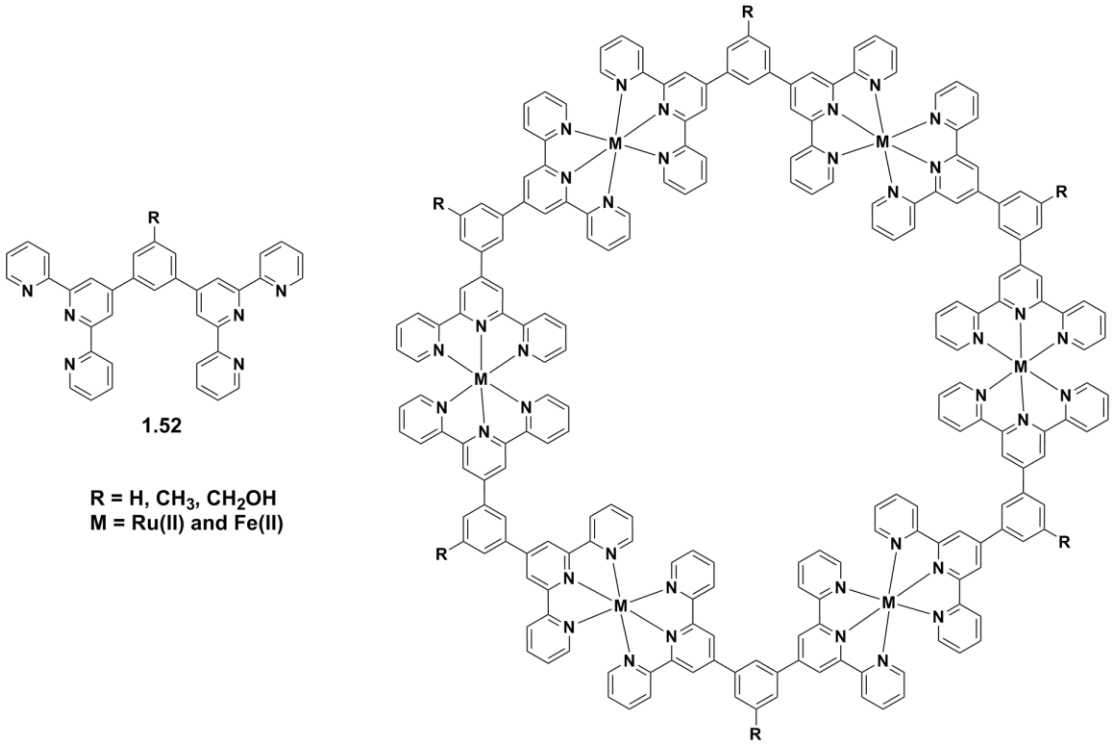

Figure 1.34. Bis-terpyridinyl monomer, 1.52, (left), The hexanuclear Ru(II) and Fe(II) wheels synthesised by Newkome et al.[159]

Hexanuclear metallocyclic wheel shaped complexes of Ru(II) and Fe(II) were self-assembled along with some directed construction using the terpyridine-based ligand **1.52** shown in **Figure 1.34**.[159] In this case, self-assembly of the macrocycles was effected by a combination of equimolar mixtures of bis-metalated and non-metalated bis-(terpyridinyl) monomers each possessing the essential planar, 60°, terpyridine-metal-terpyridine connectivity.

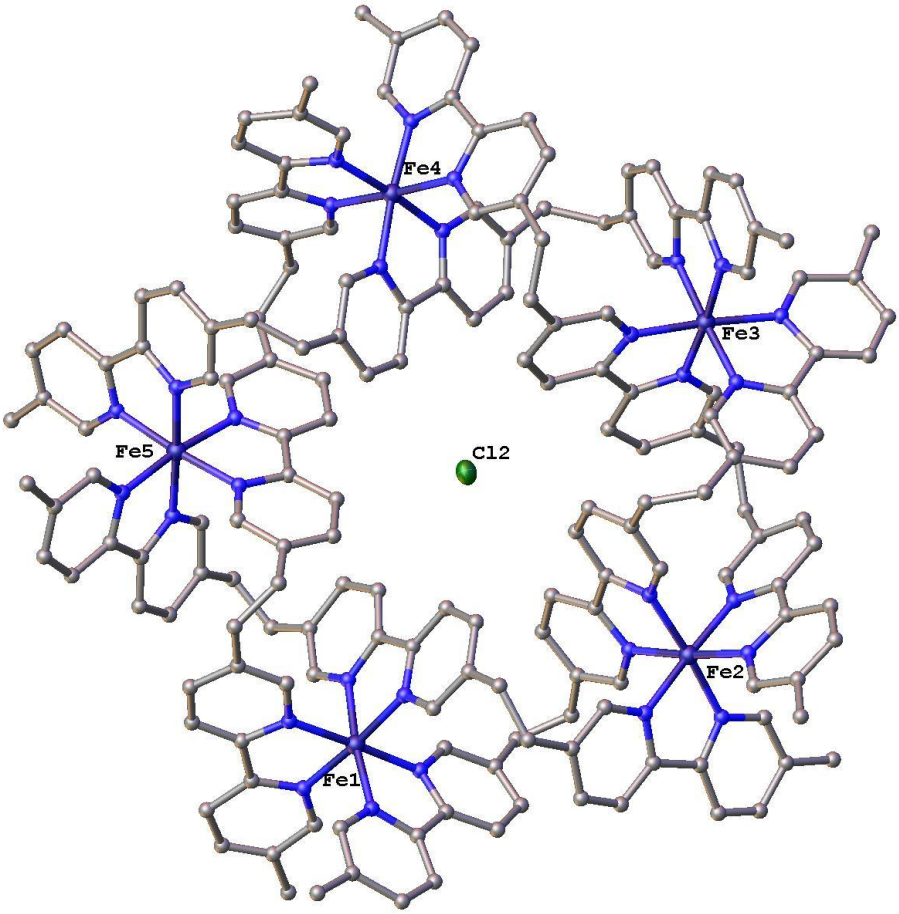

Figure 1.35. Double stranded helical wheel shaped pentanuclear Fe(II) complex synthesised by Lehn et al.[153]

A circular double helicates based on a tris-bipyridine ligand strands and six-coordinate Fe(II) ions were self assemble, **Figure 1.35**. A chloride ion was held in the middle of the cavity of one macrocycle.[152, 153]

There are no reported wheel shaped complexes with terpyridine-bipyridine type binding reported in the literature, so the decanuclear Ni(II) wheel shaped complexes synthesised in this project are the first precedents of their category.

1.7. Thesis coverage

This thesis describes the synthesis and characterisation of a number of novel polydentate terpyridine-based bridging ligands, with two non-equivalent binding sites, and their coordination chemistry. The synthesis and characterisation of mononuclear, dinuclear, and larger wheel and box-shaped transition metal complexes of the prepared ligands is also described. The kinetic studies of hydrolysis of phosphate diester studies have been performed using dinuclear complexes, and the rates of these reactions are compared with those of analogous mononuclear complexes.

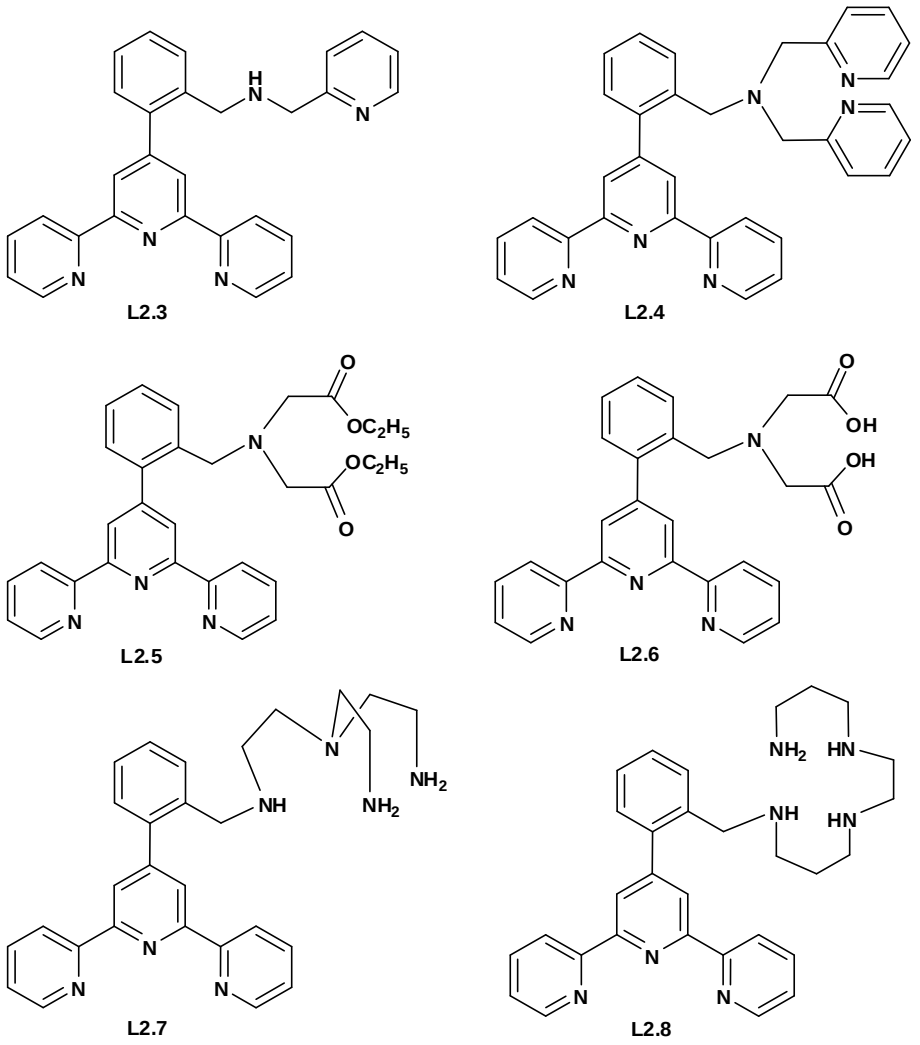

Figure 1.36. The novel polydentate ligands synthesised and characterised in this project.

Chapter 2 describes the synthesis of all the ligands prepared in this research, **Figure 1.36**. The chapter includes ligand design and retrosynthetic analysis for the proposed ligands. Along with their brief syntheses, crystal structures of some of the ligands will also be discussed in detail.

Chapter 3 includes investigation of the coordination chemistry of ligand 4'-(2'''-toluyl)-2,2':6',2''-terpyridine, **L2.1**, with different metal ions such Cu(II), Zn(II), Ni(II) and Ag(I). A range of coordination complexes were crystallised and characterised by X-ray crystallography and other techniques. Ni(II) and Cu(II) results in formation of a variety of complexes depending upon the ratio of the metal and ligand, the solvent and anions used. Zn(II) gave simple trigonal biyramidal mononuclear complexes and beautiful spirals were crystallised by using Ag(I) ions.

In Chapter 4, the Cu(II) and Zn(II) dinuclear complexes are discussed. All of the complexes were characterised by X-ray crystallography and with other analysis techniques.

Chapter 5 presents the kinetics of hydrolysis of phosphate diesters and relevant structural aspects. Catalytic behaviours of both Cu(II) and Zn(II) complexes of 2,2':6',2''-terpyridine, **L2.1**, picolylamine and the polydentate ligands **L2.3**, and **L2.4** was investigated. X-ray crystal structures of some Cu(II) complexes are discussed in detail where phosphate diester group coordinate with the metal ion.

Chapter 6 deals with the preparation and characterisation of the remarkable polynuclear box and wheel shaped self-assemblies formed from ligand **L2.3**. The ligand **L2.3** acts as a bridging ligand between different metal ions and undergoes HH-TT-HH-TT or $(HT)_{10}$ bridging and results in formation of the tetranuclear box shaped M_4L_4 or decanuclear Ni(II) wheel shaped $M_{10}L_{10}$ complexes.

Both homo-metallic and hetero-metallic box shaped complexes were synthesised. Addition of a divalent transition metal ion (M_2) to a solution of M_1(**L2.3**)$_2$ complex, in the presence of $[PF_6]^-$ ions, resulted in formation of $[M_1M_2(\mathbf{L2.3})_4X_2]^{6+}$ box complexes, where X = Cl^-, Br^-, CH_3COO^-; M_1 = Zn(II), Fe(II); and M_2 = Zn(II), Ni(II), Cu(II). The bis-bidentate bridging ligand terephthalate was also deliberately encapsulated in the middle of the Fe_2Zn_2(**L2.3**)$_4$ box to produce the complex where X_2 = terephthalate ion. These structures invite speculation that it may be possible to bind and react molecules within these boxes.

In a more fortuitous outcome Ni(II) ions bind to both sites of the ligand to give, exclusively, an unprecedented decanuclear structure, $[Ni_{10}(\mathbf{L2.3})_{10}(OH_2)_7X_3]^{17+}$ where X is Cl^- and/or Br^-. The structure has ten exchangeable ligands coordinated to each Ni(II)

located around the wheel. A Br^- ion occupies the central position in the wheel in preference to a Cl^- ion. The wheel shaped complex co-crystallise with a huge amount of water molecules around it. Three different wheel shaped complexes are discussed in Chapter 6.

The preceding chapters will be summarised in Chapter 7 and this chapter also provides a discussion on possible avenues of further research related to hydrolysis of phosphate diesters or supramolecular chemistry, and all experimental data is given in Chapter 8.

Graphs and tables reporting kinetics data, coordination bond details and crystallographic information are all provided in Appendices I-III.

CHAPTER 2

SYNTHESIS & CHARACTERISATION OF THE POLYDENTATE LIGANDS

2.1. Introduction

The aim of this research was to synthesise the hydrolytic model enzymes as dinuclear metal complexes where two metal ions bind in non-identical binding sites. The key component in the design and synthesis of the model compounds was the polydentate bridging ligands. These are the bridging ligands which must be able to bind two or more metal centres to enhance the rate of hydrolysis of phosphate diester groups similar to those present in DNA and RNA. The potential bonus of the different binding sites in such ligands is to create supramolecular assemblies discussed in Chapter 6.

Many previous kinetic studies of hydrolysis reactions have been performed using complexes with more than one identical metal binding site, as discussed in Chapter 1.[58, 160-162] This research has instead focused on synthesis of the complexes where two metal ions are bound in non-identical metal binding sites.

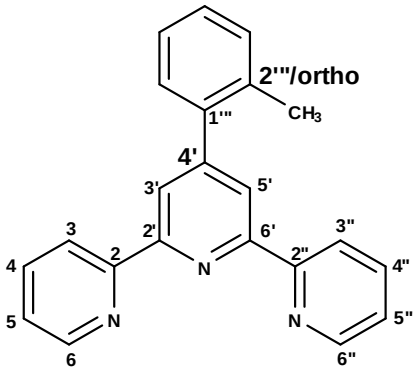

*Figure 2.1.The unsubstituted structure of 4'-(2'''-toluyl)-2,2':6',2''-tepyridine, **L2.1**, different functionalities can be introduced at 2'''- positions of the ligand.*

We began our research by continuing from the experiments performed in our group by a previous student, Paul Thornley, who was working towards the functionalisation of terpyridine ligands at the 4' position. Thornley attempted to synthesise 4'-arylterpyridines, where the *ortho* site of the aryl group was exploited to introduce different amine functionalities. Both 4' and 2''' (ortho) positions of **L2.1** are highlighted in **Figure 2.1**. Exploitation of the *ortho* methyl group was required so that the second polydentate metal binding site can be directed towards the meridional coordination site of the terpyridine group. There have been several reviews published about the synthesis and properties of the 4'-substituted 2,2':6',2''-terpyridine derivatives in the past.[71, 163, 164] The 4'- substituted terpyridine derivatives are relatively easy to synthesise *via* cross coupling or central ring closure methods and the required aldehyde and pyridine starting materials are easily

available. In this chapter the synthetic strategies involved in synthesis of the polydentate bridging ligands, containing both terpyridine and amine groups will be outlined. The isolated ligands were characterised by NMR (appendix IV), mass spectroscopy, IR and elemental analysis. Some of the ligands produced X-ray quality crystals, and their solid state structures were elucidated by X-ray crystallography.

2.2. The Proposed Ligand

The first step to approach our goal was to design the polydentate ligands. Two examples of the proposed polydentate ligand **L2.3** and **L2.8** that may bridge between two metal centres are shown in **Figure 2.2.**

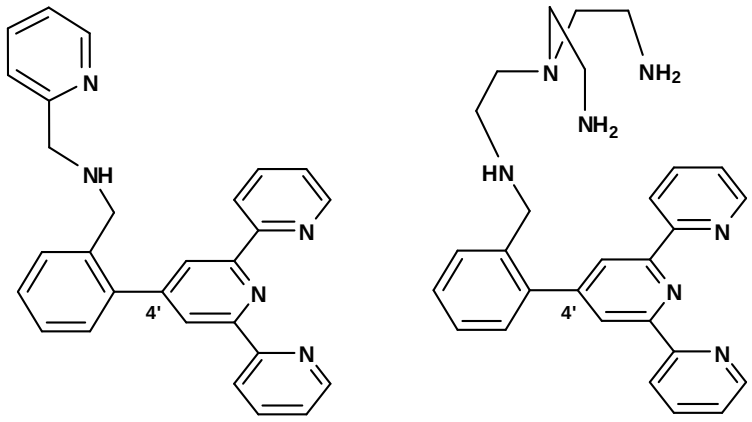

L2.3 **L2.7**

*Figure 2.2. The proposed ligands, 4'-[2'''-{(2-pyridylmethyl)aminomethyl}phenyl]-2,2':6',2''-terpyridine, **L2.3** and4'-[2'''- {5-(2-aminoethyl) 7-amino-2,5-diazaheptyl}-phenyl] -2,2':6',2''-terpyridine, **L2.7**.*

In each of the ligands shown in **Figure 2.2** there are two different types of potential metal binding site connected to each other. The ligands **L2.3** and **L2.7**, each contain two different ligating groups– one terpyridine ligand, 4'-(2'''-toluyl)-2,2':6',2''-terpyridine and the second polyamine *N,N*-bis(2-aminoethyl)ethane-1,2-diamine (tren), or (2-pyridylmethyl)amine, respectively.

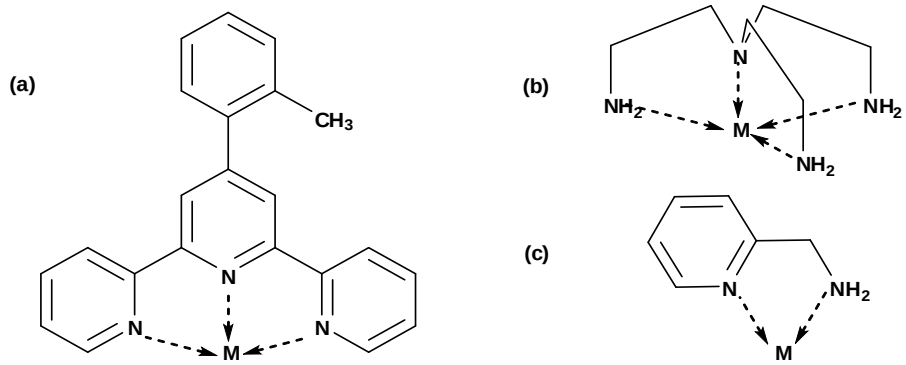

Figure 2.3. Illustration of metal binding sites of ligands 4'-(2'''-toluyl)-2,2':6',2''-tepyridine (a),N,N'-bis(2-aminoethyl)ethane-1,2-diamine (b), (2-pyridylmethyl)amine (c).

All of the ligands we proposed were based upon 2,2':6',2''-terpyridine as the common motif unit. The terpyridine unit is mostly planar, and tridentate with fixed meridional coordination to the metal centre, as shown in **Figure 2.3 (a)**. Also, as the ligand lacks a high degree of flexibility, it reduces the possibility for isomer formation.

However, the metal binding sites selected to substitute at the *ortho* methyl position were much more flexible about their coordination. The ligands **L2.3** and **L2.7**, shown in **Figure 2.2**, contain different types of amine ligands at the *ortho* position of the main 2,2':6',2''-terpyridine-like unit. In **L2.3**, the bidentate (2-pyridylmethyl)amine may coordinate to a metal ion using both of its nitrogen atoms, as shown in **Figure 2.3(c)**. In **L2.7** the polyamine *N*,*N*-bis(2-aminoethyl)ethane-1,2-diamine (tren) has a branched tripodal geometry, and contains four nitrogen donor atoms. This may lead to coordination of another metal ion in the tetradentate binding site, where all nitrogen atoms can participate in the metal binding as shown in **Figure 2.3(b)**.

As discussed in previous chapter both of metal ions can participate to enhance the rate of hydrolysis of phosphate diester group. There is a possibility that this type of ligands could produce dimers, trimers, or even larger species when coordinating with metal ions. Formation of oligomeric, polymeric or supramolecular species is also possible as discussed in Chapter 1.

Synthesis of these ligands is a multistep process. A retrosynthetic analysis of the proposed polydentate ligands is shown in **Figure 2.4**.

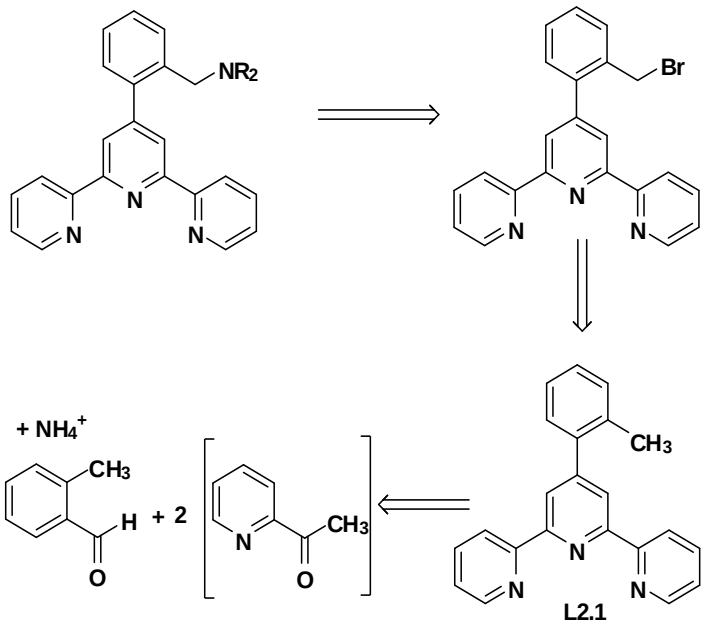

*Figure 2.4.Retrosynthetic analysis of proposed system, where NR_2= groups shown in **Figure 2.5**.*

Various amine groups (NR_2) chosen for functionalisation of **L2.1** are shown in **Figure 2.5**. Three different stages involved in synthesis of the final polydentate ligand system are – synthesis of **L2.1**; bromination of the methyl group of **L2.1**; and nucleophilic substitution of the polyamine ligands shown in **Figure 2.5**.

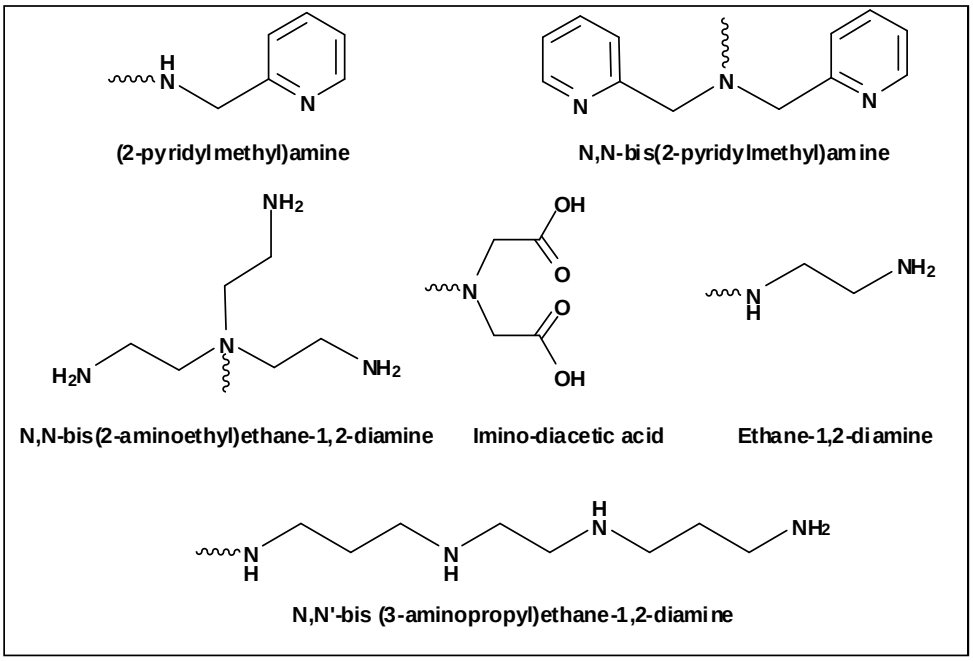

*Figure 2.5. Various (NR_2) amine functionalities used to introduce on **L2.1***

2.3. Methods for Synthesis of Terpyridine Ligands

The terpyridine ligand was first discovered in 1932 by Morgan and Burstall.[165] Heating pyridine with anhydrous iron(II) chloride at 340 °C in an autoclave, 50 atm, for 36 hours produced 2,2':6',2''-terpyridine (tpy), along with bipyridines and other by-products. A range of different methods for the synthesis of the terpyridine ligands have been described in the literature.[77, 78, 165-178] The two basic synthetic approaches to terpyridine ligands involves either assembly of the central ring, **Figure 2.6 (a)**, or coupling of the three pyridine rings as illustrated in **Figure 2.6 (b)**. Examples of the ring assembly approach include: the Kröhnke reaction, the Potts methodology, the Jameson methodology and cyclo-condensation (the Sauer methodology). The metal mediated coupling methods include nickel-mediated reactions, and palladium mediated reactions (Suzuki- reaction and Stille coupling reaction).[179-183]

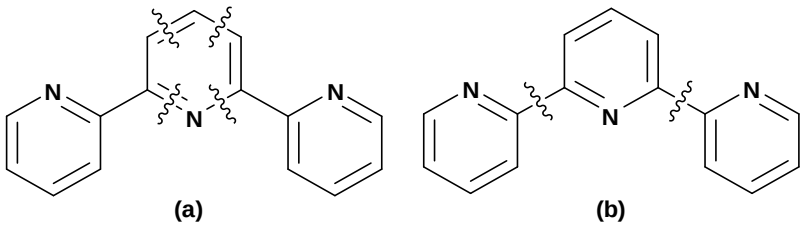

Figure 2.6. Illustration of central ring assembly (a) and coupling ring methodology (b) for synthesis of terpyridine ligands.

*2.3.1. Methods for Synthesis of 4'-(2'''-toluyl)-2,2':6',2''-Terpyridine (**L2.1**)*

The key step towards synthesis of an aryl-terpyridine, such as **L2.1**, is the condensation of two equivalents of 2-acetylpyridine with an appropriate aryl aldehyde (in this case *o*-toluylaldehyde), followed by ring closure in the presence of an ammonia source at high temperatures. Various different methods for the synthesis of substituted and un-substituted aryl-terpyridines have been described in the literature.[166, 169-171, 173, 184-193] A brief review of the methods we explored during this research is briefly discussed below.

2.3.1.1. The Kröhnke Methodology

In 1976 F. Kröhnke developed a condensation methodology leading to substituted terpyridines (oligopyridines).[174] This method is now a widely used and well known method to synthesise substituted terpyridines. Appropriate aldehydes and pyridines can be used as starting materials, under basic conditions, to synthesise particular terpyridines. In this method, the first step is that we require formation of the α,β-unsaturated ketone or enone **2.3** by an aldol condensation between *o*-toluylaldehyde and 2-acetylpyridine in basic aqueous or alcoholic medium, as shown in **Figure 2.7.**

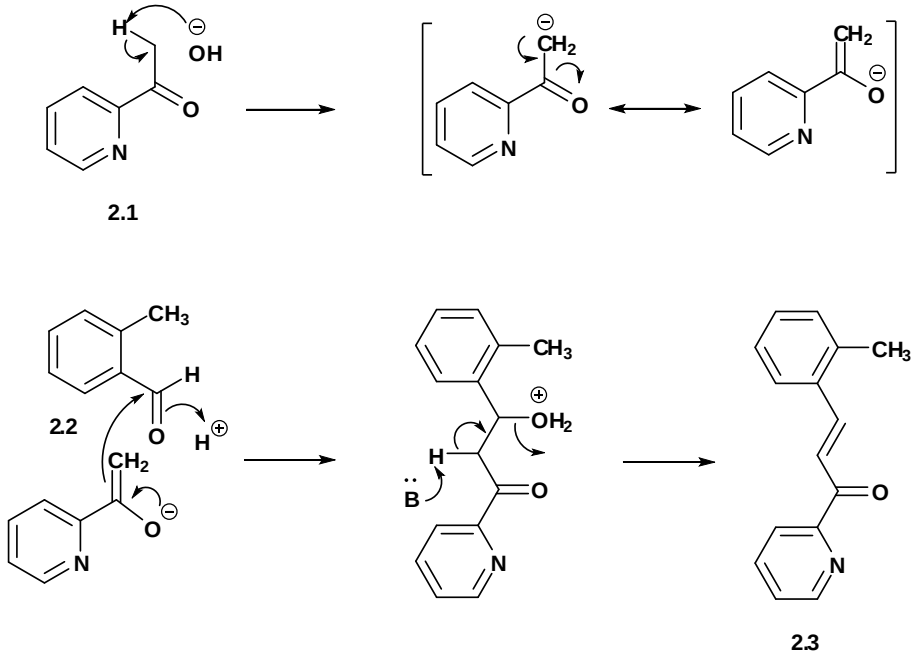

Figure 2.7. Mechanism for the formation of (E)-1-(pyridine-2-yl)-3-o-toluylprop-2-en-1-one

The enone **2.3** is isolated and then reacted with (2-pyridylacyl)pyridinium iodide **2.4** (synthesised by reacting 2-acetylpyridine with iodine and pyridine)[74], resulting in formation of a 1,5 diketone *via* a Micheal addition, as shown in **Figure 2.8**. The final ring closure can be achieved by the addition of ammonium acetate, and the resulting dihydropyridine is oxidised by O_2 *in situ* to produce the desired terpyridine, **L2.1**.

The main advantage of the Kröhnke methodology is that this method is excellent to synthesise a range of substituted or un-substituted terpyridines. This is usually achieved by reacting appropriately substituted 2-acetylpyridine and appropriate aromatic aldehydes to synthesise different enones, and which then can be reacted with a variety of pyridinium ions.[171] This means that the Kröhnke methodology can be used to tune the

terpyridine molecules to adjust their properties suitable for the applications of terpyridines.

The disadvantage of the Kröhnke method is that this method is a comparatively time consuming process for the synthesis of the terpyridines where the terminal/non-central rings are identical (symmetrical terpyridines). This is due to the multi-step process, and the yield of the reaction sequence is still lower than some other methods.

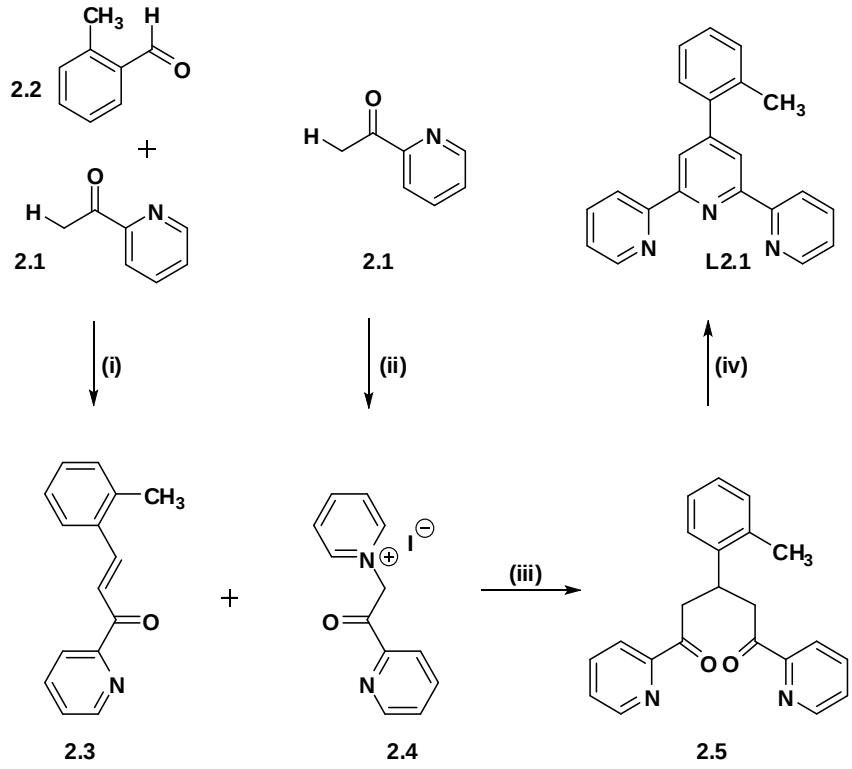

Figure 2.8. The Kröhnke methodology for synthesis of 4'-(2'''-toluyl)-2,2':6',2''-terpyridine, (i) NaOH, Ethanol, 0°C; (ii) I_2, Pyridine, 80°C, 4 hours; (iii) Ethanol, reflux; (iv) $NH_{3(aq)}$

The Kröhnke ring closure methodology has been altered in a variety of ways to improve certain aspects such as yield of the reaction, reaction duration, and isolation for particular desired products. In 2000 Cave, Scott & Raston developed an environment friendly 'green' solvent free method, and methanol was used for the central ring closure.[194-196] Recently in 2012 Husson and Knorr reintroduced the use of alumina as a base in the solvent free Kröhnke synthesis.[173] The terpyridine synthesis was reproducible using alumina as a base and better promoter for solvent free aldol and Micheal addition type reactions.[192, 197-199] Field *et al.* and Ballardini *et al*. also used Kröhnke methodology to synthesise 4'-(2'''-toluyl)-2,2':6',2''-terpyridine (**L2.1**) and the overall yield was reported to be 30% –50%.

2.3.1.2. "One-Pot" Syntheses

L2.1 is a symmetrical ligand with identical non-central rings, which means that the multi-step Kröhnke synthesis is not essential and it can also be synthesised using "one-pot" reactions. This method was first developed by Potts *et al.*[200] and further improved by many others such as Case *et al.*, Collin *et al.*, Hanan *et al.*, and Calzaferri *et al.*[78, 193, 201, 202]The key advantage of using these methods is that the reaction can be carried out in a single vessel and in a much shorter time than the related Kröhnke sequence. However, the disadvantage is the formation of two isomers of terpyridine, and isolation of the desired ligand is again a multistep process with greater time consumption.

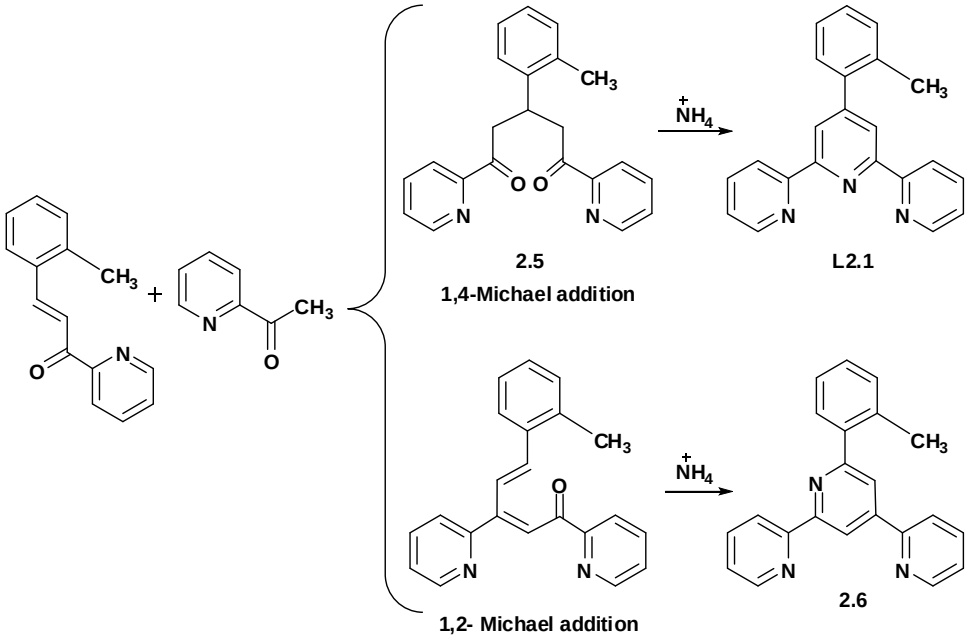

Figure 2.9. General representation of intermediates formed during 1,4- and 1,2- Michael addition reaction for symmetrical and unsymmetrical terpyridine.

During this research, at first we used Hanan and Wang's "one-pot" method to synthesise **L2.1**, where one molar equivalent of *o*-toluylaldehyde was reacted with two molar equivalents of 2-acetylpyridine in ethanol, potassium hydroxide and aqueous ammonia. Nearly four hours of reflux results in formation of a mixture of two isomers with **L2.1** as the major isomer and 6'-(2'''-toluyl)-2,2':6',2''-tepyridine, **2.6**, as the minor isomer shown in **Figure 2.9**. Similar results were produced by previous students in our group using another "one-pot" synthesis developed by Collin, Balzani and Sauvage.

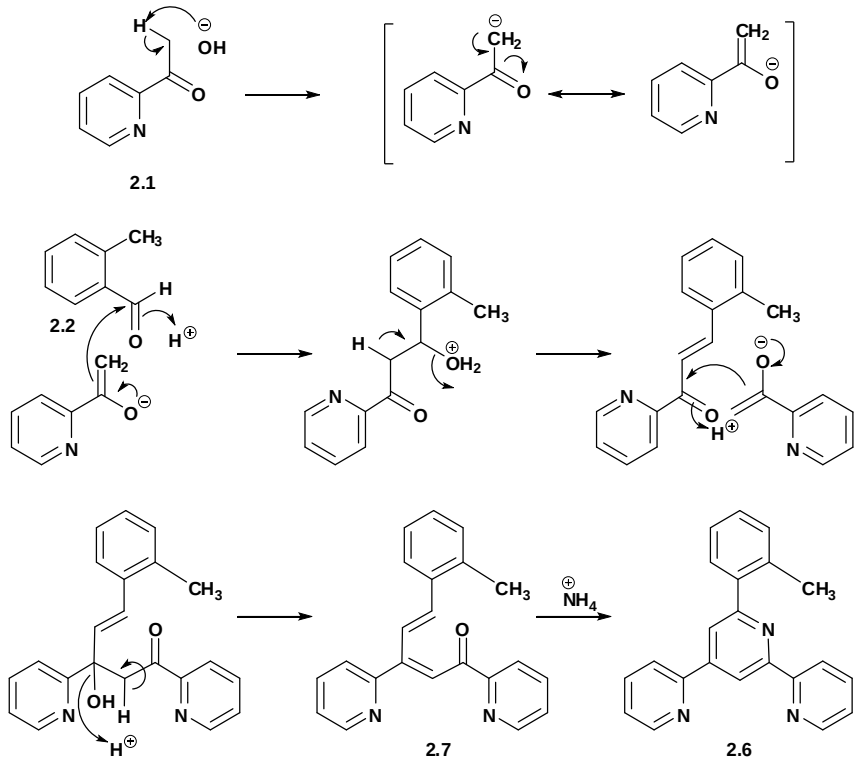

Figure 2.10. Mechanism for the formation of 6'-(2'''-toluyl)-2,2':4',2''-terpyridine via 1,2- Michael addition reaction.

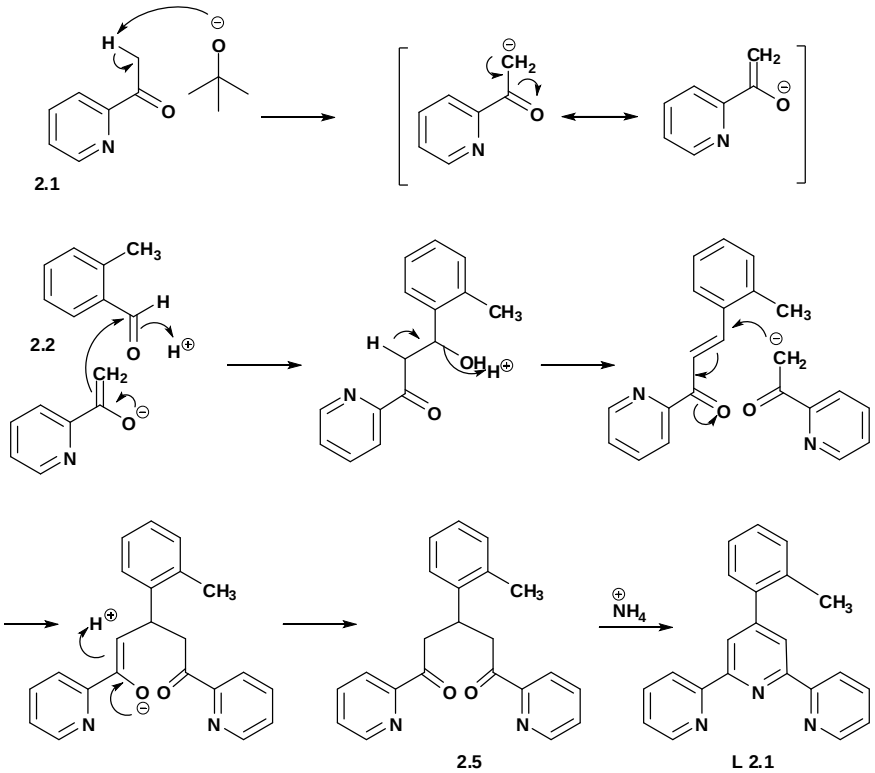

Figure 2.11. Mechanism for the formation of symmetrical isomer 4'-(2'''-toluyl)-2,2':6',2''-tepyridine via 1,4-Michael addition.

The mechanism of formation of unsymmetrical isomer terpyridine **2.6** is shown in **Figure 2.10**, and that for symmetrical isomer **L2.1** is shown in **Figure 2.11**.

Isolation of terpyridine isomers using recrystallisation methods or column chromatography (alumina or silica) is not that straight-forward. However the literature describes isolation of both isomers based upon their different coordination properties.[176] As shown in **Figure 2.12** the unsymmetrical isomer 6'-(2'''-toluyl)-2,2':4',2''-terpyridine (**2.6**) is a bidentate ligand, and the symmetrical isomer 4'-(2'''-toluyl)-2,2':6',2''-tepyridine (**L2.1**) is a tridentate ligand. Both isomers have different binding abilities and these can be isolated by exploiting the difference in their binding domains. The addition of a Fe(II) salt preferentially results in the formation of a highly stable purple coloured complex $[Fe(\mathbf{L2.1})_2]^{2+}$. The unsymmetrical bidentate isomer, **2.6**, can be extracted from the filtrate by toluene washes. The ligand **L2.1** can be liberated from iron complex $[Fe(\mathbf{L2.1})_2](PF_6)_2$ by slow addition of hydrogen peroxide under alkaline conditions, where the peroxide oxidises Fe(II) to Fe(III).[176]

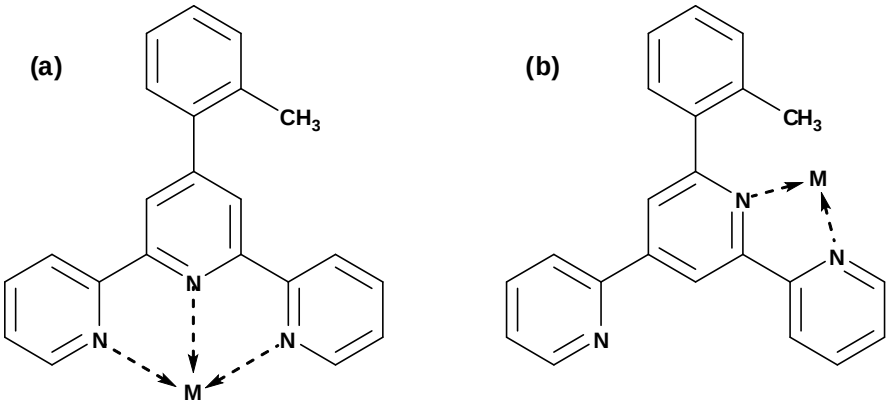

Figure 2.12. Illustration of tridentate (a) and bidentate (b) binding sites of both the isomers.

Later we tried the synthesis of **L2.1** using another "one-pot" literature method with a variation in the bases used. This method was developed by Calzaferri *et al.* to synthesise 4'-pentafluorophenyl-2,2':6',2''-terpyridine. Following this method, *o*-toluylaldehyde was mixed with 2-acetylpyridine in the presence of potassium *tert*-butoxide salt and THF. Condensation of intermediate α,β-unsaturated ketone with potassium salt of 2-acetylpyridine *via* 1,4-Michael addition and *in-situ* ring closure by addition of ammonium acetate/acetic acid/ethanol solution results in formation of symmetrical tridentate **L2.1**. The yellowish white precipitate of **L2.1** was obtained after pouring the reaction mixture into a ten-fold excess of ice cold water.

The advantage of using this method was that pure product (in nearly 70% yield) was synthesised. By scaling up the reaction, nearly 15 g of **L2.1** was also synthesised at

once. This method was reproducible and efficient towards synthesis of 4'-(2'''-toluyl)-2,2':6',2''-terpyridine in high yields.

2.3.2. Functionalisation of 4'-(2'''-Toluyl)-Terpyridine Ligands

Further functionalisation of **L2.1** was required in order to introduce the second metal binding domain for the ligands to act in a bridging capacity. Functionalisation of **L2.1** was achieved by either using different aromatic aldehydes during synthesis of various ligands, or by introducing functionality after the ligand synthesis as briefly outlined in **Section 2.2**. There have been several methods reported for synthesis of phenyl-substituted terpyridines; however the most versatile method to functionalise these ligands is a two-step process:

1. Radical bromination of the methyl group[134, 184, 203-209] (**Figure 2.13**), and

2. Nucleophilic substitution by nitrogen containing heterocyclic/acyclic/or macrocyclic compounds[75, 90, 210-213] (**Figure 2.14**)

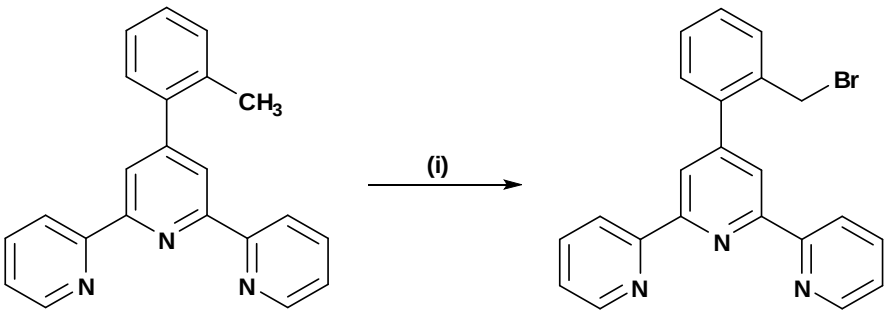

Figure 2.13. Radical bromination of L2.1 (i) N-bromosuccinimide (NBS), dibenzoyl peroxide, dry CCl_4, hv, 35°C, 20hr.

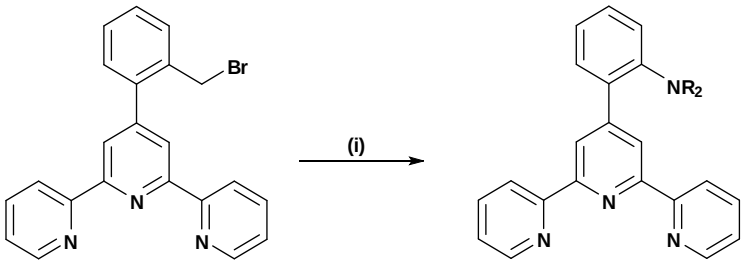

NR_2	Compound	NR_2	Compound
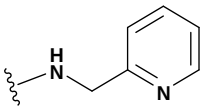	2.12	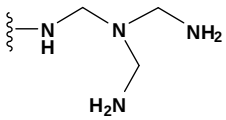	2.15
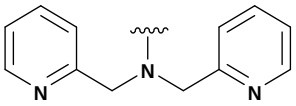	2.13	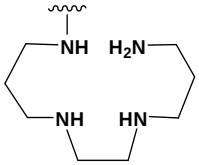	2.16
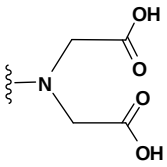	2.14	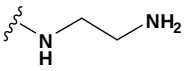	2.17

Figure 2.14.(i) base (K_2CO_3), dry CH_3CN, 35-50°C, 20-48 hrs, and in-boxed scheme numbers represents polydentate ligands synthesised using those different amine groups (NR_2).

The bromomethyl group is found to be highly reactive towards nucleophiles and can be reacted with a variety of nitrogenous or oxygen containing heterocyclic/acyclic or macrocyclic compounds under basic conditions.[75, 89, 90, 210-214]

2.3.2.1. Bromination of 4'-(2'''-toluyl)-2,2':6',2''-terpyridine

The methyl group of **L2.1** can be brominated using N-bromosuccinimide as a source of bromine. In order to initiate this reaction a catalytic amount of dibenzoyl peroxide was added and the solution was irradiated using a tungsten lamp while stirring at 35 °C, under nitrogen. A detailed mechanism of a radical bromination reaction is shown in **Figure 2.15**.

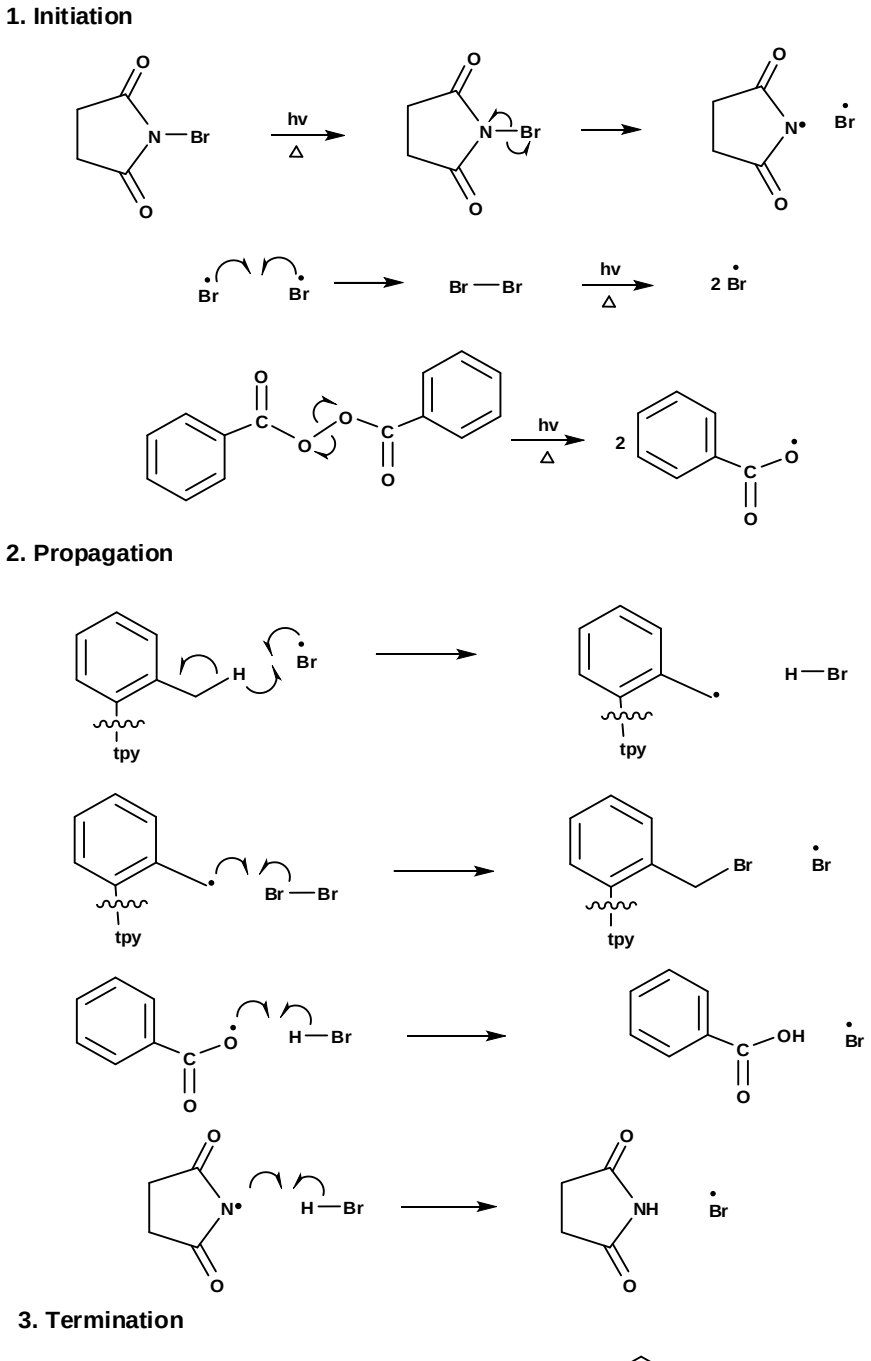

Figure 2.15. A mechanism showing the initiation, propagation and termination steps of the free radical bromination reactions.

All of the reactants, the solvent and the reaction vessel were completely dried. Either benzene or carbon tetrachloride can be used as the solvent but using carbon tetrachloride provided a better yield.

During the first few attempts of the bromination reaction we observed that the direct heating of the round bottom flask by the tungsten lamp was causing decomposition of the brominated terpyridine. To overcome this, the reaction vessel was immersed in an oil bath. Temperature of the oil bath was maintained at approximately 35 °C. This system improved the product quality and yield up to 60-70% but again due to delicacy of the reaction, the yield did vary on some occasions.

Reaction progress was monitored using ^{1}H NMR spectroscopy; proton signals due to the methylene group alpha to the bromo substituent appear as a new singlet at ~4.45 ppm. The bromination reactions were considered to be complete when the **L2.1** methyl singlet was no longer detectable in the ^{1}H spectra. On many occasions the bromination yields were lower (sometimes only in the 20–40 % range). Fortunately, mixtures obtained from incomplete reactions can be resubmitted to the reaction conditions in order to achieve better yields.

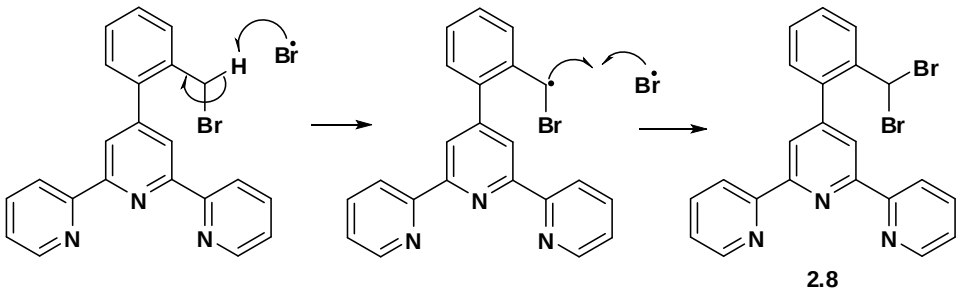

*Figure 2.16. Propagation and termination steps for formation of the by-product **2.8**.*

The bromination reactions were usually performed at a smaller scale (with 2.0 g **L2.1**) to get higher yields. Prolonged reaction time over a period of 24 hours under UV irradiations also improved the yield of reaction. It was also observed that the reaction yield was also sensitive to the amount of NBS used. Through multiple attempts, the best way to maximise the yield was to use a small excess of NBS (1.1 equivalent). Using exactly one equivalent of NBS resulted in only 70-80% yield with unreacted methyl group, whereas a larger amount (>1.1 eq.) of NBS usually results in further bromination of the mono-brominated methyl group. The propagation and termination mechanistic

steps for dibromo compound are shown in **Figure 2.16**. The dibromo by-product **2.8** was isolated when a larger excess of NBS was used.

The brominated product was collected from the filtrate by removing CCl_4 *via* rotary evaporation. Any CCl_4 collected in solvent trap was distilled and reused. The crude product could be recrystallised from a 2:1 mixture of EtOH and acetone, but this results in lower yields due to decomposition of the product. Column chromatography also proved to be ineffective in terms of separation of the desired monobromo and dibromo species. Therefore, the oily crude product containing 4'-[2-(bromomethyl)phenyl]-2,2':6',2''-terpyridine was used crude as soon as possible for the next step due to its tendency to decompose.

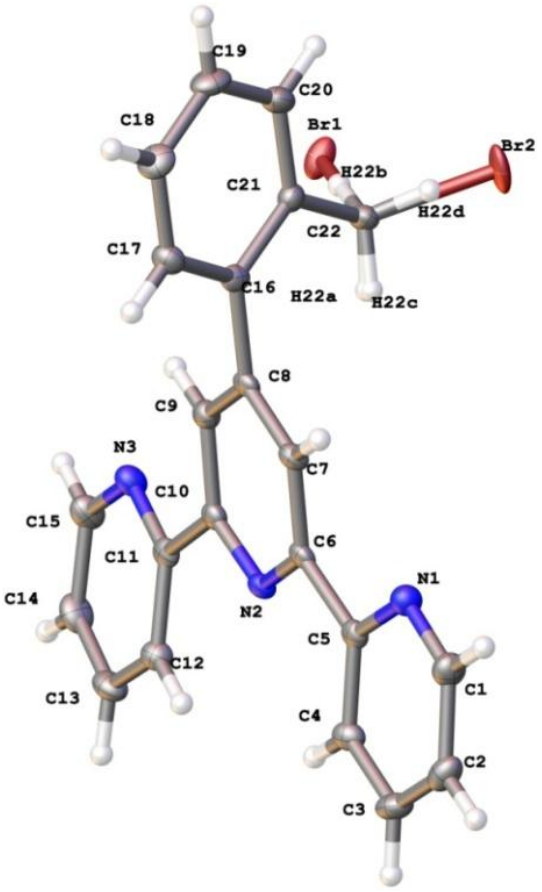

*Figure 2.17. X-ray crystal structure of di-bromo ligand **2.8.***

The compound **2.8** was synthesised by reacting two equivalents of NBS with one equivalent of **L2.1**. X-ray quality crystals of di-bromo ligand **2.8** were formed by recrystallisation of the ligand from hot ethanol. The X-ray crystal structure was solved and refined in the monoclinic space group $P2_1/c$. The crystal structure of **2.8** is shown in **Figure 2.17**.

The structure was solved to an R-factor of 5.13% using Olex 2.1.2. The bromine atoms were highly disordered. Assigning full occupancy to both the bromine atoms, results in high U_{max} to U_{min} ratio for bromine atoms and low U_{max} to U_{min} ratio for all other atoms including carbon and nitrogen atoms and for some atoms thermal ellipsoids become non-positive definite. The disorder was solved by refining the occupancy of both the bromine atoms to 0.85, and that of the hydrogen atoms H22b and H22d to 0.15, and H22a and H22c to 0.5. This disorder shows that the sample was contaminated with the possible reaction side product, the mono-brominated ligand. The final model of crystal structure is refined as $C_{22}H_{15.3}N_3Br_{1.7}$. However, the elemental analysis of the bulk crystalline sample is consistent with $C_{22}H_{15}N_3Br_2$.

Bond lengths and bond angles are similar to the parent ligand **L2.1**.[85] The terpyridine unit is almost planar with slight torsion of 9.5(5)° to 10.1(5)° between the central and terminal rings. The planar toluyl ring is twisted with an angle of 74.0(5)° with respect to the terpyridine plane.

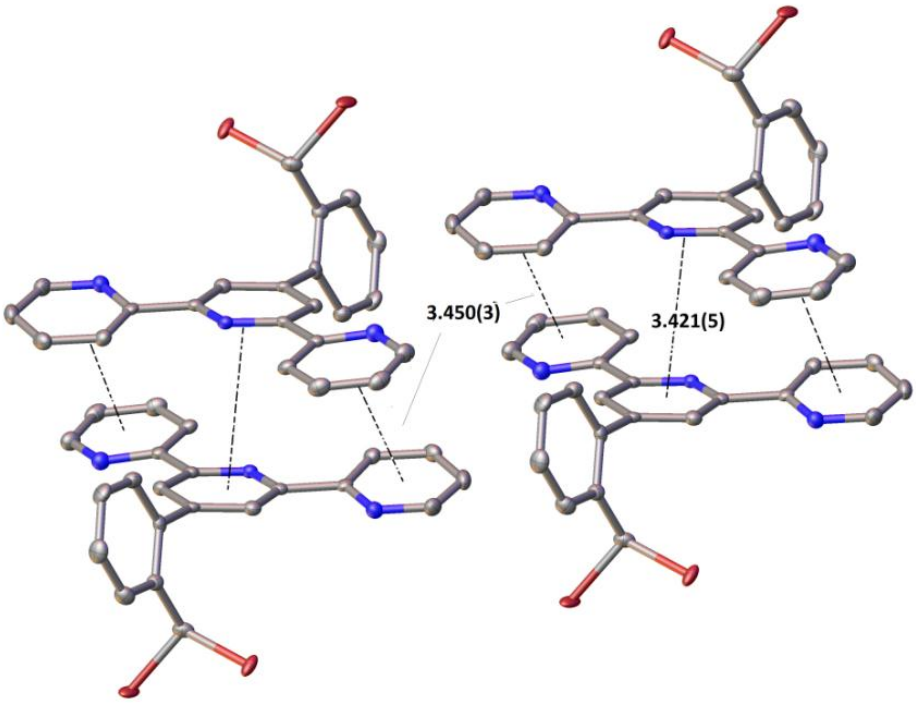

*Figure 2.18. Packing diagram of **2.8** showing inter-molecular π-π stacking between terpyridine rings. Hydrogen atoms omitted for clarity.*

The molecules in the crystal lattice are efficiently packed with π-π stacking (~3.4 Å) between pyridine rings of adjacent molecules as shown in **Figure 2.18**. Bromine and nitrogen atoms make short contacts with aromatic hydrogen atoms of adjacent molecules with distances in the range of 2.605(3) Å to 2.951(5) Å.

*2.3.2.2. Amination of 4'-{2'''-(bromomethyl)phenyl}-2,2':6',2''-terpyridine (**L2.2**)*

The last step in the preparation of the proposed polydentate ligands was amination of crude 4'-(2'''-(bromomethyl)phenyl)-2,2':6',2''-terpyridine. The bromo methyl group of **L2.2** was found to be reactive towards nucleophiles. The bromide leaving group can be replaced *via* nucleophilic substitution by a number of nitrogen containing molecules under the basic conditions.[75, 89, 90, 210-214]

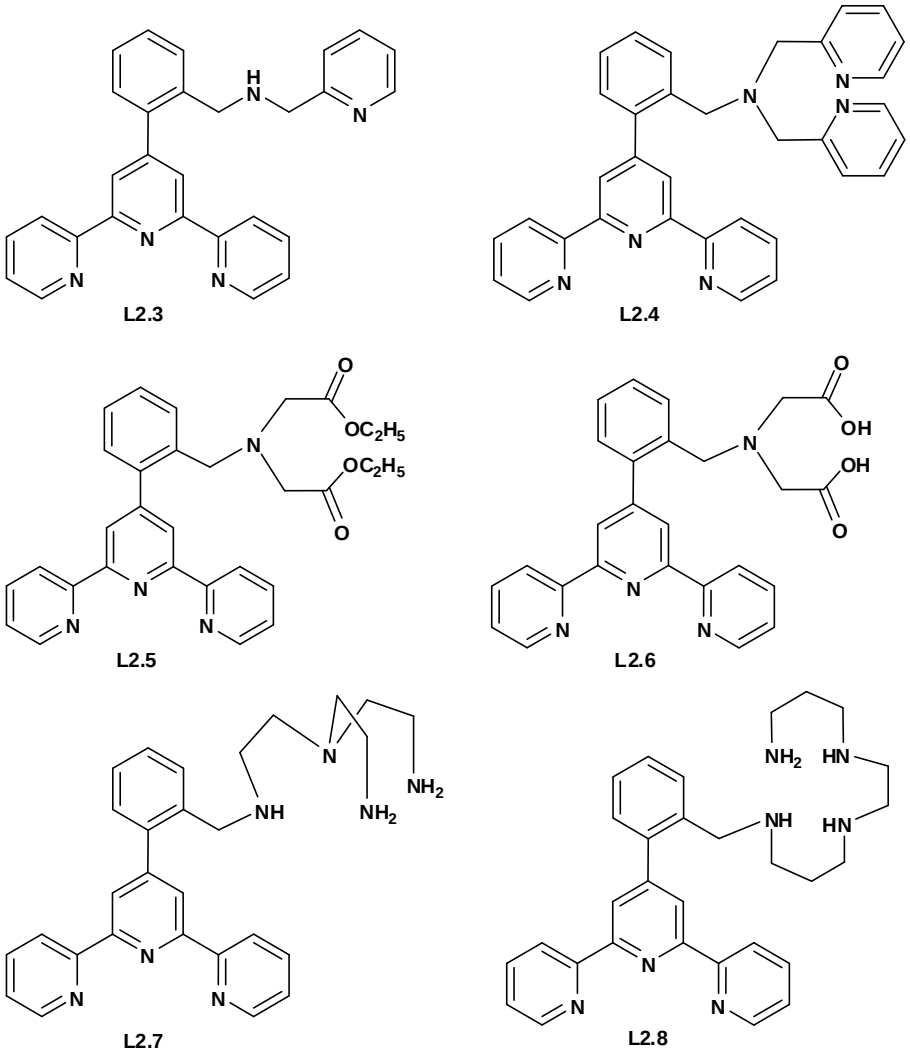

Figure 2.19. Various polydentate ligands synthesised and characterised during this project

A variety of amines (**Figure 2.5**) were selected for reaction with the bromomethyl group. The polydentate ligands synthesised, characterised and isolated are shown in **Figure 2.19**. Most of the ligands were isolated and characterised by NMR (appendix IV), elemental analysis, mass spectroscopy and melting point. X-ray crystallography was also

performed on those ligands that produced good quality crystals. Details of the syntheses and characterisation of the polydentate ligands are discussed in the following sections.

2.3.2.2.1. Synthesis of 4'-[2"'-{(2-pyridylmethyl)aminomethyl}phenyl]-2,2':6',2"-terpyridine, L2.3 and 4'-[2'"{bis(2-pyridylmethyl)aminomethyl}phenyl]-2,2':6',2"-terpyridine, L2.4

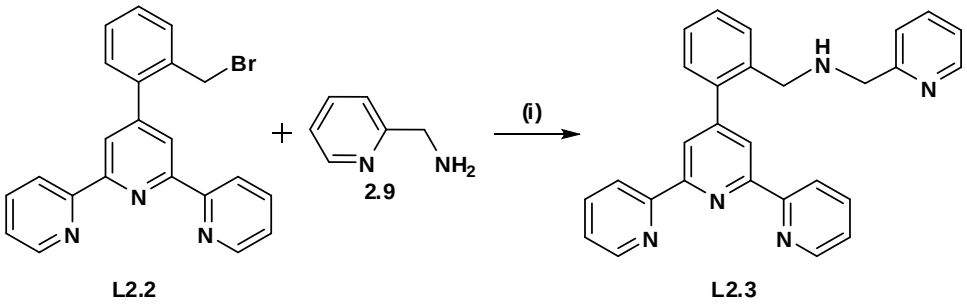

L2.2 L2.3

*Figure 2.20. Synthesis of ligand **L2.3** (i) K_2CO_3, CH_3CN, 4 days,50°C*

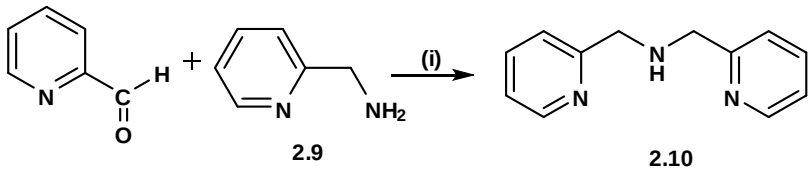

2.9 2.10

Figure 2.21. Synthesis of bis-picolylamine[215, 216] 2.10 (i) $NaBH_4$ at 0°C, dry methanol, 15 hrs, Conc. HCl, sat. NaOH.

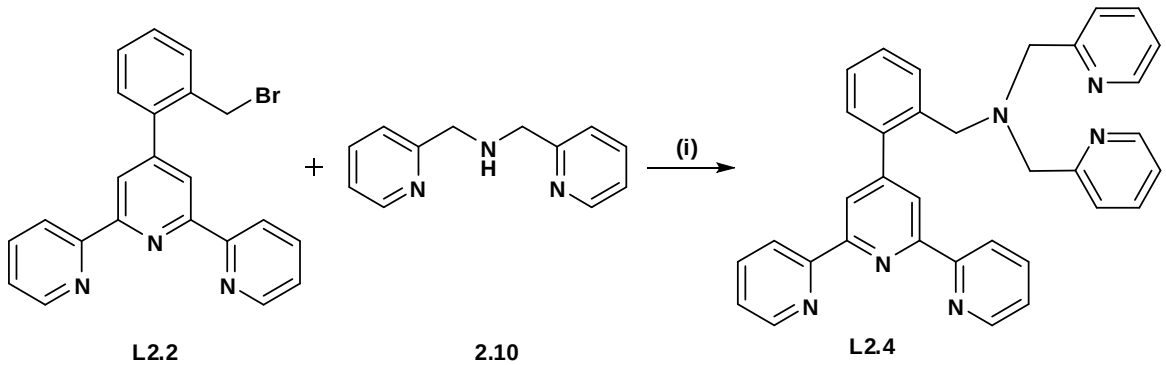

L2.2 2.10 L2.4

*Figure 2.22. Synthesis of ligand **L2.4** (i) K_2CO_3, dry CH_3CN, 4 days, 50°C.*

The ligands **L2.3** was synthesised by direct alkylation of (2-pyridylmethyl)amine with mono-bromo compound **L2.2** as shown in **Figure 2.20**. Similarly **L2.4** was synthesised using bis(2-pyridylmethyl)amine, **2.9**, **Figure 2.22**.

The known amine **2.10** required for the synthesis of **L2.4** was synthesised using a literature method.[215, 216] The amination reactions were carried out in dry CH_3CN and in the presence of K_2CO_3 to afford the desired products in good yields (75-80%). In these substitution reactions K_2CO_3 is used to neutralise the HBr salt formed during the reaction.

The amination reactions were run until all the mono-bromo species (**L2.2**) were consumed. It was observed that prolonged reactions (up to 4 days) and also using a small excess (1.2 equivalents) of the amines resulted in the best yields. The crude ligands were extracted from filtrates of reaction mixtures as crude yellow oils. Both **L2.3** and **L2.4** were purified by column chromatography. Alumina was used as a stationary phase, and initial elution with DCM removed any di-brominated compound, **2.8**, as a white powder. The ligands **L2.3** and **L2.4** were collected by eluting 1% MeOH:DCM mixture. Slow evaporation of DCM produced X-ray quality crystals of both **L2.3** and **L2.4**. The ligands were characterised using ^{1}H, and ^{13}C NMR spectroscopy, HSQC, COSY, NOESY, electron spray ionisation mass spectrometry, and CHN analysis.

2.3.2.2.2. Crystal structures and NMR of L2.3 and L2.4

The X-ray quality crystals of **L2.3** and **L2.4** were obtained by slow evaporation of their dichloromethane solutions. The crystal structure of **L2.3** was solved in the monoclinic space group $P2_1/c$ (R-factor of 3.91%) and **L2.4** was solved in the triclinic space group $P\bar{1}$ with an R-factor of 4.33%. The crystal structures of the ligands are shown below in **Figure 2.23**.

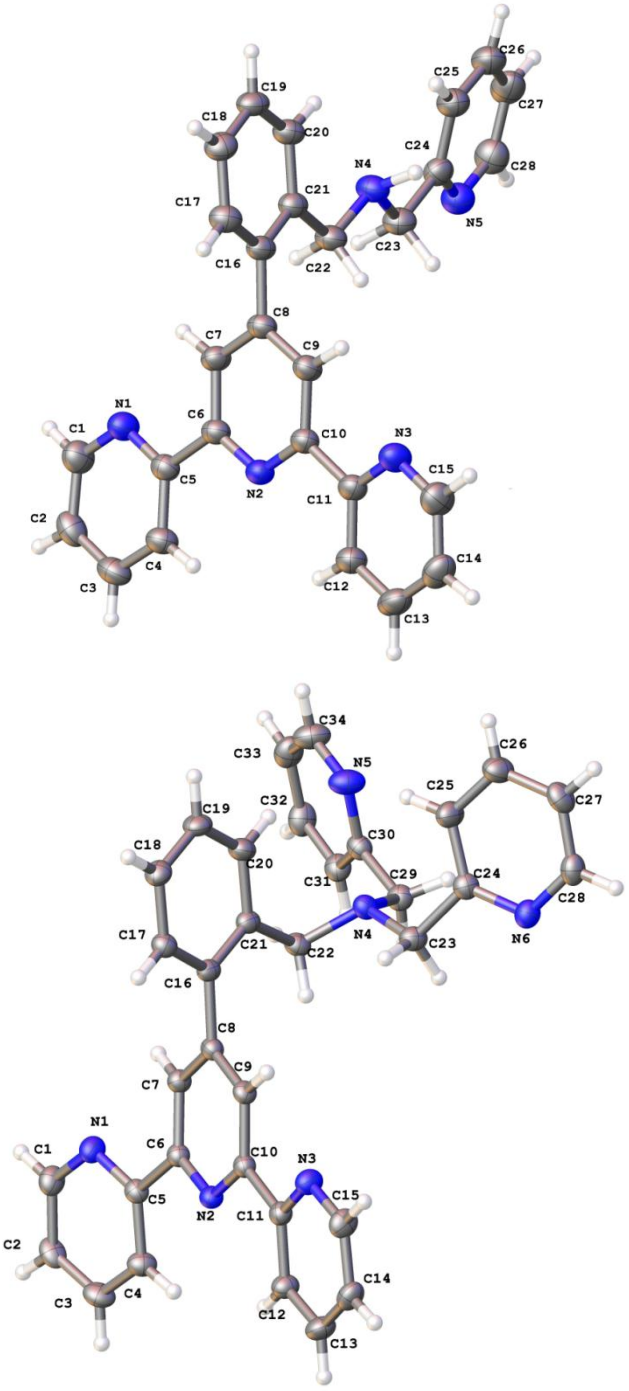

*Figure 2.23. Crystal structures of **L2.3** (top), and **L2.4** (bottom).*

Similar to any other neutral 2,2':6',2''-terpyridines, the terminal aromatic pyridine rings of terpyridine rotate around C-C single bond to avoid hydrogen-hydrogen interactions between the hydrogen atoms attached to C4-C7 and C9-C12. The most stable conformation is found to be *trans-trans*, when nitrogen atoms of the outer pyridine rings lie *anti*-periplanar to that of central pyridine and many examples have been reported in the literature.[76, 83, 217-220]

The phenyl rings in both ligands twist around with respect to central pyridine ring of the terpyridine unit to reduce steric hindrance between central ring protons and the ortho groups of the phenyl ring. The torsion angle C21-C16-C8-C9 is 102.45° and 109.78° for **L2.3** and **L2.4**, respectively. In both, the aromatic amine substituents lie almost perpendicular to the terpyridine unit, which is again for minimal intramolecular repulsive interactions. The inter-annular C-C bonds, C5-C6 and C10-C11, are in the range of 1.490-1.492 Å in both of the ligands. The three pyridine rings are not completely coplanar and the torsion angles C4-C5-C6-N1 and C12-C11-C10-N1 are 2.58° and 2.47° in **L2.3**, and those in **L2.4** are 5.55° and 11.32° respectively. These deviations from planarity are typical of other similar terpyridine ligands.[85, 218]

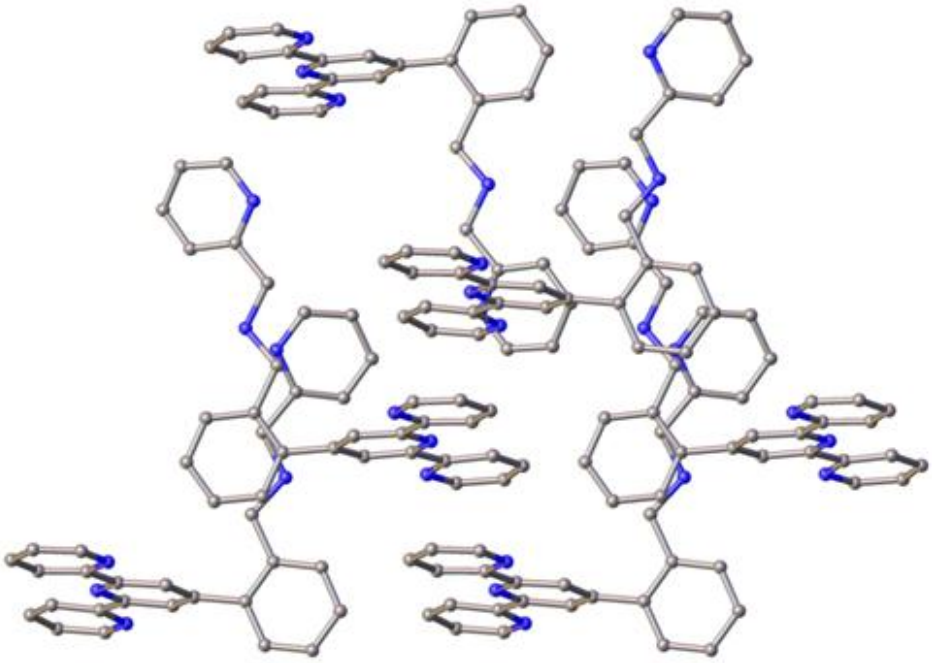

*Figure 2.24. The packing diagram of ligand **L2.3**. The hydrogen atoms omitted for clarity.*

The intermolecular π-π stacking ranges from 2.4 Å to 2.8 Å in **L2.3** and 3.8 Å to 4.3 Å in **L2.4**, as shown in packing diagrams in **Figure 2.24** and **Figure 2.25**. The nitrogen atoms make short contacts with aromatic hydrogen atoms of adjacent molecules. Various N···H-C short contacts lie between the range of 2.4 Å to 3.2 Å. All these packing interactions presumably play a role in stabilization of the crystal lattice.

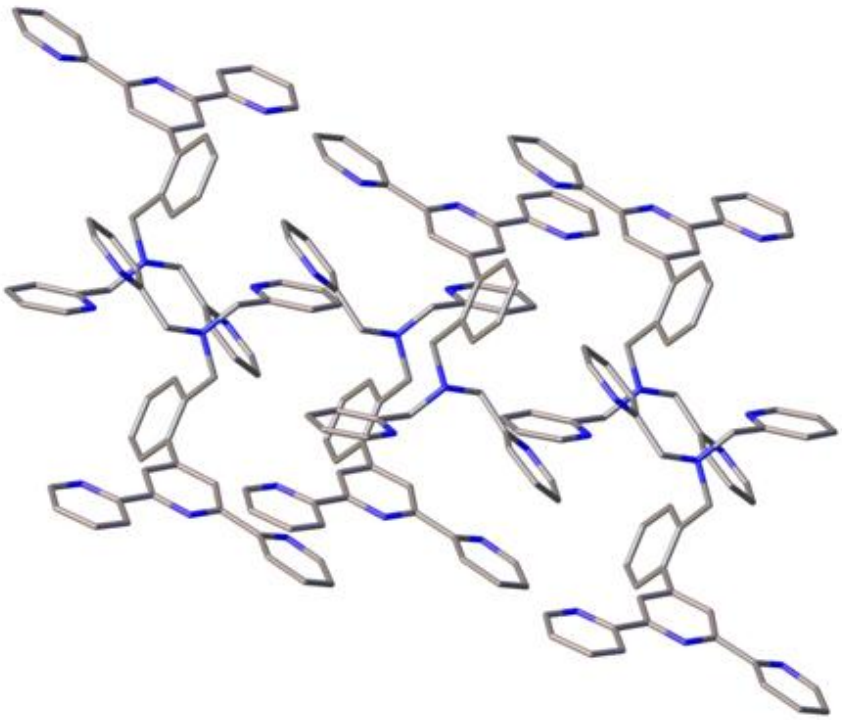

*Figure 2.25. The packing diagram of ligand **L2.4**. Hydrogen atoms are omitted for clarity.*

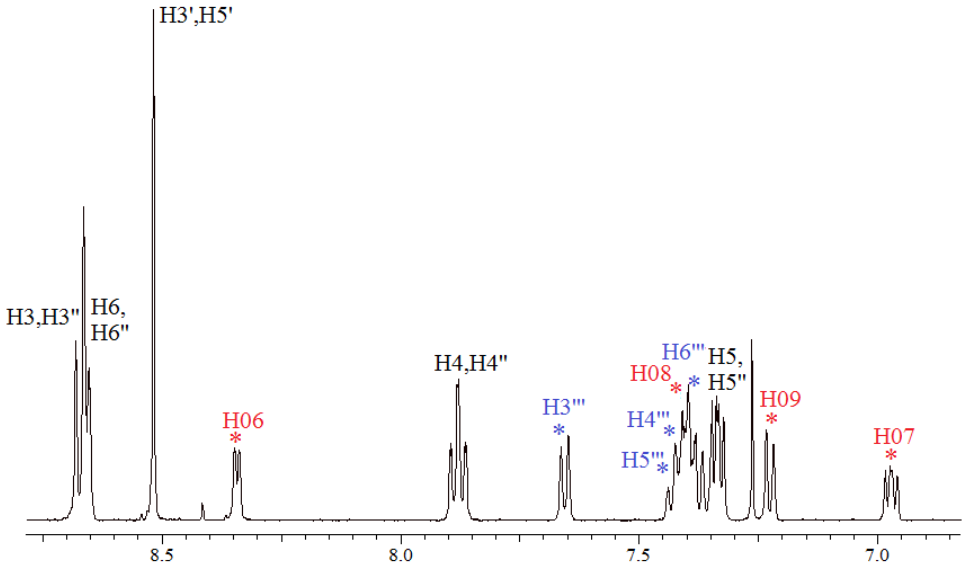

*Figure 2.26. The aromatic region of the ^{1}H NMR spectrum of **L2.3**.*

The aromatic region of the ^{1}H NMR spectrum of **L2.3**, as shown in **Figure 2.26**, displays 18 proton signals corresponding to three pyridine and one benzene ring environments. The individual ring systems were identified by a gCOSY experiment, as shown in **Figure 2.27**. The H3 and H3" protons (8.63 ppm) of the terminal pyridine rings of the terpy unit are involved in hydrogen bonding with the central pyridine nitrogen atom and are shifted downfield. This also confirms that the terminal rings of the terpy

unit are *anti*-periplanar to the central pyridine ring, as discussed in the X-ray crystal structure of **L2.3**. The terpy pyridyl H6 and H6" protons points away from the shielding environment due to the twisted conformation of the terminal rings and are assigned as the second downfield resonance at 8.65 ppm. The proton resonances at 8.34 ppm and 7.23 ppm are assigned as the H06 and H09 protons with the latter experiencing through-space ring-current effects as it lies in close proximity to the adjacent phenyl ring, also seen from the X-ray crystal structure of **L2.3**. NMR of **L2.4** is similar to **L2.3** and is given in appendix IV.

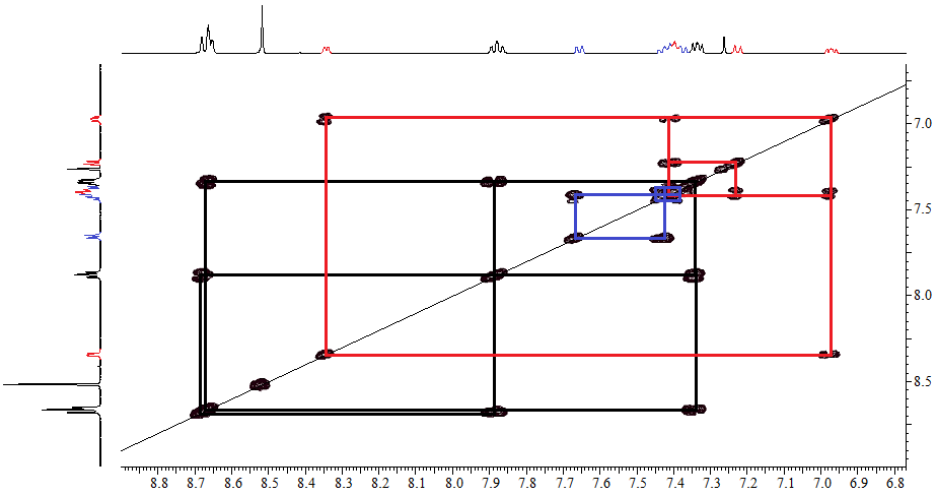

*Figure 2.27. The gCOSY spectrum of **L2.3**, showing the different ring systems.*

2.3.2.2.3. Synthesis of 4'-[2"'-{N,N-bis(carboxymethyl)aminomethyl}phenyl]-2,2':6',2"-terpyridine, L2.6, and intermediate ligand, L2.5

Iminodiacetic acid (IDA) contains a secondary amino group and two carboxylic acid groups. IDA can act as a tridentate ligand in slightly basic conditions and that may form a metal complex with two, fused, five member chelating rings. Due to chelating properties the iminodiacetic acid complexes are used for applications such as metal extraction and water purification etc.[24, 25, 34, 41, 221].

In aqueous medium IDA can produce zwitterions with an unequal charge distribution. Due to its polar nature IDA is soluble in aqueous medium only. However, the mono-bromo ligand **L2.2** is soluble only in non-polar organic solvents. Therefore, it was compulsory to substitute the polar carboxylic ends of IDA with some non-polar

group to make it soluble in non-polar solvent. The easiest method in terms of reaction workup and time was esterification of the carboxylic acid using alcohol *via* a dehydration reaction under acidic conditions. A literature method[222] was used to synthesise diethyl iminodiacetate **2.12 (Figure 2.28).** The secondary amine group in **2.12** was directly alkylated by bromo compound **L2.2**.

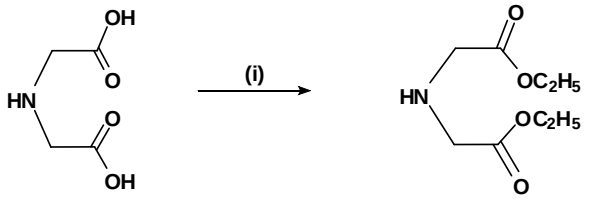

2.11 **2.12**

Figure 2.28. Synthesis of diethyl iminodiacetate[222] ***2.12****. (i) Ethanol, H_2SO_4, reflux, 2 days*

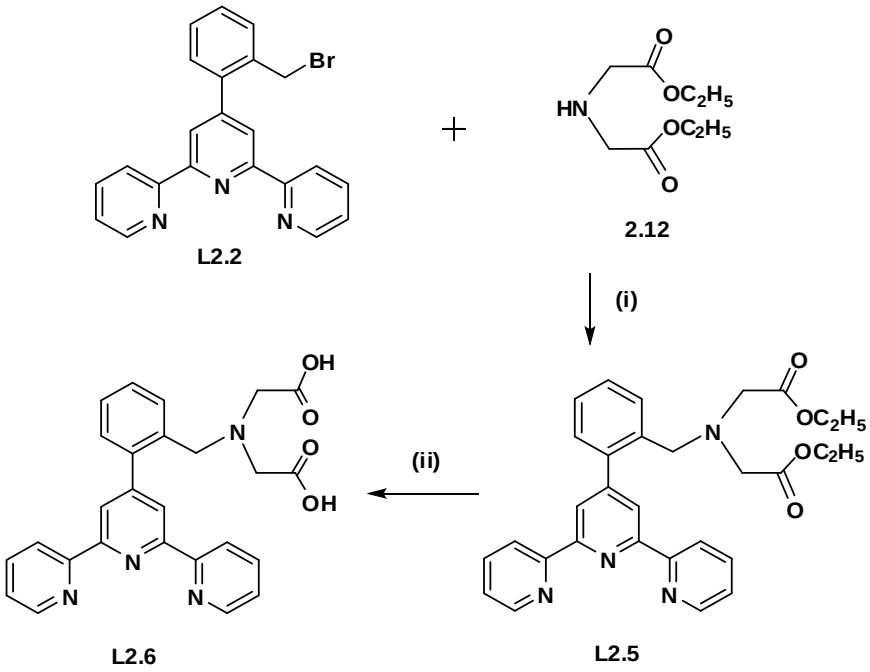

Figure 2.29. Synthesis of ligand ***L2.5*** *and* ***L2.6*** *(i) K_2CO_3, dry CH_3CN, 50°C, 12 hr. (ii) Conc. HCl, 80°C reflux, 3 days*

After synthesising the esterified compound **2.12**, it was used for direct alkylation under basic conditions in CH_3CN. One equivalent of K_2CO_3 was used to neutralise any acid formed during the reaction. Direct alkylation of **2.12** with brominated ligand **L2.2** resulted in formation of the intermediate alkylated product **L2.5** as pale yellow oil (**Figure 2.29**). The intermediate ligand **L2.5** was purified *via* column chromatography (alumina, 50% DCM:Hexane, and then only DCM). Purified **L2.5** was treated with conc.

HCl to hydrolyse the ester group. The hydrochloride salt of **L2.6** was neutralised by washing with 0.1 M NaOH and water. The ligand was collected in chloroform, washed with brine solution and then dried over $MgSO_4$. The neutral ligand was dried by rotary evaporation. Both **L2.5** and **L2.6** were characterised by ^{1}H, ^{13}C NMR, and elemental analysis.

2.3.2.2.4. Synthesis of 4'-[2'"-(5-(2-aminoethyl)-7-amino-2,5-diazaheptyl)-phenyl]-2,2':6',2"-terpyridine , L2.7

To synthesise the ligand **L2.7**, *N*,*N*-bis(2-aminoethyl)ethane-1,2-diamine (tren) was used after drying over sodium hydroxide pellets. Tren contains one tertiary amine nitrogen atom and three primary amine nitrogen atoms. All three primary amine nitrogen atoms are reactive and undergo nucleophilic substitution reactions. However, to synthesise the polydentate ligand **L2.7**, only one primary nitrogen atom is required to perform nucleophilic substitution on the brominated carbon of **L2.2**. This means the primary nitrogen atoms should be protected. Although there are a number of strategies available in literature, the selective mono-N-functionalisation of the polyamines (such as tren) is a continuing synthetic challenge due to lack of differentiation between the identical amine arms. Alternatively, when a polyamine is commercially available, one common method involves direct alkylation of a large excess of polyamine relative to the alkyl halide in order to limit N-derivatisation to only one reactive site. Hence, to ensure selective mono-N-functionalisation of polyamine, a large excess of polyamine tren was added to the reaction mixture. The excess of starting amines was recovered and reused.

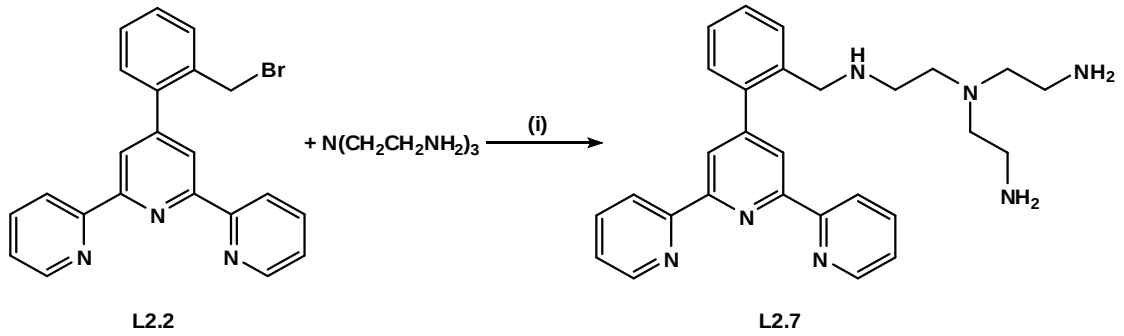

*Figure 2.30. Synthesis of **L2.7** via nucleophilic substitution, (i) dry CH_3CN, 35°C, 24 hours*

Proton NMR of the crude sample was complicated and multiple peaks in both aromatic and aliphatic regions indicate the presence of more than one molecules in the sample. ESI-MS of the crude sample show *m/z* peaks beyond 900 which indicate the

presence of larger molecules in the crude product. The purification of **L2.7** was a challenge because of possible mono-, di-, or tri-N-functionalisation of the polyamine. Although an excess of the polyamine was used to ensure mono-N-derivatisation, some bigger species were formed in the reaction mixture. Based on this knowledge, column chromatography was chosen to collect the desired ligand. As the ligand **L2.7** contains primary, secondary and tertiary amine groups there was a possibility for the amines to "stick" if silica was used as the stationary phase. Therefore alumina was used as a stationary phase, and different solvent combinations were tried to find a mobile phase for the column but none of the methods worked for purification of the polyamine ligand **L2.7**. Finally ion exchange chromatography was used, as the nitrogen atoms in the ligand protonate in the acidic medium and can be retained in the stationary phase. The stationary phase used was DOWEX 50WX2-200 cation exchange resin and the eluent used was hydrochloric acid of different concentrations. The ligand was collected as its hydrochloride salt by eluting with 4M HCl.

2.3.2.2.5. Crystal structure and NMR of $[L2.7H_6]Cl_6 \cdot 8H_2O$

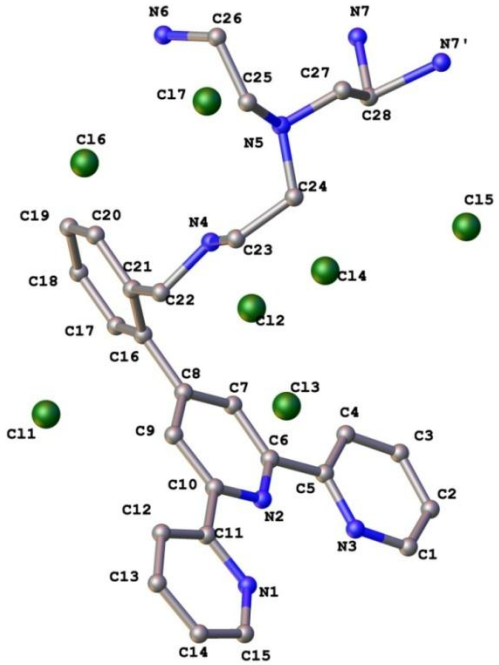

*Figure 2.31. The crystal structure of the chloride salt of **L2.7**, all solvent molecules and hydrogen atoms omitted for clarity.*

The solid state structure of **L2.7** was elucidated *via* single X-ray crystallography. Thin needle shaped X-ray quality crystals of the ligand salt were grown by evaporation of the

aqueous solution of the ligand salt inside a tightly closed glass vial containing $CaCO_3$. The crystal structure was solved in the monoclinic space group *C*2/*c* with an R-factor of 6.75%. The asymmetric unit contains one ligand with protonated nitrogen atoms, six disordered chloride ions and co-crystallised water molecules. The crystal structure of the ligand salt is shown in **Figure 2.31.**

Due to some disorder associated with chloride ions and water molecules; it was challenging to model the crystal structure. The terminal free arms of polyamine were also disordered over two positions and which were modelled by refining the occupancy of the nitrogen atoms (N7 and N7') each with 0.6:0.4 occupancy. The six hydrogen atoms on the nitrogen atoms were located in the difference electron density map. The occupancy of the disordered chloride ions Cl4, Cl5 and Cl2 was refined to give occupancy 0.5, 0.7 and 0.8, respectively.

All other chloride ions were well ordered. Other than chloride ions there were several small electron density peaks, which we tried to assign to low-occupancy water molecules as a possible solvent. However, the anisotropic displacement parameters of the disordered O atoms were large. Several attempts at defining additional sites or using lower site-occupation factors for the solvent atoms yielded inferior results. Indeed, omitting the disordered water molecules resulted in an incomplete refinement with a higher R-factor (6.75% *vs.* 10.76%).

Finally the crystal structure was solved as [**L2.7**H_6]Cl_6. The elemental analysis of the bulk sample is consistent with [**L2.7**](HCl)$_7$·8H_2O. We also tried to grow better crystals in three different experiments, but the crystallographic data obtained was same in all attempts. This type of water-chloride disorder is common in other crystals that contain a large number of chloride ions and water molecules.[223-229] More crystal structures with similar disorder are described in Chapter 4 and Chapter 6 involving larger molecules.

In contrast to the *trans-trans* confirmation in neutral ligands, **L2.3** and **L2.4**, the three pyridine rings in **L2.7**·6HCl exists in a *cis-cis* conformation due to two protonated nitrogen atoms. In the literature there is evidence where in terpyridine units only one, two or all three nitrogen atoms are protonated; in mono-protonated terpyridine compounds crystals form with *cis-trans* geometry, and both in di- or tri-protonated terpyridines the crystals form in *cis-cis* geometry.[230-232]

The geometry of the ligand **L2.7**·6HCl was considered to be *cis-cis* after looking at the different factors in the crystal structure. If we swap C4 and C12 to N atoms, this increases the R-factor by 0.24% and the thermal parameter for C atoms become too small when we assign C at the place of N3 and N1 positions. The protons were found from the electron density map but due to disordered structure, we used calculated positions to add hydrogen atoms. Also, in the packing diagram in **Figure 2.32** for N3-H···Cl3 and N1-H···Cl3 hydrogen bonds, the N-Cl distances are smaller than 3 Å and are similar to standard N-H···Cl distances reported in literature.[233]

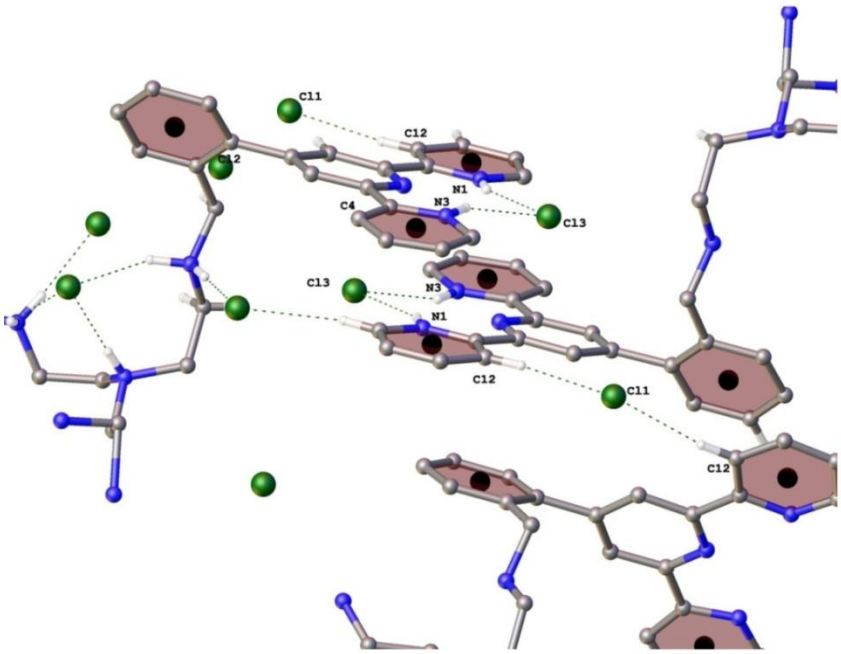

*Figure 2.32. Packing diagram of the chloride salt of **L2.7** showing various hydrogen bonding, π-π stacking and other short contact. The solvent molecules and hydrogen atoms not involved in hydrogen bonding and short contacts are omitted for clarity.*

The pyridine rings are again coplanar and the torsion angles N3-C5-C6-N2 and N1-C11-C10-N2 are 1.6° and 5.4° respectively. The torsion angle C9-C8-C16-C21 between the toluyl ring and the central pyridine ring is 54.6°. The inter-annular C-C bonds in **L2.7**·7HCl, C5-C6, 1.49Å and C10-C11, 1.48 Å, are within the range of other reported terpyridine ligands in this thesis.

The molecules in the crystal lattice are held together by hydrogen bonding, and electrostatic interactions between chloride ions and aromatic hydrogen atoms. All of the hydrogen atoms attached to nitrogen atoms are involved in hydrogen bonding with

chloride ions within the range of 2.116 Å to 2.295 Å, **Figure 2.32**. The hydrogen atoms and other short contacts range between 2.0 Å-3.0 Å. The intermolecular π-π stacking between terminal pyridine rings and the phenyl rings ranges from 3.8-3.9 Å.

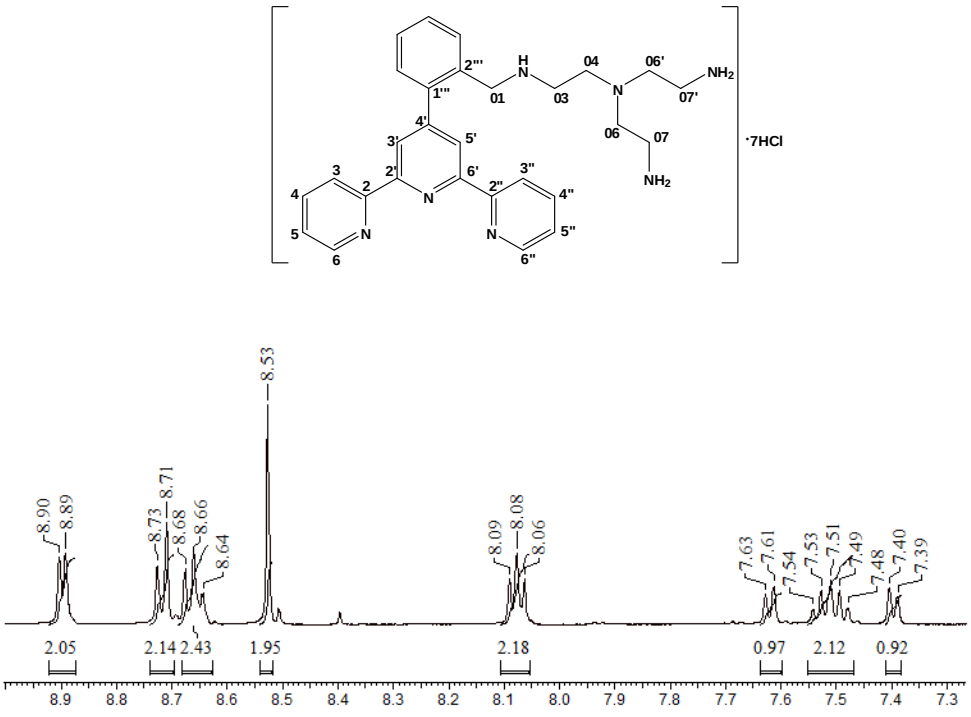

*Figure 2.33. The aromatic region of the ^{1}H NMR spectrum of **L2.7***

Figure 2.33 shows the ^{1}H NMR spectrum of **L2.7** in D_2O. The spectrum displays 28 proton signals corresponding to two pyridine and one benzene ring environments. Contrary to the ligand **L2.3**, the terpy pyridyl H6 and H6" protons experience downfield shifts and are assigned as the proton resonance at 8.90 ppm. Interestingly, due to the protonation of the terminal pyridine nitrogen atoms, as also seen from the X-ray crystal structure (**Figure 2.31**), the pyridine rings of the terpy unit adopts *cis-cis* conformation, contrary to the ligand **L2.3**. As a result, the second downfield resonance at 8.72 ppm is assigned as the H3 and H3" protons of the terminal pyridine rings of the terpy unit.

2.3.2.2.6. Synthesis of 4'-(2"'-(12-amino-2,6,9-triazadodecyl)-phenyl)-2,2':6',2"-terpyridine, L2.8

Synthesis of **L2.8** was again challenging due to the presence of more than one type of reactive group in the amine to be used for functionalisation. Addition of the tail *N,N'*-bis(3-aminopropyl)ethane-1,2-diamine (3,2,3-tet or 1,5,8,12-tetraazadodecane) or more precisely, the site at which the addition took place on 3,2,3-tet was an issue. For selective mono-N-derivatisation, it was required to protect secondary amines in 3,2,3-tet. A synthetic route similar to that which has been used to produce macrocyclic polyamines was employed as shown below in **Figure 2.34**. The polyamine 3,2,3-tet undergoes a double condensation reaction with glyoxal and forms a cyclic structure (bisaminal). In this reaction primary amines convert to secondary amines and the secondary amines convert to tertiary amines. This reaction gives dual benefit of protecting the secondary amine and producing more reactive terminal amines.

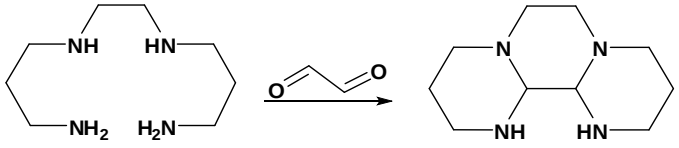

2.13 **2.14**

*Figure 2.34.Protection of 2° amine via Claudon et al. preparation.[234] 3° amines were formed by condensation reaction between 3,2,3-tet and glyoxal to produce the cyclic bisaminal **2.14**.*

The selective mono-*N*-alkylation of the primary amines of classically protected linear polyamines (with, for example, the Ts and Boc groups) is tricky because the independent reactions of the two terminal nitrogen atoms lead to mixtures of products and lower the yields.[234] This issue could be considerably controlled by making a sterically hindered rigid intermediate, where secondary amines interact with each other through a bisaminal bridge as shown in **Figure 2.35**. In this way, the alkylation of the first secondary amine could sterically influence the alkylation of the second one, and thus limit its reactivity. Moreover, preparation of the bisaminal intermediates is quantitative and, after reaction, they can easily be deprotected.

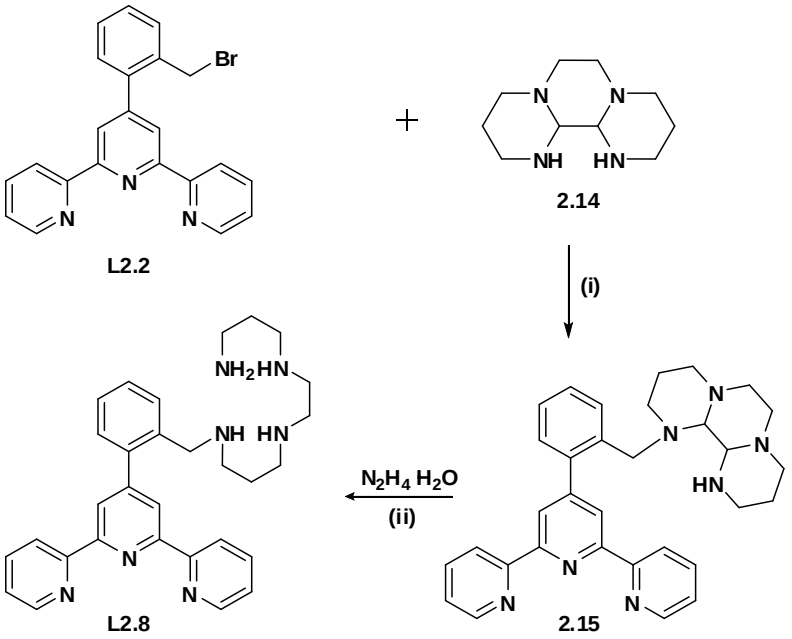

*Figure 2.35. Addition of brominated ligand to the protected tetramine, and then deprotection of the "tail" to synthesise ligand **L2.8**. (i) glyoxal, ethanol, 2.5 hr at R.T. (ii) dry CH_3CN, overnight reflux, hydrazine monohydrate, 2 hr reflux.*

In order to synthesise **L2.8**, the mono-bromo compound, **L2.2,** was added to the bisaminal of 1,5,8,12-tetraazadodecane and the reaction progress was monitored *via* TLC. The substituted bisaminal (**2.15**) was deprotected using hydrazine monohydrate. Ion exchange chromatography was used for purification and the ligand was collected as its hydrochloride salt when eluted with 4M HCl solution. Characterisation was performed using NMR, ESI-MS and elemental analysis. The ESI-MS peak of 518.30 corresponds to [**L2.8**+Na^+]. Elemental analysis of the bulk sample is consistent with **L2.8**·7HCl·6H_2O.

2.4. Conclusion

The polydentate ligands (**L2.3** – **L2.8**) based upon 2,2':6',2''-terpyridine and different amine ligands were synthesised in preparation for a study of the kinetics of hydrolysis of phosphate diesters. Different amines used to substitute at brominated position of **L2.2** were picolylamine (in **L2.3**), bis-picolylamine (**L2.4**), *N*,*N*-bis(2-aminoethyl)ethane-1,2-diamine (in **L2.8**), Imino-diacetic acid (in **L2.6**) and *N*,*N'*-bis(3-aminopropyl)ethane-1,2-diamine (in **L2.7**). The ligands were characterised using various analysis techniques such as ^{1}H NMR, ^{13}C NMR, gCOSY, HSQC, HMBC, elemental analysis, mass spectrometry, and melting point. The parent ligand 4'-(o-toluyl)-2,2':6',2''-tepyridine (**L2.1**) was synthesised using a slightly modified "one-pot" literature procedure.[169] Bromination reaction of the methyl group in **L2.1** was improved based upon observation of the nature of the reaction during various attempts in this project. The di-bromo side product **2.8** of the bromination reaction was isolated and characterised using different techniques including X-ray crystallography.

All of the polydentate ligands were purified using column chromatography, ligands **L2.3**– **L2.4** were purified as neutral ligands using alumina column, and other polydentate ligands **L2.7** and **L2.8** were purified using Dowex ion exchange column chromatography as their hydrochloride salts. Another intermediate ligand **L2.5** formed during the synthesis of **L2.6** was isolated and characterised. Crystals of polydentate ligands, **L2.3**, **L2.4**, and **L2.7** were successfully grown and their crystal structures are discussed in this chapter.

CHAPTER 3

SYNTHESIS AND CHARACTERISATION OF Ni(II), Cu(II), Zn(II), & Ag(I) COMPLEXES OF 4'-(2'''-TOLUYL)-2,2':6',2''-TERPYRIDINE

3.1. Introduction

As discussed in previous chapters the aim of this research project was to study the rate of hydrolysis of phosphate diesters using dinuclear complexes in comparison to their mononuclear analogues. The dinuclear complexes were synthesised from different polydentate ligands discussed in Chapter 2. The ligand, 4'-(2'''-toluyl)-2,2':6',2''-terpyridine), **L2.1**, was a pivotal ligand in synthesis of all these polydentate ligands. Each polydentate ligand was synthesised by introducing some amine functionality to the *ortho*-methyl group of 4'-(2'''-toluyl)-2,2':6',2''-terpyridine) *via* an intermediate bromination reaction.

This project was largely based upon the coordination behaviour of the polydentate ligands (**L2.3**-**L2.8**) with different metal ions, therefore understanding the coordination chemistry of **L2.1** was also of interest for this project.

To study the coordination chemistry of 4'-(2'''-toluyl)-2,2':6',2''-terpyridine, a number of complexes were synthesised using different metal ions including Cu(II), Ni(II), Zn(II) and Ag(I). These complexes were characterised using techniques such as NMR, mass spectrometry, elemental analysis, IR and melting point. Most of the complexes were crystallised from their bulk solutions and X-ray diffraction experiments were also performed. Crystal structure analysis reveals formation of a variety of discrete nickel, copper and zinc complexes with **L2.1** (**3.1**-**3.12**). A fascinating spiral polymer **3.13** was formed when **L2.1** was reacted with Ag(I).

This chapter includes a brief discussion of the synthesis and characterisation of complexes **3.1** – **3.13**, including their crystal structures. The bulk characterisation of the isolated material from all syntheses was performed by CHN elemental analysis. The sample was dried overnight under vacuum before sending for the analysis. In most of the cases the analysis was consistent with the crystal structures. However, in some cases, the co-crystallised solvent such as methanol and acetonitrile were evaporated and analysis was consistent with the presence of some water molecules that could be due to the atmospheric water absorbed by crystals. Other techniques such as NMR, mass spectrometry, IR and melting point were also used for characterisation of the complexes where appropriate.

3.2. Results and Discussion

3.2.1. Ni(II) Complexes

An overview of the syntheses of four different complexes prepared from Ni(II) and **L2.1** is presented below in **Figure 3.1**. Structural studies reveal that in all of the nickel complexes, the Ni(II) ion is six-coordinate and has an approximately octahedral geometry. In all the obtained structures three sites of the octahedral nickel centre are occupied by **L2.1** through its pyridine-type nitrogen atoms. The remaining octahedral sites are occupied either by neutral/anionic ligands such as chloride (**3.2**), and water (**3.3**) or by another **L2.1** ligand (**3.1**) and (**3.4**), as shown in **Figure 3.1**.

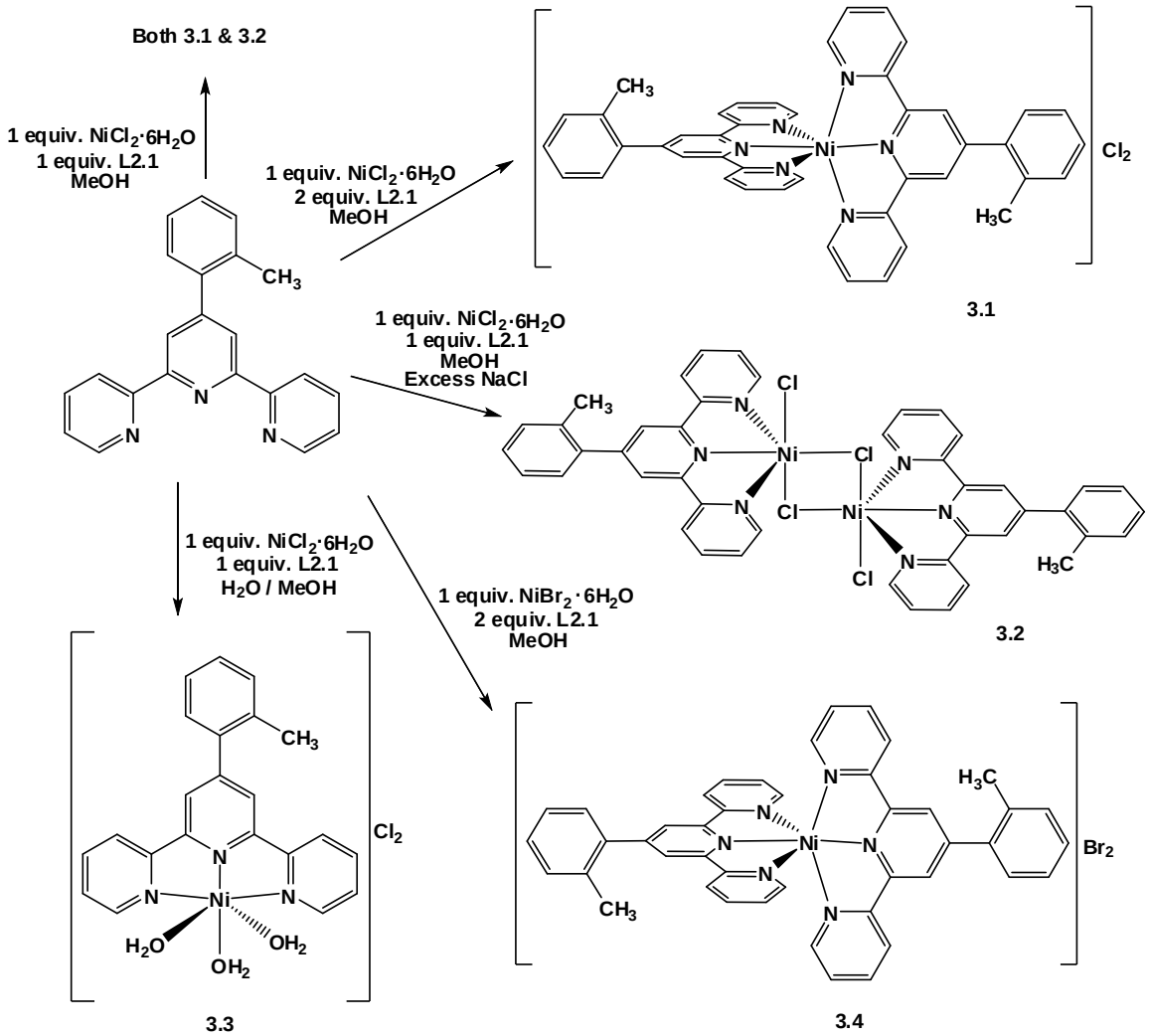

*Figure 3.1. Ni(II)-**L2.1** complexes and brief description of their syntheses.*

*3.2.1.1. [Ni(**L2.1**)$_2$Cl$_2$·4H$_2$O·2CH$_3$OH]– Complex **3.1** & [Ni(**L2.1**)$_2$]Br$_2$– Complex **3.4***

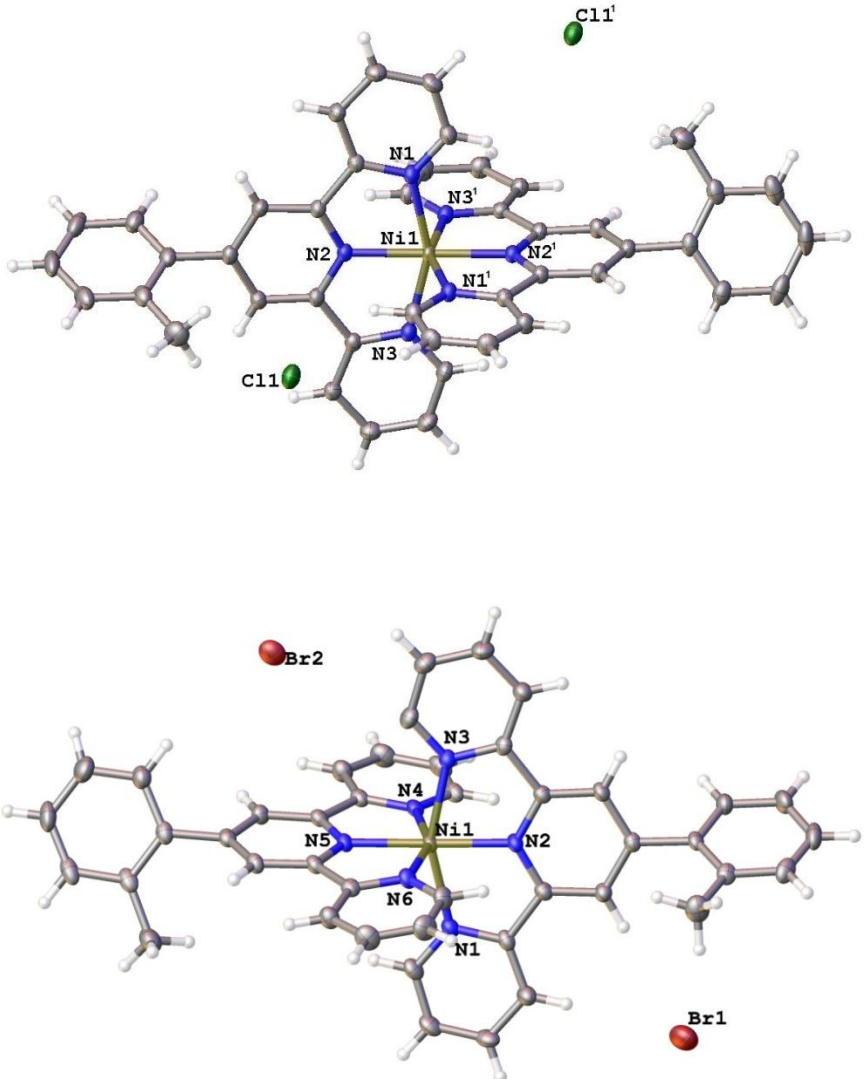

*Figure 3.2. The crystal structures of the bis(**L2.1**)-Ni(II) complex as its chloride and bromide salts **3.1**(top) and **3.4**(bottom). Solvent molecules have been omitted for clarity. The selected bond lengths and bond angles are given in Appendix III, Table A12 & A15.*

Complex **3.1** was synthesised by mixing two equivalents of **L2.1** with one equivalent of $NiCl_2·6H_2O$ in a dichloromethane/methanol solution. The X-ray quality orange-brown block shaped crystals were formed by vapour diffusion of diethyl ether into the resulting green solution. The crystal structure of complex **3.1** was solved in the monoclinic space group *C*2/c and refined to an R-factor of 3.84%. Another similar bis-**L2.1** nickel complex, **3.4**, [Ni(**L2.1**)$_2$]Br$_2$ was synthesised by mixing two equivalents of **L2.1** with one equivalent of $NiBr_2·3H_2O$ in a dichloromethane/methanol solution. Vapour diffusion of diethyl ether into resulting pale green solution produced X-ray quality hexagonal orange-brown crystals. The crystal structure was solved in the monoclinic space group

$P2_1/n$ and refined to an R-factor of 5.37%. The crystal structures of bis-**L2.1** nickel complexes **3.1**, $[Ni(\mathbf{L2.1})_2]Cl_2$ and **3.4**, $[Ni(\mathbf{L2.1})_2]Br_2$ are shown in **Figure 3.1**.

In complex **3.1**, the hydrogen atoms attached to the oxygen atoms of the solvent molecules were located from the electron density map and the DFIX restraint was applied to fix the O-H distances to the standard 0.84 Å.

In complex **3.4**, overall structure of the cation and anions was well ordered. However, some residual electron density peaks were present in a small volume of the electron density map. Due to overlapping and poor ordering of the peaks it was not possible to model the structure. Two solvent voids of 466 $Å^3$ containing 132 electrons were calculated, which indicate the presence of a large amount of solvent molecules accumulated in the small area. In this case as Z=4, there are 33 electrons per asymmetric unit. The possible solvents could be a combination of low occupancy water (10 electrons) or methanol (18 electrons), as these were used at different stages of the synthesis. The disordered peaks were masked; R-factor reduced to 5.37% from 5.98%. The CHN elemental analysis performed on the bulk material was consistent with a composition of $C_{44}H_{34}N_6NiBr_2 \cdot 3H_2O$. This difference in composition compared to that derived from the single crystal analysis may be a result of the drying procedures employed on the sample.

In both of these complexes, the nickel centre coordinates to two *meridional* **L2.1** ligands through six pyridine-type nitrogen atoms. Two non-coordinating chloride or bromide ions were located around the cation in the asymmetric unit.

In complex **3.1** both of the ligands lie almost perpendicular to each other with central pyridine plane-to-plane angle of 88.97(9)°. In complex **3.4** the ligands deviate from orthogonality and the central pyridine plane-to-plane angle shifts to 75.34(13)°. Both complexes occupy a distorted octahedral geometry with D_{2d} symmetry around the metal centre, which is typical of bis-terpyridine-type metal complexes such as $[Fe(tpy)_2]^{2+}$, $[Co(tpy)_2]^{2+}$, $[Ni(tpy)_2]^{2+}$and $[Cu(tpy)_2]^{2+}$ reported previously[72, 73, 79, 235-238] and the other bis-**L2.1** complexes **3.8** and **3.10** reported in this chapter. Some bis-terpyridine type Ni(II) complexes reported are $[Ni(tpy)_2](PF_6)_2$,[72] $[Ni(phtpy)_2](NO_3)_2$,[79] and $[Ni(phtpy)_2]Cl_2 \cdot 10H_2O$.[79, 235] In these literature complexes, the Ni-N bond lengths lie in a range of 1.996(4) Å to 2.14(2) Å, similar to complexes **3.1** and **3.4**.

*3.2.1.2. $[Ni_2(\mathbf{L2.1})_2(\mu\text{-}Cl)_2]Cl_2{\cdot}4CH_3OH$ – Complex **3.2***

Complex **3.2** was synthesised by mixing one equivalent each of **L2.1** and $NiCl_2{\cdot}6H_2O$ in dichloromethane/methanol solution. Two drops of saturated aqueous NaCl was also added and slow evaporation of the resulting green solution produced green rectangular X-ray quality crystals. The crystal structure of **3.2** was solved in the triclinic space group $P\overline{1}$ and refined to an R-factor of 4.40%. The solvent was modelled as methanol and hydrogen atoms were located from the electron density map and refined with a DFIX constraint of 0.84 Å. The crystal structure of the complex **3.2** is shown **Figure 3.3**.

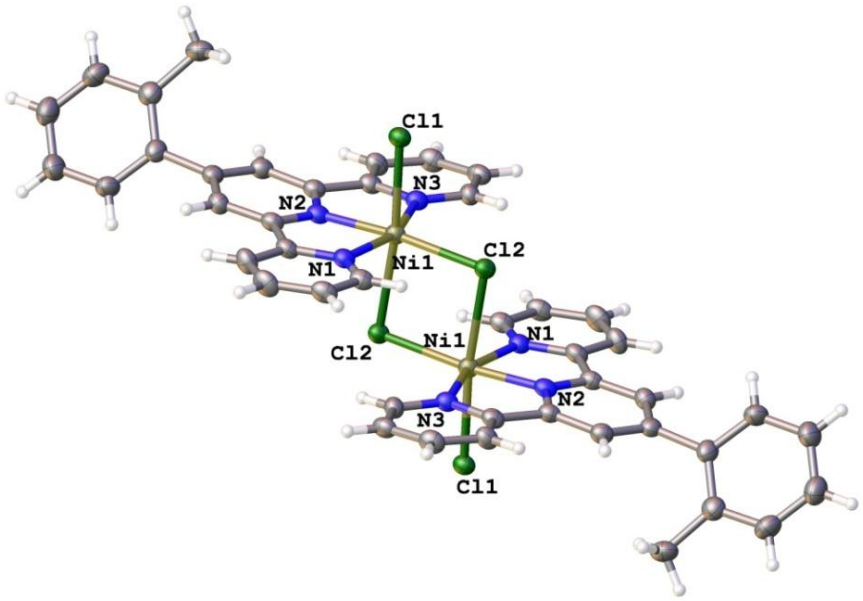

*Figure 3.3. The crystal structure of Ni(II)-**L2.1** complex **3.2**. The selected bond lengths and bond angles are given in Appendix III, Table A13.*

The asymmetric unit of **3.2** contains half of the molecule and both halves coordinate to each other by double Ni-Cl-Ni bridging. Each of the nickel centres is bonded to the tridentate terpyridine metal-binding domain of **L2.1**. The remaining coordination sites on each Ni(II) are occupied by one terminal and two bridging chloride ligands. The bridging $\{Ni(\mu\text{-}Cl)_2Ni\}$ structural motif has Ni-Cl2 bond lengths of 2.343 Å and 2.572 Å, one bond length of these is shorter than terminal Ni-Cl1, 2.457Å. These bond lengths are typical and comparable to literature complexes $[Ni_2(pttp)_2(\mu\text{-}Cl)_2Cl_2]$[210] (two bridging Ni-Cl bonds: 2.3449(7) Å and 2.6231(8) Å; terminal Ni-Cl bond: 2.3980(8) Å), where phtpy is 4'-(4'''-toluyl)-2,2':6',2''-terpyridine); and $[Ni_2(phtpy)_2(\mu\text{-}Cl)_2Cl_2]$ dimeric complex[239] (two bridging Ni-Cl bonds: 2.3666(11) Å and 2.5309(12) Å; terminal

Ni-Cl bond:2.4082(12) Å). The Ni···Ni distance is 3.548 Å, which is comparable to the inter-metallic distance observed in other similar di-nickel complexes.[80, 240-244] One somewhat longer Ni···Ni distance (3.642 Å) was found in $[Ni_2(phtpy)_2(\mu\text{-}Cl)_2Cl_2]$, where phtpy is 4'-(phenyl)-2,2':6',2''-terpyridine).[239]

*3.2.1.3. [Ni(**L2.1**)(OH$_2$)$_3$]Cl$_2$·3H$_2$O – Complex **3.3***

Complex **3.3** was synthesised by mixing one equivalent of **L2.1** in dichloromethane/methanol with one equivalent of aqueous $NiCl_2 \cdot 6H_2O$ solution. The green filtrate was allowed to evaporate slowly and green-blue rectangular X-ray quality crystals were formed. The crystal structure of **3.3** was solved in the orthorhombic space group $P2_12_12_1$ and refined to an R-factor of 2.99%. The hydrogen atoms for all the coordinating and non-coordinating water molecules were located from the electron density map and the O-H distances were fixed with a DFIX constraint of 0.84 Å. The crystal structure of the complex **3.3** is shown **Figure 3.4.**

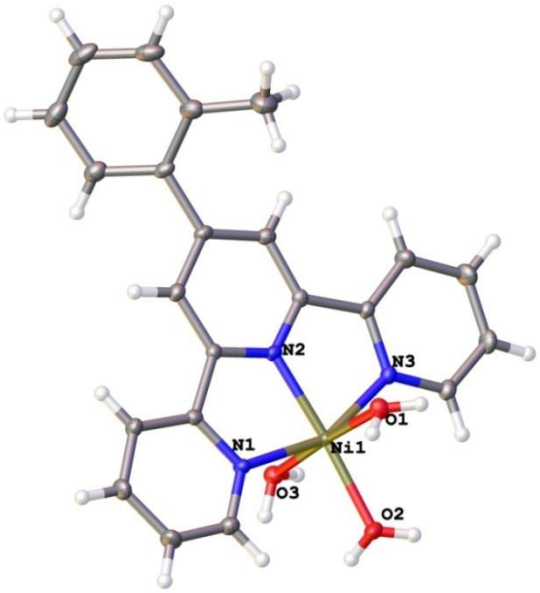

*Figure 3.4. The molecular structure of the 4'-(2'''-Toluyl)-2,2':6',2''-terpyridine Ni(II) octahedral complex **3.3**. The chloride ions and solvent have been removed for clarity. The selected bond lengths and bond angles are given in Appendix III, Table A14.*

The geometry around the nickel centre can be described as a distorted octahedron formed by the coordination of one **L2.1** ligand which functions as a tridentate ligand with nitrogen donor atoms in a meridional fashion. Three coordinated water molecules and two chloride counter-ions stabilise the structure of the dication in the asymmetric unit.

The distance between the Ni(II) and the central nitrogen donor N1 is 1.987(18) Å; whereas the distance between the terminal nitrogen donors N1 and N3 are longer at 2.102(2) Å and 2.114(2) Å, respectively. The Ni-O distances vary from 2.057 to 2.114 Å; with Ni-O2 being shortest. All the water molecules and chloride ions present in the lattice are involved in a hydrogen bonding network that runs along the a-axis of the unit cell.

3.2.2. Cu(II) Complexes

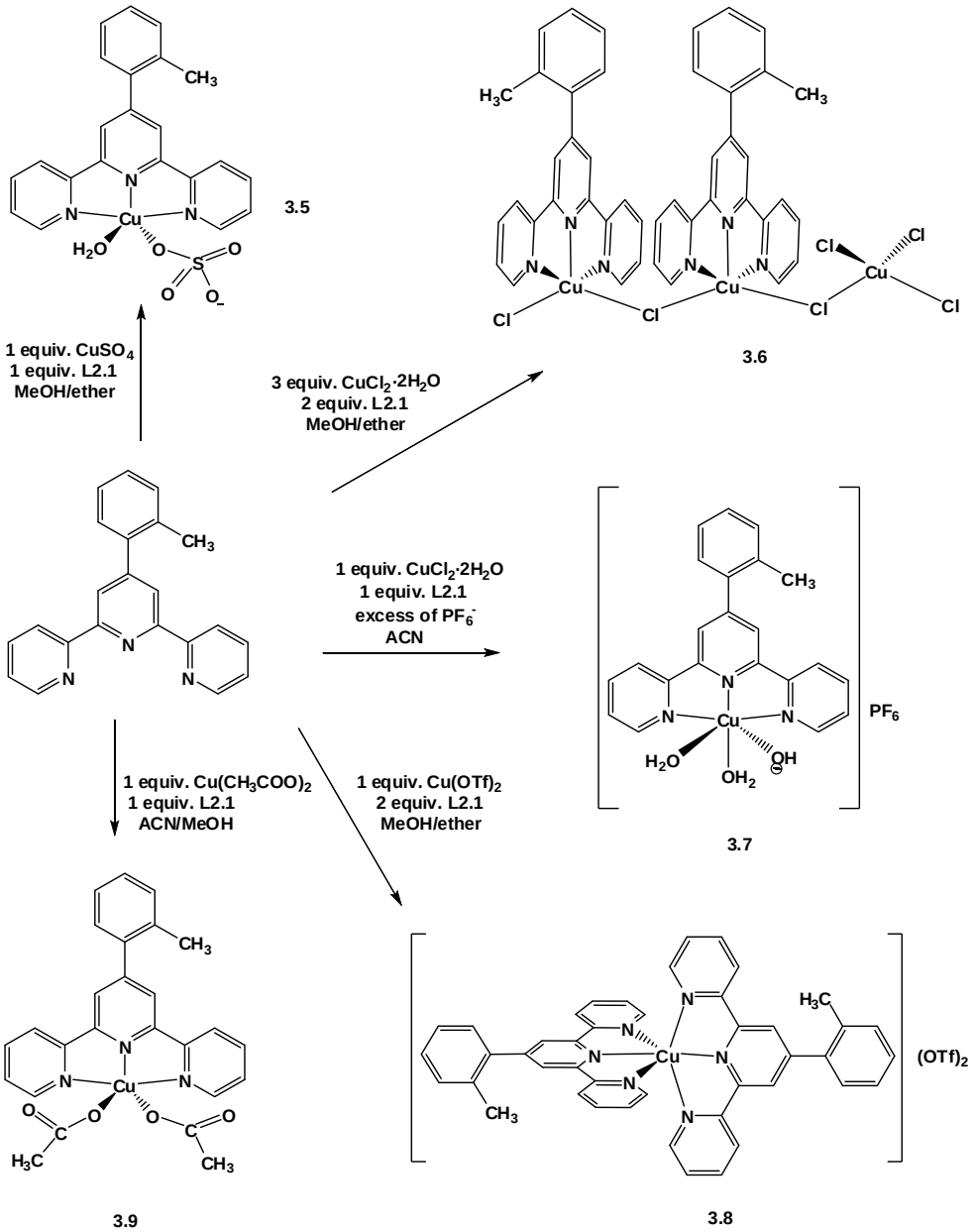

*Figure 3.5. Syntheses of Cu(II)-**L2.1** complexes. For complex **3.7** and **3.8**, refinements were poor; the structural identification of these complexes remains tentative.*

The Cu(II) complexes prepared using **L2.1** are outlined in **Figure 3.5**. The Cu(II) centre is five-coordinate in three of the five structures and six-coordinate in the remaining two. In each complex, three coordination sites of copper are occupied by three pyridine nitrogen atoms of the ligand and the remaining sites are occupied by other neutral or anionic ligands. The bis-**L2.1** Cu(II) complex **3.8** is octahedral and, unsurprisingly, the structure is very similar to that of the Ni complexes **3.1** and **3.4** reported in this chapter and other similar bis-terpyridine type metal complexes reported in literature.[72, 73, 79, 235-238]

*3.2.2.1. [Cu(**L2.1**)(OSO_3)(OH_2)]·4H_2O – Complex **3.5***

Complex **3.5** was synthesised by mixing one equivalent of **L2.1** with one equivalent of $CuSO_4$ in dichloromethane/methanol solution, resulting in formation of a blue green solution. Vapour diffusion of diethyl ether into the resulting solution produced X-ray quality thin needle shaped crystals in 85% yield. The CHN elemental analysis of the bulk sample was consistent with that of the crystal structure. The crystal structure of **3.5** was solved in the orthorhombic chiral space group *Pna*2_1 and refined to an R-factor of 4.56%.

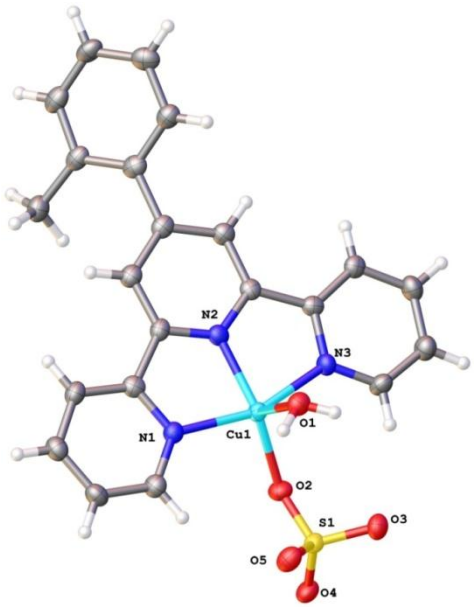

*Figure 3.6.The crystal structure of the Cu(II) complex **3.5**. The solvent molecules have been omitted for clarity. The selected bond lengths and bond angles are given in Appendix III, Table A16.*

The asymmetric unit of **3.5** contains one **L2.1** ligand coordinated to Cu(II) through three terpyridine nitrogen donor atoms, a water and a O-coordinating sulfate ion, and is shown in **Figure 3.6**. The Cu(II) is five-coordinate and has an intermediate geometry

between ideal trigonal bipyramidal (TBPY) and ideal square pyramidal (SP) geometries. A slight change in coordination environment can distort the five-coordinate geometries from ideal TBPY or SP to an intermediate shape. A geometric parameter, τ, has been defined for such five-coordinate structures by Addison *et al*.[69] This parameter is defined as $\tau = (\beta-\alpha)/60$, and represents an index of the degree of trigonality, within the structural continuum between TBPY and SP. The angles α and β are the two largest angles around the metal atom. If $\tau = 0$ the coordination geometry is an ideal square pyramidal, and if $\tau = 1$ the coordination is an ideal trigonal bipyramid. In this Cu(II) complex, the angles are (N1-Cu1-N3) =159.79° and (N2-Cu1-O2) = 151.83, giving a geometric parameter τ of 0.13, which is closer to ideal square pyramidal geometry.

Three nitrogen atoms from the terpyridine site and an oxygen atom of the sulphate ion are located at the equatorial positions. The axial position of the square pyramidal geometry is occupied by a water ligand. Based on the short contacts, each hydrogen atom of the coordinated water molecule is hydrogen bonded to a sulfate oxygen atom, and a network of hydrogen bonded atoms of water and sulphate molecules runs along c-axis.

*3.2.2.2. $[Cu_2(\mathbf{L2.1})_2(\mu\text{-}Cl)_2CuCl_4]\cdot 0.25(CH_3OH)\cdot 0.4(CHCl_3)$– Complex **3.6***

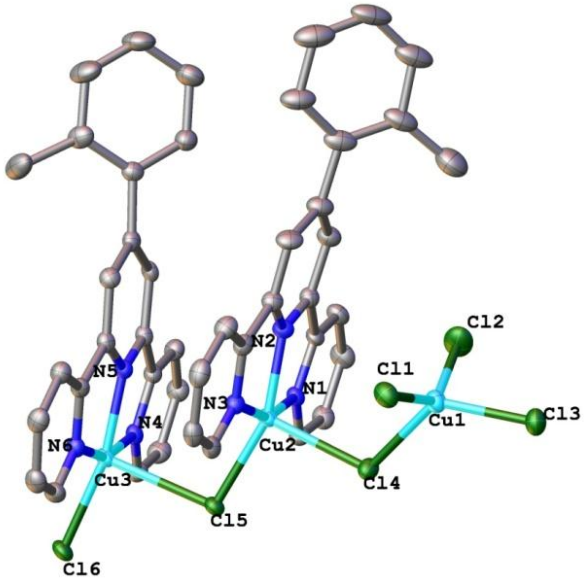

*Figure 3.7. The crystal structure of Cu(II) complex **3.6**. The hydrogen atoms and solvent molecules have been omitted for clarity. The selected bond lengths and bond angles are given in Appendix III, Table A17.*

Complex **3.6** was synthesised by mixing a chloroform solution of two equivalents of **L2.1** with three equivalents of $CuCl_2 \cdot 2H_2O$ in methanol. Vapour diffusion of diethyl ether into the resulting mixture produce X-ray quality needle shaped crystals. The crystal structure of **3.6** was solved in the triclinic space group $P\bar{1}$ and refined to an R-factor of 4.83%.

The trinuclear Cu(II) complex with six chloride ions was well-ordered but there is some disorder associated with solvent molecules. A large number of electron density peaks were located close to each other. The solvent was modelled as 40% chloroform and 25% methanol which were disordered over the same position, having a common carbon atom of 65% occupancy. The model was developed based on inspection of the size and distribution of the electron density peaks and subsequent refinements. Due to very small electron density disordered carbon and oxygen were handled with thermal ellipsoid restraint (ISOR), and occupancy of O2 was refined without any hydrogen atoms.

The crystal structure of the complex **3.6** is shown in **Figure 3.7**. The crystal structure contains a trinuclear discrete $[Cu_3(\mathbf{L2.1})_2Cl_6]$ unit. Each complex contains two **L2.1** ligands, three Cu(II) ions and six chloride ions. Two Cu(II) ions are coordinated in each tridentate site through terpyridine-type nitrogen donor atoms. All of the Cu(II) centres are in different coordination environments. Two copper ions, Cu3 and Cu2, are five-coordinate and occupy approximately square pyramidal geometries with the trigonality index, τ, 0.126 and 0.003, respectively. The third copper centre, Cu1, has coordination number four and is coordinated to four chloride ions in a distorted tetrahedral geometry. All three copper centres interact with neighbouring ions through Cu-Cl-Cu bridges, and the chloride ions Cl4 and Cl5 act as bridging ligands between copper ions. The Cu(II) and chloride ions in the Cl6-Cu3-Cl5-Cu2-Cl4-Cu1-Cl3 chain are almost coplanar with each other and lie in a zig-zag manner as shown in **Figure 3.7**. The bond lengths and bond angles between copper and nitrogen atoms in **3.6** are similar of those found in a literature mononuclear $[Cu(\mathbf{L2.1})Cl_2]$ complex.[85]

The Cl-Cu-Cl bond angles of the distorted tetrahedral $[CuCl_4]$ unit are in a range of 97°-139°. The Cu2 and Cu3 lie at a distance of 3.815 Å and the distance between Cu2 and Cu1 is 4.027 Å.

*3.2.2.3. [Cu(**L2.1**)(OH_2)(OH)]PF_6·2H_2O – Complex **3.7***

Complex **3.7** was synthesised by mixing one equivalent of **L2.1** with one equivalent of $CuCl_2$·2H_2O in dichloromethane/methanol solution. Addition of aqueous ammonium hexafluoridophosphate resulted in formation of a green precipitate. Vapour diffusion of diethyl ether into an acetonitrile solution of the precipitate produced X-ray quality blue plate shaped crystals. The crystal structure of **3.7** was solved in the monoclinic with space group $P2_1/c$ and refined to an R-factor of 9.03%. The crystal structure was well ordered, and modelled easily except for a low occupancy electron density peak located at 1.8760(17) Å to O3. Attempts were made to refine occupancy to this electron density peak to a small amount (10% to 20%) of water but there was no information about any hydrogen atoms around it. Therefore, the peak was left unmodelled.

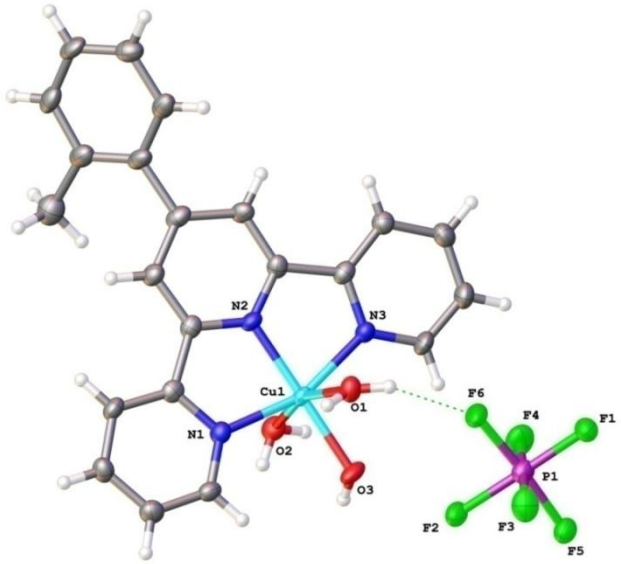

*Figure 3.8. The molecular structure of Cu(II) complex **3.7** with the ligand **L2.1**. The selected bond lengths and bond angles are given in Appendix III, Table A18.*

The X-ray crystal structure of complex **3.7** contains **L2.1** ligand and two water ligands, one non-coordinated hexafluoridophosphate ion and one hydroxide ion coordinated to the Cu(II) centre. The Cu(II) is six-coordinate and is in the centre of a distorted octahedron of three terpyridine-type nitrogen atoms, two water ligands and one hydroxide ion. The crystal lattice also contains two solvent water molecules. The crystal structure of **3.7** is shown in **Figure 3.8**.

The Cu1-N2 and Cu1-O3 bond lengths are shorter than other Cu-N and Cu-O bond lengths in **3.7**. This shortening of Cu-N2 and Cu-O3 may be attributed to three factors.

Firstly, the *trans*-out Jahn Teller effect in d^9 octahedral complexes can cause lengthening of the *trans* bond lengths. Secondly, as discussed for other complexes in this article, the central terpyridine N-metal bond is always shorter than those of the other pyridine donor groups, and thirdly, Cu-O3 might have shortened due to the negative charge on the hydroxide ion attached to the copper centre.

*3.2.2.4. [Cu(**L2.1**)(CH$_3$COO)$_2$]CH$_3$CN·2H$_2$O – Complex **3.9***

Complex **3.9** was synthesised by mixing one equivalent of **L2.1** with one equivalent of $Cu_2(CH_3COO)_4$ in dichloromethane/methanol solution. X-ray quality needle shaped crystals were formed overnight. The crystal structure was solved in the triclinic space group $P\bar{1}$ and refined to an R-factor of 4.07%. The solvent acetonitrile was disordered in two different orientations over same position. The carbon atom C1 was split over two positions by restraining their occupancies to 50% each.

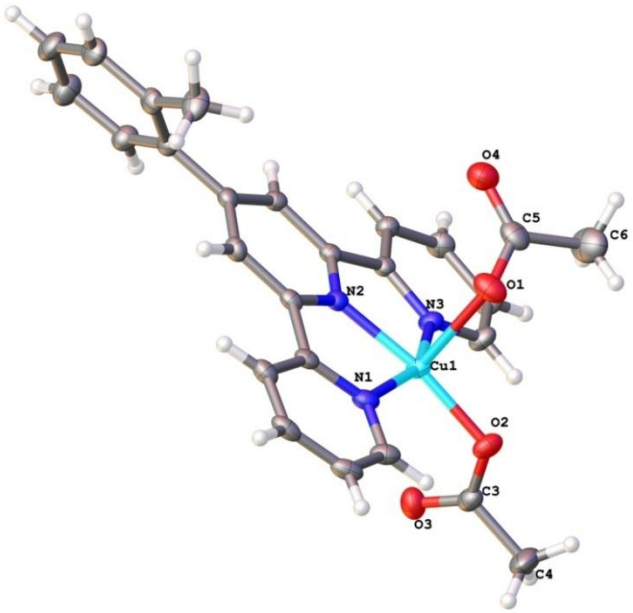

*Figure 3.9. The crystal structure of Cu(II) complex **3.9**. The hydrogen atoms and solvent omitted for clarity. The selected bond lengths and bond angles are given in Appendix III, Table A19.*

The copper centre in **3.9** is five-coordinate, where the geometry around the Cu(II) centre can be described as approximately square pyramidal with a τ value of 0.22. The crystal structure is shown in **Figure 3.9**. The asymmetric unit contains a copper-bound ligand **L2.1**, two copper-bound acetate ions, one water molecule and one disordered acetonitrile molecule. Three terpyridine-type nitrogen donor atoms and an acetate ion

occupy the equatorial positions and the second acetate ion is located in the axial position. The axial Cu1-O2 bond is relatively longer, 2.2183(15) Å, than the equatorial Cu1-O1 bond, 1.91445(17) Å.

3.2.3. Zn(II) Complexes

The Zn(II) complexes **3.10 – 3.12** synthesised using **L2.1** are outlined below in **Figure 3.10**.

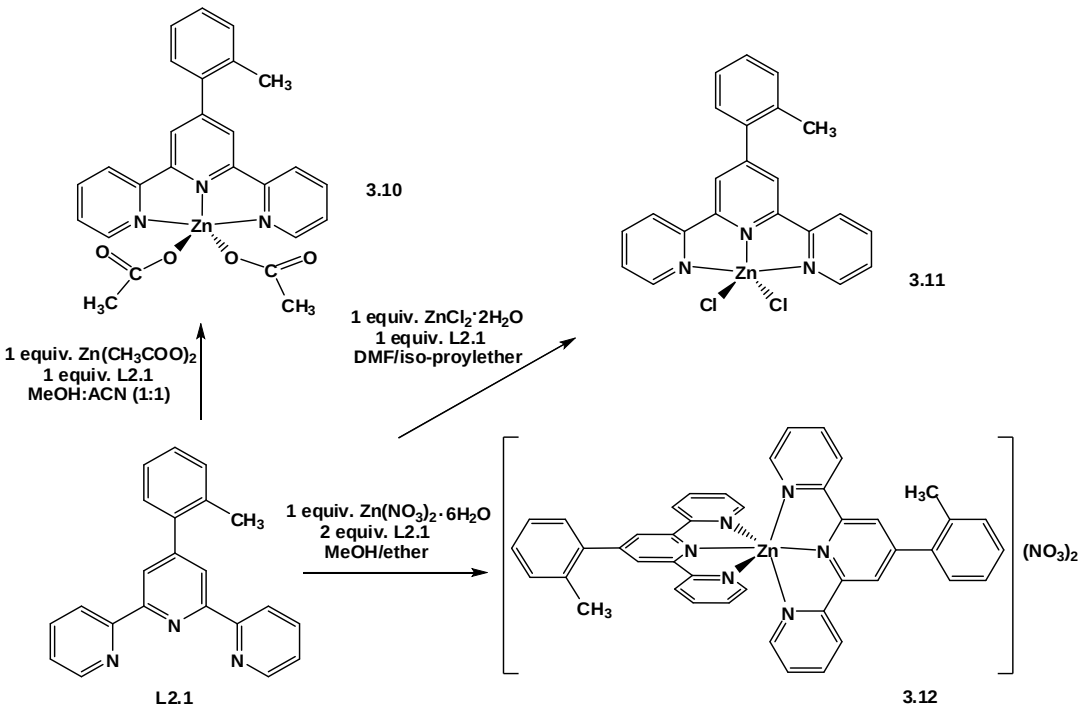

*Figure 3.10. Complexes **3.10**-**3.12** synthesised by using Zn(II) and **L2.1**.*

While studying the coordination chemistry of **L2.1**, the synthesis of various Zn(II) complexes was also attempted. The complexes [Zn(**L2.1**)$(CH_3COO)_2$] (**3.10**), [Zn(**L2.1**)Cl_2] (**3.11**), [Zn(**L2.1**)$_2$]$(NO_3)_2$ (**3.12**) were successfully synthesised and characterised. Due to poor crystal quality refinement, the crystal structure of complex **3.12** remained incomplete. The X-ray crystal structure analysis of complex **3.10** and **3.11** confirms the formation of the five-coordinated [Zn(**L2.1**)$(CH_3COO)_2$], and [Zn(**L2.1**)Cl_2] complexes.

*3.2.3.1. [Zn(**L2.1**)(CH$_3$COO)$_2$]·CH$_3$CN – Complex **3.10** & [Zn(**L2.1**)Cl$_2$] – Complex **3.11***

Complex **3.10** was synthesised by mixing one equivalent of **L2.1** with one equivalent of $Zn(CH_3COO)_2 \cdot 2H_2O$ in dichloromethane/methanol solution. X-ray quality block shaped crystals of **3.10** were formed by slow evaporation of the resulting solution.

Complex **3.11** was formed by mixing one equivalent of **L2.1** with one equivalent of $ZnCl_2 \cdot 2H_2O$ in dichloromethane/methanol solution, resulting in formation of a white precipitate. Vapour diffusion of di-isopropyl ether into a hot DMF solution of the white precipitate produced thin X-ray quality crystals.

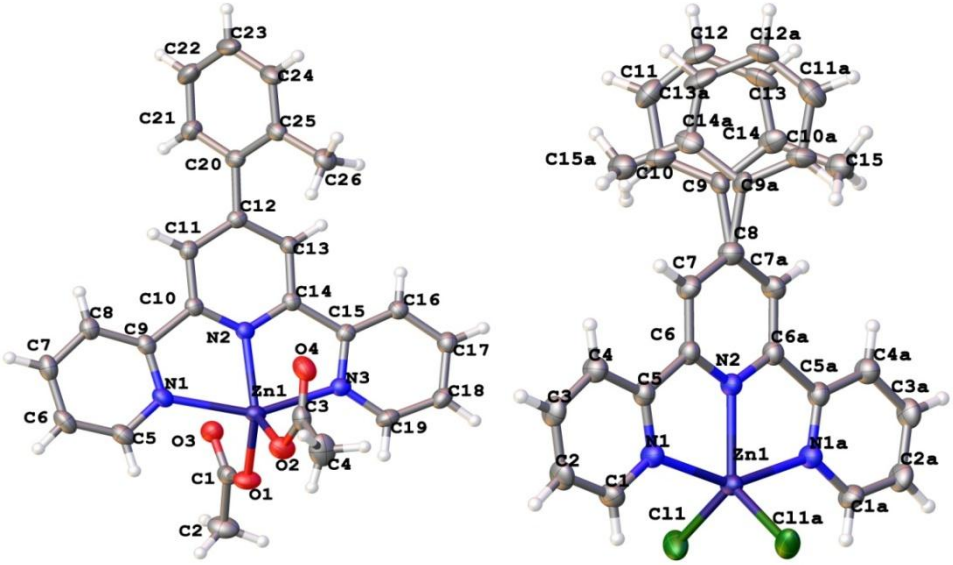

*Figure 3.11. The X-ray crystal structures of Zn(II) complex **3.10** (left) and complex **3.11** (right). The solvent molecules have been omitted for clarity. The selected bond lengths and bond angles are given in Appendix III, Table A20 & A21.*

The crystal structure of **3.10** was solved in the monoclinic space group $P2_1/c$ and that for complex **3.11** was solved in the monoclinic space group $C2/c$. In both complexes the zinc metal centre is five-coordinate and geometry lies between trigonal bipyramidal and square pyramidal geometries. The zinc centres in **3.10** and **3.11** are nearly square pyramidal with τ values 0.21 and 0.41, respectively; however **3.10** is more square pyramidal than **3.11**.[69]

In each case three coordination sites of Zn(II) are occupied by terpyridine-type nitrogen donor atoms of **L2.1** and the remaining coordination sites are occupied either by acetate ions (complex **3.10**) or chloride ions (complex **3.11**), **Figure 3.11.**

In complex **3.11** the asymmetric unit contains only one half of the molecule. The atoms Zn1, N2, C8, C9 and C12 are located on the special positions in the unit cell along C2-axis.The toluyl ring is disordered over two positions occupying either position half of the time. The molecule lacks planarity with the fact that both positions of disordered toluyl group lie either side of the plane of terpyridine unit. The modelled crystal structure of complex **3.11** is shown in **Figure 3.11(b)**. The zinc centre occupies five-coordinate geometry, where central nitrogen N2, Cl1 and Cl1a occupy the equatorial positions and the terminal pyridine nitrogen atoms N1 and N3 occupy the axial positions.

*3.2.4. Structural Trends in Ni(II), Cu(II) & Zn(II) complexes of **L2.1***

In all of the Ni(II), Cu(II) and Zn(II) complexes synthesised here, the 2,2':6',2''-terpyridine fragment of **L2.1** binds in a tridentate fashion with the metal centre through its nitrogen donor atoms. In each complex the metal-N bond lengths for central pyridine rings are smaller than that for the terminal metal-N bonds shown in **Table 3.1**. This observation is consistent with the vast majority of literature data for metal complexes containing 2,2':6',2''-terpyridine fragment.[68, 72, 73, 75, 92, 204, 218, 236, 237, 239, 241-243, 245-254]

*Table 3.1. Selected bond lengths (Å) for the Ni(II),Cu(II), and Zn(II) complexes of **L2.1***

Complex / **Metal-N**	**Complex 3.1**	**Complex 3.2**	**Complex 3.3**	**Complex 3.4**	**Complex 3.5**
M-N$_{central}$	2.001(15)	1.977(3)	1.9875(18)	1.998(3) 1.994(3)	1.938(4)
M-N$_{terminal}$	2.1112(16)	2.068(2)	2.102(2)	2.122(3) 2.115(3)	2.030(4)
M-N$_{terminal}$	2.1142(16)	2.071(2)	1.9875(18)	1.994(3) 2.111(3)	2.038(4)
	Complex 3.6	**Complex 3.7**	**Complex 3.9**	**Complex 3.10**	**Complex 3.11**
M-N$_{central}$	1.935(3) 1.946(3)	1.944(5)	1.9393(18)	2.0748(16)	2.119(4)
M-N$_{terminal}$	2.032(3) 2.027(3)	2.030(6)	2.0374(19)	2.1863(17)	2.194(3)
M-N$_{terminal}$	2.041(3) 2.023(3)	2.034(6)	2.0366(19)	2.1774(17)	2.194(3)

The shortening of metal-N bond length of central pyridine is usually attributed to a greater π-bonding component of the 4'-phenyl substituted terpyridine ligands. The positive charge of the metal ion favours conjugation of the 4'-phenyl substituent with the ring, thus increasing the multiple-bond character of the metal-N bond.[84, 166, 243] The central metal-N shortening could also be due to the geometric constraints imposed by rigid geometry of terpyridine. However, this was not the case in the Ag(I) complex **3.13**, discussed in the next section, where the central nitrogen of the terpyridine binds to two silver metal centres and the central Ag2-N6 2.548(5) Å, Ag1-N6 2.555(5) Å bond lengths are longer than the terminal Ag1-N5 2.245(6) Å, Ag2-N4 2.234(6) Å bond lengths.

*Table 3.2 (X) Torsion angle (°) between terminal and central rings of terpyridine-type ligand **L2.1**, and (Y) torsion angle (°) between the o-toluyl ring and central ring plane of the Ni(II), Cu(II), Zn(II) and Ag(I) complexes **3.1-3.7**, **3.9-3.11** and **3.13**.*

Complex	**X (°)**	**Y (°)**	**Complex**	**X (°)**	**Y (°)**
3.1	3.45-5.31	67.21	**3.7**	0.21-4.80	47.5
3.2	2.31-5.73	51.35	**3.9**	1.71-2.52	50.3
3.3	3.17-3.27	552.41	**3.10**	2.34-3.15	55.33
3.4	0.85-5.71/1.49-6.10	60.3/61.9	**3.11**	0.18	57.17
3.5	1.36-1.41	42.7	**3.13**	29.0-31.0	53.19/63.19
3.6	2.47-4.01/2.56-2.22	47.73/38.47			

X = Interannular torsion angle between terminal and central rings of terpyridine unit
Y = Torsion angle due to the twist of o-toluyl ring from the plane of the central ring

In all of the Ni(II), Cu(II), and Zn(II) complexes reported in this chapter, the terpyridine unit is approximately planar, and the terminal rings show a small deviation from the plane of the central pyridine ring. The terminal and central pyridine rings in these complexes form dihedral angles in the range of 0.81° to 5.73° shown in **Table 3.2**.

In each case, the *o*-toluyl ring also twists away from the plane of the central pyridine ring of the terpyridine unit. The inter-annular torsion angles around the C-C bond between *o*-toluyl ring and the central pyridine are in the range of 42.7° (complex **3.5**) to 63.19° (complex **3.13**). The similar torsion angles of the phenyl ring from the central pyridine ring have been also observed in other previously reported 4'-phenyl-terpyridine complexes.[85, 255] However, the twist is much larger in case of **L2.1** metal complexes reported in this thesis than that found in 4'-phenyl substituted and 4'-*p*-toluyl

substituted terpyridine literature complexes. The larger twist presumably minimises the steric hindrance (H-H contacts and π-π overlap) between the *o*-toluyl ring and the hydrogen atoms of the central pyridine ring.

Each pyridine ring of the ligand is almost planar in all the complexes; however, the pyridine rings are tilted with respect to each other. The tilting between adjacent pyridine rings within a ligand is essentially confined to a twist about the intervening C-C bond. The relevant interannular torsional angles range from 0.85° to 5.73° in these complexes. The torsion angles for the complexes discussed in this chapter are shown in **Table 3.2**. All of the Ni(II), Cu(II) and Zn(II) complexes are packed in their crystal lattice through various packing interactions such as hydrogen bonding, π-π stacking and short contacts between different atoms.

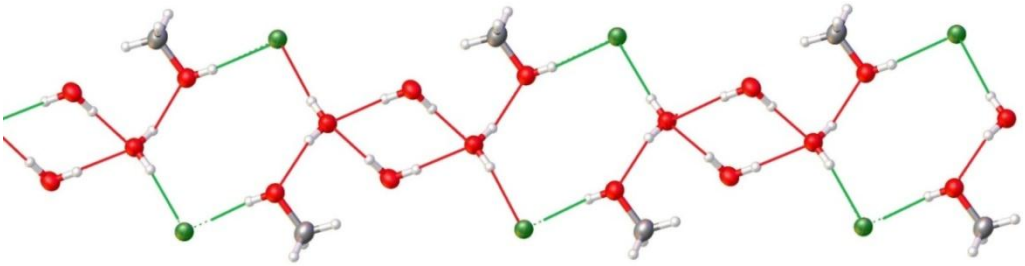

*Figure 3.12. Representation of the hydrogen bonded tapes in complex **3.2** exhibiting alternate hexagonal and rectangular geometries, formed by hydrogen bonding network between water, chloride ions and methanol. The cations have been excluded for clarity. The hydrogen bonds have also been darkened for clarity.*

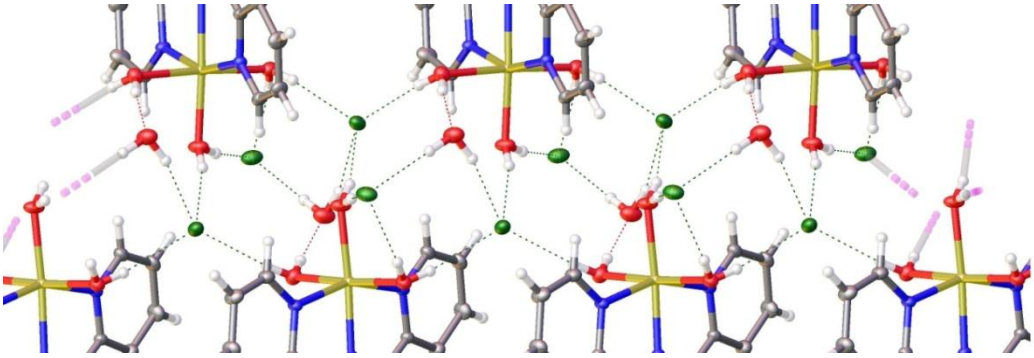

*Figure 3.13. Hydrogen bonded network in complex **3.3**, where alternate pentagonal and rectangular geometries of hydrogen network make tapes of Cl ions and H_2O molecules. Portions of the cations have been excluded for clarity*

In complexes **3.2** and **3.3**, the hydrogen bonded molecules make an infinite tape network of alternative pentagonal, rectangular or hexagonal geometries shown in **Figure 3.12** and **Figure 3.13**, respectively.

In the case of Ni(II) complexes, the π-π stacking of 3.414 Å were observed in **3.4** only. However, inter-molecular π-π stacking ranging from 3.4 Å to 4.1 Å was observed in all the Cu(II) and Zn(II) complexes. The Cu(II) complex **3.6** exhibits additional intramolecular face-to-face π-π stacking between the pyridine rings, as shown in **Figure 3.14**, where rings are labelled as A, B, C, A', B', and C' to allow reference to the various π-π stacking parameters for **3.6** that are shown in **Table 3.3**.

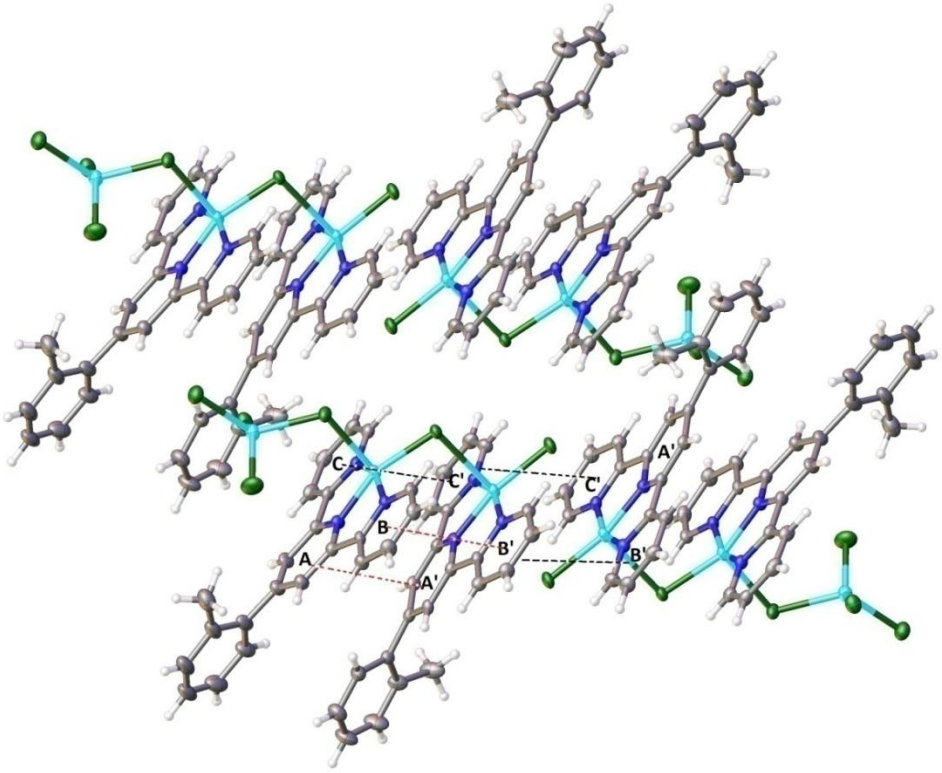

*Figure 3.14. Packing diagram showing both inter- and intra- molecular π-π stacking between adjacent pyridine rings in **3.6***

*Table 3.3.The π-π stacking parameters for Cu(II)-**L2.1** complex **3.6**.*

Ring system	Centroid-Centrod distance (A°)	Plane-Plane distance (A°)	Shift distance (A°)
A-A'	4.0115 (19)	3.8371 (3)	1.996 (5)
B-B'	3.8035 (19)	3.3901 (3)	1.7241 (5)
C-C'	3.8002 (19)	3.4572 (3)	1.7827 (5)
B'-B'/C'-C'	4.1971 (2)	3.5601 (3)	2.5629 (5)

*3.2.5. Synthetic Trends in Ni(II), Cu(II) & Zn(II) complexes of **L2.1***

Although the reaction conditions and the molar ratio of metal-to-ligand used were almost the same for all of the complexes, it is not always possible to predict the exact reaction outcomes; however, considering some general principles at least we can rationalise the kind of molecules that will be found.

A reaction of **L2.1** with $NiCl_2$ in 1:1 molar ratio produced a mixture of two complexes $[Ni(\mathbf{L2.1})_2]Cl_2$, **3.1** and $[Ni(\mathbf{L2.1})Cl_2]_2$, **3.2**. The complex **3.1** consists of 1:2 Ni(II):**L2.1** ratio and the complex **3.2** is made of 1:1 Ni(II):**L2.1** molar ratio. The reaction mixture contains 1:1 Ni(II): **L2.1** ratio, so the formation of two complexes **3.1** and **3.2** may be attributed to an equilibrium that depends upon the chloride ion concentration. The equilibrium and the controlled synthesis of **3.1** and **3.2** is shown in **Figure 3.15**.

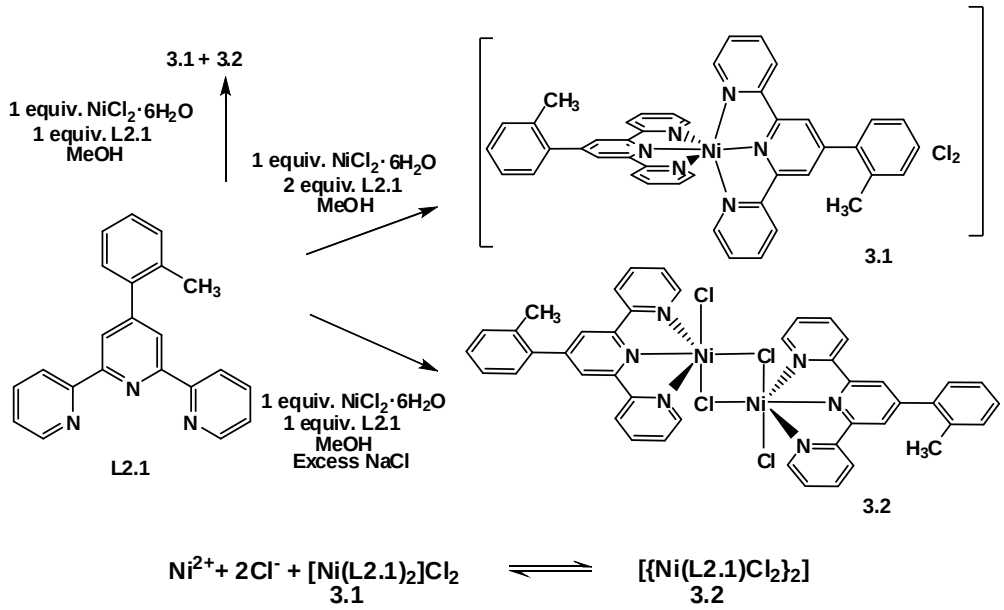

*Figure 3.15. The controlled syntheses, and presentation of equilibrium between complexes **3.1** and **3.2**.*

When an equal concentration of both, **L2.1** and $NiCl_2$, were present in the system there might have been an equilibrium which might have favoured formation of the bis-**L2.1** nickel complex **3.1** owing to higher stability of the bis-tpy complexes in comparison to mono-tpy complexes.[256] After formation of bis-**L2.1** complex **3.1**, the solution is left with a higher chloride ion concentration compared to the ligand concentration in the solution. This high chloride concentration may have favoured the formation of the 1:1 M:L molar ratio complex **3.2**.

A reaction between 1:2 Ni(II):**L2.1** produced only bis-**L2.1** nickel complex **3.1**, and addition of an extra chloride ion to the reaction mixture resulted in formation of dinuclear bridging nickel complex **3.2** in approximately 75% yield.

In the case of the complex of $NiBr_2$, a change in the ratio of metal-to-ligand did not affect the resulting complex formation. During each attempt bis-**L2.1** nickel complex **3.4** was isolated when $NiBr_2$ was added to a solution of **L2.1** regardless of the ratio of metal and ligand used, and same as other nickel complexes in this chapter a dominant *m/z* peak at 352.10 was obtained. However, the maximum yield of the complex **3.4** was isolated when 1:2 Ni(II):**L2.1** was used. In all of the nickel complexes reported in this article, only complex **3.4** is the one where molecules are packed *via* both hydrogen bonding network and π-π interactions. This could lead to greater stability of the crystal lattice, lower solubility, and could lead to the observed isolation of the bis-**L2.1** complex **3.4**.

The tris-aqua complex **3.3** was formed when 1:1 Ni(II):**L2.1** ratio was used and crystals were isolated from aqueous medium. Using same ratio of Ni(II):**L2.1** in methanol produced crystals of **3.1** and **3.2**. The use of alcohol as a solvent might have displaced the water ligands in **3.1** and **3.2**.

Ni(II) always prefer octahedral geometry with terpyridine-based ligands, regardless of the anion, solvent or metal-to-ligand ratio used. However, both Cu(II) and Zn(II) can adopt either a five-coordinate or six-coordinate geometry based upon the metal-to-ligand ratio, and binding ability of the anions used. The Cu(II) chemistry of **L2.1** was explored using different Cu(II) metal salts in different ratios. The mononuclear complex [Cu(**L2.1**)Cl_2] was previously synthesised in our group by using 1:1 ratio of $CuCl_2$ and **L2.1**,[85] which was consistent with formation of other similar $[Cu(tpy)]^{2+}$ type complexes formed by Cu(II) and terpyridine-based ligands.[87, 249] In these literature complexes Cu(II) occupies a five-coordinate geometry, where three coordination sites are occupied by pyridine type nitrogen atoms and remaining positions are occupied by the anions or solvent. Consistent with previous copper complexes, reaction between 1:1 ratio of **L2.1** with Cu(II) acetate and Cu(II) sulfate resulted in formation of five-coordinate Cu(II) complexes **3.9** and **3.5**, respectively.

Addition of an excess of $CuCl_2$ to **L2.1**, in this project, resulted an unexpected complex **3.6**, containing a [Cu_2(**L2.1**)$_2$(μ-Cl)$_2$$CuCl_4$] unit. Two Cu(II) centres which were

coordinated to terpyridine units were five-coordinated and the third Cu(II) ion occupied a four-coordinate geometry. The same complex was again crystallised when 3:1, 4:1 and 3:2 Cu(II):**L2.1** ratio were used under identical conditions. Unsurprisingly, the highest yield (90%) was collected when a 3:2 Cu(II):**L2.1** ratio was used.

Similar to Cu(II), the metal ion Zn(II) also produces five-coordinate $[Zn(tpy)X_2]$ complexes when 1:1 ratio of Zn(II) metal salts and **L2.1** are mixed, where X is chloride and acetate ion as used in this project.

The octahedral Cu(II) and Zn(II) complexes $[Cu(\mathbf{L2.1})(OH_2)(OH)]PF_6$, **3.7**, $[Cu(\mathbf{L2.1})_2](OTf)_2$, **3.8**, and $[Zn(\mathbf{L2.1})_2](NO_3)_2$, **3.12** were formed when relatively non-coordinating anions were used regardless of the concentration of the metal and ligand. However, the highest yield for bis-L2.1 complexes was obtained from the experiments when 1:2 M(II):**L2.1** ratio was used**.**

3.2.6. Ag(I) Complex – $[Ag_2(\mathbf{L2.1})_2NO_3]_n[NO_3]_n\cdot(2CH_3CN)_n$ – Complex ***3.13***

A reaction of one equivalent of **L2.1** in chloroform with 1 equivalent of $AgNO_3$ in ethanol produced thin and long needle shaped crystalline material. The X-ray diffraction experiment revealed a fascinating Ag(I)-**L2.1** polymeric complex of stoichiometry $[Ag_2(\mathbf{L2.1})_2NO_3]_n[NO_3]_n\cdot(2CH_3CN)_n$ that was solved in the hexagonal chiral space group $P6_1$and refined to an R-factor of 3.22% (**Figure 3.16**).

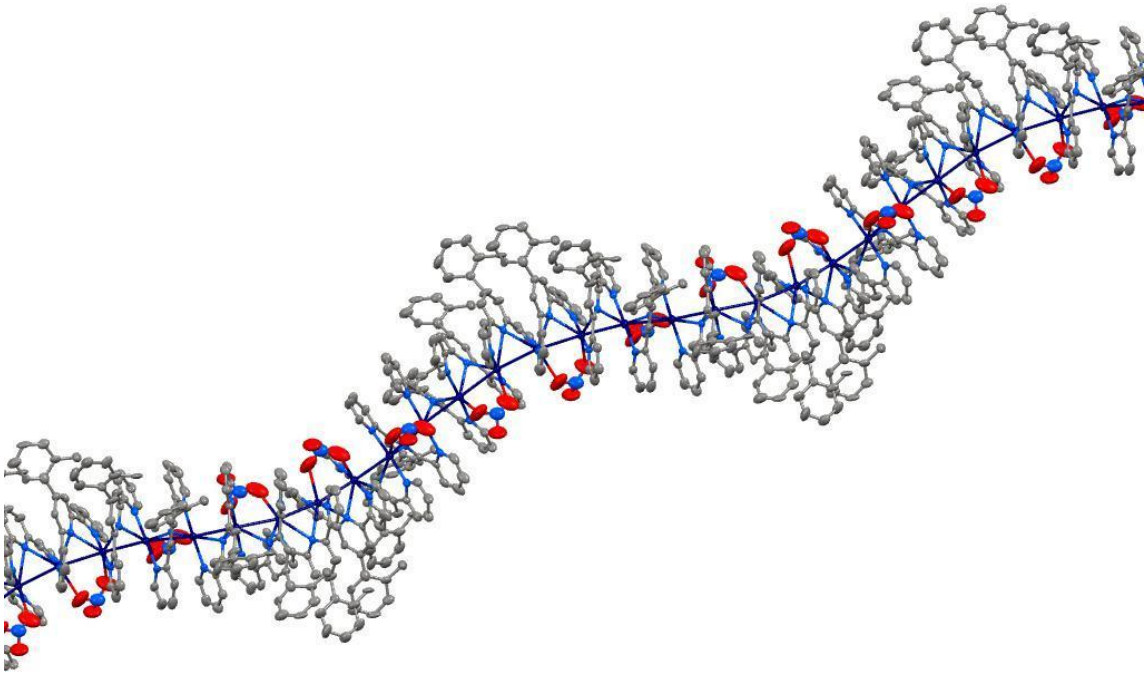

Figure 3.16. Crystal structure of $[Ag_2(\mathbf{L2.1})_2NO_3]_n[NO_3]_n$ as infinite spiral. The solvent and free nitrate anion and hydrogen atoms have been omitted for clarity. The selected bond lengths and bond angles are given in Appendix III, Table A22.

The asymmetric unit of **3.13** is shown in **Figure 3.17.** In this spiral complex all terpyridine-type ligands bridge two metal centres as a bis-bidendate ligand with the middle pyridine bound to both silver centres. Binding to two silver atoms is a rare behaviour for sp^2 nitrogen atoms. The term "hyperdentate" has been introduced recently for such situation where an atom binds to more metal ions than normal.[257]

The asymmetric unit shown in **Figure 3.17** clearly shows that the terpyridine ligand is non-planar and twists around the mean spiral axis to bridge between two Ag(I) centres. There are two distinct silver centres with coordination number of seven, including short Ag···Ag interactions. The alternating silver-silver distances are 3.148 Å and 2.995 Å. These Ag···Ag contacts are a common feature in Ag(I) coordination chemistry.[258-260]

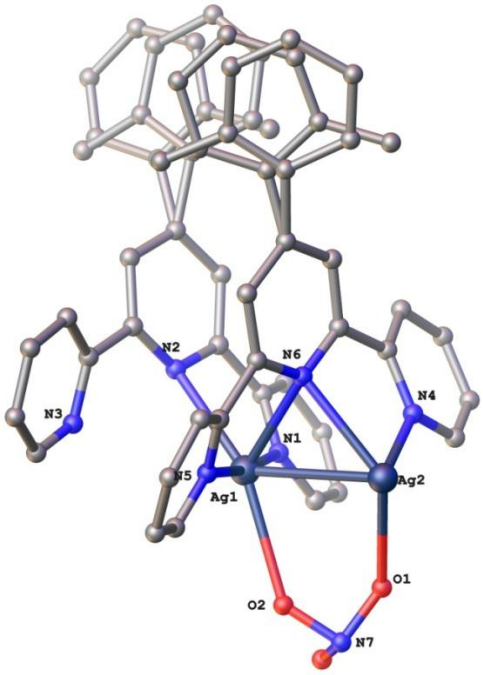

*Figure 3.17. Asymmetric unit of the Ag(I)-**L2.1** spiral. The solvent, hydrogen atoms and non-coordinating nitrate are omitted for clarity.*

To the best of our knowledge there are only five examples in the literature where pyridine nitrogen atom bridges between two metals like Cs[261], Mo[262], Ti[263] and Ag[264, 265]. Out of these, two examples are where pyridine nitrogen binds two Ag(I) atoms, one is previously reported Ag(I) spiral[265] molecule $[Ag_5L_5(CH_3CN)_3]_n[ClO_4]_{5n}$, L=4'-thiomethyl-2,2':6',2''-terpyridine; where the middle pyridine nitrogen shows short contacts towards two silver centres. The behaviour of the previously reported spiral[265] was similar to that reported here, but in spiral **3.13**, the Ag1 and Ag2 atoms define a deeper helical spiral about the axis of the array with displacements of 1.34 Å and 1.39Å, respectively, from the mean spiral axis, which is significantly greater than the 0.3-0.7 Å displacement in the previously reported spiral.[265]

The pyridine nitrogen atoms that bridge the silver atoms, N2 and N6 bind to silver atoms in at distances of 2.555(6) Å (Ag1-N6), 2.646(7) Å (Ag1-N2), 2.548(6) Å (Ag2-N6) and 2.648(7) Å (Ag2-N2). All three pyridine rings have face-face π-π stacking with the ligands both above and below in a range of 3.4 Å to 3.6 Å. The individual terpyridine units are not exactly planar and exhibit dihedral angles between the terminal rings and the central ring in the range 29.7° to 31.5°. Very extensive face-to-face stacking is found within the spiral chain, (centroid-centroid distances 3.43Å - 3.86 Å). All three pyridine-type rings of each ligand stack with the pyridine-type three rings of the ligand both above and below.

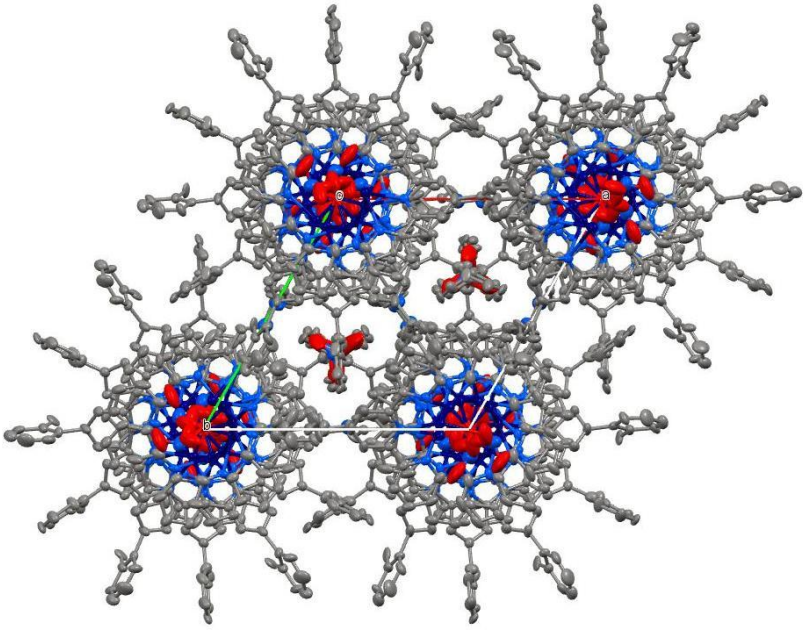

Figure 3.18. Packing of $[Ag_2(\mathbf{L2.1})_2NO_3]_n[NO_3]_n \cdot (2CH_3CN)_n$ with unit cell representation. The hydrogen atoms omitted for clarity.

The infinite spiral polymers have a pitch of 35.36 Å and thirteen **L2.1** ligands rotate around to complete one pitch. The spiral polymer chains are packed together in like a grid leaving inter-chain voids that contain the non-coordinating nitrate anions **Figure 3.18**. The nitrate anions and acetonitrile molecules make both inter- and intra- chain short contacts with aromatic C-H hydrogen atoms in 2.3 – 2.6 Å range.

The crystals were formed in a chiral space group $P6_1$. The overall structure of the spiral was well ordered except the toluyl ring of **L2.1**. The toluyl ring was disordered over two positions with 50% occupancy each. Both coordinated and non-coordinated nitrate anions were also disordered. The electron density peaks for the all disordered nitrate ions were smeared over a number of sites, so it was not possible to model the nitrate ions from the electron density map. The same disorder has been seen in previous reports of the similar spirals.[265] Despite the Flack parameter being very close to zero, -0.14(5), the low data parameter ratio means that the absolute chirality of the molecules cannot be determined. The bulk crystals were looked under a microscope for chiral resolution. The same method was used by Louis Pasteur to separate both enantiomers of sodium ammonium tartrate. Different mirror image crystals of different enantiomers were picked under the plane polarised light. However, we were not able to distinguish different crystals based upon their mirror image due to their thin needle shape.

The elemental analysis was consistent with [Ag(**L2.1**)(NO_3)] and ESI-MS spectrum shows *m/z* peaks at 430.05, 753.19 and 922.08 corresponding to $[Ag+L]^+$, $[Ag+2L]^+$ and $[2Ag+2L+NO_3]^+$. The mass spectroscopy results indicate the presence of the nitrate ions.

3.3. Conclusion

4'-(2'''-toluyl)-2,2':6',2''-terpyridine, **L2.1**, is the core ligand in synthesis of polydentate ligands discussed in Chapter 2. To explore coordination chemistry of the divalent metal ions with **L2.1**, thirteen Cu(II), Ni(II), Zn(II) and Ag(I) complexes of 4'-(2'''-toluyl)-2,2':6',2''-terpyridine, **L2.1**, have been prepared and characterised using X-ray crystallography.

The Ni(II) produced octahedral 1:1 and 1:2 (M:L) stoichiometry complexes with **L2.1**. The 1:1 and 1:2 stoichiometry complexes [Ni(**L2.1**)$_2$]Cl_2 and [{Ni(**L2.1**)Cl_2}$_2$] were in equilibrium and either product forms based upon the chloride ion concentration in the solution.

Both Cu(II) and Zn(II) produce five- and six-coordinate complexes of 1:1 and 1:2 (M:L) stoichiometry. The 1:2 (M:L) stoichiometry bis-**L2.1** complexes were formed with non-coordinating counter-ion regardless of the ratio of metal-to-ligand used.

A trinuclear Cu(II) complex, **3.6**, with 3:2 (M:L) stoichiometry was crystallised from the reaction mixture when an excess of metal salt was added to the ligand. The notable feature of the complex is that two terpyridine coordinated Cu(II) ions are five-coordinated and the third is four-coordinate. All the Cu(II) and chloride ions are connected by single Cu-Cl-Cu bridging.

Ag(I) produced fascinating polymeric complex **3.13**, where terpyridine binds as a unusual bis-bidenate ligand. The central nitrogen acts as a hyperdentate ligand where it binds to two silver ions. The bond lengths and bond angles in **3.13** are exceptionally different from usual 2,2':6',2''-terpyridine type metal complexes.

These studies were helpful in understanding the behaviour of **L2.1** with different metal salts. Since **L2.1** is the pivotal unit of the polydentate ligands synthesised in this project, we proposed that the terpyridine-type binding site in these ligands will adopt the

similar coordination geometries with Cu(II), Zn(II) and Ni(II) as **L2.1** has adopted. As proposed, all the dinuclear complexes synthesised with Cu(II) and Zn(II) occupy five-coordinate geometry in their terpyridine-type (head) binding sites. The synthesis and characterisation of these dinuclear complexes is discussed in Chapter 4. A comparison of the rate of phosphate diester hydrolysis of BNPP using dinuclear (Zn_2**L2.3**) and mononuclear (Zn**L2.1**) complexes is discussed in Chapter 5.

CHAPTER 4

THE DI- & TETRA- NUCLEAR COMPLEXES – SYNTHESES, CHARACTERISATION & CRYSTAL STRUCTURES

4.1. Introduction

As discussed in Chapter 1, the goal of this research was to synthesise dinuclear metal complexes to study kinetics of hydrolysis of the DNA model compound, bis(*p*-nitrophenyl) phosphate (BNPP). The phosphate diesters are exceptionally stable, so are used by nature as the backbone for genetic material for the integrity and maintenance of the living system. The half-life of a typical DNA phosphate diester bond under physiological conditions is estimated to be on the order of thousands of year.[266] Nature possesses many enzymes like polymerases, nucleases, recombinases, topoisomerases, and others to catalyse phosphate diester cleavage efficiently under physiological conditions. Many enzymes utilize metal ions in their active site, and metal ions act as cofactors.

In order to better understand the precise role of metal ions, several studies have been done by using model compounds of transition metal ions such as Fe(III)/Fe(II),[33, 267] Fe (III),[268, 269] Cu(II),[270] Co(II),[271, 272] Co(III),[25, 39, 47-49, 52, 54, 55, 273, 274] Cu(II),[38, 40, 92, 94, 96, 98, 106, 160, 161, 272, 275] Mn(II),[272, 276] Ni(II),[272] Zn(II),[32, 35, 36, 41, 67, 98, 277-279] and lanthanide ions.[280] These compounds are reported to catalyse hydrolysis of phosphate diester model systems, and most of these show a significant increase in the rate of hydrolysis over their analogous mononuclear complexes.[22, 27, 44, 50, 281-284] Many previous kinetic studies of hydrolysis reactions have been performed using complexes with more than one identical metal binding site, as discussed in Chapter 1.[58, 160-162] The aim of this research is to understand the catalytic behaviour of dinuclear complexes where two metal ions are bound in non-identical metal binding sites of a ligand. The synthesis of such polydentate ligands is discussed in Chapter 2.

This chapter will focus on synthesis and structural analysis of dinuclear Zn(II) and Cu(II) complexes of two polydentate ligands – 4'-[2'''-{(2-pyridylmethyl)aminomethyl}phenyl]-2,2':6',2''-terpyridine, **L2.3**, and 4'-[2'''-{bis(2-pyridylmethyl)aminomethyl}phenyl]-2,2':6',2''-terpyridine, **L2.4** (**Scheme 4.1**). Each ligand possesses two potential metal binding sites, where the symmetrical tridentate metal binding site 2,2':6′,2″-terpyridine, head (H), is a common feature of both ligands. The tail (T) is the bidentate picolylamine group in **L2.3** and the tridentate bis(picolylamine) group in **L2.4**. The head and tail binding sites of both **L2.3** and **L2.4** are shown in **Scheme 4.1** using bold arrows. In the presence of different solvents and anions, a metal ion can join

these ligands in different coordination modes. The coordination modes, such as Head-to-Head (HH), Tail-to-Tail (TT) and Head-to-Tail (HT), result in formation of the dinuclear, tetranuclear, and decanuclear metal complexes in this project. Both **L2.3** and **L2.4** possess amine groups capable of metal binding, which can rotate around the C-C and C-N bonds shown with curly arrows in **Scheme 4.1**. Due to flexible nature of the ligand the complexes formed can acquire different shapes.

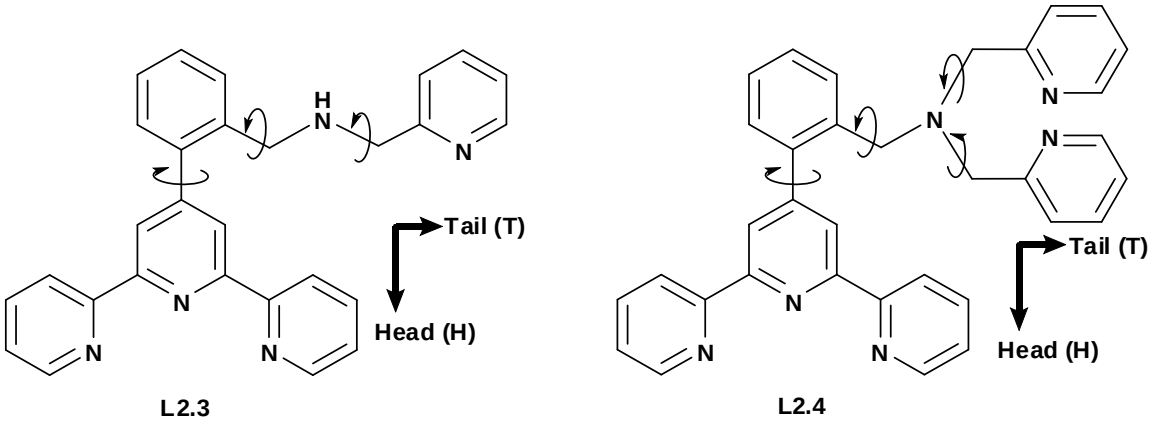

*Scheme 4.1. The polydentate ligands **L2.3** and **L2.4** with non-equivalent metal binding domains, denoted as head and tail using the bold arrows. Flexibility of the tail groups to twist around C-N bonds is represented with the curved arrows.*

The 2,2′:6′,2″-terpyridine is a symmetrical group which usually coordinates as a chelating tridentate ligand. The purple bis(terpyridine) octahedral complexes formed with Fe(II)[204, 285, 286] are probably among the most studied complexes of terpyridine-like ligands. With Cu(II), terpyridine ligands can produce square pyramidal, trigonal bipyramidal or even square planar complexes.[287-294] Octahedral bis(terpyridine) and trigonal bipyramidal complexes of Co(II) and Zn(II)[285, 286] have been studied also. In most of the complexes all three pyridine rings of the terpyridine group remain almost co-planar to each other with a small torsion between the rings.

The tail groups, picolylamine and bis(picolylamine) most often coordinate as chelating bidentate and tridentate ligands by forming one and two five-member rings, respectively. These ligands also produce a variety of square pyramidal, trigonal bipyramidal, tetrahedral, and octahedral complexes with a range of metal ions such as, Cu(II), Ni(II), Zn(II), Rh(II), Hg(II), Pt(II), Pd(II), and Cd(II) metal ions.[295-308] A variety of complexes with bridging and non-bridging halide ions can form in the presence of different CuX_2 salts, where X is a Cl or Br ion. Both mono-μ-halide and di-μ-halide

bridging complexes are reported in literature with Cu(II) chloride salts.[301, 303, 307] In most of the picolylamine complexes hydrogen bonds are formed between the amine hydrogen (-NH) and the counter ions or solvent molecules.

In this project, a variety of complexes have been synthesised and characterised using these ligands. A range of tetranuclear M_4L_4 and decanuclear $M_{10}L_{10}$ complexes synthesised will be discussed further in Chapter 6. Here in this chapter, six different dinuclear M_2L and tetranuclear M_4L_2 complexes of **L2.3** and **L2.4** are discussed. When only one ligand bridges between two Zn(II) or two Cu(II) ions using both head and tail binding sites, dinuclear Zn(II) complexes **4.1**, **4.2** or a dinuclear Cu(II) complex **4.3** are formed. With CuX_2 salts (X=Cl), di-μ-halide tail-to-tail bridging complexes **4.4**, **4.5** and mono-μ-halide head-to-tail bridging complex **4.6** were synthesised. All of the complexes were characterised using a range of techniques such as NMR, mass spectrometry, IR, melting point and elemental analysis. Single crystal X-ray crystallographic structural analysis is discussed in detail for all of the complexes.

4.2. Results and Discussion

*4.2.1. Dinuclear Zn(II) & Cu(II) Complexes of **L2.3** & **L2.4***

*4.2.1.1. $[Zn_2(\mathbf{L2.3})Cl_4]\cdot 3CH_3CN$ – Complex **4.1** & $[Zn_2(\mathbf{L2.4})Cl_4]\cdot 2CH_3OH$ – Complex **4.2***

The dinuclear complex **4.1** was synthesised by mixing one equivalent of **L2.3** with two equivalents of $ZnCl_2\cdot 2H_2O$ in a chloroform-methanol (1:1) mixture. The creamy white precipitate was formed. Overnight, slow evaporation of an acetonitrile solution of the precipitate yielded irregular crystals suitable for structural analysis *via* single crystal X-ray diffraction.

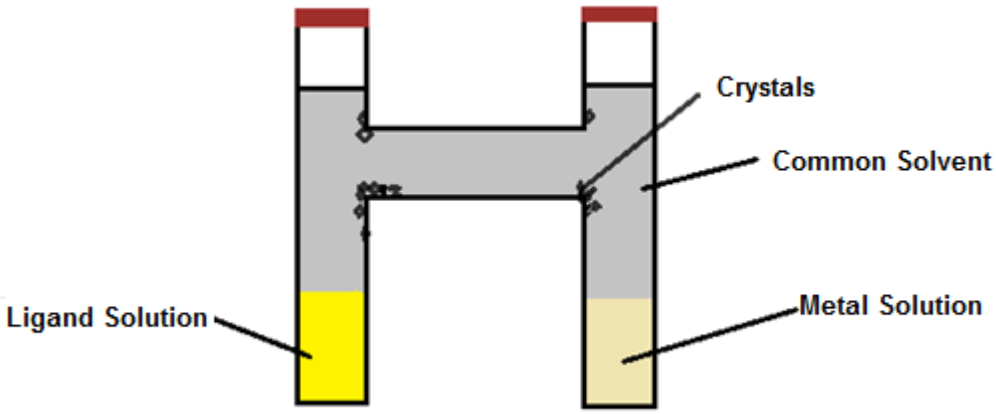

Figure 4.1. A schematic diagram of the H-tube crystallisation method.

Complex **4.2** was also synthesised by mixing one equivalent of the appropriate ligand (**L2.4**) with two equivalents of $ZnCl_2\cdot 2H_2O$ in chloroform-methanol (1:1) mixture. Following the exactly the same procedure as for the complex **4.1**, a white precipitate was collected. The initial white precipitate was almost insoluble in any of the common solvents and characterisation of the complex was limited to infrared and mass spectrometry techniques. Therefore, different crystallisation techniques such as solvent layering and H-tube crystallisation were used to grow crystals of complex **4.2**. The H-tube method produced high quality colourless blocks. In this method, a chloroform solution of ligand **L2.3** was added to the bottom of one branch of the H-tube and a methanol solution of $ZnCl_2\cdot 2H_2O$ was added to the second branch of the tube. The H-

tube was held vertically and filled with pure methanol. Both ends of the tube were sealed with a rubber bung. Over 2 weeks, crystals of **4.2** formed at the edges of the bridging tube. A diagram of the experimental set up is shown in **Figure 4.1**.

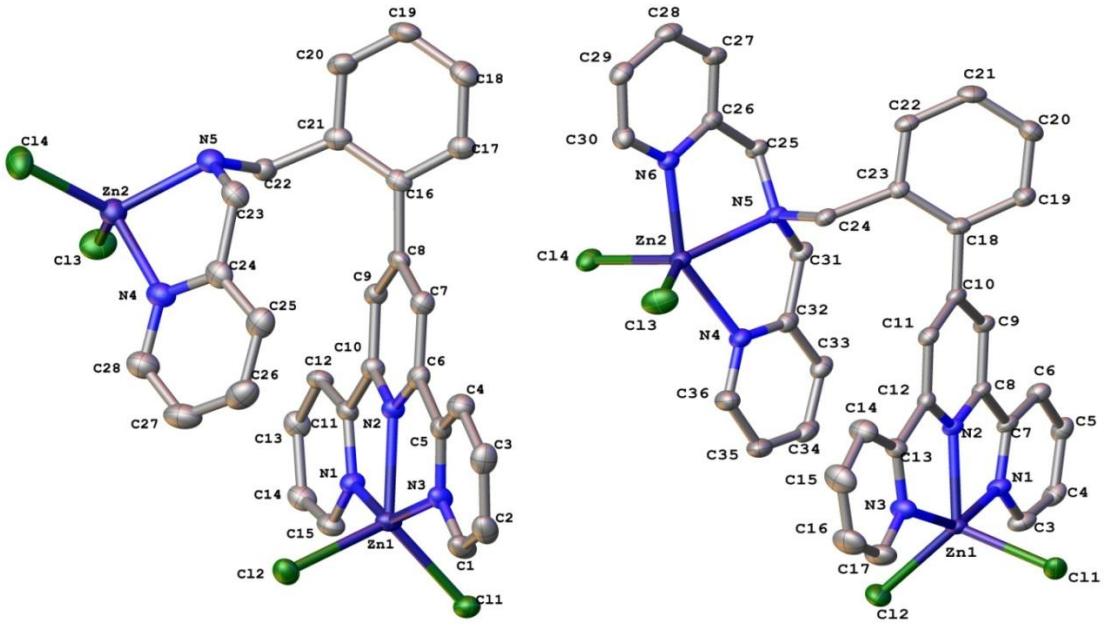

*Figure 4.2. Crystal structures of the dinuclear complexes; [Zn_2(**L2.3**)Cl_4]·3CH_3CN, **4.1**,(left)and [Zn_2(**L2.4**)Cl_4]·2CH_3OH, **4.2**,(right). The H atoms and solvent molecules omitted for clarity. The selected bond lengths and bond angles are given in Appendix III, Table A23 & A24.*

The solid state structures of **4.1** and **4.2** were elucidated *via* single crystal analysis using X-ray crystallography. Both crystal structures were solved and refined in the monoclinic space group $P2_1/n$. Complex **4.1** was refined to an R-factor 4.47%, and **4.2** was refined to R-factor 3.44% using SHELXL in the Olex2 program. In each case, the ligand bridges two Zn atoms, with Zn1 in the head terpyridine-like binding site and Zn2 coordinates in the tail amine binding site. The crystal structures of both **4.1** and **4.2** are shown in **Figure 4.2**.

The Zn1 ion in the tridentate terpyridine-like binding site of **4.1** and **4.2** is five-coordinate, and the geometry lies between trigonal bipyramidal and square pyramidal geometries with τ value of 0.61 and 0.54 (for ideal square pyramidal geometry τ = 0, and for ideal trigonal bipyramidal geometry τ = 1)[69] in the respective complexes with the three terpyridine nitrogen atoms and two chloride ions completing the coordination sphere. Similar Zn-terpyridine coordination is observed in many Zn(II) literature complexes of both substituted and unsubstituted 2,2':6',2''-terpyridine ligands.[219, 309-312]

The Zn1-N distances in the terpyridine-like binding sites of **4.1** and **4.2**, are all within the range of 2.194(3) – 1.996(6) Å. The central Zn-N bond in the terpyridine is shorter than the terminal Zn-N bond lengths, which is typical of all the terpyridine-type complexes reported in literature.[109, 110, 219, 309-316] The Zn1-Cl distances in **4.2** are shorter than in **4.1** and **3.11** (Zn-Cl_1: 2.248(7), 2.276 (10), 2.267(10) Å, and Zn-Cl_2: 2.238(7), 2.274 (11) and 2.267(10) Å, respectively). The terpyridine groups are almost coplanar with their central pyridine ring with slight deviation from planarity. The torsion angles between the central and terminal pyridine rings of terpyridine in **4.2**, 0.0(3)° and 3.9(3)°, are less than those in **4.1**, -3.7(5)° and 8.0(5)°.

The zinc centre, Zn2, in **4.1** is four-coordinate, and occupies a distorted tetrahedral geometry in the bidentate picolylamine binding site. The nitrogen atoms (N4 and N5) and chloride ions (Cl3 and Cl4) occupy four positions of the tetrahedral geometry as shown in **Figure 4.2**. The Zn2 ion exhibits deviation from the ideal tetrahedral coordination geometry to reduce steric repulsion around the coordination environment. The picolylamine bite angle N4-Zn2-N5 (82.30°) is smaller than the Cl3-Zn2-Cl4 angle (117.17°) and these angles are significantly different from the angles of a regular tetrahedron (109.5°). Distortion from perfect tetrahedron is also reflected by the angle between the $ZnCl_2$ and ZnN_2 planes, which is 86.09°. This is often seen in L_2ZnX_2 type complexes, where L_2 is a nitrogen donor bidentate ligand and X is a halogen ion. Similar observations have been made of other four-coordinate zinc complexes of 2-picolylamine-type ligands discussed in the literature.[296, 299]

The bond lengths for Zn2-N4 and Zn2-N5 in **4.1** are 2.051(4) Å and 2.085(3) Å, respectively. Similar results have been reported previously in the literature for Cu(II) and Zn(II) dihalide complexes. The slightly shorter Zn2-N4 bond relative to that of Zn2-N5 might be due to the electronic properties of pyridine nitrogen N4 in contrast to the amine group N5. The pyridine-type strong field ligands make stronger metal-ligand bonds due to π-back bonding than the corresponding amine-type ligands.[298, 304]

In complex **4.2**, Zn2 is five-coordinated at the tail end of the ligand by three nitrogen atoms (N4, N5 and N6) and two chloride ions (Cl3 and Cl4) as shown in **Figure 4.2**. The geometry of Zn2 lies between the ideal trigonal bipyramidal and square pyramidal geometries with a τ value of 0.57. The terminal Zn2-N3 and Zn2-N4 bond lengths are shorter than the central Zn2-N5 bond lengths in bis(picolylamine) site of **4.2,**

due to stronger pi-back bonding donation in pyridine-type ligands. Similar behaviour was observed in the picolylamine-like coordination site of **4.1** and other literature complexes.[300]

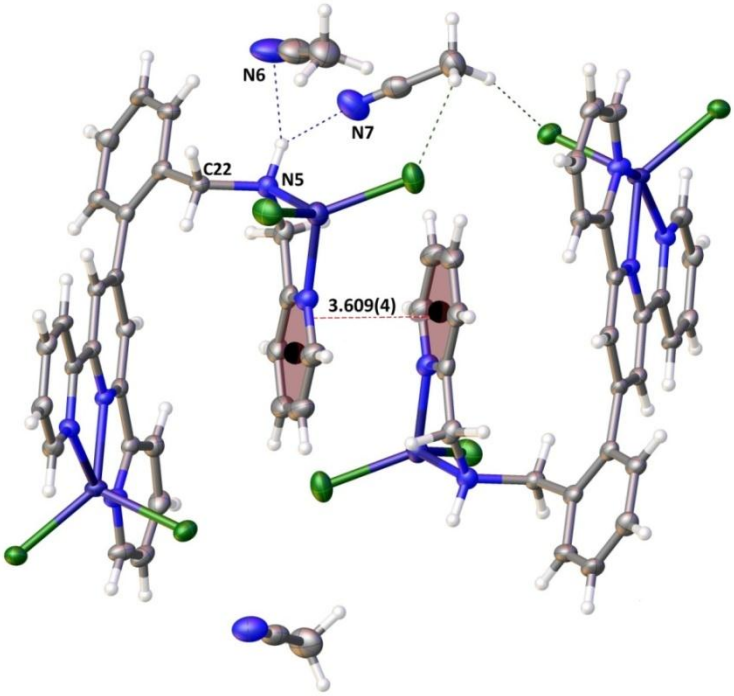

*Figure 4.3. The packing diagram of **4.1**, showing π-π stacking, H-bonding and other short C-H···Cl contacts.*

The picolylamine group twists around the N5-C22 bond in order to make intermolecular parallel-displaced π-π stacking at 3.609(4) Å between the adjacent pyridine rings as shown in **Figure 4.3**. The terminal terpyridine rings are also involved in parallel displaced π-π stacking interactions at 3.368(3) Å with an interplanar angle of 6.13°. The acetonitrile solvent molecules are involved in intermolecular hydrogen bonds to the hydrogen donating secondary amine; N5-H5···N6, 2.384(4) Å and N5-H5···N7, 2.492(5) Å. The molecules in crystal lattice are packed so that the chloride ligands have short contacts with the acetonitrile hydrogen atoms and some aromatic hydrogen atoms within the range of 2.738(10) Å to 3.017(12) Å.

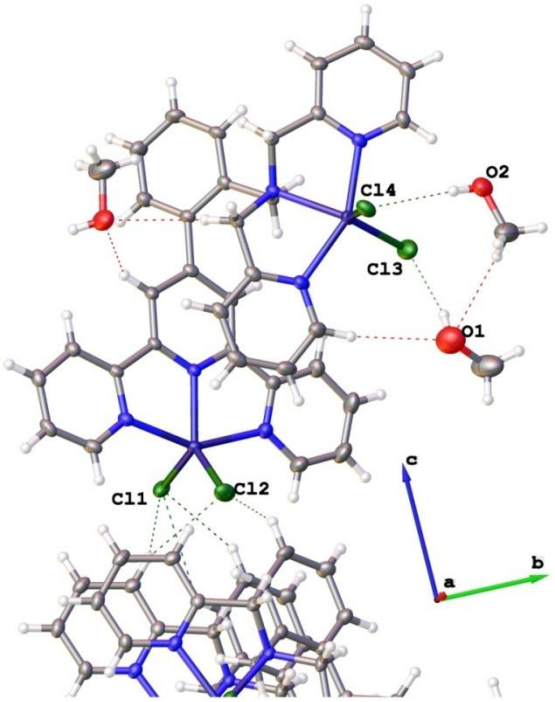

*Figure 4.4. Diagram of **4.2** showing Cl··H-O bonding and some C-H···Cl and C-H···O short contacts. Portions of the ligands were omitted for clarity.*

In complex **4.2**, the chloride ligands and hydrogen donor methanol molecules participate in hydrogen bonding interactions. Several short contacts between chloride ligands, water, and aromatic hydrogen atoms also stabilise the crystal structure. Extensive inter-molecular π-π stacking ranging from *ca*. 3.3 Å -4.3 Å are also observed between the terminal rings of bis(picolylamine) and terpyridine units. The interplanar angle between stacked rings varies from *ca.* 15° to 20.6°. The Zn2 coordinated bis(picolylamine) group twists around the C24-N5 bond to make intermolecular hydrogen bonding between the chloride ligands and hydrogen donor water molecules, O2-H2···Cl4, 2.45(2) Å and O1-H1···Cl3, 2.147(8) Å (**Figure 4.4**). The chloride ions coordinated to Zn1 in the terpyridine binding site do not participate in hydrogen bonding but instead make short contacts with aromatic hydrogen atoms ranging from 2.6433(5) Å to 2.9379(5) Å.

*4.2.1.2. [Cu_2(**L2.3**)($CH_3COO)_4$(H_2O)]·3H_2O –Complex **4.3***

The dinuclear complex **4.3** was synthesised by mixing one equivalent of ligand **L2.3** in chloroform with two equivalents of [$Cu_2(CH_3COO)_4$]·4H_2O in methanol, followed by heating at reflux. Vapour diffusion of acetone into the resulting green solution produced thin needle shaped crystals suitable for structural analysis *via* single crystal X-ray diffraction.

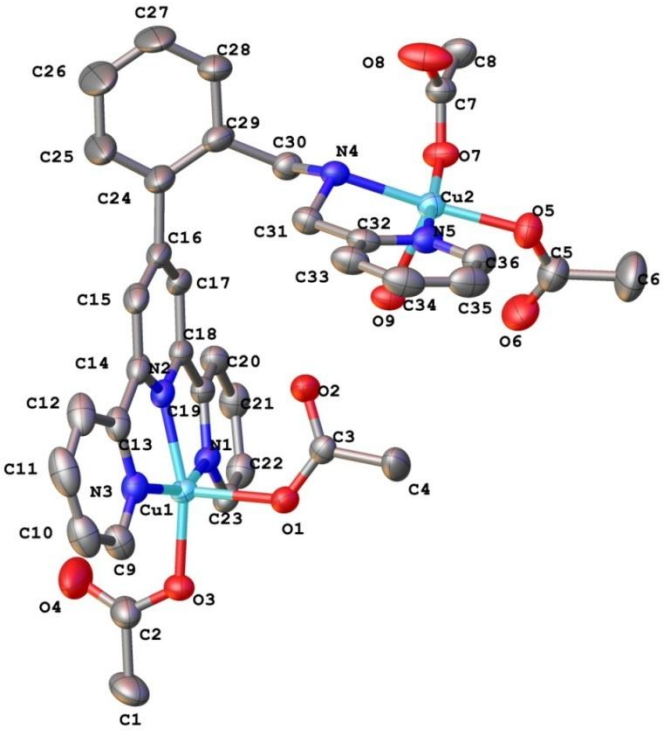

*Figure 4.5. The crystal structure of **4.3**, [Cu_2(**L2.3**)($CH_3COO)_4$(H_2O)]·3H_2O. Solvent molecules and hydrogen atoms have been omitted for clarity. The selected bond lengths and bond angles are given in Appendix III, Table A25.*

The crystal structure for **4.3** was solved and refined in the triclinic space group $P\bar{1}$. Similar to **4.1** and **4.2**, the ligand bridges between two divalent metal ions, resulting in a Cu_2L type dinuclear complex. The crystal structure of **4.3** is shown in **Figure 4.5**. The solvent molecules in the lattice were disordered and the disorder was modelled with one fully occupied water, a second water equally distributed over two positions, and a third water with occupying two different positions which refined to 75% and 25% occupancies. All three water molecules were refined without any hydrogen atoms due to the reduced occupancy and poor ordering. No electron density for hydrogen atoms could be seen in the electron density difference map.

The Cu1 ion coordinated to the terpyridine binding site is five-coordinate and is similar to that found in, [Cu(**L2.1**)$(CH_3COO)_2$] complex **3.9** reported in this thesis. The geometry of Cu1 is approximately square pyramidal with a τ value of 0.13, where all three nitrogen atoms of the terpyridine-type binding site and two monodentate oxygen coordinated acetate ions bind to Cu1. The terpyridine type nitrogen atoms (N1-N3) and the acetate oxygen atom (O3) occupy the equatorial positions, and the second acetate ligand's oxygen donor (O1) provides the axial position of the square pyramidal geometry.

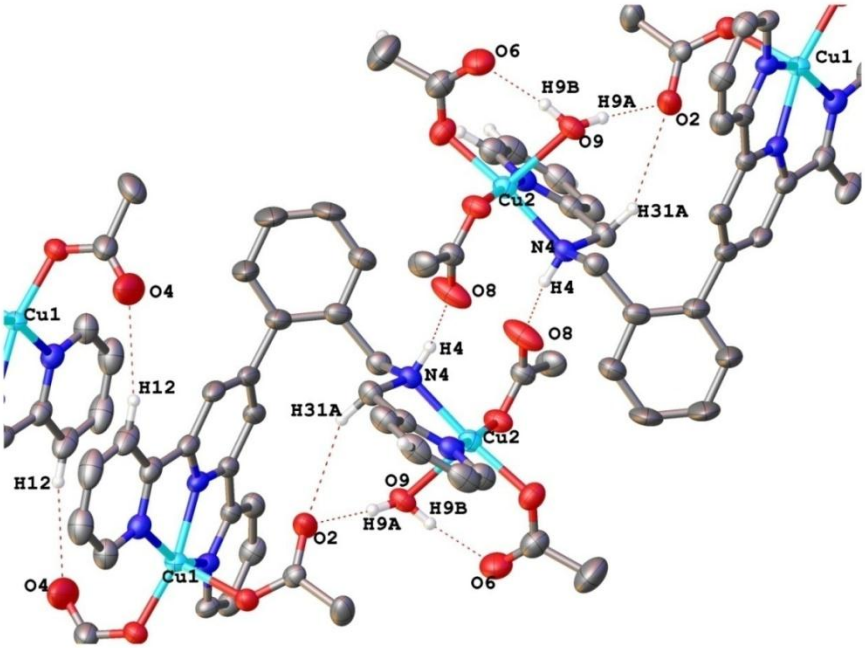

*Figure 4.6. Packing diagram of the complex **4.3** showing hydrogen bonds and other short contacts between O, H and N atoms. Solvent molecules and hydrogen atoms not involved in packing interactions have been omitted for clarity.*

The second copper ion (Cu2) coordinates to the picolylamine metal binding site of the ligand, and again has a square pyramidal geometry with a τ value 0.013. Both nitrogen atoms (N4, N5) and the acetate oxygen atoms (O7, O5) are located in the equatorial positions of the square pyramidal geometry. The axial position is occupied by a coordinating water molecule (O9).

All the Cu1-N and Cu1-O bond lengths in terpyridine group in **4.3** are very similar to those in complex, [Cu(**L2.1**)$(CH_3COO)_2$], **3.9**. The axial Cu1-O1 bond is longer than all other Cu1-O and Cu1-N bonds due to trans-out Jahn Teller distortion of the square pyramidal geometry. However, the Cu1-O1 bond, 2.158(2) Å, in **4.3** is shorter than the comparable bond, 2.218(17) Å, in **3.9**. This shortening of the Cu1-O1 bond may be attributed to intra-molecular hydrogen bonding (**Figure 4.6**) between the acetate oxygen

atoms and water molecule coordinated to the other copper centre, Cu2 (O9-H9···O2 of 1.83(2) Å). In the case of **3.9**, the above mentioned H-bonding is intermolecular, involving non-coordinated water molecules.

Furthermore, the acetate oxygen atom O8 makes a hydrogen bond with the adjacent molecule through the hydrogen donating secondary amine nitrogen N4. The intermolecular N4-H4···O8 hydrogen bond is 2.04(4) Å long. The acetate oxygen atoms also make short contacts with aromatic hydrogen atoms, C12-H12···O4 and C31-H31···O2 are 2.616(4) Å and 2.658(3) Å respectively. Along with this extensive hydrogen bonding and short contacts, some inter-molecular π-π stacking of 3.699(3) Å are also observed between the terminal rings of terpyridine units with an interplanar angle of 15.25(11)°.The torsion angle C30-N4-C31-C32 is 165.7(3)°. The Cu2-N and Cu2-O bond lengths are in the range of 1.93 Å to 2.25 Å and are similar to literature picolylamine complexes.[298, 304, 305]

*4.2.2. Tetranucelar Cu(II) Bridging Complexes of **L2.3** & **L2.4***

*4.2.2.1. $[Cu_4(\mathbf{L2.3})_2(\mu_2\text{-}Cl)_2Cl_6(CH_3OH)_2]\cdot 2\ CH_3OH$ – Complex **4.4** & $[Cu_4(\mathbf{L2.3})_2(\mu_2\text{-}Cl)_2Cl_6]$ – Complex **4.5***

Complex **4.4** was synthesised by mixing one equivalent of ligand **L2.3** in chloroform with two equivalents of $CuCl_2\cdot 2H_2O$ in methanol. Vapour diffusion of diethyl ether into the resulting green solution produced green block shaped crystals suitable for X-ray crystallographic analysis. Complex **4.5** was also crystallised from the same reaction mixture. The green reaction mixture slowly evaporated over a period of 3 months to yield green square blocks of X-ray quality crystals.

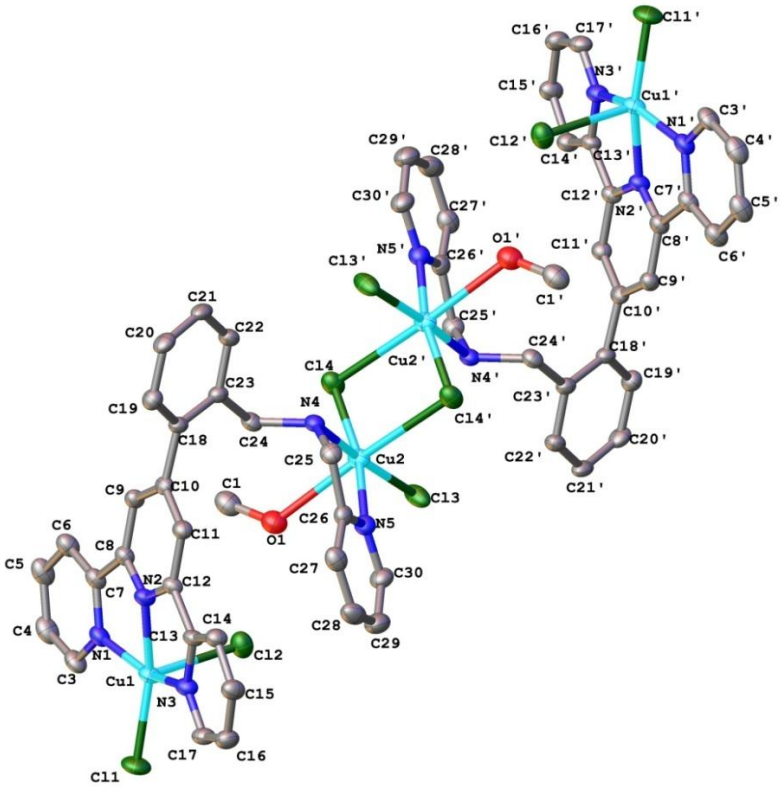

*Figure 4.7. The crystal structure of Cu(II) complex **4.4**. Solvent and hydrogen atoms are omitted for clarity. The selected bond lengths and bond angles are given in Appendix III, Table A26.*

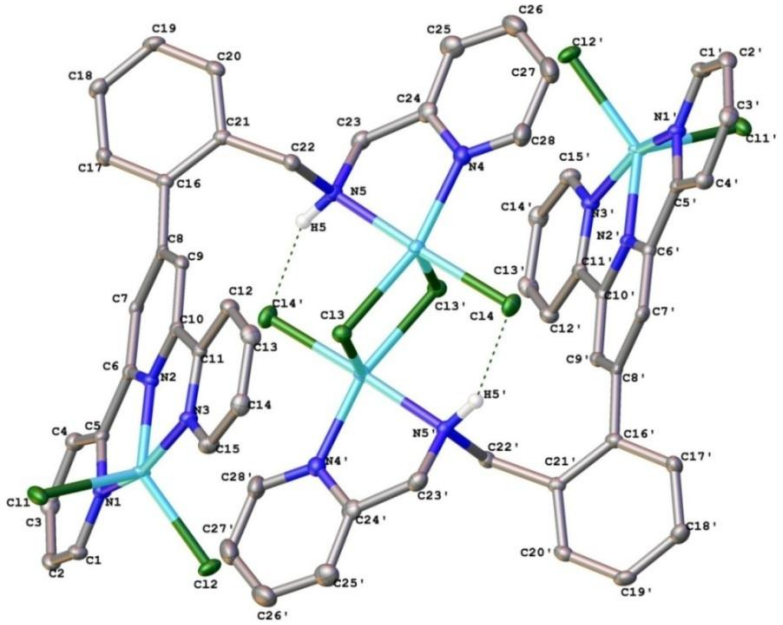

*Figure 4.8. The crystal structure of Cu(II) complex **4.5** showing intra-molecular, N-H···Cl, H-bonding. Hydrogen atoms not involved in hydrogen bonding have been omitted for clarity. The selected bond lengths and bond angles are given in Appendix III, Table A27.*

The crystal structure of **4.4** was solved and refined in the triclinic space group $P\bar{1}$ with an R-factor of 3.79%. The crystal structure of **4.5** was solved and refined in the

monoclinic space group $P2_1/c$ with an R-factor of 2.55%. The crystal structures of complexes **4.4** and **4.5** are illustrated in **Figure 4.7** and **Figure 4.8**, respectively.

As with the previous complexes **L2.3** again acts as a bridging ligand. Each ligand is coordinated to two Cu(II) ions to produce dinuclear Cu_2L units. However, in both **4.4** and **4.5**, each dinuclear unit bridges through the Cu2 centres in their picolylamine binding sites resulting in formation of Cu-Cl-Cu double μ-chloro bridging. This tail-to-tail Cu-Cl-Cu double bridging of two dinuclear units result in formation of Cu_4L_2 tetranuclear complexes as shown in **Figure 4.7** and **Figure 4.8**.

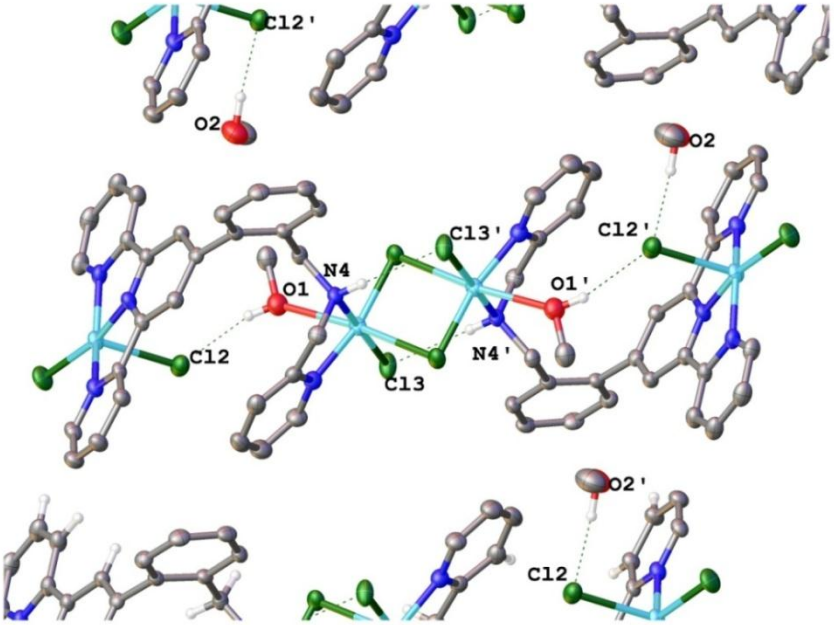

*Figure 4.9. Illustration of hydrogen bonding interactions in complex **4.4** between Cl and hydrogen donor N and O atoms. Hydrogen atoms not involved in bonding have been omitted.*

In both complexes, the Cu(II) centres (Cu1 and Cu1') coordinated in the terpyridine-type binding sites are related by symmetry. All three terpyridine nitrogen atoms and two chloride ligands in each case make five-coordinate geometries. In **4.4**, the Cu1 and Cu1' occupy approximately square pyramidal geometries with τ value of 0.15, whereas the geometry around Cu1 and Cu1' in **4.5** is intermediate between the ideal square pyramidal and trigonal bipyramidal geometries with a τ value of 0.41. The higher square pyramidal character (or lower trigonal distortion) of Cu1 and Cu1' geometry in **4.4** could be attributed to the intra-molecular hydrogen bonding interactions between Cu1 bound chloride ion and the methanol molecule bound to Cu2 within the same ligand as shown in **Figure 4.9**. Similar higher square pyramidal character of the Cu1 coordination

geometry was reported in complexes [Cu(4′-toluyl-2,2′:6′,2″-terpyridine)Cl_2],[85] and [Cu(4′-chloro-2,2′:6′,2″-terpyridine)Cl_2],[317] where the axial chloride ions are hydrogen bonded to the water molecules.

In **4.4**, the Cu2 and Cu2' ions coordinated in the picolylamine binding sites occupy the distorted octahedral geometry. Three terpyridine nitrogen atoms, two chloride ions and a methanol are coordinated to each copper centre. Both copper centres interact with chloride ions Cl4 and Cl4', respectively, at a distance of 2.881(2) Å and 2.264(2) Å. The Cl4 and Cl4' ions act as bridging ligands, resulting in formation Cu_4L_2 complexes with double-μ-chloro (tail-to-tail) bridging. The Cu2-Cu2' distance is 3.551(8) Å and Cu2-Cl4-Cu2' bond angle is 86.42(3)°. The Cu1-N bond lengths and angles in terpyridine group in **4.4** are close to typical Cu(II)-terpyridine complexes reported in literature.[85] Torsion angle C24-N4-C25-C26 and C24'-N4'-C25'-C26' both are 92.6(3)°.

In **4.5**, the Cu2 and Cu2' ions in the picolylamine binding sites are five-coordinate geometries using two picolylamine-type nitrogen atoms and three chloride ions. The geometries are approximately square pyramidal with τ values of 0.25 each. The chloride ions Cl3 and Cl3' participate in Cu-Cl-Cu bridging. The Cu2-Cu2' distance 3.272(5) Å and Cu2-Cl3-Cu2' bond angle 81.558(16)° are smaller than these angles observed in complex **4.4**.

Complex **4.4** crystallises with four methanol molecules, of which two act as coordinating ligands and other two are present in the crystal lattice as non-coordinating solvent molecules, and are involved in hydrogen bonding. The terminal chloride ions coordinated in the picolylamine binding sites also hydrogen bond with the secondary amine nitrogen atoms (N4'-H4'⋯Cl3 and N4-H4⋯Cl3') both at a distance of 2.610(18) Å, and this sort of hydrogen bonding is a common feature of picolylamine complexes reported in literature.[298, 304]Along with the hydrogen bonding interactions and other short contacts, some π-π stacking is also observed in adjacent molecules. The terminal pyridine rings of each terpyridine stack with the terminal pyridine rings of the adjacent molecules within the crystal lattice, the centroid-centroid distance is 3.477(2) Å with an inter-planar angle of 7.74(9) Å.

In complex **4.5** only the bridging chloride ions Cl4 and Cl4' participate in hydrogen bond formation, N5'-H5'⋯Cl4 and N5-H5⋯Cl4' both 2.435(5) Å, through hydrogen

donor secondary amine nitrogen atoms. The torsion angles C22-N5-C23-C24 and C22'-N5'-C23'-C24' are both of 84.18(18)°. Molecules in the crystal lattice are efficiently packed so terpyridine coordinated chloride ions have short contacts with some aromatic hydrogen atoms of adjacent molecules within a range of 2.691(5) Å to 2.754(5) Å. The face-to-face displaced aromatic π-π stacking between the terminal and central ring of terpyridine groups of adjacent molecules also results in efficient packing of the molecules in the crystal lattice. The plane containing C12-C11-N3-C15-C14-C13 atoms stacks over C3-C4-C5-N1-C1-C2 plane of the adjacent molecule at 3.376(19) Å with an inter-planar angle of 9.625(6)°. The same plane C12-C11-N3-C15-C14-C13 further show some π-π stacking with C8-C7-C6-N2-C10-C9 plane of another molecule 3.433(14) Å with an inter-planar angle of 4.997(6)°.

*4.2.2.2. $[Cu_4(\mathbf{L2.4})_2(\mu\text{-}Cl)Cl_{6.5}(H_2O)_{1.8}]Cl_{1.5}\cdot 1H_2O$ – Complex **4.6***

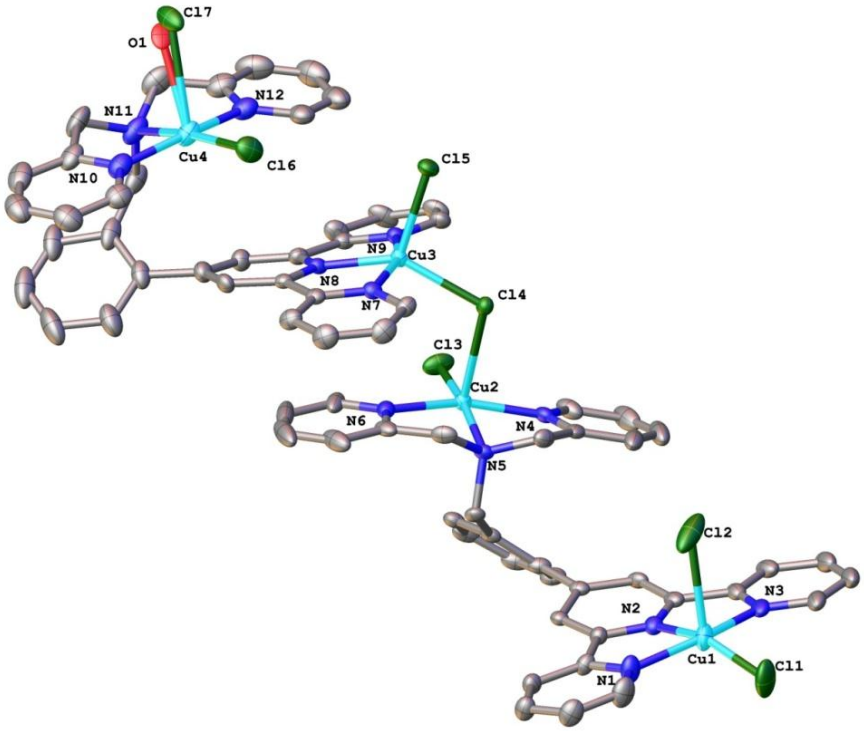

*Figure 4.10. The crystal structure of Cu(II) complex **4.6**. The hydrogen atoms, uncoordinated chloride and water have been omitted for clarity. The selected bond lengths and bond angles are given in Appendix III, Table A28.*

As with the previous complexes discussed in this chapter, complex **4.6** was also synthesised by mixing one equivalent of ligand (**L2.4**) dissolved in chloroform with two equivalents of $CuCl_2\cdot 2H_2O$ dissolved in methanol. Average quality blue plates of crystals

were formed in the aqueous filtrate after 3 weeks time. A small piece of a crystal suitable for structural analysis by X-ray crystallography was carefully cut from one of the overlapped large crystals.

The crystal structure for complex **4.6** (**Figure 4.10**) was solved and refined in the triclinic space group $P\bar{1}$ with an R-factor of 5.85%. As with the previous complexes **4.4** and **4.5**, Cu_4L_2Complex was formed. However, in **4.6** both two dinuclear units bridge to each other by head-to-tail coordination mode, which is different from that observed tail-to-tail coordination in **4.4** and **4.5**.

Contrary to the double-μ-chloro bridging in **4.4** and **4.5**, the mono-μ-Chloro bridging is present in **4.6**. However, in Cu(II) halide complexes, the mono-μ-Cl bridging mode is not unusual, a similar arrangement was reported in Cu(II) complexes of bis(picolylamine) containing ligands, **Figure 4.11**.[303, 307]

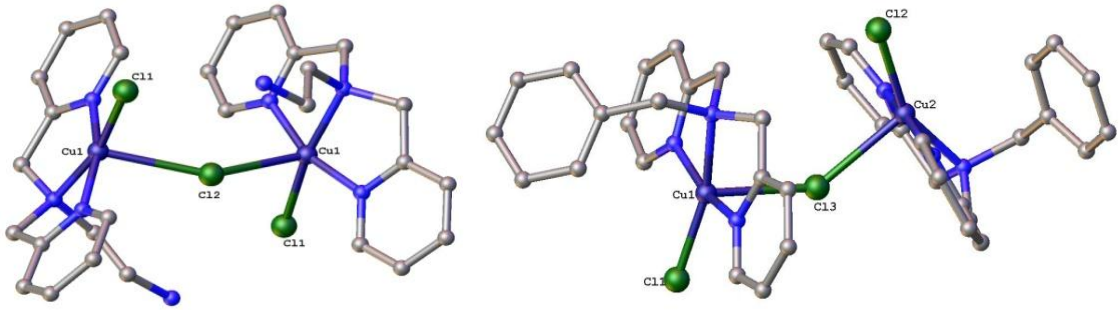

Figure 4.11. Literature complexes showing mono-μ-chloro, Cl-Cu-Cl, bridging.[303, 307]

The asymmetric unit of **4.6** contains two ligands, four Cu(II) ions, eight chloride ions and some reduced occupancy disordered water molecules. The elemental analysis of the bulk sample was consistent with the presence of eight water molecules; the sample was dried overnight under vacuum prior sending for elemental analysis.

Due to some serious disorder associated with water and chloride ions, it was difficult to model all the closely spaced electron density peaks. Several attempts were made to grow better quality crystals using different solvents and techniques, none of which were successful. The analysis of the crystallographic data for each attempt shows that the cation $[Cu_4(\mathbf{L2.4})_2]^{8+}$ was well ordered but water and chloride ions were always severely disordered.

All of the Cu(II) ions are five-coordinate and occupy approximately square pyramidal geometries with τ values of 0.03, 0.09, 0.25 and 0.13 for Cu1, Cu2, Cu3 and

Cu4, respectively. In case of Cu1, Cu2, and Cu3, three positions of the five-coordinate geometries are occupied by three nitrogen atoms and the other two by the chloride ions. In the case of Cu4, three nitrogen atoms, one chloride ion, one 50% occupancy water molecule and another 50% occupancy chloride ion completes the five-coordinate geometry. The metal ions Cu2 and Cu3 are involved in head-to-tail bridging through chloride ion Cl4. The Cu2-Cu3 distance is 4.010(10) Å, and Cu2-Cl4-Cu3 angle is 105.71(4)°.

The chloride ions coordinated to the middle metal ions (Cu2 and Cu3) were well ordered but the thermal ellipsoid for the chloride ion coordinated to outer metal ions (Cu4 and Cu1) was larger than other atoms in the model. Two large residual electron density peaks of 4.4 eA^{-3} and 4.9 eA^{-3} were located at a distance of 2.2973(7) Å and 2.404(13) Å from their corresponding Cu ions and, 0.5 Å and 0.9 Å from the nearest chloride ions. These peaks were left unmodelled due to some persistent and severe disorder associated with the model.

The additional electron density peaks near the chlorides could be expected to be a disorder with a water molecule. However refining the occupancy of the chlorides and water lead to chemically impossible (occupancies greater than one or less than one) solutions or improbable thermal ellipsoids. Presence of chloride and water is supported by microanalysis ($C_{68}H_{56}N_{12}Cu_4Cl_8 \cdot 8H_2O$), and refinement with bromide lead to NPD.

Overall residual electron density present for the ligands around Cu1 was larger and around Cu4 was smaller than that required for any possible combination of the ligands such as chloride ion and water. The chloride ions (Cl1, Cl2) were modelled with full occupancy, leaving one big residual electron density peak unmodelled near Cl2. One chloride ion (Cl6) was modelled with full occupancy and the second chloride (Cl7) was modelled at 50% occupancy as coordinated with Cu4. One water molecule (O1) coordinated to Cu4 was modelled with occupancy 50% to balance the overall charge of the cation; however the thermal ellipsoid for O1 was almost flat and small. Two large electron density peaks in the crystal lattice were modelled as non-coordinating chloride ions, Cl8 with full occupancy and Cl7' at 50% occupancy.

Most of the solvent was also highly disordered. Only well ordered peaks were modelled and the remaining solvent was removed using solvent mask option in OLEX2.

This type of disorder is found to be common in complexes containing a large number of water molecules and chloride ions, because two closely located electron density peaks could be either disordered chloride ions with occupancy 0.5 or it could be two disordered water molecules.[223-229] More crystal structures with similar disorder are discussed in Chapter 6 involving larger polynuclear complexes.

4.2.3. Characterisation of the Di- and Tetra- Nuclear Cu(II) Complexes

All Cu(II) and Zn(II) complexes were characterised by a combination of elemental analysis, mass spectrometry, and IR. The Zn(II) complex **4.1** was characterised by ^{1}H and ^{13}C NMR as well. Complex **4.2** was only sparingly soluble in the common NMR solvents so NMR analysis was not possible.

The ESI-MS spectrum of complex **4.1** shows a *m/z* signal at 528.09 which corresponds to $[Zn+\mathbf{L2.3}+Cl]^{+}$. The elemental analysis results for the bulk sample of **4.1** was different ($C_{28}H_{23}N_5Zn_2Cl_4\cdot 2H_2O$) from that found ($C_{28}H_{23}N_5Zn_2Cl_4\cdot 3CH_3CN$) in the crystal structure, because the bulk sample sent for elemental analysis was dried under vacuum in a desiccator, which suggests that the co-crystallised solvent might have evaporated, and two water molecules can possibly come from the atmospheric moisture. The *m/z* signals at 753.00 and 619.13 in ESI-MS spectrum of **4.2** correspond to $[2Zn+\mathbf{L2.3}+3Cl]^{+}$ and $[Zn+\mathbf{L2.3}+Cl]^{+}$, respectively. The elemental analysis result of the bulk sample of **4.2** was consistent with the crystal structure.

The ESI-MS peak of *m/z* 358.01 correspond to $[2Cu+\mathbf{L2.4}+2Cl]^{2+}$ in **4.6**. For both **4.4** and **4.5** the ESI-MS spectrum shows *m/z* signal at 312.49 which correspond to $[2Cu+\mathbf{L2.3}+2Cl]^{+}$ owing to their same dinuclear species present in solution. The elemental analysis of **4.4** shows loss of one crystallised methanol and increase in water content in the bulk sample. As explained in previous complexes the bulk sample sent for elemental analysis was dried under vacuum in a desiccator, which suggests that the co-crystallised methanol might have evaporated, and the water content in molecules can possibly increase due to atmospheric moisture.

4.3. Conclusion

As proposed in this project, dinuclear complexes of the polydentate ligands were synthesised and characterised including some tetranuclear complexes. The solid state structure of the complexes was analysed by single crystal X-ray crystallography. The bulk characterisation of the isolated material was consistent with formation of the dinuclear complexes where both coordination sites of the ligands were occupied by metal ions. Mass spectroscopy data shows formation of M_2(**L2.3**) and M_2(**L2.4**) species in solution for both Cu(II) and Zn(II) complexes discussed in this chapter.

Both dinuclear and tetranuclear μ-chlorido bridging complexes of **L2.3** and **L2.4** were synthesised using Zn(II) and Cu(II) metal ions. All complexes were synthesised by mixing one equivalent of ligand with two equivalents of the metal ions. Single crystals were produced using different crystallisation methods like slow evaporation, vapour diffusion and H-tube crystallisation.

In all the complexes discussed in this chapter, each ligand bridges between two metal ions, where one metal ion binds in the tridentate terpyridine (head) binding site and another metal ion binds either in bidentate picolylamine or in tridentate bis(picolylamine) tail binding site.

The Zn(II) complexes $[Zn_2(\mathbf{L2.3})Cl_4]\cdot 3CH_3CN$, **4.1** and $[Zn_2(\mathbf{L2.4})Cl_4]\cdot 2CH_3OH$, **4.2**, synthesised using $ZnCl_2$ were crystallised as discrete dinuclear units. Similarly, the Cu(II) complex $[Cu_2(\mathbf{L2.3})(CH_3COO)_4(H_2O)]\cdot 3H_2O$, **4.3**, was also crystallised as discrete dinuclear units.

However, the Cu(II) complexes $[Cu_4(\mathbf{L2.3})_2(\mu_2\text{-}Cl)_2Cl_6(CH_3OH)_2]\cdot 2CH_3OH$, **4.4**, $[Cu_4(\mathbf{L2.3})_2(\mu_2\text{-}Cl)_2Cl_6]$, **4.5**, and $[Cu_4(\mathbf{L2.4})_2(\mu\text{-}Cl)Cl_{6.5}(H_2O)_{1.8}]Cl_{1.5}\cdot 1H_2O$, **4.6**, synthesised using $CuCl_2\cdot 2H_2O$, were crystallised as tetranuclear complexes. In these complexes two dinuclear units were bridged together through Cu-Cl-Cu bridging. In the case of **4.4** and **4.5**, ligands interact *via* double μ-chloro (tail-to-tail) Cu-Cl-Cu bridging, whereas in **4.6** the mono μ-chloro (head-to-tail) Cu-Cl-Cu bridging was observed between each dinuclear unit.

In all the complexes of **L2.3**, except **4.2**, hydrogen bonding was observed between the –NH hydrogen atoms of the ligands and the counter ions or solvent molecules. Other

than this other various packing interactions such as π-π stacking and short contacts were also observed in all complexes discussed in this chapter.

CHAPTER 5

PHOSPHATE DIESTERS HYDROLYSIS: KINETICS AND RELEVANT STRUCTURAL STUDIES

5.1. Introduction

In nature, phosphate diester bonds exist ubiquitously.[318] They are found in the form of nucleoside phosphates (nucleotides) as components of DNA and RNA.[319] To maintain the integrity of genetic substances, nature could hardly have devised more suitable links than phosphate diester bonds in DNA, RNA and proteins.[14] The phosphate diesters in DNA are stable towards hydrolysis under physiological conditions, with a half-life for spontaneous hydrolysis estimated to be in the range of 10 million to 16 million years.[9, 320] A series of enzymes (such as alkaline phosphatase, phospholipase C and P1 nucleases, DNases, RNases, restriction endonucleases, exonucleases, ribonucleases) developed by nature to catalyse the phosphate diester hydrolysis contain metal ions in their active sites.[321-324] Many enzymes that catalyse other functions such as replication of DNA, and transesterification of RNA are also activated by more than one metal ion.[325]

Most of these hydrolytic enzymes use metal ions as cofactors. The metal ions effectively control an enzyme-catalysed reaction. There are three direct modes of activation. First, increased acidity of coordinated water ligands promotes the formation of hydroxide, which is a stronger nucleophile. Second, bonding of a metal atom to the anionic oxygen of the substrate increases the electrophilic susceptibility of the neighbouring atom for the nucleophilic attack. Third, the metal ion can stabilise the leaving group by interaction with the partial negative charge on the leaving oxygen, in the transition state.[326-328] Two indirect modes of activation are where metal coordinated hydroxide can act as an intramolecular general base catalyst, or metal coordinated water can act as a general acid catalyst. Different modes of activation by metal ions are shown in detail in Chapter 1. Since there can be more than one metal centre in an enzyme, each metal centre can have multiple interactions with the phosphate, so it is important to be able to study the model enzymes in order to understand the importance of each contact separately and cooperatively. It has been widely studied that more than one metal ion can cooperatively activate the hydrolysis reaction.

The reason for working with model systems is that the relationship between the structure and reactivity is much easier to understand and study in simple model compounds than in the enzymes themselves. Fundamental knowledge gained from such studies may provide valuable insights into how the enzymes function. Many metal ion

based model systems have been reported, and some related to this research have been briefly discussed in Chapter 1. These model systems generally feature tridentate or tetradentate coordination sites, and a metal centre containing exchangeable ligands.[42, 277, 278, 328, 329]. Some examples of such model systems are shown in **Figure 5.1**. In these examples, the complexes formed are symmetrical and two metal ions bind in an identical environment. The two metal ions may interact with the substrate (phosphate diester) simultaneously during the hydrolysis reactions in solution.

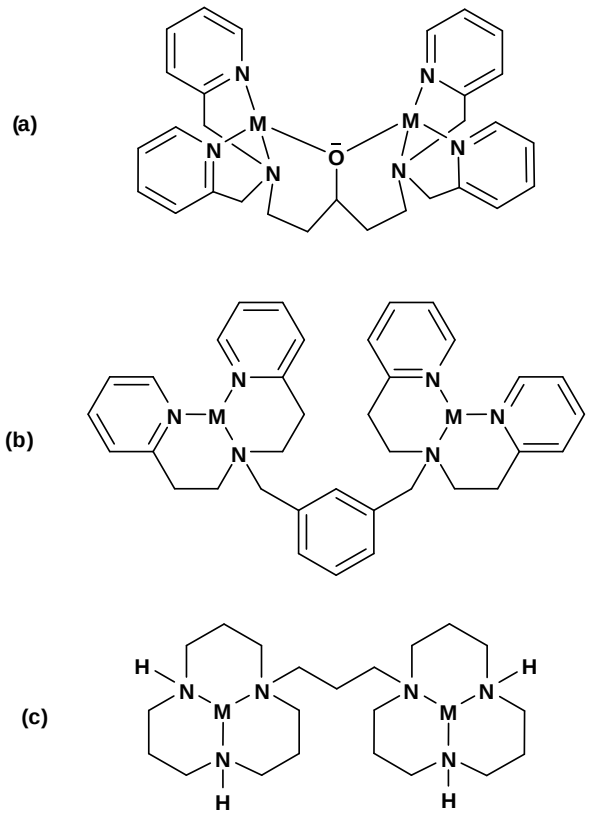

Figure 5.1. Dinuclear models with identical metal binding sites used to study kinetics of phosphate hydrolysis. M = Zn(II),Cu(II),Co(III)[42, 278, 328]

The proposed general mechanism of the hydrolysis reaction promoted by complexes of the ligands in **Figure 5.1** is based on the Lewis acid character of the metal ion reducing pK_a of the coordinated water.

This provides a metal-bound hydroxide nucleophile at neutral pH and, at the same time, both metal ions activate a coordinated substrate (phosphate diester) towards nucleophilic attack by charge neutralization as shown in **Figure 5.2**.[14, 42, 278, 328]

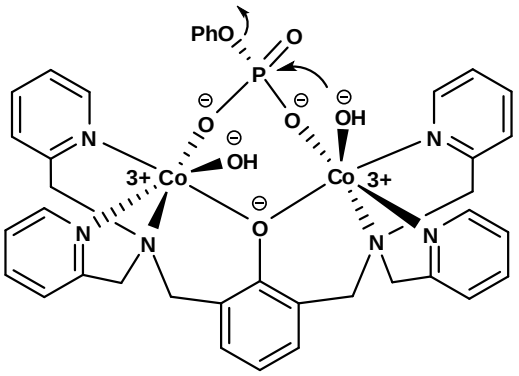

Figure 5.2. Lewis acid activation and metal-coordinated hydroxide involved in hydrolysis of phosphate diester.

With the aim of developing more efficient metal complexes possessing hydrolytic activity under physiological conditions, we have studied the systems where two metals bind in a different environment (**Figure 5.3**). A variety of Cu(II) and Zn(II) dinuclear complexes have been synthesised and characterised, as described in Chapter 4, along with their X-ray crystal structures.

The dinuclear model systems in this research possess two entirely different metal binding sites, the tridentate terpyridine binding site and the bidentate picolylamine or tridentate bis(picolylamine) binding sites, as shown in **Figure 5.3**.

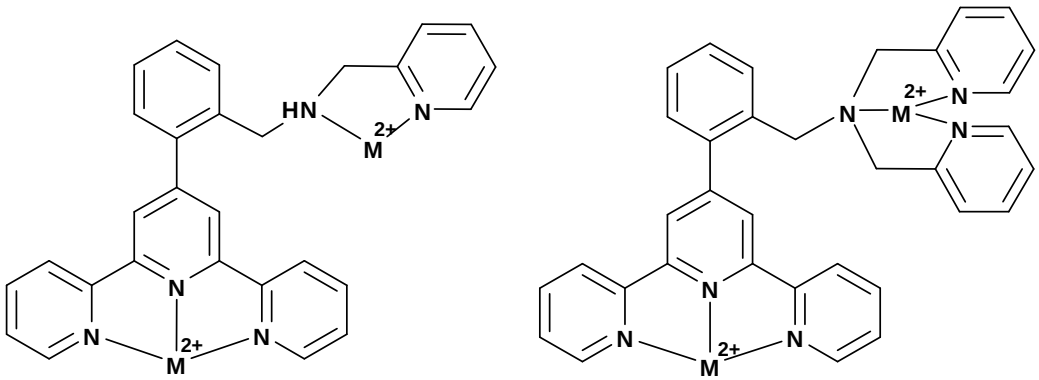

Figure 5.3. A diagrammatic representation of the model dinuclear systems studied for hydrolytic catalysis in this research.

The solid state crystal structures of the dinuclear complexes in Chapter 4, and mononuclear complexes Chapter 2, mass spectroscopy data and elemental analyses are consistent with Zn(II) and Cu(II) ions in terpyridine binding sites. There are a number of complexes in literature where Zn(II) and Cu(II) bind in a five-coordinate geometry with

terpyridine type ligands.[85, 90, 163, 202, 209, 214, 217, 219, 242, 330, 331] In most of the terpyridine-type five-coordinate complexes, three sites of the coordination geometry are occupied by terpyridine nitrogen atoms, and the two are occupied by other counter-ions or the solvent molecules present in the reaction mixture.

Picolylamine and bis(picolylamine) type ligands make a variety of metal complexes with different metal ions and are reported to have tetrahedral, square pyramidal and trigonal bipyramidal geometries.[295, 296, 298-300, 303-306, 308, 332] In the solution state, such complexes may exchange counter ions and may provide coordination sites for substrate binding. There is also a possibility of equilibria involving between complexes of more than one ligand, as shown in equations 1-3. In case of picolylamine one metal ion may bind with one, two or three ligands shown in **Figure 5.4**.

$$Zn^{2+} + L \rightleftharpoons ZnL \qquad (1)$$

$$ZnL + L \rightleftharpoons ZnL_2 \qquad (2)$$

$$ZnL_2 + L \rightleftharpoons ZnL_3 \qquad (3)$$

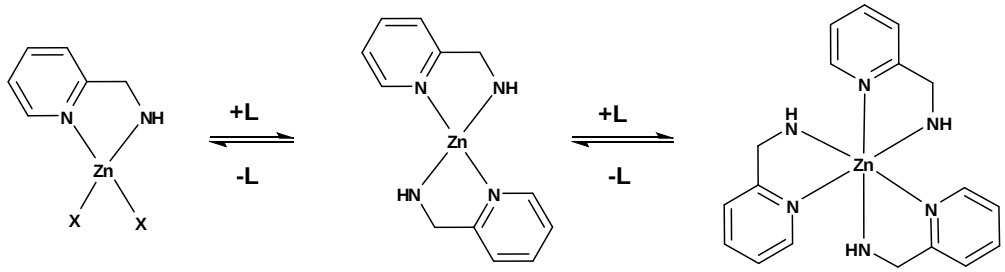

Figure 5.4. Illustration of equilibria between metal complexes of more than one picolylamine ligands.

This chapter presents our kinetic studies on hydrolysis of phosphate diesters using dinuclear Zn(II) complexes of the ligands **L2.3** and **L2.4** and comparisons with the analogous mononuclear complexes. The phosphate diester substrate bis(*p*-nitrophenyl)phosphate (BNPP) was used as a model of RNA/DNA. The aim of these studies was to look for changes in the rate of hydrolysis of phosphate diesters when dinuclear complexes with flexible and entirely different two metal centres were used in comparison to their mononuclear analogues.

When Cu(II) complexes of **L2.1** were mixed with the solution of BNPP, some precipitate was formed. Due to this precipitation problem, it was not possible to measure the rate of hydrolysis of BNPP with the spectrophotometer. The precipitate formed was crystallised and analysed using X-ray crystallography. The substrate coordinated Cu(II) complexes of **L2.1**, the complexes **5.1** and **5.2** were characterised. The crystal structures of the complexes are also discussed in this chapter.

5.2. Results and Discussion

5.2.1. Development of the Experimental Methodology

Both Cu(II) and Zn(II) metal ions were used in attempts to study the kinetics of hydrolysis of the phosphate diester compound, BNPP, in this project. Zn(II) was mainly used because many natural enzymes possess it in their active sites. For example carboxypeptidase A, carbonic anhydrase, and purple acid phosphatase, alkaline phosphatase, P1 nucleases are the enzymes which consist of Zn(II) as a cofactor in their active sites.[328, 333]

Cu(II) and Zn(II) ions produce the proposed dinuclear complexes in this research. Other metal ions such as Fe(II) and Ni(II) usually give bis-terpyridine type octahedral complexes with the ligands synthesised in this project and Ni(II) can give even bigger complexes (Chapter 6). The Fe(II) complexes of **L2.3** do not possess any coordination site available for the substrate binding during hydrolysis reactions. The dinuclear Cu(II) and Zn(II) complexes are discussed in Chapter 4, the terpyridine-type binding sites of **L2.3** and **L2.4** form part of a five-coordination geometry with Cu(II) and Zn(II) metal ions, where three coordination sites are occupied by three terpyridine-type nitrogen atoms and the remaining sites are occupied by exchangeable ligands such as chloride, water or acetate. The picolylamine-type and bis-picolylamine-type ligands participate in four and five-coordinate geometries, respectively, and in each case two coordination sites on the metal ions are occupied by exchangeable ligands. This means dinuclear Zn(II) and Cu(II) complexes can possibly exchange ligands in hydrolytic reactions for substrate binding or to produce metal coordinated stronger nucleophiles. Therefore, the dinuclear Cu(II) and

Zn(II) complexes of **L2.3** and **L2.4** were used for hydrolysis experiment of BNPP in this project.

Experiments in the kinetics of hydrolysis of phosphate diesters were performed using spectrophotometric methods. In general for these experiments, a solution of complex is mixed with the solution of BNPP in the presence of a buffer at a certain temperature and pH, and a change in absorbance of the solution is observed at 430 nm due to formation of ionic *p*-nitrophenolate. Therefore, the reactant and products must be all soluble in some solvent to get a clear reaction mixture for accurate absorbance measurements.

The dinuclear complexes used to study catalysis in this research were all soluble in hot DMSO, and addition of aqueous buffer caused precipitation of the complexes. It was not possible to use the isolated complexes directly for the experiments. Therefore the complexes were prepared *in situ* by mixing a solution of metal (in acetonitrile) and the ligand (in a minimum amount of DMF) in UV quartz cuvettes prior to addition of the aqueous buffer, and the substrate for each experiment.

The use of chloride ions was avoided in our experiments, because some previous studies discuss that chloride ions can inhibit the hydrolysis of BNPP performed in the presence of terpyridine-type complexes. [91, 93] In these literature experiments 0.1 M KCl solution was used to maintain the ionic strength of the reaction mixture, and Cu(II) complex of 2,2':6',2''-terpyridine (tpy) was used as a catalyst. The rate of hydrolysis of BNPP was slow, which took 2-3 days to complete 1% of the reaction at pH 10.5, and no hydrolysis was observed at lower pH (7.0). In that case [Cu(tpy)(BNPP)Cl] complex was precipitated from the reaction mixture. Similar complexes **5.1** and **5.2** were crystallised from hydrolysis experiments performed in this research when Cu(II) complexes of **L2.1** were used.

To avoid this sort of problems, the sulfonic acid derivative buffers such as HEPES (pH 6.8-8.0) and TAPS (pH 7.7-9.1) were used. The pH was adjusted using aqueous sodium hydroxide solution, the ionic strength of the solutions was maintained using 0.1 M $NaClO_4$ solution, as perchlorate ions are relatively non-coordinating anion in comparison to chloride ions. The Zn(II) complexes used were synthesised with acetate counter-ions.

Another problem arose on mixing the aqueous buffer with aqueous BNPP solution, which leads to quick precipitation of BNPP in the aqueous reaction mixtures. Using different type of buffers was ineffective towards the resulting precipitation. This sort of solubility problem was not explained in any related journal articles, but many similar experimental studies were performed using a mixture of solvents such as 75% ethanol,[92, 93] 20% methanol,[58] 50% acetonitrile,[326] and 33% DMF[334] aqueous solutions at different temperatures between 25 °C to 40 °C. Therefore, 45% acetonitrile-5% DMF aqueous solution was used to avoid BNPP precipitation. Even under these conditions there was some turbidity in the solution beyond pH 9, so the experiments were performed in the range of pH 7-9 at 35 °C.

Typically, for each experiment, a solution of the ligand (5 mM), a solution of the metal salt (10 mM), buffers HEPES or TAPS (0.2 M at pH range of 7-9, I= 0.2 M $NaClO_4$), and BNPP (250 mM) were prepared in bulk. The bulk solutions were freshly prepared prior the experiments. In each experiment, the ligand solution (40 µl) was mixed with the metal solution (40 µl for dinuclear complexes, and 20 µl for mononuclear complexes), followed by addition of the buffer (450 µl) and acetonitrile (430 µl for mononuclear complexes, and 450 µl for dinuclear complexes) into a 1 cm cuvette with 1.5 mL capacity. The cuvette, stoppered with a Teflon stopper, was inverted to allow the solutions to mix. The solution temperature was allowed to reach to equilibrium for 5 min prior addition of the solution of BNPP (40 µl, final conc. 10 mM) to the cuvette. Ultimately the reaction solutions contained 0.4 mM complex, 0.9 M buffer at I = 0.9 M $NaClO_4$, and 10 mM BNPP.

The molar absorptivity of p-nitrophenol was calculated at the experimental temperature and pH values ranging from 7-9; ε (mol $L^{-1}cm^{-1}$) = 25100, 28400, 30000, 30700, and 33100 at pH 7, 7.5, 8, 8.5, and 9 respectively.

Blank experiments were performed to measure the auto-hydrolysis of BNPP and p-nitrophenol. These experiments show a lack of auto-hydrolysis in BNPP. Therefore correction for the spontaneous (auto) hydrolysis of the substrate by the solvent or the buffer was accomplished by using a reference cell containing all the reactants and solvents except the catalyst under the same conditions.

Due to the solubility issues of the complexes and very low rates of hydrolysis of BNPP, both substrate and complex concentration based kinetic studies were not possible. Any experiment with a higher concentration of the substrate or complex resulted in precipitation of complex and unstable spectrophotometric results. As discussed in the next section, the increase in absorbance due to hydrolysis of BNPP was very low and the extent of the reaction was very small. A decrease in the concentration of substrate or complex would give even more errors in the slope.

5.2.2. Analysis of Results

The rate of hydrolysis was observed by monitoring the increase in absorbance at 400 nm, following formation of the yellow coloured *p*-nitrophenolate ions in the solution. In these experiments, due to the low rate of hydrolysis of phosphate diester (BNPP), the data points in A *vs.* T graphs were very noisy and the slope was almost flat due to the very low hydrolysis rate of the phosphate diesters (Appendix I). There was no supplementary information available in previous research articles about the raw data graphs of A *vs.* t, and authors of some recent journal articles[272, 279, 320] were contacted by email to get more information about the raw data and they mentioned their graphs too were almost flat and A *vs.* t graphs are not included in the supplementary information (Zhao M., private communication, November 5, 2013), (Hanafy A.I., private communication, January 14, 2014).

The first 0.2 min of each experiment was excluded due to very abrupt changes in absorbance due to mixing effects. These mixing phase changes were common in each experiment on addition of any solvent. A few examples of the raw graphs are shown below in **Figure 5.5** and **5.6**. Similar mixing behaviour was also observed in blank experiments, **Figure 5.7**.

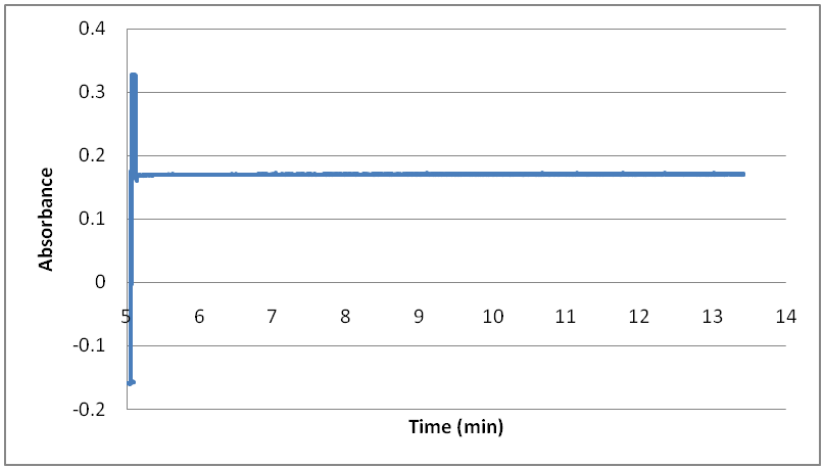

Figure 5.5. The expanded absorbance vs. time raw graph showing large changes in absorbance during the mixing phase.

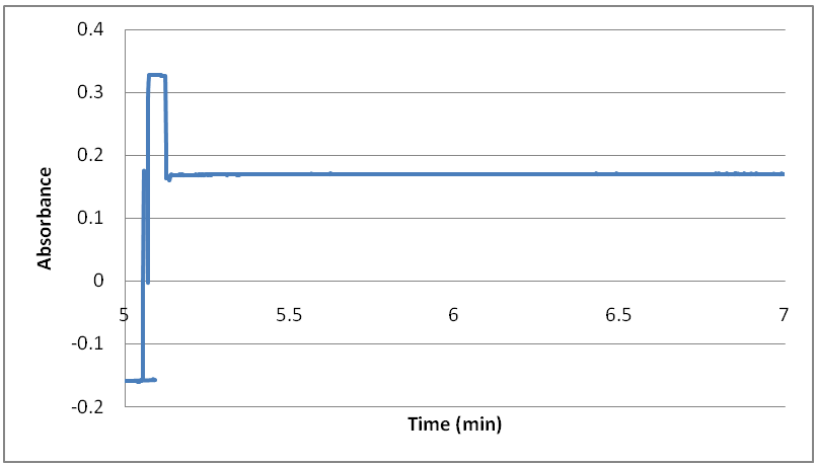

Figure 5.6. The expanded absorbance vs. time graph showing abrupt initial changes at the mixing phase.

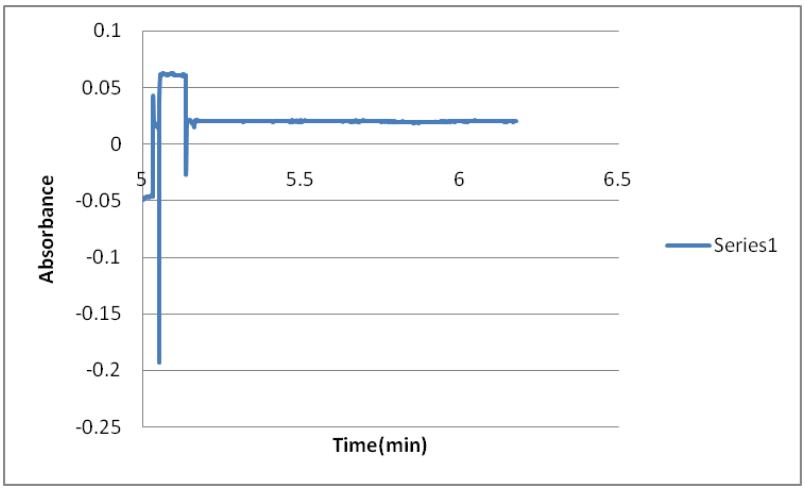

Figure 5.7. The expanded absorbance vs. time graph showing initial mixing phase in a reference experiment.

The reactions were performed under pseudo-first order conditions using an initial concentration of BNPP (10 mM) in large excess compared to the complex concentration (0.4 mM). The concentration of BNPP remains almost constant at early times of the experiment, and consumption of a small amount of BNPP does not affect the rate of reaction. The rate depends upon the metal complex concentration only, which does not change during the reaction, so that the linear slope of the A *vs.* t graphs can provide the rate of reaction.

5.2.3. Comparison of the rate of hydrolysis of bis(p-nitrophenyl)phosphate promoted by the mononuclear and dinuclear metal complexes

The rate of hydrolysis of the DNA model compound BNPP was observed using a spectrophotometer in the presence of the mononuclear Zn(II) complexes of **L2.1**, picolylamine (**pa**) and the dinuclear Zn(II) complexes of **L2.3** and **L2.4**.

The pseudo-first order rates of hydrolysis of BNPP were calculated from the slope of A *vs.* t graphs for different complexes and are given in **Table 5.1**. The solutions of both mononuclear and dinuclear complexes used in each experiment were of the same concentration. That means, solutions of the dinuclear complexes contained two times of the Zn(II) ions in comparison to those in the mononuclear complexes. To compare the rate of hydrolysis on a per zinc basis, we compared the rate of each dinuclear complex with the sum of the rates of both analogous mononuclear complexes. Adding the rates of the mononuclear complexes should give the same result as the dinuclear complex if the dinuclear complex is behaving as two independent reaction sites. **Table 5.1** includes the individual observed rates of hydrolysis of BNPP with the mononuclear and dinuclear complexes ($k_{ZnL2.1}$, k_{Znpa}, $k_{ZnL2.3}$, and $k_{ZnL2.4}$) and also the comparison of the dinuclear complexes rate with sum ($k_{ZnL2.1} + k_{Znpa}$) of the mononuclear complex rate.

$k_{ZnL2.1}$ = Pseudo-first order rate observed for hydrolysis of BNPP in the presence of mononuclear Zn(II) complex of **L2.1**

k_{Znpa} = Pseudo-first order rate observed for hydrolysis of BNPP in the presence of mononuclear Zn(II) complex of **pa**

$k_{ZnL2.3}$ = Pseudo-first order rate observed for hydrolysis of BNPP in the presence of dinuclear Zn(II) complex of **L2.3**

$k_{ZnL2.4}$ = Pseudo-first order rate observed for hydrolysis of BNPP in the presence of dinuclear nuclear Zn(II) complex of **L2.4**

*Table 5.1. Showing rate of hydrolysis of BNPP using mononuclear Zn(II) complexes of **L2.1** and **pa** in comparison to the dinuclear Zn(II) complexes of **L2.3** and **L2.4**.The rate of hydrolysis in the case of dinuclear complexes is slightly higher in comparison to the mononuclear complexes.*

Rate (s^{-1}) / pH	$k_{ZnL2.1}$	k_{Znpa}	$k_{ZnL2.3}$	$k_{ZnL2.4}$	$k_{ZnL2.1} + k_{Znpa}$	$k_{ZnL2.3} / (k_{ZnL2.1} + k_{Znpa})$	$k_{ZnL2.4} / (k_{ZnL2.1} + k_{Znpa})$
7	(4.54±0.75)E-06	(5.46±0.19)E-07	(7.82±0.37)E-06	(8.08±0.73)E-06	(5.09±0.36)E-06	1.53	1.59
7.5	(5.71±0.58)E-06	(1.66±0.16)E-06	(9.01±0.51)E-06	(2.64±0.29)E-05	(7.36±0.21)E-06	1.22	3.53
8	(7.10±0.68)E-06	(9.79±0.10)E-06	(7.17±0.96)E-05	(9.32±0.14)E-05	(1.79±0.03)E-05	4.01	5.33
8.5	(1.32±0.64)E-05	(1.46±0.10)E-06	(2.20±0.79)E-04	(1.66±0.07)E-04	(2.89±0.29)E-05	7.61	5.74
9	(4.96±0.54)E-05	(3.52±0.11)E-05	(2.74±0.87)E-04	(2.44±0.12)E-04	(8.48±0.21)E-05	3.21	2.88

Note: Average rates and standard deviations were calculated from the data sets taken from the experiments performed on different days. Data points within the experiments performed on the same day were close to each other whereas data from different days were more, different probably due variation in solution concentrations. As we were working with very dilute systems, the errors in concentration of the complexes and BNPP are more likely to happen. Also there could be some spectrophotometric instrumental error as well.

As can be seen from **Table 5.1**, the dinuclear Zn(II) complexes of **L2.3** and **L2.4** increase the rate of hydrolysis of BNPP by 1.5- to 7.6- fold at different pH values, relative to mononuclear Zn(II) complexes of **L2.1** and **pa**. These levels of rate enhancement are comparable to those observed for some low activity dinuclear complexes reported previously[57, 66, 335] where the rate of hydrolysis of the phosphate diester by the macrocyclic dinuclear Zn(II) complexes of **1.21** and **1.28** was compared with the analogous mononuclear Zn(II) complexes of **1.22** and **1.29**, respectively.

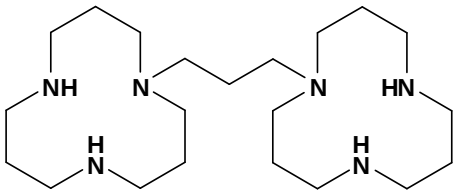

1.21

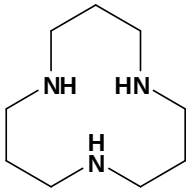

1.22

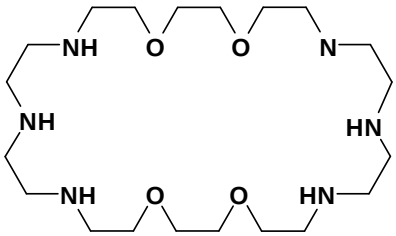

1.28

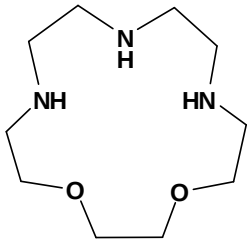

1.29

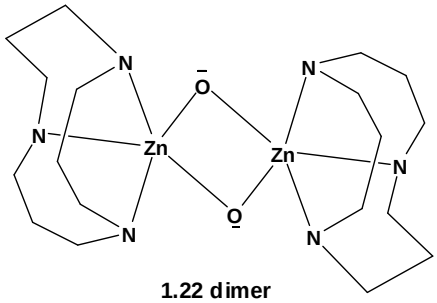

1.22 dimer

In the case of Zn(II) complex of **1.21**, the rate given in the literature[57, 335] was slightly (1.2 fold) higher than the mononuclear complex of **1.22** at pH 7, 34 °C. The rates were compared between the same metal ions concentration, which means that in terms of the number of reactive sites the rate obtained with the dinuclear complex is actually slower than that with the mononuclear complex. The low activity was attributed to two factors: first, dimerization of the complexes with dihydroxy bridging and second, a change in pK_a of the metal coordinated water.[57, 335] Due to dimer formation, no catalytic sites are available for hydrolysis.

In this case also, a complete pH-profile with the dinuclear complexes was not obtained due to precipitation at a pH higher than pH 7.2. However, the pK_a of the water molecule coordinated to the dinuclear complex was estimated to be slightly lower than 7.3 – the reported pK_a of the water molecule bound to the mononuclear complex. So it was proposed that a 1.2 fold rise in hydrolysis is merely due to lowering of the pK_a of a coordinated water molecule. This means there may be no cooperation between the metal ions in dinuclear complexes, as if there is any effect of dinuclearity on the rate of hydrolysis of phosphate diesters then the rate enhancement should have been significantly larger based on the similar previous studies.[58, 95, 96, 106]

The dinuclear Zn(II) complexes of **1.28** were almost 10 times more active than their analogous mononuclear Zn(II) complexes of **1.29** at pH 10 and 10.5, 30 °C, the rates were compared between same concentration of Zn(II) in different complexes.[66] The sigmoidal pH-rate profile curve of complexes of **1.28** and **1.29** showed that metal coordinated hydroxide were the active species for hydrolysis of phosphate diester. The pK_a of the metal coordinated water molecule in **1.28** and **1.29** was 7.6 and 8.8, respectively. Stability constants for complexes of **1.28** and **1.29** were studied potentiometrically, which showed that zinc coordinated monohydroxide and dihydroxide species form in aqueous solution. Therefore, it was possible for dinuclear species to at least double the rate enhancement in comparison to the mononuclear species at a lower pH (due to low pK_a). However in this case the actual rate enhancement by dinuclear complexes was about 10 times more than the mononuclear complexes, so it was proposed that there is some cooperation between the metal ions**.** The mechanism proposed was that two metal ions can participate in double Lewis acid activation and metal coordinated hydroxide can attack the positively charged P atom of phosphate diester simultaneously. This observation was also supported by the crystal structure where BNPP was coordinated to two zinc ions.[66]

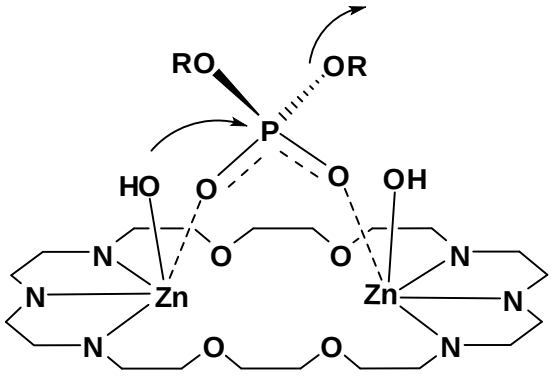

In this research, to gain some insight into the mechanisms by which the metal ions promote hydrolysis of BNPP, pH-rate profiles for mononuclear complexes of **L2.1** and **pa** as well as for dinuclear complexes of **L2.3** and **L2.4** were obtained. The pH-rate profiles for hydrolysis of BNPP in the presence of the mononuclear and the dinuclear complexes are given in **Figures 5.8** to **Figure 5.11**.

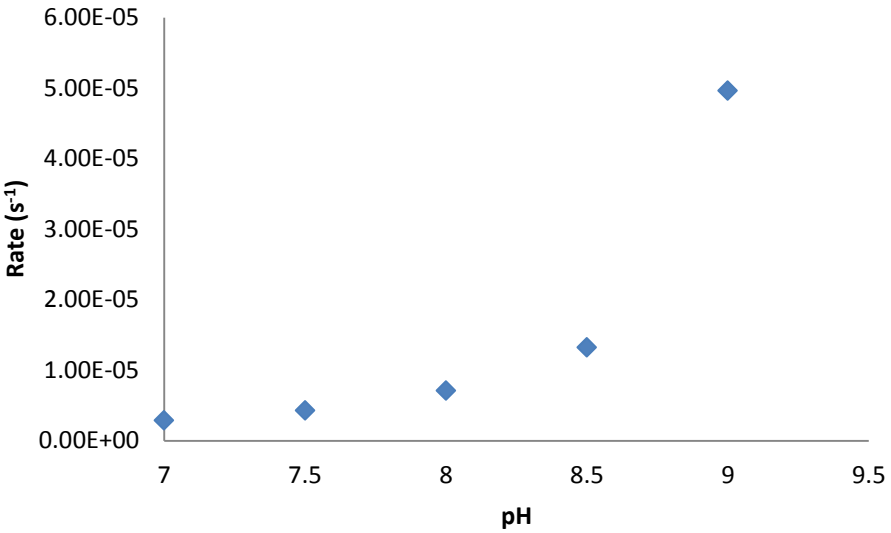

*Figure 5.8. pH-Rate profile for hydrolysis of BNPP (10 mM) using mononuclear Zn(II)-**L2.1** (0.4 mM) complex at 35 °C and I = 0.09 M $NaClO_4$ in 45% CH_3CN-5% DMF aqueous solution.*

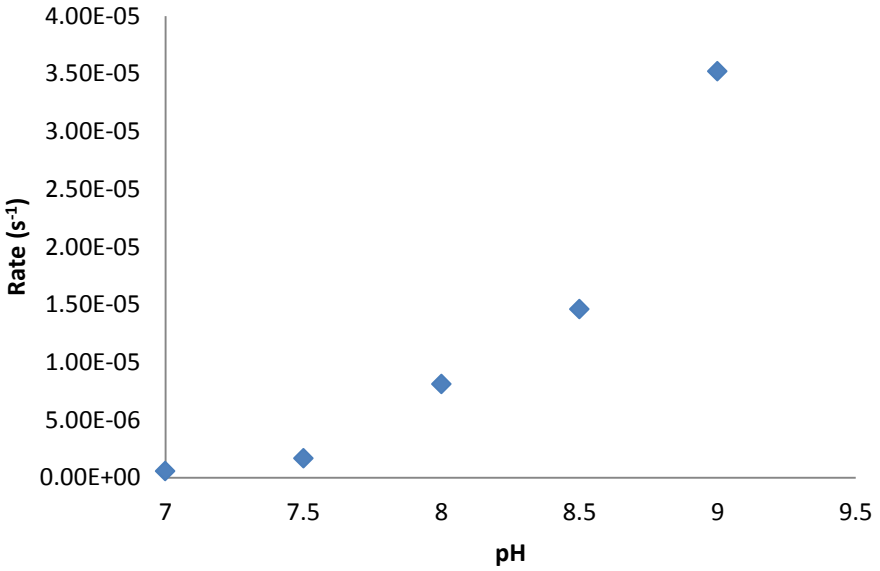

*Figure 5.9. pH-Rate profile for hydrolysis of BNPP (10 mM) using mononuclear Zn(II)-**pa** (0.4 mM) complex at 35 °C and I = 0.09 M $NaClO_4$ in 45% CH_3CN-5% DMF aqueous solution.*

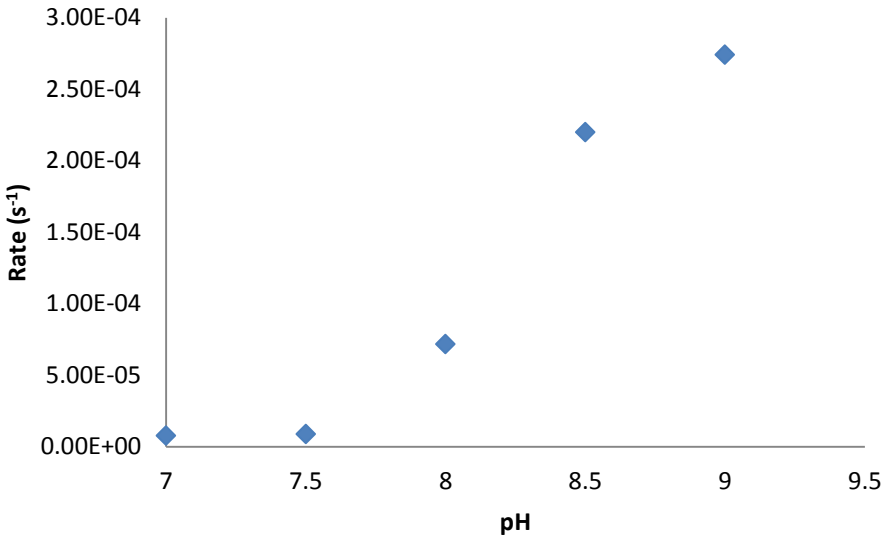

*Figure 5.10. pH-Rate profile for hydrolysis of BNPP (10 mM) using dinuclear Zn(II)-**L2.3** (0.4 mM) complex at 35 °C and I = 0.09 M $NaClO_4$ in 45% CH_3CN-5% DMF aqueous solution.*

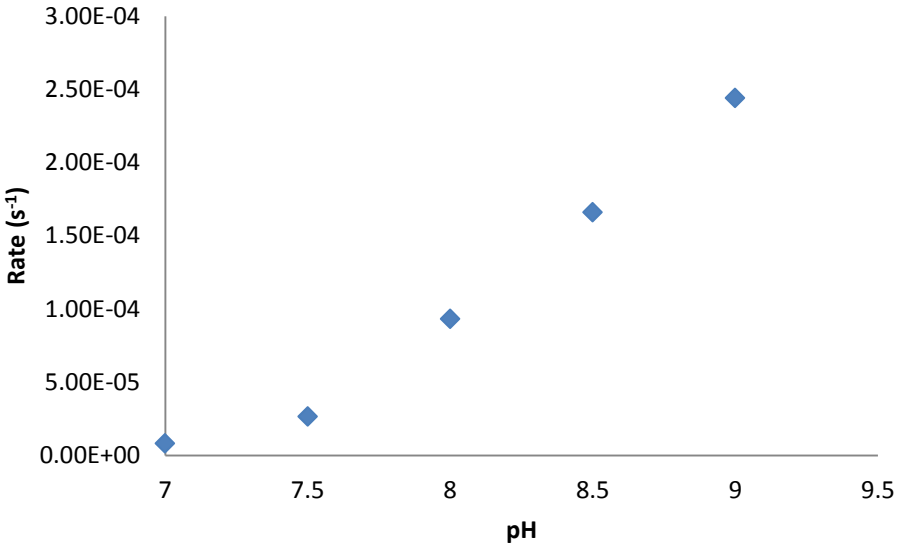

*Figure 5.11. pH-Rate profile for hydrolysis of BNPP (10 mM) using dinuclear Zn(II)-**L2.4** (0.4 mM) complex at 35 °C and I = 0.09 M $NaClO_4$ in 45% CH_3CN-5% DMF aqueous solution.*

The derived pH-rate profiles (**Figure 5.8- 5.11**) show an increase in the observed rate with the increase in pH and there is a sharp rise in rate after certain pH values. In the case of mononuclear Zn(II) complexes the sharp increase in rate occurs above pH 8.5 (**Figure 5.8** and **Figure 5.9**) and for the dinuclear complexes a sharp increase in rate occurs above pH 8 (**Figure 5.10** and **Figure 5.11**). Some precipitation was observed in the reaction mixture at pH values above 9, so it was not possible to get any reliable kinetic data beyond this pH. We believe that the derived pH-rate profiles are a portion of sigmoid functions. The sigmoid

shaped pH-rate profile curves observed in the literature are a characteristic of a kinetic process controlled by an acid-base equilibrium and which exhibit inflection points corresponding to the pK_a values for a complex. Often this pK_a is assigned to deprotonation of coordinated water molecules of the corresponding metal complexes.[53, 66, 96, 106, 273]

It was also not possible to calculate pK_a of the zinc coordinated water molecules by potentiometric titrations due to their insolubility in the aqueous solutions. So, from the pH-rate profile it can be estimated that the pK_a of the coordinated water molecule in mononuclear complexes is about 8.5 and that of dinuclear complexes is around 8 – which is lower than the mononuclear complexes. This lowering of pK_a in the dinuclear complexes can be attributed to higher charge on the metal centres.

The pH-rate profiles obtained in these kinetic experiments were similar to those found in some literature studies, so it can be concluded that the metal coordinated hydroxide is the active species which hydrolyses the BNPP.[67] The increase in rate with increasing pH means more Zn-OH^- species form in the reaction mixture. This is consistent with the observation that metal ions are more efficient promoters of hydrolysis at pH values close to their pK_a due to formation of maximum M-OH^- species. In the literature many precedents are available where metal-coordinated hydroxide ions promote hydrolysis of phosphate diesters and a sharp increase in rate occurs at the pH close to pK_a.[266, 272, 280, 320, 328, 329, 336]

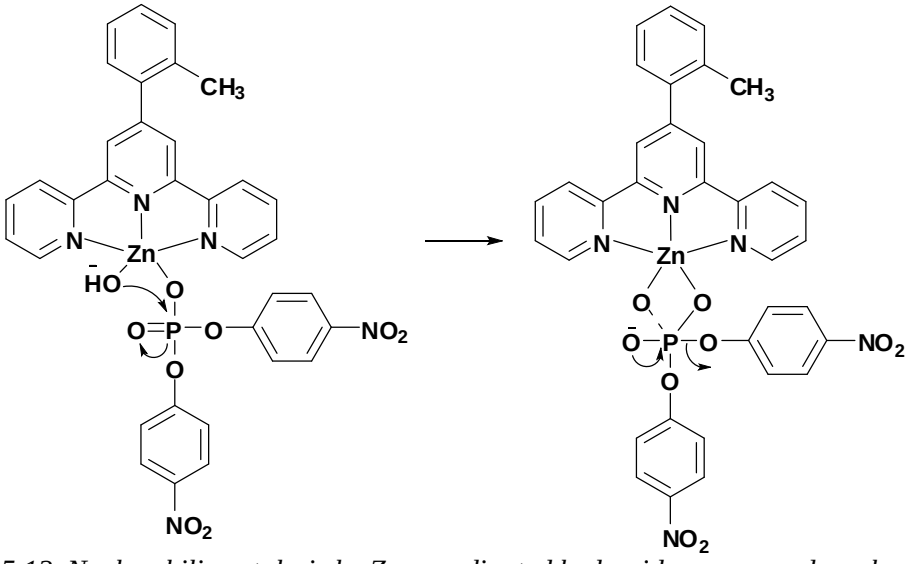

*Figure 5.12. Nucleophilic catalysis by Zn-coordinated hydroxide – proposed mechanism for hydrolysis of BNPP by mononuclear Zn(II) complex of **L2.1**.*

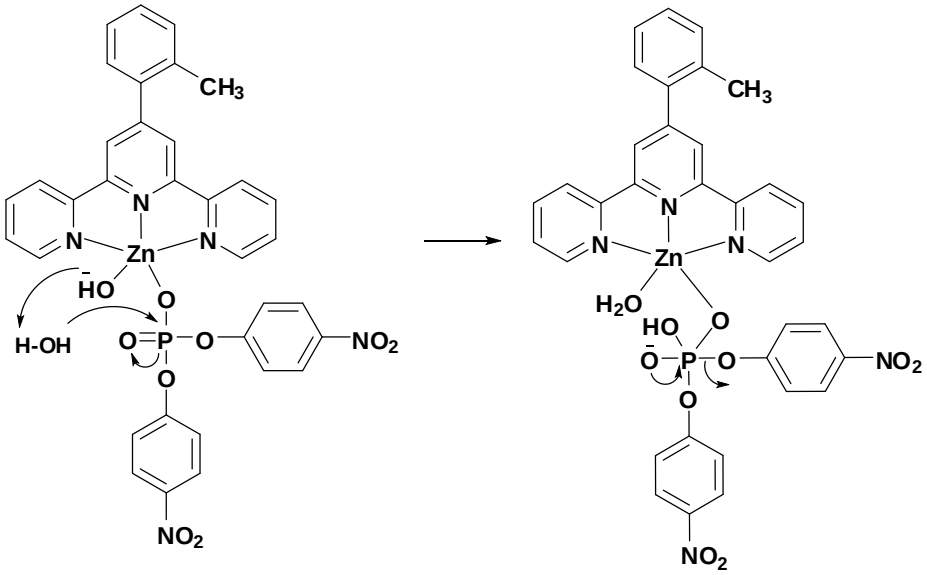

*Figure 5.13. General base catalysis by Zn-coordinated hydroxide–proposed mechanism for hydrolysis of BNPP by mononuclear Zn(II) complex of **L2.1**.*

The kinetics data in **Table 5.1** show that the rate of hydrolysis of BNPP in the case of dinuclear complexes is slightly higher (1.5- to 7.6- fold at different pH values) than that of the mononuclear complexes. The rates are compared on a per Zn basis. If a dinuclear complex behaves as two independent reaction sites, addition of the rates by the corresponding mononuclear complexes should be equal to that of the dinuclear complex. Based upon on the results, this slight rate enhancement in dinuclear complexes could be either due to a small extent of cooperation between the metal ions or that could be due to lower pK_a of the coordinated water molecules in dinuclear complexes.

According to some literature studies, the rate enhancement by dinuclear species could be upto 70- to 600- fold if there is proper cooperation between two metal ions.[58, 95, 96, 106] For the dinuclear Zn(II) complexes of **L2.3** and **L2.4** the rate enhancement is only slightly larger than that due to the corresponding mononuclear complexes. This means there could be some or no cooperation between the metal ions in dinuclear complexes studied here.

However, the rate enhancement is not very high by dinuclear complexes, which may mean there is no cooperation between the metal ions, and the rate enhancement could only be due to lowering of the pK_a of the water molecules coordinated to metal centre in the dinuclear complexes.

5.3. Substrate (BNPP) Coordinated Cu(II) Complexes

Hydrolysis of BNPP in the presence of Cu(II) complexes was not measurable due to some precipitate formation during the experiments. In the case of Cu(II) complexes of **L2.3** or **L2.4**, a bluish white precipitate was obtained from the turbid reaction mixture, but it was not possible to characterise the precipitate due to its insolubility in common solvents. However, formation of the bluish colour precipitate may indicate some Cu(II) complex was formed after addition of BNPP.

The Cu(II) complexes of **L2.1** also produced some bluish white precipitate during BNPP hydrolysis studies. In this case, the precipitate was recrystallised from DMF/acetonitrile mixture by vapour diffusion of diethyl ether. The crystal analysis revealed formation of complex **5.1** discussed in the next section. Similar complexes were crystallised in a previous kinetic study of hydrolysis of BNPP in the presence of the Cu(II) complex of 2,2':6',2''-terpyridine (tpy). In that study, the Cu(II) complexes show no hydrolysis of BNPP at pH 7 and [Cu(tpy)(BNPP)Cl] crystallises from the solution.[92] In another literature study an enhanced rate of BNPP hydrolysis was observed with Cu-terpyridine complexes at pH 10.5 (pK_a 7.98) in 75% ethanol solution.[93]

*5.3.1. [Cu(**L2.1**)(BNPP)Cl] – Complex **5.1***

As mentioned above, the crystals of complex **5.1** were obtained from recrystallisation of the precipitates from a kinetics experiment, where 1 eq. of $CuCl_2 \cdot 2H_2O$ was mixed with 1 eq. of **L2.1**, followed by addition of the HEPES buffer (pH 7) and BNPP. The precipitate formed was recrystallised by vapour diffusion of diethyl ether into the filtered DMF/acetonitrile solution of the precipitate and a small yield of blue crystals was obtained. Later, a high yield of the same crystals was obtained by mixing $CuCl_2 \cdot 2H_2O$ with **L2.1** and aqueous BNPP at approximate pH 7.5. Vapour diffusion of diethyl ether to the resulting solution produced blue X-ray quality crystals within a period of 3 weeks.

The crystal structure was solved and refined in the triclinic space group $P\bar{1}$ with an R-factor of 3.80%. Each complex contains a copper-bound ligand **L2.1**, one copper-bound

chloride ion, and one coordinating ligand BNPP (**Figure 5.14**). The Cu(II) ion occupies a five-coordinate geometry that lies between the ideal trigonal bipyramidal and square pyramidal geometries with a τ value of 0.052, close to square pyramidal geometry (angle α, N2-Cu1-O1 is 155.46° and the angle β, N3-Cu1-N1, is 158.59°).

Three terpyridine nitrogen atoms and a chloride ion are located at the base of the square pyramidal geometry. The axial position of the geometry is occupied by oxygen atom of the substrate BNPP. Although both oxygen atoms of BNPP that are not involved in ester linkages are equivalent, only one is coordinated to the copper ion.

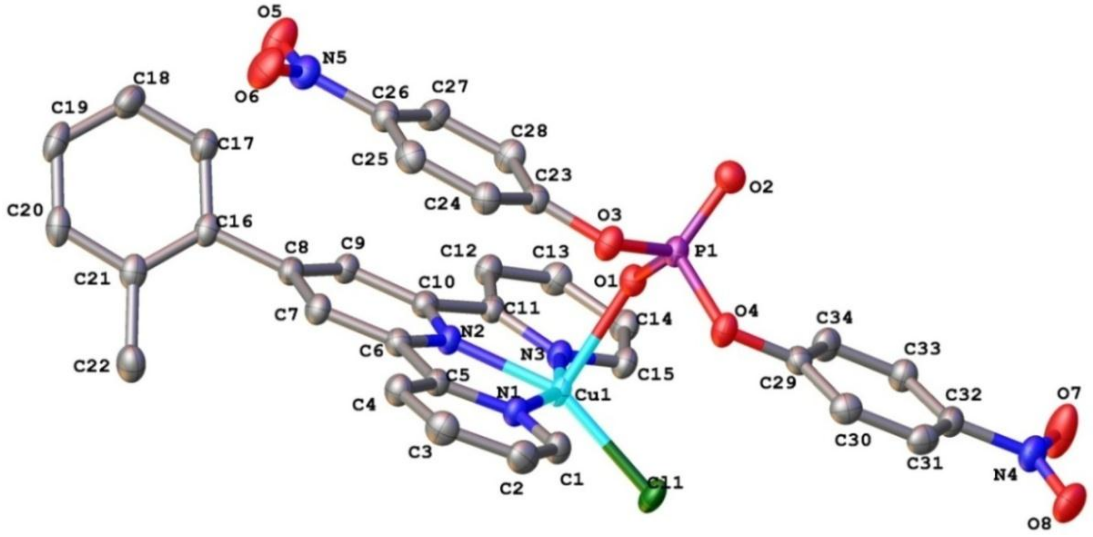

*Figure 5.14. The crystal structure of [Cu(**L2.1**)(Cl)(BNPP)] complex. Hydrogen atoms have been omitted for clarity. The selected bond lengths and bond angles are given in Appendix III, Table A29.*

The structure follows the trends observed in a number of other five-coordinate nearly square pyramidal terpyridine-copper complexes reported in literature.[85, 172, 215, 337] The Cu-N1 and Cu-N3 bonds are slightly longer than the Cu-N2 bond by 1.0 Å and 0.07 Å, respectively. The axial Cu1-O1 bond is nearly 0.2 Å longer than a normal Cu-O bond, 2.159 Å *versus* 1.95 Å. The bond lengths and bond angles in copper coordination site are similar to those in terpyridine-Cu(II) complexes with coordinated BNPP and DPP (di-phenylphosphate ester) reported previously. The literature crystal structures [Cu(tpy)(BNPP)Cl] and [Cu(tpy)(DPP)] are very similar to each other, and the metal-ligand coordination sphere is also very similar to complex **5.1**, however the literature complexes differ from **5.1** in terms of orientation of BNPP. In these literature complexes, only one phenyl ring of BNPP and DPP lies in plane of terpyridine for intramolecular π-π stacking with one terminal ring of the ligand. In **5.1**, both *p*-nitrophenyl rings of BNPP lie in plane with the central ring of terpyridine-type unit. The

packing diagram (**Figure 5.15**) shows how all of the terpyridine-type and BNPP aromatic rings are involved in inter- and intra- molecular π-π stacking. The aromatic hydrogen atoms are involved in short contacts with oxygen, chlorine and nitrogen atoms but no hydrogen bonding interactions are available.

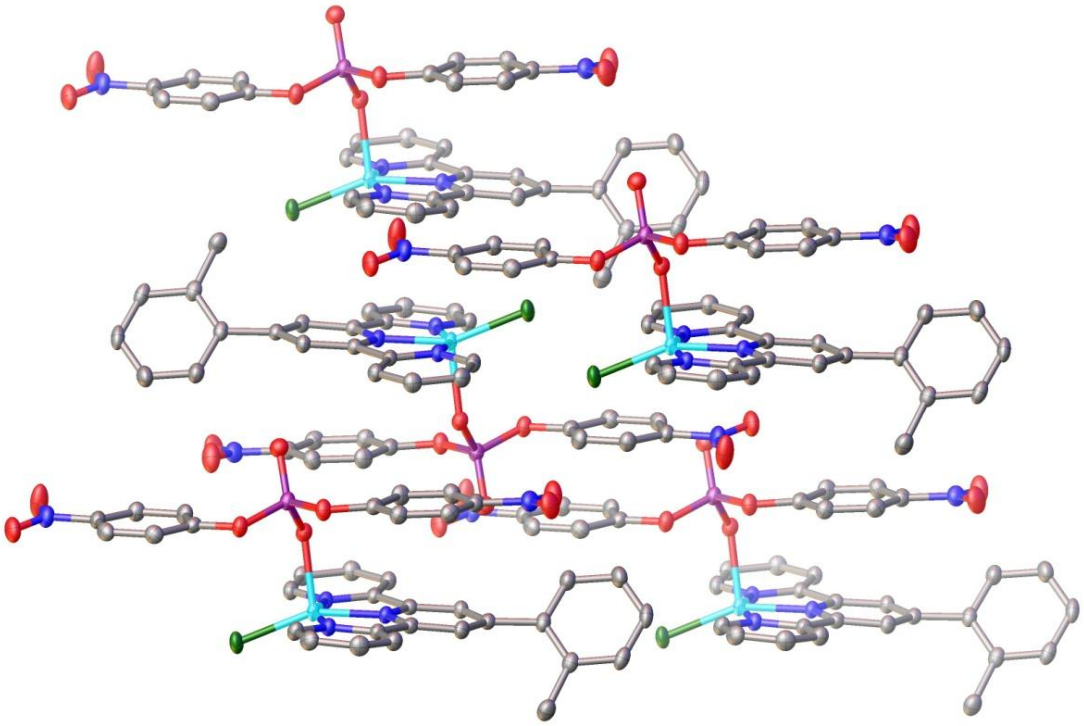

Figure 5.15. Packing diagram showing inter- and intra- molecular π-π stacking between terpyridine-type and BNPP rings.

*5.3.2. [Cu(**L2.1**)(BNPP)(H_2O)]PF_6·0.4H_2O – Complex **5.2***

Complex **5.2** was prepared by addition of hexafluoridophosphate ions into the reaction mixture of complex **5.1**. A few drops of aqueous ammonium hexafluoridophosphate solution were added to the blue solution of **5.1**, and resulted in formation of a green precipitate. The precipitate was dissolved in acetonitrile and slow evaporation over a period of two weeks produced pale green blocks of X-ray quality crystals.

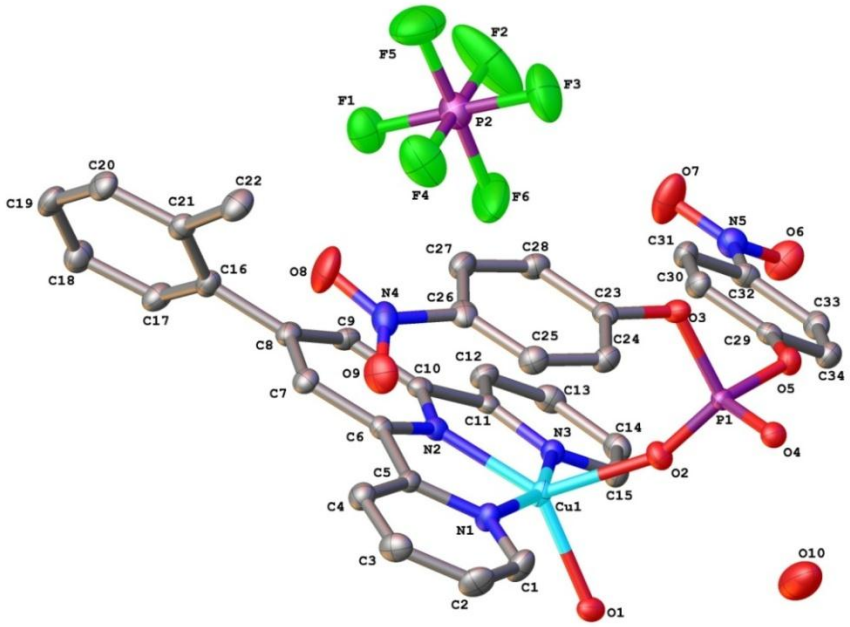

*Figure 5.16. The crystal structure of complex **5.2**, [Cu(**L2.1**)(BNPP)(H_2O)]PF_6·0.4H_2O. The hydrogen atoms have been omitted for clarity. The selected bond lengths and bond angles are given in Appendix III, Table A30.*

The solid state structure of the complex was solved and refined in the orthorhombic space group $P2_12_12_1$ with an R-factor of 2.60%. Each complex contains one **L2.1** ligand, one Cu(II) ion coordinated in the tridentate terpyridine binding site of **L2.1**, Cu(II) coordinated water and BNPP, and a non coordinating hexafluoridophosphate ion, as shown in **Figure 5.16**. A small electron density peak located near the copper centre was modelled as 40% occupancy oxygen presumably part of a water molecule. No residual electron density peaks for hydrogen atoms were found in the electron density map, so oxygen was modelled as an isolated atom without any hydrogen atoms.

The Cu(II) ion occupies a five-coordinate geometry that lies between the square pyrdamial and trigonal bipyramidal with τ value of 0.31 with β (N3-Cu1-N1) and α (N2-Cu1-

O1) of 160.2° and 141.44°, respectively. Three terpyridine nitrogen atoms, one BNPP and a water molecule make the five-coordination sphere of Cu(II). In comparison to **5.1**, the chloride ion in this complex has been replaced with a water molecule in the presence of an excess of non-coordinating hexafluoridophosphate ions. The difference in packing of the molecules in **5.2** from that in **5.1** appears to be due to addition of the non-coordinating hexafluoridophosphate ion and hydrogen bonded water molecules.

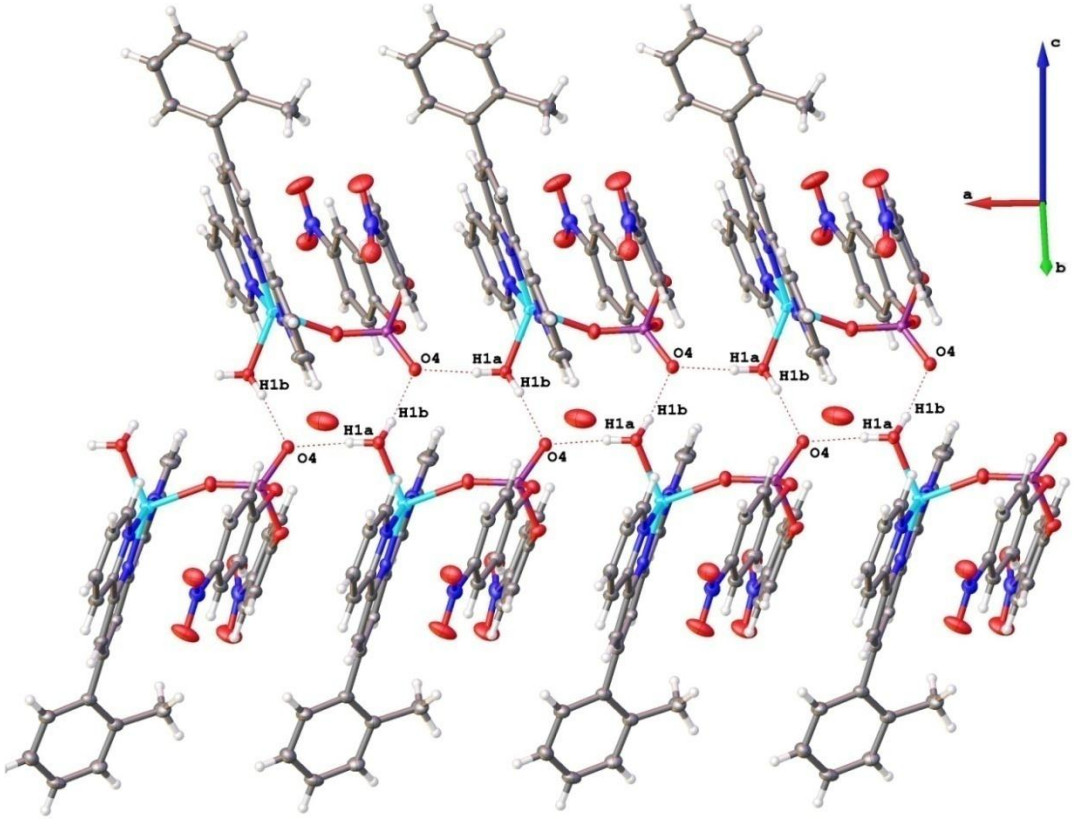

*Figure 5.17. Packing diagram of complex **5.2**, showing inter- and intra- molecular π-π stacking along with hydrogen bonding interactions.*

Molecules in the crystal lattice are packed efficiently both *via* inter- and intra-molecular π-π stacking and the hydrogen bonding interactions. The oxygen atoms of BNPP which are not involved in ester linkage are inequivalent, one is coordinating to copper and the other, O4, is involved in double hydrogen bonding interactions with hydrogen atoms of water in adjacent molecules, **Figure 5.17**. The hydrogen bonds O4···H1a-O1 and O4···H1b-O1 are 1.815(2) Å and 1.844(2) Å, respectively.

5.4. Conclusion

The Zn(II) dinuclear complexes were synthesised using polydentate ligands **L2.3** and **L2.4**. The X-ray crystal structures of such Zn(II) complexes are discussed in Chapter 4, which confirms the five-coordinate trigonal bipyramidal geometries of the terpyridine and bis-picolylamine binding sites, and four-coordinate tetrahedral geometry of the picolylamine-binding site. Two positions on each metal ion are occupied by exchangeable chloride ligands in their solid structures. These chloride ions can be replaced by water or hydroxide ions in aqueous solutions. This structural information was then used to rationalise the ability of these complexes to carry out hydrolysis of the phosphate diesters.

This chapter describes the studies of the kinetics of hydrolysis of the phosphate diester compound BNPP in the presence of dinuclear Zn(II) complexes of **L2.3** and **L2.4**. The rates were compared with corresponding mononuclear Zn(II) complexes of **L2.1** and **pa**. The pseudo-first order rate of hydrolysis of BNPP was calculated from the slope of absorbance *versus* time graphs measured using a spectrophotometer. The kinetics data shows a slight increase in the rate of hydrolysis of BNPP in case of dinuclear complexes (1.5- to 7.6- fold at different pH values) compared to the mononuclear complexes, **Table 5.1**.

The derived pH-rate profiles show an increase in the observed rate of hydrolysis with the increase in pH, with sharp rise in rate after certain pH values. In the case of the mononuclear complexes, the sharp rise was at pH 8.5 and that in case of dinuclear complexes was at pH 8.0, **Figure 5.8** to **Figure 5.11**. The portion of sigmoid shaped pH-rate profile curves observed were interpreted as being characteristic of a kinetic process controlled by an acid-base equilibrium, which exhibit inflection points corresponding to the pK_a values for a complex. Since the rate enhancement by the dinuclear complexes over the mononuclear complexes was not too high, based on literature we concluded that there is slight or no effect of dinuclearity on the rate of hydrolysis. This level of rate enhancement may be due to lowering of pK_a of metal coordinated hydroxide species in dinuclear complexes.

The kinetics of hydrolysis in the presence of Cu(II) ions was not successful due to some precipitation. However, formation of the complexes [Cu(**L2.1**)(Cl)(BNPP)], **5.1** and [Cu(**L2.1**)(BNPP)(H_2O)]PF_6·0.4H_2O , **5.2** shows that substrate BNPP binds to the metal centre in these complexes.

CHAPTER 6

DELIBERATE BOXES AND ACCIDENTAL WHEELS

6.1. Introduction

The novel 2,2′:6′,2″-terpyridine–picolylamine-based bridging ligand, **L2.3**, has been synthesised and fully characterised using a variety of techniques including single crystal X-ray diffraction (Chapter 2). As shown in **Figure 6.1**, the ligand has two metal binding sites: the tridentate terpyridine-type (Head) and the bidentate picolylamine-type (Tail). The coordination properties of such terpyridine and picolylamine ligands are discussed in previous chapters. Both of these ligands can adopt different coordination modes depending upon the metal ion, anions, solvent and the reaction conditions used.[71, 88, 89, 176, 209, 241, 253, 258, 259, 300, 301, 306, 308] Some of the common binding modes are shown in **Figure 6.2**.

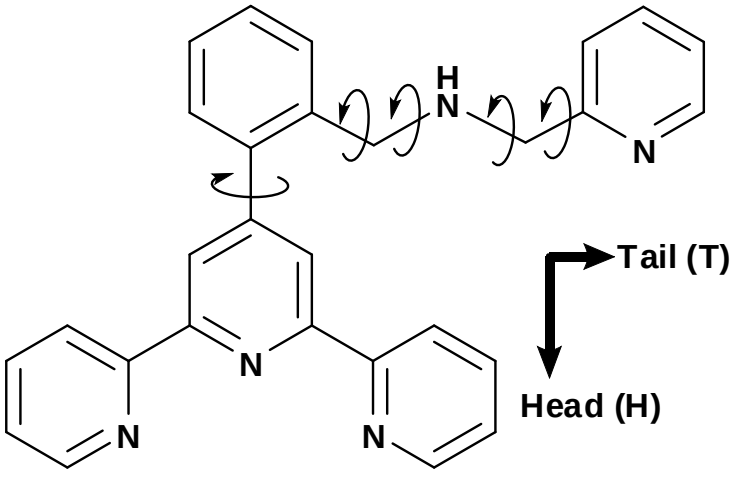

L2.3

*Figure 6.1.The polydentate ligands **L2.3** with terpyridine-type and picolylamine-type metal binding domains, denoted as head and tail using the bold arrows. Flexibility of the tail groups to twist around C-N and C-C bonds is represented with the curved arrows.*

In **L2.3**, both metal binding sites are available for coordination with various metal ions adopting different coordination modes, as shown in **Figure 6.2**. A range of dinuclear Zn(II) and Cu(II) complexes (M_2**L2.3**) were synthesised and characterised (Chapter 4), where both the binding sites coordinate with metal ions, as illustrated in **Figure 6.2(a)** and **(b)**. The crystal structures of the dinuclear complexes demonstrate that **L2.3** has the potential to adopt different orientations due to the flexibility of the C-N_{amine}-C and C-C bonds shown in **Figure 6.1**. In the dinuclear metal complexes the ligand acts as a bridging ligand between two metal ions.

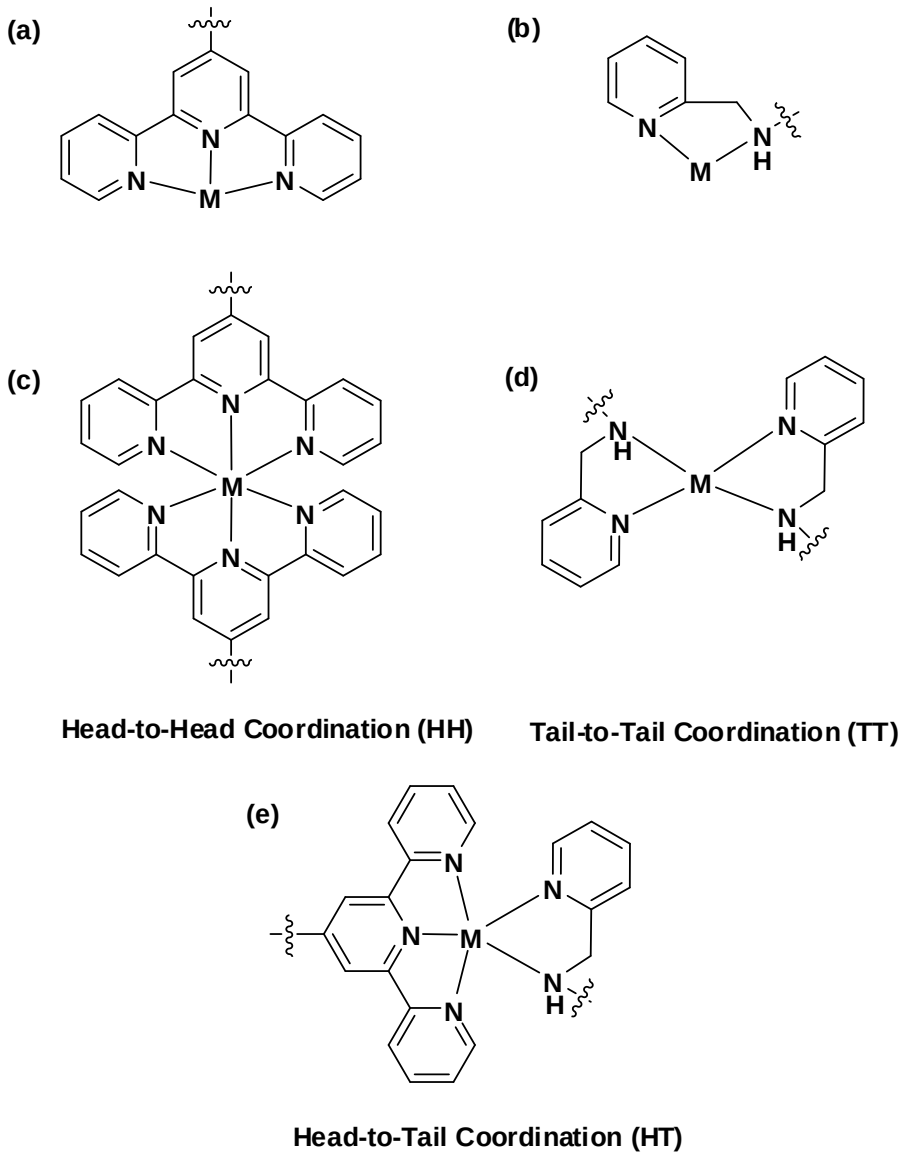

Figure 6.2. The most common coordination modes of terpyridine and picolylamine ligands metal complexes containing picolylamine- and terpyridine-type ligands. The complexes discussed in this chapter adopt (c), (d) or (e) coordination mode to produce large supramolecular assemblies.

In this chapter we report systems which combine the structural and reactive sites of the dinucleating terpyridine-picolylamine ligand (**Figure 6.1**) with the coordination preferences and flexibilities of particular divalent metal ions to form a series of closely related box structures in a deliberate fashion. The ligand also produces unprecedented decanickel wheel complexes, in what is a more serendipitous outcome.

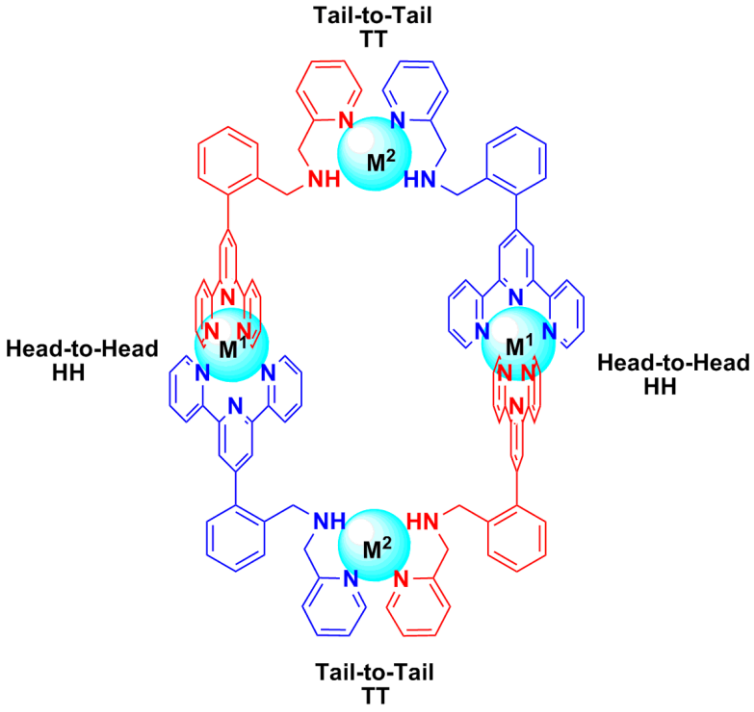

*Figure 6.3. Schematic representation of the HH-TT-HH-TT coordination mode in box shaped complexes of **L2.3**.*

This chapter is divided into two main sections – the first on boxes and the second on wheels. In each section, individual crystal structures are discussed in detail followed by overall discussion of the chemistry involved in formation of these remarkable supramolecular assemblies. In the case of boxes, spectrophotometric studies are also discussed, including those of Job's method of continuous variations.

Tetranuclear box shaped complexes, $[M^1_2M^2_2(\mathbf{L2.3})_4]$ were synthesised by using known octahedral and flexible metal coordination geometries. The boxes form through HH-TT-HH-TT coordination mode as illustrated in **Figure 6.3**. In this case one metal ion binds between two terpyridine-type sites *via* Head-to-Head (HH) binding at the metal, and the second metal ion binds between the picolylamine-type binding sites *via* Tail-to-Tail (TT) binding.

The decanuclear wheel shaped complexes $Ni_{10}(\mathbf{L2.3})_{10}$ form through $(HT)_{10}$ coordination mode, where ten Ni(II) ions bind between the tridentate and the bidentate binding sites of ten **L2.3** ligands and assemble themselves in a remarkable wheel shape.

6.2. The Tetranuclear Boxes – HH-TT-HH-TT Coordination Mode

6.2.1. Synthesis and Crystal Structures

6.2.1.1. $[Fe_2Zn_2(\mathbf{L2.3})_4Cl_2](PF_6)_6 \cdot 4H_2O$ – Complex **6.1**

The box complex $[Fe_2Zn_2(\mathbf{L2.3})_4Cl_2]^{6+}$, **6.1**, was synthesised by mixing one equivalent of a methanolic solution of $FeCl_2 \cdot 2H_2O$ with two equivalents of **L2.3** in chloroform. The resulting purple solution of the complex was treated with one equivalent of $ZnCl_2 \cdot 2H_2O$. An excess of aqueous ammonium hexafluoridophosphate solution was added for precipitation of the complex. The dark purple precipitate was collected and dissolved in acetonitrile. Small purple plate shaped X-ray quality single crystals were collected, following vapour diffusion of ethyl acetate into the acetonitrile solution, with 60% yield.

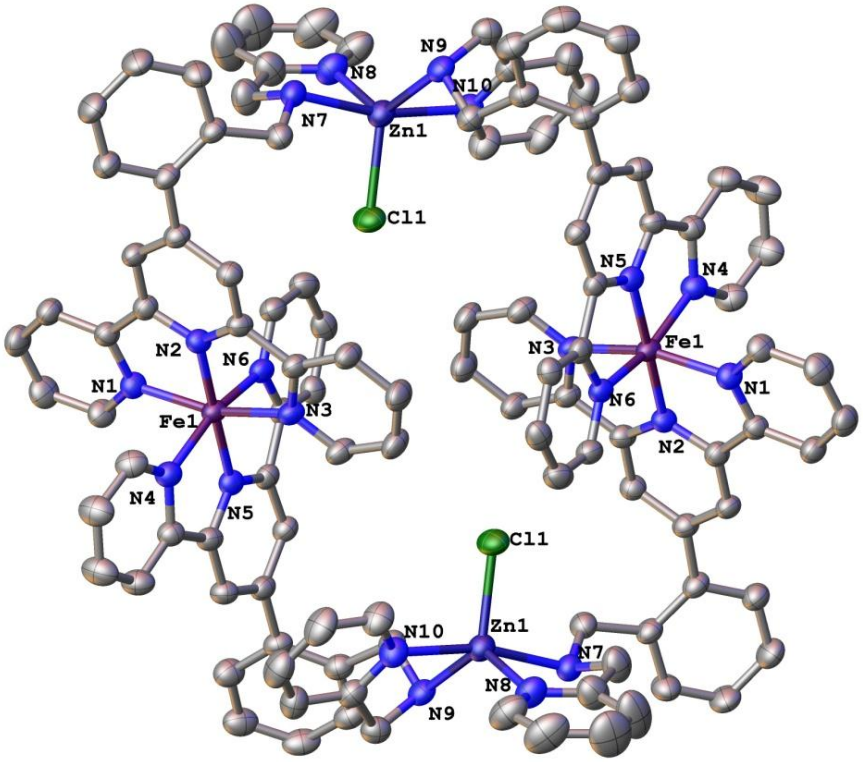

Figure 6.4. The crystal structure of $[Fe_2Zn_2(\mathbf{L2.3})_4Cl_2](PF_6)_6 \cdot 2H_2O.CH_3CH_2COOCH_3$. The PF_6 ions, the hydrogen atoms, and the solvents- water and ethyl acetate have been omitted for clarity. The selected bond lengths and bond angles are given in Appendix III, Table A31.

The X-ray crystal structure of **6.2** reveals formation of a di-iron, di-zinc box shaped complex cation, $[Fe_2Zn_2(\mathbf{L2.3})_4]^{6+}$ (**Figure 6.4**). The crystal structure was solved in the triclinic space group $P\bar{1}$ with an R-factor 5.36%. The overall cation and the anions were well ordered but all the solvent molecules were significantly disordered. Due to low electron

density peaks available, one low occupancy ethyl acetate was refined to 30%, 30%, 20% and 20% at four different positions. Two water molecules were also disordered and modelled by refining the occupancies to 50% over four different positions. The half occupancy water molecules were refined without any hydrogen atoms because of insufficient electron density located around the donor atoms to locate hydrogen atoms.

In the $[Fe_2Zn_2(\mathbf{L2.3})_4Cl_2]^{6+}$ complex cation, each Fe(II) coordinates to two **L2.3** ligand molecules through their terpyridine-type nitrogen atoms *via* head-head binding. The six-coordinate Fe(II) ions occupy a distorted octahedral geometry, where the two ligands are arranged in the classic bis(terpyridine) meridional fashion. Two Fe(**L2.3**)$_2$ units bind to two Zn(II) ions in tail-to-tail coordination mode through their picolylamine-type nitrogen atoms, resulting in formation of the box shaped complex **6.1**. The Zn(II) ions occupy a geometry intermediate between trigonal bipyramidal and square pyramidal geometry with a τ value of 0.67. The zinc coordinated Cl^- ions point inside the cavity which is hydrophobic in character, due to the aromatic groups that make up the ligands. The Zn1-Zn1 distance is 11.6574(12) Å and the Cl1-Cl1 atoms are 7.449(5) Å apart from each other. The Fe1-Fe1 distance is 9.3708(10) Å.

The asymmetric unit of complex **6.1** consists of exactly one half of the molecule. Both halves of the molecule are related to each other through an inversion centre at the mid-point of the assembly. The molecules in the crystal lattice are packed by a number of atomic interactions such as hydrogen bonding, π-π stacking and other short contacts. The terpyridine rings of all four **L.23** ligands are stacked parallel to the opposite rings at distances 4.9697(7) Å and 8.349(3) Å (**Figure 6.5 top**).

The fluorine atoms of hexafluoridophosphate ions make multiple hydrogen bonds with the hydrogen atom of the secondary amines. The amine hydrogen atom interacts with two to three fluorine atoms ranging from 2.134(9) Å to 2.580(7) Å with a shortest F···N distance of 3.003(4) Å. The molecules are stabilised by various other weak inter- and intra-molecular short interactions between the solvent molecules, anions and aromatic hydrogen atoms such as N···H-C, F···H-C and Cl···H-C ranging from 2.266 Å to 3.164 Å as shown in (**Figure 6.5 bottom**).

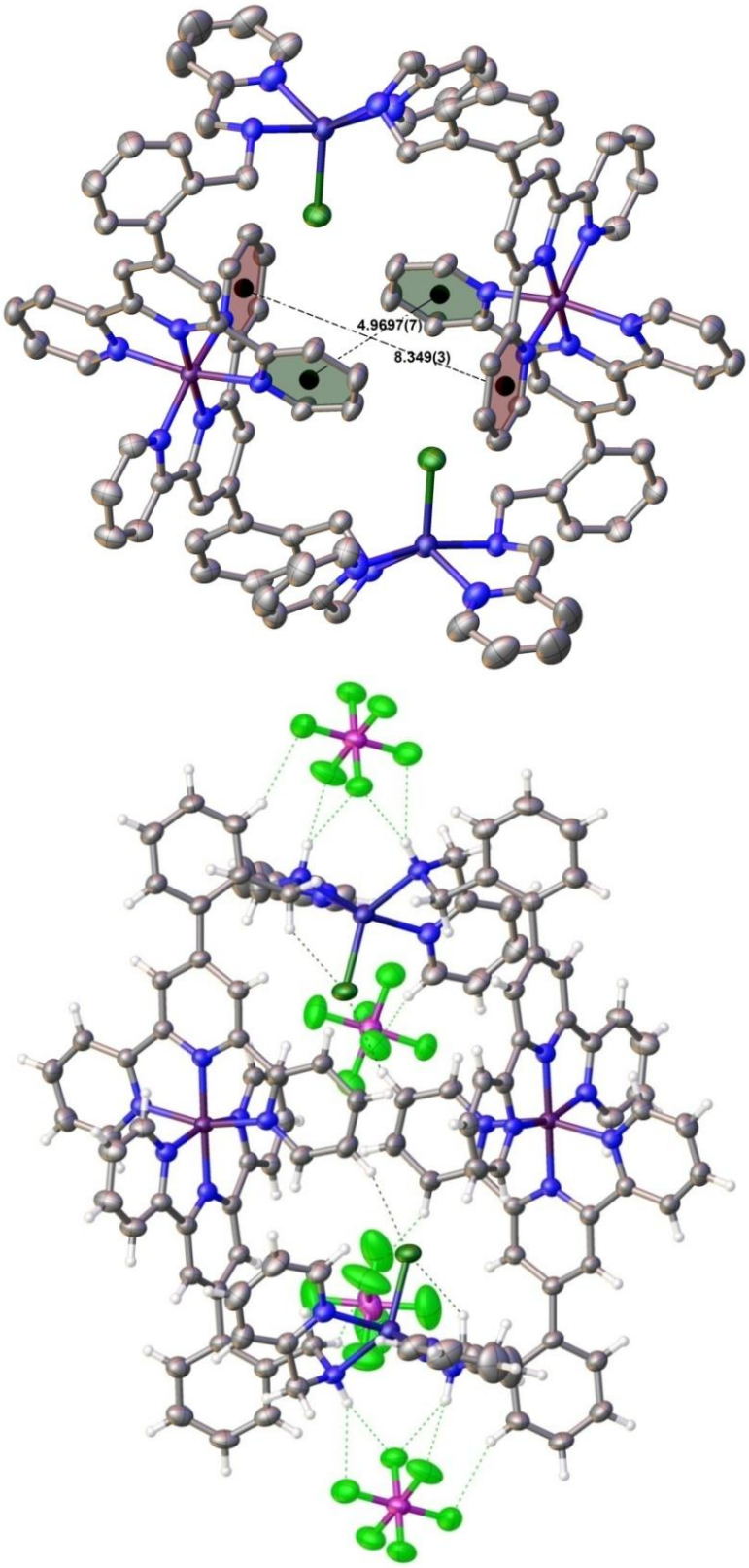

Figure 6.5. The diagram showing terpyridine rings stacking (top) and Cl···H-C, F···H-N, F···H-C interactions (bottom) which hold the boxes together in the crystal lattice. Some anions, hydrogen atoms and solvent molecules are omitted for clarity.

*6.2.1.2. [Zn_4(**L2.3**)$_4$($CH_3COO)_2$]($PF6)_6$·2CH_3CN – Complex **6.2***

The complex **6.2** was prepared in a similar way as **6.1** by using $Zn(CH_3COO)_2.2H_2O$ and **L2.3** followed by ammonium hexafluoridophosphate resulting in formation of a white precipitate. The slow diffusion of di-isopropyl ether into the acetonitrile solution produced X-ray quality single crystals of complex **6.2**.

The X-ray crystal structure of **6.2**, a tetra zinc box shaped complex, $[Zn_4(\mathbf{L2.3})_4(CH_3COO)_2]^{6+}$ is shown in **Figure 6.6**. The crystal structure was solved in monoclinic space group *C*2/c to an R-factor of 7.07%. It is similar to that of **6.1**, except the presence of two coordinated acetate ions instead of the chloride ions.

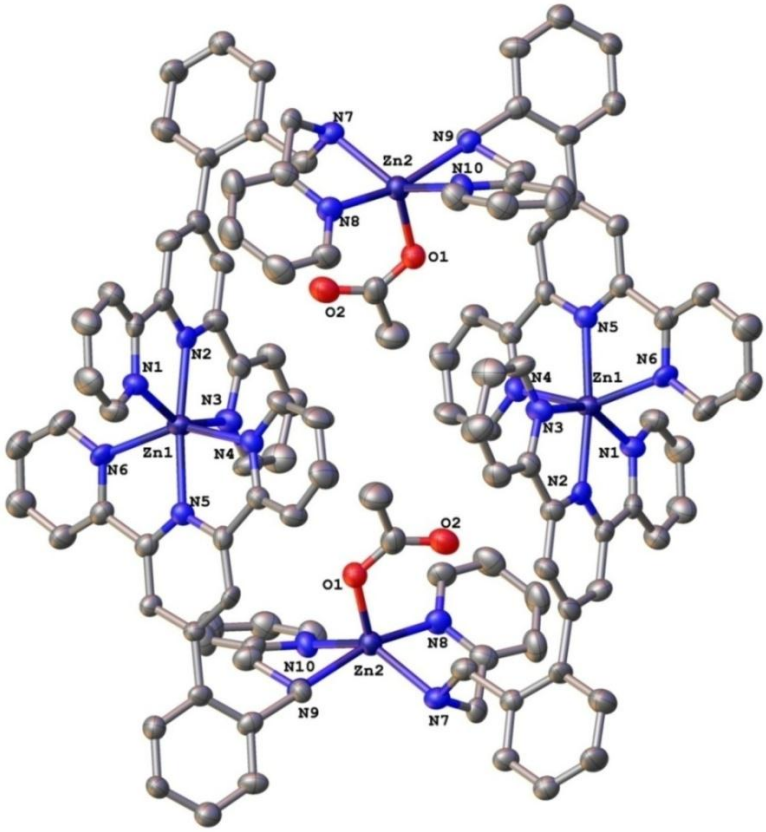

*Figure 6.6. A view of the molecular structure of [Zn_4(**L2.3**)$_4$($CH_3COO)_2$]($PF_6)_6$·2CH_3CN. The hydrogen atoms, PF_6 ions and the solvent molecules have been omitted for clarity. The selected bond lengths and bond angles are given in Appendix III, Table A32.*

The structures of the complex cation and anions were well ordered but some residual electron density peaks were apparent in the electron density map. Due to reduced occupancy and poor ordering it was not possible to model the residual electron density peaks any more. The disordered and diffused peaks were masked using the 'solvent mask' option in Olex2,

which only reduced the R-factor to 7.02% from 7.07%. A solvent void of 173 $Å^3$ containing 10.5 electrons was calculated, which indicates the presence of some low occupancy solvent molecules similar to the previous complex.

Each of the four Zn(II) ions bridges between two ligands through HH or TT bridging. Both the Zn1 ions bind in terpyridine-type sites (Head) of two **L2.3** ligands in six-coordinate distorted octahedral geometry, resulting in formation of the bis-terpyridine type Zn(**L2.3**)$_2$ geometry. The Zn2 ions link the picolylamine-type binding sites of two Zn(**L2.3**)$_2$ geometries occupying five-coordinate geometries. Both five-coordinate geometries are intermediate between the square pyramidal and trigonal bipyramidal geometries with a τ value of 0.42. The acetate ions act as monodentate ligands and bind the fifth position of both the five-coordinate geometries.

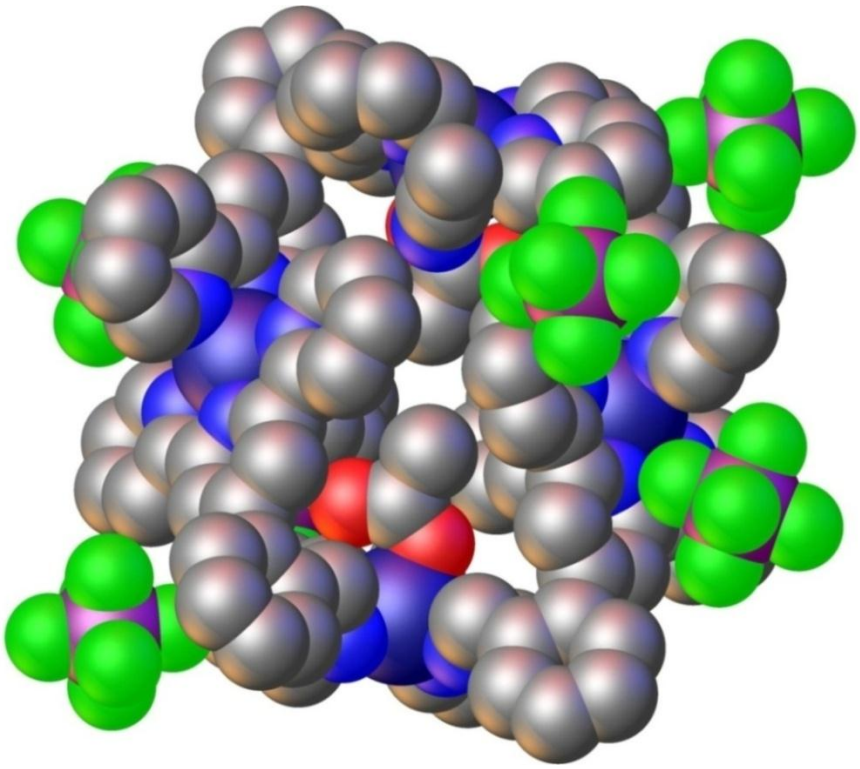

*Figure 6.7. Space-fill model of the complex **6.2**, the side view showing the empty space inside the ring. The hydrogen atoms have been omitted for clarity.*

The Zn2 coordinated acetate ions point inside the cavity in a hydrophobic, aromatic environment. The distance between the coordinating oxygen atoms is 8.171(10) Å. The distance between two Zn1 atoms coordinated to the terpyridine binding sites is 9.678(2) Å. The Zn2-Zn2 distance is 11.878(2) Å and the sp^3 carbons (methyl) of two acetate counter-ions are 3.781(16) Å apart from each other. There is no other solvent molecule or anion

present in the cavity, other than coordinated acetate ions as shown in the space-filling model of **6.2** in **Figure 6.7**.

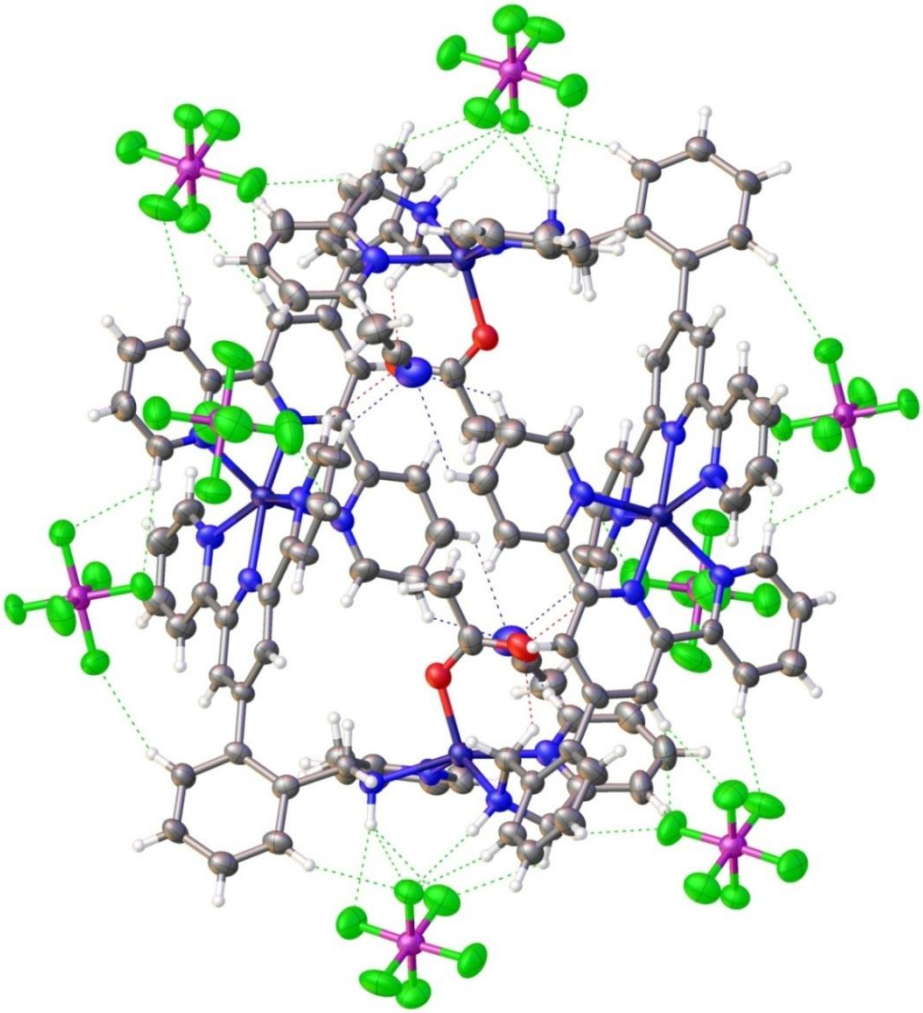

*Figure 6.8. The packing structure of complex **6.2** showing hydrogen bonding and other short contacts.*

The crystal packing of **6.2** is shown in **Figure 6.8** and is similar to that seen in **6.1**. The fluorine atoms of the PF_6 ions participate in multiple hydrogen bonding interactions through hydrogen atoms of the secondary amines. The multiple F···H-N bonds range from 2.101(4) Å to 2.531(4) Å. The terpyridine rings of the opposite ligands within a box are stacked parallel to each other at 3.925(4) Å and 7.284(6) Å.

*6.2.1.3. $[Fe_2Zn_2(\mathbf{L2.3})_4(C_8H_4O_4)]\ (PF_6)_6$ – Complex **6.3***

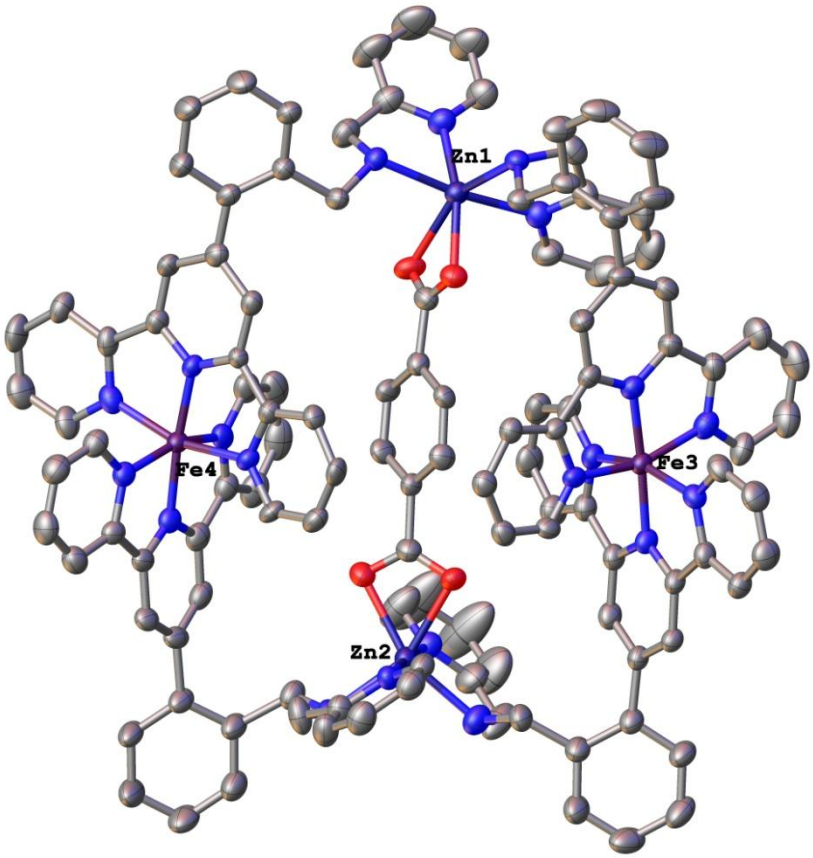

*Figure 6.9. The crystal structure of **6.3** showing a terephthalate ion in the box cavity. The hydrogen atoms, uncoordinated anions and the solvent molecules have been omitted for clarity.*

The complex **6.3** was synthesised by mixing a methanolic solution of one equivalent of $(NH_4)_2Fe(SO_4)_2{\cdot}6H_2O$ with two equivalents of ligand **L2.3**. After heating gently for 30 mins an excess of sodium terephthalate was added, followed by addition of $Zn(NO_3)_2{\cdot}6H_2O$. The complex was precipitated by addition of an excess of ammonium hexafluoridophosphate solution. Purple coloured X-ray quality crystals were produced by vapour diffusion of ethyl acetate into a very dilute acetonitrile solution of the complex over a period of three-four weeks.

The crystal structure of complex cation $[Fe_2Zn_2(\mathbf{L2.3})_4(C_8H_4O_4)]^{6+}$, **6.3**, was solved in the monoclinic space group $P2_1/n$ with an R-factor 7.07%, **Figure 6.9**. As described previously **L2.3** has two binding sites, the terpyridine-type "head" and picolylamine-type "tail" and similar to previous complexes Fe(II) and Zn(II) coordinated to four ligands resulting in formation of **6.3**.

A remarkable achievement in the synthesis of this box complex was that a molecule of terephthalate is encapsulated in the central cavity. The geometry of both the Zn(II) ions is distorted octahedral and is different from the previous complexes due to presence of the bidentate terephthalate ion. In each Zn(II) ion, four positions of the octahedral geometry are occupied by nitrogen atoms from the picolylamine binding sites of the coordinating ligands. The fifth and sixth positions are occupied by the bridging terephthalate ion through coordinating oxygen atoms. In contrast to the previous boxes, the inversion centre in the middle of the complex is no longer present.

The aromatic ring of terephthalate is located parallel to one of the terpyridine plane and are involved in π-π interactions with stacking distance of 3.270(15) Å. The distance between the Zn1-Zn2 is 10.7593(15) Å and the Fe1-Fe2 distance is 10.7858(19) Å. A discussion about the choice of terephathalate ion and comparison of the box geometry with other similar complexes is given in **section 6.2.3.**

The structure of the cationic part of complex is well ordered. Only four hexafluoridophosphate ions were modelled easily. The electron density peaks for remaining anions and the solvent molecules were diffused and smeared over each other. One nitrate was disordered over two positions and its occupancy was refined to 50% at each position. Similarly one hexafluoridophosphate was also modelled with 50% occupancy at two positions.

The elemental analysis performed for the bulk material is consistent with presence of six hexafluoridophosphate ions.

*6.2.1.4. $[Fe_2Cu_2(\mathbf{L2.3})_4Cl_2](PF_6)_6 \cdot 2CH_3CN \cdot 0.5(CH_3CH_2)_2O$ – Complex **6.4***

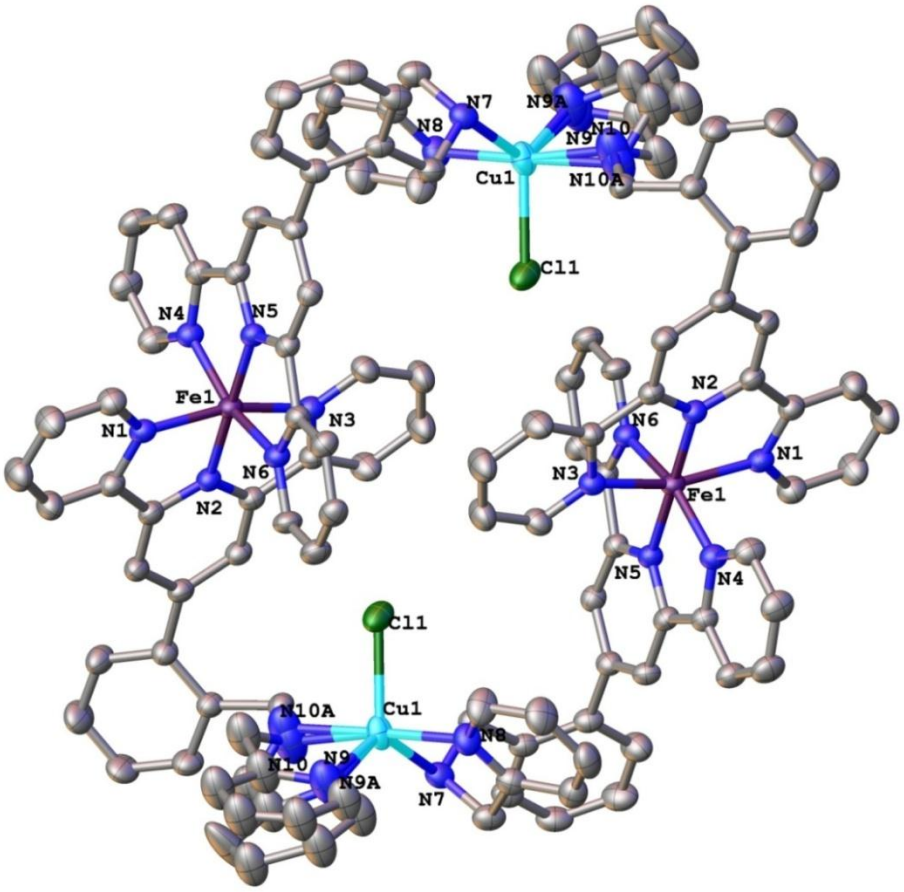

*Figure 6.10. The crystal structure of the hetero-metallic tetranuclear box complex $[Fe_2Cu_2(\mathbf{L2.3})_4Cl_2]^{2+}$, **6.4**, showing disorder at the tail binding site. The hydrogen atoms, anions and solvent have been omitted for clarity. The selected bond lengths and bond angles are given in Appendix III, Table A33.*

The titled box complex, **6.4**, was synthesised using the same procedure as **6.1**, with $ZnCl_2$ replaced with $CuCl_2$. The dark purple precipitate collected was dissolved in acetonitrile and purple crystals of X-ray quality were collected, by vapour diffusion of diethyl ether into the acetonitrile solution with 70% yield. The crystal structure of complex $[Fe_2Cu_2(\mathbf{L2.3})_4Cl_2]^{6+}$ is shown in **Figure 6.10**.

The crystal structure was solved in the triclinic space group $P\overline{1}$ and refined to an R-factor of 6.36%. Similar to previous structures there was significant disorder associated with the solvent molecules. Due to low electron density peaks available, the occupancy of one acetonitrile and one diethyl ether was refined to 50% each. Another acetonitrile was disordered into two different orientations with nitrogen atoms positioned very close to each

other. The occupancy of two parts was refined to 50% each. Unlike any other box complexes crystallised in this project, some disorder was also associated with the cationic part of the complex **6.4**. One picolylamine-part of one **L2.4** in the box was disordered over two orientations which was modelled with 50% occupancy in each orientation as shown in **Figure 6.11**.

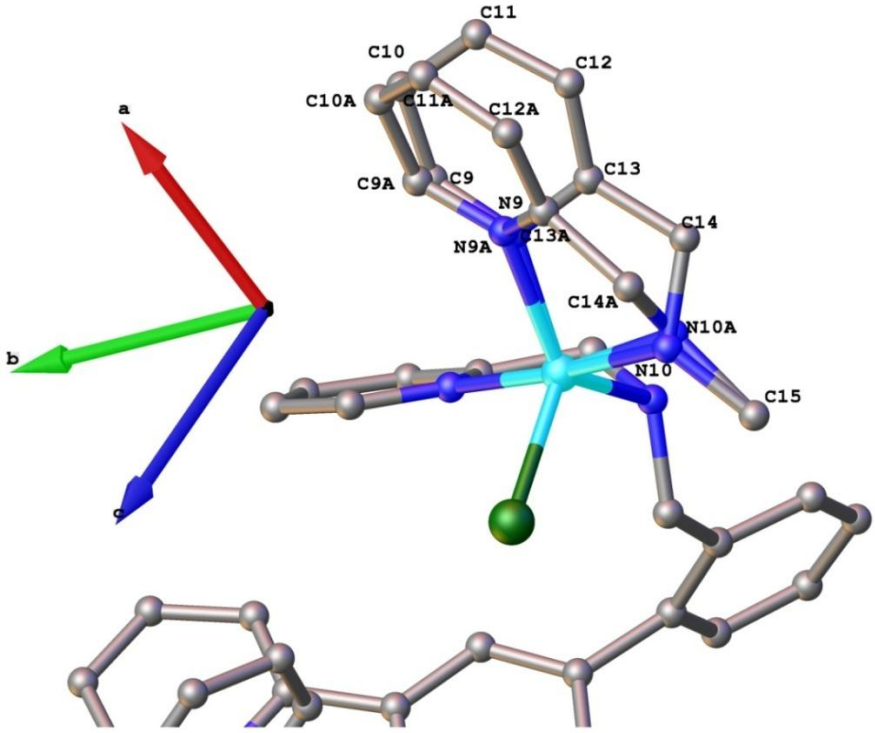

*Figure 6.11. Ball-stick model of complex **6.4** showing the disordered picolylamine-part of **L2.3**. Rest of the complex, hydrogen atoms, solvent and other anions omitted for clarity.*

In this box, similar to **6.1** and **6.2**, Fe(II) is coordinated in the octahedral geometry between two **L2.3** ligands through HH coordination mode. The Cu(II) has five-coordinate geometry through TT coordination mode and Cl^- anion. In **6.4** the τ values for five-coordinate geometries are between 0.70 and 0.87 due to two orientations of the disordered picolylamine. Similar to previous complexes a number of packing forces such as hydrogen binding, π-π stacking and short contacts between F, N, O and H are available.

*6.2.1.5. $[Ni_2Zn_2(\mathbf{L2.3})_4Cl_2](PF_6)_6 \cdot 4CH_3CN \cdot 2(CH_3CH)_2O \cdot 2H_2O$ – Complex **6.5***

The box complex **6.5** was synthesised by mixing the methanolic solution of one equivalent of $NiCl_2.6H_2O$ with two equivalents of **L2.3**. The resulting pale green solution of the complex was treated with $ZnCl_2 \cdot 2H_2O$ followed by addition of an excess of hexafluoridophosphate ions. The irregular pale green single crystals of X-ray quality were formed by vapour diffusion of diethyl ether into the acetonitrile solution of the complex in 65% yield.

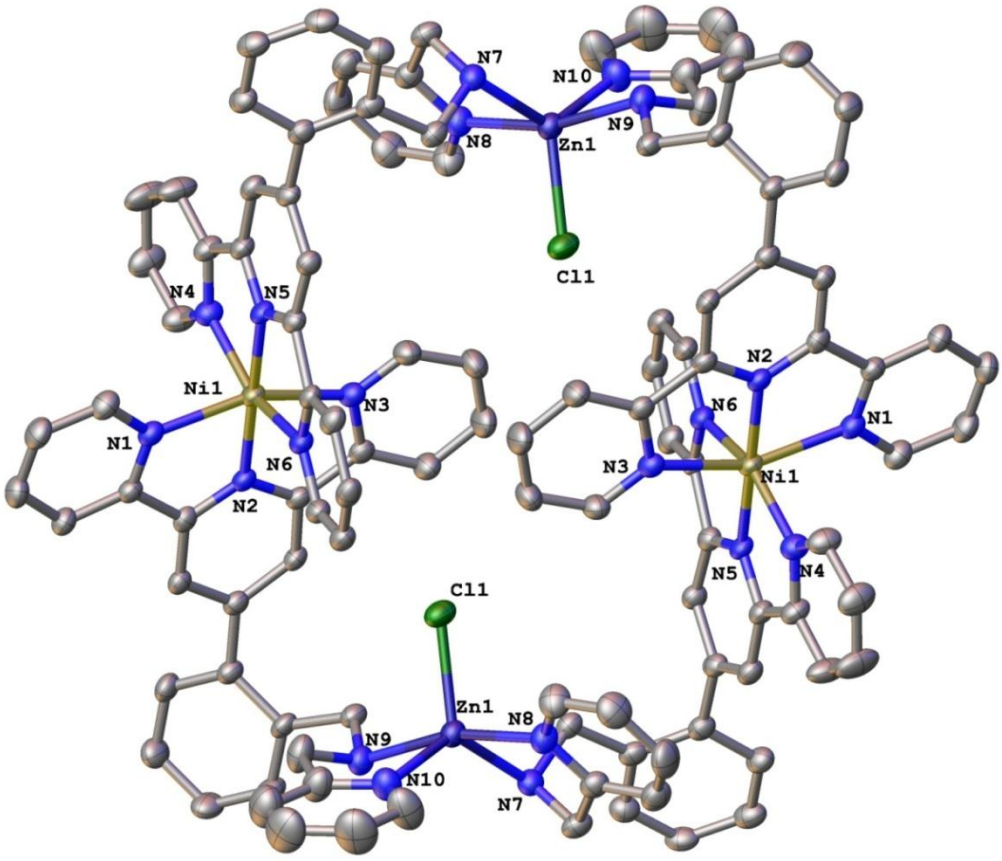

*Figure 6.12. The crystal structure of the hetero-nuclear box complex $[Ni_2Zn_2(\mathbf{L2.3})_4Cl_2]^{2+}$, **6.5**. The hydrogen atoms, anions and solvent have been omitted for clarity. The selected bond lengths and bond angles are given in Appendix III, Table A34.*

X-ray diffraction studies of the crystal shows formation of a new hetero-metallic box complex containing both Ni(II) and Zn(II) ions. The crystal structure was solved in the triclinic space group $P\bar{1}$ with an R-factor 7.97%. The crystal structure of complex $[Ni_2Zn_2(\mathbf{L2.3})_4Cl_2]^{6+}$ is shown in **Figure 6.12**. It consists of four **L2.3** ligands, two Ni(II) ions, and two Zn(II) ions. The Ni(II) is present in octahedral geometry and Zn(II) occupies a five-coordinate geometry. There is literature evidence for Ni(II) to prefer to bind in a octahedral geometry[72, 79, 252, 285] and Zn(II) in five-coordinate geometries.[209, 312, 315] The

chloride ions are coordinated to Zn(II) ions which point towards the ring cavity in a similar fashion as acetate and chloride ions in the previous box complexes.

The cationic structure we are interested in is well ordered. One acetonitrile solvent was also well ordered, but all other solvent molecules were severely disordered. The occupancy of all disordered molecules was refined with fixed thermal parameters before fixing the occupancy and refining the thermal parameters. The occupancies of C1, C2 and N12 atoms of the disordered acetonitrile were refined to 50% each, due to low electron density peaks available. The half occupancy diethyl ether molecule was refined isotropically without hydrogen. The half occupancy water, O2, was also refined without any hydrogen atoms because there was insufficient electron density located around the donor atoms to located hydrogen atoms.

The asymmetric unit contains exactly half of the box complex. Each ligand bridges between one Ni(II) and one Zn(II) ions. In each box, the Ni(II) bridge two tridentate terpyridine sites of two adjacent **L2.3** ligands in a six-coordinate distorted octahedral geometry through the HH bridging mode. Both terpyridine-type ligands lie nearly perpendicular to each other with an inter-planar angle of 91.82(10) Å.

In each of the picolylamine bidentate site of the ligand, Zn(II) binds to two ligands through four nitrogen atoms and a chloride counter-ion. The Zn(II) binds in a five-coordinate geometry, intermediate between trigonal bipyramidal and square pyramidal geometries with a τ value of 0.63. The chlorine atom (Cl1), the amine nitrogen (N7) from one **L2.3** and pyridine-type nitrogen (N10) of another **L2.3** occupies the equatorial positions, and the N8 and N9 occupy the axial positions of the trigonal bipyramidal geometry.

The inter-molecular hydrogen bonding F···H-N between the fluorine atoms of the hexafluoridophosphate and the secondary amine hydrogen atoms ranges from 2.103(3) Å to 2.850(5) Å. Various other inter- and intra-molecular short contacts between F, O, N and H atoms ranging from 2.436 Å to 3.772 Å.

*6.2.1.6. $[Zn_4(L2.3)_4Br_2](PF_6)_6 \cdot 2CH_3CN \cdot 0.5(C_2H_6CH)_2O$ – Complex **6.6***

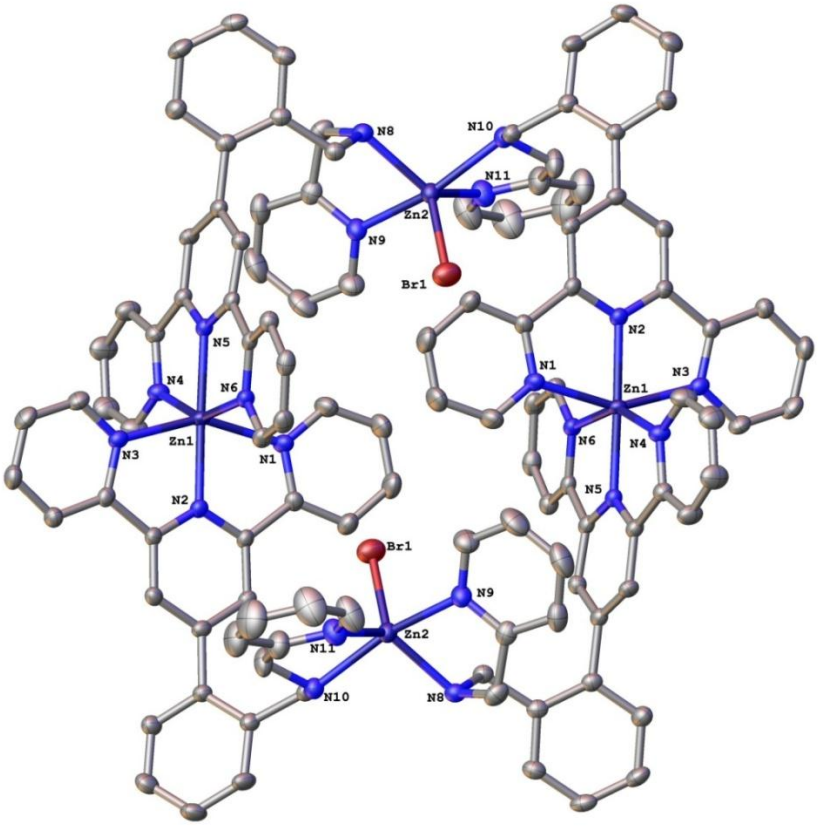

*Figure 6.13. The Crystal structure of $[Zn_4(\mathbf{L2.3})_4Br_2]^{6+}$,**6.6**. The solvent molecules, hydrogen atoms and anions have been omitted for clarity. The selected bond lengths and bond angles are given in Appendix III, Table A35.*

The complex **6.6** was synthesised by mixing one equivalent of **L2.3** with methanolic $ZnBr_2$. The pale white precipitate was collected by addition of an excess of hexafluoridophosphate solution. The X-ray quality crystals were formed by vapour diffusion of di-isopropyl ether into acetonitrile solution of the complex.

The crystal structure of the complex **6.6** was solved in the triclinic space group $P\bar{1}$ with an R-factor of 5.80%. The structure of the cation and the coordinating anions was well ordered but solvent molecules- one di-isopropyl ether and one acetonitrile were disordered. The occupancy of all disordered molecules was refined with fixed thermal parameters before fixing the occupancy and refining the thermal parameters. Two parts of acetonitrile were disordered over two orientations at the same positions with 60:40 occupancy ratio. All the atoms in di-isopropyl ether were modelled with half occupancy and the diffuse electron density around di-isopropyl ether were not attempted. Four fluorine atoms bonded in one

plane in hexafluoridophosphate ion were also disordered. The disordered fluorine atom was modelled by splitting over two positions with an occupancy ratio of 50:50.

The two Zn(II) ions are coordinated between tridentate terpyridine binding sites of four ligands in the six-coordinate octahedral geometry through an HH binding mode. The other two Zn(II) ions coordinate between the picolylamine binding sites of four ligands through TT bridging mode with five-coordinate geometries. Both of the five-coordinate Zn(II) geometries are intermediate between the ideal trigonal bipyramidal and square pyramidal geometries with τ values of 0.68, however closer to the trigonal bipyramidal geometry.

The crystal structure of the box cation $[Zn_4(\mathbf{L2.3})_4Br_2]^{6+}$ is similar to that of **6.2** except the bromide ion coordinated to five-coordinate Zn(II) ions instead of the acetate ions. Similar to acetate ions in **6.2** the bromide ions point towards the centre of the cavity in hydrophobic aromatic environment. The Zn2-Zn2 distance is 11.744(11) Å, and the Zn1-Zn1 distance is 9.622(11) Å. The bromide to bromide distance is 7.271(12) Å.

The molecules in the crystal lattice are packed by a number of atomic interactions such as hydrogen bonding, π-π stacking and other short contacts. The terpyridine rings of all four **L2.3** ligands involved in box geometry participate in π-π stacking and the distances between the rings of the opposite ligands in the range of 4.853(7) Å and 7.804(5) Å. The fluorine atoms of hexafluoridophosphate ions make multiple hydrogen bonds with hydrogen atoms of the secondary amines. Each amine hydrogen atom interacts with two or three fluorine atoms ranging from 2.116(3) Å to 2.770(5) Å with a shortest F···N distance of 3.081(4) Å. The molecules are stabilised by both inter- and intra-molecular short interactions between the solvents, anions and aromatic hydrogen atoms such as N···H-C, F···H-C and Br···H-C ranging from 2.266 Å to 3.164 Å.

A lower yield of the similar complex was crystallised when the reaction was performed using either $Zn(NO_3)_2$ or $Zn(OTf)_2$ salts in the presence of hexafluoridophosphate ions with **L2.3** containing a small amount of bromide impurity of the ligand. The cation and anions in these crystal structures were the same except for the co-crystallised solvent molecules.

6.2.2. Spectrophotometric Studies

6.2.2.1. Job's method analysis

The spectrophotometric method of continuous variation, also known as Job's method, was used to study formation of the complexes in solution. Initially in 1912, the method of continuous variation was worked out by Denison[338] in connection with his studies of compound formation in liquid mixtures. Later it was applied by Job[339] to the spectrophotometric determination of the empirical formulas of complexes that are products of incomplete equilibrium reactions. Job's method, as it is now called, has been commonly used in laboratory experiments in instrumental analysis classes to determine metal-to-ligand ratios in complex formation reactions.[340] The method enables one to determine the ratio of metal and ligand (M:L) of the complex formed by the mixing the two solutions. Since in using this method the property to be measured should be additive, Job chose to study the absorption of light by solutions of the complexes. The equation for an equilibrium reaction may be written as:

$$A + nB \leftrightharpoons ABn$$

According to the principle of the method of continuous variation, when different amount of A and B are mixed together in solution, with the imposed restriction that the sum of their original concentrations is fixed constant in all cases, then the concentration of the complex produced at equilibrium will approach a maximum value as the ratio of the original concentrations $\left[\frac{B_0}{A_0}\right]$ becomes equal.[341]

Practically, in this technique the total amount of ligand and metal are held constant in a series of solutions of constant volume, whereas the individual amounts of the ligand and metal are varied constantly. A physical property, such as the absorbance is measured for each solution. The absorbance *versus* mole fraction of one species (either metal or ligand) plot gives a curve with ascending, and then descending branches. The extrapolation of the sides meets at a point of maximum absorbance of the solution. This point corresponds to the optimum mole fraction of the metal at which complete formation of complex occurs, and hence the formula of the complex can be calculated. This technique may be applied to the determination of the formula of any ionic compound, provided some physical characteristic of the compound may be measured.[340, 342, 343]

In general, when terpyridine-type ligands and Fe(II) solutions are mixed, purple coloured complexes form, which absorb the visible light at 559 nm; typical of the $[Fe(tpy)_2]^{2+}$ chromophore.[108, 131] In our case, **L2.3** was mixed with different Fe(II) salts, the same purple solution was formed indicating formation of $[Fe(\mathbf{L2.3})_2]^{2+}$complexes in solution. However, this complex was not able to be characterised by ^{1}H NMR spectroscopy, so the Fe(II) complex of **L2.3** was analysed spectrophotometrically in the solution state using Job's method.

Equimolar concentration stock solutions (2.9×10^{-5}M) of **L2.3** and $FeCl_2\cdot4H_2O$ were prepared in 5% $CHCl_3$methanol solution. Two stock solutions were mixed in varying ratios and 25 different mole fraction solutions were prepared starting from 0 to 1 mole fraction of **L2.3**. The absorbance of each purple solution was determined at 559 nm. The six-coordinate picolylamine-Fe(II) literature complexes absorb the visible light at 647, 676 and 830 nm[344, 345]and no absorbance was seen in that region in these experiments. The Job plot of absorbance *versus* mole fraction (A *vs.* n) of the ligand **L2.3** is shown in **Figure 6.14**.

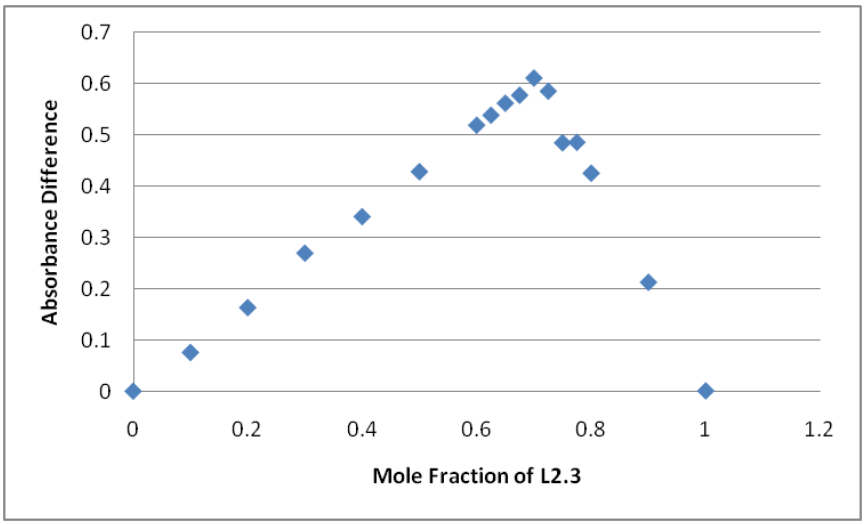

*Figure 6.14. The Job's plot according to the method of continuous variations, indicating the 2:1 stoichiometry of the **L2.3**-Fe(II) complex. The total concentration of **L2.3** and Fe(II) ion is 2.9×10^{-5}M.*

The Job plot of **L2.3**-Fe(II) complex shows optimum absorbance when 0.670 mole fraction solution of **L2.3** was mixed with 0.330 mole fraction solution of Fe(II). This means that the maximum amount of the complex which absorbs at 559 nm is formed of 2:1 stoichiometry. The MS-ESI spectra of the solution is consistent with the formulation $[Fe(\mathbf{L2.3})_2]^{2+}$ complex with *m/z* peaks at 457.16 and 305.11 which correspond to

[Fe+2(**L2.3**)]$^{2+}$ and [Fe+2(**L2.3**)]$^{3+}$ fragments. The complex with the experimentally determined stoichiometry is shown in **Figure 6.15**.

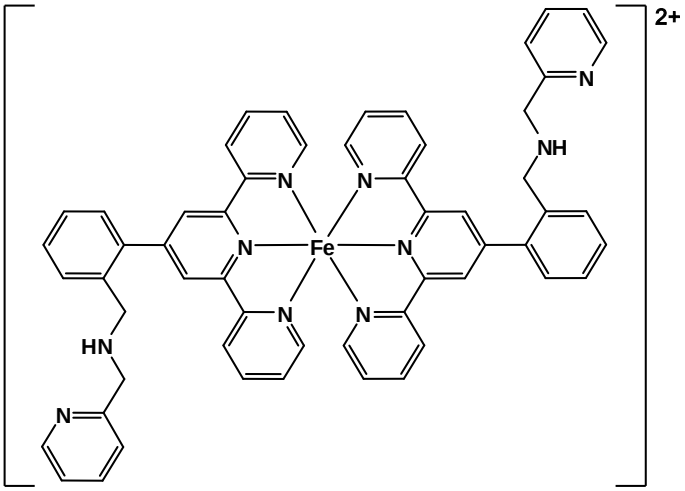

*Figure 6.15. Diagrammatic representation of 2:1 (M:L) stoichiometry complex formed in solution in Job's experiment of **L2.3**-Fe(II) complex.*

6.2.2.2. The UV-vis analysis of Mixed Fe(II)Zn(II) systems

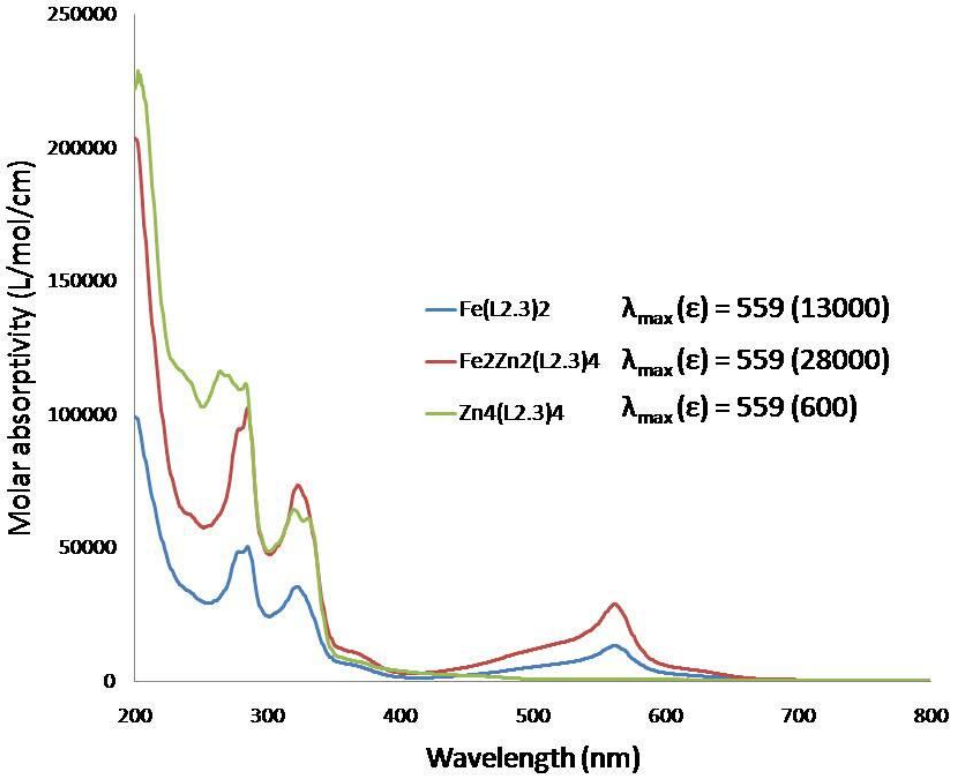

*Figure 6.16.This molar absorptivity graph illustrates increase in absorption of UV-light Zn_4(**L2.3**)$_4$, Fe_2**L2.3**, and Fe_2Zn_2(**L2.3**)$_4$ complexes.*

Presence of Fe(II) in terpyridine-type binding sites of the Fe_2Zn_2(**L2.3**)$_4$ mixed metal systems was confirmed on the basis of the UV-vis measurements (**Figure 6.16**), molar absorptivity data. The UV-vis spectrum of [Fe_2Zn_2(**L2.3**)$_4Cl_2$]PF_6, **6.1**, and [Fe_2Zn_2(**L2.3**)$_4$($C_8H_4O_4$)]PF_6, **6.3** have a metal to ligand charge transfer (MLCT) band at a wavelength of 559 nm, which can be assigned principally to the d-π^* transition of the Fe(II)-bisterpyridine chromophore based on literature precedents.[81, 252, 256] Since the complex [Zn_4(**L2.3**)$_4Cl_2$]$(PF_6)_6$, **6.5** is colourless there is no absorption band observed in the visible region. The Fe_2Zn_2(**L2.3**)$_4$ complexes have molar absorptivity (28000 $L^{-1}mol^{-1}cm$) slightly larger than twice the extinction coefficient of Fe(**L2.3**)$_2$ complex (13000 $L^{-1}mol^{-1}cm$). This confirms that in these Fe(II)Zn(II) systems, Fe(II) preferably binds in terpyridine-type binding sites and that there is no scrambling of metal ions between the binding sites in the boxes. These results were consistent with literature where bis-terpyridine Fe(II) complexes are discussed to be most stable (due to their higher stability constant) in comparison to analogous Cu(II), Zn(II) or Ni(II) complexes.[71, 256, 346-348]

6.2.3. Discussion of the Box Complexes

The novel ligand **L2.3** contains two binding sites, the tridentate terpyridine-type metal binding site (head or H) and the bidentate picolylamine-type binding site (tail or T) as shown earlier in this chapter, **Figure 6.1**. The terpyridine site coordinate using the three nitrogen atoms leading to the formation of bis-terpyridine complex $[M(\mathbf{L2.3})_2]^{2+}$, and the picolylamine binding site is flexible for its geometry depending upon the metal and anion used.

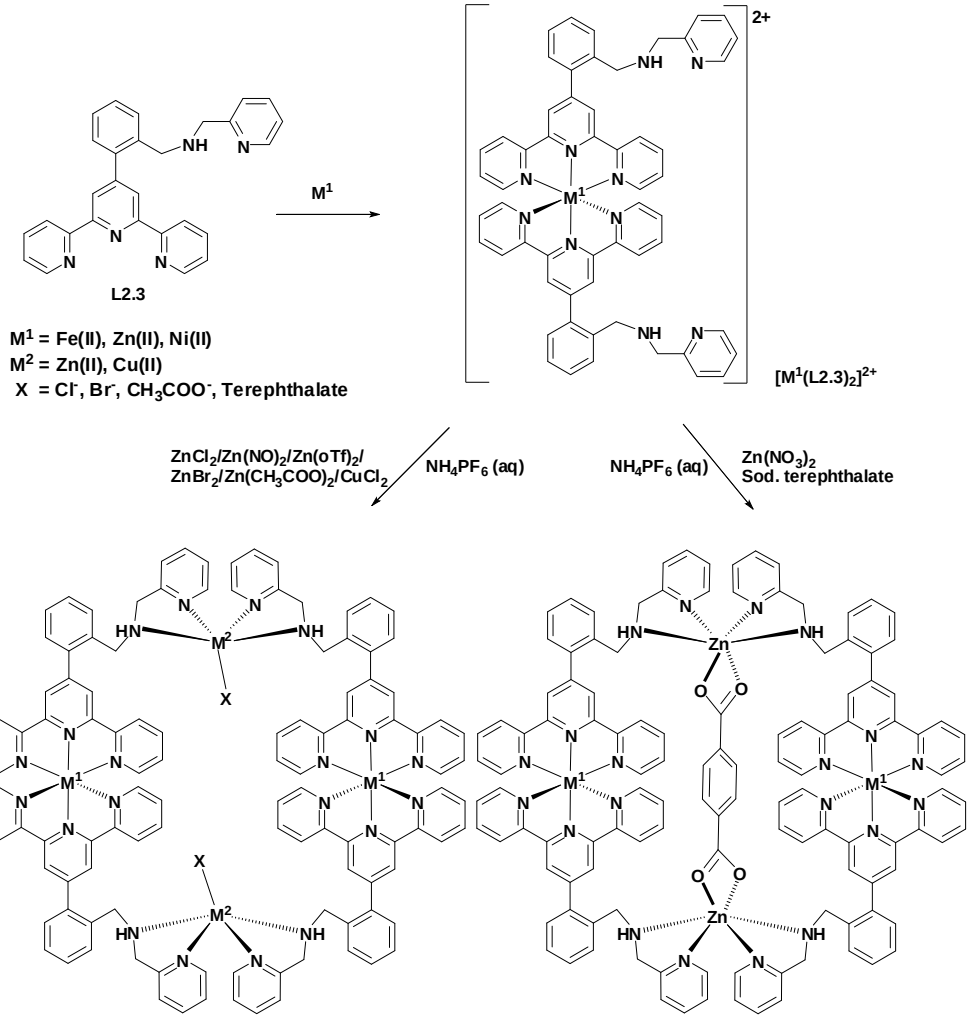

Figure 6.17.The schematic diagram of formation of $[M^1{}_2M^2{}_2(\mathbf{L2.3})_4(X)_2]^{6+}$ box shaped complexes, via formation of the intermediate $[M^1(\mathbf{L2.3})_2]^{2+}$ complexes.

To achieve control over the coordination chemistry of the ligand **L2.3**, appropriate metal ions were used which can preferentially bind two ligands through their terpyridine-type binding site; for example Fe(II). As shown in **Figure 6.17**, head-to-head bridging of **L2.3** was achieved by making $[M(\mathbf{L2.3})_2]^{2+}$ complexes using Fe(II), Ni(II) and Zn(II) ions based on the fact that 2,2′:6′,2″-terpyridine group can make a range of different complexes with almost any metal ion in the periodic table, including bis-terpyridine complexes of Fe(II), Ni(II), Zn(II),

Ru(II) and Cu(II).[72, 73, 81, 176, 204, 209, 212, 238, 239, 252, 253] Depending upon the specific metal ions, complexes can show different stabilities, as expressed in the stability constant (K values) in **Table 6.1**, where K_1 represents mono-terpyridine complex (1:1, M:L) and K_2 represents bis-terpyridine complex (1:2, M:L) complexes.[107, 166, 256, 346-348]

Table 6.1. Stability constants for mono- and bis- terpyridine complexes measured in water.[256]

Metal ion	**logK_1**	**logK_2**
Mn(II)	4.4	-
Fe(II)	7.1	13.8
Co(II)	8.4	9.9
Ni(II)	10.7	11.1
Cu(II)	12.3	6.8
Zn(II)	6.0	5.2
Cd(II)	5.1	-

The table shows that Fe(II) bis-terpyridine complexes are more stable than the others. The bis-terpyridine complexes are highly stable due to strong metal-ligand (d-π*) back donation and a strong chelate effect. The purple colored bis-terpyridyl octahedral complexes formed with Fe(II) are probably among the most studied complexes of terpyridine derivatives and can be isolated easily.

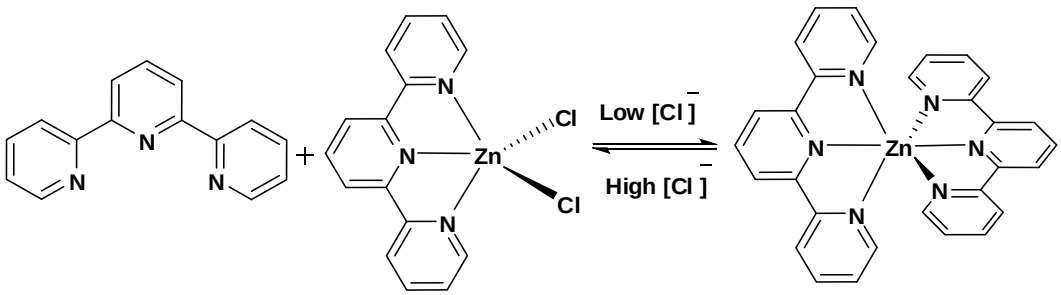

Figure 6.18. Equilibrium between mono- and bis- terpyridine Zn(II) complexes.

In the case of Zn(II), bis-terpyridine complexes are in equilibrium with mono-terpyridine complexes as illustrated in **Figure 6.18**. The zinc-terpyridine complexes are labile in comparison to the iron complexes,[346] therefore the Zn(II) complex formation can be reversed more easily. Zinc complexes exist in a dynamic equilibrium and thus exchange

rapidly. In $[M(\mathbf{L2.3})_2]^{2+}$ complexes, the picolylamine-type metal binding sites (Tail) are free to coordinate with other metal ions such as Zn(II), which can adopt different coordination numbers and geometries due to its full d orbital.

Table 6.2 Change in metal-metal distance (Å) by a changing the coordinating ligand (X). For an easier approach a diagrammatic sketch of the box complexes is shown as well. The different metal ions are represented as M^1 and M^2.

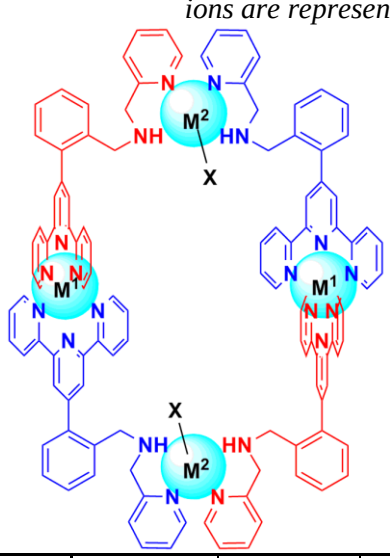

6.1 - $[Fe_2Zn_2(L2.3)_4Cl_2]^{6+}$

6.2 - $[Zn_4(L2.3)_4(CH_3COO)_2]^{6+}$

6.3 - $[Fe_2Zn_2(L2.3)_4(C_8H_4O_4)]^{6+}$

6.4 - $[Fe_2Cu_2(L2.3)_4Cl_2]^{6+}$

6.5 - $[Ni_2Zn_2(L2.3)_4Cl_2]^{6+}$

6.6 - $[Zn_4(L2.3)_4Br_2]^{6+}$

Complex / Distance(Å)	6.1	6.2	6.3	6.4	6.5	6.6
M^1- M^1 (terpyridine site)	9.428(18)	9.678(2)	10.782(3)	9.058(12)	9.489(14)	9.622(11)
M^2-M^2 (picolylamine site)	11.633(17)	11.878(2)	10.763(3)	11.926(14)	11.615(12)	11.744(11)
X-X (anion - anion)	7.456(3)	8.171(10)	7.323(13)	7.533(2)	7.393(2)	7.271(12)

Six different tetranuclear, both homo-metallic and hetero-metallic, box shaped complexes were isolated, the crystal structures of which are described earlier in this chapter. For hetero-metallic box shaped complexes, the ligand **L2.3** was reacted with half an equivalent of $FeCl_2$. The reaction mixture immediately turned purple, indicating formation of $[Fe(\mathbf{L2.3})_2]^{2+}$ complex in solution through HH coordination mode. The picolylamine binding site was reacted with Zn(II) and Cu(II) salts. Addition of an excess of hexafluoridophosphate ions resulted in precipitation of the boxes $[Fe_2Zn_2(\mathbf{L2.3})_2Cl_2](PF_6)_6$, **6.1** and $[Fe_2Cu_2(\mathbf{L2.3})_2Cl_2]PF_6$, **6.4**, respectively, which could then be crystallised by vapour diffusion methods. Similarly, when Ni(II) was used instead of Fe(II), the box $[Ni_2Zn_2(\mathbf{L2.3})_4Cl_2]PF_6$, **6.5**, was formed. The homo-metallic box complexes $[Zn_4(\mathbf{L2.3})_4(OAc)_2]PF_6$, **6.2**, and$[Zn_4(\mathbf{L2.3})_4Br_2]PF_6$, **6.6**, were formed when only Zn(II) metal salts of the respective anions were used.

In all the boxes except **6.3**, the dimensions of the box skeleton are similar to each other **Table 6.2**. The average metal-metal distances between the octahedral metals is 9.5 Å, between the five-coordinate metals is 11.7 Å, and the anion-anion distances measured between the cavity are 7.3 Å. Based on the nature of the boxes and cavity size, especially the complex **6.2** which contains two coordinated acetate ions pointing in to the cavity, we explored whether it was possible to insert a dicarboxylate ion into the cavity, **Figure 6.19**.

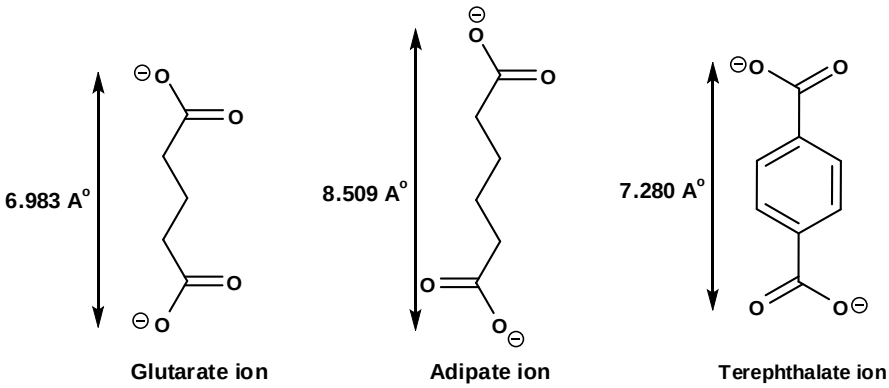

Figure 6.19. Possible dicarboxylate anions to fit in the box cavity, coordinating oxygen to oxygen distances are given.

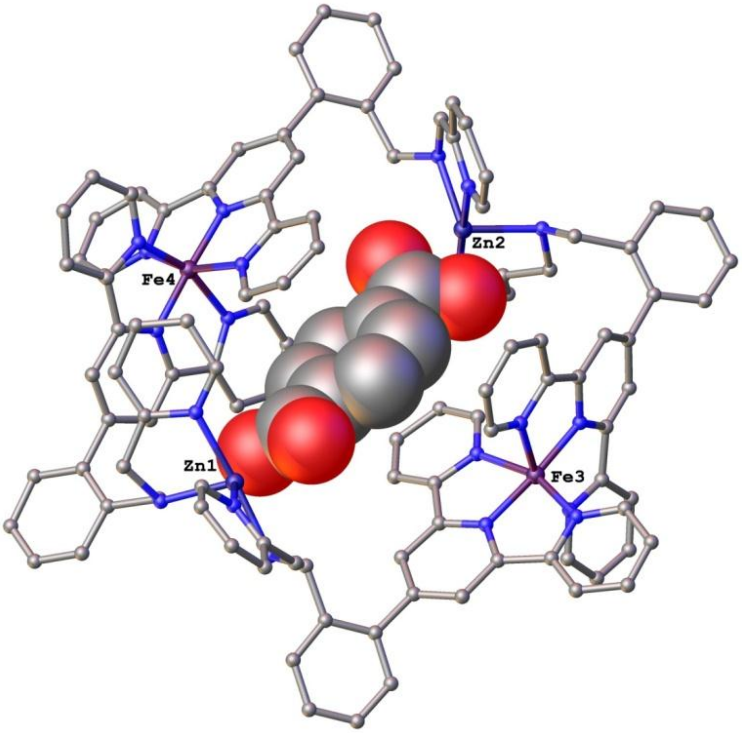

*Figure 6.20. The crystal structure of box **6.3**, showing π-π stacked terephthalate ion. Hydrogen atoms, solvent and non-coordinated ions are omitted for clarity.*

Theoretically, all three dicarboxylate ions, glutarate, adipate and terephthalate ions may be able to fit in the box cavity. However, practically terephthalate ion was inserted successfully in the cavity due to π-stacking interactions with the aromatic terpyridine rings

and its rigid nature resulting in formation of the box, $[Fe_2Zn_2(C_8H_4O_4)](PF_6)_6$, **6.3**, **Figure 6.20**. Due to similar π-stacking interactions with neighbouring aromatic rings terephthalate was referred as 'a very welcome guest' in a 2006 communication, where terephthalate dianion template assisted synthesis of some macrocycles.[349]

During the initial attempts to synthesise boxes containing dicarboxylate ions $FeCl_2$ and $ZnCl_2$ salts were used as a source of Fe(II) and Zn(II) ions, which resulted in consistent formation of the box **6.1**, $[Fe_2Zn_2(\mathbf{L2.3})_2Cl_2]^{6+}$, with no terephthalate present. Finally, the use of $(NH_4)_2Fe(SO_4)_2$ and $Zn(NO_3)_2$ salts resulted in the formation of box **6.3**. Use of $ZnCl_2$ repeatedly produced box **6.1**, even in the presence of excess terephthalate ions. This shows that terephthalate only coordinates to the metal centre in the presence of large weakly-coordinating anions such as SO_4^{2-} or NO_3^-. In the presence of strongly coordinating ions such as Cl^-, terephthalate does not take part in coordination. The halide ion preference was also observed when an excess of NO_3^- or ClO_4^{2-} counter-ions (relatively non-coordinating) were used in the presence of a small amount of bromide ion impurity, and the complex **6.6**, $[Zn_4(\mathbf{L2.3})_4Br_2]^{6+}$, was crystallised. There is a possibility of some sort equilibrium between the different types of box complexes, but it was experienced that the chloride and bromide ions are preferably the best fit anions to crystallise the boxes.

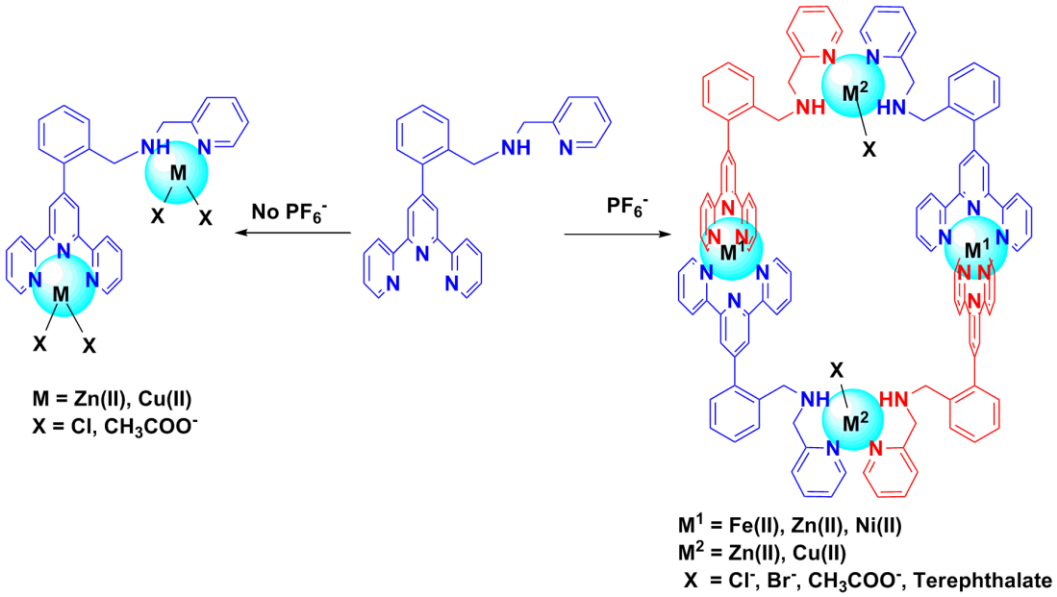

Figure 6.21. Diagram showing formation of the dinuclear and box complexes governed by hexafluoridophosphate ions.

Another interesting aspect of these box shaped tetranuclear structures is the possible templating effect of hexafluoridophosphate anion that appears to be required in syntheses of

the boxes. Without hexafluoridophosphate ions simple dinuclear complexes are formed, **Figure 6.21**. Those dinuclear complexes [Zn_2(**L2.3**)Cl_4], [Cu_2(**L2.3**)Cl_4] and [Cu_2(**L2.3**)$(CH_3COO)_4$] are discussed in Chapter 4 .

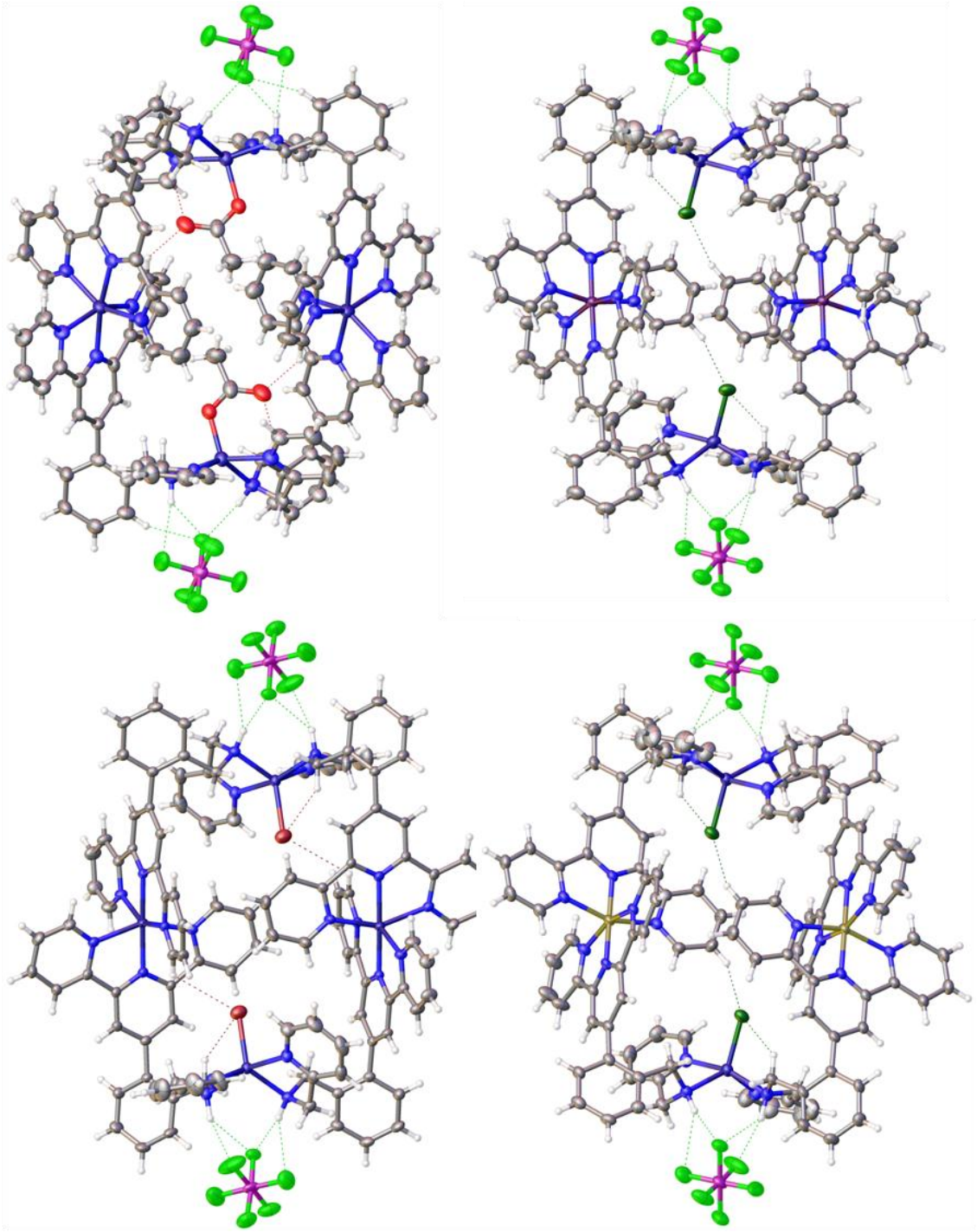

*Figure 6.22. Various box complexes showing multiple F···H-N hydrogen bonding interactions. (Top): left **6.2**, right **6.1** and (Bottom): left **6.6**, right **6.5**. The PF_6^- ions not involved hydrogen bonding and the solvents have been excluded for clarity.*

In all the boxes hexafluoridophosphate ions, located above and below the box, participate in F···H-N hydrogen bonding interactions (2.0 Å – 2.3 Å). All four amine hydrogen atoms of each box participate in multiple hydrogen bonding interactions to different fluorine atoms of the same anions located near the coordination sites, **Figure 6.22**.

6.2.3.1. The Mysterious Box

At different stages of this research work, experiments aimed at the crystallisation of the bis-terpyridine type complex $[Fe(\mathbf{L2.3})_2]^{2+}$ were conducted. Similar to other Fe(II) containing terpyridine complexes, dark purple coloured small plate shaped crystals were formed during each attempt. The yield of the crystals formed was very low in all attempts. The X-ray crystallographic analysis of the crystals revealed that box shaped $[M^1{}_2M^2{}_2(\mathbf{L2.3})_4]^{6+}$ complexes, **6.7**, were crystallised from each experiment. Each crystal structure contains two octahedral M^1 metal ions, two five-coordinate M^2 metal ions, four **L2.3** ligands, two chloride and six hexafluoridophosphate ions, along with a number of low occupancy disordered solvent molecules, which is consistent with other boxes synthesised in this project.

As the experiments were performed in the presence of added Fe(II) metal salts, the crystals were intense purple, and the bond lengths and angles were also in the range of bis-terpyridine-Fe(II) complexes, we conclude that M^1 is an Fe(II) ion. However, it was important to question the actual identity of M^2 in these experiments. Since no other metal ion was added deliberately to the reaction mixtures and the results were consistent in all attempts, there is a possibility that M^2 in these structures is a five-coordinate Fe(II) ion.

Generally, formation of five-coordinate Fe(II) complexes is not common due to d^6 electronic configuration which generally results in formation of stable, low spin, octahedral geometry.[350] A Cambridge Crystallographic Data Centre (CCDC) search of complexes of iron coordinating with two picolylamine ligands and one chloride ion yields 70 entries, out of which only 4 journal articles reported 7 complexes containing five-coordinate Fe(II) ions.[351-354] Out of these, only four complexes have a chloride ligand coordinated to the Fe(II) centre, and these are shown in **Figure 6.23**, together with their Fe-Cl bond lengths.

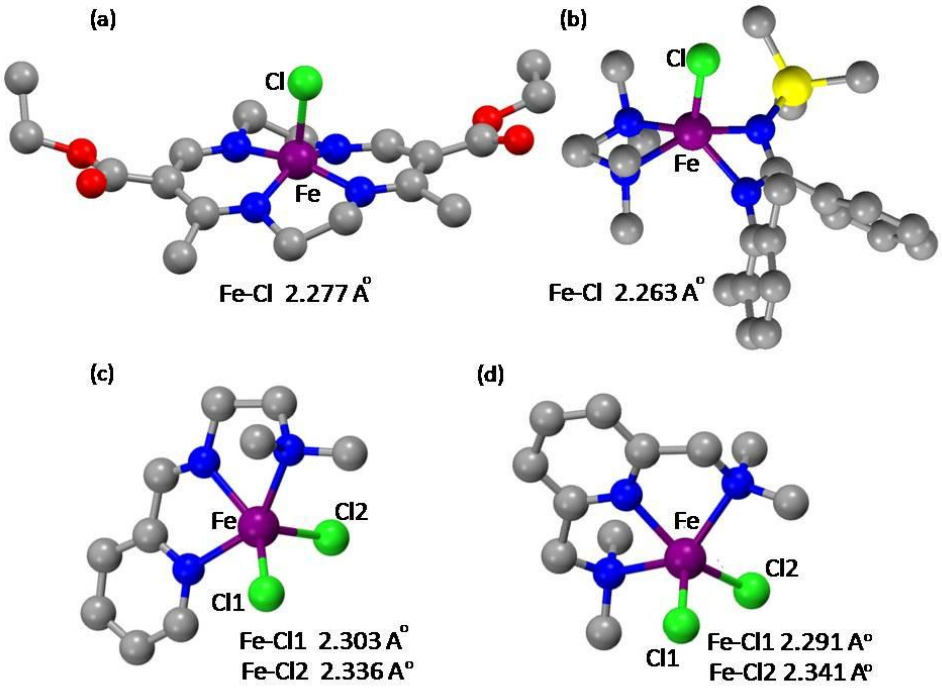

Figure 6.23. Five-coordinate Fe(II) literature complexes showing Fe-Cl bond lengths.[351, 353, 354]

Since the CCDC search revealed only a few Fe(II) five-coordinate complexes, the low yielding complex **6.7** reported in this thesis having Fe(II) in five-coordinate geometry must be looked at suspiciously. There is a possibility of having an impurity such as Cu(II), Ni(II) or Zn(II) metal ion in the five-coordination geometry, consistent with the low yield. However, the repeated synthesis of the same complex should rule out the possibility of non-iron metal salt impurity to some extent, unless the impurity was reproducibly introduced through a contaminated sample/reagent. Due to the very low yield of the crystals elemental analysis, ESI-MS, UV or Mossbauer analysis was not possible. The elemental analysis of the non-crystalline bulk is consistent with $[Fe(\mathbf{L2.3})_2](PF_6)_2 \cdot 4H_2O$.

However, an explanation of formation of Fe(II) five-coordinate geometry in **6.7** can come from the role played by hexafluoridophosphate ions in crystallising the box geometry. As discussed earlier, the hexafluoridophosphate ions make multiple hydrogen bonds with the secondary amine hydrogen atoms of **L2.3** ligands (**Figure 6.22**). We speculate that due to multiple hydrogen bonding of hexafluoridophosphate being important in stabilising box structures, there is no room for the sixth ligand to coordinate with Fe(II) ions. This might have led to preferred five-coordinate geometry of Fe(II) in "the mysterious box" **6.7**.

Table 6.3. A comparison of the crystallographic parameters such as R-factor, thermal parameter (Ueq), and bond length when different box models were refined using Fe(II), Co(II), Ni(II), Cu(II) and Zn(II).

Complex	M^1	M^2	M^2-N_{py} (Å)	M^2-N_{am} (Å)	M^2-Cl/Br (Å)	R (%)	Ueq $M^1 - M^2$
6.7, $Fe_2M^2_2(L2.3)_2Cl_2$	Fe(II)	Zn(II)	2.141(5)	2.130(4)	2.272(14)	7.22	0.025-0.033
	Fe(II)	Fe(II)	2.140(5)	2.128(5)	2.273(14)	7.43	0.028-0.024
	Fe(II)	Co(II)	2.140(5)	2.128(5)	2.272(14)	7.44	0.028-0.022
	Fe(II)	Cu(II)	2.142(4)	2.130(4)	2.272(14)	7.12	0.025-0.028
	Fe(II)	Ni(II)	2.142(5)	2.128(4)	2.272(14)	7.27	0.027-0.020
6.1, $Fe_2Zn_2(L2.3)_2Cl_2$	Fe(II)	Zn(II)	2.134(4)	2.153(4)	2.269(13)	5.61	0.024-0.030
	Fe(II)	Fe(II)	2.134(5)	2.149(5)	2.269(15)	6.14	0.028-0.019
	Fe(II)	Co(II)	2.134(5)	2.149(5)	2.269(15)	6.16	0.028-0.017
	Fe(II)	Cu(II)	2.134(4)	2.151(4)	2.269(13)	5.56	0.025-0.024
	Fe(II)	Ni(II)	2.134(5)	2.149(5)	2.269(15)	5.95	0.027-0.016
6.5, $Ni_2Zn_2(L2.3)_2Cl_2$	Ni(II)	Zn(II)	2.148(3)	2.130(3)	2.261(11)	7.52	0.025-0.029
	Ni(II)	Fe(II)	2.145(4)	2.128(4)	2.262(13)	7.98	0.027-0.020
	Ni(II)	Co(II)	2.145(4)	2.128(4)	2.262(13)	8.10	0.028-0.018
	Ni(II)	Cu(II)	2.147(3)	2.129(3)	2.261(11)	7.51	0.025-0.024
	Ni(II)	Ni(II)	2.145(4)	2.128(4)	2.262(11)	7.87	0.027-0.016
6.4, $Fe_2Cu_2(L2.3)_2Cl_2$	Fe(II)	Cu(II)	1.990(3)	2.149(3)	2.329(13)	6.40	0.025-0.037
	Fe(II)	Fe(II)	1.991(4)	2.149(3)	2.329(13)	6.72	0.026-0.037
	Fe(II)	Co(II)	1.990(4)	2.149(4)	2.329(13)	6.78	0.026-0.035
	Fe(II)	Zn(II)	1.991(3)	2.149(3)	2.329(12)	6.40	0.025-0.040
	Fe(II)	Ni(II)	1.991(3)	2.149(3)	2.329(12)	6.49	0.025-0.033
6.6, $Zn_4(L2.3)_4Br_2$	Zn(II)	Zn(II)	2.146(4)	2.131(3)	2.378(5)	5.84	0.021-0.023
	Zn(II)	Fe(II)	2.144(4)	2.133(4)	2.378(8)	6.36	0.023-0.014
	Zn(II)	Co(II)	2.144(4)	2.133(4)	2.378(8)	6.84	0.023-0.014
	Zn(II)	Cu(II)	2.145(4)	2.131(3)	2.378(8)	5.80	0.022-0.018
	Zn(II)	Ni(II)	2.145(4)	2.131(4)	2.378(8)	6.48	0.023-0.010

Therefore, the only structural confirmation came from the single crystal analysis from different experiments. Refinement of the crystallographic models for **6.7** after assigning different metal ions to the five-coordinate M^2 site does not cause any significant change in M^2-N and M^2-Cl bond lengths. **Table 6.3** lists the results of these refinements, the crystallographic parameters of the well-characterised boxes are also compared by changing the M^2 to different metal ions. In all cases the lowest R-factor comes when M^2 is refined as Cu(II) regardless of the actual metal present in the molecule. This shows crystallographic methods are not adequate to determine the 5-coordinate metal in **6.7**.

Table 6.4.Unit cell dimensions, volume and the space group of the halide containing boxes

Complex	Space group	a(Å)	b(Å)	c(Å)	α(°)	β(°)	γ(°)	V(Å^3)
6.1, $Fe_2Zn_2(L2.3)_2Cl_2$	$P\bar{1}$	12.863	14.281	18.956	76.07	83.14	82.37	3335.94
6.4, $Fe_2Cu_2(L2.3)_2Cl_2$	$P\bar{1}$	13.465	14.223	19.014	74.174	82.329	81.481	3448.32
6.5, $Ni_2Zn_2(L2.3)_2Cl_2$	$P\bar{1}$	13.048	14.625	19.191	74.338	82.18	82.769	3478.53
6.6, $Zn_4(L2.3)_4Br_2$	$P\bar{1}$	13.099	14.698	19.357	75.148	82.755	83.518	3561.19
6.7, $[Fe_2M^2{}_2(L2.3)_4]^{6+}$	$P\bar{1}$	13.146	14.558	19.094	74.648	82.357	83.046	3478.64

So based on the repeated crystallisation of the same complex **6.7**, and persistent multiple F···H-N hydrogen bonding interactions in the boxes, We speculate that M^2 is Fe(II) and the box complex $[Fe_4(\mathbf{L2.3})_4Cl_2]PF_6$ containing five-coordinate Fe(II) has been formed. However, the bond lengths and other crystallographic parameters across all the halide containing boxes given in **Table 6.3** and **Table 6.4** are so similar that no conclusions can be drawn about identity of M^2 in box **6.7**.

6.3. The Decanickel Wheels – $(HT)_{10}$ Coordination Mode

All the dinuclear and box shaped complexes discussed earlier in thesis were formed by mixing the ligand **L2.3** with different metal ions such as Fe(II), Zn(II) and Cu(II) under different conditions. However, the Ni(II) ion produced something remarkable – self assembled decanickel wheels. These wheels are the first precedent complexes with terpyridine-picolylamine type binding. The detailed crystal structures, characterisation and an overview of the wheels are discussed in the following sections.

6.3.1. Synthesis and Crystal Structures

*6.3.1.1. $[Ni_{10}(\mathbf{L2.3})_{10}Br_4(H_2O)_6]Br_{16}\cdot 68H_2O$ – Complex **6.8***

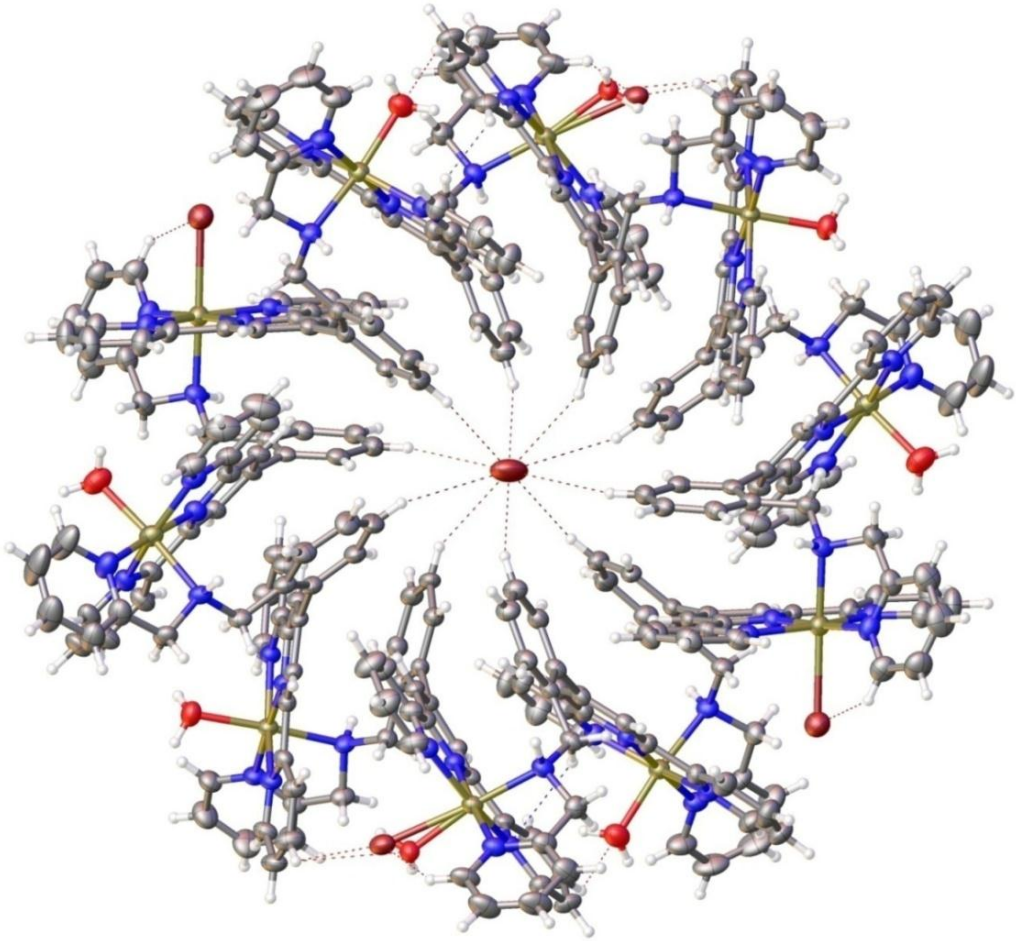

*Figure 6.24. The crystal structure wheel complex $[Ni_{10}(\mathbf{L2.3})_{10}B_{2.1}(H_2O)_6]Br_{17.9}$, **6.8**. The solvent molecules and the uncoordinated bromide ions are omitted for clarity. The central Br···C-H interactions range between 3.0 Å to 3.3 Å.*

The complex $[Ni_{10}(\mathbf{L2.3})_{10}Br_{2.1}(H_2O)_{7.9}]Br_{17.9}$, **6.8** was synthesised by mixing of $NiBr_2\cdot 3H_2O$ in water (10 ml) with the ligand **L2.3** in dichloromethane : methanol (1:5) solution. The

resulting green solution was heated to reflux for 1 hr and then reduced to 1 ml from the mixture by rotary evaporation. The pale green block shaped crystals suitable for X-ray crystallographic analysis were obtained by slow evaporation of an aqueous solution in about 3 weeks time with 90% yield. The X-ray crystal structure of the complex was solved in the triclinic space group $P\bar{1}$, **Figure 6.24**. The complex contains ten **L2.3** ligand molecules, ten Ni(II) ions, twenty bromide ions and a large number of water molecules around the wheel. Nineteen bromide ions lie outside the wheel cavity and one bromide ion is held in the centre with Br···H-C interactions.

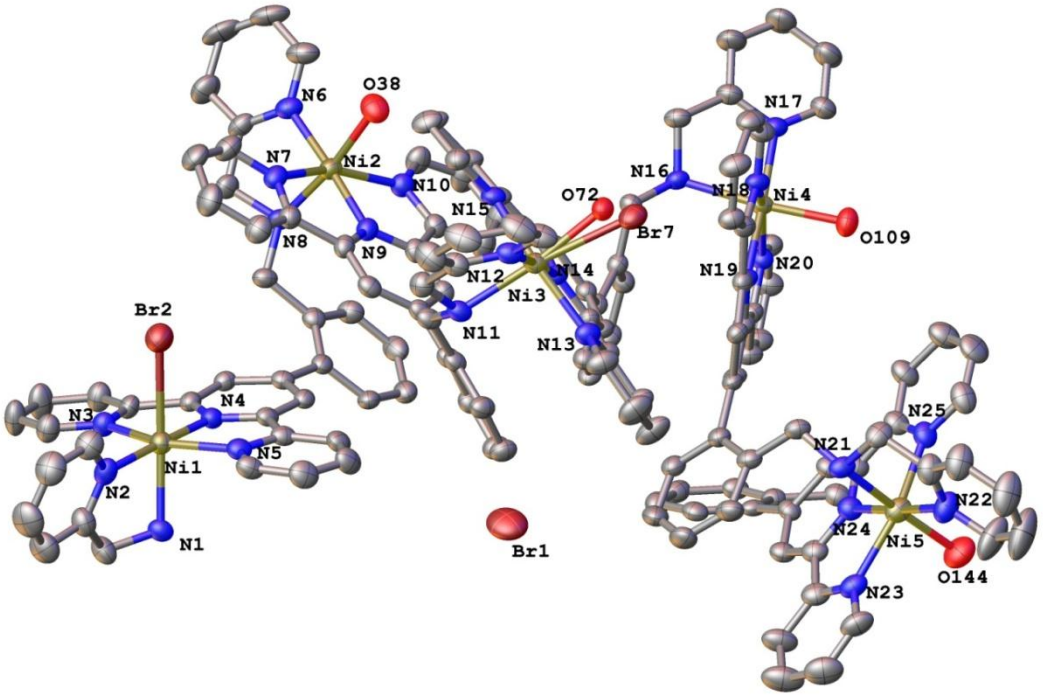

*Figure 6.25. The asymmetric unit of the complex **6.8**, showing Head-to-tail bridging of the ligands.*

The Ni(II) ions are six-coordinate with slightly distorted octahedral geometry. Each Ni(II) ion is coordinated to two **L2.3** ligands *via* HT coordination mode (**Figure 6.2e**), where it coordinate through terpyridine-type binding site (head or H) of one ligand and picolylamine-type binding site (tail or T) of the second ligand. Each wheel is assembled remarkably with ten such HT coordination modes, referred to as a $(HT)_{10}$ coordination mode. In each coordination site, five-positions are occupied by three terpyridine-type and two picolylamine-type nitrogen atoms, and the sixth position was either occupied by a bromide ion (on two of the ten nickel centres), a water molecule (on six of the ten nickel centres) or both bromide and water (on two of the ten nickel ions) when disordered, shown in the

asymmetric unit of **6.8** in **Figure 6.25**. In the octahedral geometries a bromide ion/water ligand and a picolylamine nitrogen atom occupy the axial positions. The equatorial positions are occupied by four nitrogen atoms (all three terpyridine-type nitrogen atoms and one of the picolylamine-type nitrogen atoms). In an asymmetric unit, the ligands on the sixth axial position of the Ni(II) octahedral geometry are arranged in an order of halide – water – halide/water – water – water.

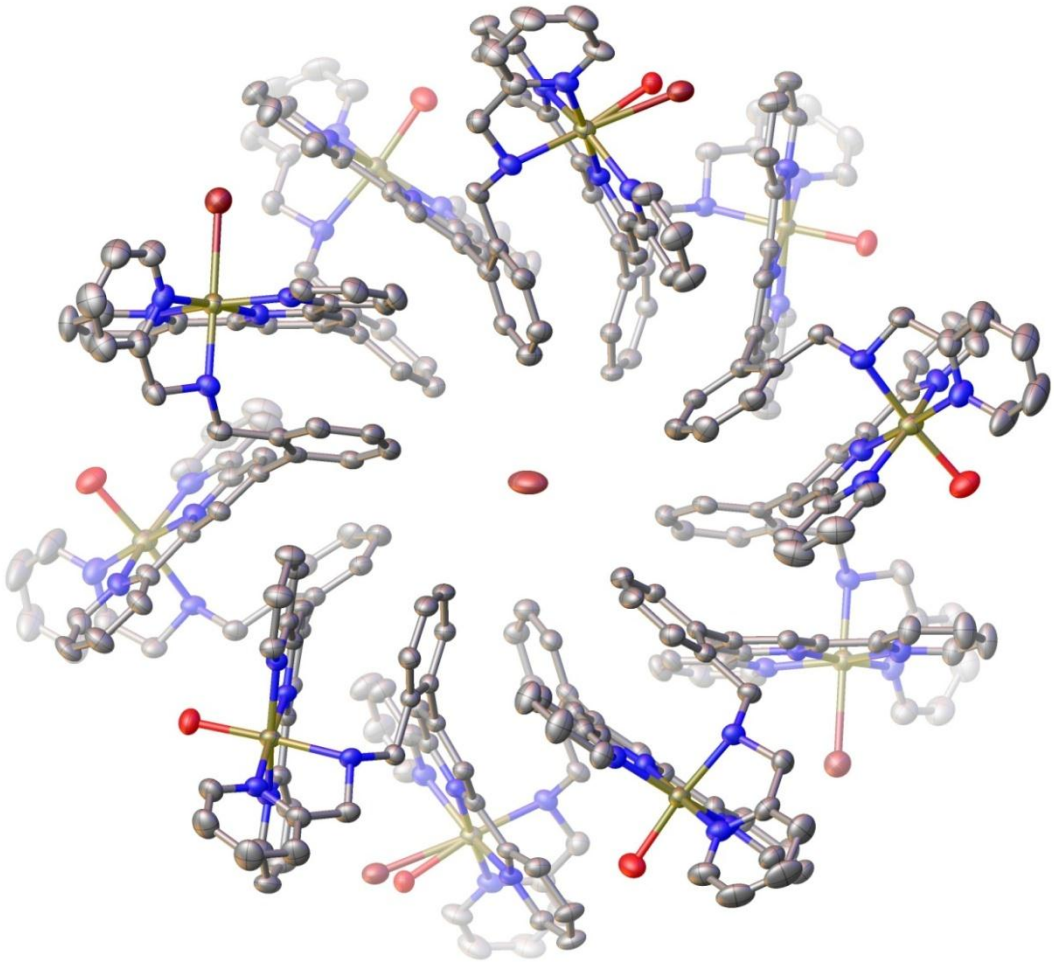

*Figure 6.26. The alternative metal-ligands units of **6.8** assembled above (dark atoms) and below (fainted atoms) the plane of the wheel. The phenyl ring of the terpyridine units of **L2.3** are nearer to the centre of the ring. The halide or water ligands lie above and below the plane of wheel alternatively. The solvent molecules, H atoms, and all non-coordinating bromide ions except the one in centre have been omitted for clarity.*

The water or bromide ligands reach around the next Ni(II) ion from the outside of the wheel, while the terpyridine units are nearer the centre of the wheel (**Figure 6.26**). All of the metal coordination spheres alternatively lie above and below of the plane of the wheel as shown in **Figure 6.26**. The adjacent ligands twist around up and down alternatively to assemble itself in the shape of wheel. The inter-planar angle between the terpyridine planes

of the adjacent **L2.3** ligands varies from 26.20° to 47.32°. Each ligand twists with a torsion angle C-N-C-C (between phenyl and amine functionality) ranging from 163.4(4)° to 163.6(4)°. In each wheel the water and halide ligands attached to Ni(II) are oriented in the same direction like wings of a windmill. Ignoring the chloride and water ligands attached to nickel, the molecule has D_{5d} symmetry.

A bromide ion is present inside the wheel cavity held tightly with a number of interactions with hydrogen atoms of the phenyl rings near the cavity (**Figure 6.24**). The wheel shape Ni_{10}**L2.3**$_{10}$ metal-ligand assembly of the complex seems to form with Br···H-C interactions, where a bromide ion is held in the centre of the cavity. The Br···C-H interactions with aromatic hydrogen atoms of the phenyl rings of the ligands are shown in crystal structure of **6.8**, which range between 3.324(13) Å to 4.279(19) Å.

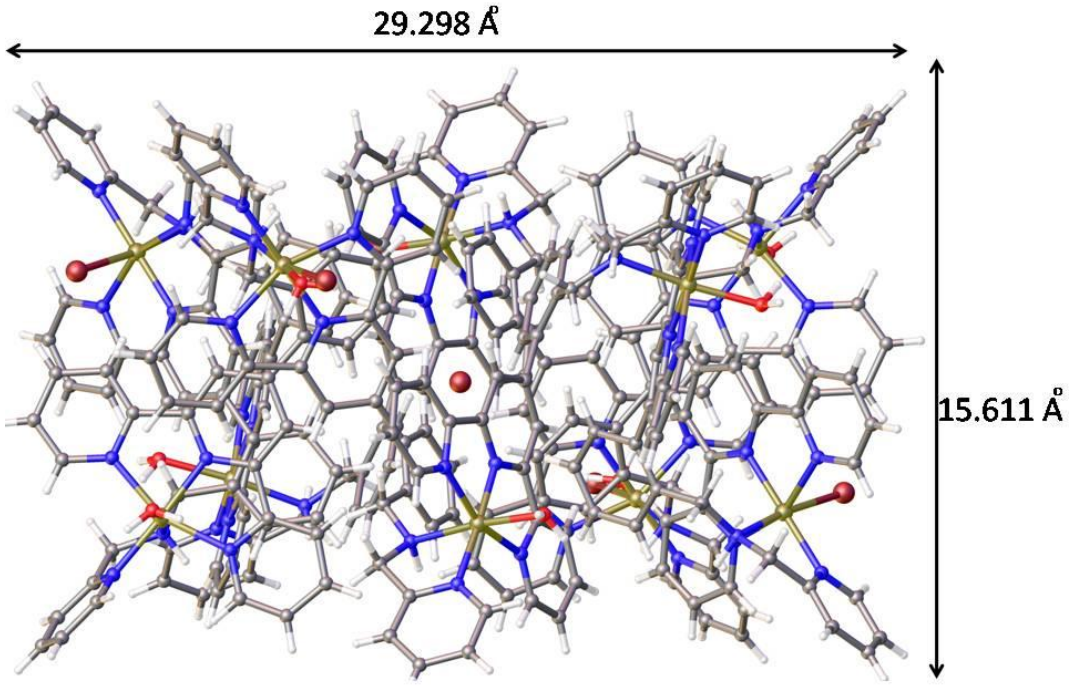

*Figure 6.27. The lateral view of the wheel shaped complex **6.8** showing depth and diameter of the ring.*

The wheel is approximately circular with an inner diameter measured between the symmetry equivalent hydrogen atoms of 7.693(3) Å to 6.006(15) Å and the distances between symmetry equivalent nickel ions of 18.934(2) Å to 20.217 (19) Å. The outer diameter of the ring varies from 29.298 Å to 26.515 Å and the ring is 15.611 Å deep (rim

thickness) shown in **Figure 6.27**. Fifteen uncoordinated bromide ions are present around the wheel for charge balance of the complex.

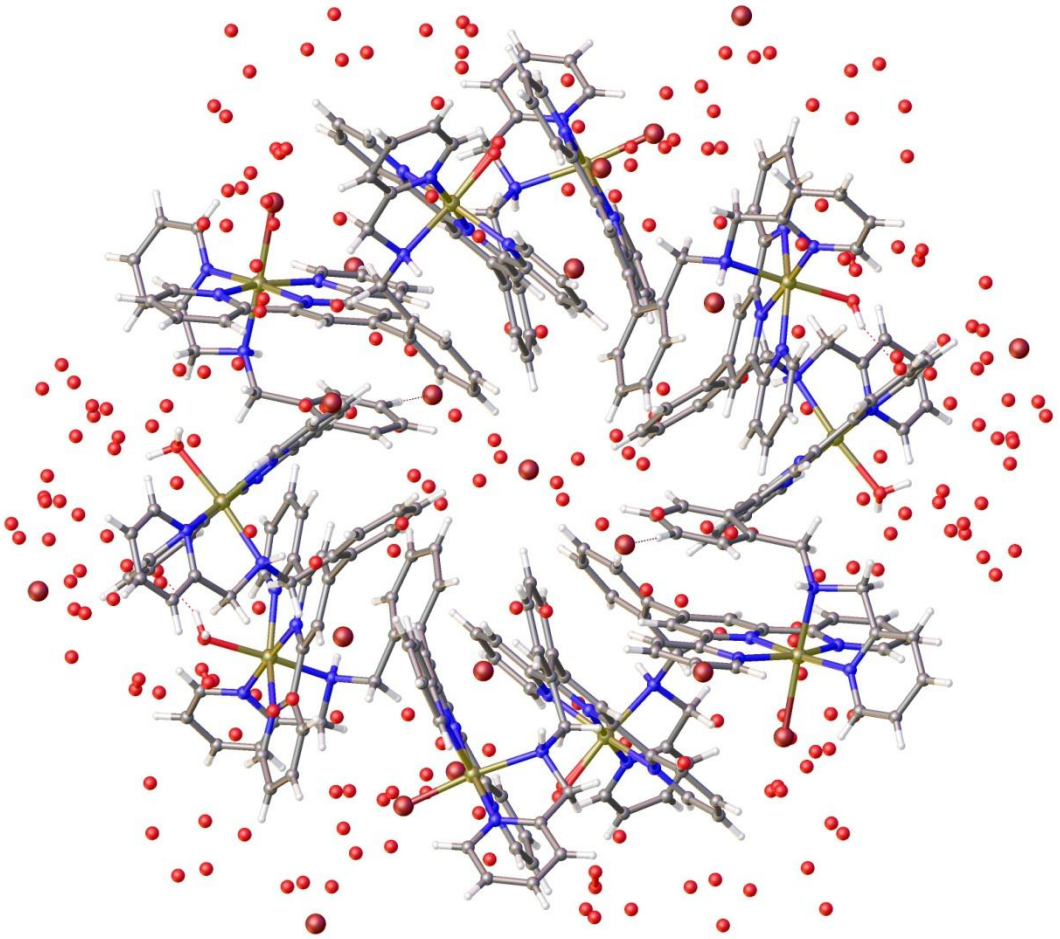

*Figure 6.28. A view of the complex **6.8** showing incredibly large amount of solvent water molecules scattered randomly around the wheel.*

Each decanickel complex contains a remarkably large amount of solvent that contains approximately 182 water molecules (calculated from crystal cell volume) scattered randomly in between the molecules shown **Figure 6.28**. This wheel type structure is linked in a 3D network by the hydrogen bond interactions between various atoms. However, due to disorder associated with outer bromide and water molecules, only 54 water molecules were modelled from the electron density map. More about modelling of the disorder in these crystal structures will be discussed in **section 6.3.1.4**. Different techniques used to calculate the number of water molecules present in the crystal structure will be discussed in **section 6.3.2**. Other than hydrogen bonding interactions, a number of non-covalent stacking interactions such as π-π stacking and short contacts are also involved in stabilisation of these big wheel shaped supramolecular assemblies.

Different Ni-N bond lengths range between 1.990 Å to 2.174 Å. The bond lengths between Ni(II) ions and the coordinated water molecules lie between 2.07 Å to 2.17 Å, whereas between Ni(II) and the coordinated bromide ions it varies from 2.59 Å to 2.63 Å.

*6.3.1.2. $[Ni_{10}(\mathbf{L2.3})_{10}Cl_4(H_2O)_6]Cl_{16}\cdot 88H_2O$ – Complex **6.9***

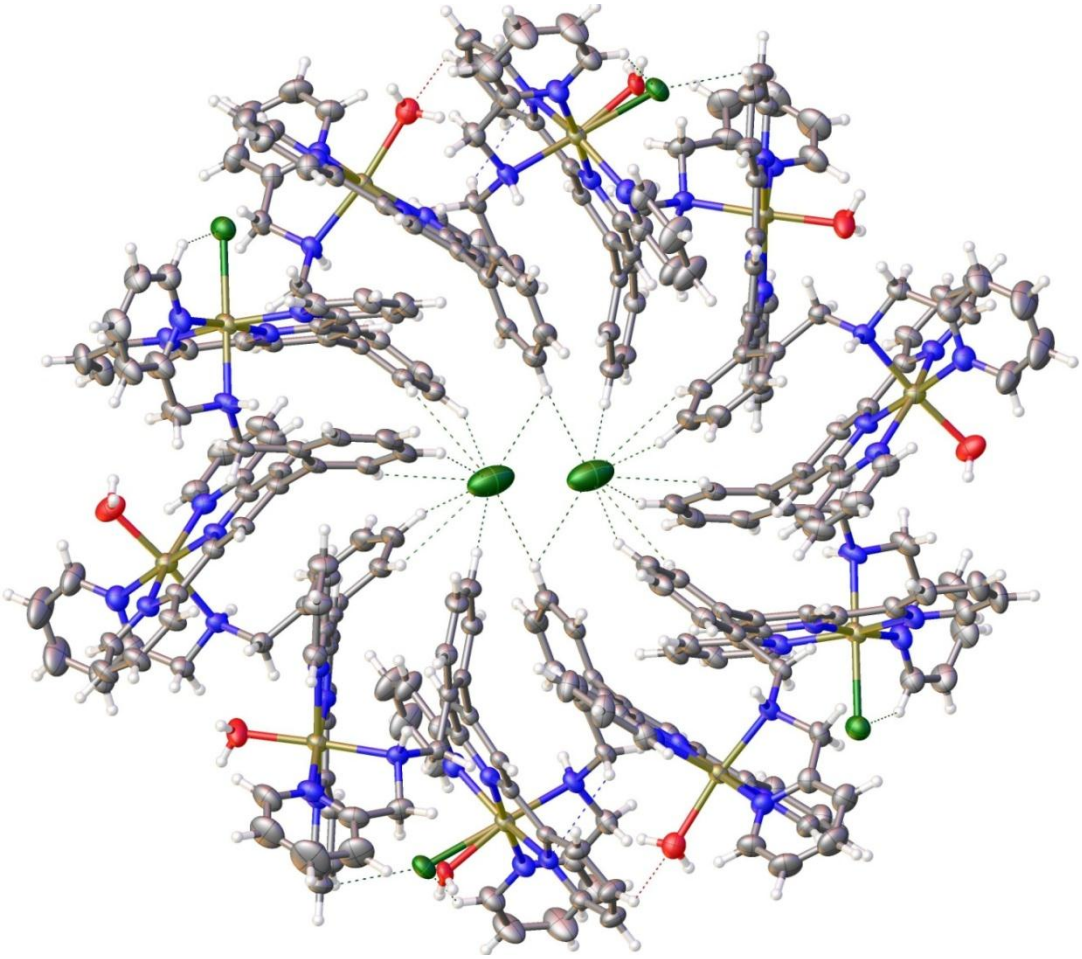

*Figure 6.29. The crystal structure for $[Ni_{10}(\mathbf{L2.3})_{10}Cl_{2.6}(H_2O)_{7.4}](Cl)_{17.4}$,**6.9**. The solvent molecules and the uncoordinated chloride ions omitted for clarity. The central Cl···C-H interactions range between 2.9 Å to 3.3 Å.*

The complex $[Ni_{10}(\mathbf{L2.3})_{10}Cl_{2.6}(H_2O)_{7.4}]Cl_{17.4}$, **6.9** was also synthesised in a same way as the previous complex **6.8** but with $NiCl_2\cdot 6H_2O$. The crystals appear after 3 weeks by slow evaporation from undisturbed aqueous solutions with 75% yield.

The crystal structure of **6.9** was solved in the triclinic space group $P\bar{1}$. This wheel also contains ten octahedral Ni(II) ions coordinated to ten **L2.3** ligands *via* $(HT)_{10}$ coordination mode, **Figure 6.29**. The sixth position on Ni(II) is occupied either by a chloride (on two of

the ten nickel centres), or a water ligand (on six of the ten nickel centres) or a water and chloride both (on two out of the ten nickel ions) when disordered. The remaining chloride ions are non-coordinating, present in crystal lattice for charge balance.

This wheel contains a disordered chloride ion in the centre of cavity held by Cl···H-C interactions. The chloride ion is disordered over two positions within the cavity, the occupancy of which was anisotropically refined to 50% at each position. The distance between two disordered chloride ions is 2.578(9) Å. In comparison to the previous wheel, the smaller size of the anion in the cavity means it is disordered over two positions to hold the round shape of the complex.

However, due to disordered chloride the wheel is not as round as the previous one. The reduction in size of the anion caused the wheel to become more elliptical in comparison to wheel **6.8**. The wheel elongates to one direction and compresses in perpendicular direction. The inner cavity is elongated to 7.747(17) Å in one diection and compressed to 5.685(9) Å in the opposite direction, with Ni to Ni distances of 18.879(11) Å to 20.274(10) Å. The rim to rim distances are of 29.886 Å to 24.551 Å. The change in dimensions of the wheel in this case indicates that these molecules are very much likely to assemble themselves in a circular form, even if the anion present in the middle is small and disordered.

Compared to previous wheels, the disordered chloride ions in the cavity are held in their place with a larger number of Cl···C-H interactions through aromatic hydrogen atoms of the phenyl rings of **L2.3**. These Cl···C-H interactions range between 2.797(5) Å to 3.015(5) Å. Different Ni-N bond lengths range between 1.990 Å to 2.174 Å. The bond lengths between Ni(II) ions and the coordinated water molecules lie between 2.06 Å to 2.17 Å, whereas between Ni(II) and the coordinated chloride ions the bond lengths vary from 2.24 Å to 2.43 Å.

*6.3.1.3. $[Ni_{10}(\mathbf{L2.3})_{10}Cl_4(H_2O)_6](Cl)_{15}Br{\cdot}91H_2O$ – Complex **6.10***

The Complex $[Ni_{10}(\mathbf{L2.3})_{10}Cl_{2.5}(H_2O)_{7.5}](Cl)_{16.5}Br$, **6.10** was crystallised by mixing of $NiCl_2{\cdot}6H_2O$ with the ligand **L2.3**, containing a small amount of bromide impurity, following the same procedure as with the previous wheels. The pale green block shaped crystals suitable for X-ray crystallographic analysis were obtained by slow evaporation of the aqueous solution over three weeks time with 90% yield.

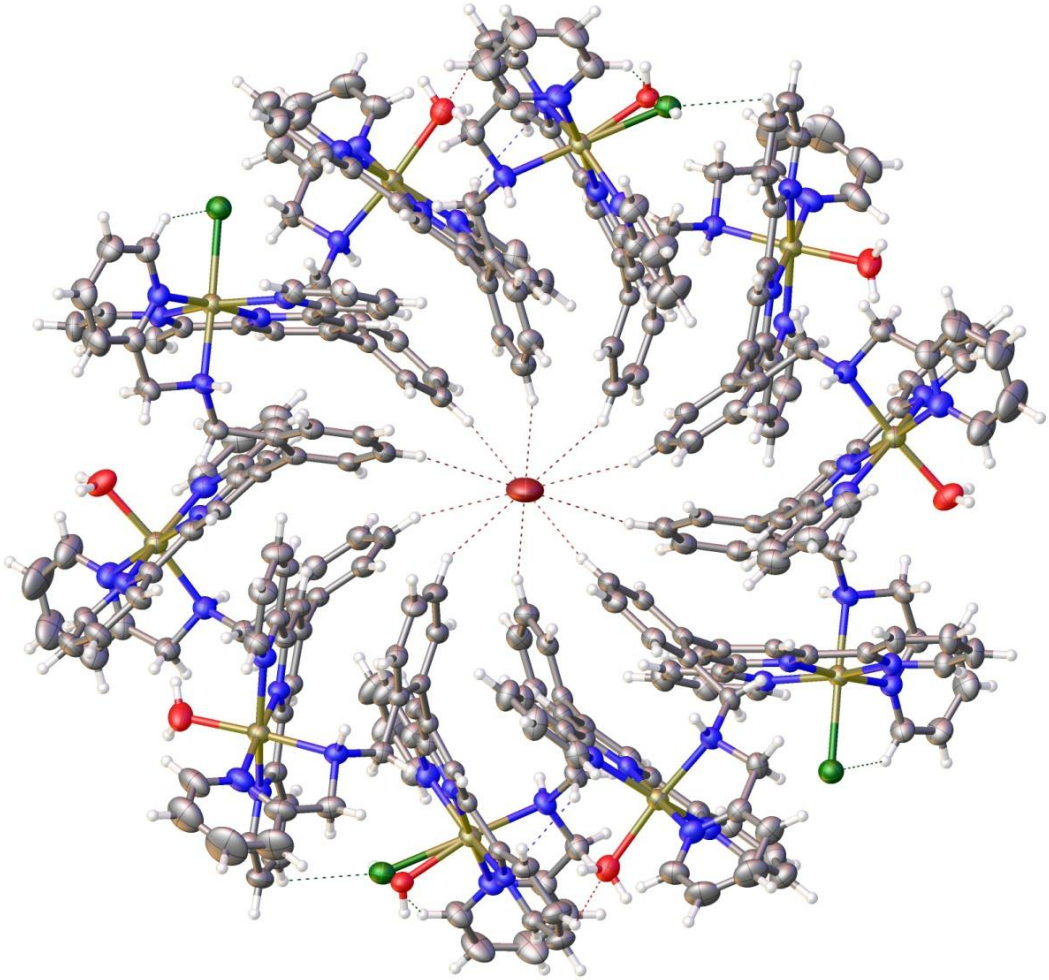

Figure 6.30. Molecular structure for $[Ni_{10}(\mathbf{L2.3})_{10}Cl_{2.5}(H_2O)_{7.5}](Cl)_{16.5}Br$. The water molecules and the uncoordinated chloride ions omitted for clarity.

The complex **6.10** was also crystallised in the triclinic space group $P\bar{1}$, which is similar to the previous wheel. However, the interesting feature of this wheel is that it contains a bromide ion in the centre of the wheel cavity and chloride ions outside. The X-ray crystal structure of decanickel wheel **6.10** is shown in **Figure 6.30**.

The Ni(II) ions occupy the octahedral geometry similar to previous wheels using terpyridine-type binding site, picolylamine-type binding site, chloride ions and water molecules as coordinating ligands. The inner cavity diameter of the wheel measured between the symmetry equivalent hydrogen atoms is 5.928 Å to 6.583 Å and the distance between the symmetry equivalent Ni(II) is 18.852 Å to 19.432 Å. The outer diameter of the ring varies from 26.228 Å to 29.281 Å and the ring is 15.768 Å deep (rim thickness). A bromide ion is present inside the wheel cavity held tightly with a number of interactions with the aromatic hydrogen atoms of the phenyl rings near the cavity (**Figure 6.30**). These Br···H-C interactions range from 3.291(11) Å to 4.027(13) Å.

Different Ni-N bond lengths range between 1.990 Å to 2.174 Å. The bond lengths between Ni(II) ions and the coordinated water molecules lie between 2.067 Å to 2.174 Å, whereas between Ni(II) and the coordinated chloride ions the bond length varies from 2.243 Å to 2.438 Å.

6.3.1.4. Disorder Modelling in Wheel Crystal Structures

In all the wheel crystal structures, the cation Ni_{10}(**L2.3**)$_{10}$ was well ordered except some occupancy problem associated with the halide ions and water molecules coordinated to two nickel centres. The halide-water ligand coordination sites triggered the Hirshfield warning for Ni-halide bond. The halide ion was split into two atoms and their free occupancies were refined isotropically with fixed thermal parameters (U_{iso}). In wheel **6.8**, the occupancies were modelled to 5% for the bromide ion and 95% for water ligand, and were refined anisotropically with fixed U_{iso}. Similarly, in **6.9** the disordered occupancies were modelled by refining the occupancy of chloride and water to 30% and 70%, respectively; and that in **6.10** was modelled by refining the occupancies of bromide and water to 25% and 75%.

Other than this, there was a severe halide/water disorder associated with all the wheel complexes due to remarkably large amount of solvent present in their crystal lattices. This type of halide/water disorder is found to be common in complexes containing a large number of water molecules and halide ions,[223-229] because two closely located electron density peaks could be either a chloride ion disordered over two positions with 50% occupancy at each position, or there could be two disordered water molecules located closely to each other.

To model this halide/water disorder, occupancy of the structure was refined isotropically. The larger electron density peaks were refined as halide ions with full occupancies and then water molecules were assigned to the smaller peaks. Removing the disordered solvent molecules using solvent mask option in Olex2, the structures were modelled to R-factor 10%, 9.1% and 5.67% for **6.8**, **6.9**, and **6.10**, respectively. The number of well ordered water molecules, modelled in the crystal structures were 54, 52 and 38 in respective wheels **6.8**, **6.9** and **6.10**.

6.3.2. Characterisation of the Wheels

6.3.2.1. Mass Spectrometry Analysis

Due to weak interactions the wheels break apart under the mass spectroscopy conditions and the mass to charge (*m/z*) signals appear only at 243.56, 261.55, 305.77, 324.41, 336.41, 458.16, 522.09, 351.75, 568.04 units, which corresponds to $[2(\mathbf{L2.3})+2Ni]^{4+}$, $[\mathbf{L2.3}+NiCl]^{2+}$-H, $[2(\mathbf{L2.3})+Ni]^{3+}+H$, $[2(\mathbf{L2.3})+2Ni]^{3+}$-H, $[2(\mathbf{L2.3})+2Ni+Cl]^{3+}$, $[2(\mathbf{L2.3})+Ni]^{2+}$, $[\mathbf{L2.3}+NiCl]^{+}$, $[2(\mathbf{L2.3})+2Ni+Br]^{3+}$, $[\mathbf{L2.3}+NiBr]^{+}$ ionic species, respectively. Ionic species containing one ligand and one metal ion shows their *m/z* peaks in ES-MSI spectra of all the wheels. A small peak due to free ligand at *m/z* 430.02, $[\mathbf{L2.3}+H]^{+}$, is always present, even if excess nickel ion is present.

6.3.2.2. Thermo Gravimetric, Elemental (CHN) & Melting Point Analyses

Through cell volume calculations in crystallographic analysis the number of water molecules calculated are 182, 190, and 184 in wheel **6.8**, **6.9** and **6.10**, respectively. However, due to the disorder associated with halide and water molecules, it was not possible to model all the water molecules. So different analyses were performed to get some information about the number of water molecules involved in these crystal structures.

Thermal gravimetric analysis (DSC-TGA) data shows that 30% of the total weight that belonged to the free water molecules around the wheel was lost around 100°C upon heating. From experimental data and calculations using molecular mass, 30% weight of a wheel

coincides with 130 water molecules. Clearly the loosely bound water molecules present in the wheel must have been evaporated within the range of first 100°C heating. All halide ions and coordinated water molecules makes 10% of the total weight of the wheel which was lost between 100-300°C heating range. The whole molecule was decomposed to 100% by heating further to higher temperatures.

The melting point results were also consistent with the DSC-TGA results. The wheel crystals start popping at around 100 °C and decompose at further heating to 250 °C.

For elemental analysis the samples were dried in a vacuum dryer from 100-150 °C. The elemental analysis method based upon "flash combustion" shows presence of 68, 88 and 91 water molecules in the respective **6.8**, **6.9** and **6.10** wheel.

These crystals lose their crystallinity when dried, which indicates that water molecules which are loosely bound in the lattice evaporates and hence crystals start converting into powder. As both elemental analysis and thermal gravimetric analysis are performed by heating the material to different temperatures in different times that may have affected the consistency between the results.

6.3.3. An Overview of the Wheels

Here we present the synthesis, crystal structures and characterisation of the unprecedented terpyridine-picolylamine based decanickel wheels. The wheels crystallised from their aqueous solutions containing 1:1 ratio of **L2.3** and Ni(II) salts. These wheel shaped complexes contain Ni_{10}**L2.3**$_{10}$ units arranged in a circular array. Each octahedral Ni(II) is coordinated between two ligands through terpyridine-type (head or H) site of the one ligand and picolylamine-type (tail or T) of the second ligand *via* HT binding mode, resulting in formation of a ring by $(HT)_{10}$ coordination mode. The sixth ligand in each coordination site is occupied either by a water or chloride. All of these crystal structures have very similar structure with very similar unit cell dimensions and space group.

Table 6.5. Showing preferred formation of wheels containing Br in the middle of the cavity.

sNo.	Reactants	Wheel (cavity anion / rim anions)	Yield
1	1 $NiCl_2 \cdot 6H_2O$ + 1 **L2.3**(Br)x + water	**6.8 (Br/Cl)**	70%
2	1 $Ni(NO_3)_2 \cdot 6H_2O$ + 1 **L2.3**(Br)x + water	**6.9 (Br/Br)**	40%
3	1 $Ni(SO_4)_2 \cdot 6H_2O$ + 1 **L2.3**(Br)x + water	**6.9 (Br/Br)**	40%
4	1 $NiBr_2 \cdot 3H_2O$ + 1 **L2.3**(Br)x + water	**6.9 (Br/Br)**	90%
5	1 $NiCl_2 \cdot 6H_2O$ + 1 **L2.3**(Br)x + water + excess NaCl	**6.10 (Br/Cl)**	90%
6	1 $NiCl_2 \cdot 6H_2O$ + 1 **L2.3** + water	**6.9 (Cl/Cl)**	75%
7	1 NiI_2 + 1 **L2.3** + water	-	-
8	1 NiF + 1 **L2.3** + water/acetone	-	-
9	**6.8** + Excess of NaCl + water	**6.10 (Br/Cl)**	90%
10	**6.9** + Excess of LiBr + water	**6.9 (Br/Br)**	90%
11	**6.8** + Pyridine/ 4-ethylpyridine + water	**6.9 (Br/Br)**	90%

Different experiments performed with both pure and impure ligand are shown in **Table 6.5**. Understanding these results, we conclude three facts about the wheel shaped complexes – 1. These wheels form only in the presence of bromide or chloride ions; 2. The preference of chloride or bromide as outer ligands always depends upon their concentration in the reaction mixture; and 3. The bromide ion is the best fit anion for the wheel cavity.

The third fact, preference of bromide ion over the chloride ion to fit in the cavity could be due to the perfect size of bromide ion to undergo H-bonding interactions with the hydrogen atoms pointing inside the cavity. However, in the presence of only chloride ions, the complexes still manage to arrange themselves in the form of a wheel but slightly elliptical. Due to smaller size of the chloride ion it is disordered over two positions each with an half occupancy. This displacement of the chloride ion over two positions enables it to undergo H-bonding interactions with maximum hydrogen atoms of the inner cavity phenyl rings; thus stabilise large wheel supramolecular architectures.

This type of template effect of anions (chloride/bromide in our case) to form supramolecular architecture (wheels in our case) has been observed in literature. Dunbar *et al.* highlighted the "anion template effect" in formation of the resulting structural motifs among M(II)−bptz complexes, where judicious choice of the anion resulted in the formation

of either a molecular square or a pentagon (where M = Ni, Zn and bptz = 3,6-bis(2pyridyl)-1,2,4,5-tetrazine).[355] Lee *et al.* reported that anion size can regulate the secondary structure of a coordination chain, from folded helical, cyclic, to unfolded linear chain conformations in the solid state.[356] Beer *et al.* have summarised their efforts in the area of anion influenced syntheses of interlocked structures, demonstrating the versatility and scope of this approach.[357]

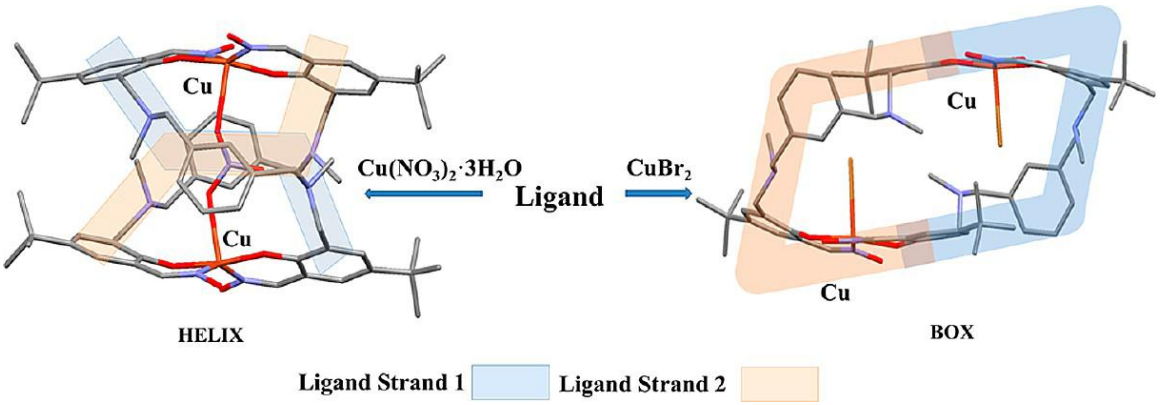

Figure 6.31. Anion governed helicate and box complexes synthesised by Plieger et al. (Picture form reference)[358]

More recently in 2013, Plieger *et al.* depicted the use of $Cu(NO_3)_2 \cdot 3H_2O$ metal salt leads to the formation of a dicopper(II) double helicate structure with aryl-linked salicylaldoxime-based ligands, whereas the use of bromide and bromide/tetrafluoroborate Cu(II) salts resulted in formation of the "boxes", showing the strong influence of anion on the structural forms adopted by the resulting complex (**Figure 6.31**).[358]

In the present work, it appears that the wheel shaped geometries are stabilised by the encapsulated halide ions due to their anion···H-C interactions. The Br···H-C interactions range between 3.003(8) Å to 3.649(9) Å; and the Cl···H-C interactions range from 2.797(5) Å to 3.015(5) Å. The space-fill model of the wheel containing bromide ion in the cavity, **6.8**, and the wheel containing disordered chloride ion in the cavity, **6.9** are shown in **Figure 6.32**.

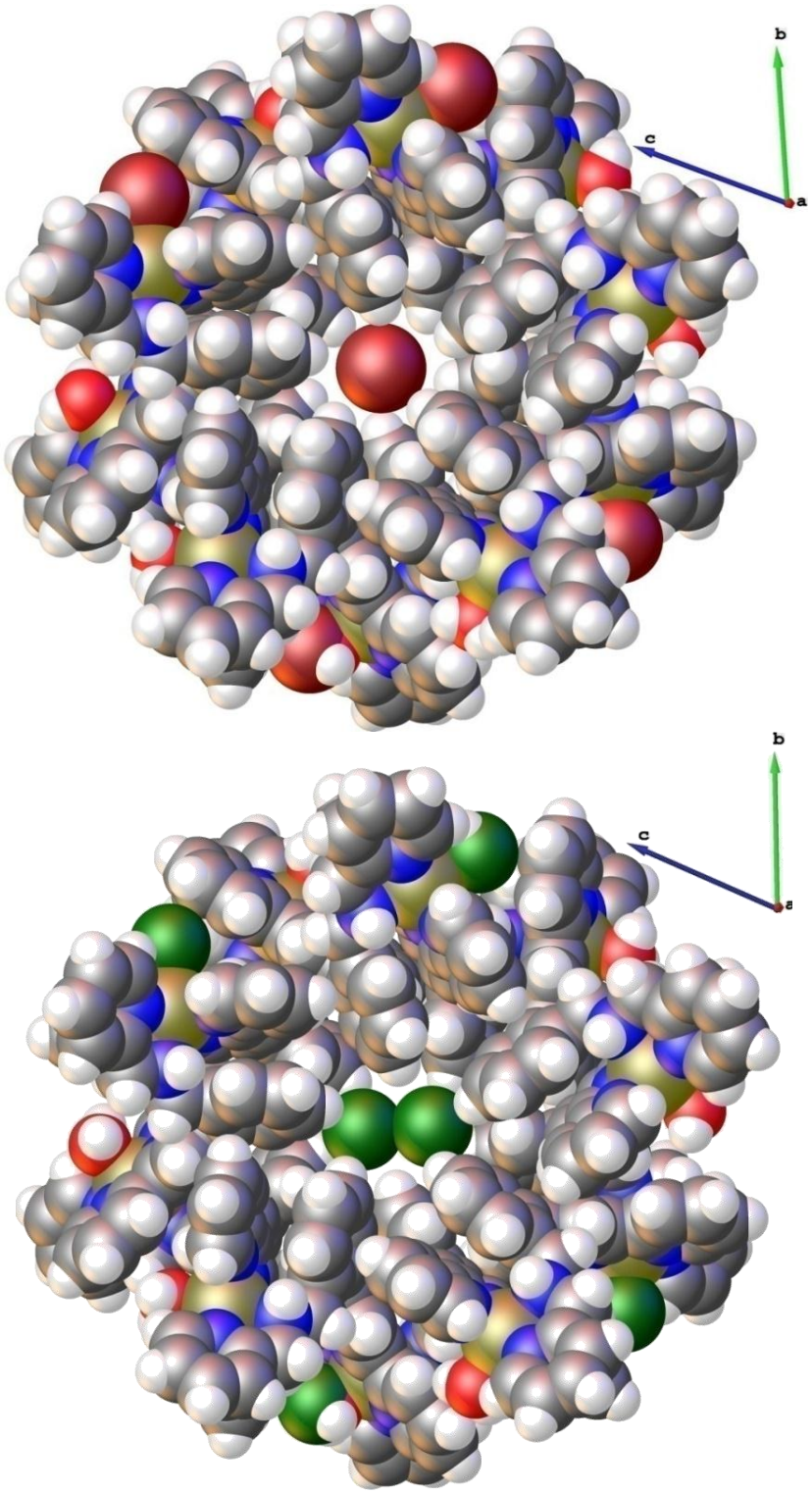

*Figure 6.32. The spacefill diagrams of complex **6.8** and **6.9** showing tightly held anions in the middle of the wheels.*

6.4. Conclusion

This chapter deals with macrocyclic supramolecular complexes synthesised during this project. The ligand **L2.3** was able to act as a bridging ligand between two metal ions and adopt different coordination modes such as HH-TT-HH-TT and $(HT)_{10}$, resulting in formation of two spectacular architectures – the boxes and the wheels.

The HH-TT-HH-TT coordination mode, **Figure 6.3**, results in formation of box shaped complexes. Six different tetranuclear, both homo-metallic and hetero-metallic, box shaped complexes were isolated, the crystal structures of which are described in detail in this chapter. For hetero-metallic box shaped complexes, the ligand **L2.3** was mixed with Fe(II). The reaction mixture immediately turned purple, indicating formation of $[Fe(\mathbf{L2.3})_2]^{2+}$ complex in solution through HH coordination mode. Formation of these 1:2 Fe:**L2.3** species in solution was confirmed with Job's method analysis and mass spectrometry.

Addition of Zn(II) and Cu(II) salts in to $[Fe(\mathbf{L2.3})_2]^{2+}$ complexes in solution produced boxes $[Fe_2Zn_2(\mathbf{L2.3})_2Cl_2](PF_6)_6$, **6.1** and $[Fe_2Cu_2(\mathbf{L2.3})_2Cl_2]PF_6$, **6.4** *via* TT coordination between free picolylamine binding sites. Addition of an excess of hexafluoridophosphate ions resulted in crystallisation of the boxes. Similarly, when Ni(II) was used instead of Fe(II), the box $[Ni_2Zn_2(\mathbf{L2.3})_4Cl_2]PF_6$, **6.5**, was formed. The homo-metallic box complexes $[Zn_4(\mathbf{L2.3})_4(OAc)_2]PF_6$, **6.2**, and $[Zn_4(\mathbf{L2.3})_4Br_2]PF_6$, **6.6**, were formed only when Zn(II) metal salts of the respective anions were used.

In all the box complexes, the metal ions bound in terpyridine binding sites occupied octahedral geometry. All the positions of octahedral geometry are occupied by terpyridine type nitrogen atoms. The metal ions in picolylamine binding sites occupied five-coordinate geometry where four positions are occupied by amine nitrogen atoms and the fifth position is occupied by monodentate coordinating anions such as chloride, bromide or acetate added as a part of the metal salt.

All the box complexes had a very similar structure with similar cavity sizes and two coordinating anions pointing into the box cavity. As an extension to complex **6.1** and **6.2**, a dicarboxylate chelating anion terephthalate was deliberately inserted in the box cavity resulting in formation of box complex **6.3**. The terephthalate ion was stacked in the cavity with π-π stacking interactions with peripheral terpyridine-type rings of **L2.3** ligands.

An interesting fact about the boxes was that they crystallise only in the presence of hexafluoridophosphate ions. The crystal structures show a number of hydrogen bonding interactions between amine hydrogen atoms of the ligands. In each complex two of the six hexafluoridophosphate ions located above and below the box geometries participate in multiple hydrogen bonding interactions with amine hydrogen atoms. When no hexaflouridophosphate ions were added, the dinuclear complexes were formed. In dinuclear complexes one metal ion binds in each binding site. Which showed that hexaflouridophosphate ions may have a templating effect on crystallisation of the box shaped complexes.

Reaction of Ni(II) ions with **L2.3** produced spectacular decanickel wheel shaped complexes, which are the first precedent wheel shaped complexes with terpyridine-picolylamine type binding. The detailed crystal structure, and characterisation are discussed in this chapter. When Ni(II) bromide or chloride salts were mixed with **L2.3** in aqueous solutions, the wheel shaped complexes $[Ni_{10}(\mathbf{L2.3})_{10}Br_{2.1}(H_2O)_{7.9}]Br_{17.9}$, **6.8**, $[Ni_{10}(\mathbf{L2.3})_{10}Cl_{2.6}(H_2O)_{7.4}](Cl)_{17.4}$, **6.9** and $[Ni_{10}(\mathbf{L2.3})_{10}Cl_{2.5}(H_2O)_{7.5}](Cl)_{16.5}Br$, **6.10** were crystallised. These wheel shaped complexes contain $Ni_{10}\mathbf{L2.3}_{10}$ units arranged in a single circular array. Each octahedral Ni(II) ion is coordinated between two ligands through terpyridine-type site (H) of the one ligand and picolylamine-type site (T) of the second ligand, (HT binding mode), resulting in formation of a $(HT)_{10}$. The sixth ligand at each metal ion site is occupied either by water or halide. A bromide or chloride ion is always present within the cavity of the wheel. These crystal structures had very similar unit cell dimensions and space groups.

A number of experiments with different Ni(II) salts and **L2.3** were performed, and in our experience the wheel shaped complexes form only in the presence of chloride or bromide ions. The preference of chloride or bromide as outer ligands was always depended upon their concentration in the reaction mixture.

Another fact of these wheel shaped complexes was preference of bromide ion over the chloride ion to fit in the cavity, which could be due to the perfect size of bromide ion to undergo H-bonding interactions with the hydrogen atoms pointing inside the cavity. However, in the presence of only chloride ions, the complexes still managed to arrange themselves in the form of a wheel, but one which is slightly elliptical. Due to smaller size of the chloride ion, it was disordered over two positions each with an half occupancy. This

displacement of the chloride ion over two positions enabled it to undergo H-bonding interactions with maximum hydrogen atoms of the inner cavity phenyl ring resulting stabilization of the large wheel supramolecular architectures. It appears that the wheel shaped geometries are stabilised by the encapsulated halide ions due to their anion···H-C interactions.

CHAPTER 7

CONCLUSIONS AND FUTURE PROSPECTS

7.1. Conclusions

This thesis describes successful synthesis of some dinuclear metal complexes and their effect on the rate of hydrolysis of the phosphate diester group in the DNA model compound, BNPP. The rate of hydrolysis was compared with those of the related analogous mononuclear complexes. This research has focused on synthesis of the complexes with non-identical metal binding sites. The initial aim of the research was fulfilled by synthesising a number of 2,2':6',2''-terpyridine-based polydentate ligands with different amine functionalities. The dinuclear complexes used for hydrolysis of phosphate diester in literature were with identical metal binding sites. [30, 38, 41, 42, 45, 57, 58, 66, 95, 106] Various polydentate ligands synthesised in this project are shown in **Figure 2.20**.

The 2,2':6',2''-terpyridine-based parent ligand 4'-(2'''-toluyl)-2,2':6',2''-terpyridine, **L2.1**, was functionalised at its 2'''-methyl group *via* a free radical bromination reaction, then different amine functionalities were introduced by nucleophilic substitution reactions. All the ligands were purified by column chromatographic techniques using alumina or Dowex ion-exchange columns. The detailed ligand syntheses are discussed in Chapter 2, with crystal structures of some isolated ligands.

All these polydentate ligands contain two binding sites – the terpyridine-type site denoted as "Head" or "H" and the amine-type bi-, tri-, or tetradentate binding sites denoted as "Tail" or "T" in this thesis. Due to these potential binding sites, a metal can bridge between two ligands through different coordination modes such as HH and TT coordination modes discussed in Chapter 4 and HH-TT-HH-TT or $(HT)_{10}$ coordination modes discussed in Chapter 6. A number of dinuclear, polynuclear and supramolecular complexes have been synthesised and characterised, during this research, where metal ion adopt these coordination modes.

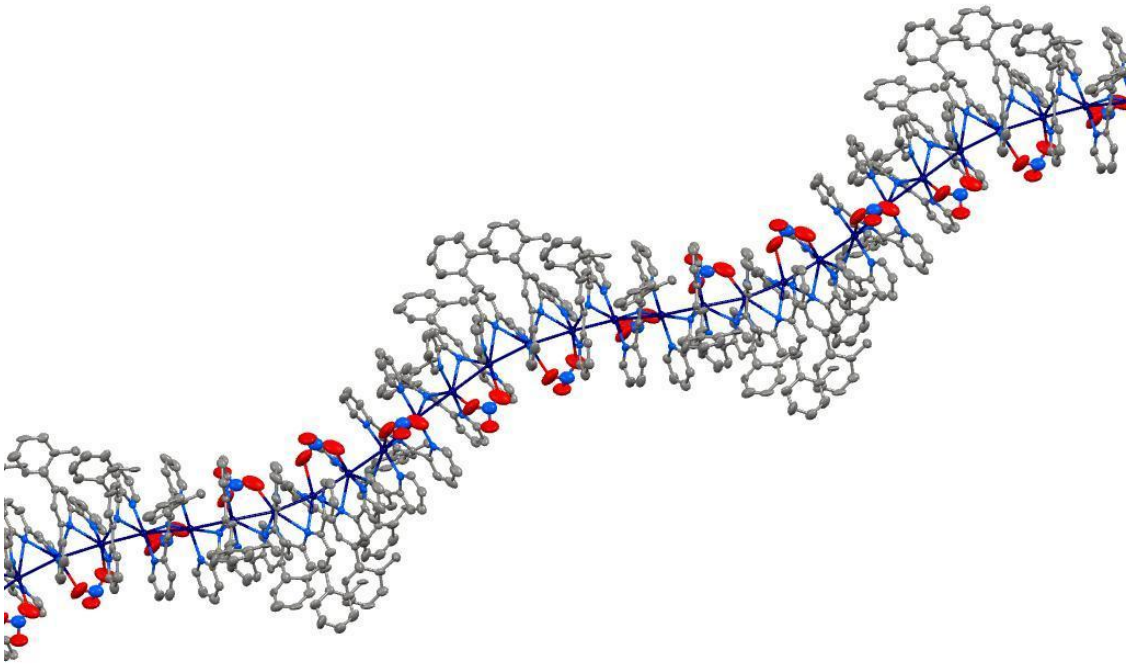

*Figure 7.1. The fascinating $[Ag_2(\mathbf{L2.1})_2NO_3]_n[NO_3]_n$ infinite Ag(I) spiral, **3.13**, synthesised during this research.*

The coordination chemistry of the parent ligand 4'-(2'''-toluyl)-2,2':6',2''-terpyridine, **L2.1**, was explored using the transition metal ions Cu(II), Ni(II), Zn(II) and Ag(I). The thirteen new metal complexes that were synthesised and characterised are discussed in Chapter 3, along with their crystal structures. Ag(I) produced a fascinating polymeric complex **3.13**, where terpyridine binds as an unusual bis-bidentate ligand, **Figure 7.1**. The central nitrogen atom acts as a "hyperdentate" ligand where it binds to two silver ions.

Ni(II) produced octahedral 1:1 and 1:2 (M:L) complexes with **L2.1**. The 1:1 and 1:2 complexes $[Ni(\mathbf{L2.1})_2]Cl_2$ and $[\{Ni(\mathbf{L2.1})Cl_2\}_2]$ were in equilibrium with the ratio of the products depending on the chloride ion concentration in solution. Both Cu(II) and Zn(II) produce five- and six-coordinate complexes of 1:1 and 1:2 (M:L) stoichiometry. The 1:2 (M:L) bis-**L2.1** complexes were formed if only non-coordinating counter-ions are used, regardless of the ratio of metal-to-ligand present.

A trinuclear Cu(II) complex, **3.6**, with 3:2 (M:L) stoichiometry was crystallised from the reaction mixture when an excess of metal salt was added to the ligand. The notable feature of the complex is that two terpyridine coordinated Cu(II) ions are five-coordinated and the third is four-coordinate. All the Cu(II) and chloride ions were connected by Cu-Cl-Cu mono-μ-chlorido bridging.

Both dinuclear and tetranuclear complexes of **L2.3** and **L2.4** were synthesised using Zn(II) and Cu(II) metal ions. In these complexes each ligand bridges between two metal ions, where one metal ion binds in the tridentate terpyridine (head) binding site and another metal ion binds either in bidentate picolylamine or in tridentate bis(picolylamine) tail binding sites. The synthesis, characterisation and crystal structures of these complexes are discussed in Chapter 4.

The Zn(II) complexes $[Zn_2(\mathbf{L2.3})Cl_4]\cdot 3CH_3CN$, **4.1**, and $[Zn_2(\mathbf{L2.4})Cl_4]\cdot 2CH_3OH$, **4.2**, synthesised using $ZnCl_2$ were crystallised as discrete dinuclear units. Similarly, the Cu(II) complex $[Cu_2(\mathbf{L2.3})(CH_3COO)_4(H_2O)]\cdot 3H_2O$, **4.3**, was also crystallised as discrete dinuclear units. However, the Cu(II) complexes $[Cu_4(\mathbf{L2.3})_2(\mu_2\text{-}Cl)_2Cl_6(CH_3OH)_2]\cdot 2CH_3OH$, **4.4**, $[Cu_4(\mathbf{L2.3})_2(\mu_2\text{-}Cl)_2Cl_6]$, **4.5**, and $[Cu_4(\mathbf{L2.4})_2(\mu\text{-}Cl)Cl_{6.5}(H_2O)_{1.8}]Cl_{1.5}\cdot 1H_2O$, **4.6**, synthesised using $CuCl_2\cdot 2H_2O$, were crystallised as tetranuclear complexes. In these complexes two dinuclear units were bridged together through Cu-Cl-Cu bridging. In the case of **4.4** and **4.5**, ligands interact *via* double μ-chlorido (tail-to-tail) Cu-Cl-Cu bridging, whereas in **4.6** the mono μ-chlorido (head-to-tail) Cu-Cl-Cu bridging was observed between each dinuclear unit.

Chapter 5 describes the studies of the kinetics of hydrolysis of the phosphate diester compound BNPP in the presence of dinuclear and analogous mononuclear Zn(II) complexes. The pseudo-first order rate of hydrolysis of BNPP was calculated from the slope of absorbance *versus* time graphs. The kinetics data shows a slight increase in the rate of hydrolysis of BNPP in case of dinuclear complexes (1.5- to 7.6- fold at different pH values) than that of the mononuclear complexes. The derived pH-rate profiles showed an increase in the observed rate with the increase in pH with a sharp rise in rate after certain pH values. In the case of the mononuclear complexes, the sharp rise was at pH 8.5 and that in case of dinuclear complexes was at pH 8.0. The portion of sigmoid shaped pH-rate profile curves observed were a characteristic of a kinetic process controlled by an acid-base equilibrium, which exhibit inflection points corresponding to the pK_a values for a complex. Since the rate enhancement by the dinuclear complexes over the mononuclear complexes was not too high, based on literature we concluded that there is slight or no effect of dinuclearity on the rate of hydrolysis. This level of rate enhancement is due to lowering of pK_a of metal coordinated hydroxide species in dinuclear complexes.

Chapter 6 discusses the supramolecular aspects of the polydentate ligands synthesised in this project. The metal complexes of **L2.3** produced impressive architectures – the boxes

and the wheels, with divalent metal ions such as Fe(II), Zn(II), Cu(II) and Ni(II). In all the box and wheel complexes **L2.3** acted as a bridging ligand between two metal ions.

The tetranuclear $M^1{}_2M^2{}_2$(**L2.3**)$_4$ box shaped complexes were formed with HH-TT-HH-TT coordination mode. In this coordination mode, two divalent M^1 ions bridge between the ligands through their terpyridine binding sites (H). This produced octahedral bis-terpyridine type complex M^1(**L2.3**)$_2$ *via* HH coordination mode leaving the picolylamine binding site free. Then two divalent M^2 ions link two M(**L2.3**)$_2$ units together through picolylamine binding sites *via* TT coordination mode, in order to produce $[M^1{}_2M^2{}_2$(**L2.3**)$_4]^{8+}$ complexes, **Figure 6.17**. The M^2 ions in each box complex adopt a five-coordinate geometry, where four positions are occupied by the nitrogen atoms from picolylamine-type binding sites, and the fifth position is occupied by a coordinating anion (chloride, bromide or acetate) introduced as a part of the metal salt.

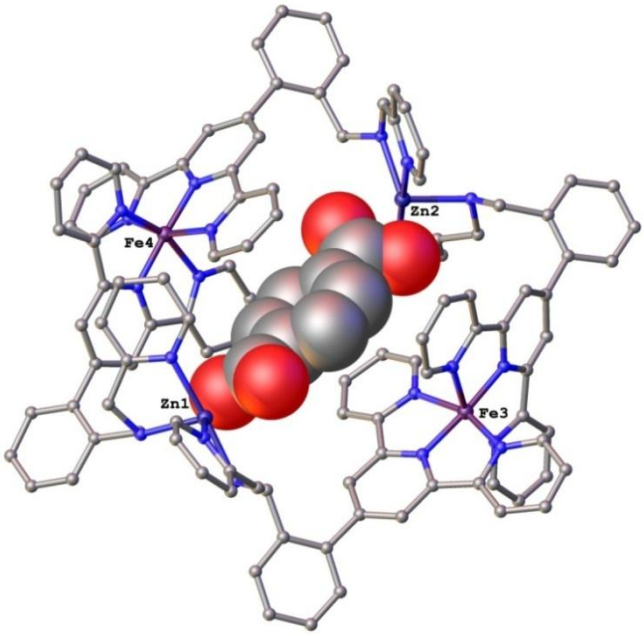

Figure 7.2. Terephthalate encapsulated box Complex 6.3 synthesised during this research.

For the hetero-metallic box shaped complexes, $[Fe_2Zn_2$(**L2.3**)$_2Cl_2](PF_6)_6$, **6.1**, and $[Fe_2Cu_2$(**L2.3**)$_2Cl_2]PF_6$, **6.4**, the ligand **L2.3** was reacted with Fe(II) to bind two terpyridine-type binding sites. The picolylamine binding sites were then linked using Zn(II) and Cu(II) salts. Addition of an excess of hexafluoridophosphate ions resulted in crystallisation of the boxes. Similarly, when Ni(II) was used instead of Fe(II), the box $[Ni_2Zn_2$(**L2.3**)$_4Cl_2]PF_6$, **6.5**, was formed. The homo-metallic box complexes $[Zn_4$(**L2.3**)$_4(OAc)_2]PF_6$, **6.2**, and $[Zn_4$(**L2.3**)$_4Br_2]PF_6$, **6.6**, were formed when only Zn(II) metal salts of the respective anions were used.

All the box complexes synthesised had similar structures with similar cavity sizes, and two coordinating anions pointing into the box cavity. A chelating bidentate terephthalate ion was inserted successfully in the cavity probably due to possible π-stacking interactions with the aromatic terpyridine rings and its rigid nature resulting in formation of the box, $[Fe_2Zn_2(C_8H_4O_4)]PF_6$, **6.3, Figure 7.3**.

The interesting feature of these boxes was that they all crystallised using hexafluoridophosphate ions. The hexafluoridophosphate ion are involved in multiple F···H-N hydrogen bonding with amine nitrogen atoms. Two of the six hexafluoridophosphate ions locate above and below the box complexes. Other than hydrogen bonding many F···H-C short contact are also involved in stabilisation of the boxes lattice. Without hexafluoridophosphate ions, simple dinuclear complexes discussed in Chapter 4 were formed. This suggested that hexafluoridophosphate ions may have a templating effect on crystallisation of the box shaped complexes.

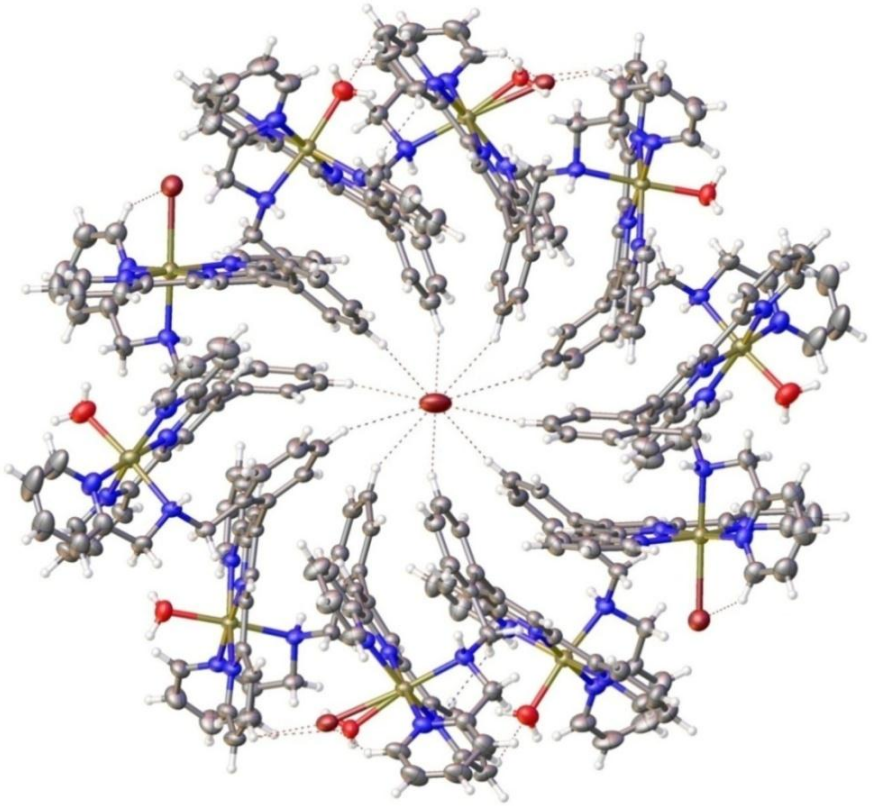

*Figure 7.3. The crystal structure of wheel shaped complex $[Ni_{10}(\mathbf{L2.3})_{10}Br_4(H_2O)_6]Br_{16}$, **6.8**. The solvent molecules and the uncoordinated bromide ions are omitted for clarity. The central Br···C-H interactions range between 3.0 Å to 3.3 Å.*

The most remarkable and fortuitous outcome of this project was formation of decanickel wheel shaped complexes. When Ni(II) bromide or chloride salts were mixed with **L2.3** in aqueous solutions, the wheel shaped complexes $[Ni_{10}(\mathbf{L2.3})_{10}Br_4(H_2O)_6]Br_{16}$, **6.8**, $[Ni_{10}(\mathbf{L2.3})_{10}Cl_4(H_2O)_6](Cl)_{16}$, **6.9** and $[Ni_{10}(\mathbf{L2.3})_{10}Cl_4(H_2O)_6](Cl)_{15}Br$, **6.10** were crystallised. These wheel shaped complexes contain $Ni_{10}\mathbf{L2.3}_{10}$ units arranged in a single circular array. Each octahedral Ni(II) ion is coordinated between two ligands through terpyridine-type site (H) of the one ligand and picolylamine-type site (T) of the second ligand *via* HT binding mode, resulting in formation of a $(HT)_{10}$ ring. The sixth ligand at each metal ion site is occupied either by a water or halide. A bromide or (two disordered) chloride ion is always present in the wheel cavity. These crystal structures had very similar unit cell dimensions and space groups.

A number of experiments with different Ni(II) salts and **L2.3** were performed, and in our experience the wheel shaped complexes form only in the presence of chloride or bromide ions. The preference of chloride or bromide as outer ligands was always depended upon their concentration in the reaction mixture.

Another fact of these wheel shaped complexes was preference of bromide ion over the chloride ion to fit in the cavity, which could be due to the perfect size of bromide ion to undergo H-bonding interactions with the hydrogen atoms pointing inside the cavity. However, in the presence of only chloride ions, the complexes still managed to arrange themselves in the form of a wheel, but one which is slightly elliptical. Due to smaller size of the chloride ion, it was disordered over two positions each with an half occupancy. This displacement of the chloride ion over two positions enabled it to undergo H-bonding interactions with maximum hydrogen atoms of the inner cavity phenyl ring resulting stabilization of the large wheel supramolecular architectures. It appears these wheels form due to templating Br···H-C or Cl···H-C interactions.

7.2. Future work

During this research the kinetics of hydrolysis was studied using Zn(II) complexes of the neutral ligands **L2.3** and **L2.4**. They showed a slight increase in rate of hydrolysis over the mononuclear complexes of analogous neutral ligands. With literature understanding and the kinetics data we concluded that the slight increase in rate is due to lowering of the pK_a in dinuclear complexes instead of cooperation between two metal ions. Similar kinetics studies can be performed using complexes of the charged ligands, **Figure 7.4**, in order to understand the relationship between rate and pK_a of the water molecules coordinated to the metal.

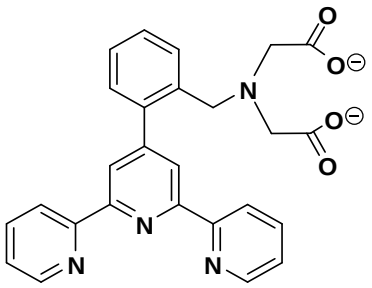

Figure 7.4. An example of a charged ligand that can be useful in understanding the relationsip between rate and pK_a of the water molecules coordinated to the metal.

In case of the box complexes, different aromatic molecules (a) to (f) can be inserted in the box cavity, **Figure 7.5**.

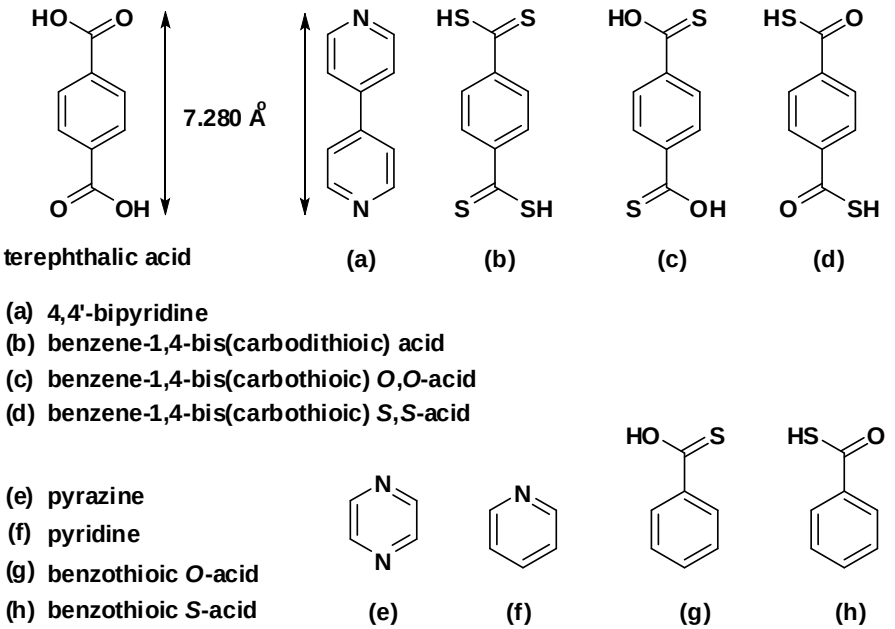

Figure 7.5. Aromatic molecules which can be encapsulate in the box shaped complexes.

Other molecules inserted in the cavity could be studied using techniques other than crystallography. NMR can be useful as aliphatic amino acids will shift peaks in the aliphatic region in comparison to the uncoordinated molecule.

Boxes can act as reaction chambers and may lead to faster reactions by fixing the two reactants in close proximity. The two reactants could have functional groups such as carboxylic acids and amines to give an amide, or primary amines and halides to give secondary amines.

The wheel shaped complexes can be decorated by incorporating different monodentate ligands at the sixth position of octahedral geometry, which is currently occupied by halide or water, and sometimes both are bound in a disordered structure.

CHAPTER 8

EXPERIMENTAL

8.1 General Information

4'-(2'''-Toluyl)-2,2':6',2''-terpyridine (**L2.1**)[169],*N*,*N'*-Bis(2-pyridylmethyl)amine, **2.10**,[215, 216]iminodiacetate, **2.12**,[222] bis(*p*-nitrophenyl)phosphate (BNPP),[359] and 1,5,8,12-tetraazadodecane, **2.14**,[234] were synthesised according to literature procedures. Dibenzoyl peroxide (BPO) and N-bromosuccinimide (NBS) were recrystallised using standard literature methods[360] and were stored in the dark, over $CaCO_3$, in a desiccator. Carbon tetrachloride (CCl_4) was dried over P_2O_5 and then distilled using Schlenk techniques, under nitrogen.

All other solvents, reagents and starting materials were reagent grade, purchased from standard suppliers and used as received. Solvents used for syntheses of complexes were analytical grade and used as received. Water was purified in-house by reverse osmosis. All anhydrous solvents used in reactions of moisture sensitive compounds were purified either in-house by passing over a sealed column of activated alumina or distilled from standard drying agents. Free radical bromination reactions were carried out under inert atmosphere of nitrogen using standard Schlenk techniques. Electrothermal Melting Point Apparatus used to record melting points. Microanalyses were performed by Campbell Microanalytical Laboratory at the University of Otago, New Zealand.

8.2 Infrared Spectroscopy

Infrared spectra were recorded either on a Perkin-Elmer Spectrum One FTIR instrument operating in a diffuse reflectance mode with samples prepared as KBr mulls (denoted KBr) or on a Bruker FTIR spectrometer equipped with Alpha's Platinum ATR single reflection diamond, and samples were placed directly on the diamond under clamp without any preparation (denoted neat). The abbreviations used are: s: strong, vs: very strong, m: medium, w: weak, sh: sharp.

8.3. Thermogravimetric analysis

Thermogravimetric analyses were performed on an Alphatech SDT Q600 TGA/DSC apparatus. All samples were heated on alumina crucibles under nitrogen flow of 100 ml/min. The heating cycle on Ramp is fixed 1 °C/min^{-1}.

8.4. Nuclear Magnetic Resonance Spectroscopy

^{1}H and ^{13}C NMR spectra were recorded on Varian INOVA 500, Varian UNITY 300, or 400 spectrometers. Spectral chemical shifts were referenced to the residual solvent resonance or, in the case of D_2O, using TPMS as an internal reference. 2D COSY, HSQC, and NOESY experiments were performed to assign proton peaks where required, using standard Varian pulse sequence. All samples were prepared in commercially available deuterated solvents.

8.5. UV-Vis Spectroscopy and Kinetic Studies

UV-Visible spectra were recorded with a Varian CARY Probe 50 UV-Visible spectrophotometer in the range of 200 – 800 nm. Samples were measured in quartz cuvettes of path length 1 cm and approximate capacity of 1 ml. Spectra were referenced to the solvent used in each experiment.

The hydrolysis rate of bis(*p*-nitrophenyl)phosphate (BNPP) in the presence of different metal complexes was measured in the pH range 7-9 by following the increase in 400 nm-absorption in 45% CH_3CN, 5% DMF aqueous solution (0.09 M HEPES, or TAPS buffer, I = 0.09 M, $NaClO_4$) at 35 °C. Typically, for each experiment, a solution of the ligand (5 mM), a solution of the metal salt (10 mM), buffer(HEPES or TAPS,0.2 M at pH range of 7-9, I= 0.2 M $NaClO_4$), and BNPP (250 mM) were prepared in bulk. The bulk solutions were freshly prepared prior the kinetics experiments. In each experiment at first the ligand solution (40 μl) was mixed with the metal solution (40 μl for dinuclear complexes, and 20 μl for mononuclear complexes), followed by addition of the buffer (450 μl) and acetonitrile (430 μl for

mononuclear complexes, and 450 μl for dinuclear complexes) into a 1 cm cuvette with 1.5 ml capacity. The cuvette, stoppered with Teflon stopper, was inverted to allow the solutions to mix. The solution temperature was allowed to reach to equilibrium for 5 min prior addition of the solution of BNPP (40 μl, final conc. 10 mM) to the cuvette. Correction of the spontaneous hydrolysis of the substrate by the solvent or the buffer was accomplished by using a reference cell containing all the reactants and solvents except the metal complex under the same conditions. The reaction solutions contained 0.4 mM complex, 0.9 M buffer at I = 0.9 M $NaClO_4$, and 10 mM BNPP.

8.6. Mass Spectrometry

Mass spectra were recorded by Dr. Marie Squire and Dr. Meike Holzenkaempher on either a BrukerMaXis4G spectrometer or DIONEX Ultimate 300 spectrometer. Both of the spectrometers were operated in a high resolution positive ion electron spray mode. Samples were prepared by dissolving and diluting to the required concentration in appropriate HPLC grade solvents.

8.7. X-Ray Crystallography

X-Ray data were collected with an Oxford-Agilent Supernova instrument with a focused microsource Mo Kα [λ = 0.71073 Å] or Cu Kα [λ = 1.5405 Å] radiation and an ATLAS CCD area detector. CrysAlisPro 171.37.31 was used for the data collection and data processing. Multi-scan absorption corrections were applied using SCALE3 ABSPACK. The crystals were mounted on nylon loop using a perfluorinated polyethylene glycol. The crystal was kept at 120.00(10) K during data collection. All structures were solved using direct methods with SHELXS[361] and refined on wF^2 using all data by full matrix least square procedures with SHELXL-14 using OLEX-2[362] for visualisation. Hydrogen atoms were included in calculated positions for carbons and manually located from residual electron density for heteroatoms, with isotropic displacement parameters 1.2 or 1.5 times the isotropic equivalent of their carrier atoms. Heteroatom hydrogens were fixed at distances, O-H 0.84 Å

and N-H 0.90 Å. Graphical presentation of crystallographic data was prepared using OLEX-2.[362]

8.8. Ligand Synthesis (Chapter 2)

4'-(2'''-Toluyl)-2,2':6',2''-terpyridine, ***L2.1***

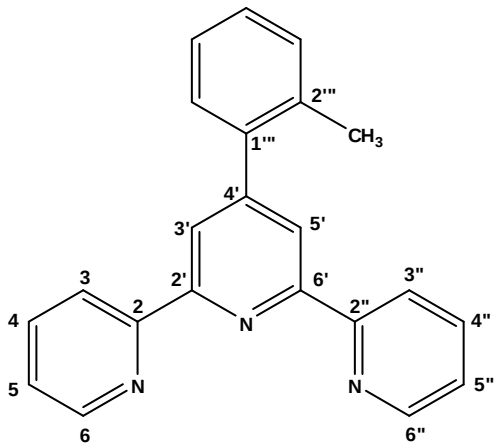

2-Acetylpyridine (2.4 g, 20 mmol) was added to a solution of potassium *t*-butoxide (3.36 g, 30 mmol) in freshly distilled dry THF (160 ml) and the resultant creamy yellow suspension was treated with *o*-tolualdehyde (1.2 g, 10 mmol) and the mixture was stirred overnight at room temperature under nitrogen. A solution of dry ammonium acetate (15.8 g) in 2:1 ethanol:acetic acid (190 ml) was then added and the clear brown mixture obtained was heated at reflux for 5 hours. The resulting orange-yellow reaction mixture was cooled to room temperature and treated with ice (500 g) and water (2000 ml) to give a yellow precipitate. The precipitate was collected by filtration. Recrystallisation from ethanol gave pure **L2.1** as pale yellow crystals. Yield: 2.5 g (68%); m.p.146-152°C; ^{1}H NMR ($CDCl_3$): δ = 8.72 (d, 2H, $H_{6,6''}$), 8.71 (d, 2H, $H_{3,3''}$), 8.49 (s, 2H, $H_{3',5'}$), 7.90 (t, 2H, $H_{4,4''}$), 7.30–7.36 (m, 6H, $H_{5,5'',toluyl}$), 2.38 (s, 3H, CH_3); ^{13}C NMR ($CDCl_3$): 156.5, 155.6, 152.2,149.4, 139.9, 137.1, 135.4, 130.7, 129.7, 128.5, 126.2, 124.1, 121.9, 121.6, 20.7 (CH_3); ESI-MS *m/z*: $[M+H]^+$ 324.13.

4'-{2'''-(Bromomethyl)phenyl}-2,2':6',2''-terpyridine, ***L2.2***

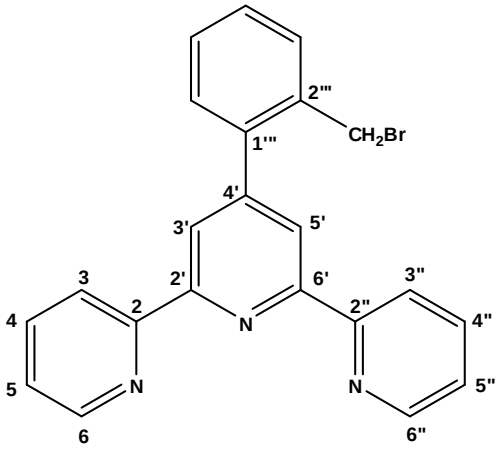

L2.1 (2.0 g, 6.1 mmol) and purified N-bromosuccinimide (1.2 g, 6.5 mmol) were added to a dry three-necked round bottom flask while flushing with N_2. Freshly distilled CCl_4 (150 ml) was also transferred to the three-necked flask while flushing under N_2. The solution was irradiated with a tungsten lamp for about 5 hours after adding a catalytic amount of dibenzoyl peroxide (0.002 g). The mixture was heated to 25°C for 12 hours under N_2. The reaction mixture was cooled to room temperature and filtered. The filtrate was concentrated under vacuum to give the crude brominated product, 4'-{2'''-(bromomethyl)phenyl}-2,2':6',2''-terpyridine as a yellow oil, which was used directly because of its tendency to decompose. Yield= 2.2 g (90%); ^{1}H NMR ($CDCl_3$) δ = 8.72 (d,2H), 8.71 (d, 2H), 8.58(s, 2H), 7.91 (t,2H), 7.58 (d,1H), 7.58 (d,1H), 7.35-7.44(m,5H), 4.45 (s, 2H, CH_2Br); ^{13}C NMR ($CDCl_3$) 156.2, 155.8, 150.5, 149.5, 140.1, 137.3, 135.3,131.2, 130.4, 129.2, 129.0, 124.2, 121.8, 121.7, 31.8 (CH_2Br); ESI-MS: *m/z* $[M+H]^+$ 402.0612.

4'-{2'''-(Dibromomethyl)phenyl}-2,2':6',2''-terpyridine, ***2.8***

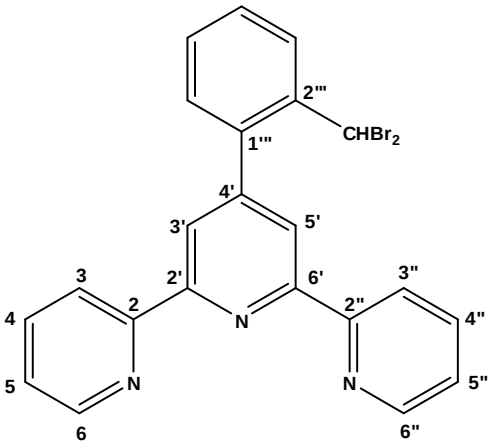

L2.1 (0.5 g, 1.5 mmol) and dry N-bromosuccinimide (0.54 g, 3.1 mmol) were added to a dry three-necked round bottom flask while flushing with N_2. Freshly distilled CCl_4 (50 ml) was also transferred to the three-necked flask while flushing under N_2. The solution was irradiated with a tungsten lamp for about 5 hours after addition of a catalytic amount of dibenzoyl peroxide (0.002 g). The mixture was heated to35°C for 4 hours under N_2. The reaction mixture was cooled to room temperature and filtered. The filtrate was concentrated under vacuum to give the crude di-brominated product, 4'-{2'''-(di-bromomethyl)phenyl}-2,2':6',2''-terpyridine, as a pale yellow oil. Yield: 0.70 g (95%); m.p.159-161°C; Elemental analysis: Found (%): C 55.14, H 3.07, N 8.71, Br 33.20, Calcd. $C_{22}H_{15}N_3Br_2$ (%): C 55.14, H 3.14, N 8.73, Br 33.21; ^{1}H NMR ($CDCl_3$) δ = 8.72 (d, 2H), 8.70 (d, 2H), 8.54 (s, 2H), 8.13 (d, 1H), 7.88 (t, 2H), 7.54 (t,1H), 7.35-7.44(m, 4H), 6.74 (s, 1H, $CHBr_2$); ^{13}C NMR ($CDCl_3$) 156.8, 156.1, 151.0, 149.8, 140.4, 136.7, 135.4, 133.6, 131.6, 129.3, 128.1, 124.2, 121.5, 120.8, 39.9 ($CHBr_2$); ESI-MS: *m/z* $[M+H]^+$ 481.9692, $[M+2H]^{2+}$ 241.4874. The crude oil was dissolved in ethanol and colourless blocks of X-ray quality crystals were collected by slow evaporation.

4'-(2'''-Formylphenyl)-2,2':6',2''-terpyridine

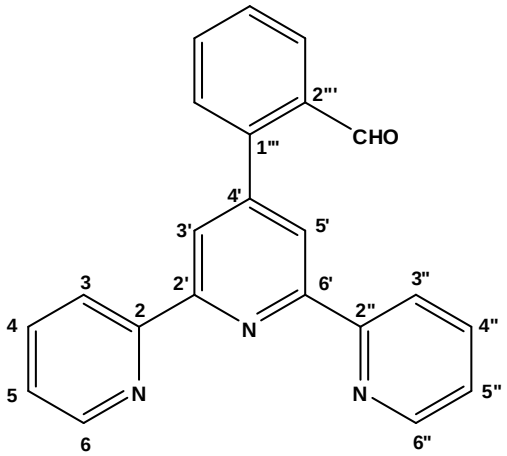

A suspension of **2.8** (0.5 g, 1.0mmol) and $CaCO_3$ (1.0 g, 10mmol) were added to a mixture of 1,4-dioxane:water (4:1, 50 ml) and heated at reflux for 30 h. The resulting mixture was then filtered. The filtrate was extracted with CH_2Cl_2 (2 × 50 ml). The extracts were combined and washed with aqueous HCl solution (0.1 M, 50ml) and then with distilled water (50 ml). Solvent was removed under vacuum after drying over dry sodium sulphate. The pale powder collected was the titled complex. Yield: 0.08 g (25%); m.p. 152-155°C; ^{1}H NMR ($CDCl_3$) δ = 8.68(d,3H), 8.50(s, 2H), 8.04 (d,2H), 7.85 (t,2H), 7.57-7.55 (m,3H), 7.31(m,2H), 10.08 (s,1H, CHO); ^{13}C NMR ($CDCl_3$) 191.33, 160.44, 155.62, 149.17, 147.96, 143.54, 137.03, 133.82, 133.78, 133.53, 130.56, 128.88, 128.10, 128.07, 124.12, 122.02, 121.49, 121.47; ESI-MS: *m/z* $[M+H]^+$ 338.130.

4'-[2'''-{5-(2-aminoethyl)-7-amino-2,5-diazaheptyl}-phenyl]-2,2':6',2''-terpyridine, ***L2.7***

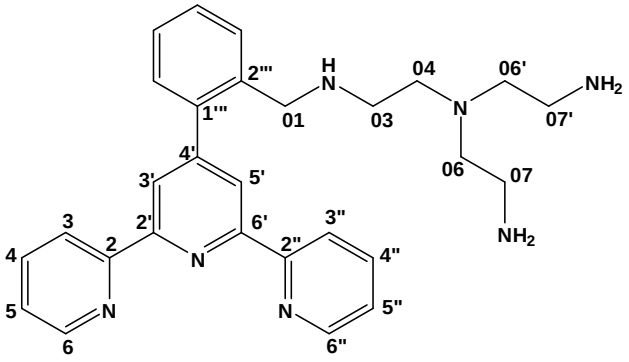

Dry *N*,*N*-bis(2-aminoethyl) ethane-1,2-diamine (3.7 g, 25 mmol) was placed in a dry two necked flask and then dry acetonitrile20 ml was added. Then **L2.2** (1.45 g, 3.5 mmol) dissolved in acetonitrile (20 ml) was added dropwise using a glass syringe equipped with a long needle. The mixture was stirred for 10 hours under nitrogen while heating at 40 °C, filtered, and the filtrate was concentrated to yield a yellow crude oil (5.02 g).

The crude yellow oil (2.0 g) was dissolved in HCl (1M, 200 ml) and adsorbed onto a H^+-Dowex column (30×3 cm). The column was initially eluted with aqueous HCl (2 M, 6 L). The eluate was collected in fractions of 500ml and taken to dryness on a rotary evaporator at 70°C. The brownish powder produced was characterised as *N*,*N*-bis(2-aminoethyl) ethane-1,2-diamine (^{1}H NMR). Increasing the concentration of the aqueous HCl eluate to 4 M washed out most of the aromatic impurities. Finally, the column was eluted with 6 M HCl and the ligand was obtained as its hydrochloride salt. Yield: 1.1 g (55%); m.p. 99-101 °C; Elemental analysis: Found (%): C 39.18, H 6.24, N 10.87, Cl 28.26, Calcd. $[C_{28}H_{32}N_7]\cdot 7HCl\cdot 8H_2O$ (%): C 38.84, H 6.40, N 10.87, Cl 28.66; ^{1}H NMR (500 MH_z, D_2O): δ = 8.91 (d, 2H,6,6"), 8.68 (m, 4H, 3,3",5,5"), 8.55 (s, 2H, 3', 5'), 8.10 (t, 2H, 4, 4"), 7.53 (m, 2H, 4''',5'''), 7.43 (d, 1H, 3'''), 4.31 (s, 2H, 01), 2.97 (t, 2H, 03), 2.93 (t, 2H, 06, 06'), 2.72 (t,2H, 04), 2.65 (t, 4H, 07, 07'); ^{13}C NMR (500MHz) 155.4, 150.8, 149.8, 148.9, 144.8, 140.5, 133.3, 132.8, 130.8, 128.7, 127.8, 51.5, 51.2, 51.0, 46.7, 38.8; ESI-MS calcd. M= 467.25, meas.: *m/z* $[M+H]^+$ 468.287, $[M+2H]^{2+}$ 234.647, $[M+Na]^+$ 490.26. X-ray quality crystals were grown as thin needles by evaporation of the aqueous solution of the ligand salt inside a tightly closed glass vial containing $CaCO_3$like a desiccator.

Synthesis of 4'-{2'''-(12-amino-2,6,9-triazadodecyl)phenyl}-2,2':6',2''-terpyridine, ***L2.8***

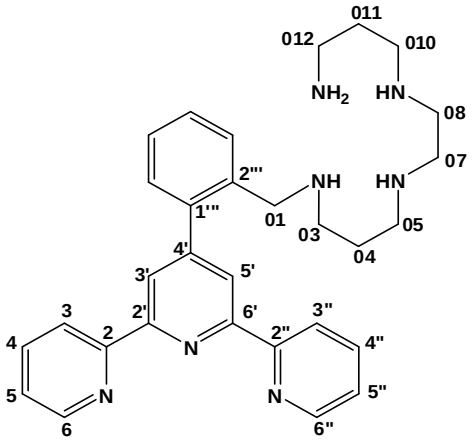

The cyclic bisaminal of 1,5,8,12-tetraazadodecane, 2.14 (0.71 g, 3.6 mmol) was added to dry CH_3CN (20 ml) while stirring and heated to reflux for 30 mins. To the stirring mixture, **L2.2** (1.45 g, 3.6 mmol) was added and the resulting mixture was heated at reflux overnight. The mixture was then cooled to room temperature and excess solvent was removed under vacuum. Hydrazine monohydrate (10 ml) was added to the residual oil and the mixture was heated at reflux for 2 hours. The solution was cooled to room temperature and the hydrazine was removed under vacuum. The residue was taken up in $CHCl_3$ and insoluble polymers were removed by filtration. Excess solvent was removed under vacuum to produce an oily residue of the ligand**L2.8**.Yield (crude): 1.46 g (65%)

The crude ligand **L2.8** (1.46 g) was dissolved in HCl (1 M, 150 ml) and adsorbed onto a H^+-form Dowex column (30×3 cm). The column was initially eluted with aqueous HCl (2 M, 4L). The eluate was collected in fractions of 250 ml and taken to dryness on a rotary evaporator at 70˚C. Then the column was eluted with aqueous HCl (4 M, 4 L; then 6 M,1 L), followed by HCl in (6M in 25% ethanol) and almost pure ligand was obtained as its hydrochloride salt from the final eluate. Yield: 0.6 g (30%); m.p. 107-110 °C; Elemental analysis: Found (%): C 41.66, H 6.31, N 11.20, Cl 28.65, Calcd. $[C_{30}H_{37}N_7]\cdot 7HCl\cdot 6H_2O$ (%): C 41.95, H 6.57, N 11.41, Cl 28.89; ^{1}H NMR (500 MH_z, D_2O): δ = 8.70 (d, 2H), 8.68 (d, 2H), 8.50 (s, 2H), 7.92 (t, 2H), 7.58 (d, 1H), 7.45 (d, 1H), 7.37-7.43 (m, 4H), 3.73 (s,2H), 2.94 (d, 2H), 2.93 (d, 2H), 2.89 & 2.71(d, 4H), 2.72 (d, 2H), 2.62 (d, 2H), 1.75 (t, 2H), 1.63 (t, 2H); ^{13}C NMR 155.1, 155.0, 150.7, 149.6, 148.6, 144.7, 140.1, 133.1, 133.0, 132.6, 130.8, 130.6, 128.5, 127.8, 56.1, 51.0, 50.8, 50.5, 49.9, 47.6, 46.8, 40.7, 23.2, 20.3; ESI-MS calcd. M= 495.31, meas.: *m/z* $[M+Na]^+$ 518.30.

Synthesis of 4'-[2'''-{(2-pyridylmethyl)aminomethyl}phenyl]-2,2':6',2''-terpyridine, ***L2.3***

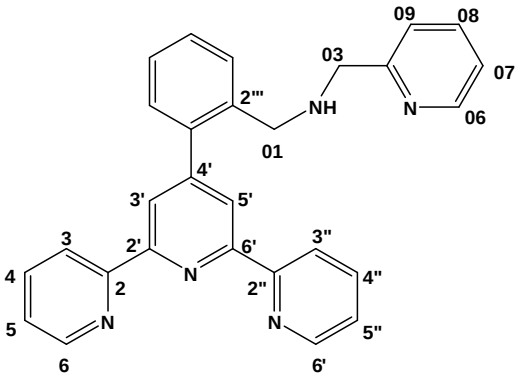

(2-Pyridylmethyl)amine (0.53 g, 4.9 mmol) was dissolved in dry CH_3CN (100 ml), with stirring, followed by the addition of K_2CO_3 (0.68 g, 4.9 mmol). The mixture was stirred for 10 mins at 35°C. **L2.2** (2.0 g, 4.9 mmol) was added to the stirring solution. The resulting mixture was heated to 50°C for 4 days under a reflux condenser, filtered and the filtrate was taken to dryness under vacuum. The residual oil was a crude product containing the **L2.3**, unreacted amine and **L2.1**. Yield (crude): 2.0 g (95%).

The ligand was purified by alumina column chromatography. Initial elution with DCM removed any unreacted **L2.1**. The desired ligand was eluted with a 0.5% MeOH:DCM mixture. The eluate was taken to dryness and the pure ligand was collected as a pale yellow fine powder. Yield 1.2 g (60%); m.p. 125-127°C; Elemental analysis: Found (%): C 78.34, H 5.61, N 16.61, Calcd. $C_{28}H_{23}N_5$ (%): C 78.44, H 5.42, N 16.34; ^{1}H NMR (500 MH_z, $CDCl_3$): δ = 8.68 (d, J=8, 2H, 3,3''), 8.65 (d, J=4, 2H, 6,6''), 8.54 (s, 2H, 3', 5'), 8.34 (d, J=5, 1H, 06), 7.86 (td, 2H, 4, 4''), 7.65 (d, J=8, 1H, 3''), 7.42-7.38 (m, 4H, 5''',6''',4'', 08), 7.34 (td, 2H, 5, 5''), 7.23 (d, J=8, 1H, 09), 6.98 (t, J=5, 1H, 07), 3.85 (d, 4H, 01, 03); ^{13}C NMR (500MHz) 158.3 (C2'''), 156.1 (2C, 2,2''), 155.3 (2C, 2', 6'), 150.9 (4'), 149.2 (2C, 6, 6''), 149.0 (6'''), 139.9 (1'''), 136.8 (2C, 4, 4''), 136.3 (06), 135.9 (010), 129.9-129.8 (2C, 09, 4'''), 128.7 (08), 127.5 (07), 123.8 (2C, 5,5''), 122.3 (3'''), 121.9 (5'''), 121.6 (2C, 3',5'), 121.3 (2C, 3', 3''), 53.9 (03), 50.5 (01); IR (KBr, cm^{-1}) 3140 m, 3055 m, 2925 m, 2854 m, 1585 s, 1567 ssh, 1541 msh, 1466 s, 1393 w, 1335 m, 1264 m, 1131 w, 992 m, 907 w, 851 m, 762 s, 652 w, 627 m, 508 w, 467 w; ESI-MS: *m/z* [$M+H^+$] 430.202, [$M+2H^{2+}$] 215.605, [$2M+H^+$] 859.396. X-ray quality crystals were formed as pale plates by slow evaporation the DCM solution of the ligand.

Synthesis of 4'-[2'''-{bis(2-pyridylmethyl)aminomethyl}phenyl]-2,2':6',2''-terpyridine, ***L2.4***

N,*N*-bis(pyridylmethyl)amine (1.23 g, 6.2 mmol) was dissolved in dry CH_3CN while stirring, followed by the addition of K_2CO_3 (0.62 g, 6.2 mmol). The mixture was stirred for 10 mins at 35°C. **L2.2** (2.5 g, 6.2 mmol) was added to the stirring solution. The resulting mixture was stirred overnight at 50°C under a reflux condenser, filtered and the filtrate was taken to dryness under vacuum. The residual oil was a crude product containing the **L2.4**, unreacted amine and **L2.1**. Yield (crude): 3.0 g (90%)

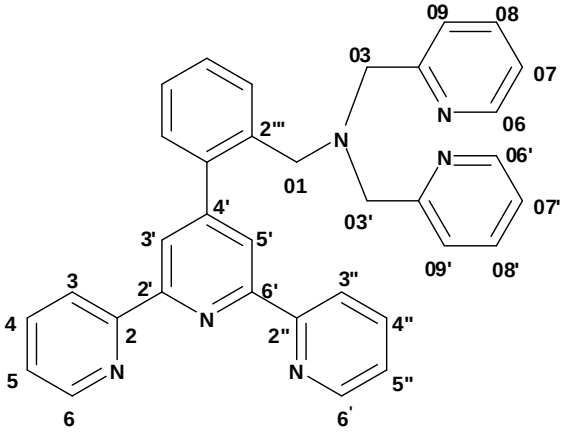

The ligand was purified by alumina column chromatography. Initial elution was done with only DCM to remove any unreacted **L2.1**. The desired ligand was eluted with a 0.1% MeOH:DCM mixture and was taken to dryness. The pure ligand was collected as a pale yellow fine powder. Yield 2.1 g (65%); m.p. 117-120 °C; Elemental analysis: Found. C 78.38, H 5.56, N 15.83, Calcd. $C_{34}H_{28}N_5$ (%): C 78.44, H 5.42, N 16.14; ^{1}H NMR (400 MH_z, $CDCl_3$): δ = 8.71 (d, J=4, 2H,6,6''), 8.66 (d, J=5, 2H, 3,3''), 8.42 (s, 2H, 3', 5'), 8.34(d, J=5, 2H, 06, 06'), 7.87 (t,J=15, 2H, 4, 4''), 7.67 (d, J=8, 1H, 3'''), 7.42-7.26 (m, 9H, 08, 08', 5''', 6''', 4''', 5, 5'', 09, 09'), 6.98 (t, J=16,2H, 07, 07'), 3.81 (s, 2H, 01), 3.70 (s, 4H, 03, 03'); ^{13}C NMR (500MHz) 158.8 (C2'''), 156.1 (2C, 2,2''), 155.0 (2C, 2', 6'), 151.5 (4'), 149.1 (2C, 6, 6''), 149.1 (2C, 6,6''), 148.4 (2C, 06, 06'), 140.5 (1'''), 136.8 (2C, 4, 4''), 136.5 (2C, 4, 4''), 130.7 (4'''), 129.8 (5'''), 128.2 (6'''), 127.3 (3'''), 123.8 (2C, 08, 08'), 122.9 (09, 09'), 121.8 (07, 07'), 121.6 (2C, 3', 5'), 121.2 (2C, 3', 3''), 59.8 (03, 03'), 56.5 (01); ESI-MS calcd. M = 520.24 meas.: *m/z* $[M+H]^+$ 521.245, $[M+2H]^{2+}$ 261.1267. X-ray quality crystals were formed as pale blocks by slow evaporation the DCM solution of the ligand.

Synthesis of 4'-[2'''-{N,N-bis(ethoxycarbonylmethyl)aminomethyl}phenyl]-2,2':6',2''-terpyridine, L2.5

Diethyl iminodiacetate 2.12 (0.83 g, 4.4 mmol) was added to dry CH_3CN (30 ml) followed by addition of anhydrous K_2CO_3 (0.60 g, 4.4 mmol) while stirring. To the resulting mixture **L2.2** (1.78 g, 4.4 mmol) was added. The reaction mixture was heated at reflux overnight, filtered, and the filtrate was concentrated under vacuum. A crude mixture of the desired ligand was collected as yellow oil.

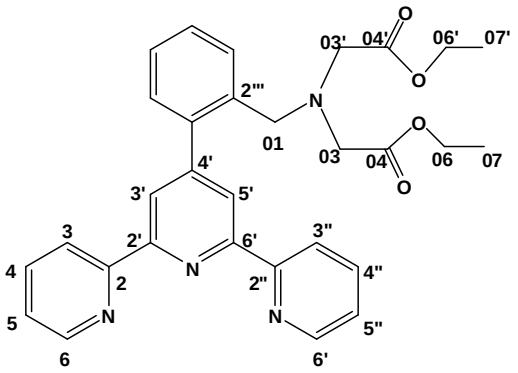

The ligand was purified using alumina column. The desired ligand was eluted using a mixture of 10% Hexane:DCM solution. The solvent was removed by rotary evaporation and the ligand was collected as colourless oil. Yield: 1.8 g (80%); m.p. 121-122 °C; Elemental Analysis: Found: C 69.62, H 5.81, N 10.73, Calcd. $C_{30}H_{30}N_4O_4$ (%): C 70.51, H 5.92, N 10.94; ^{1}H NMR (500 MH_z, $CDCl_3$): δ = 8.69 (d, 2H), 8.68 (d, 2H), 8.45 (s, 2H), 7.86 (t, 2H), 7.74 (d, 1H), 7.42 (d, 1H), 7.36-7.33 (m, 3H), 7.27 (d, 1H) 4.18 (s,4H), 3.98-3.95 (m, 6H), 3.44 (s, 6H); ^{13}C NMR (500 MHz, $CDCl_3$)171.1 (2C, 04, 04'), 156.2, 155.3, 151.3, 149.2, 140.5, 136.9, 135.9, 130.3, 129.8, 128.6, 127.5, 123.9, 121.7, 121.3, 60.3 (2H, 06, 06'), 55.0 (01), 54.2 (2H, 03, 03'), 14.2 (2C, 07, 07'); ESI-MS calcd. = 510.58, meas.: *m/z* $[M+H]^+$ 511.23, $[M+2H]^{2+}$ 256.11, $[M+Na]^+$ 533.21.

Synthesis of 4'-[2'''-{N,N-bis(carboxymethyl)aminomethyl}phenyl]-2,2':6',2''-terpyridine, ***L2.6***

Pure **L2.9** (0.2 g, 0.97 mmol) was added to conc. HCl (20 ml). The mixture was heated at reflux for 3 days. A water soluble creamy white precipitate was formed on evaporation to dryness using rotary evaporator. The ligand was recrystallised from 50% ethanol:water mixture as a hydrochloride salt. Yield 0.19 g (90%); m.p. 109-111 °C; ^{1}H NMR (400 $MH_{z,}$ D_2O): δ = 8.94 (d, 2H), 8.70 (td, 4H), 8.59 (s, 2H), 8.11 (dt, 2H), 7.71 (dd, 1H), 7.72-7.60 (m, 2H), 7.48 (dd, 1H), 3.86 (s, 4H); ^{13}C NMR (400 MHz, D_2O)167.9, 152.4, 148.1, 147.3, 146.1, 139.2, 133.0, 131.3, 130.8, 130.6, 128.1, 125.9, 125.5, 125.0, 55.2, 53.7; ESI-MS calcd. M= 454.16, meas.: *m/z* [$M+H^{+}$] 455.162, [$M+2H^{2+}$] 228.081.

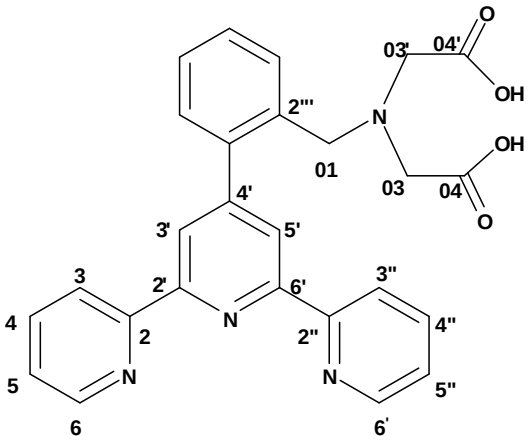

8.9. Complex Synthesis (Chapter 3)

*[Ni(**L2.1**)$_2$]Cl$_2$·4H$_2$O·2CH$_3$OH – Complex **3.1***

A methanol/DCM mixture (1.00 ml, 1:1) of **L2.1** (0.010 g, 0.030 mmol) was added to a methanolic solution of $NiCl_2·6H_2O$ (0.004 g, 0.015 mmol). The mixture was heated for 10 min to remove DCM from the mixture. Vapour diffusion of ether into the resulting green methanolic solution produced hexagonal orange-brown X-ray quality block shaped crystals. Yield: 0.015 g, 80%; m.p. >300 °C; Elemental analysis: Found (%): C 62.52, H 5.48, N 9.71, Calcd. $C_{44}H_{42}N_6O_3NiCl_2·CH_3OH$ (%): C 62.52, H 5.36, N 9.72; IR (neat, cm^{-1}): 3352 w, 3050 w, 1599 m, 1544 sh, 1514 m, 1489 sh, 1473 m, 1415 m, 1344 s, 1218 s, 1158 m, 1111 w, 1097 w, 1081 w, 1014 m, 910 s, 849 m, 797 s,763 s, 749 s, 739 s, 725 sh, 654 m, 573 w, 532 w, 450 w, 419 s; ESI-MS (CH_3OH): *m/z* $[Ni+2L]^{2+}$ 352.10.

*[Ni$_2$(**L2.1**)$_2$(μ-Cl)$_2$]·4CH$_3$OH – Complex **3.2***

A methanol/DCM mixture (1.00 ml, 1:1) of **L2.1** (0.010 g, 0.030 mmol) was added to a methanolic solution of $NiCl_2·6H_2O$ (0.007 g, 0.030 mmol) and two drops of saturated $NaCl_{(aq)}$ were also added. The mixture was heated to remove DCM. Slow evaporation of resulting green solution produced green rectangular blocks X-ray quality crystals. Yield: 0.009 g, 75%; m.p. >300 °C; Elemental analysis: Found (%): C 53.37, H 4.53, N 8.29, Calcd. $C_{46}H_{42}N_6O_2Ni_2Cl_4·4H_2O$ (%): C 53.02, H 4.84, N 8.06; IR (neat, cm^{-1}): 3340 w, 3051 w, 1600 s, 1570 wsh, 1470 m, 1413 m, 1302 w, 1244 m, 1157 w, 1015 s, 897 w, 843 w, 797 s, 763, s, 739 m, 641 m, 556 w, 510 w, 452 w, 423 m; ESI-MS (CH_3OH): *m/z* $[Ni+L]^{2+}$ 190.53.

*Alternative method for both complexes **3.1** and **3.2***

A methanol/DCM mixture (1.00 ml, 1:1) of **L2.1** (0.010 g, 0.030 mmol) was added to a methanolic solution of 0.007 g (0.003 mmol) of $NiCl_2·6H_2O$. The mixture was heated for 10 min to remove DCM from the mixture. Vapour diffusion of ether into resulting green methanolic solution produced both hexagonal orange-brown plates of **3.1** and green rectangular blocks of **3.2**. Both type of crystals proved to be of X-ray quality.

*[Ni(**L2.1**)(OH$_2$)$_3$]Cl$_2$·H$_2$O – Complex **3.3***

A methanol/DCM mixture (1.00 ml, 1:1) of **L2.1** (0.010 g, 0.030 mmol) was added to an aqueous solution of $NiCl_2 \cdot 6H_2O$ (0.007 g, 0.030 mmol). The green filtrate was allowed to evaporate slowly, and pale green blue rectangular X-ray quality crystals were formed in a period of 10 days. Yield: 0.008 g, 50%; m.p. 220 – 225 °C; Elemental analysis: Found (%): C 50.06, H 4.87, N 8.46, Calcd. $C_{22}H_{25}N_3O_4NiCl_2$ (%): C 50.33, H 4.80, N 8.00; IR (neat, cm^{-1}): 3361 w, 3051 w, 1620 m, 1519 m, 1475 w, 1465 m, 1419 m, 1349 s, 1217 s, 1153 m, 1097 w, 1081 w, 1014 m, 910 s, 849 m, 797 s,763 s, 749 s, 739 s, 728 s, 657 m, 575 w, 535 w, 441 w, 413 m; ESI-MS (CH_3CN): *m/z* $[Ni+L+CH_3CN]^{2+}$ 211.05.

*[Ni(**L2.1**)$_2$]Br$_2$ – Complex **3.4***

A methanol/DCM mixture (1.00 ml, 1:1) of **L2.1** (0.010 g, 0.030 mmol) was added to a methanolic solution of $NiBr_2 \cdot 3H_2O$ (0.004 g, 0.015 mmol). DCM was removed from the mixture by heating and vapour diffusion of ether in resulting green solution produced hexagonal orange-brown X-ray quality plates. Yield: 0.020 g, 85%; m.p. >300 °C; Elemental analysis: Found (%):C 57.54, H 4.5, N 9.26, Calcd. $C_{44}H_{34}N_6NiBr_2 \cdot 3H_2O$ (%): C 57.48, H 4.39, N 9.14; IR (net) (ν, cm^{-1}): 3383 w, 3050 w, 1598 m, 1543 sh, 1515 m, 1492 sh, 1472 m, 1415 s, 1348 m, 1245 m, 1156 m, 1112 m, 1096 w, 1052 w, 1013 m, 969 sh, 898 m, 797 s, 763 s, 738 s, 725 sh, 654 m, 629 m, 580 w, 556 w, 510 w, 452 w, 419 s; ESI-MS (CH_3OH): *m/z* $[Ni+2L]^{2+}$ 352.10.

*[Cu(**L2.1**)(OSO_3)(OH_2)]·4H_2O – Complex **3.5***

A methanol/DCM mixture (1.00 ml, 1:1) of **L2.1** (0.037 g, 0.11 mmol) was added to a methanolic solution of $CuSO_4$ (0.018 g, 0.11 mmol). The blue green solution was heated for 10 min at 40°C. Vapour diffusion of diethyl ether in to the filtered blue green reaction mixture produced thin needle shaped X-ray quality crystals. Yield: 0.055 g, 85%; m.p. 240 – 244 °C; Elemental analysis: Found (%): C 47.60, H 4.62, N 7.23, Calcd. $C_{22}H_{25}N_3CuSO_8$ (%): C 47.69, H 4.54, N 7.57; IR (neat, cm^{-1}): 3050 w, 2160 w, 2080 w, 1687 m, 1604 m, 1462 m, 1433 m, 1245 w, 1145 m, 1108 w, 1051 w, 1028 m, 995 m, 838 s, 801 msh, 639 w, 556 s, 479 w, 419 m; ESI-MS (CH_3OH): *m/z* $[Cu+L]^{2+}$ 193.04.

*[Cu_2(**L2.1**)$_2$(μ-Cl)$_2CuCl_4$]·CH_3OH – Complex **3.6***

A methanol/DCM mixture (1.00 ml, 1:1) of **L2.1**was added dropwise to (0.010 g, 0.030 mmol) a methanolic solution of $CuCl_2·2H_2O$ (0.033 g, 0.020 mmol). The resulting solution was heated at reflux for 30 min, and then DCM was evaporated by further heating. The methanolic green reaction mixture was cooled to RT and vapour diffusion of ether into the solution produced X-ray quality green needle shape crystals. The slow evaporation method also produced same crystals within a period of two weeks. Yield: 0.020 g, 90%; m.p. 210 – 213°C; Elemental analysis: Found (%): C 48.33, H 3.26, N 7.89, Calcd. $C_{44}H_{34}N_6Cu_3Cl_6·2H_2O$ (%): C 48.65, H 3.53, N 7.74; IR (neat, cm^{-1}): 3339 w, 3063 w, 1598 s, 1539 m, 1470 w, 1403 w, 1359 s, 1298 w, 1234 m, 1160 w, 1119 w, 1020 s, 906 w, 867 w, 761 s, 732 w, 694 w, 441 w, 418 m; ESI-MS (CH_3OH): *m/z* $[(Cu+L+Cl]^+$ 421.04, $[Cu+L]^{2+}$ 193.04; UV-vis (CH_3CN): λ_{max}= 720, 435, 345, 330, 288, 278, 266, 220 nm.

*[Cu(**L2.1**)(OH_2)$_2$(OH)]PF_6·2H_2O – Complex **3.7***

L2.1 (0.030 g, 0.10 mmol) was dissolved in a small amount of DCM/methanol mixture and then a methanolic solution of $CuCl_2·2H_2O$ (0.015 g, 0.10 mmol) was added. The mixture was heated to remove any DCM present. Addition of a few drops of saturated aqueous ammonium hexafluoridophosphate resulted in formation of green precipitate, which was filtered and washed with methanol and ether. Vapour diffusion of ether to an acetonitrile solution of the

precipitate produced X-ray quality crystals. Yield: 0.019 g, 40%; m.p. 225 – 228 °C; Elemental analysis: Found (%): C 43.82, H 4.25, N 7.1, Calcd. $C_{22}H_{25}N_3O_4CuPF_6$ (%): C 43.75, H 4.17, N 6.96; IR (neat, cm^{-1}): 3501 w, 3083 w, 2163 w, 2083 w, 1608 s, 1573 m, 1557 w, 1478 m, 1420 m, 1247 m, 1021bs, 790 s, 632 w, 520 w, 419 m; ESI-MS (CH_3OH): *m/z* $[Cu+L]^{2+}$ 193.04.

*[Cu(**L2.1**)$_2$](OTf)$_2$ – Complex **3.8***

L2.1 (0.010 g, 0.030 mmol) was dissolved in mixture of DCM: methanol (2 ml, 1:1). To the mixture $Cu(OTf)_2$ (0.006 g, 0.015 mmol) was added dropwise. The mixture was heated for 10 mins, filtered and slow evaporation of solvent produced very thin overlapped plates of crystals. X-ray quality crystals were carefully collected from the bulk. Yield: 0.025 g, 80%; m.p. >300 °C; Elemental analysis: Found (%): C 53.88, H 3.50, N 8.20, Calcd. $C_{44}H_{34}N_6Cu(CF_3SO_3)_2 \cdot H_2O$ (%): C 53.82, H 3.53, N 8.19; IR (neat, cm^{-1}): 3063 w, 2164 w, 1598 m, 1573 w, 1544 w, 1544 w, 1416 m, 1258 s, 1222 wsh, 1145 s, 1055 s, 929 w, 891 w, 844 m, 794 m, 632 s, 571 m, 515 m, 454 w, 413 m; ESI-MS (CH_3OH): *m/z* $[Cu+2L]^{2+}$ 354.60; UV-vis (CH_3CN): λ_{max}= 680, 285, 276, 267, 226, 213 nm.

*[Cu(**L2.1**)(CH$_3$CO$_2$)$_2$]·2H$_2$O – Complex **3.9***

A chloroform solution (1 ml) of **L2.1** (0.016 g, 0.049 mmol) was added dropwise to a methanolic solution of $Cu(CH_3CO_2)_2$ (0.015 g, 0.049 mmol) while stirring. The resulting blue green mixture was heated for 1 hour at 35°C and then acetonitrile (5 ml) was added. Slow evaporation of the solvent overnight produced X-ray quality blue-green crystals. Yield: 0.020 g, 85%; m.p. 230 – 233 °C; Elemental analysis: Found (%): C 54.34, H 5.27, N 7.30, Calcd. $C_{26}H_{23}N_3CuO_4 \cdot 4H_2O$ (%): C 54.11, H 5.41, N 7.28; IR (neat, cm^{-1}): 3383 w, 3079 w, 2160 w, 1603 m, 1547 s, 1476 m, 1392 s, 1340 m, 1305 w, 1264 w, 1166 w, 1021 s, 1893 w, 763 s, 736 s, 640 m, 571 s, 421 w, 421 m; ESI-MS (CH_3CN): *m/z* $[(Cu+L+CH_3CN]^+$ 427.10, $[Cu+L+CH_3CN]^{2+}$ 213.54; UV-vis (CH_3CN): λ_{max}= 680, 285, 275, 267, 226, 213 nm.

*[Zn(**L2.1**)(CH_3CO_2)$_2$]·CH_3CN – Complex **3.10***

A dichloromethane solution of **L2.1** (0.013 g, 0.040 mmol) was mixed with a methanol:acetonitrile solution (1:1, 2 ml) of $Zn(CH_3CO_2)_2 \cdot 2H_2O$ (0.0084 g, 0.040 mmol). The mixture was heated for 15 mins, and filtered. The slow evaporation of the solvents produced X-ray quality crystals over a period of one week. Yield: 0.008 g, 70%; m.p. 258 – 261 °C; Elemental analysis: Found (%): C 61.68, H 4.62, N 10.13, Calcd. $C_{28}H_{26}N_4O_4Zn$ (%): C 61.38, H 4.75, N 10.25; ^{1}H NMR (CD_3CN): 2.11 (s, 6H), 2.62 (s, 3H), 7.43 (m, 2H), 7.57 (m, 3H), 7.66 (d, 1H), 7.91 (d, 2H), 8.15 (t, 2H), 8.62 (d, 2H), 8.77 (s, 2H); ^{13}C NMR (CD_3CN): 158.03, 149.31, 148.13, 147.91, 141.27, 137.52, 135.71, 131.21, 129.99, 129.63, 127.52, 126.63, 124.22, 123.18, 29.89, 19.52; IR (neat, cm^{-1}): 3395 w, 3059 w, 2979 w, 2244 w, 1730 w, 1594 s, 1547 m, 1475 w, 1372 s, 1249 m, 1150 m, 1047 w, 1023 s, 922 w, 843 m, 795 m, 764 m, 692 s, 657 m, 637 msh, 452 w, 412 m; ESI-MS (CH_3CN): *m/z* $[Zn+L]^{2+}$ 193.53.

*[Zn(**L2.1**)Cl_2] – Complex **3.11***

A dichloromethane/methanol solution of **L2.1** (0.106 g, 0.32 mmol) was added drop-wise to a methanolic solution of $ZnCl_2 \cdot 2H_2O$ (0.044 g, 0.32 mmol). The mixture was heated to 35°C for 5 mins. A white precipitate formed upon cooling the mixture to room temperature. The precipitate was filtered and dissolved in hot DMF. In a period of 2 days, vapour diffusion of di-isopropyl ether into resulting DMF solution produced fragile X-ray quality colourless plates. Yield: 0.096 g, 65%; m.p. 272 – 275 °C; Elemental analysis: Found (%): C 57.46, H 3.69, N 9.24, Calcd. for $C_{22}H_{17}N_3ZnCl_2$ (%): C 57.48, H 3.73, N 9.14; ^{1}H NMR (DMSO): 2.41 (s, 3H), 7.43 (m, 3H), 7.52 (d, 1H), 7.86 (t, 2H), 8.26 (t, 2H), 8.83 (d, 6H); IR (neat, cm^{-1}): 3453 w, 3070 w, 2163 w, 1655 s, 1611 w, 1597 s, 1570 m, 1547 m, 1494 m, 1457 m, 1437 s, 1410 s, 1387 m, 1292 s, 1245 w, 1162 w, 1096 m, 1011 s, 953 w, 798 m, 764 m, 733 w, 692 m, 657 m, 511 w, 412 m; ESI-MS (CH_3CN): *m/z* [Zn+L+Cl]+ 422.0397.

*[Zn(**L2.1**)$_2$](NO$_3$)$_2$ – Complex **3.12***

A methanolic solution of $Zn(NO_3)_2 \cdot 6H_2O$ (0.004 g, 0.015 mmol) was added drop-wise to a hot methanolic solution of **L2.1** (0.010 g, 0.030 mmol). Resulting solution was heated at 35°C to remove DCM. Vapour diffusion of diethyl ether to the resulting solution produced X-ray quality irregular shaped crystals. Yield: 0.013 g, 65%; m.p. >300 °C; Elemental analysis: Found (%): C 58.62, H 3.64, N 12.42, Calcd. $C_{44}H_{34}N_8O_6Zn$ (%): C 58.78, H 3.81, N 12.47; IR (neat, cm^{-1}): 3455 w, 3069 w, 1625 s, 1558 s, 1493 s, 1328 s, 1248 m, 1163 s, 1100 m, 1017 s, 896 m, 790 m, 733 w, 511 w, 419 m; ESI-MS (CH_3CN): *m/z* $[Zn+2L]^{2+}$ 355.10.

*[Ag$_2$(**L2.1**)$_2$(NO$_3$)]$_n$(NO$_3$)$_n$·(2CH$_3$CN)$_n$ – Complex **3.13***

L2.1 (0.010 g, 0.030 mmol) was dissolved in chloroform (1ml). A drop-wise addition of ethanolic solution of $AgNO_3$ (0.005g, 0.030 mmol, 1ml) under dark conditions produced a white fibrous precipitate. The precipitate was filtered and dissolved into 1ml of acetonitrile solution and vapour diffusion of di-isopropyl ether into the resulting solution produced colourless needle shaped crystal of the polymeric title compound. Yield: 0.011g, 70%; m.p. 123-125°C; Elemental analysis: found (%): C 53.68, H 3.50, N 11.24, Calcd. $AgC_{22}H_{17}N_4O_3$ (%): C 53.57, H 3.47, N 11.36; ^{1}H NMR (CD_3CN) 2.42 (s, 3H), 7.45 (m, 4H), 7.55 (t, 2H), 8.20 (t, 2H), 8.26 (s, 2H), 8.30 (d, 2H), 8.59 (d, 2H); IR (neat, cm^{-1}): 3439 w, 3018 w, 2251 w, 1754 s, 1602 w, 1567 w, 1539 w, 1518 m, 1333 bs, 1242 w, 1190 w, 1099 w, 1006 m, 885 w, 787 m, 745 s, 684 w, 633 w, 504 m, 419 m; ESI-MS (CH_3CN): *m/z* $[Ag+L]^+$ 430.05, $[Ag+2L]^+$ 753.19, $[2Ag+2L+NO_3]^+$ 922.08.

8.10. Complex Synthesis (Chapter 4)

*[Zn2(**L2.3**)Cl4]·3CH3CN – Complex **4.1***

A chloroform solution (0.50 ml) of **L2.3** (0.010 g, 0.023 mmol) was mixed with a methanolic solution of $ZnCl_2 \cdot 2H_2O$ (0.0064 g, 0.046 mmol). The mixture was heated gently for 1 hour. Cooling to room temperature resulted in formation of white precipitate. The precipitate was

washed with diethyl ether and dissolved in acetonitrile. The X-ray quality crystals were produced overnight by slow evaporation of acetonitrile. Yield: 0.012 g (80%); m.p. 257-260 °C; Elemental analysis: Found (%): C 45.73, H 3.49, N 9.46, Calcd. $C_{28}H_{23}N_5Zn_2Cl_4 \cdot 2H_2O$ (%): C 45.84, H 3.71, N 9.55; ^{1}H NMR (DMSO) δ = 8.84 (d,2H), 8.80 (d,2H), 8.69 (d, 2H), 8.36 (s,H), 8.24 (t, 2H), 7.84 (t, 2H), 7.75 (d, 1H), 7.67 (t, 1H), 7.58-7.54 (m, 4H), 7.31 (d, 1H), 7.22 (t, 1H), 3.91 (s, 2H), 3.79 (s, 2H); IR (neat, cm^{-1}): 3060 w, 2921 w, 1600 m, 1572 w, 1477 m, 1415 m, 1366 w, 1308 w, 1250 w, 1166 w, 1150 m, 1020 m, 790 m, 774 s, 759 w, 671 m, 532 w, 503 w, 450 m, 413 s; ESI-MS (CH_3CN): *m/z* $[Zn+L+Cl]^+$ 528.0905.

*$[Zn_2$(**L2.4**)$Cl_4]\cdot 2CH_3OH$ – Complex **4.2***

L2.4 (0.016 g, 0.030 mmol) was dissolved in a minimum amount of chloroform and added to one branch of the H-tube. To the second branch of H-tube, a methanolic solution of $ZnCl_2 \cdot 2H_2O$ (0.08 g, 0.062 mmol) was added. Then, H-tube was filled slowly with dry methanol so that the ligand and metal layers remain undisturbed. Both openings of the H-tube were closed properly with parafilm plastic wraps, and left undisturbed on a stand. After a period of a week colourless blocks of crystals were formed in the middle branch at interface and also in the branch containing the ligand. Yield: 0.020 g (81%); m.p. >300 °C; Elemental analysis: Found (%): C50.67, H 4.22, N 9.72, Calcd. $C_{34}H_{28}N_6Zn_2Cl_4 \cdot 2CH_3OH$ (%): C 50.70, H4.25, N9.86; IR (KBr, cm-1): 3060 w, 2920 w, 1606 s, 1572 w, 1546 w, 1466 m, 1366 s, 1250 w, 1050 m, 893 w, 831 s, 799 s, 759 sh, 738 msh, 670 m, 503 w, 413 s; ESI-MS (CH_3CN/DMSO): *m/z* $[2Zn+L+3Cl]^+$753.0018, $[Zn+L+Cl]^+$ 619.1350.

*$[Cu_2$(**L2.3**)$(OCH_3CO)_4(OH_2)]\cdot 3H_2O$ – Complex **4.3***

A chloroform solution of **L2.3** (0.010 g, 0.023 mmol) was mixed with a methanolic solution of $Cu(OCH_3CO)_2.2H_2O$ (0.0064 g, 0.046 mmol). The resulting green mixture was heated gently for 1 hour, and reduced to 1 ml by rotary evaporation. A slow diffusion of acetone into the resulting green methanolic solution produced a few X-ray quality green crystals over a period of 3 months. Yield: 0.08 g (27%); m.p. 249-252°C; Elemental analysis: Found (%): C 53.19, H 4.40, N 8.64, Calcd. $C_{28}H_{37}N_5Cu_2O_9$ (%): C 53.39, H 4.60, N 8.65; IR (neat, cm^{-1}):

3108 w, 3035 w, 1655 s, 1608 w, 1595 w, 1505 m, 1537 m, 1419 w, 1343 w, 1245 w, 1154 w, 1020 m, 790 m, 774 s, 759 w, 738 w, 646 m, 513 w, 505 w, 417 m; UV-vis (CH_3CN): λ_{max} = 720, 323, 287, 275, 215 nm.

*$[Cu_4(\mathbf{L2.3})_2Cl_8]\cdot 4CH_3OH$ – Complex **4.4** & $[Cu_4(\mathbf{L2.3})_2Cl_8]$ – Complex **4.5***

A chloroform solution of **L2.3** (0.020 g, 0.046 mmol) was mixed with a methanolic solution of $CuCl_2\cdot 2H_2O$ (0.015 g, 0.093 mmol). The resulting green mixture was heated gently for 1 hour, and reduced to 1 ml by rotary evaporation. A slow diffusion of diethyl ether into half of the methanolic solution produced X-ray quality green crystals of 4.4 over a period of 2 weeks. Yield: 0.09 g (40%); m.p. 233-235 °C; Elemental analysis: Found (%): C 47.51, H 3.63, N 9.81, Calcd. $(C_{28}H_{23}N_5Cu_2Cl_4)_2\cdot CH_3OH\cdot H_2O$ (%): C 47.50, H 3.63, N 9.72; IR (neat, cm^{-1}): 3179 w, 3047 w, 1600 m, 1554 w, 1471 m, 1427 m, 1416 w, 1343 w, 1245 w, 1154 w, 1020 m, 790 m, 774 s, 759 w, 646 m, 532 w, 507 w, 415 m; ESI-MS (CH_3CN): *m/z* $[Cu+L+Cl]^+$ 527.0933, $[Cu+L+Cl]^{2+}$ 263.5464, $[2Cu+L+2Cl]^{2+}$ 312.4956; UV-vis (CH_3CN): λ_{max}= 720, 320, 285, 275, 215 nm.

Slow evaporation of other half of methanolic solution produced green blocks of X-ray quality crystals of 4.5 over a period of 3 months. Yield: 0.013 g (45%); m.p. 232-235 °C; Elemental analysis: Found (%): C 48.25, H 3.52, N 9.93, Calcd. $(C_{28}H_{23}N_5Cu_2Cl_4)_2$ (%): C 48.35, H 3.33, N 10.07; IR (neat, cm^{-1}): 3185 w, 3052 w, 1606 m, 1544 w, 1492 m, 1435 m, 1423 w, 1334 w, 1256 w, 1155 w, 1030 m, 794 m, 772 s, 764 w, 652 m, 536 w, 509 w, 416 m; ESI-MS (CH_3CN): *m/z* $[Cu+L+Cl]^+$ 527.0933, $[Cu+L+Cl]^{2+}$ 263.5464, $[2Cu+L+2Cl]^{2+}$ 312.4956; UV-vis (CH_3CN): λ_{max}= 720, 320, 285, 275,215 nm.

*$[Cu_4(\mathbf{L2.4})_2Cl_{6.5}(OH_2)_{0.75}]Cl_{1.5}\cdot 1H_2O$ – Compex **4.6***

A chloroform solution of **L2.4** (0.050 g, 0.096 mmol) was dissolved in a methanolic solution of $CuCl_2\cdot 2H_2O$ (0.032 g, 0.19 mmol). The resulting green solution was heated gently for 1 hr and taken to dryness by rotary evaporation. The resulting green paste was dissolved in water and the blue aqueous solution formed was filtered. Slow evaporation of the blue solution produced blue plates of crystal suitable of X-ray crystallography. Yield: 0.12 g (75%); m.p.

220-223 °C; Elemental analysis: Found (%): C 47.68, H 4.22, N 9.79, Calcd. $C_{68}H_{56}N_{12}Cu_4Cl_8 \cdot 8H_2O$ (%): C 47.55, H 4.22, N 9.79. IR (neat, cm-1): 3397 w, 3058 w, 1633 s, 1606 m, 1570 m, 1553 m, 1475 m, 1416 w, 1305 w, 1284 m, 1158 m, 1951 s, 767 s, 724 m, 487 w, 422 w; ESI-MS (CH_3CN): *m/z* $[2Cu+L+2Cl]^{2+}$ 358.0167; UV-vis (H_2O): λ_{max}= 670, 345, 330, 289, 278, 256, 213 nm.

8.11. Complex Synthesis (Chapter 5)

*[Cu(**L2.1**)(BNPP)Cl] – Complex **5.1***

L2.1 (0.010 g, 0.030 mmol) was dissolved in chloroform:methanol (1:1, 2 ml) solution and aqueous BNPP (0.09 g, 0.030 mmol) was added. While stirring and heating the mixture, $CuCl_2 \cdot 2H_2O$ (0.05 g, 0.030 mmol) was added. The reaction mixture was heated gently for 2 hrs. Filtered and vapour diffusion of diethyl ether into the blue filtrate produced rectangular green blocks of crystals suitable for X-ray diffraction experiment. Yield: 0.020 g (85%); m.p. >300 °C; Elemental analysis: Found (%): C 52.1, H 3.71, N 8.69, Calcd. $C_{34}H_{25}N_5O_8PCuCl \cdot H_2O$ (%): C 52.43, H: 3.49, N 8.99; IR (neat, cm-1): 3109 w, 1606 m, 1587 m, 1488 m, 1414 w, 1338 s, 1233 s, 1166 w, 1090 m, 1020 w, 886 s, 848 s, 748 s, 623 m, 529 m, 487 w, 468 w, 420 w; UV-vis (CH_3CN): λ_{max}= 695, 345, 330, 288, 280, 268, 218 nm.

*[Cu(**L2.1**)(BNPP)(OH_2)]PF_6 – Complex **5.2***

L2.1 (0.010 g, 0.030 mmol) was dissolved in chloroform methanol (1:1 v/v) solution and aqueous BNPP (0.09 g, 0.030 mmol) was added at pH 7.5. While stirring and heating the mixture, $CuCl_2 \cdot 2H_2O$ (0.05 g, 0.030 mmol) was added. After 2 hrs heating, few drops of aqueous ammonium hexafluoridophosphate solution were added and light green precipitate formed was filtered, washed with methanol/ether solution. The precipitate was dissolved in acetonitrile, filtered and left for slow evaporation. After a period of two weeks pale green blocks of crystals suitable of X-ray crystallography were collected. Yield: 0.010 g (75%); m.p. 270 - 272 °C; Elemental analysis: Found (%): C 45.48, H 2.98, N 7.97, Calcd. $C_{34}H_{27}N_5O_9CuPF_6$ (%): C 45.94, H 3.06, N 7.88.IR (neat, cm-1): 3080 w, 1605 m, 1553 m, 1520 m, 1477 w, 1342 s, 1242 m, 1213 m, 1094 m, 1024 w, 901 m, 831 s, 764 m, 688 m, 554

m, 455 w, 419 w; ESI-MS (CH_3CN): *m/z* $[(Cu+L+BNPP-H_2O]^+$ 725.073; UV-vis (CH_3CN): λ_{max}= 686, 343, 330, 288, 280, 219 nm.

8.12. Complex Synthesis (Chapter 6)

$[Fe(\mathbf{L2.3})_2](PF_6)_2 \cdot 4(H_2O)$

$FeCl_2.2H_2O$ (0.05 g, 0.025 mmol) in methanol was added to a solution of **L2.3** (0.02 g, 0.05 mmol) in methanol to give a purple solution, immediately. The solution was heated for 1h while stirring and then cooled to room temperature, followed by addition of few drops of a concentrated methanolic solution of ammonium hexafluoridophosphate. An excess of cold water was also added to enhance the precipitation of complex. The purple complex was collected by centrifugation from the aqueous solution, washed with ether : methanol (2:1) solution, dried under N_2 stream. Yield 0.030 g, 75%; m.p. 255-260°C; Elemental analysis Found (%): C 52.41, H 4.13, N 10.61, Calcd. $C_{56}H_{46}N_{10}FeP_2F_{12} \cdot 4H_2O$ (%): C 52.63, H 4.26, N 10.97.^{13}C NMR (CD_3CN) δ: 160.0, 157.8, 153.2, 149.8, 148.9, 138.8, 137.5, 132.1, 131.1, 130.9, 130.4, 129.7, 127.4, 124.4, 124.0, 123.3, 122.8, 51.7, 49.7; IR (KBr, cm-1) 3635 s, 3064 w, 1608 m, 1573 w, 1613 m, 1545 w,1469 m, 1423 w, 1365 m, 1288 s, 1163 w, 1056 w, 1028 w, 1000 s, 830 vs, 790 w, 754 m, 654 w, 558 s, 497 w, 458 w; ESI-MS (CH_3CN): *m/z* $[Fe+2L]^{2+}$ 457.1623, $[Fe+2L+PF_6+H]^{2+}$ 530.1483, $[Fe+2L]^{2+}$ 305.1106; UV-vis (CH_3CN): λ_{max} (ε) = 275 (45789), 287 (47872), 322 (34159), 561 (13238), nm (L mol^{-1} cm^{-1}).

*$[Fe_2Zn_2(\mathbf{L2.3})_4Cl_2](PF_6)_6 \cdot 4H_2O$ – Complex **6.1***

$FeCl_2.2H_2O$ (0.05 g, 0.025 mmol) in methanol was added to a solution of **L2.3** (0.02 g, 0.05 mmol) in methanol to give a purple solution, immediately. The resulting purple complex solution was treated with an excess of methanolic $ZnCl_2 \cdot H_2O$. The mixture was heated for 1h while stirring and then cooled to room temperature, followed by addition of few drops of a concentrated methanolic solution of ammonium hexafluoridophosphate. An excess of cold water was also added to enhance the precipitation of complex. The complex was collected by centrifugation from the aqueous solution, washed with ether : methanol (2:1) solution, dried under N_2 stream. The X-ray quality single crystals as purple fragile plates were formed by

vapour diffusion of ethyl acetate into the acetonitrile solution of the complex. Yield 0.056 g, 60%; m.p. >280 °C; Elemental analysis: Found (%): C 44.71, H 3.40, N 9.40, Calcd. $C_{112}H_{92}N_{20}Zn_2Fe_2Cl_2P_6F_{36}\cdot 5H_2O$ (%): C 44.97, H 3.44, N 9.36; IR (KBr, cm-1) 3340 s, 2368 w, 1844 w, 1611 m, 1535 w,1468 w, 1368 w, 1040 w, 794 s, 626 w, 558 m, 497 w, 458 w; UV-vis (CH_3CN): λ_{max} (ε) = 275 (88851), 287 (95819), 322 (73242), 561 (28724), nm (L mol^{-1} cm^{-1}).

*$[Zn_4$(**L2.3**)$_4(OCH_3CO)_2](PF_6)_6\cdot 2CH_3CN$ – Complex **6.2***

A methanolic solution of $Zn(OCH_3CO)_2.2H_2O$ (0.01 g, 0.046mmol) was mixed with a methanolic solution of **L2.3** (0.010g, 0.023mmol), resulting in a pale yellow solution. The solution was then treated with a concentrated methanolic solution of ammonium hexafluoridophosphate. Later addition of an excess of cold water resulted in formation of the white precipitates. The precipitates were collected by centrifugation, and washed with methanol and ether. Vapour diffusion of di-isopropyl ether into an acetonitrile solution of the white precipitates produced colourless blocks of X-ray quality crystals within two days. Yield 0.012 g, 63%; m.p. 245 - 248 °C; Elemental analysis: Found (%): C 46.17, H 3.34, N 9.37, Calcd. $C_{116}H_{98}N_{20}Zn_4O_4P_6F_{36}\cdot 2H_2O$ (%): C 46.40, H 3.42, N 9.34; ^{1}H NMR (DMSO) δ = 8.86 (d,2H), 8.83 (d,2H), 8.69 (d, 3H), 8.23 (d,3H), 7.85 (s, 1H), 7.67 (t, 2H), 7.54-7.46 (m, 5H), 7.17 (d, 1H), 6.98 (t, 1H), 3.80 (s, 2H), 3.76 (s, 2H); IR (KBr, cm^{-1}) 3675 w, 3340 s, 2542 w, 1866 w, 1603 s, 1575 w, 1549 w, 1478 s, 1419 w, 1371 w, 1325 w, 1248 m, 794 s, 764 w,739 w, 658 w, 559 s, 469 w; UV-vis (CH_3CN): λ_{max} (ε) = 275 (111208), 287 (96801), 322 (63446), 561 (668) nm (L mol^{-1} cm^{-1}).

*$[Fe_2Zn_2$(**L2.3**)$_4(C_8H_4O_4)](PF_6)_6$ – Complex **6.3***

To a methanolic solution of **L2.3** (30 mg, 0.070 mmol), methanolic $(NH_4)_2Fe(SO_4)_2\cdot 6H_2O$ (9 mg, 0.035 mmol)was added, to produce a purple solution, immediately. A solution of an excess of sodium terephthalate in methanol was added. After stirring for 30 mins, a methanolic solution of $Zn(NO_3)_2\cdot 6H_2O$ (20 mg, 0.070 mmol) was added. The mixture was heated at reflux for 8 hrs and then cooled to room temperature, followed by addition of few

drops of a concentrated methanolic solution of ammonium hexafluoridophosphate. An excess of cold water was also added to enhance the precipitation of the complex. The precipitate was collected by centrifugation from the aqueous solution, washed with ether:methanol (2:1) solution, and dried under a stream of N_2. The X-ray quality purple square shaped plates were formed by slow diffusion of ethyl acetate into a dilute acetonitrile solution of the complex over a period of 3 weeks. Yield 0.056 g, 60%; m.p. >280 °C; Elemental analysis: Found (%): C 47.42, H 3.72, N 8.89, Calcd. $C_{112}H_{92}N_{20}Fe_2Zn_2C_8H_4O_4P_6F_{36}\cdot 2.5H_2O$ (%): C 45.90, H 3.35, N 9.22; IR (neat, cm-1) 3340 s, 2368 w, 1844 w, 1698 w,1557 s, 1551 m, 1504 w, 1381 w, 1020 w, 823 s, 789 s, 653 w, 556 m, 447 w; UV-vis (CH_3CN): λ_{max} (ε) = 275 (88300), 287 (94830), 322 (71800), 561 (24720) nm (L mol^{-1} cm^{-1}).

*$[Fe_2Cu_2(\mathbf{L2.3})_4Cl_2](PF_6)_6\cdot 2CH_3CN\cdot(C_2H_5)_2O$ – Complex **6.4***

$FeCl_2.2H_2O$ (0.023 g, 0.011 mmol) in methanol was added to a solution of **L2.3** (0.010 g, 0.023 mmol) in methanol to give a purple solution, immediately. The resulting purple complex solution was treated with an excess of methanolic $CuCl_2\cdot 2H_2O$. The mixture was heated for 1h while stirring and then cooled to room temperature, followed by addition of few drops of concentrated methanolic solution of hexafluoridophosphate. An excess of cold water was also added to enhance the precipitation of complex. The complex was collected by centrifugation from the aqueous solution, washed with 3 ml of ether methanol (2:1 v/v) solution, and dried under N_2 stream. The X-ray quality single crystals as purple blocks were formed by slow diffusion of diethyl ether into a dilute acetonitrile solution of the complex. Yield: 0.011 g (70%); m.p. >280 °C; Elemental analysis: Found (%): C 44.68, H 3.03, N 9.58, Calcd. $C_{112}H_{92}N_{20}Fe_2Cu_2Cl_2P_6F_{36}\cdot 5H_2O$ (%): C 45.03, H 3.44, N 9.38; IR (neat, cm^{-1}) 3637 w, 1608 m, 1485 m, 1443 m, 1411 w, 1367 m, 1287 w, 1160 w, 1102 w, 1056 w, 1023 w, 982 w, 878 vs, 756 s, 737 s, 639 w, 555 s, 486 w, 428 w, 409 w; UV-Vis (CH_3CN):λ_{max} (ε) = 275 (88860), 287 (95825), 322 (73251), 561 (28739), nm (L mol^{-1} cm^{-1}).

*$[Ni_2Zn_2(\mathbf{L2.3})_4Cl_2](PF_6)_6 \cdot 4CH_3CN \cdot 2(CH_3CH)_2O \cdot 2H_2O$ – Complex **6.5***

A methanolic solution of $NiCl_2 \cdot H_2O$ (0.0027 g, 0.012 mmol) was mixed with a methanolic solution of **L2.3** (0.010 g, 0.023 mmol), resulting in a pale green solution. The solution was heated for 30 minutes and then $ZnCl_2 \cdot 2H_2O$ (0.0035 g, 0.012 mmol) in methanol was added. The mixture was heated to reflux for 2 hours. Cooled to room temperature and then treated with a concentrated methanolic solution of ammonium hexafluoridophosphate. Later addition of an excess of cold water resulted in formation of the very pale green precipitates. The precipitates were collected by centrifugation, and washed with methanol (1 ml) and ether (5 ml). Vapour diffusion of diethyl ether into acetonitrile solution of the precipitates produced X-ray quality crystals in 3-4 days. Yield 0.009 g (63%); m.p. 262-265 °C; Elemental analysis: Found (%): C 46.02, H 3.31, N 9.59, Calcd. $C_{112}H_{92}N_{20}Ni_2Zn_2Cl_2P_6F_{36} \cdot 2H_2O$ (%): C 45.90, H 3.39, N 9.41.

*$[Zn_4(\mathbf{L2.3})_4Br_2](PF_6)_6 \cdot 4CH_3CN \cdot 2(C_3H_7OC_3H_7)$ – Complex **6.6***

A methanolic solution of $Zn(Br)_2$ (0.01 g, 0.046 mmol) mixed with a methanolic solution of **L2.3** (0.010 g, 0.023 mmol) resulting in a clear solution. The solution was then treated with a concentrated methanolic solution of ammonium hexafluoridophosphate. Later addition of an excess of cold water resulted in formation of the white precipitates. The precipitates were collected by centrifugation, and washed with methanol and ether. An undisturbed slow diffusion of di-isopropyl ether into acetonitrile solution of the white precipitates produced colourless blocks of X-ray quality crystals within two days. Yield 0.012 g, 63%; Elemental analysis: Found (%): C 44.7, H 3.08, N 9.31, Calcd. $C_{112}H_{92}N_{20}Zn_4Br_2P_6F_{36} \cdot H_2O$ (%): C 44.44, H 3.13, N 9.25.

*[Zn_4(**L2.3**)$_4Br_2$](PF_6)$_6$·2$CH_3COOC_2H_5$*

A methanolic solution of $Zn(OTf)_2$ (0.01 g, 0.027 mmol) was mixed with a methanolic solution of **L2.3**·1/4HBr (0.011g, 0.027 mmol), resulting in a clear solution. The solution was then treated with a concentrated methanolic solution of ammonium hexafluoridophosphate. Later addition of an excess of cold water resulted in formation of the white precipitates. The precipitates were collected by centrifugation, and washed with methanol and ether. Vapour diffusion of ethyl acetate into an acetonitrile solution of the white precipitates produced colourless blocks of X-ray quality crystals within two days. Yield 0.008 g, 45%; Elemental analysis: Found (%): C 44.62, H 3.21, N 9.17, Calcd. $C_{112}H_{92}N_{20}Zn_4Br_2P_6F_{36}$ (%): C 44.79, H 3.09, N 9.33.

*[Ni_{10}(**L2.3**)$_{10}Br_4$(OH_2)$_6$]Br_{16}·68H_2O – Complex **6.8***

A 10 ml of aqueous solution of $NiBr_2·3H_2O$ (0.008 g, 0.029 mmol) was added to **L2.3** (0.006 g, 0.014 mmol) in 5 ml DCM:methanol (1:4) solution, heated to reflux for 30 mins. The yellow green solution of the complex reduced to 1 ml under vacuum rotary evaporation. The solution was filtered and left for slow evaporation, which resulted in formation of blocks of pale green X-ray quality crystals over a period of 3 weeks. Yield 0.013 g, 90%; Elemental analysis: Found (%): C 43.91, H 4.86, N 9.18, Calcd. $C_{280}H_{230}N_{50}Ni_{10}Br_{20}·68H_2O$ (%): C 43.65, H 4.80, N 9.09; IR (KBr, cm^{-1}) 3645 w, 3190 s, 1605 s, 1550 w, 1470 m, 1417 w, 1302 w, 1247 m, 1162 w, 1055 w, 1016 s, 890 w, 772 s, 645 w, 598 w, 548 w, 516 w, 499 w, 481 w, 465 w.

*[$Ni_{10}L_{10}Cl_4$(H_2O)$_6$]Cl_{16}·88H_2O – Complex **6.9***

A 5 ml DCM:methanol (1:4) solution of **L2.3** (0.006 g, 0.014 mmol) was mixed with a 10 ml aqueous solution of $NiCl_2·6H_2O$ (0.003 g, 0.014 mmol). To the resulting mixture an excess of aqueous solution of NaCl was added and heated to reflux for 1 h, then reduced to 1 ml by rotary evaporation. Within a period of 3 weeks rectangular blocks of pale green crystals were formed. Yield 0.008 g, 80%; Elemental analysis: Found (%): C 47.16, H 4.83, N 9.97, Calcd. $C_{280}H_{230}N_{50}Ni_{10}Cl_{20}·88H_2O$ (%): C 46.86, H 5.71, N 9.76; IR (KBr, cm^{-1}) 3628 w, 3199 s,

3050 w, 1604 s, 1550 w, 1460 s, 1416 m, 1300 w, 1245 m, 1162 w, 1053 w, 1017 s, 891 w, 795 w, 770 s, 739 msh, 645 w, 598 w, 548 w, 516 w, 499 w, 465 w.

*[Ni_{10}(**L2.3**)$_{10}Cl_4$(H2O)$_6$](Cl)$_{15}$Br ·91H_2O – Complex **6.10***

A 5 ml of DCM:methanol (1:4) solution of **L2.3**·¼HBr (0.023 g, 0.053 mmol) was mixed with an 10 ml aqueous solution of $NiCl_2·6H_2O$ (0.013 g, 0.053 mol). The resulting green mixture was heated at reflux for 1 h, and then reduced to 1 ml by rotary evaporation. The final green solution was filtered and left aside for evaporation. Within a period of three weeks fragile rectangular blocks of pale green X-ray quality crystals were formed. Yield 0.030 g, 80%; Elemental analysis: Found (%): C 46.32, H 5.72, N 9.65, Calcd. $C_{280}H_{230}N_{50}Ni_{10}Cl_{19}Br·91H_2O$ (%): C 46.23, H 5.71, N 9.63; IR (KBr, cm^{-1}): 3854 w, 3202 s, 2003 w, 1605 m, 1551 w, 1474 m,1416 w, 1303 w, 1245 m, 1161 w, 1055 w, 1017 m, 893 w, 738 s, 643 w, 540 w, 508 w,470 w, 460 m.

8.13. Miscellaneous complexes

*[Cu(**L2.5**)Cl_2]·CH_3CN·($C_2H_5OC_2H_5$)*

A chloroform solution of **L2.5** (0.010 g, 0.020 mmol) was added to a methanolic solution of $CuCl_2·2H_2O$ (0.033 g, 0.020 mmol) resulting in a green solution. The mixture was heated for 1 hr at reflux and reduced to 1 ml by rotary evaporation. Overnight slow diffusion of diethyl ether into the methanolic complex solution resulted in formation of green blocks of X-ray quality crystals. Yield: 0.010 g (85%); m.p. 206-209 °C; Elemental analysis: Found (%): C 55.88, H 4.73, N 8.79. Calcd. $C_{30}H_{30}N_4O_4CuCl_2$ (%): C 55.97, H 4.70, N 8.70; IR (KBr, cm^{-1}) 3671 w, 3290 s, 2640 w, 1859 w, 1655 sh, 1607 m, 1575 w, 1549 w, 1478 s, 1419 w, 1371 w, 1325 w, 1248 m, 784 s, 772 w,721 w, 655 w, 559 s, 414 m; ESI-MS (CH_3CN): *m/z* $[Cu+L+Cl]^+$ 608.13, $[Cu+L+Cl+H]^{2+}$ 304.5659.

*[{Cu_2(**L2.6**)Cl_4}H^+Cl^-]·CH_3CN·($C_2H_5OC_2H_5$)*

An aqueous solution of **L2.6** (0.010 g, 0.021 mmol) was added to a methanolic solution of $CuCl_2·2H_2O$ (0.075 g, 0.044 mmol) and a green precipitate was produced. The green precipitate was filtered, dried and dissolved in acetonitrile. Slow diffusion of diethyl ether in acetonitrile solution produced green needle shaped X-ray quality crystals over a period of 4 days. Yield: 0.008 g (55%); m.p. 134-136 °C; Elemental analysis: Found (%): C 36.23, H 3.96, N 6.44, Calcd. $C_{26}H_{23}N_4O_4Cu_2Cl_5(H_2O)_5$ (%): C 36.88, H 3.93, N 6.62; IR (KBr, cm^{-1}) 3633 w, 3060 s, 1821 w, 1650 s, 1600 m, 1572 w, 1546 w, 1477 s, 1413 w, 1371 w, 1306 w, 1248 m, 794 s, 764 w,799 w, 738 m, 671 m, 503 w, 412 m; ESI-MS (CH_3CN); *m/z* $[Cu+L+Cl]^+$ 552.0620.

APPENDIX I

Absorbance *vs.* Time graphs for the kinetics of hydrolysis experiments performed using Zn(II) complexes (0.4 mM), BNPP (10 mM), pH 7-9 (HEPES, I = 0.1 M $NaClO_4$), 45% CH_3CN-5% DMF at 35 °C. (Related to Table 5.1. in Chapter 5)

A *vs.* T graph for Zn-**L2.1**, pH 7

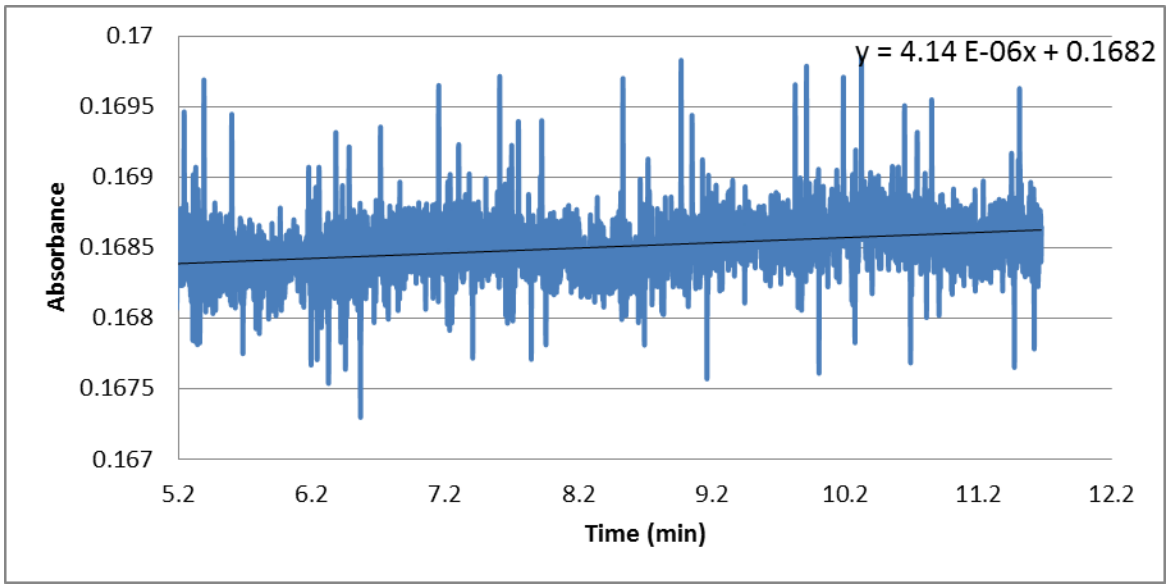

A *vs.* T graph for Zn-**L2.1**, pH 7.5

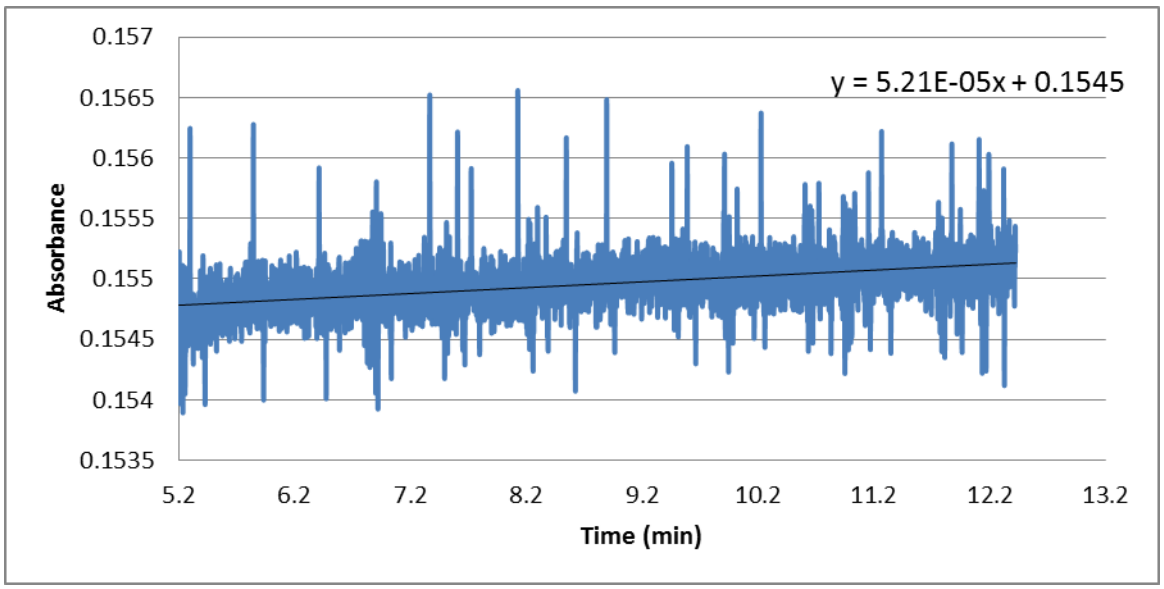

A *vs.* T graph for Zn-**L2.1**, pH 8

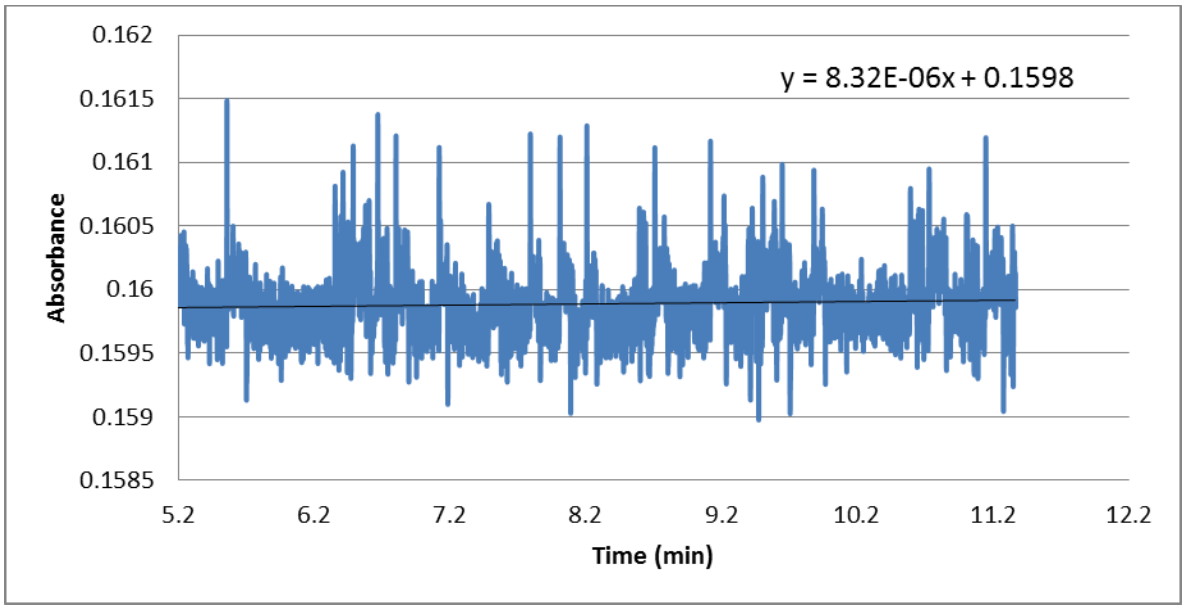

A *vs.* T graph for Zn-**L2.1**, pH 8.5

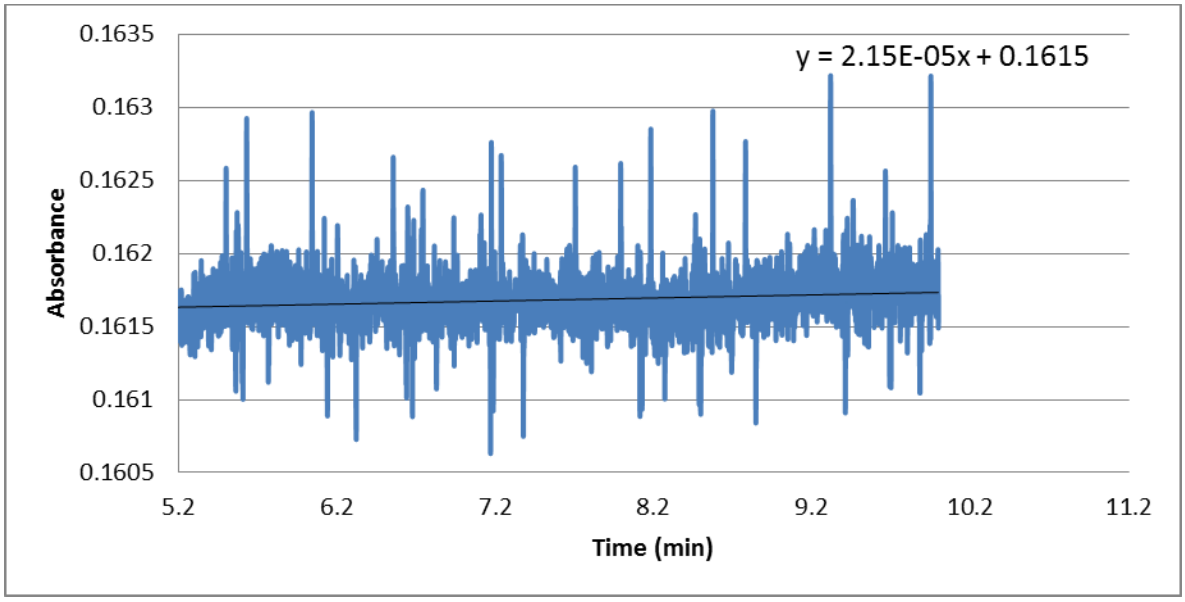

A *vs.* T graph for Zn(II)-**L2.1**, pH 9

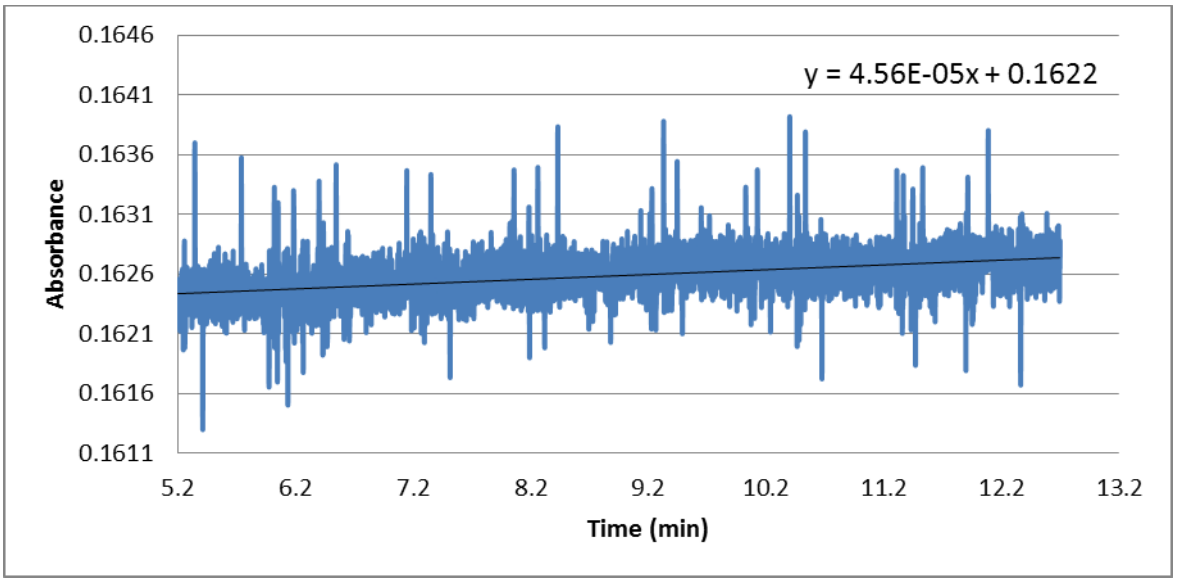

A *vs.* T for Zn-**pa,** pH 7

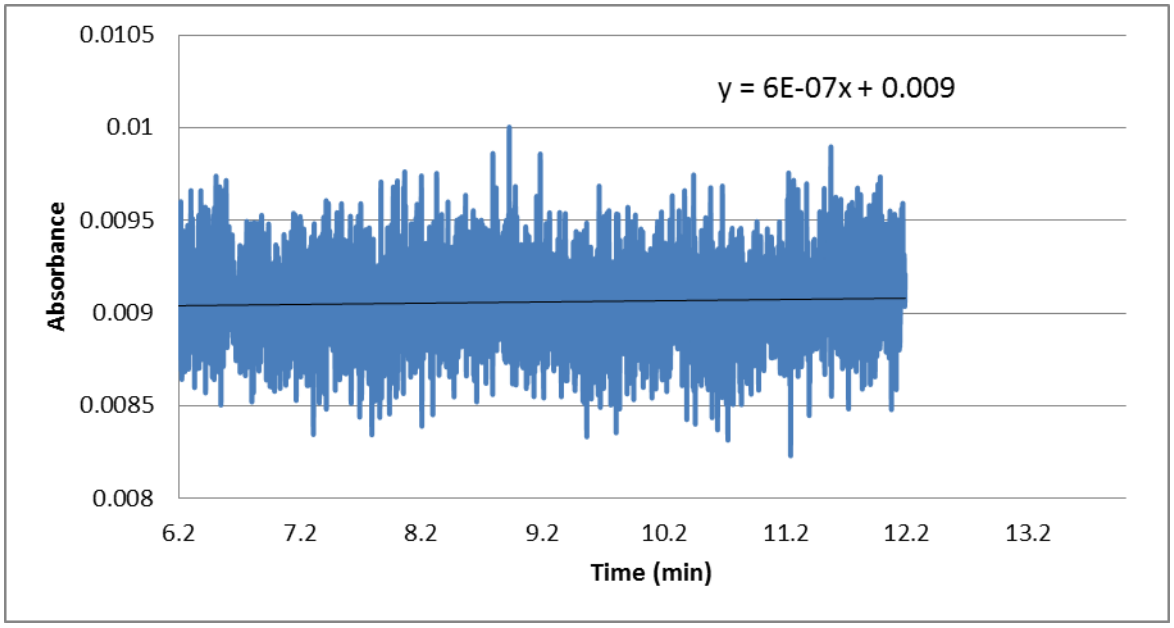

A vs. T graph for Zn-**pa**, pH 7.5

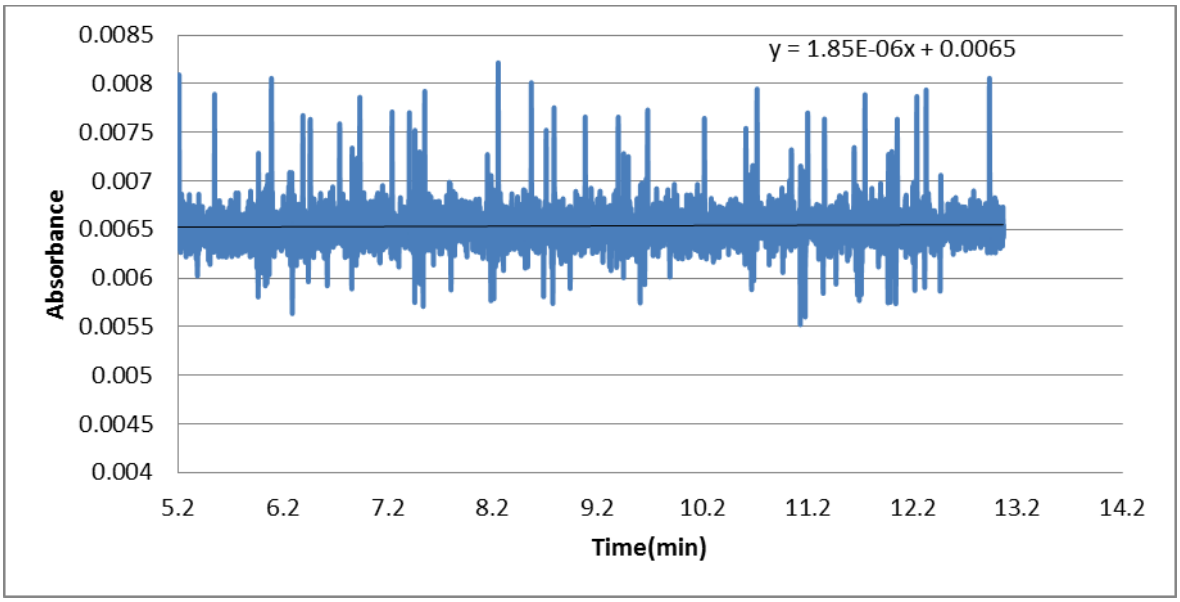

A *vs.* T graph for Zn-**pa**, pH 8

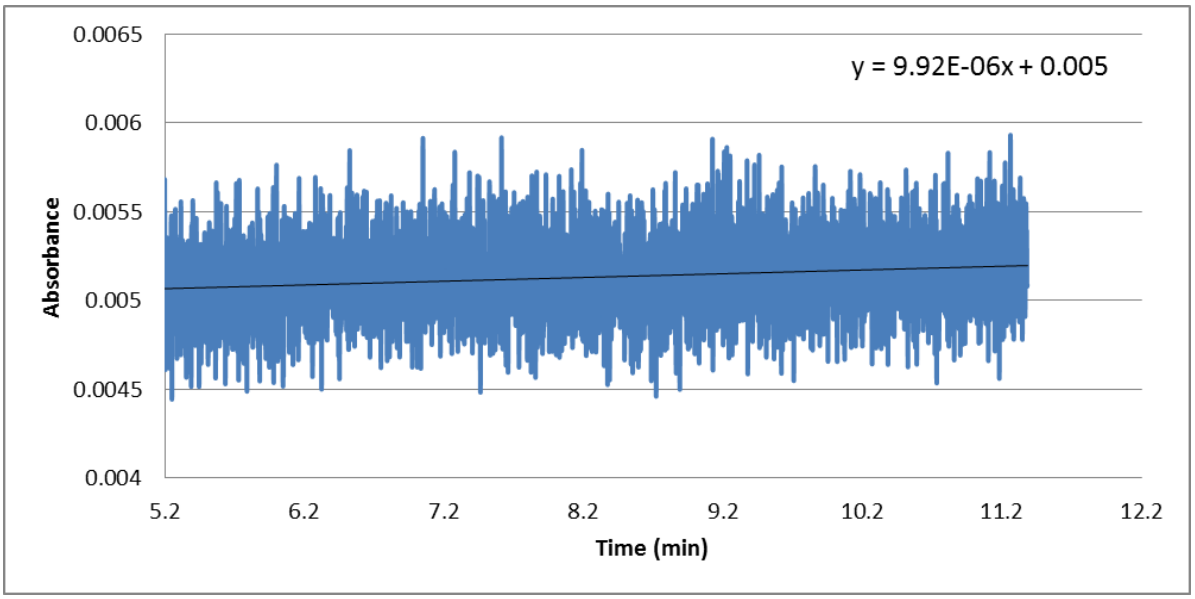

A vs. T graph for Zn-**pa**, pH 8.5

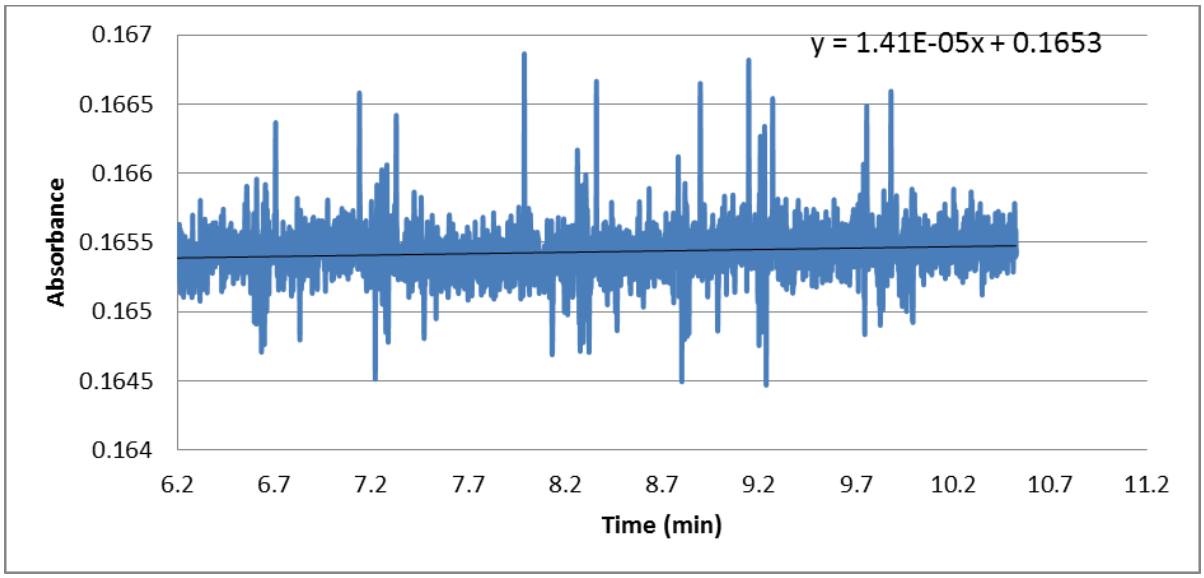

A vs. T graph for Zn(II)-**pa**, pH 9

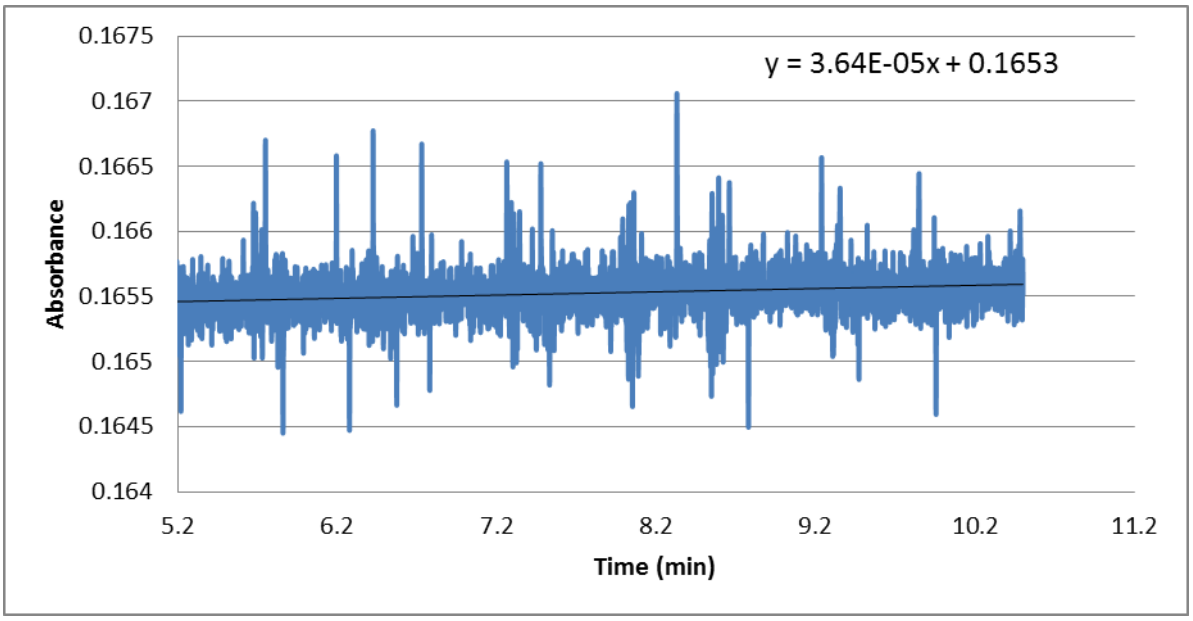

A vs. T graph for Zn(II)-**L2.3**, pH 7

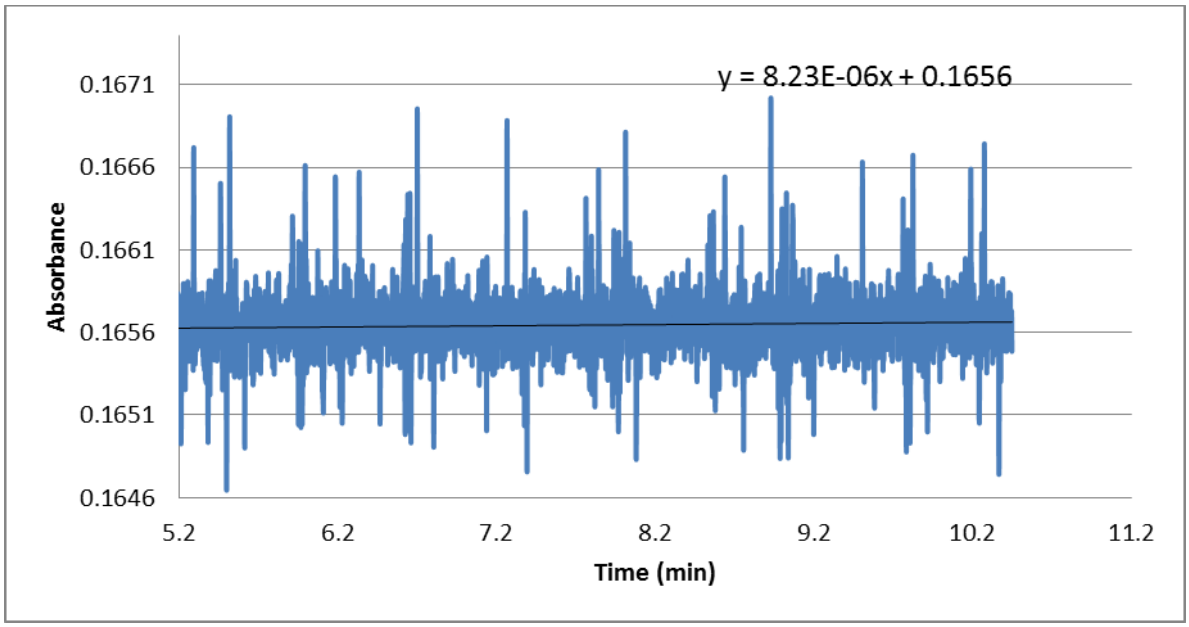

A vs. T graph for Zn(II)-**L2.3**, pH 7.5

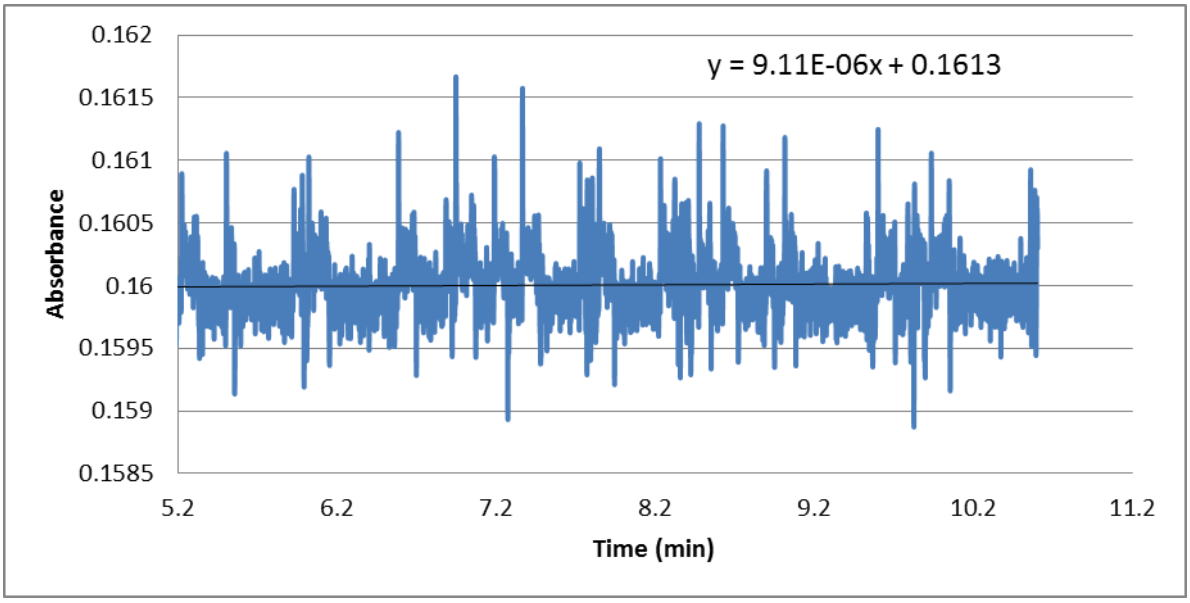

A vs. T graph for Zn(II)-**L2.3**, pH 8

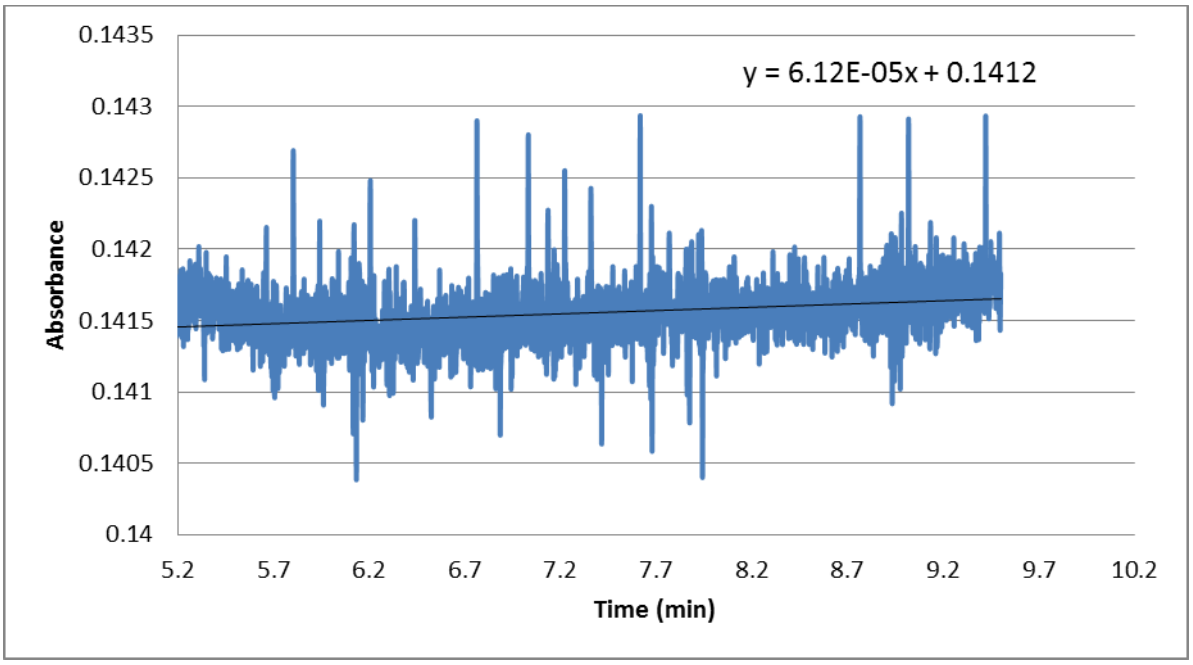

A vs. T graph for Zn(II)-**L2.3**, pH 8.5

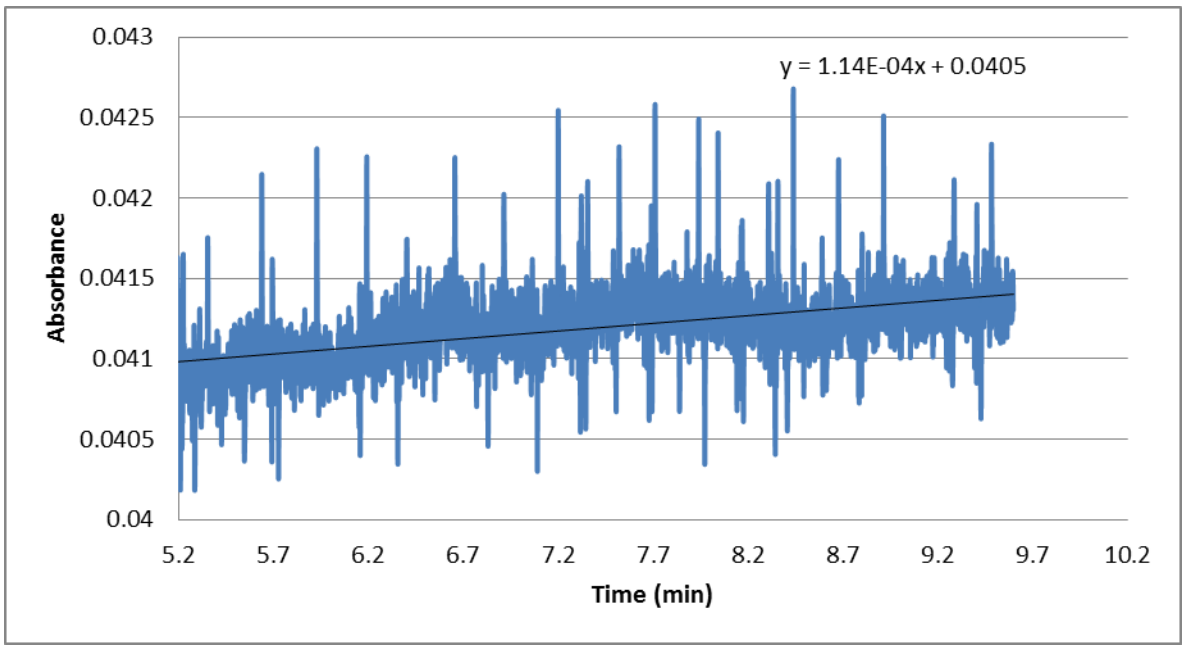

A vs. T graph for Zn(II)-**L2.3**, pH 9

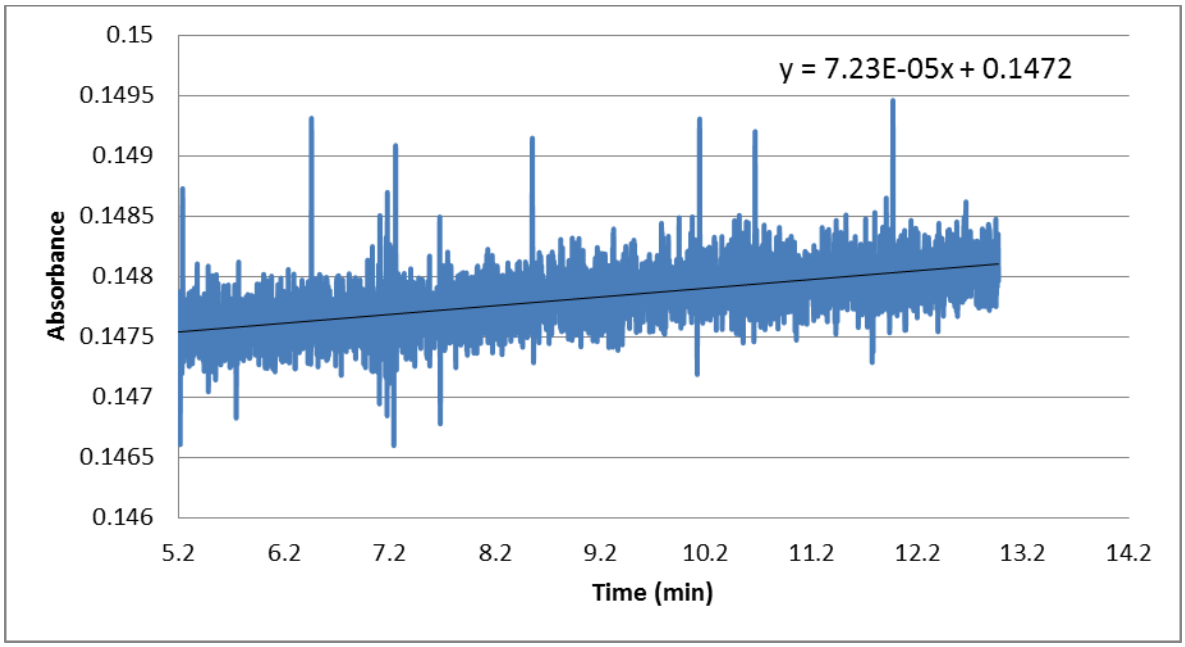

A vs. T graph for Zn(II)-**L2.4**, pH 7

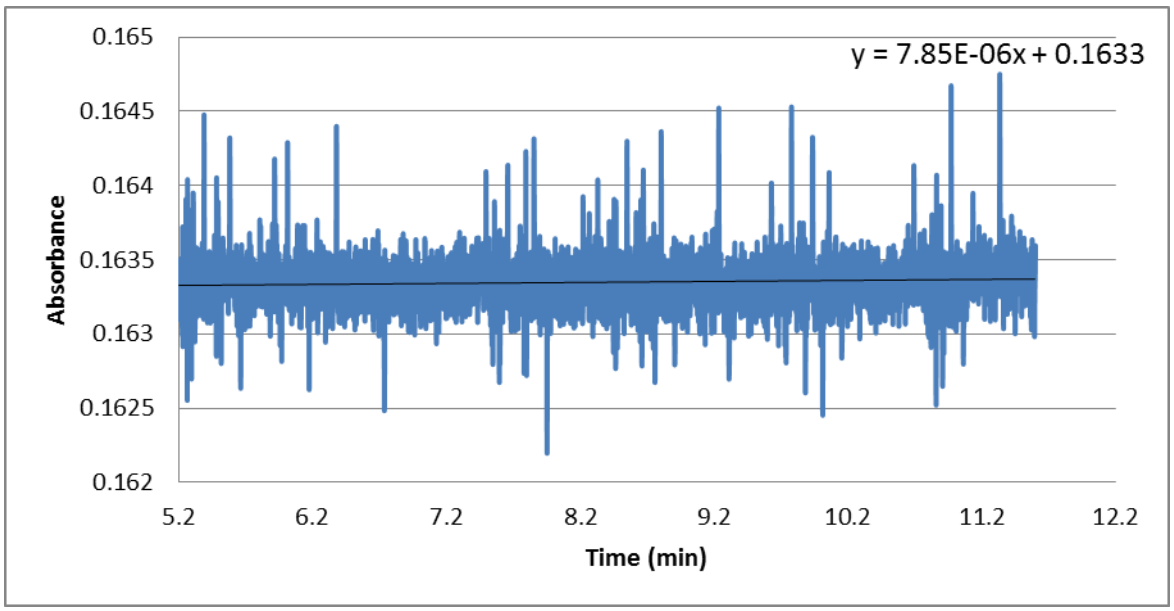

A vs. T graph for Zn(II)-**L2.4**, pH 7.5

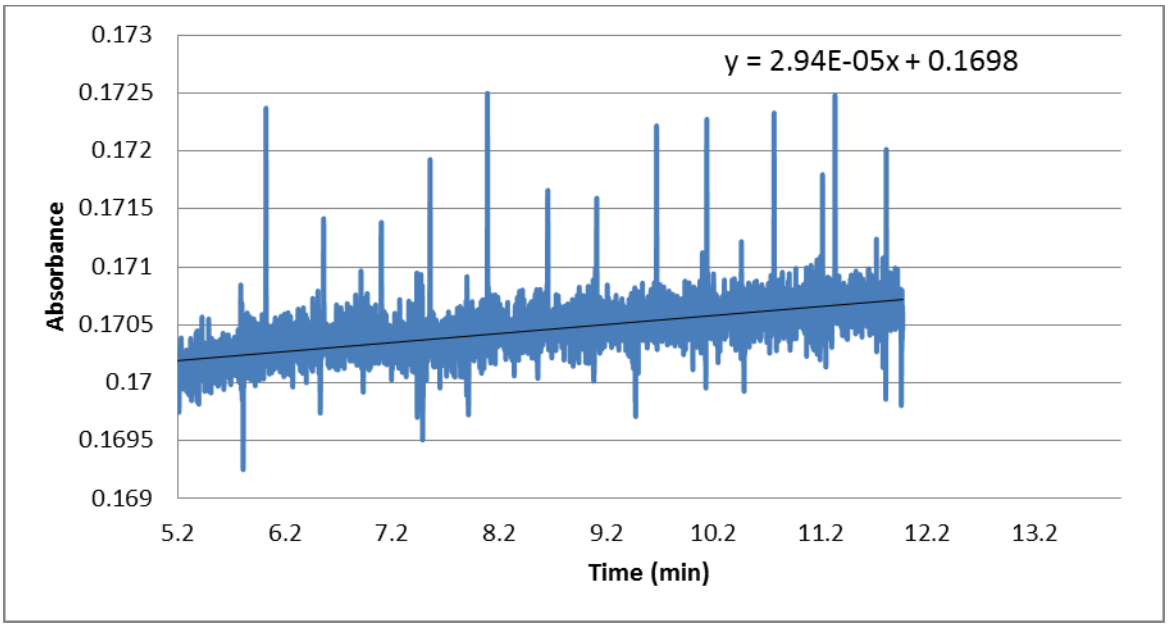

A vs. T graph for Zn(II)-**L2.4**, pH 8

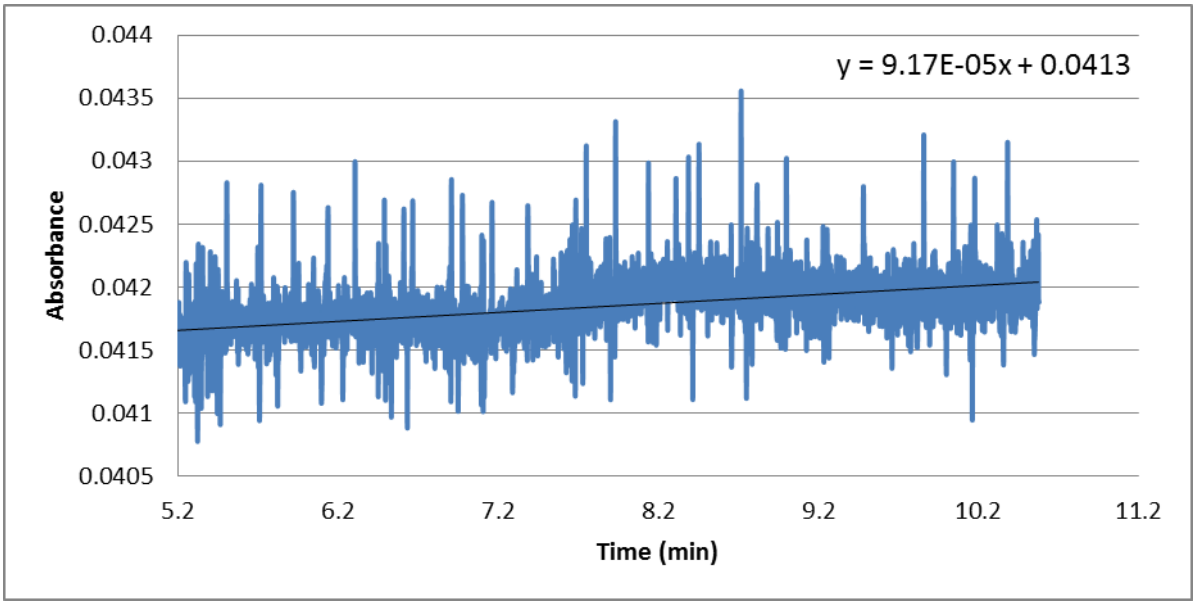

A vs. T graph for Zn(II)-**L2.4**, pH 8.5

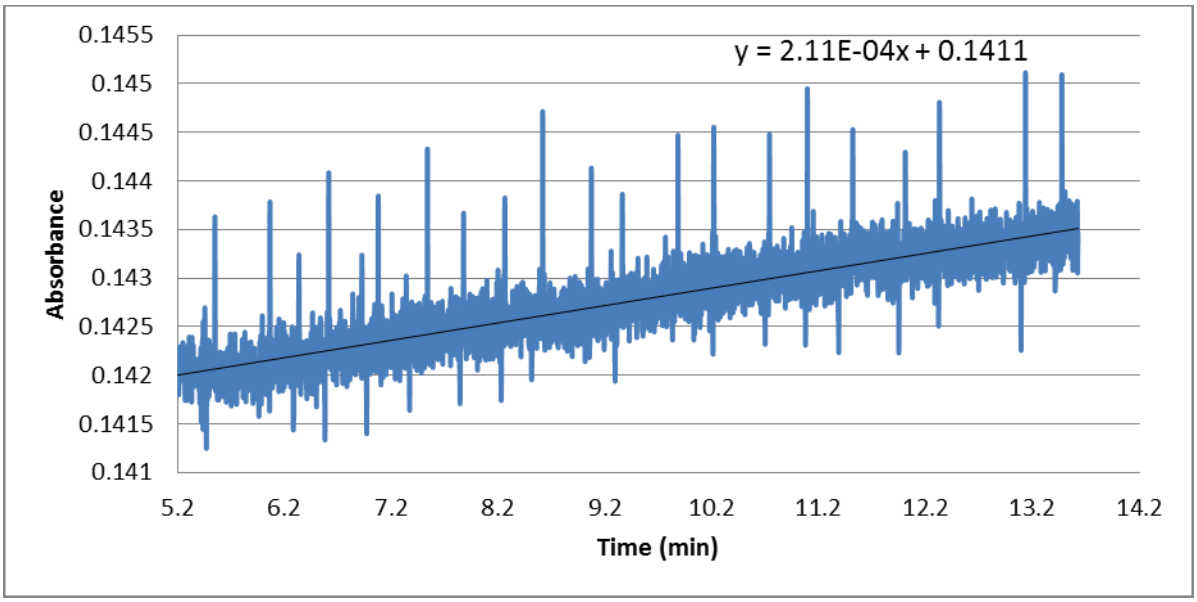

A vs. T graph for Zn(II)-**L2.4**, pH 9

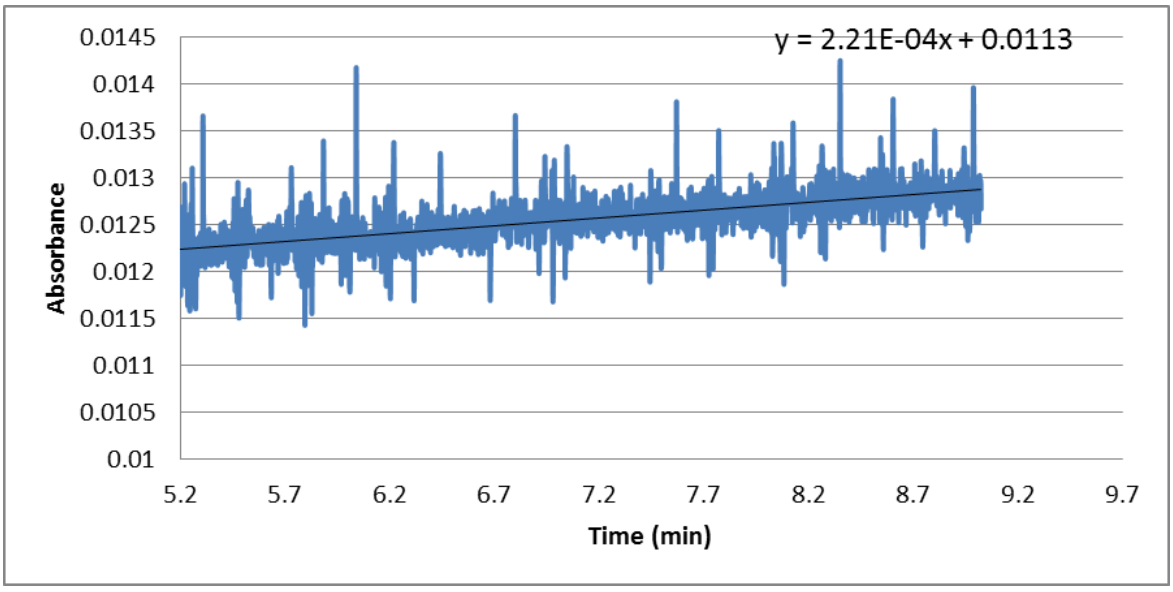

APPENDIX II

Table – A1 Crystal data and X-ray experimental data for compounds L2.3, L2.4 and L2.7

Compound	**L2.3**	**L2.4**	**L2.7**
Identification code	GK4	GKA55	GKA2R
Empirical formula	$C_{28}H_{23}N_5$	$C_{34}H_{28}N_6$	$C_{28}H_{34}Cl_6N_7$
Formula weight	429.51	520.62	681.32
Temperature/K	120.01(10)	120.01(10)	120.01(10)
Crystal system	monoclinic	triclinic	monoclinic
Space group	$P2_1/c$	P-1	C2/c
a/Å	18.1292(5)	10.25418(15)	29.1603(4)
b/Å	11.5151(2)	10.51097(15)	13.5818(2)
c/Å	10.8978(3)	14.04166(18)	22.1714(4)
α/°	90	68.4172(13)	90
β/°	107.376(3)	84.4281(12)	93.4419(15)
γ/°	90	68.9351(14)	90
Volume/$Å^3$	2171.20(9)	1312.20(4)	8765.1(3)
Z	4	2	8
$\rho_{calc}g/cm^3$	1.314	1.318	1.033
μ/mm^{-1}	0.626	0.627	3.759
F(000)	904.0	548.0	2824.0
Crystal size/mm^3	0.35 × 0.1 × 0.05	0.35 × 0.24 × 0.13	0.2 × 0.08 × 0.04
Radiation	CuKα (λ = 1.54184)	CuKα (λ = 1.54184)	CuKα (λ = 1.54184)
2Θ range for data collection/°	9.226 to 147.658	6.776 to 147.734	6.072 to 130.992
Index ranges	$-22 \le h \le 22$, $-14 \le k \le 14$, $-11 \le l \le 13$	$-12 \le h \le 12$, $-11 \le k \le 12$, $-17 \le l \le 17$	$-36 \le h \le 35$, $-16 \le k \le 12$, $-27 \le l \le 27$
Reflections collected	24681	67308	30695
Independent reflections	4336 [R_{int} = 0.0236, R_{sigma} = 0.0141]	5275 [R_{int} = 0.0497, R_{sigma} = 0.0175]	7537 [R_{int} = 0.0315, R_{sigma} = 0.0270]
Data/restraints/parameters	4336/1/390	5275/0/361	7537/15/416
Goodness-of-fit on F^2	1.086	1.038	1.089
Final R indexes [I>=2σ (I)]	R_1 = 0.0392, wR_2 = 0.1118	R_1 = 0.0433, wR_2 = 0.1188	R_1 = 0.0675, wR_2 = 0.2068
Final R indexes [all data]	R_1 = 0.0473, wR_2 = 0.1172	R_1 = 0.0474, wR_2 = 0.1227	R_1 = 0.0779, wR_2 = 0.2171
Largest diff. peak/hole / e $Å^{-3}$	0.24/-0.21	0.23/-0.28	1.63/-0.64

Table – A2 Crystal data and X-ray experimental data for compounds 2.8, 3.1 and 3.2

Compound	**2.8**	**3.1**	**3.2**
Identification code	GKA85	GKA94	GKA93R
Empirical formula	$C_{22}H_{15.3}Br_{1.7}N_3$	$C_{46}H_{50}Cl_2N_6NiO_6$	$C_{48}H_{50}Cl_4N_6Ni_2O_4$
Formula weight	457.52	912.53	1034.16
Temperature/K	120.02(10)	120.01(10)	120.01(10)
Crystal system	monoclinic	monoclinic	triclinic
Space group	$P2_1/c$	C2/c	P-1
a/Å	10.31992(15)	22.6989(5)	8.3237(6)
b/Å	7.79812(11)	9.7944(2)	8.4445(6)
c/Å	23.7839(4)	20.4780(5)	18.0119(14)
α/°	90	90	96.892(6)
β/°	99.9708(15)	95.324(2)	95.155(6)
γ/°	90	90	106.782(6)
Volume/$Å^3$	1885.12(5)	4533.08(17)	1193.00(16)
Z	4	4	1
$\rho_{calc}g/cm^3$	1.612	1.337	1.439
μ/mm^{-1}	4.788	2.142	3.444
F(000)	911.0	1912.0	536.0
Crystal size/mm^3	0.5 × 0.3 × 0.2	0.17 × 0.1 × 0.03	0.3 × 0.15 × 0.06
Radiation	CuKα (λ = 1.54184)	CuKα (λ = 1.54184)	CuKα (λ = 1.54184)
2Θ range for data collection/°	10.49 to 147.64	7.824 to 134.986	9.98 to 134.95
Index ranges	$-12 \le h \le 12$, $-9 \le k \le 9$, $-29 \le l \le 20$	$-25 \le h \le 27$, $-11 \le k \le 8$, $-24 \le l \le 24$	$-9 \le h \le 9$, $-7 \le k \le 10$, $-21 \le l \le 21$
Reflections collected	10580	8270	7536
Independent reflections	3705 [R_{int} = 0.0332, R_{sigma} = 0.0261]	4081 [R_{int} = 0.0279, R_{sigma} = 0.0375]	4276 [R_{int} = 0.0379, R_{sigma} = 0.0511]
Data/restraints/parameters	3705/0/244	4081/5/298	4276/4/298
Goodness-of-fit on F^2	1.046	1.028	1.043
Final R indexes [I>=2σ (I)]	R_1 = 0.0513, wR_2 = 0.1435	R_1 = 0.0384, wR_2 = 0.0984	R_1 = 0.0440, wR_2 = 0.1169
Final R indexes [all data]	R_1 = 0.0524, wR_2 = 0.1443	R_1 = 0.0444, wR_2 = 0.1039	R_1 = 0.0591, wR_2 = 0.1284
Largest diff. peak/hole / e $Å^{-3}$	1.66/-0.74	0.58/-0.32	0.72/-0.44

Table – A3 Crystal data and X-ray experimental data for compounds 3.3, 3.4 and 3.5

Compound	**3.3**	**3.4**	**3.5**
Identification code	GKA87	GKA51B	GKA104B
Empirical formula	$C_{22}H_{25}Cl_2N_3NiO_4$	$C_{44}H_{34}Br_2N_6Ni$	$C_{22}H_{25}CuN_3O_9S$
Formula weight	525.06	865.30	571.05
Temperature/K	120.01(10)	120.02(10)	120.01(10)
Crystal system	orthorhombic	monoclinic	orthorhombic
Space group	$P2_12_12_1$	$P2_1/n$	$Pna2_1$
a/Å	8.1869(2)	12.51123(12)	16.4533(5)
b/Å	16.6367(4)	16.11054(18)	19.2409(8)
c/Å	16.9708(4)	21.8742(2)	7.3408(2)
α/°	90	90	90
β/°	90	93.8121(9)	90
γ/°	90	90	90
Volume/Å^3	2311.47(10)	4399.26(8)	2323.93(14)
Z	4	4	4
ρ_{calc}g/cm^3	1.509	1.306	1.632
μ/mm^{-1}	1.105	3.035	2.700
F(000)	1088.0	1752.0	1180.0
Crystal size/mm^3	0.3 × 0.11 × 0.11	0.3 × 0.14 × 0.05	0.26 × 0.13 × 0.04
Radiation	MoKα (λ = 0.71073)	CuKα (λ = 1.54184)	CuKα (λ = 1.54184)
2Θ range for data collection/°	5.39 to 59.996	6.82 to 147.584	7.07 to 129.956
Index ranges	$-11 \le h \le 10$, $-11 \le k \le 23$, $-23 \le l \le 23$	$-15 \le h \le 15$, $-19 \le k \le 17$, $-27 \le l \le 26$	$-19 \le h \le 19$, $-19 \le k \le 22$, $-8 \le l \le 8$
Reflections collected	11026	44288	9268
Independent reflections	6540 [R_{int} = 0.0237, R_{sigma} = 0.0393]	8758 [R_{int} = 0.0371, R_{sigma} = 0.0230]	3727 [R_{int} = 0.0449, R_{sigma} = 0.0415]
Data/restraints/parameters	6540/8/314	8758/0/480	3727/9/336
Goodness-of-fit on F^2	1.050	1.041	1.057
Final R indexes [I>=2σ (I)]	R_1 = 0.0299, wR_2 = 0.0702	R_1 = 0.0537, wR_2 = 0.1520	R_1 = 0.0456, wR_2 = 0.1208
Final R indexes [all data]	R_1 = 0.0324, wR_2 = 0.0718	R_1 = 0.0589, wR_2 = 0.1563	R_1 = 0.0467, wR_2 = 0.1231
Largest diff. peak/hole / e Å^{-3}	0.43/-0.26	1.13/-1.50	0.67/-0.39
Flack Parameter	-0.008(6)		0.00(2)

Table – A4 Crystal data and X-ray experimental data for compounds 3.6, 3.7 and 3.9

Compound	**3.6**	**3.7**	**3.9**
Identification code	GKA75	GKA101B	GKA89B
Empirical formula	$C_{45.65}H_{38}Cl_{7.2}Cu_3N_6O_{1.25}$	$C_{22}H_{26}CuF_6N_3O_5P$	$C_{28}H_{28}CuN_4O_5$
Formula weight	1136.48	620.97	564.08
Temperature/K	120.01(10)	120.0(2)	120.01(10)
Crystal system	triclinic	monoclinic	triclinic
Space group	P-1	$P2_1/c$	P-1
a/Å	10.0369(4)	12.7656(3)	7.9367(3)
b/Å	11.0646(4)	7.53655(11)	12.2373(5)
c/Å	22.0870(7)	25.5833(4)	15.0660(5)
α/°	98.170(3)	90	111.031(3)
β/°	101.712(3)	94.4076(16)	103.423(3)
γ/°	98.342(3)	90	92.955(3)
Volume/$Å^3$	2338.82(14)	2454.06(7)	1313.74(9)
Z	2	4	2
$\rho_{calc}g/cm^3$	1.614	1.681	1.426
μ/mm^{-1}	5.720	2.669	0.877
F(000)	1147.0	1268.0	586.0
Crystal size/mm^3	0.3 × 0.2 × 0.05	0.1 × 0.1 × 0.08	0.25 × 0.2 × 0.05
Radiation	CuKα (λ = 1.54184)	CuKα (λ = 1.54184)	MoKα (λ = 0.71073)
2Θ range for data collection/°	8.206 to 147.456	6.93 to 147.706	5.712 to 54.998
Index ranges	$-12 \le h \le 12$, $-11 \le k \le 13$, $-23 \le l \le 27$	$-14 \le h \le 15$, $-9 \le k \le 9$, $-31 \le l \le 31$	$-10 \le h \le 10$, $-15 \le k \le 15$, $-17 \le l \le 19$
Reflections collected	19441	18034	12630
Independent reflections	9168 [R_{int} = 0.0384, R_{sigma} = 0.0469]	4890 [R_{int} = 0.0309, R_{sigma} = 0.0261]	6041 [R_{int} = 0.0245, R_{sigma} = 0.0368]
Data/restraints/parameters	9168/13/601	4890/11/380	6041/2/373
Goodness-of-fit on F^2	1.055	1.195	1.107
Final R indexes [I>=2σ (I)]	R_1 = 0.0483, wR_2 = 0.1327	R_1 = 0.0903, wR_2 = 0.2497	R_1 = 0.0407, wR_2 = 0.1065
Final R indexes [all data]	R_1 = 0.0609, wR_2 = 0.1405	R_1 = 0.0933, wR_2 = 0.2513	R_1 = 0.0449, wR_2 = 0.1097
Largest diff. peak/hole / e $Å^{-3}$	1.27/-0.65	2.44/-0.92	1.17/-0.56

Table – A5 Crystal data and X-ray experimental data for compounds 3.10, 3.11 and 3.13

Compound	**3.10**	**3.11**	**3.13**
Identification code	GKA109	GKA115	GKA114
Empirical formula	$C_{28}H_{26}N_4O_4Zn$	$C_{22}H_{17}N_3Cl_2Zn$	$C_{48}H_{39}Ag_2N_{10}O_6$
Formula weight	547.90	459.65	1067.63
Temperature/K	119.99(10)	120.02(10)	120.01(10)
Crystal system	monoclinic	monoclinic	hexagonal
Space group	$P2_1/c$	C2/c	$P6_1$
a/Å	14.5212(2)	11.0438(7)	14.82092(16)
b/Å	8.80738(13)	13.5326(6)	14.82092(16)
c/Å	21.2301(3)	13.1994(7)	35.3634(4)
α/°	90	90	90
β/°	106.8569(18)	100.129(6)	90
γ/°	90	90	120
Volume/$Å^3$	2598.54(8)	1941.94(19)	6727.20(16)
Z	4	4	6
$\rho_{calc}g/cm^3$	1.400	1.572	1.581
μ/mm^{-1}	1.652	4.383	7.518
F(000)	1136.0	936.0	3234.0
Crystal size/mm^3	0.16 × 0.15 × 0.05	0.2 × 0.06 × 0.02	0.3 × 0.03 × 0.03
Radiation	CuKα (λ = 1.54184)	CuKα (λ = 1.54184)	CuKα (λ = 1.54184)
2Θ range for data collection/°	6.36 to 148.944	10.438 to 133.914	6.886 to 133.948
Index ranges	$-18 \le h \le 17$, $-10 \le k \le 10$, $-25 \le l \le 26$	$-13 \le h \le 11$, $-16 \le k \le 16$, $-14 \le l \le 15$	$-17 \le h \le 17$, $-17 \le k \le 17$, $-42 \le l \le 37$
Reflections collected	32570	5449	32313
Independent reflections	5250 [R_{int} = 0.0296, R_{sigma} = 0.0173]	1701 [R_{int} = 0.0331, R_{sigma} = 0.0295]	7157 [R_{int} = 0.0327, R_{sigma} = 0.0279]
Data/restraints/parameters	5250/0/338	1701/0/165	7157/9/728
Goodness-of-fit on F^2	1.034	1.095	1.047
Final R indexes [I>=2σ (I)]	R_1 = 0.0352, wR_2 = 0.0907	R_1 = 0.0487, wR_2 = 0.1276	R_1 = 0.0322, wR_2 = 0.0815
Final R indexes [all data]	R_1 = 0.0387, wR_2 = 0.0934	R_1 = 0.0523, wR_2 = 0.1305	R_1 = 0.0343, wR_2 = 0.0833
Largest diff. peak/hole / e $Å^{-3}$	0.87/-0.46	1.47/-0.69	0.96/-0.60
Flack Parameter			-0.014(5)

Table – A6 Crystal data and X-ray experimental data for compounds 4.1, 4.2 and 4.3

Compound	**4.1**	**4.2**	**4.3**
Identification code	GKA20	GKA60	GKA35
Empirical formula	$C_{34}H_{32}Cl_4N_8Zn_2$	$C_{36}H_{36}Cl_4N_6O_2Zn_2$	$C_{36}H_{37}Cu_2N_5O_9$
Formula weight	825.21	857.25	810.78
Temperature/K	120.01(10)	290.82(10)	120.01(10)
Crystal system	monoclinic	monoclinic	triclinic
Space group	$P2_1/n$	$P2_1/n$	P-1
a/Å	8.4399(4)	7.40640(7)	8.6292(10)
b/Å	14.9784(5)	19.66830(18)	12.0438(13)
c/Å	28.9572(9)	25.2756(2)	19.221(3)
α/°	90	90	79.962(10)
β/°	94.594(4)	96.3220(9)	89.491(10)
γ/°	90	90	73.915(10)
Volume/Å^3	3648.9(2)	3659.53(6)	1888.3(4)
Z	4	4	2
ρ_{calc}g/cm^3	1.502	1.556	1.426
μ/mm^{-1}	4.604	4.639	1.885
F(000)	1680.0	1752.0	836.0
Crystal size/mm^3	0.2 × 0.04 × 0.04	0.24 × 0.12 × 0.08	? × ? × ?
Radiation	CuKα (λ = 1.54184)	CuKα (λ = 1.54184)	CuKα (λ = 1.54184)
2Θ range for data collection/°	6.648 to 134.986	5.706 to 137.992	7.764 to 134.99
Index ranges	$-8 \le h \le 10$, $-17 \le k \le 16$, $-23 \le l \le 34$	$-8 \le h \le 6$, $-23 \le k \le 21$, $-30 \le l \le 30$	$-7 \le h \le 10$, $-14 \le k \le 14$, $-22 \le l \le 23$
Reflections collected	15741	24830	13167
Independent reflections	6553 [R_{int} = 0.0448, R_{sigma} = 0.0617]	6782 [R_{int} = 0.0375, R_{sigma} = 0.0309]	6785 [R_{int} = 0.0321, R_{sigma} = 0.0492]
Data/restraints/parameters	6553/1/440	6782/1/458	6785/2/516
Goodness-of-fit on F^2	1.037	1.043	1.049
Final R indexes [I>=2σ (I)]	R_1 = 0.0446, wR_2 = 0.1018	R_1 = 0.0344, wR_2 = 0.0897	R_1 = 0.0447, wR_2 = 0.1212
Final R indexes [all data]	R_1 = 0.0654, wR_2 = 0.1170	R_1 = 0.0390, wR_2 = 0.0929	R_1 = 0.0526, wR_2 = 0.1281
Largest diff. peak/hole / e Å^{-3}	0.61/-0.70	1.07/-0.55	0.55/-0.51

Table – A7 Crystal data and X-ray experimental data for compounds 4.4, 4.5 and 4.6

Compound	**4.4**	**4.5**	**4.6**
Identification code	GKA10	GKA50	GKA70-R
Empirical formula	$C_{60}H_{62}Cl_8Cu_4N_{10}O_4$	$C_{56}H_{46}Cl_8Cu_4N_{10}$	$C_{68}H_{58}Cl_8Cu_4N_{12}O_{1.5}$
Formula weight	1524.95	1396.79	1605.02
Temperature/K	120.01(10)	120.01(10)	120.01(10)
Crystal system	triclinic	monoclinic	triclinic
Space group	P-1	$P2_1/c$	P-1
a/Å	9.0859(8)	14.20516(11)	10.9040(3)
b/Å	9.7087(8)	12.74024(8)	15.4257(5)
c/Å	17.9955(15)	15.16100(9)	22.4889(8)
α/°	84.863(7)	90	87.327(3)
β/°	89.138(7)	95.1715(6)	83.923(3)
γ/°	79.810(7)	90	74.313(3)
Volume/$Å^3$	1556.1(2)	2732.62(3)	3620.7(2)
Z	1	2	2
$\rho_{calc}g/cm^3$	1.627	1.698	1.472
μ/mm^{-1}	5.153	5.752	4.446
F(000)	776.0	1408.0	1628.0
Crystal size/mm^3	0.52 × 0.24 × 0.04	0.27 × 0.13 × 0.06	0.11 × 0.026 × 0.02
Radiation	CuKα (λ = 1.54184)	CuKα (λ = 1.54184)	CuKα (λ = 1.54184)
2Θ range for data collection/°	9.292 to 130.986	6.248 to 130.952	5.952 to 130.998
Index ranges	$-8 \le h \le 10$, $-11 \le k \le 11$, $-21 \le l \le 21$	$-16 \le h \le 13$, $-15 \le k \le 15$, $-17 \le l \le 17$	$-13 \le h \le 7$, $-19 \le k \le 18$, $-26 \le l \le 28$
Reflections collected	13937	24402	25753
Independent reflections	5238 [R_{int} = 0.0428, R_{sigma} = 0.0435]	4700 [R_{int} = 0.0332, R_{sigma} = 0.0183]	12399 [R_{int} = 0.0310, R_{sigma} = 0.0421]
Data/restraints/parameters	5238/2/402	4700/1/356	12399/2/868
Goodness-of-fit on F^2	1.034	1.051	1.077
Final R indexes [I>=2σ (I)]	R_1 = 0.0379, wR_2 = 0.0939	R_1 = 0.0254, wR_2 = 0.0702	R_1 = 0.0598, wR_2 = 0.1586
Final R indexes [all data]	R_1 = 0.0477, wR_2 = 0.0999	R_1 = 0.0262, wR_2 = 0.0709	R_1 = 0.0705, wR_2 = 0.1660
Largest diff. peak/hole / e $Å^{-3}$	0.87/-0.47	0.38/-0.43	4.33/-2.88

Table – A8 Crystal data and X-ray experimental data for compounds 5.1, 5.2 and 6.1

Compound	**5.1**	**5.2**	**6.1**
Identification code	GKA10	GKA78	GKA26A
Empirical formula	$C_{60}H_{62}Cl_8Cu_4N_{10}O_4$	C34H25ClCuN5O8P	$C_{58}H_{50}ClF_{18}FeN_{10}O_2P_3Zn$
Formula weight	1524.95	761.55	1510.66
Temperature/K	120.01(10)	120	293(2)
Crystal system	triclinic	triclinic	triclinic
Space group	P-1	P-1	P-1
a/Å	9.0859(8)	12.4163(8)	12.863
b/Å	9.7087(8)	12.5679(7)	14.281
c/Å	17.9955(15)	12.6914(7)	18.956
α/°	84.863(7)	74.535(5)	76.07
β/°	89.138(7)	62.048(6)	83.14
γ/°	79.810(7)	65.220(6)	82.37
Volume/$Å^3$	1556.1(2)	1582.25(19)	3335.9
Z	1	2	2
$\rho_{calc}g/cm^3$	1.627	1.598	1.504
μ/mm^{-1}	5.153	2.776	4.120
F(000)	776.0	778.0	1528.0
Crystal size/mm^3	0.52 × 0.24 × 0.04	0.116 × 0.063 × 0.039	0.1988 × 0.0519 × 0.0309
Radiation	CuKα (λ = 1.54184)	CuKα (λ = 1.54184)	CuKα (λ = 1.54184)
2Θ range for data collection/°	9.292 to 130.986	7.778 to 130.99	6.414 to 147.964
Index ranges	$-8 \le h \le 10$, $-11 \le k \le 11$, $-21 \le l \le 21$	$-14 \le h \le 14$, $-14 \le k \le 11$, $-14 \le l \le 14$	$-12 \le h \le 15$, $-16 \le k \le 17$, $-23 \le l \le 23$
Reflections collected	13937	11925	33745
Independent reflections	5238 [R_{int} = 0.0428, R_{sigma} = 0.0435]	5439 [Rint = 0.0319, Rsigma = 0.0398]	13091 [R_{int} = 0.0418, R_{sigma} = 0.0504]
Data/restraints/parameters	5238/2/402	5439/0/452	13091/2/943
Goodness-of-fit on F^2	1.034	1.053	1.038
Final R indexes [I>=2σ (I)]	R_1 = 0.0379, wR_2 = 0.0939	R1 = 0.0380, wR2 = 0.0979	R_1 = 0.0536, wR_2 = 0.1410
Final R indexes [all data]	R_1 = 0.0477, wR_2 = 0.0999	R1 = 0.0438, wR2 = 0.1020	R_1 = 0.0788, wR_2 = 0.1609
Largest diff. peak/hole / e $Å^{-3}$	0.87/-0.47	0.65/-0.47	0.75/-0.57

Table – A9 Crystal data and X-ray experimental data for compounds 4.4, 4.5 and 4.6

Compound	6.2	6.3	6.4
Identification code	GKA21	GKA116a	GKA61
Empirical formula	$C_{60}H_{55}F_{17}N_{12}O_2P_3Zn_2$	$C_{122}H_{99}F_{30}Fe_2N_{22}O_7P_5Zn_2$	$C_{122}H_{101}Cl_2F_{36}N_{23}Ni_2O_2P_6Zn_2$
Formula weight	1522.81	2952.52	3110.13
Temperature/K	120.01(10)	173.35(10)	290.82(10)
Crystal system	monoclinic	monoclinic	triclinic
Space group	C2/c	$P2_1/n$	P-1
a/Å	35.189(2)	20.9518(10)	13.0486(8)
b/Å	14.8680(6)	19.8601(6)	14.6255(7)
c/Å	26.4641(16)	36.0894(12)	19.1917(9)
α/°	90	90	74.338(4)
β/°	109.638(7)	101.626(4)	82.180(5)
γ/°	90	90	82.769(4)
Volume/Å^3	13040.6(14)	14708.9(10)	3478.5(3)
Z	8	4	1
ρ_{calc}g/cm^3	1.551	1.333	1.485
μ/mm^{-1}	2.503	3.260	2.628
F(000)	6184.0	5992.0	1574.0
Crystal size/mm^3	0.05 × 0.03 × 0.01	0.1981 × 0.1494 × 0.0135	0.18 × 0.08 × 0.04
Radiation	CuKα (λ = 1.54184)	CuKα (λ = 1.54184)	CuKα (λ = 1.54184)
2Θ range for data collection/°	5.332 to 130.992	5.398 to 148.856	6.304 to 130.992
Index ranges	$-41 \le h \le 31$, $-9 \le k \le 17$, $-29 \le l \le 31$	$-26 \le h \le 25$, $-24 \le k \le 22$, $-29 \le l \le 44$	$-15 \le h \le 15$, $-12 \le k \le 17$, $-17 \le l \le 22$
Reflections collected	23225	62630	26099
Independent reflections	11241 [R_{int} = 0.0862, R_{sigma} = 0.1318]	28900 [R_{int} = 0.0582, R_{sigma} = 0.0798]	11992 [R_{int} = 0.0527, R_{sigma} = 0.0604]
Data/restraints/parameters	11241/0/867	28900/4/1712	11992/0/896
Goodness-of-fit on F^2	1.029	0.993	1.087
Final R indexes [I>=2σ (I)]	R_1 = 0.0707, wR_2 = 0.1838	R_1 = 0.0707, wR_2 = 0.1861	R_1 = 0.0798, wR_2 = 0.2178
Final R indexes [all data]	R_1 = 0.1341, wR_2 = 0.2412	R_1 = 0.1124, wR_2 = 0.2075	R_1 = 0.0936, wR_2 = 0.2363
Largest diff. peak/hole / e Å^{-3}	0.84/-0.86	0.80/-0.99	1.68/-0.79

Table – A10 Crystal data and X-ray experimental data for compounds 4.4, 4.5 and 4.6

Compound	6.5	6.6	6.8
Identification code	GKA119	GKA31	GKA39a
Empirical formula	$C_{122.08}H_{105.69}Cl_2Cu_2F_{36}Fe_2N_{23}OP_6$	$C_{63}H_{59}BrF_{18}N_{12}O_{0.5}P_3Zn_2$	$C_{280}H_{245.8}Br_{20}N_{50}Ni_{10}O_{53.9}$
Formula weight	3090.39	1637.78	7358.75
Temperature/K	120.01(10)	278.17(10)	286.13(10)
Crystal system	triclinic	triclinic	triclinic
Space group	P-1	P-1	P-1
a/Å	13.4651(4)	13.0995(3)	16.9013(4)
b/Å	14.2236(5)	14.6987(4)	25.0753(7)
c/Å	19.0141(7)	19.3570(4)	26.0861(7)
α/°	74.174(3)	75.148(2)	65.062(3)
β/°	82.329(3)	82.7551(19)	85.547(2)
γ/°	81.481(3)	83.518(2)	82.033(2)
Volume/Å^3	3448.3(2)	3561.19(16)	9925.6(5)
Z	1	2	1
ρ_{calc}g/cm^3	1.488	1.527	1.231
μ/mm^{-1}	3.943	2.972	3.365
F(000)	1565.0	1654.0	3687.0
Crystal size/mm^3	? × ? × ?	0.41 × 0.36 × 0.22	0.3128 × 0.1667 × 0.0883
Radiation	CuKα (λ = 1.54184)	CuKα (λ = 1.54184)	CuKα (λ = 1.54184)
2Θ range for data collection/°	6.504 to 148.912	6.242 to 130.996	5.28 to 147
Index ranges	$-12 \le h \le 16$, $-17 \le k \le 17$, $-23 \le l \le 23$	$-15 \le h \le 15$, $-16 \le k \le 17$, $-22 \le l \le 17$	$-15 \le h \le 20$, $-31 \le k \le 29$, $-32 \le l \le 30$
Reflections collected	33790	30732	89188
Independent reflections	13749 [R_{int} = 0.0283, R_{sigma} = 0.0335]	12263 [R_{int} = 0.0212, R_{sigma} = 0.0245]	38714 [R_{int} = 0.0378, R_{sigma} = 0.0396]
Data/restraints/parameters	13749/0/931	12263/0/998	38714/0/1828
Goodness-of-fit on F^2	1.024	1.056	1.366
Final R indexes [I>=2σ (I)]	R_1 = 0.0636, wR_2 = 0.1843	R_1 = 0.0580, wR_2 = 0.1755	R_1 = 0.1000, wR_2 = 0.3087
Final R indexes [all data]	R_1 = 0.0737, wR_2 = 0.1941	R_1 = 0.0638, wR_2 = 0.1811	R_1 = 0.1149, wR_2 = 0.3323
Largest diff. peak/hole / e Å^{-3}	1.01/-0.93	1.18/-1.96	5.59/-2.16

Table – A11 Crystal data and X-ray experimental data for compounds 4.4, 4.5 and 4.6

Compound	6.9	6.10
Identification code	GKA57a	GKA36a
Empirical formula	$C_{280}H_{244.8}Cl_{20}N_{50}Ni_{10}O_{51.4}$	$C_{280}H_{245}BrCl_{19}N_{50}Ni_{10}O_{37.5}$
Formula weight	6428.54	6250.81
Temperature/K	120.02(10)	120.00(10)
Crystal system	triclinic	triclinic
Space group	P-1	P-1
a/Å	16.7862(2)	16.7973(4)
b/Å	24.9108(4)	24.9735(6)
c/Å	26.1281(5)	25.9840(6)
α/°	64.9465(18)	64.918(2)
β/°	85.1949(14)	84.7335(19)
γ/°	81.8728(13)	81.464(2)
Volume/Å^3	9794.8(3)	9757.7(4)
Z	1	1
ρ_{calc}g/cm^3	1.090	1.064
μ/mm^{-1}	2.267	2.289
F(000)	3306.0	3213.0
Crystal size/mm^3	0.3677 × 0.211 × 0.1418	0.2477 × 0.2167 × 0.1058
Radiation	CuKα (λ = 1.54184)	CuKα (λ = 1.54184)
2Θ range for data collection/°	6.24 to 147.732	5.322 to 147.974
Index ranges	$-20 \leq h \leq 19$, $-31 \leq k \leq 31$, $-32 \leq l \leq 32$	$-19 \leq h \leq 20$, $-26 \leq k \leq 30$, $-30 \leq l \leq 32$
Reflections collected	111735	69359
Independent reflections	38593 [R_{int} = 0.0367, R_{sigma} = 0.0401]	38286 [R_{int} = 0.0343, R_{sigma} = 0.0531]
Data/restraints/parameters	38593/0/1800	38286/5/1757
Goodness-of-fit on F^2	1.092	1.072
Final R indexes [I>=2σ (I)]	R_1 = 0.0801, wR_2 = 0.2399	R_1 = 0.0781, wR_2 = 0.2390
Final R indexes [all data]	R_1 = 0.0928, wR_2 = 0.2548	R_1 = 0.0948, wR_2 = 0.2569
Largest diff. peak/hole / e Å^{-3}	3.48/-0.79	1.74/-1.03

APPENDIX III

Table – A12 Bond Lengths (Å) & Angles (°) for Compound 3.1

	Bond Lengths (Å)		
Ni1─N2[1]	2.0007(15)	Ni1─N3	2.1112(16)
Ni1─N2	2.0007(15)	Ni1─N1[1]	2.1142(16)
Ni1─N3[1]	2.1112(16)	Ni1─N1	2.1142(16)
	Bond Angles (°)		
N2[1]─Ni1─N2	179.79(9)	N2─Ni1─N1	77.82(6)
N2[1]─Ni1─N3[1]	77.88(6)	N3─Ni1─N3[1]	94.92(8)
N2[1]─Ni1─N3	101.97(6)	N3─Ni1─N1[1]	90.27(6)
N2─Ni1─N3[1]	101.97(6)	N3[1]─Ni1─N1[1]	155.71(6)
N2─Ni1─N3	77.88(6)	N3─Ni1─N1	155.71(6)
N2[1]─Ni1─N1[1]	77.82(6)	N3[1]─Ni1─N1	90.27(6)
N2[1]─Ni1─N1	102.32(6)	N1[1]─Ni1─N1	94.69(8)
N2─Ni1─N1[1]	102.32(6)		

Table – A13 Bond Lengths (Å) & Angles (°) for Compound 3.2

	Bond Lengths (Å)		
Ni1─Cl1	2.4570(8)	Ni1─N1	2.067(2)
Ni1─Cl2[1]	2.3428(8)	Ni1─N2	1.976(3)
Ni1─Cl2	2.5720(8)	Ni1─N3	2.071(2)
	Bond Angles (°)		
Cl1─Ni1─Cl2	173.52(3)	N2─Ni1─Cl2[1]	173.53(7)
Cl2[1]─Ni1─Cl1	98.75(3)	N2─Ni1─Cl2	85.85(7)
Cl2[1]─Ni1─Cl2	87.68(3)	N2─Ni1─N1	79.40(10)
N1─Ni1─Cl1	87.98(7)	N2─Ni1─N3	79.34(10)
N1─Ni1─Cl2[1]	100.64(7)	N3─Ni1─Cl1	89.67(7)
N1─Ni1─Cl2	90.12(7)	N3─Ni1─Cl2[1]	100.65(7)
N1─Ni1─N3	158.69(10)	N3─Ni1─Cl2	89.86(7)
N2─Ni1─Cl1	87.72(7)		

Table – A14 Bond Lengths (Å) & Angles (°) for Compound 3.3

	Bond Lengths (Å)		
Ni1─O1	2.0707(19)	Ni1─N3	2.114(2)
Ni1─O2	2.0569(17)	Ni1─N2	1.9876(18)
Ni1─O3	2.1143(18)	Ni1─N1	2.102(2)
	Bond Angles (°)		
O1─Ni1─O3	176.67(8)	N2─Ni1─O1	90.43(8)
O1─Ni1─N3	87.75(8)	N2─Ni1─O2	175.20(8)
O1─Ni1─N1	92.06(8)	N2─Ni1─O3	92.90(8)
O2─Ni1─O1	89.34(8)	N2─Ni1─N3	78.48(8)
O2─Ni1─O3	87.32(8)	N2─Ni1─N1	78.88(8)
O2─Ni1─N3	106.30(8)	N1─Ni1─O3	88.38(8)
O2─Ni1─N1	96.34(8)	N1─Ni1─N3	157.36(7)
O3─Ni1─N3	93.11(8)		

Table – A15 Bond Lengths (Å) & Angles (°) for Compound 3.4

Bond Lengths (Å)			
Ni1─N1	2.117(3)	Ni1─N4	1.998(2)
Ni1─N2	2.118(3)	Ni1─N5	2.109(3)
Ni1─N3	2.120(3)	Ni1─N6	1.999(2)
Bond Angles (°)			
N1─Ni1─N2	86.91(10)	N5─Ni1─N1	98.15(10)
N1─Ni1─N3	155.71(10)	N5─Ni1─N2	156.00(10)
N2─Ni1─N3	97.75(10)	N5─Ni1─N3	87.27(10)
N4─Ni1─N1	77.93(10)	N6─Ni1─N1	101.34(10)
N4─Ni1─N2	101.64(10)	N6─Ni1─N2	78.16(10)
N4─Ni1─N3	77.79(10)	N6─Ni1─N3	102.95(10)
N4─Ni1─N5	102.36(10)	N6─Ni1─N5	77.83(10)
N4─Ni1─N6	179.26(11)		

Table – A16 Bond Lengths (Å) & Angles (°) for Compound 3.5

Bond Lengths (Å)			
Cu1─N2	1.937(4)	S1─O3	1.472(4)
Cu1─N1	2.029(4)	S1─O5	1.461(4)
Cu1─O1	2.201(4)	S1─O2	1.501(4)
Cu1─O2	1.936(3)	S1─O4	1.471(4)
Cu1─N3	2.037(4)		
Bond Angles (°)			
N2─Cu1─N1	79.87(16)	O2─Cu1─N3	98.19(16)
N2─Cu1─O1	103.30(15)	N3─Cu1─O1	90.22(15)
N2─Cu1─N3	80.20(17)	O3─S1─O2	108.9(2)
N1─Cu1─O1	97.55(15)	O5─S1─O3	110.3(2)
N1─Cu1─N3	159.79(17)	O5─S1─O2	109.4(2)
O2─Cu1─N2	151.83(17)	O5─S1─O4	112.1(2)
O2─Cu1─N1	97.80(16)	O4─S1─O3	109.8(2)
O2─Cu1─O1	104.83(14)	O4─S1─O2	106.2(2)

Table – A17 Bond Lengths (Å) & Angles (°) for Compound 3.6

Bond Lengths (Å)			
Cu2─Cl5	2.2533(9)	Cu3─N6	2.024(3)
Cu2─Cl4	2.5194(10)	Cu3─N4	2.026(3)
Cu2─N1	2.032(3)	Cu3─N5	1.946(3)
Cu2─N3	2.041(3)	Cu1─Cl1	2.2286(10)
Cu2─N2	1.937(3)	Cu1─Cl2	2.2064(12)
Cu3─Cl5	2.6949(10)	Cu1─Cl3	2.2702(11)
Cu3─Cl6	2.2282(9)	Cu1─Cl4	2.3012(10)
Bond Angles (°)			
Cl5─Cu2─Cl4	97.34(3)	Cl6─Cu3─Cl5	94.29(3)
N1─Cu2─Cl5	97.80(8)	N6─Cu3─Cl5	90.43(9)
N1─Cu2─Cl4	95.97(9)	N6─Cu3─Cl6	99.53(9)
N1─Cu2─N3	158.62(12)	N6─Cu3─N4	159.31(12)
N3─Cu2─Cl5	98.92(9)	N4─Cu3─Cl5	96.92(9)
N3─Cu2─Cl4	94.99(9)	N4─Cu3─Cl6	99.17(9)
N2─Cu2─Cl5	158.43(10)	N5─Cu3─Cl5	98.81(9)
N2─Cu2─Cl4	104.22(9)	N5─Cu3─Cl6	166.88(9)

Continued....

N2─Cu2─N1	79.68(12)	N5─Cu3─N6	79.87(12)
N2─Cu2─N3	79.87(12)	N5─Cu3─N4	79.91(12)

Table – A18 Bond Lengths (Å) & Angles (°) for Compound 3.7

	Bond Lengths (Å)		
Cu1─N2	1.944(5)	Cu1─N3	2.034(6)
Cu1─O3	1.979(5)	Cu1─N1	2.031(6)
Cu1─O1	2.390(6)	Cu1─O2	2.417(6)
	Bond Angles (°)		
N2─Cu1─O3	179.2(2)	O3─Cu1─O2	81.6(2)
N2─Cu1─O1	98.9(2)	O1─Cu1─O2	163.27(18)
N2─Cu1─N3	79.8(2)	N3─Cu1─O1	86.3(2)
N2─Cu1─N1	79.9(2)	N3─Cu1─O2	94.6(2)
N2─Cu1─O2	97.7(2)	N1─Cu1─O1	96.1(2)
O3─Cu1─O1	81.8(2)	N1─Cu1─N3	159.7(2)
O3─Cu1─N3	100.4(2)	N1─Cu1─O2	88.8(2)
O3─Cu1─N1	99.9(2)		

Table – A19 Bond Lengths (Å) & Angles (°) for Compound 3.9

	Bond Lengths (Å)		
Cu1─O2	1.9146(16)	Cu1─N2	1.9393(18)
Cu1─N3	2.0366(19)	Cu1─O1	2.2183(17)
Cu1─N1	2.0374(19)		
	Bond Angles (°)		
O2─Cu1─N3	101.01(7)	N3─Cu1─O1	93.89(7)
O2─Cu1─N1	98.23(8)	N1─Cu1─O1	95.11(7)
O2─Cu1─N2	170.89(7)	N2─Cu1─N3	79.41(7)
O2─Cu1─O1	97.05(7)	N2─Cu1─N1	79.77(8)
N3─Cu1─N1	157.55(8)	N2─Cu1─O1	91.99(7)

Table – A20 Bond Lengths (Å) & Angles (°) for Compound 3.10

	Bond Lengths (Å)		
Zn1─O1	1.9628(13)	Zn1─N3	2.1776(16)
Zn1─N2	2.0750(15)	Zn1─N1	2.1862(17)
Zn1─O2	1.9665(14)		
	Bond Angles (°)		
O1─Zn1─N2	137.50(6)	N2─Zn1─N1	75.01(6)
O1─Zn1─O2	97.47(6)	O2─Zn1─N2	125.02(6)
O1─Zn1─N3	98.61(6)	O2─Zn1─N3	98.60(6)
O1─Zn1─N1	100.32(6)	O2─Zn1─N1	101.08(6)
N2─Zn1─N3	75.76(6)	N3─Zn1─N1	150.54(6)

Table – A21 Bond Lengths (Å) & Angles (°) for Compound 3.11

	Bond Lengths (Å)		
Zn1─Cl1	2.2672(10)	Zn1─N1	2.194(3)
Zn1─Cl1^{1}	2.2672(10)	Zn1─N2	2.119(4)
Zn1─N1^{1}	2.194(3)		
	Bond Angles (°)		
Cl1^{1}─Zn1─Cl1	112.14(6)	N1^{1}─Zn1─N1	148.09(16)
N1─Zn1─Cl1^{1}	100.04(8)	N2─Zn1─Cl1	123.93(3)
N1^{1}─Zn1─Cl1	100.04(8)	N2─Zn1─Cl1^{1}	123.93(3)
N1^{1}─Zn1─Cl1^{1}	97.62(8)	N2─Zn1─N1^{1}	74.05(8)
N1─Zn1─Cl1	97.62(8)	N2─Zn1─N1	74.05(8)

Table – A22 Bond Lengths (Å) & Angles (°) for Compound 3.13

	Bond Lengths (Å)		
Ag1─N6	2.555(5)	Ag1─Ag2^{1}	2.9955(7)
Ag1─N1	2.229(6)	Ag1─Ag2	3.1481(7)
Ag1─N5	2.245(6)		
	Bond Angles (°)		
N6─Ag1─Ag2^{1}	134.18(13)	N5─Ag1─N6	69.8(2)
N6─Ag1─Ag2	51.80(13)	N5─Ag1─Ag2^{1}	96.04(15)
N1─Ag1─N6	105.49(19)	N5─Ag1─Ag2	78.13(15)
N1─Ag1─N5	172.39(19)	Ag2^{1}─Ag1─Ag2	169.80(2)
N1─Ag1─Ag2^{1}	82.98(15)	Ag2─N6─Ag1	76.19(13)
N1─Ag1─Ag2	103.90(15)		

Table – A23 Bond Lengths (Å) & Angles (°) for Compound 4.1

	Bond Lengths (Å)		
Zn1─Cl1	2.2769(10)	Zn2─Cl4	2.2128(11)
Zn1─Cl2	2.2745(11)	Zn2─Cl3	2.2083(11)
Zn1─N3	2.182(3)	Zn2─N5	2.085(4)
Zn1─N2	2.100(3)	Zn2─N4	2.051(4)
Zn1─N1	2.191(3)		
	Bond Angles (°)		
Cl2─Zn1─Cl1	111.33(4)	N1─Zn1─Cl1	97.21(8)
N3─Zn1─Cl1	99.04(9)	N1─Zn1─Cl2	102.22(9)
N3─Zn1─Cl2	97.11(9)	Cl3─Zn2─Cl4	117.17(5)
N3─Zn1─N1	148.13(12)	N5─Zn2─Cl4	112.73(9)
N2─Zn1─Cl1	133.60(9)	N5─Zn2─Cl3	116.18(10)
N2─Zn1─Cl2	115.06(9)	N4─Zn2─Cl4	114.68(10)
N2─Zn1─N3	74.49(12)	N4─Zn2─Cl3	108.77(10)
N2─Zn1─N1	74.42(12)	N4─Zn2─N5	82.27(14)

Table – A24 Bond Lengths (Å) & Angles (°) for Compound 4.2

	Bond Lengths (Å)		
Zn1─Cl1	2.2484(7)	Zn2─Cl4	2.2814(7)
Zn1─Cl2	2.2385(7)	Zn2─Cl3	2.2634(7)
Zn1─N2	2.0946(19)	Zn2─N6	2.160(2)
Zn1─N1	2.230(2)	Zn2─N4	2.173(2)
Zn1─N3	2.200(2)	Zn2─N5	2.204(2)
	Bond Angles (°)		
Cl2─Zn1─Cl1	116.06(3)	Cl3─Zn2─Cl4	117.52(3)
N2─Zn1─Cl1	112.59(6)	N6─Zn2─Cl4	95.14(6)
N2─Zn1─Cl2	131.28(6)	N6─Zn2─Cl3	97.42(6)
N2─Zn1─N1	74.28(7)	N6─Zn2─N4	151.84(8)
N2─Zn1─N3	74.91(8)	N6─Zn2─N5	76.27(7)
N1─Zn1─Cl1	100.30(6)	N4─Zn2─Cl4	98.29(6)
N1─Zn1─Cl2	99.05(6)	N4─Zn2─Cl3	98.12(6)
N3─Zn1─Cl1	95.96(6)	N4─Zn2─N5	75.72(8)
N3─Zn1─Cl2	97.41(6)	N5─Zn2─Cl4	112.84(6)
N3─Zn1─N1	148.79(8)	N5─Zn2─Cl3	129.62(6)

Table – A25 Bond Lengths (Å) & Angles (°) for Compound 4.3

	Bond Lengths (Å)		
Cu1─N1	2.030(2)	Cu2─O5	1.953(2)
Cu1─O1	2.1570(19)	Cu2─O7	1.939(2)
Cu1─N2	1.945(2)	Cu2─O9	2.258(2)
Cu1─O3	1.9155(19)	Cu2─N5	2.009(2)
Cu1─N3	2.039(2)	Cu2─N4	2.042(2)
	Bond Angles (°)		
N1─Cu1─N3	156.32(9)	O5─Cu2─N5	89.94(10)
N2─Cu1─N1	79.60(9)	O5─Cu2─N4	169.11(9)
N2─Cu1─O1	104.26(8)	O7─Cu2─O5	90.25(10)
N2─Cu1─N3	79.04(10)	O7─Cu2─O9	92.27(8)
O3─Cu1─N1	99.79(9)	O7─Cu2─N5	168.20(9)
O3─Cu1─O1	91.19(8)	O7─Cu2─N4	96.56(9)
O3─Cu1─N2	164.44(9)	N5─Cu2─O9	99.37(9)
O3─Cu1─N3	98.04(10)	N5─Cu2─N4	81.66(9)
N3─Cu1─O1	94.98(8)	N4─Cu2─O9	89.69(9)
O5─Cu2─O9	98.55(9)		

Table –A26 Bond Lengths (Å) & Angles (°) for Compound 4.4

	Bond Lengths (Å)		
Cu1─Cl1	2.2217(8)	Cu2─Cl4^{1}	2.8807(8)
Cu1─Cl2	2.5455(9)	Cu2─Cl3	2.2796(8)
Cu1─N2	1.957(2)	Cu2─O1	2.596(2)
Cu1─N1	2.039(2)	Cu2─N4	2.054(2)
Cu1─N3	2.047(3)	Cu2─N5	2.018(3)
Cu2─Cl4	2.2637(8)	Cl4─Cu2^{1}	2.8807(8)
	Bond Angles (°)		
Cl1─Cu1─Cl2	105.55(3)	Cl3─Cu2─Cl4^{1}	92.92(3)
N2─Cu1─Cl1	166.06(7)	Cl3─Cu2─O1	91.51(6)
N2─Cu1─Cl2	88.39(7)	O1─Cu2─Cl4^{1}	170.97(6)

Continued...

N2─Cu1─N1	79.31(9)	N4─Cu2─Cl4	89.43(7)
N2─Cu1─N3	79.51(9)	N4─Cu2─Cl4[1]	80.99(6)
N1─Cu1─Cl1	99.38(7)	N4─Cu2─Cl3	173.50(7)
N1─Cu1─Cl2	92.52(7)	N4─Cu2─O1	94.22(8)
N1─Cu1─N3	156.97(10)	N5─Cu2─Cl4[1]	93.27(7)
N3─Cu1─Cl1	98.98(7)	N5─Cu2─Cl4	168.14(7)
N3─Cu1─Cl2	95.83(7)	N5─Cu2─Cl3	96.09(7)
Cl4─Cu2─Cl4[1]	93.58(3)	N5─Cu2─O1	78.44(9)
Cl4─Cu2─Cl3	93.22(3)	N5─Cu2─N4	82.09(9)
Cl4─Cu2─O1	94.02(6)	Cu2─Cl4─Cu2[1]	86.42(3)

Table – A27 Bond Lengths (Å) & Angles (°) for Compound 4.5

	Bond Lengths (Å)		
Cl2─Cu1	2.2740(5)	Cu1─N2	1.9646(15)
Cl1─Cu1	2.3918(5)	Cu1─N1	2.0250(16)
Cl4─Cu2	2.2672(5)	Cu2─Cl3[1]	2.6979(5)
Cl3─Cu2	2.2894(5)	Cu2─N4	2.0113(17)
Cl3─Cu2[1]	2.6979(5)	Cu2─N5	2.0414(16)
Cu1─N3	2.0360(16)		
	Bond Angles (°)		
Cu2─Cl3─Cu2[1]	81.557(16)	Cl4─Cu2─Cl3[1]	93.359(17)
Cl2─Cu1─Cl1	108.64(2)	Cl4─Cu2─Cl3	93.778(19)
N3─Cu1─Cl2	97.32(5)	Cl3─Cu2─Cl3[1]	98.442(16)
N3─Cu1─Cl1	95.43(5)	N4─Cu2─Cl4	96.81(5)
N2─Cu1─Cl2	133.40(5)	N4─Cu2─Cl3	162.53(5)
N2─Cu1─Cl1	117.96(5)	N4─Cu2─Cl3[1]	94.78(5)
N2─Cu1─N3	79.05(6)	N4─Cu2─N5	80.82(7)
N2─Cu1─N1	79.03(6)	N5─Cu2─Cl4	177.57(5)
N1─Cu1─Cl2	95.63(5)	N5─Cu2─Cl3[1]	87.39(5)
N1─Cu1─Cl1	97.30(5)	N5─Cu2─Cl3	88.40(5)
N1─Cu1─N3	157.89(6)		

Table – A28 Bond Lengths (Å) & Angles (°) for Compound 4.6

	Bond Lengths (Å)		
Cu2─Cl4	2.7037(12)	Cu3─Cl4	2.3194(11)
Cu2─Cl3	2.2356(12)	Cu3─N8	1.951(4)
Cu2─N5	2.049(3)	Cu3─N9	2.025(4)
Cu2─N6	1.995(4)	Cu3─N7	2.013(4)
Cu2─N4	1.996(4)	Cu4─Cl6	2.2377(14)
Cu1─Cl1	2.2240(15)	Cu4─N12	1.992(4)
Cu1─N2	1.937(4)	Cu4─N10	1.979(5)
Cu1─N1	2.044(4)	Cu4─N11	2.069(4)
Cu1─N3	2.042(4)	Cu4─Cl7	2.793(5)
Cu1─Cl2	2.5803(19)	Cu4─O1	2.404(13)
Cu3─Cl5	2.3888(12)		
	Bond Angles (°)		
Cl3─Cu2─Cl4	99.70(4)	N8─Cu3─N9	79.55(14)
N5─Cu2─Cl4	92.11(10)	N8─Cu3─N7	79.17(14)
N5─Cu2─Cl3	168.15(11)	N9─Cu3─Cl5	96.96(11)

Continued....

N6─Cu2─Cl4	92.39(11)	N9─Cu3─Cl4	95.92(11)
N6─Cu2─Cl3	98.82(12)	N7─Cu3─Cl5	97.04(11)
N6─Cu2─N5	81.57(15)	N7─Cu3─Cl4	97.72(11)
N6─Cu2─N4	162.19(16)	N7─Cu3─N9	158.04(15)
N4─Cu2─Cl4	93.36(11)	Cl6─Cu4─Cl7	96.47(14)
N4─Cu2─Cl3	96.80(12)	Cl6─Cu4─O1	103.3(3)
N4─Cu2─N5	81.39(15)	N12─Cu4─Cl6	97.22(14)
Cl1─Cu1─Cl2	108.38(7)	N12─Cu4─N11	81.47(18)
N2─Cu1─Cl1	160.42(13)	N12─Cu4─Cl7	86.96(16)
N2─Cu1─N1	79.46(16)	N12─Cu4─O1	89.1(4)
N2─Cu1─N3	79.78(16)	N10─Cu4─Cl6	97.14(13)
N2─Cu1─Cl2	91.11(12)	N10─Cu4─N12	163.44(18)
N1─Cu1─Cl1	99.08(12)	N10─Cu4─N11	83.11(18)
N1─Cu1─Cl2	97.91(14)	N10─Cu4─Cl7	99.57(17)
N3─Cu1─Cl1	98.58(13)	N10─Cu4─O1	95.6(4)
N3─Cu1─N1	158.49(17)	N11─Cu4─Cl6	171.48(13)
N3─Cu1─Cl2	88.04(12)	N11─Cu4─Cl7	91.88(19)
Cl4─Cu3─Cl5	101.65(4)	N11─Cu4─O1	85.1(3)
N8─Cu3─Cl5	115.58(11)	O1─Cu4─Cl7	7.5(4)
N8─Cu3─Cl4	142.76(11)	Cu3─Cl4─Cu2	105.71(4)

Table – A29 Bond Lengths (Å) & Angles (°) for Compound 5.1

	Bond Lengths (Å)		
Cu1─O1	2.020(2)	Cu1─O2	2.066(2)
Cu1─N2	1.931(2)	Cu1─N1	2.023(2)
Cu1─N3	2.010(2)		
	Bond Angles (°)		
O1─Cu1─O2	88.51(9)	N2─Cu1─N1	80.31(10)
O1─Cu1─N1	100.51(10)	N3─Cu1─O1	92.97(10)
N2─Cu1─O1	141.43(10)	N3─Cu1─O2	97.35(10)
N2─Cu1─N3	80.14(10)	N3─Cu1─N1	160.23(11)
N2─Cu1─O2	129.89(10)	N1─Cu1─O2	97.39(10)

Table – A30 Bond Lengths (Å) & Angles (°) for Compound 5.2

	Bond Lengths (Å)		
Cu1─Cl1	2.2303(7)	Cu1─N1	2.040(2)
Cu1─O1	2.1593(17)	Cu1─N2	1.9528(19)
Cu1─N3	2.027(2)		
	Bond Angles (°)		
O1─Cu1─Cl1	105.33(5)	N2─Cu1─N1	79.45(8)
N3─Cu1─Cl1	100.50(6)	O2─P1─O1	119.25(10)
N3─Cu1─O1	88.02(7)	O2─P1─O4	111.21(10)
N3─Cu1─N1	158.59(8)	O2─P1─O3	110.65(10)
N1─Cu1─Cl1	98.08(6)	O1─P1─O4	109.55(10)
N1─Cu1─O1	97.27(7)	O1─P1─O3	110.11(9)
N2─Cu1─Cl1	155.46(6)	O4─P1─O3	92.95(9)
N2─Cu1─O1	99.19(7)	P1─O1─Cu1	132.38(10)
N2─Cu1─N3	79.23(8)		

Table – A31 Bond Lengths (Å) & Angles (°) for Compound 6.1

	Bond Lengths (Å)		
Zn35─Cl1	2.2696(10)	Fe1─N62	1.884(3)
Zn35─N43	2.143(3)	Fe1─N2	1.980(3)
Zn35─N36	2.134(3)	Fe1─N51	1.979(3)
Zn35─N27	2.171(3)	Fe1─N68	1.977(3)
Zn35─N34	2.092(3)	Fe1─N13	1.878(3)
Fe1─N19	1.970(3)		
	Bond Angles (°)		
N43─Zn35─Cl1	122.11(9)	N62─Fe1─N19	100.42(12)
N43─Zn35─N27	96.52(12)	N62─Fe1─N2	97.69(12)
N36─Zn35─Cl1	97.30(9)	N62─Fe1─N51	81.02(12)
N36─Zn35─N43	77.48(12)	N62─Fe1─N68	81.21(13)
N36─Zn35─N27	165.99(13)	N51─Fe1─N2	89.94(12)
N27─Zn35─Cl1	96.60(9)	N68─Fe1─N2	95.25(13)
N34─Zn35─Cl1	111.84(11)	N68─Fe1─N51	162.00(12)
N34─Zn35─N43	125.98(13)	N13─Fe1─N19	81.06(12)
N34─Zn35─N36	94.04(14)	N13─Fe1─N62	178.39(12)
N34─Zn35─N27	79.14(13)	N13─Fe1─N2	80.84(12)
N19─Fe1─N2	161.87(12)	N13─Fe1─N51	99.61(12)
N19─Fe1─N51	92.12(12)	N13─Fe1─N68	98.23(13)
N19─Fe1─N68	88.28(13)		

Table – A32 Bond Lengths (Å) & Angles (°) for Compound 6.2

	Bond Lengths (Å)		
Zn2─O1	1.964(5)	Zn1─N6	2.215(7)
Zn2─N9[1]	2.227(6)	Zn1─N5	2.065(6)
Zn2─N8	2.137(7)	Zn1─N3	2.245(6)
Zn2─N10[1]	2.095(7)	Zn1─N1	2.166(6)
Zn2─N7	2.124(6)	Zn1─N4	2.191(7)
Zn1─N2	2.071(6)		
	Bond Angles (°)		
O1─Zn2─N9[1]	89.7(2)	N2─Zn1─N4	103.5(2)
O1─Zn2─N8	107.6(2)	N6─Zn1─N3	89.5(2)
O1─Zn2─N10[1]	106.1(2)	N5─Zn1─N2	169.9(2)
O1─Zn2─N7	115.9(2)	N5─Zn1─N6	75.0(2)
N8─Zn2─N9[1]	162.6(2)	N5─Zn1─N3	94.6(2)
N10[1]─Zn2─N9[1]	77.6(2)	N5─Zn1─N1	114.1(2)
N10[1]─Zn2─N8	95.0(2)	N5─Zn1─N4	76.3(2)
N10[1]─Zn2─N7	137.5(2)	N1─Zn1─N6	98.0(2)
N7─Zn2─N9[1]	95.9(2)	N1─Zn1─N3	151.4(2)
N7─Zn2─N8	78.8(2)	N1─Zn1─N4	88.0(2)
N2─Zn1─N6	105.8(2)	N4─Zn1─N6	150.6(2)
N2─Zn1─N3	75.4(2)	N4─Zn1─N3	98.9(2)
N2─Zn1─N1	76.0(2)		

Table – A33 Bond Lengths (Å) & Angles (°) for Compound 6.4

	Bond Lengths (Å)		
Zn1─Cl1	2.2621(12)	Ni1─N1	2.107(4)
Zn1─N8	2.146(4)	Ni1─N3	2.108(4)
Zn1─N9	2.189(4)	Ni1─N2	1.991(3)
Zn1─N7	2.128(4)	Ni1─N6	2.118(4)
Zn1─N10	2.079(4)	Ni1─N4	2.101(4)
Ni1─N5	1.995(3)		
	Bond Angles (°)		
N8─Zn1─Cl1	97.49(11)	N5─Ni1─N4	78.54(14)
N8─Zn1─N9	164.31(15)	N1─Ni1─N3	156.56(14)
N9─Zn1─Cl1	98.02(11)	N1─Ni1─N6	93.08(13)
N7─Zn1─Cl1	119.92(10)	N3─Ni1─N6	89.71(14)
N7─Zn1─N8	77.79(14)	N2─Ni1─N5	178.34(14)
N7─Zn1─N9	96.40(14)	N2─Ni1─N1	78.15(14)
N10─Zn1─Cl1	113.25(13)	N2─Ni1─N3	78.46(14)
N10─Zn1─N8	93.75(15)	N2─Ni1─N6	100.56(14)
N10─Zn1─N9	77.94(16)	N2─Ni1─N4	103.01(14)
N10─Zn1─N7	126.78(16)	N4─Ni1─N1	91.53(14)
N5─Ni1─N1	101.32(14)	N4─Ni1─N3	95.16(14)
N5─Ni1─N3	102.02(14)	N4─Ni1─N6	156.42(14)
N5─Ni1─N6	77.88(14)		

Table – A34 Bond Lengths (Å) & Angles (°) for Compound 6.5

	Bond Lengths (Å)		
Fe1─N2	1.882(3)	Cu1─N8	1.990(3)
Fe1─N5	1.882(3)	Cu1─N7	2.148(3)
Fe1─N3	1.979(3)	Cu1─N9A	1.974(16)
Fe1─N1	1.978(3)	Cu1─N10	2.019(15)
Fe1─N6	1.976(3)	Cu1─N10A	2.049(15)
Fe1─N4	1.974(3)	Cu1─N9	2.106(15)
Cu1─Cl1	2.3297(12)		
	Bond Angles (°)		
N2─Fe1─N3	80.94(12)	N8─Cu1─N7	79.42(12)
N2─Fe1─N1	80.81(12)	N8─Cu1─N10	170.1(4)
N2─Fe1─N6	99.16(12)	N8─Cu1─N10A	175.1(4)
N2─Fe1─N4	99.12(12)	N8─Cu1─N9	94.3(5)
N5─Fe1─N2	179.35(13)	N7─Cu1─Cl1	114.86(9)
N5─Fe1─N3	98.43(12)	N9A─Cu1─Cl1	122.1(6)
N5─Fe1─N1	99.82(12)	N9A─Cu1─N8	94.2(6)
N5─Fe1─N6	80.71(12)	N9A─Cu1─N7	123.0(6)
N5─Fe1─N4	81.01(12)	N9A─Cu1─N10A	81.2(7)
N1─Fe1─N3	161.74(12)	N10─Cu1─Cl1	95.6(4)
N6─Fe1─N3	91.29(12)	N10─Cu1─N7	98.7(5)
N6─Fe1─N1	91.00(12)	N10─Cu1─N9	79.2(7)
N4─Fe1─N3	92.29(12)	N10A─Cu1─Cl1	86.8(4)
N4─Fe1─N1	91.20(12)	N10A─Cu1─N7	104.7(5)
N4─Fe1─N6	161.70(12)	N9─Cu1─Cl1	116.4(6)
N8─Cu1─Cl1	94.05(10)	N9─Cu1─N7	128.7(6)

Table – A35 Bond Lengths (Å) & Angles (°) for Compound 6.6

	Bond Lengths (Å)		
Zn1─N5	2.075(3)	Zn1─N3	2.178(3)
Zn1─N1	2.175(3)	Zn1─N6	2.193(3)
Zn1─N4	2.162(3)	Zn1─N2	2.061(3)
	Bond Angles (°)		
N5─Zn1─N1	104.04(12)	N4─Zn1─N6	151.94(12)
N5─Zn1─N4	76.38(12)	N3─Zn1─N6	93.61(12)
N5─Zn1─N3	103.93(12)	N2─Zn1─N5	177.22(13)
N5─Zn1─N6	75.56(12)	N2─Zn1─N1	75.95(12)
N1─Zn1─N3	151.86(12)	N2─Zn1─N4	106.40(13)
N1─Zn1─N6	90.44(13)	N2─Zn1─N3	75.96(12)
N4─Zn1─N1	96.18(13)	N2─Zn1─N6	101.67(12)
N4─Zn1─N3	93.23(12)		

APPENDIX IV

^{1}H NMR of **L2.3**

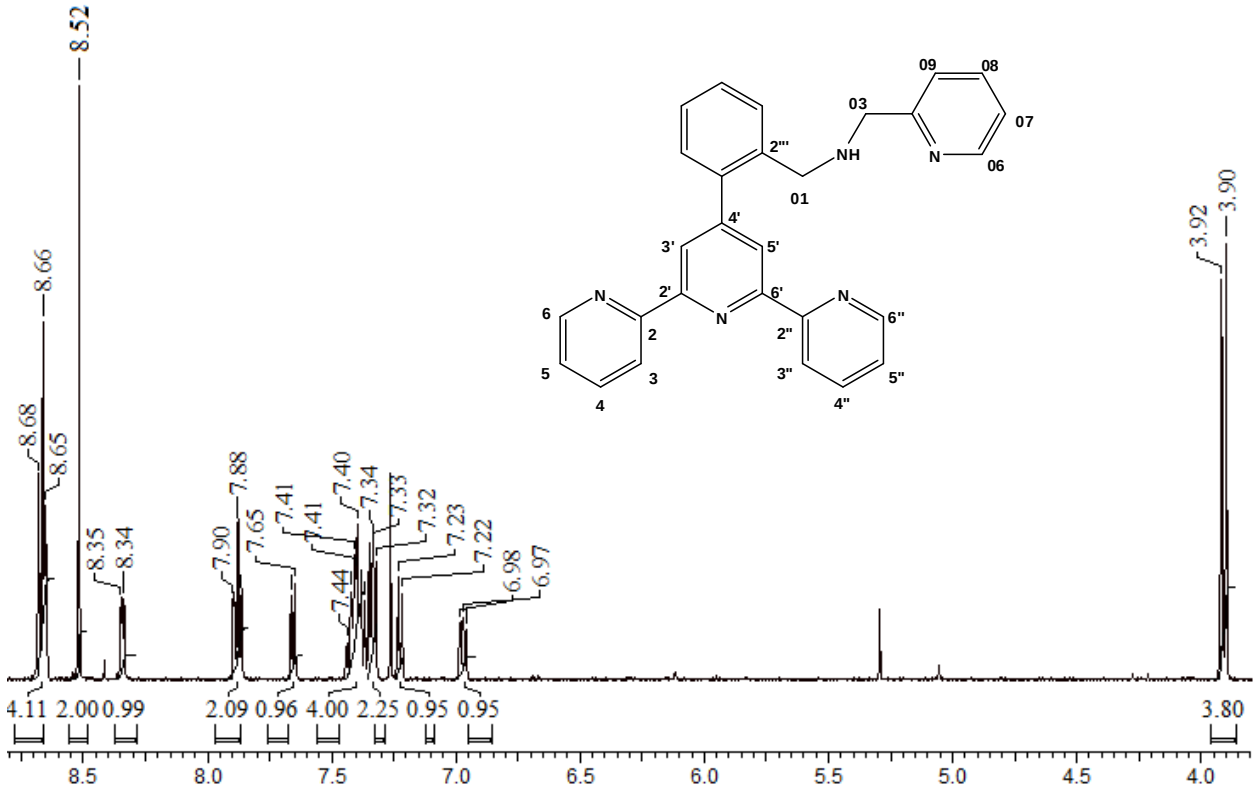

^{13}C NMR of **L2.3**

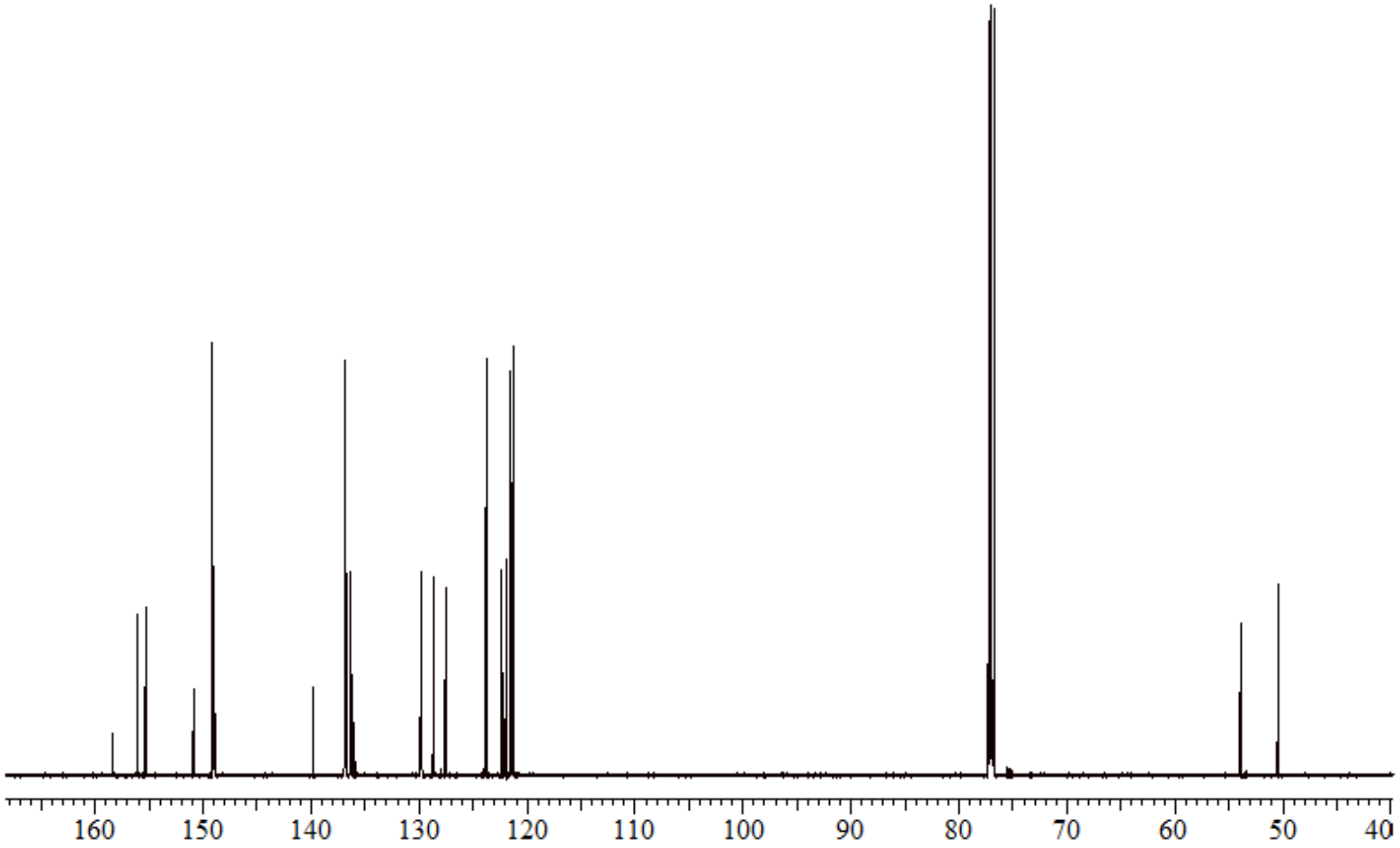

^{1}H NMR of **L2.4**

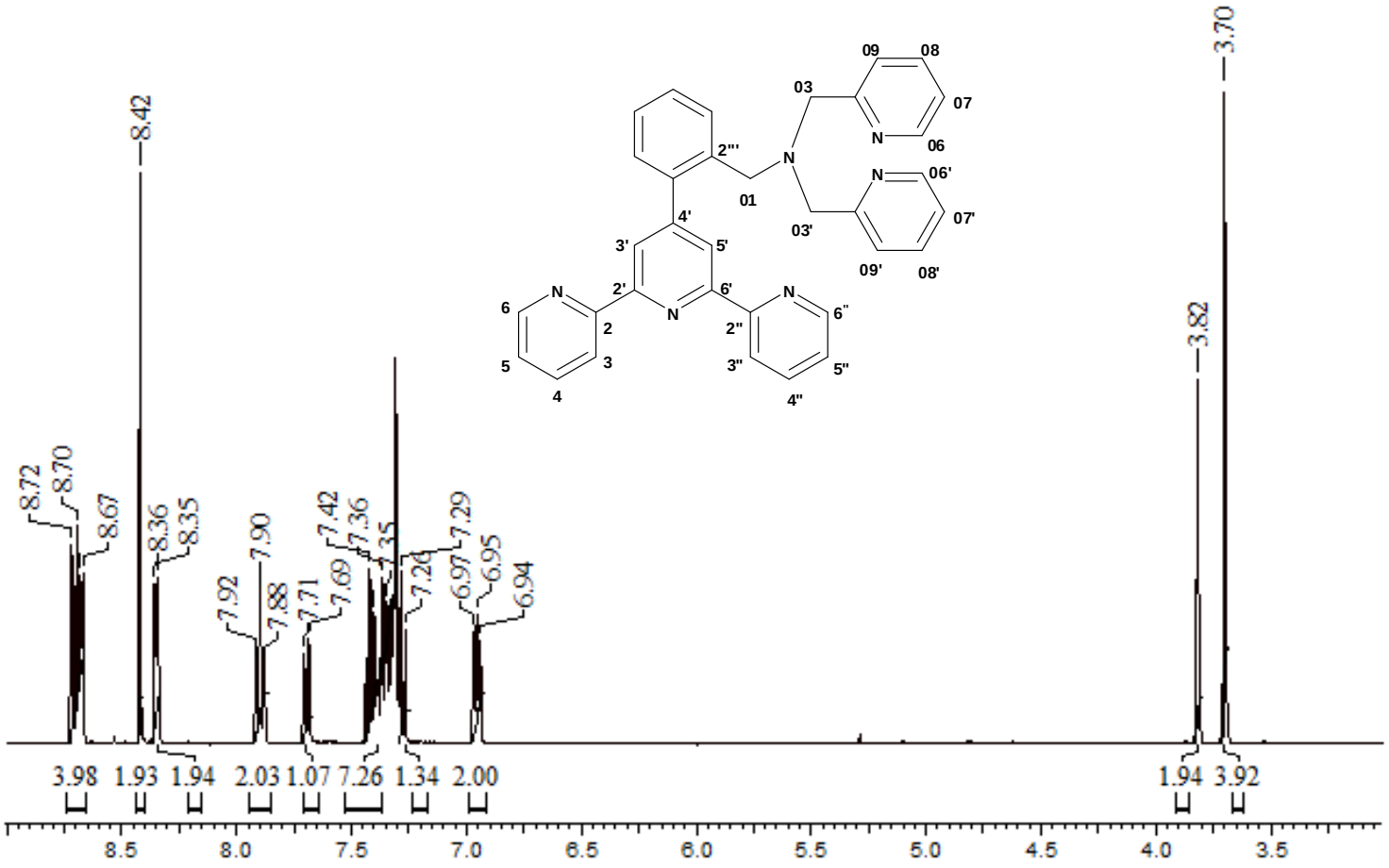
8.72
8.70
8.67
8.42
8.36
8.35
7.92
7.90
7.88
7.71
7.69
7.42
7.36
7.35
7.24
6.97
7.29
6.95
6.94
3.82
3.70
3.98
1.93
1.94
2.03
1.07
7.26
1.34
2.00
1.94
3.92
8.5
8.0
7.5
7.0
6.5
6.0
5.5
5.0
4.5
4.0
3.5

^{13}C NMR of **L2.4**

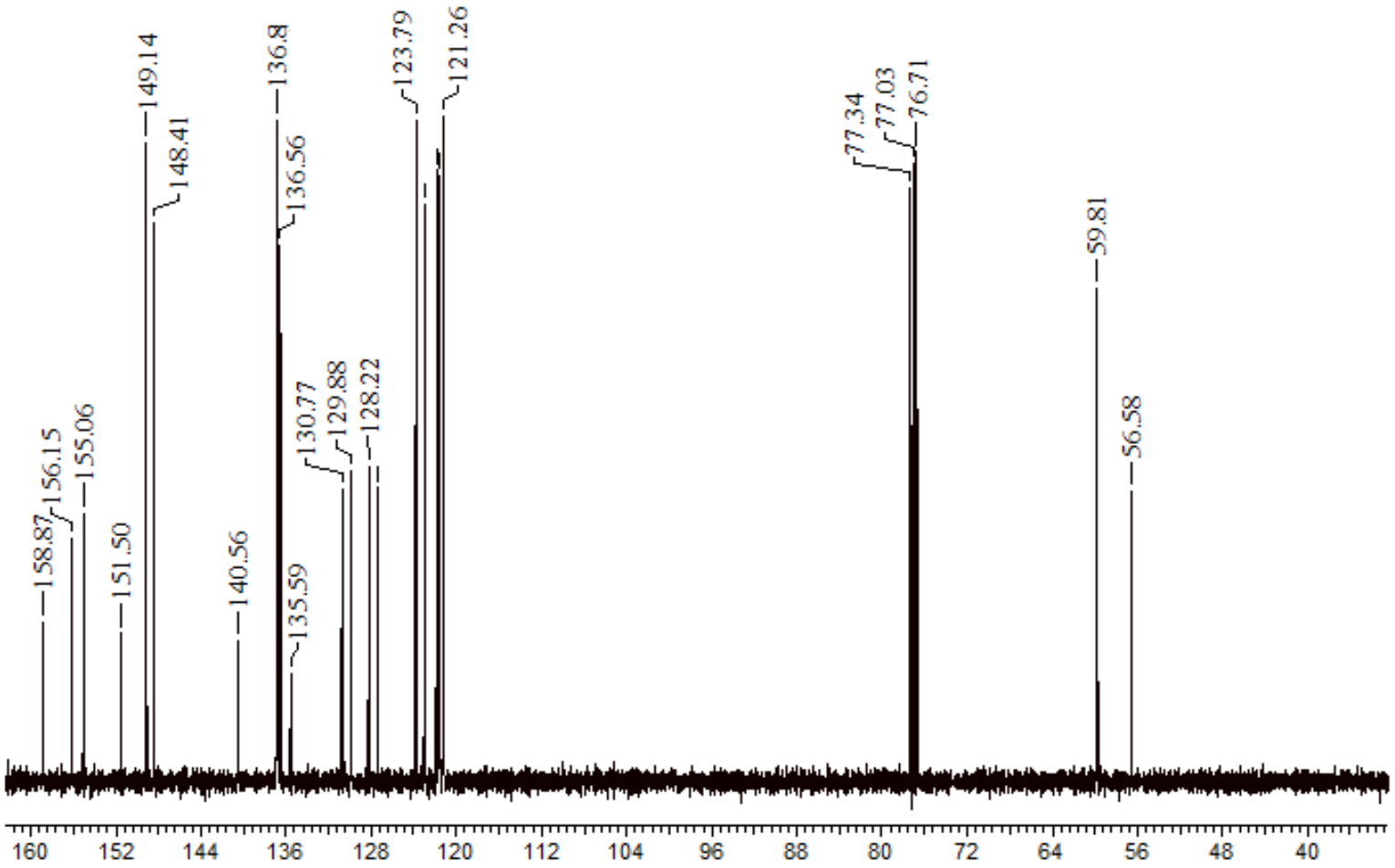

^{1}H NMR of **L2.5**

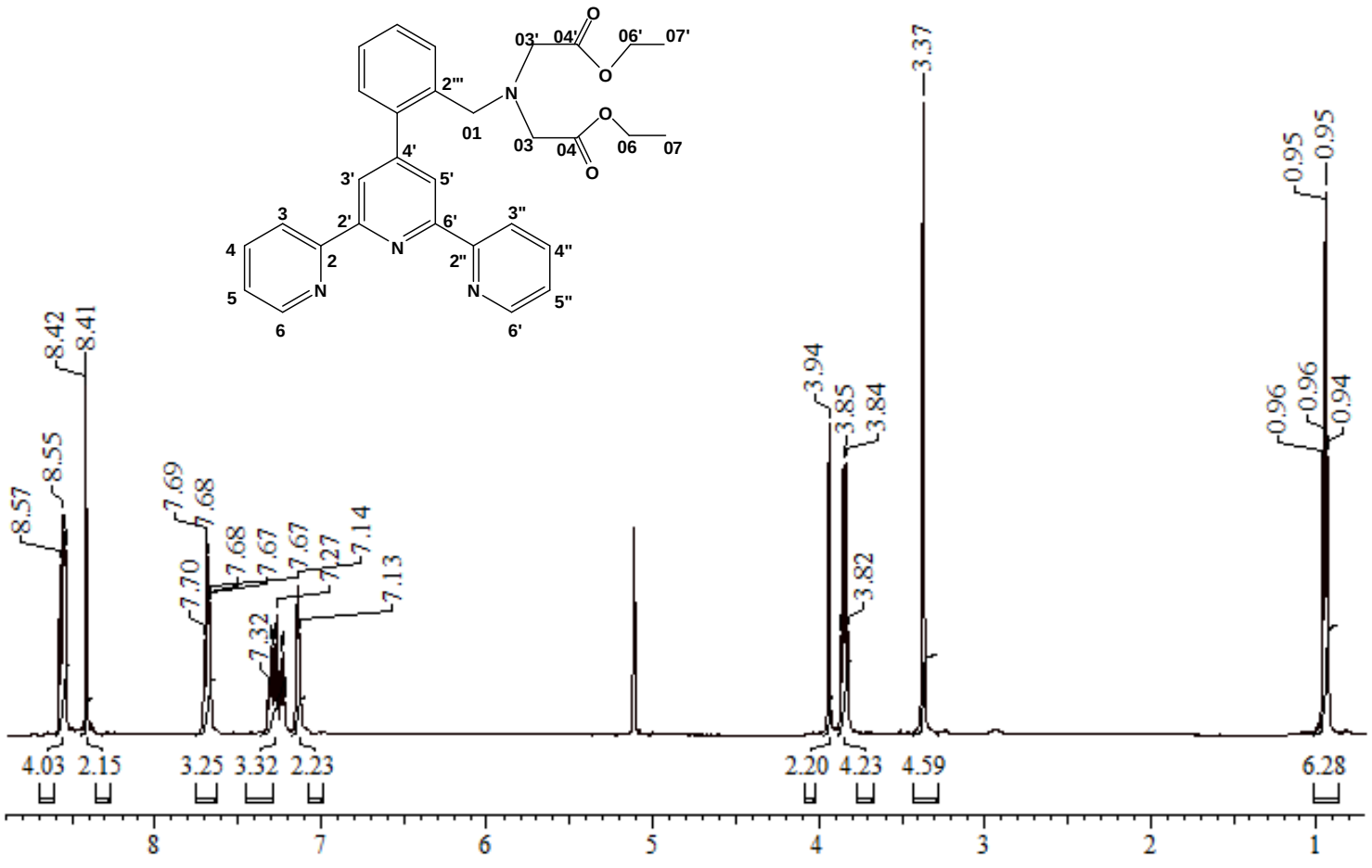
8.57
8.55
8.42
8.41
7.70
7.69
7.68
7.68
7.67
7.67
7.32
7.27
7.14
7.13
3.94
3.85
3.84
3.82
3.37
0.96
0.96
0.94
0.95
0.95
4.03
2.15
3.25
3.32
2.23
2.20
4.23
4.59
6.28
8
7
6
5
4
3
2
1

^{13}C NMR of **L2.5**

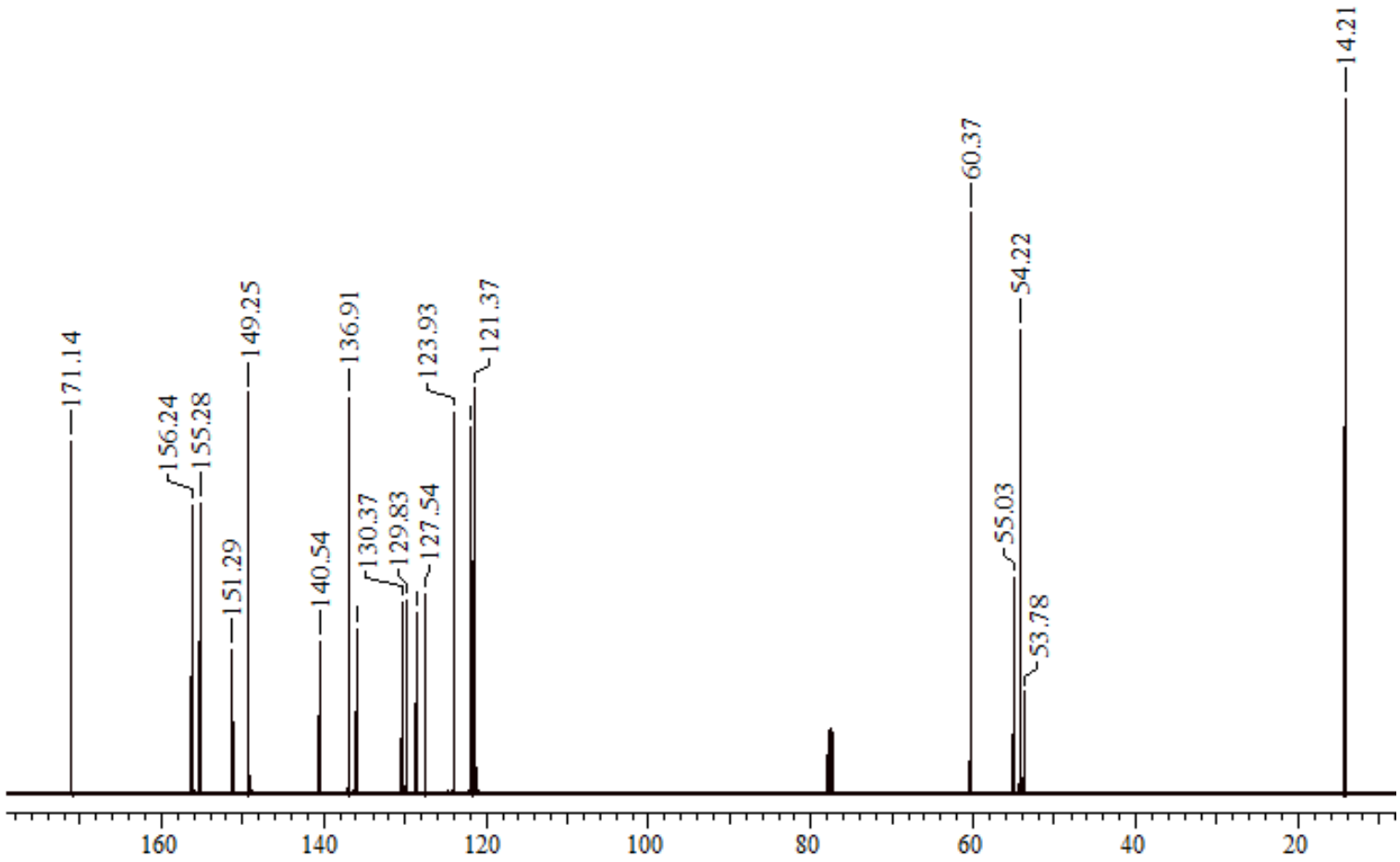

^{1}H NMR of **L2.6**

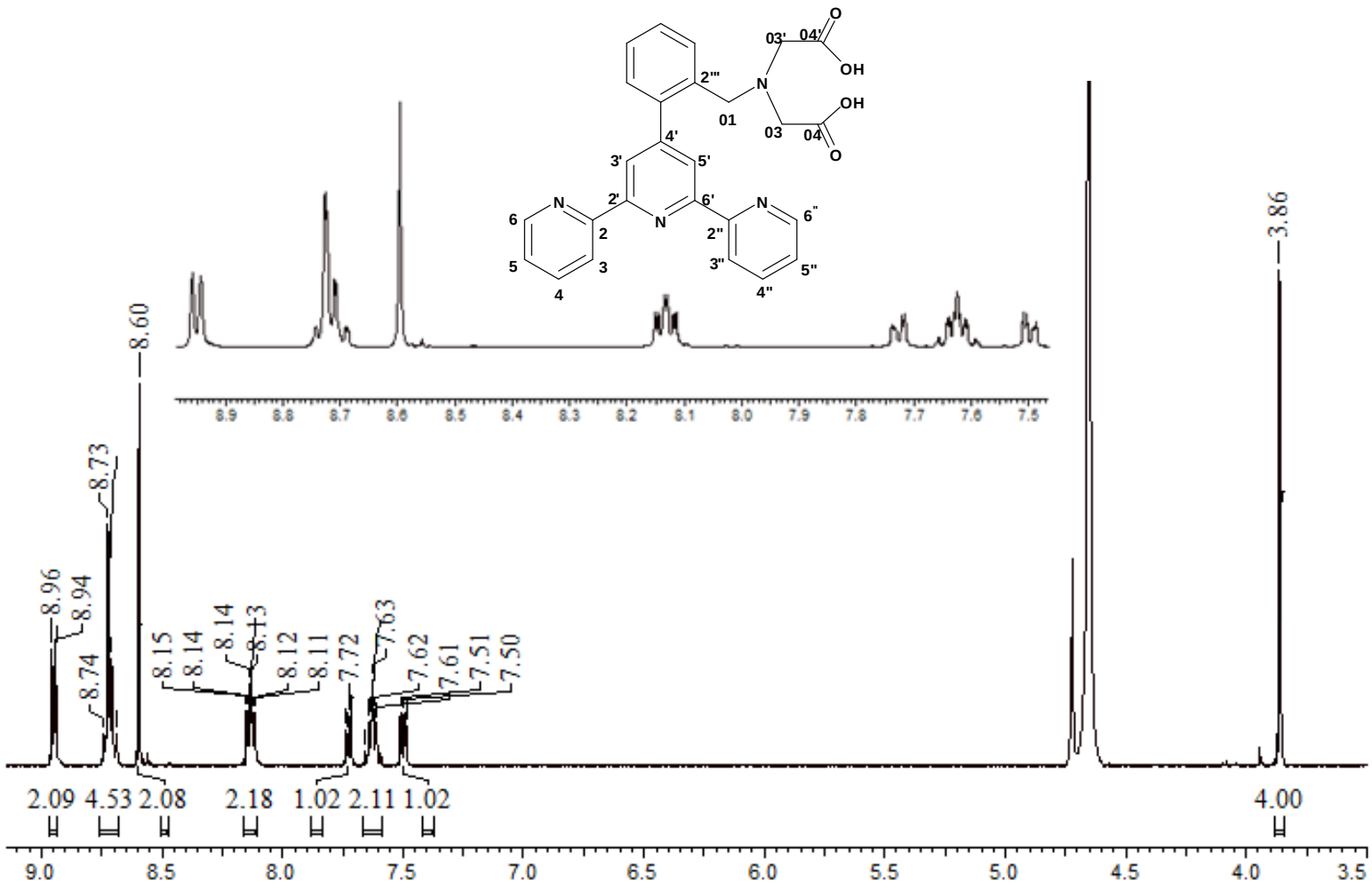
8.96
8.94
8.74
8.73
8.60
8.15
8.14
8.14
8.13
8.12
8.11
7.72
7.63
7.62
7.61
7.51
7.50
3.86
2.09
4.53
2.08
2.18
1.02
2.11
1.02
4.00
9.0
8.5
8.0
7.5
7.0
6.5
6.0
5.5
5.0
4.5
4.0
3.5

^{13}C NMR of **L2.6**

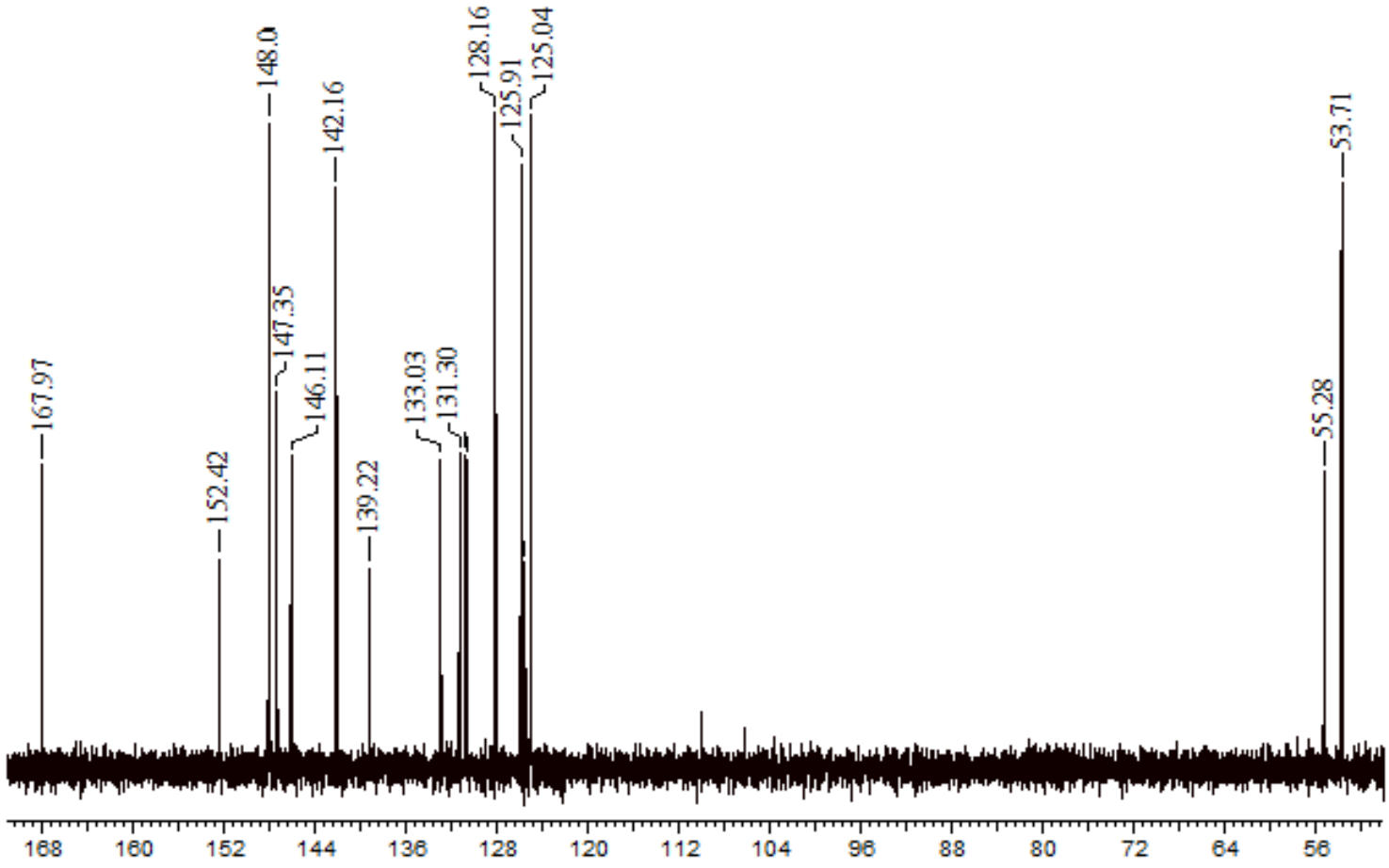

^{1}H NMR of **L2.7**

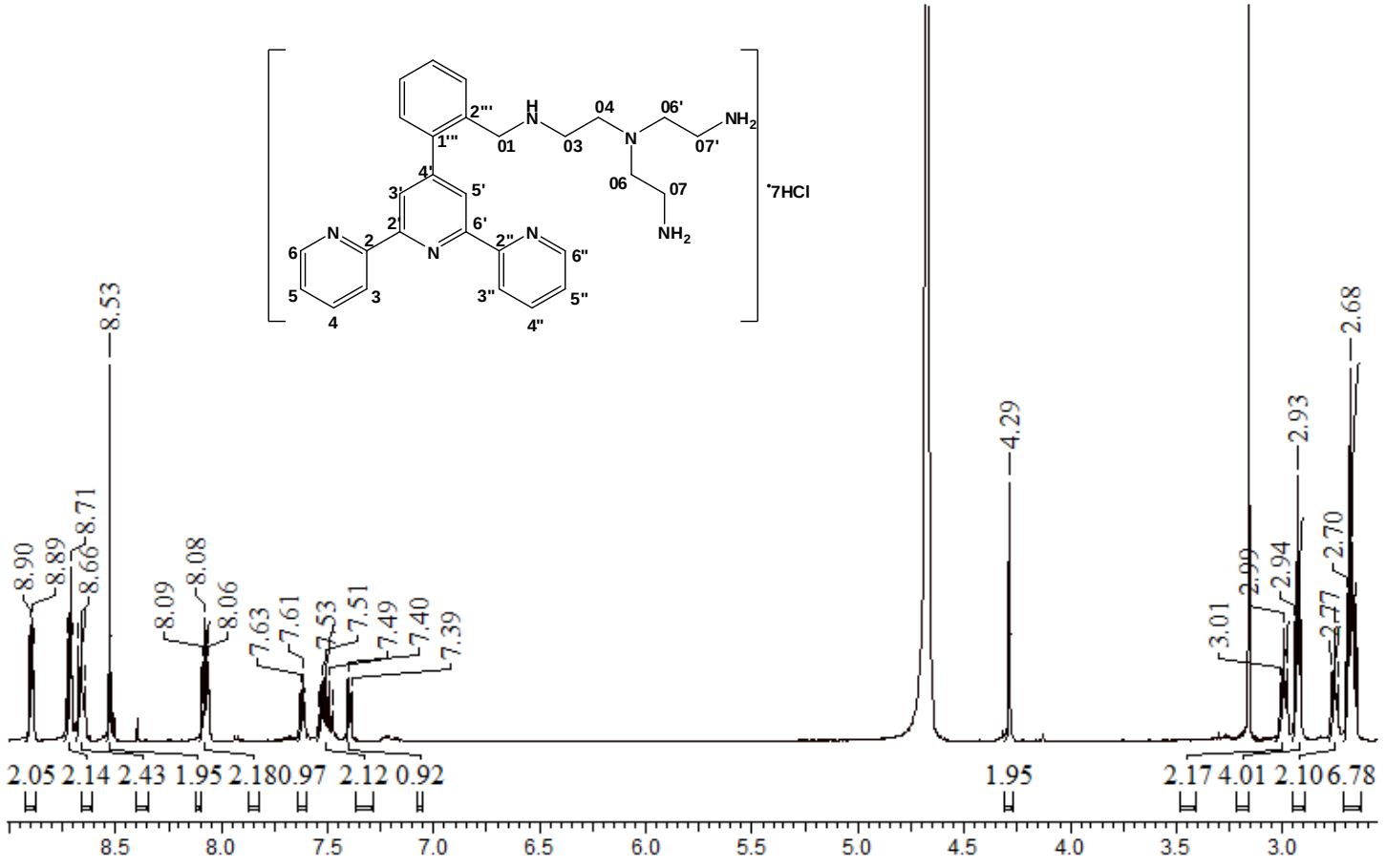
8.90
8.89
8.71
8.66
8.53
8.09
8.08
8.06
7.63
7.61
7.53
7.51
7.49
7.40
7.39
4.29
3.01
2.99
2.94
2.93
2.77
2.70
2.68
2.05 2.14 2.43 1.95 2.18 0.97 2.12 0.92
1.95
2.17 4.01 2.10 6.78
8.5 8.0 7.5 7.0 6.5 6.0 5.5 5.0 4.5 4.0 3.5 3.0
·7HCl

^{13}C NMR of **L2.7**

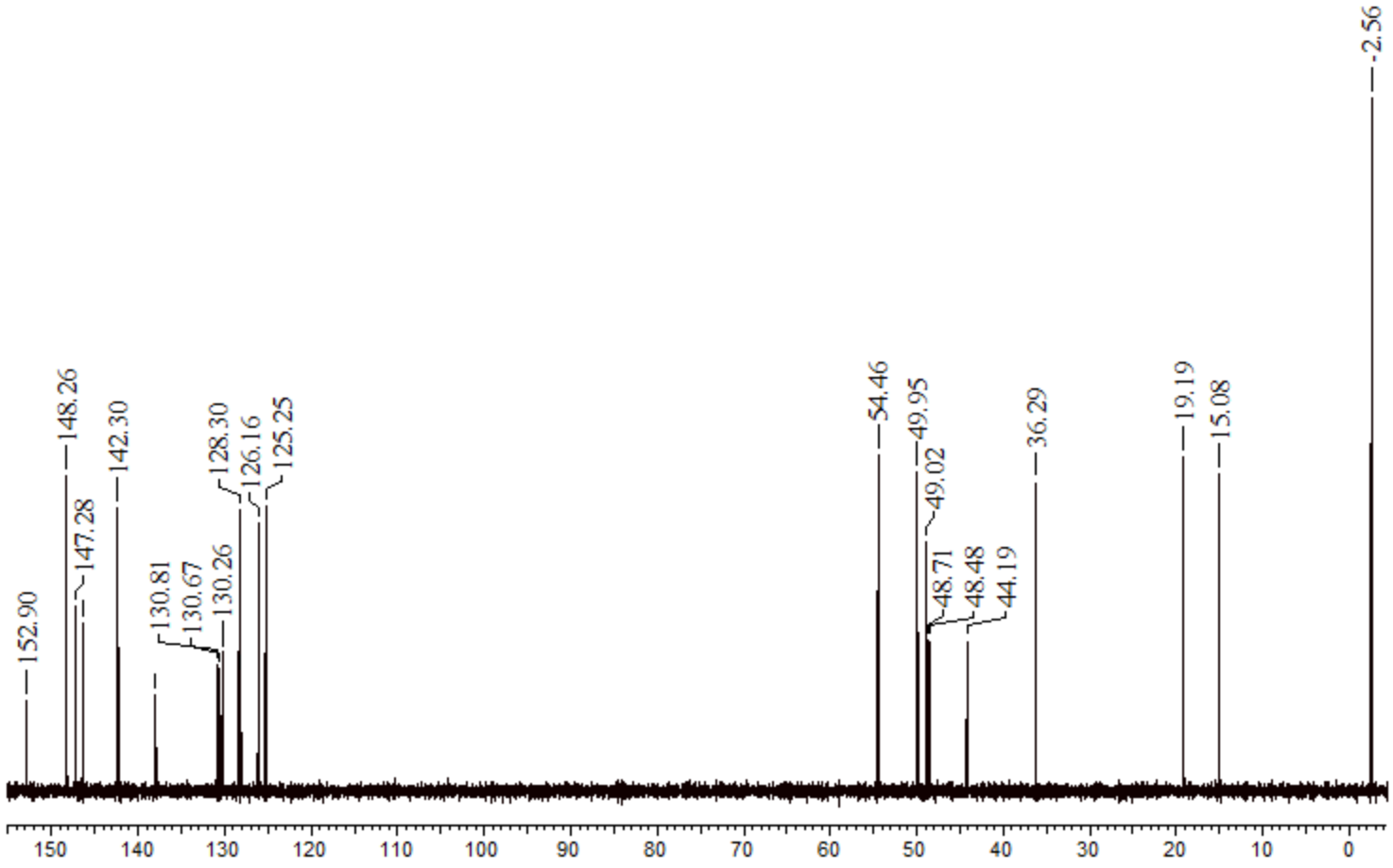

^{1}H NMR of **L2.8**

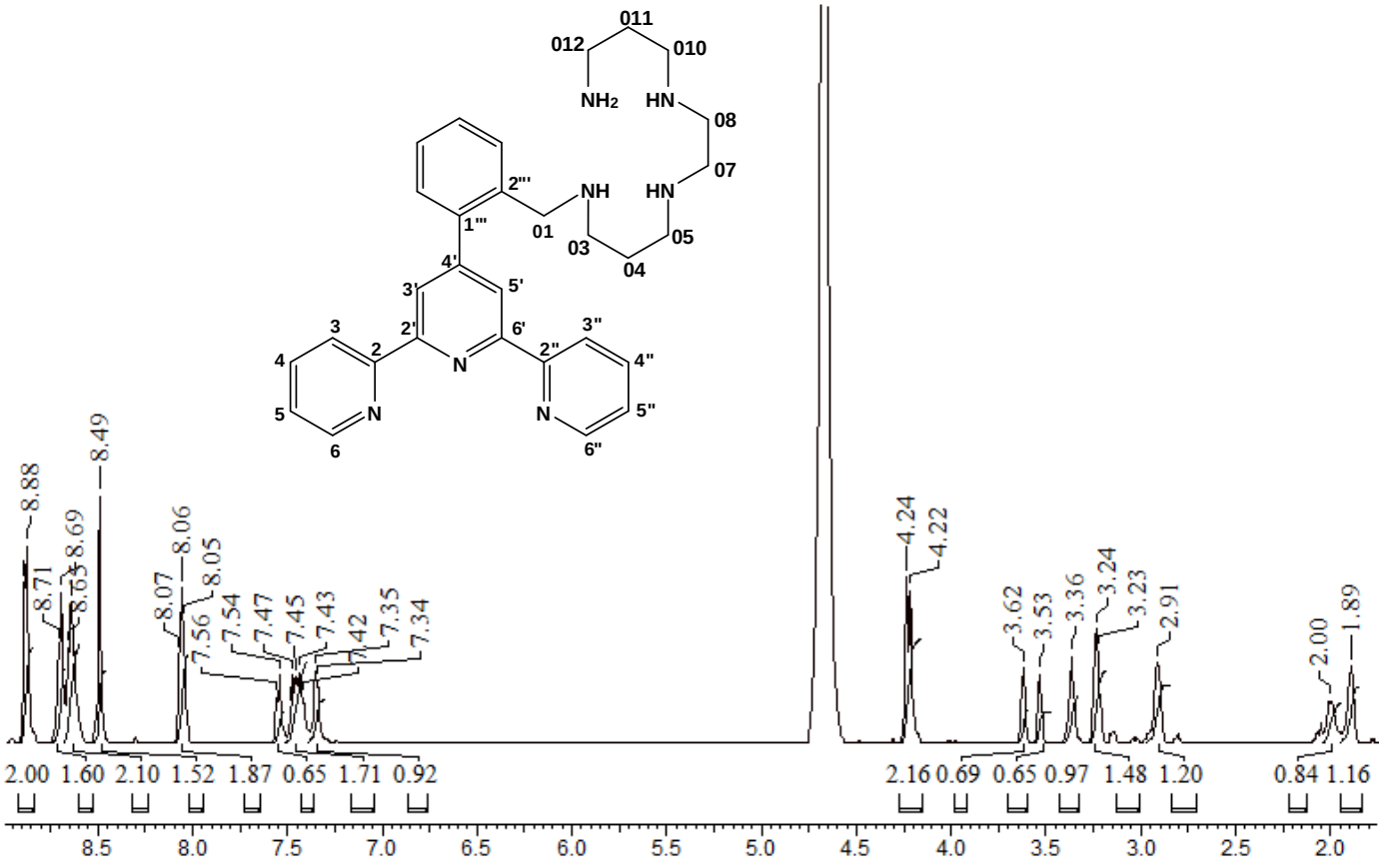
011
012
010
NH2
HN
08
07
NH
HN
2'''
1'''
01
03
05
04
4'
3'
5'
3
2'
6'
3''
2
2''
4''
4
5
N
N
5''
6
6''
8.88
8.71
8.69
8.65
8.49
8.07
8.06
8.05
7.56
7.54
7.47
7.45
7.43
7.42
7.35
7.34
4.24
4.22
3.62
3.53
3.36
3.24
3.23
2.91
2.00
1.89
2.00 1.60 2.10 1.52 1.87 0.65 1.71 0.92
2.16 0.69 0.65 0.97 1.48 1.20
0.84 1.16
8.5
8.0
7.5
7.0
6.5
6.0
5.5
5.0
4.5
4.0
3.5
3.0
2.5
2.0

^{13}C NMR of **L2.8**

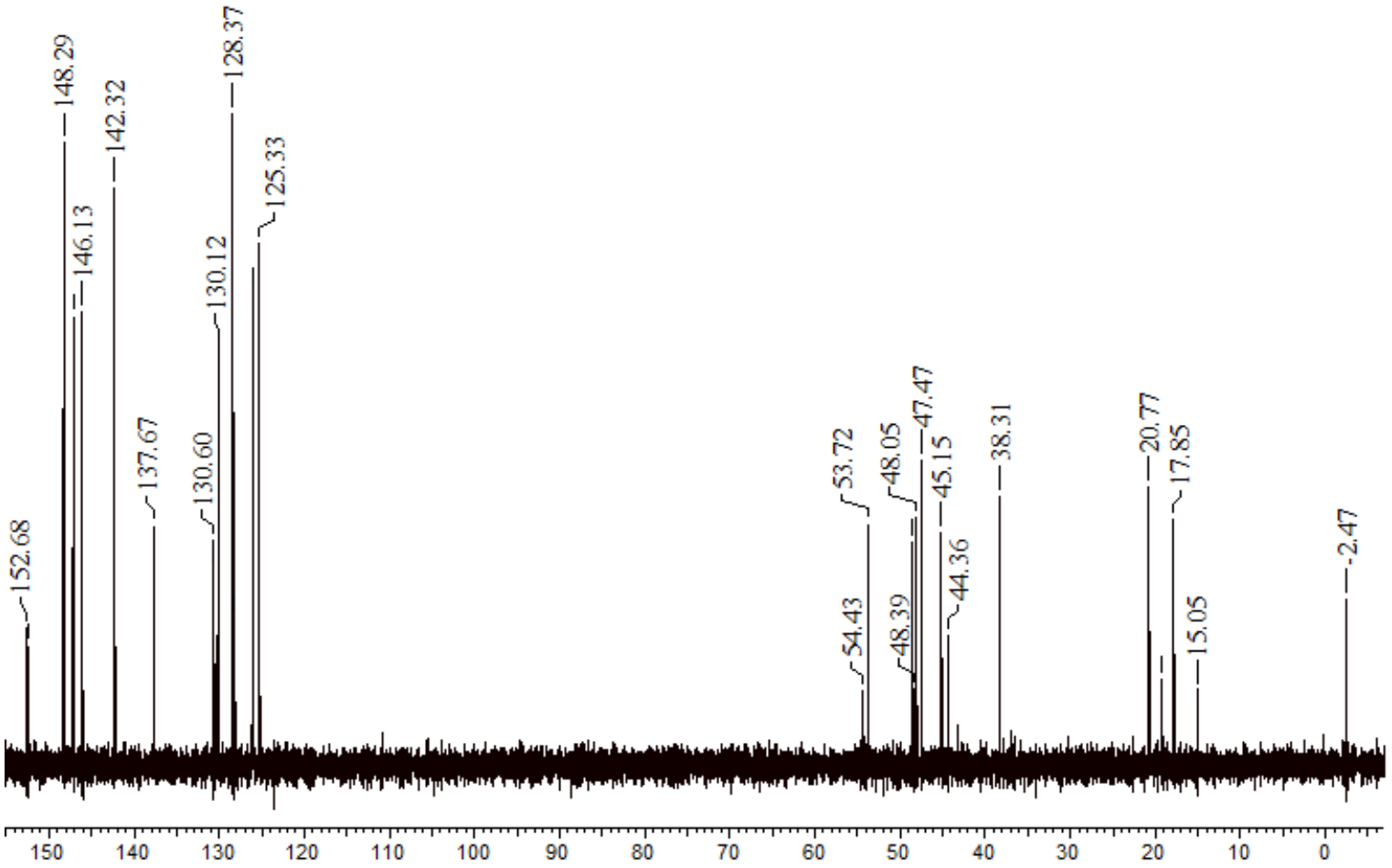

REFERENCES

1. D. Voet, C. W. Pratt and J. G. Voet, *Principles of Biochemistry*, John Wiley & Sons, Limited, 2013.
2. F. H. Westheimer, *Science*, **1987**, 235, 1173-1178.
3. H. Shim, S.-B. Hong and F. M. Raushel, *J. Biol. Chem.*, **1998**, 273, 17445-17450.
4. A. J. Pratt, *J. Cosmol.*, **2010**, 13, 3601-3605.
5. R. Kramer, *Coord. Chem. Rev.*, **1999**, 182, 243-261.
6. J. Chin, M. Banaszczyk, V. Jubian and X. Zou, *J. Am. Chem. Soc.*, **1989**, 111, 186-190.
7. R. Kramer, *Coord. Chem. Rev.*, **1999**, 182, 243-261.
8. K. S. Dickson, C. M. Burns and J. P. Richardson, *J. Biol. Chem.*, **2000**, 275, 15828-15831.
9. R. Wolfenden, *Chem. Rev. (Washington, DC, U. S.)*, **2006**, 106, 3379-3396.
10. N. Williams and J. Chin, *Chem. Commun. (Cambridge, U. K.)*, **1996**, 131-132.
11. F. Mancin, P. Scrimin and P. Tecilla, *Chem. Commun. (Cambridge, U. K.)*, **2012**, 48, 5545-5559.
12. G. K. Schroeder, C. Lad, P. Wyman, N. H. Williams and R. Wolfenden, *Proc. Natl. Acad. Sci. U. S. A.*, **2006**, 103, 4052-4055.
13. T. Lindahl and B. Nyberg, *Biochemistry*, **1972**, 11, 3610-3618.
14. C. Liu and L. Wang, *Dalton Trans.*, **2009**, 227-239.
15. M. R. Tock, E. Frary, J. R. Sayers and J. A. Grasby, *EMBO J.*, **2003**, 22, 995-1004.
16. R. A. Anderson, W. F. Bosron, F. S. Kennedy and B. L. Vallee, *Proc. Natl. Acad. Sci. U. S. A.*, **1975**, 72, 2989-2993.
17. J. W. Pyrz, J. T. Sage, P. G. Debrunner and L. Que, Jr., *J. Biol. Chem.*, **1986**, 261, 11015-11020.
18. S. C. L. Kamerlin, P. K. Sharma, R. B. Prasad and A. Warshel, *Q. Rev. Biophys.*, **2013**, 46, 1-132.
19. G. Parkin, *Chem. Rev.*, **2004**, 104, 699-767.
20. Y. Zhang, J. Y. Liang, S. Huang, H. Ke and W. N. Lipscomb, *Biochemistry*, **1993**, 32, 1844-1857.
21. J. F. Davies, II, Z. Hostomska, Z. Hostomsky, S. R. Jordan and D. A. Matthews, *Science*, **1991**, 252, 88-95.
22. G. H. Rawji, M. Yamada, N. P. Sadler and R. M. Milburn, *Inorg. Chim. Acta*, **2000**, 303, 168-174.
23. L. R. Gahan, S. J. Smith, A. Neves and G. Schenk, *Eur. J. Inorg. Chem.*, **2009**, 2745-2758.
24. N. Mitic, S. J. Smith, A. Neves, L. W. Guddat, L. R. Gahan and G. Schenk, *Chem. Rev.*, **2006**, 106, 3338-3363.
25. N. H. Williams, W. Cheung and J. Chin, *J. Am. Chem. Soc.*, **1998**, 120, 8079-8087.
26. N. H. Williams, A.-M. Lebuis and J. Chin, *J. Am. Chem. Soc.*, **1999**, 121, 3341-3348.
27. N. H. Williams, B. Takasaki, M. Wall and J. Chin, *Acc. Chem. Res.*, **1999**, 32, 485-493.
28. J. Chin, *Artificial phosphoesterase: metal activation by strain, PhD Thesis*, McGill Univ., 1993.
29. D. E. Wilcox, *Chem. Rev. (Washington, D. C.)*, **1996**, 96, 2435-2458.
30. R. J. Geue, A. M. Sargeson and R. Wijesekera, *Aust. J. Chem.*, **1993**, 46, 1021-1040.
31. L. J. Daumann, G. Schenk, D. L. Ollis and L. R. Gahan, *Dalton Trans.*, **2014**, 43, 910-928.
32. L. J. Daumann, L. Marty, G. Schenk and L. R. Gahan, *Dalton Trans.*, **2013**, 42, 9574-9584.
33. P. Comba, L. R. Gahan, V. Mereacre, G. R. Hanson, A. K. Powell, G. Schenk and M. Zajaczkowski-Fischer, *Inorg. Chem.*, **2012**, 51, 12195-12209.
34. G. Schenk, N. Mitic, L. R. Gahan, D. L. Ollis, R. P. McGeary and L. W. Guddat, *Acc. Chem. Res.*, **2012**, 45, 1593-1603.

35. L. J. Daumann, K. E. Dalle, G. Schenk, R. P. McGeary, P. V. Bernhardt, D. L. Ollis and L. R. Gahan, *Dalton Trans.*, **2012**, 41, 1695-1708.
36. R. R. Buchholz, M. E. Etienne, A. Dorgelo, R. E. Mirams, S. J. Smith, S. Y. Chow, L. R. Hanton, G. B. Jameson, G. Schenk and L. R. Gahan, *Dalton Trans.*, **2008**, 6045-6054.
37. N. Mitic, S. J. Smith, A. Neves, L. W. Guddat, L. R. Gahan and G. Schenk, *Chem. Rev. (Washington, DC, U. S.)*, **2006**, 106, 3338-3363.
38. R. L. Gustafson and A. E. Martell, *J. Am. Chem. Soc.*, **1959**, 81, 525-529.
39. B. Anderson, R. M. Milburn, J. M. Harrowfield, G. B. Robertson and A. M. Sargeson, *J. Am. Chem. Soc.*, **1977**, 99, 2652-2661.
40. H.-C. Liang, Y. Zhang and M. M. Hetu, *Inorg. Chem. Commun.*, **2007**, 10, 204-208.
41. Y. Zhang and H.-C. Liang, *Inorg. Chem. Commun.*, **2006**, 9, 460-463.
42. Y. Gultneh, A. R. Khan, D. Blaise, S. Chaudhry, B. Ahvazi, B. B. Marvey and R. J. Butcher, *J. Inorg. Biochem.*, **1999**, 75, 7-18.
43. Y. Gultneh, Allwar, B. Ahvazi, D. Blaise, R. J. Butcher, J. Jasinski and J. Jasinski, *Inorg. Chim. Acta*, **1996**, 241, 31-38.
44. C. Piovezan, L. F. Silva, F. S. Nunes and S. M. Drechsel, *Transition Met. Chem.*, **2011**, 36, 79-85.
45. E. Longhinotti, J. B. Domingos, B. Szpoganicz, A. Neves and F. Nome, *Inorg. Chim. Acta*, **2005**, 358, 2089-2092.
46. P. Hendry and A. M. Sargeson, *Prog. Inorg. Chem.*, **1990**, 38, 201-258.
47. D. R. Jones, L. F. Lindoy and A. M. Sargeson, *J. Am. Chem. Soc.*, **1984**, 106, 7807-7819.
48. J. S. Seo, R. C. Hynes, D. Williams, J. Chin and N.-D. Sung, *J. Am. Chem. Soc.*, **1998**, 120, 9943-9944.
49. J. S. Seo, N.-D. Sung, R. C. Hynes and J. Chin, *Inorg. Chem.*, **1996**, 35, 7472-7473.
50. J. S. Seo, D. Williams and J. Chin, *J. Inorg. Biochem.*, **1997**, 67, 241.
51. R. Wijesekera, P. Hendry and A. M. Sargeson, *Aust. J. Chem.*, **1992**, 45, 1189-1190.
52. P. Hendry and A. M. Sargeson, *Inorg. Chem.*, **1990**, 29, 92-97.
53. P. Hendry and A. M. Sargeson, *J. Am. Chem. Soc.*, **1989**, 111, 2521-2527.
54. J. A. Connolly, J.-H. Kim, M. Banaszczyk, M. Drouin and J. Chin, *Inorg. Chem.*, **1995**, 34, 1094-1099.
55. D. Wahnon, A.-M. Lebuis and J. Chin, *Angew. Chem., Int. Ed. Engl.*, **1995**, 34, 2412-2414.
56. N. Straeter, T. Klabunde, P. Tucker, H. Witzel and B. Krebs, *Science*, **1995**, 268, 1489-1492.
57. J. Kim and H. Lim, *Bull. Korean Chem. Soc.*, **1999**, 20, 491-493.
58. J. Chen, X. Wang, Y. Zhu, J. Lin, X. Yang, Y. Li, Y. Lu and Z. Guo, *Inorg. Chem.*, **2005**, 44, 3422-3430.
59. W. N. Lipscomb and N. Straeter, *Chem. Rev. (Washington, D. C.)*, **1996**, 96, 2375-2433.
60. N. C. Horton and J. J. Perona, *Nat. Struct. Biol.*, **2001**, 8, 290-293.
61. Y. Takagi, M. Warashina, W. J. Stec, K. Yoshinari and K. Taira, *Nucleic Acids Res.*, **2001**, 29, 1815-1834.
62. E. E. Kim and H. W. Wyckoff, *J. Mol. Biol.*, **1991**, 218, 449-464.
63. N. Straeter, W. N. Lipscomb, T. Klabunde and B. Krebs, *Angew. Chem., Int. Ed. Engl.*, **1996**, 35, 2025-2055.
64. S.-I. Kawahara and T. Uchimaru, *Eur. J. Inorg. Chem.*, **2001**, 2437-2442.
65. W. H. Chapman, Jr. and R. Breslow, *J. Am. Chem. Soc.*, **1995**, 117, 5462-5469.
66. C. Bazzicalupi, A. Bencini, A. Bianchi, V. Fusi, C. Giorgi, P. Paoletti, B. Valtancoli and D. Zanchi, *Inorg. Chem.*, **1997**, 36, 2784-2790.
67. L. Bonfa, M. Gatos, F. Mancin, P. Tecilla and U. Tonellato, *Inorg. Chem.*, **2003**, 42, 3943-3949.
68. K. Abdi, H. Hadadzadeh, M. Salimi, J. Simpson and A. D. Khalaji, *Polyhedron*, **2012**, 44, 101-112.
69. A. W. Addison, T. N. Rao, J. Reedijk, J. Van Rijn and G. C. Verschoor, *J. Chem. Soc., Dalton Trans.*, **1984**, 1349-1356.
70. M. A. Al-Anber, T. Rüffer, M. Al-Noaimi and H. Lang, *Arabian J. Chem.*, **2012**.
71. P. R. Andres, R. Lunkwitz, G. R. Pabst, K. Boehn, D. Wouters, S. Schmatloch and U. S. Schubert, *Eur. J. Org. Chem.*, **2003**, 3769-3776.

72. M. I. Arriortua, T. Rojo, J. M. Amigo, G. Germain and J. P. Declercq, *Bull. Soc. Chim. Belg.*, **1982**, 91, 337-338.
73. A. T. Baker and H. A. Goodwin, *Aust. J. Chem.*, **1985**, 38, 207-214.
74. R. Ballardini, V. Balzani, M. Clemente-Leon, A. Credi, M. T. Gandolfi, E. Ishow, J. Perkins, J. F. Stoddart, H.-R. Tseng and S. Wenger, *J. Am. Chem. Soc.*, **2002**, 124, 12786-12795.
75. S. Bianco, C. Musetti, A. P. Krapcho, M. Palumbo and C. Sissi, *Chem. Commun. (Cambridge, U. K.)*, **2013**, 49, 8057-8059.
76. M. A. Bork, H. B. Vibbert, D. J. Stewart, P. E. Fanwick and D. R. McMillin, *Inorg. Chem.*, **2013**, 52, 12553-12560.
77. F. H. Burstall, *J. Chem. Soc.*, **1938**, 1662-1672.
78. F. H. Case, *J. Org. Chem.*, **1962**, 27, 640-641.
79. G.-J. Chen, Z.-G. Wang, Y.-Y. Kou, J.-L. Tian and S.-P. Yan, *J. Inorg. Biochem.*, **2013**, 122, 49-56.
80. R. Cortés, M. I. Arriortua, T. Rojo, D. Beltrán and T. Debaerdemaeker, *Transition Met. Chem.*, **1986**, 11, 238-239.
81. C. W. Machan, M. Adelhardt, A. A. Sarjeant, C. L. Stern, J. Sutter, K. Meyer and C. A. Mirkin, *J. Am. Chem. Soc.*, **2012**, 134, 16921-16924.
82. D. Maity, S. Das, S. Mardanya and S. Baitalik, *Inorg. Chem.*, **2013**, 52, 6820-6838.
83. S. Martinez-Vargas, A. I. Martinez, J. Valdes-Martinez and D. L. Perry, *J. Mol. Struct.*, **2013**, 1033, 34-39.
84. K. Suntharalingam, A. J. P. White and R. Vilar, *Inorg. Chem.*, **2010**, 49, 8371-8380.
85. P. A. Thornley, J. C. Starkey, R. Zibaseresht, M. I. J. Polson, J. L. Wikaira and R. M. Hartshorn, *J. Coord. Chem.*, **2011**, 64, 145-158.
86. N. Tuccitto, I. Delfanti, V. Torrisi, F. Scandola, C. Chiorboli, V. Stepanenko, F. Wuerthner and A. Licciardello, *Phys. Chem. Chem. Phys.*, **2009**, 11, 4033-4038.
87. H. Z. Xie and D. Y. Wei, *Russ. J. Coord. Chem.*, **2011**, 37, 600-605.
88. S. Yuan and X. Ge, *Daxue Huaxue*, **2008**, 23, 37-42, 54.
89. M. Zaarour, A. Singh, C. Latouche, J. A. G. Williams, I. Ledoux-Rak, J. Zyss, A. Boucekkine, B. H. Le, V. Guerchais, C. Dragonetti, A. Colombo, D. Roberto and A. Valore, *Inorg. Chem.*, **2013**, 52, 7987-7994.
90. W. Zhou, X. Wang, M. Hu and Z. Guo, *J. Inorg. Biochem.*, **2013**, 121, 114-120.
91. L. A. Jenkins, J. K. Bashkin, J. D. Pennock, J. Florian and A. Warshel, *Inorg. Chem.*, **1999**, 38, 3215-3222.
92. J. K. Bashkin and L. A. Jenkins, *J. Chem. Soc., Dalton Trans.*, **1993**, 3631-3632.
93. P. E. Jurek and A. E. Martell, *Inorg. Chem.*, **1999**, 38, 6003-6007.
94. S. Liu, Z. Luo and A. D. Hamilton, *Angewandte Chemie International Edition in English*, **1997**, 36, 2678-2680.
95. L. Maanpää, V. Luzet, G. Guillaume, S. Taherpour, E. Maeki and S. Mikkola, *New J. Chem.*, **2009**, 33, 1853-1858.
96. S. Liu and A. D. Hamilton, *Tetrahedron Lett.*, **1997**, 38, 1107-1110.
97. B. N. Trawick, T. A. Osiek and J. K. Bashkin, *Bioconjugate Chem.*, **2001**, 12, 900-905.
98. A. Stachelska-Wierzchowska, Z. J. Wieczorek and J. Wierzchowski, *Nucleosides, Nucleotides Nucleic Acids*, **2012**, 31, 61-71.
99. C. Bazzicalupi, A. Bencini, A. Bianchi, A. Danesi, C. Giorgi, C. Lodeiro, F. Pina, S. Santarelli and B. Valtancoli, *Chem. Commun. (Cambridge, U. K.)*, **2005**, 2630-2632.
100. J. R. Morrow and W. C. Trogler, *Inorg. Chem.*, **1988**, 27, 3387-3394.
101. V. M. Shelton and J. R. Morrow, *Inorg. Chem.*, **1991**, 30, 4295-4299.
102. R. S. Brown, J. C. Dewan and A. Klug, *Biochemistry*, **1985**, 24, 4785-4801.
103. B. Linkletter and J. Chin, *Angew. Chem., Int. Ed. Engl.*, **1995**, 34, 472-474.
104. J. K. Bashkin, E. I. Frolova and U. Sampath, *J. Am. Chem. Soc.*, **1994**, 116, 5981-5982.
105. V. Jubian, A. Veronese, R. P. Dixon and A. D. Hamilton, *Angew. Chem., Int. Ed. Engl.*, **1995**, 34, 1237-1239.
106. S. Liu and A. D. Hamilton, *Bioorg. Med. Chem. Lett.*, **1997**, 7, 1779-1784.
107. E. C. Constable, *Adv. Inorg. Chem. Radiochem.*, **1986**, 30, 69-121.

108. E. C. Constable, B. A. Hermann, C. E. Housecroft, M. Neuburger, S. Schaffner and L. J. Scherer, *New J. Chem.*, **2005**, 29, 1475-1481.
109. J.-J. Liu, Y.-J. Lin and G.-X. Jin, *Organometallics*, **2014**, 33, 1283-1290.
110. S. Vaddypally, C. Xu, S. Zhao, Y. Fan, C. E. Schafmeister and M. J. Zdilla, *Inorg. Chem.*, **2013**, 52, 6457-6463.
111. D. J. Cardenas, J.-P. Collin, P. Gavina, J.-P. Sauvage, A. De Cian, J. Fischer, N. Armaroli, L. Flamigni, V. Vicinelli and V. Balzani, *J. Am. Chem. Soc.*, **1999**, 121, 5481-5488.
112. A. Livoreil, J.-P. Sauvage, N. Armaroli, V. Balzani, L. Flamigni and B. Ventura, *J. Am. Chem. Soc.*, **1997**, 119, 12114-12124.
113. S.-S. Zhang, S.-Z. Zhan, M. Li, R. Peng and D. Li, *Inorg. Chem.*, **2007**, 46, 4365-4367.
114. M. Beyler, V. Heitz and J.-P. Sauvage, *J. Am. Chem. Soc.*, **2010**, 132, 4409-4417.
115. G. D. Harzmann, M. Neuburger and M. Mayor, *Eur. J. Inorg. Chem.*, **2013**, 2013, 3334-3347.
116. J. D. Megiatto, D. I. Schuster, S. Abwandner, G. de Miguel and D. M. Guldi, *J. Am. Chem. Soc.*, **2010**, 132, 3847-3861.
117. J. D. Megiatto, Jr. and D. I. Schuster, *New J. Chem.*, **2010**, 34, 276-286.
118. J.-F. Ayme, J. Lux, J.-P. Sauvage and A. Sour, *Chem. - Eur. J.*, **2012**, 18, 5565-5573.
119. E. C. Constable, E. Figgemeier, I. A. Hougen, C. E. Housecroft, M. Neuburger, S. Schaffner and L. A. Whall, *Dalton Trans.*, **2005**, 1168-1175.
120. H. S. Chow, E. C. Constable, C. E. Housecroft, M. Neuburger and S. Schaffner, *Polyhedron*, **2006**, 25, 1831-1843.
121. R. Chotalia, E. C. Constable, M. Neuburger, D. R. Smith and M. Zehnder, *J. Chem. Soc., Dalton Trans.*, **1996**, 4207-4216.
122. E. C. Constable, K. Harris, C. E. Housecroft and M. Neuburger, *Dalton Trans.*, **2011**, 40, 1524-1534.
123. E. C. Constable, M. D. Ward, M. G. B. Drew and G. A. Forsyth, *Polyhedron*, **1989**, 8, 2551-2555.
124. I. Eryazici, P. Wang, C. N. Moorefield, M. Panzer, S. Durmus, C. D. Shreiner and G. R. Newkome, *Dalton Trans.*, **2007**, 626-628.
125. P. K.-K. Ho, S.-M. Peng, K.-Y. Wong and C.-M. Che, *J. Chem. Soc., Dalton Trans.*, **1996**, 1829-1834.
126. J. C. Loren, P. Gantzel, A. Linden and J. S. Siegel, *Org. Biomol. Chem.*, **2005**, 3, 3105-3116.
127. C. B. Smith, E. C. Constable, C. E. Housecroft and B. M. Kariuki, *Chem. Commun. (Cambridge, U. K.)*, **2002**, 2068-2069.
128. E. C. Constable, A. J. Edwards, P. R. Raithby and J. V. Walker, *Angew. Chem.*, **1993**, 105, 1486-1487 (See also Angew. Chem., Int. Ed. Engl., 1193, 1432(1410), 1465-1467).
129. E. C. Constable, C. E. Housecroft, J. R. Price and J. A. Zampese, *Inorg. Chem. Commun.*, **2010**, 13, 683-685.
130. S. Maji, I. López, F. Bozoglian, J. Benet-Buchholz and A. Llobet, *Inorg. Chem.*, **2013**, 52, 3591-3593.
131. G. L. Abbati, A. Cornia, A. C. Fabretti, W. Malavasi, L. Schenetti, A. Caneschi and D. Gatteschi, *Inorg. Chem.*, **1997**, 36, 6443-6446.
132. O. Waldmann, R. Koch, S. Schromm, J. Schülein, P. Müller, I. Bernt, R. W. Saalfrank, F. Hampel and E. Balthes, *Inorg. Chem.*, **2001**, 40, 2986-2995.
133. L. Cronin, *Annual Reports Section "A" (Inorganic Chemistry)*, **2003**, 99, 289-347.
134. X. Lu, X. Li, Y. Cao, A. Schultz, J.-L. Wang, C. N. Moorefield, C. Wesdemiotis, S. Z. D. Cheng and G. R. Newkome, *Angew. Chem. Int. Ed. Engl.*, **2013**, 52, 7728-7731.
135. Y. H. Kan, K. C.-H. Tso, S. L.-F. Chan, X. Guan and C.-M. Che, *New J. Chem.*, **2013**, 37, 1811-1816.
136. T. C. Stamatatos, A. G. Christou, C. M. Jones, B. J. O'Callaghan, K. A. Abboud, T. A. O'Brien and G. Christou, *J. Am. Chem. Soc.*, **2007**, 129, 9840-9841.
137. P. King, T. C. Stamatatos, K. A. Abboud and G. Christou, *Angew. Chem., Int. Ed.*, **2006**, 45, 7379-7383.
138. T. C. Stamatatos, S. Mukherjee, K. A. Abboud and G. Christou, *Chem. Commun. (Cambridge, U. K.)*, **2009**, 62-64.

139. A. J. Tasiopoulos, A. Vinslava, W. Werndorfer, K. A. Abboud and G. Christou, *Angew. Chem., Int. Ed.*, **2004**, 43, 2117-2121.
140. L. Cronin, *Annu. Rep. Prog. Chem., Sect. A: Inorg. Chem.*, **2004**, 100, 323-383.
141. Z.-G. Song, C.-H. Geng, J.-P. Ma and Y.-B. Dong, *Inorg. Chem. Commun.*, **2010**, 13, 809-813.
142. S. J. Shah, C. M. Ramsey, K. J. Heroux, A. G. DiPasquale, N. S. Dalal, A. L. Rheingold, E. del Barco and D. N. Hendrickson, *Inorg. Chem.*, **2008**, 47, 9569-9582.
143. S. J. Shah, C. M. Ramsey, K. J. Heroux, J. R. O'Brien, A. G. DiPasquale, A. L. Rheingold, E. del Barco and D. N. Hendrickson, *Inorg. Chem.*, **2008**, 47, 6245-6253.
144. J.-L. Wang, X. Li, X. Lu, I. F. Hsieh, Y. Cao, C. N. Moorefield, C. Wesdemiotis, S. Z. D. Cheng and G. R. Newkome, *J. Am. Chem. Soc.*, **2011**, 133, 11450-11453.
145. M. Schmittel and P. Mal, *Chem. Commun. (Cambridge, U. K.)*, **2008**, 960-962.
146. X.-Y. Chen, Y. Bretonniere, J. Pecaut, D. Imbert, J.-C. Buenzli and M. Mazzanti, *Inorg. Chem.*, **2007**, 46, 625-637.
147. G. J. E. Davidson and S. J. Loeb, *Dalton Trans.*, **2003**, 4319-4323.
148. Y. Bretonniere, M. Mazzanti, J. Pecaut and M. M. Olmstead, *J. Am. Chem. Soc.*, **2002**, 124, 9012-9013.
149. J.-M. Kern, L. Raehm, J.-P. Sauvage, B. Divisia-Blohorn and P.-L. Vidal, *Inorg. Chem.*, **2000**, 39, 1555-1560.
150. J. Fielden, M. Speldrich, C. Besson and P. Kogerler, *Inorg. Chem.*, **2012**, 51, 2734-2736.
151. S. G. Baca, S. Breukers, A. Ellern and P. Koegerler, *Acta Crystallogr., Sect. C: Cryst. Struct. Commun.*, **2011**, 67, m371-m374.
152. B. Hasenknopf, J.-M. Lehn, N. Boumediene, A. Dupont-Gervais, A. Van Dorsselaer, B. Kneisel and D. Fenske, *J. Am. Chem. Soc.*, **1997**, 119, 10956-10962.
153. B. Hasenknopf, J.-M. Lehn, B. O. Kneisel, G. Baum and D. Fenske, *Angew. Chem., Int. Ed. Engl.*, **1996**, 35, 1838-1840.
154. L. F. Jones, A. Batsanov, E. K. Brechin, D. Collison, M. Helliwell, T. Mallah, E. J. L. McInnes and S. Piligkos, *Angew. Chem., Int. Ed.*, **2002**, 41, 4318-4321.
155. G. L. Abbati, A. Caneschi, A. Cornia, A. C. Fabretti and D. Gatteschi, *Inorg. Chim. Acta*, **2000**, 297, 291-300.
156. S. P. Watton, P. Fuhrmann, L. E. Pence, A. Caneschi, A. Cornia, G. L. Abbati and S. J. Lippard, *Angew. Chem., Int. Ed. Engl.*, **1998**, 36, 2774-2776.
157. V. Mougel, L. Chatelain, J. Pecaut, R. Caciuffo, E. Colineau, J.-C. Griveau and M. Mazzanti, *Nat. Chem.*, **2012**, 4, 1011-1017.
158. A. Mueller, E. Krickemeyer, J. Meyer, H. Boegge, F. Peters, W. Plass, E. Diemann, S. Dillinger, F. Nonnenbruch and a. et, *Angew. Chem., Int. Ed. Engl.*, **1995**, 34, 2122-2124.
159. G. R. Newkome, T. J. Cho, C. N. Moorefield, R. Cush, P. S. Russo, L. A. Godinez, M. J. Saunders and P. Mohapatra, *Chem. - Eur. J.*, **2002**, 8, 2946-2954.
160. K. A. Deal and J. N. Burstyn, *Inorg. Chem.*, **1996**, 35, 2792-2798.
161. K. A. Deal, A. C. Hengge and J. N. Burstyn, *J. Am. Chem. Soc.*, **1996**, 118, 1713-1718.
162. L. Zhu, O. Dos Santos, C. W. Koo, M. Rybstein, L. Pape and J. W. Canary, *Inorg. Chem.*, **2003**, 42, 7912-7920.
163. L. A. Saghatforoush, L. Valencia, F. Chalabian and S. Ghammamy, *Bioinorg. Chem. Appl.*, **2011**, 803292, 803297 pp.
164. U. S. Schubert and C. Eschbaumer, *Angew. Chem., Int. Ed.*, **2002**, 41, 2892-2926.
165. G. T. Morgan and F. H. Burstall, *J. Chem. Soc.*, **1932**, 20-30.
166. C. Bazzicalupi, A. Bencini, A. Bianchi, A. Danesi, E. Faggi, C. Giorgi, S. Santarelli and B. Valtancoli, *Coord. Chem. Rev.*, **2008**, 252, 1052-1068.
167. L. Chenneberg, J. G. Ferreira and G. S. Hanan, *Acta Crystallographica Section C: Crystal Structure Communications*

2011, 67, m81-m84.
168. E. C. Constable, *Coord. Chem. Rev.*, **2008**, 252, 842-855.
169. E. C. Constable, B. Kariuki and A. Mahmood, *Polyhedron*, **2003**, 22, 687-698.
170. R.-A. Fallahpour, *Synthesis*, **2003**, 155-184.

171. J. S. Field, R. J. Haines, D. R. McMillin and G. C. Summerton, *J. Chem. Soc., Dalton Trans.*, **2002**, 1369-1376.
172. H. Hofmeier and U. S. Schubert, *Chem. Soc. Rev.*, **2004**, 33, 373-399.
173. J. Husson and M. Knorr, *Beilstein J. Org. Chem.*, **2012**, 8, 379-389, No. 341.
174. F. Kroehnke, *Synthesis*, **1976**, 1-24.
175. A. Mishra, E. Mena-Osteritz and P. Baeuerle, *Beilstein J. Org. Chem.*, **2013**, 9, 866-876, No. 100.
176. E. C. Constable, M. D. Ward and S. Corr, *Inorg. Chim. Acta*, **1988**, 141, 201-203.
177. D. L. Jameson and L. E. Guise, *Tetrahedron Lett.*, **1991**, 32, 1999-2002.
178. K. T. Potts, *Bull. Soc. Chim. Belg.*, **1990**, 99, 741-768.
179. K. Itami and J.-i. Yoshida, *Bull. Chem. Soc. Jpn.*, **2006**, 79, 811-824.
180. N. Miyaura, *Top. Curr. Chem.*, **2002**, 219, 11-59.
181. N. Miyaura and A. Suzuki, *Chem. Rev. (Washington, D. C.)*, **1995**, 95, 2457-2483.
182. E.-i. Negishi, *Bull. Chem. Soc. Jpn.*, **2007**, 80, 233-257.
183. K. Tamao and N. Miyaura, *Top. Curr. Chem.*, **2002**, 219, 1-9.
184. D. J. Bray, J. K. Clegg, K. A. Jolliffe, L. F. Lindoy and G. Wei, *J. Coord. Chem.*, **2008**, 61, 3-13.
185. M. Chisholm, C. Hadad, K. Heinze, K. Hempel, N. Singh and S. Vyas, *J. Cluster Sci.*, **2008**, 19, 209-218.
186. E. C. Constable, *Chem. Soc. Rev.*, **2007**, 36, 246-253.
187. E. C. Constable, T. Kulke, M. Neuburger and M. Zehnder, *Chem. Commun. (Cambridge, U. K.)*, **1997**, 489-490.
188. M. Heller and U. S. Schubert, *Eur. J. Org. Chem.*, **2003**, 947-961.
189. X.-H. Li, Z.-Q. Liu, F.-Y. Li, X.-F. Duan and C.-H. Huang, *Chin. J. Chem* . **2007**, 25, 186-189.
190. U. S. Schubert, C. Eschbaumer, O. Hien and P. R. Andres, *Tetrahedron Lett.*, **2001**, 42, 4705-4707.
191. A. M. W. C. Thompson, *Coord. Chem. Rev.*, **1997**, 160, 1-52.
192. R. S. Varma, G. W. Kabalka, L. T. Evans and R. M. Pagni, *Synth. Commun.*, **1985**, 15, 279-284.
193. J. Wang and G. S. Hanan, *Synlett*, **2005**, 1251-1254.
194. G. W. Cave, C. L. Raston and J. L. Scott, *Chem Commun (Cambridge United Kingdom)*, **2001**, 2159-2169.
195. G. W. V. Cave and C. L. Raston, *Chem. Commun. (Cambridge, U. K.)*, **2000**, 2199-2200.
196. G. W. V. Cave, C. L. Raston and J. L. Scott, *Chem. Commun. (Cambridge, U. K.)*, **2001**, 2159-2169.
197. S. Etienne and M. Beley, *Inorg. Chem. Commun.*, **2006**, 9, 68-71.
198. J. Husson, E. Migianu, M. Beley and G. Kirsch, *Synthesis*, **2004**, 267-270.
199. B. C. Ranu and S. Bhar, *Tetrahedron*, **1992**, 48, 1327-1332.
200. K. T. Potts, D. A. Usifer, A. Guadalupe and H. D. Abruna, *J. Am. Chem. Soc.*, **1987**, 109, 3961-3967.
201. J. P. Collin, P. Gavina, V. Heitz and J. P. Sauvage, *Eur. J. Inorg. Chem.*, **1998**, 1-14.
202. W. Spahni and G. Calzaferri, *Helv. Chim. Acta*, **1984**, 67, 450-454.
203. H. Hofmeier, P. R. Andres, R. Hoogenboom, E. Herdtweck and U. S. Schubert, *Aust. J. Chem.*, **2004**, 57, 419-426.
204. J. E. Beves, P. Chwalisz, E. C. Constable, C. E. Housecroft, M. Neuburger, S. Schaffner and J. A. Zampese, *Inorg. Chem. Commun.*, **2008**, 11, 1009-1011.
205. M. E. Padilla-Tosta, J. M. Lloris, R. Martinez-Manez, A. Benito, J. Soto, T. Pardo, M. A. Miranda and M. D. Marcos, *Eur. J. Inorg. Chem.*, **2000**, 741-748.
206. M. Beley, J. P. Collin, J. P. Sauvage, H. Sugihara, F. Heisel and A. Miehe, *J. Chem. Soc., Dalton Trans.*, **1991**, 3157-3159.
207. M. L. Turonek, P. Moore and W. Errington, *Dalton*, **2000**, 441-444.
208. M. E. Padilla-Tosta, J. M. Lloris, R. Martinez-Manez, M. D. Marcos, M. A. Miranda, T. Pardo, F. Sancenon and J. Soto, *Eur. J. Inorg. Chem.*, **2001**, 1475-1482.

209. Y. H. Lee, E. Kubota, A. Fuyuhiro, S. Kawata, J. M. Harrowfield, Y. Kim and S. Hayami, *Dalton Trans.*, **2012**, 41, 10825-10831.
210. Y.-L. Chen, B.-Z. Li, P. Yang and J.-Z. Wu, *Acta Crystallogr. Sect. C: Cryst. Struct. Commun.*, **2009**, 65, m238-m240.
211. F. Dumur, C. R. Mayer, E. Dumas, F. Miomandre, M. Frigoli and F. Secheresse, *Org. Lett.*, **2008**, 10, 321-324.
212. G. Sathyaraj, T. Weyhermueller and B. U. Nair, *Eur. J. Med. Chem.*, **2010**, 45, 284-291.
213. Q.-H. Wei, S. P. Argent, H. Adams and M. D. Ward, *New J. Chem.*, **2008**, 32, 73-82.
214. M.-J. Li, T.-Y. Lan, Z.-S. Lin, C. Yi and G.-N. Chen, *JBIC, J. Biol. Inorg. Chem.*, **2013**, 18, 993-1003.
215. M. A. R. Raycroft, C. I. Maxwell, R. A. A. Oldham, A. S. Andrea, A. A. Neverov and R. S. Brown, *Inorg. Chem.*, **2012**, 51, 10325-10333.
216. V. Tiwow, G. A. Lawrance, M. Maeder and P. Jensen, *J. Coord. Chem.*, **2011**, 64, 3637-3651.
217. T.-H. Huang, M.-H. Zhang, C.-Y. Gao and L.-T. Wang, *Inorg. Chim. Acta*, **2013**, 408, 91-95.
218. R.-h. Jia and S.-j. Tu, *Xuzhou Shifan Daxue Xuebao, Ziran Kexueban*, **2007**, 25, 52-54,64.
219. Z. Ma, B. Liang, M. Yang and L. Lu, *Acta Crystallogr. Sect. Sect. E: Struct. Rep. Online*, **2012**, 68, m298-m299.
220. J. Novales, N. Jonkhoff and J. H. Acquaye, *Polyhedron*, **2013**, 62, 148-157.
221. T. Konno, K. Koide and T. Ishida, *Chem. Commun. (Cambridge, U. K.)*, **2013**, 49, 5156-5158.
222. N. M. El-Ashgar and M. S. Abdel-Latif, *Anal. Lett.*, **2008**, 41, 3074-3087.
223. D. N. Adhikesavalu, D. Mastropaolo, A. Camerman and N. Camerman, *Acta Crystallogr., Sect. C: Cryst. Struct. Commun.*, **2001**, 57, 657-659.
224. S.-Q. Bai, G. Y. H. Quek, L. L. Koh and T. S. A. Hor, *CrystEngComm*, **2010**, 12, 226-233.
225. M. Benslimane, H. Merazig, J.-C. Daran and O. Zeghouan, *Acta Crystallogr. Sect. Sect. E: Struct. Rep. Online*, **2012**, 68, m1342-m1343.
226. J. R. Butchard, O. J. Curnow, D. J. Garrett and R. G. A. R. Maclagan, *Angew. Chem., Int. Ed.*, **2006**, 45, 7550-7553.
227. A. V. Polishchuk, A. V. Gerasimenko, K. A. Gayvoronskaya and E. T. Karaseva, *Acta Crystallogr. Sect. Sect. E: Struct. Rep. Online*, **2008**, 64, m931-m932.
228. R. Tian, Y. Yan, C. Zhang, L. Wang and Q. Pan, *Acta Crystallogr. Sect. Sect. E: Struct. Rep. Online*, **2012**, 68, m914-m915.
229. J. Xing, *Acta Crystallogr. Sect. Sect. E: Struct. Rep. Online*, **2009**, 65, m468.
230. H. S. Chow, E. C. Constable, C. E. Housecroft, M. Neuburger and S. Schaffner, *Dalton Trans.*, **2006**, 2881-2890.
231. A. Kochel, *Acta Crystallogr. Sect. Sect. E: Struct. Rep. Online*, **2006**, 62, m37-m38.
232. A. Hergold-Brundic, Z. Popovic and D. Matkovic-Calogovic, *Acta Crystallogr. Sect. C: Cryst. Struct. Commun.*, **1996**, C52, 3154-3157.
233. T. Steiner, *Angew. Chem., Int. Ed.*, **2002**, 41, 48-76.
234. G. Claudon, N. Le Bris, H. Bernard and H. Handel, *Eur. J. Org. Chem.*, **2004**, 2004, 5027-5030.
235. E. C. Constable, J. Lewis, M. C. Liptrot and P. R. Raithby, *Inorg. Chim. Acta*, **1990**, 178, 47-54.
236. B. N. Figgis, E. S. Kucharski and A. H. White, *Aust. J. Chem.*, **1983**, 36, 1563-1571.
237. B. N. Figgis, E. S. Kucharski and A. H. White, *Aust. J. Chem.*, **1983**, 36, 1537-1561.
238. K. V. Reddy, T. Satyanarayana, N. R. Anipindi and R. N. Reddy, *Oxid. Commun.*, **2011**, 34, 38-43.
239. E. C. Constable, D. Phillips and P. R. Raithby, *Inorg. Chem. Commun.*, **2002**, 5, 519-521.
240. G. Aullon, D. Bellamy, A. Guy Orpen, L. Brammer and A. B. Eric, *Chem. Commun.*, **1998**, 653-654.
241. N. Baidya, M. Olmstead and P. K. Mascharak, *Inorg. Chem.*, **1991**, 30, 929-937.
242. R. Cortes, M. I. Arriortua, T. Rojo, X. Solans, C. Miravitlles and D. Beltran, *Acta Crystallogr. Sect. C: Cryst. Struct. Commun.*, **1985**, 41, 1733-1736.
243. R. Cortes, L. Lezama, J. I. R. Larramendi, M. Insausti, J. V. Folgado, G. Madariaga and T. Rojo, *J. Chem. Soc., Dalton Trans.*, **1994**, 2573-2579.

244. M. Gotzone Barandika, R. Cortes, L. Lezama, M. Karmele Urtiaga, M. Isabel Arriortua and T. Rojo, *J. Chem. Soc., Dalton Trans.*, **1999**, 2971-2976.
245. G. Gasser, G. Labat and H. Stoeckli-Evans, *Acta Crystallogr. Sect. Sect. E: Struct. Rep. Online*, **2004**, 60, m244-m246.
246. X.-H. Jin, L.-X. Cai, J.-K. Sun, Z.-F. Ju and J. Zhang, *Inorg. Chem. Commun.*, **2010**, 13, 86-89.
247. T. Rojo, M. I. Arriortua, J. Ruiz, J. Darriet, G. Villeneuve and D. Beltran-Porter, *J. Chem. Soc., Dalton Trans.*, **1987**, 285-291.
248. J. Valdes-Martinez, D. Salazar-Mendoza and R. A. Toscano, *Acta Crystallogr. Sect. Sect. E: Struct. Rep. Online*, **2002**, 58, m712-m714.
249. V. M. Manikandamathavan, V. Rajapandian, A. J. Freddy, T. Weyhermuller, V. Subramanian and B. U. Nair, *Eur. J. Med. Chem.*, **2012**, 57, 449-458.
250. K. Suntharalingam, D. J. Hunt, A. A. Duarte, A. J. P. White, D. J. Mann and R. Vilar, *Chem. - Eur. J.*, **2012**, 18, 15133-15141.
251. M. Walesa-Chorab, A. R. Stefankiewicz, A. Gorczynski, M. Kubicki, J. Klak, M. J. Korabik and V. Patroniak, *Polyhedron*, **2011**, 30, 233-240.
252. M. Chiper, M. A. R. Meier, J. M. Kranenburg and U. S. Schubert, *Macromol. Chem. Phys.*, **2007**, 208, 679-689.
253. E. C. Constable, A. H. Redondo, C. E. Housecroft and M. Neuburger, *Inorg. Chem. Commun.*, **2010**, 13, 70-73.
254. R. Dobrawa, P. Ballester, C. R. Saha-Moeller and F. Wuerthner, *ACS Symp. Ser.*, **2006**, 928, 43-61.
255. Z. Ma, Y. Cao, Q. Li, d. S. M. F. C. Guedes, d. S. J. J. R. Frausto and A. J. L. Pombeiro, *J. Inorg. Biochem.*, **2010**, 104, 704-711.
256. U. S. Schubert, H. Hofmeier and G. R. Newkome, in *Modern Terpyridine Chemistry*, Wiley-VCH Verlag GmbH & Co. KGaA, 2006, pp. 1-6, 37-38.
257. R. Puttreddy and P. J. Steel, *CrystEngComm*, **2014**, 16, 556-560.
258. E. C. Constable, A. J. Edwards, G. R. Haire, M. J. Hannon and P. R. Raithby, *Polyhedron*, **1997**, 17, 243-253.
259. M. Munakata, L. P. Wu, K. Sugimoto, T. Kuroda-Sowa, M. Maekawa, Y. Suenaga, N. Maeno and M. Fujita, *Inorg. Chem.*, **1999**, 38, 5674-5680.
260. M. A. Omary, T. R. Webb, Z. Assefa, G. E. Shankle and H. H. Patterson, *Inorg. Chem.*, **1998**, 37, 1380-1386.
261. G. W. Rabe, H. Heise, G. P. A. Yap, L. M. Liable-Sands, I. A. Guzei and A. L. Rheingold, *Inorg. Chem.*, **1998**, 37, 4235-4245.
262. M. G. B. Drew, P. C. H. Mitchell and A. R. Read, *J. Chem. Soc., Chem. Commun.*, **1982**, 238-239.
263. T. J. Boyle, L. A. M. Ottley, S. M. Hoppe and C. F. Campana, *Inorg. Chem.*, **2010**, 49, 10798-10808.
264. G. A. Bowmaker, Effendy, P. J. Harvey, P. C. Healy, B. W. Skelton and A. H. White, *J. Chem. Soc., Dalton Trans.*, **1996**, 2459-2465.
265. M. J. Hannon, C. L. Painting, E. A. Plummer, L. J. Childs and N. W. Alcock, *Chem. - Eur. J.*, **2002**, 8, 2225-2238.
266. S. Cai, W. Hu, J. Li, B. Xie, L. He and X. Zhang, *J. Dispersion Sci. Technol.*, **2013**, 35, 93-97.
267. A. Neves, A. J. Bortoluzzi, R. Jovito, R. A. Peralta, B. de Souza, B. Szpoganicz, A. C. Joussef, H. Terenzi, P. C. Severino, F. L. Fischer, G. Schenk, M. J. Riley, S. J. Smith and L. R. Gahan, *J. Braz. Chem. Soc.*, **2010**, 21, 1201-1212.
268. A. K. Boudalis, R. E. Aston, S. J. Smith, R. E. Mirams, M. J. Riley, G. Schenk, A. G. Blackman, L. R. Hanton and L. R. Gahan, *Dalton Trans.*, **2007**, 5132-5139.
269. A. Kantacha, R. Buchholz, S. J. Smith, G. Schenk and L. R. Gahan, *JBIC, J. Biol. Inorg. Chem.*, **2011**, 16, 25-32.
270. A. Prokofieva, A. I. Prikhod'ko, E. A. Enyedy, E. Farkas, W. Maringgele, S. Demeshko, S. Dechert and F. Meyer, *Inorg. Chem.*, **2007**, 46, 4298-4307.

271. L. J. Daumann, P. Comba, J. A. Larrabee, G. Schenk, R. Stranger, G. Cavigliasso and L. R. Gahan, *Inorg. Chem.*, **2013**, 52, 2029-2043.
272. A. I. Hanafy, A. M. A. Hassan, S. A. Shama, H. K. Thabet and H. M. Z. El-Alfy, *Eur. J. Chem.*, **2013**, 4, 157-161.
273. D. R. Jones, L. F. Lindoy and A. M. Sargeson, *J. Am. Chem. Soc.*, **1983**, 105, 7327-7336.
274. S. Moghaddas, P. Hendry, R. J. Geue, C. Qin, A. M. T. Bygott, A. M. Sargeson and N. E. Dixon, *Dalton*, **2000**, 2085-2089.
275. F. Mancin and P. Tecilla, *New J. Chem.*, **2007**, 31, 800-817.
276. S. J. Smith, M. J. Riley, C. J. Noble, G. R. Hanson, R. Stranger, V. Jayaratne, G. Cavigliasso, G. Schenk and L. R. Gahan, *Inorg. Chem.*, **2009**, 48, 10036-10048.
277. G. Feng, D. Natale, R. Prabaharan, J. C. Mareque-Rivas and N. H. Williams, *Angew. Chem., Int. Ed.*, **2006**, 45, 7056-7059.
278. C. T. Liu, A. A. Neverov and R. S. Brown, *J. Am. Chem. Soc.*, **2008**, 130, 13870-13872.
279. S.-P. Tang, Y.-H. Zhou, H.-Y. Chen, C.-Y. Zhao, Z.-W. Mao and L.-N. Ji, *Chem. - Asian J.*, **2009**, 4, 1354-1360.
280. B.-y. Jiang, J. Du, C.-w. Hu, X.-c. Zeng and Y.-s. Cao, *Transition Met. Chem. (Dordrecht, Neth.)*, **2004**, 29, 361-367.
281. A. Jancso, I. Torok, K. Hegetschweiler and T. Gajda, *ARKIVOC (Gainesville, FL, U. S.)*, **2008**, 217-224.
282. M. J. Young and J. Chin, *J. Am. Chem. Soc.*, **1995**, 117, 10577-10578.
283. B. K. Takasaki and J. Chin, *J. Am. Chem. Soc.*, **1994**, 116, 1121-1122.
284. F. Verge, C. Lebrun, M. Fontecave and S. Menage, *Inorg. Chem.*, **2003**, 42, 499-507.
285. E. C. Constable, J. Lewis, M. C. Liptrot and P. R. Raithby, *Inorg. Chim. Acta*, **1990**, 178, 47-54.
286. Y. Yin, *Wuli Huaxue Xuebao*, **1999**, 15, 629-635.
287. C. Wang, Y. Zhang, B. Yuan and J. Zhao, *J. Mol. Catal. A: Chem.*, **2010**, 333, 173-179.
288. J. R. Allan, G. H. W. Milburn, F. Richmond, D. L. Gerrard, J. Birnie and A. S. Wilson, *Eur. Polym. J.*, **1991**, 27, 907-910.
289. M. Barquin, G. M. J. Gonzalez, L. Larrinaga, E. Pinilla and M. R. Torres, *Inorg. Chim. Acta*, **2009**, 362, 2334-2340.
290. V. C. Copeland, W. E. Hatfield and D. J. Hodgson, *Inorg. Chem.*, **1973**, 12, 1340-1343.
291. D. Y. Jeter, W. E. Hatfield and D. J. Hodgson, *J. Phys. Chem.*, **1972**, 76, 2707-2710.
292. Y. I. Kim and W. E. Hatfield, *Inorg. Chim. Acta*, **1991**, 189, 237-241.
293. M. L. Niven, G. C. Percy and D. A. Thornton, *J. Mol. Struct.*, **1980**, 68, 73-80.
294. C. J. O'Connor, E. E. Eduok, F. R. Fronczek and O. Kahn, *Inorg. Chim. Acta*, **1985**, 105, 107-113.
295. D. C. Bebout, E. V. Bowers, R. E. Freer, M. E. Kastner, D. A. Parrish and R. J. Butcher, *J. Chem. Crystallogr.*, **2013**, 43, 108-115.
296. J. Boerner, I. dos Santos Vieira, M. D. Jones, A. Doering, D. Kuckling, U. Floerke and S. Herres-Pawlis, *Eur. J. Inorg. Chem.*, **2011**, 2011, 4441-4456.
297. D. A. Cavarzan, F. D. Fagundes, O. Fuganti, C. W. P. da Silva, C. B. Pinheiro, D. F. Back, A. Barison, A. L. Bogado and M. P. de Araujo, *Polyhedron*, **2013**, 62, 75-82.
298. K.-Y. Choi, Y.-M. Jeon, K.-C. Lee, S.-N. Choi, M.-W. Kim, H.-H. Lim and M.-J. Kim, *Transition Met. Chem. (Dordrecht, Neth.)*, **2004**, 29, 405-410.
299. A. Congreve, R. Kataky, M. Knell, D. Parker, H. Puschmann, K. Senanayake and L. Wylie, *New J. Chem.*, **2003**, 27, 98-106.
300. L. Götzke, K. Gloe, K. A. Jolliffe, L. F. Lindoy, A. Heine, T. Doert, A. Jäger and K. Gloe, *Polyhedron*, **2011**, 30, 708-714.
301. P. Hirva, A. Nielsen, A. D. Bond and C. J. McKenzie, *J. Phys. Chem. B*, **2010**, 114, 11942-11948.
302. Y. K. Kang, Q. T. Nguyen, R.-E. Lee, H. Lee and J. H. Jeong, *Bull. Korean Chem. Soc.*, **2009**, 30, 257-260.
303. Y. Kani, S. Ohba, S. Ito and Y. Nishida, *Acta Crystallogr. Sect. C: Cryst. Struct. Commun.*, **2000**, C56, e195.

304. H.-W. Lee, H.-J. Seo, H.-J. Kim, S. K. Kang, J. Y. Heo and Y.-I. Kim, *Bull. Korean Chem. Soc.*, **2007**, 28, 855-858.
305. D. S. Marlin, D. G. Cabrera, D. A. Leigh and A. M. Z. Slawin, *Angew. Chem., Int. Ed.*, **2006**, 45, 77-83.
306. T. Mukherjee, B. Sen, E. Zangrando, G. Hundal, B. Chattopadhyay and P. Chattopadhyay, *Inorg. Chim. Acta*, **2013**, 406, 176-183.
307. M. Schatz, M. Leibold, S. P. Foxon, M. Weitzer, F. W. Heinemann, F. Hampel, O. Walter and S. Schindler, *Dalton Trans.*, **2003**, 1480-1487.
308. L. Yang, W. Chen, Y. Chen, W. Liu, T. Lei, L. Li, M. Lin, J. Wu, Y. Cao, W. Li and Y. Li, *Z. Anorg. Allg. Chem.*, **2012**, 638, 1833-1838.
309. W. Chu, Y. Wang, S. Liu, X. Yang, S. Wang, S. Li, G. Zhou, X. Qin, C. Zhou and J. Zhang, *Bioorg. Med. Chem. Lett.*, **2013**, 23, 5187-5191.
310. E. C. Constable, C. E. Housecroft, N. S. Murray and J. A. Zampese, *Polyhedron*, **2013**, 54, 110-118.
311. Z. Ma, W. Lu, B. Liang and A. J. L. Pombeiro, *New J. Chem.*, **2013**, 37, 1529-1537.
312. S. Wang, W. Chu, Y. Wang, S. Liu, J. Zhang, S. Li, H. Wei, G. Zhou and X. Qin, *Appl. Organomet. Chem.*, **2013**, 27, 373-379.
313. L. Gou, *Z. Kristallogr. - New Cryst. Struct.*, **2013**, 228, 15-16.
314. A. Juneja, T. S. Macedo, D. R. M. Moreira, M. B. P. Soares, A. C. L. Leite, J. K. d. A. L. Neves, V. R. A. Pereira, F. Avecilla and A. Azam, *Eur. J. Med. Chem.*, **2014**, 75, 203-210.
315. Y. H. Lee, V. N. Nguyen, M. J. Go, J. Lee, S. U. Lee and M. H. Lee, *Organometallics*, **2014**, 33, 753-762.
316. N. Zhang, J. Yang, R.-X. Hu and M.-B. Zhang, *Z. Anorg. Allg. Chem.*, **2013**, 639, 197-202.
317. E. J. Cho, S. Jung, K. Lee, H. J. Lee, K. C. Nam and H.-J. Bae, *Chem. Commun. (Cambridge, U. K.)*, **2010**, 46, 6557-6559.
318. M. Subat, K. Woinaroschy, C. Gerstl, B. Sarkar, W. Kaim and B. König, *Inorg. Chem.*, **2008**, 47, 4661-4668.
319. M. Arca, A. Bencini, E. Berni, C. Caltagirone, F. A. Devillanova, F. Isaia, A. Garau, C. Giorgi, V. Lippolis, A. Perra, L. Tei and B. Valtancoli, *Inorg. Chem.*, **2003**, 42, 6929-6939.
320. S.-P. Tang, S. Chen, G.-F. Wu, H.-Y. Chen, Z.-W. Mao and L.-N. Ji, *Inorg. Chem. Commun.*, **2011**, 14, 184-188.
321. M. Wall, B. Linkletter, D. Williams, A.-M. Lebuis, R. C. Hynes and J. Chin, *J. Am. Chem. Soc.*, **1999**, 121, 4710-4711.
322. Anon, *Met.-Based Drugs*, **1997**, 4, 111-112.
323. J. P. Glusker, A. K. Katz and C. W. Bock, *Rigaku J.*, **1999**, 16, 8-16.
324. P. Tomasik and P. Tomasik, *Chem. Inz. Ekol.*, **1996**, 3, 279-301.
325. M. Livieri, F. Manicin, G. Saielli, J. Chin and U. Tonellato, *Chem. - Eur. J.*, **2007**, 13, 2246-2256.
326. C. Piovezan, F. Silva Lisboa, F. S. Nunes and S. M. Drechsel, *Transition Met. Chem. (Dordrecht, Neth.)*, **2011**, 36, 79-85.
327. E. Kimura, *Curr. Opin. Chem. Biol.*, **2000**, 4, 207-213.
328. J. Chin, 1996.
329. C. Liu, M. Wang, T. Zhang and H. Sun, *Coord. Chem. Rev.*, **2004**, 248, 147-168.
330. L. Infantes, J. Chisholm and S. Motherwell, *CrystEngComm*, **2003**, 5, 480-486.
331. S. K. Padhi, R. Sahu and V. Manivannan, *Polyhedron*, **2008**, 27, 2221-2225.
332. K.-y. Choi, H. Ryu, N.-d. Sung and M. Suh, *J. Chem. Crystallogr.*, **2003**, 33, 947-950.
333. K. M. J., M. M. T. and P. M. J., in *Ellis Harwood Series in Inorganic Chemistry*, Ellis Horwood Limited, 1992, ch. 83-147, pp. 83-147.
334. J. W. Mao, H. Zhou, Y. F. Chen, G. Z. Cheng and Z. Q. Pan, *Transition Met. Chem. (Dordrecht, Neth.)*, **2012**, 37, 385-391.
335. E. Kimura, I. Nakamura, T. Koike, M. Shionoya, Y. Kodama, T. Ikeda and M. Shiro, *J. Am. Chem. Soc.*, **1994**, 116, 4764-4771.
336. S. Aoki and E. Kimura, *Chem. Rev.*, **2004**, 104, 769-788.
337. H. Hofmeier, R. Hoogenboom, M. E. Wouters and U. S. Schubert, *J. Am. Chem. Soc.*, **2005**, 127, 2913-2921.

338. W. R. Carmody, *J. Chem. Educ.*, **1964**, 41, 615-616.
339. P. Job, *Ann. Chim. Appl.*, **1928**, 9, 113-203.
340. W. R. Furlong, M. A. Rubinski and R. Indralingam, *J. Chem. Educ.*, **2013**, 90, 937-940.
341. W. C. Vosburgh and G. R. Cooper, *J. Am. Chem. Soc.*, **1941**, 63, 437-442.
342. J. R. Masaguer Fernandez, M. V. Coto and J. S. Casas, *J. Chem. Educ.*, **1975**, 52, 387.
343. C. Airoldi, *J. Chem. Educ.*, **1976**, 53, 268.
344. H. Ando, Y. Nakao, H. Sato and S. Sakaki, *Dalton Trans.*, **2010**, 39, 1836-1845.
345. C. Enachescu, U. Oetliker and A. Hauser, *J. Phys. Chem. B*, **2002**, 106, 9540-9545.
346. R. H. Holyer, C. D. Hubbard, S. F. A. Kettle and R. G. Wilkins, *Inorg. Chem.*, **1966**, 5, 622-625.
347. P. R. Andres, H. Hofmeier, B. G. G. Lohmeijer and U. S. Schubert, *Synthesis*, **2003**, 2865-2871.
348. U. S. Schubert, C. Eschbaumer, P. Andres, H. Hofmeier, C. H. Weidl, E. Herdtweck, E. Dulkeith, A. Morteani, N. E. Hecker and J. Feldmann, *Synth. Met.*, **2001**, 121, 1249-1252.
349. M. Bru, I. Alfonso, M. I. Burguete and S. V. Luis, *Angew. Chem., Int. Ed.*, **2006**, 45, 6155-6159.
350. E. Wiberg, N. Wiberg and H. A. F., *Inorganic Chemistry*, Academic Press, W. de Gruyter, San Diego, California. : Berlin, 2001.
351. H. K. Lee, T. S. Lam, C.-K. Lam, H.-W. Li and S. M. Fung, *New J. Chem.*, **2003**, 27, 1310-1318.
352. B. Weber, I. Kaepplinger, H. Goerls and E.-G. Jaeger, *Eur. J. Inorg. Chem.*, **2005**, 2794-2811.
353. W.-F. Liaw, J.-H. Lee, H.-B. Gau, C.-H. Chen, S.-J. Jung, C.-H. Hung, W.-Y. Chen, C.-H. Hu and G.-H. Lee, *J. Am. Chem. Soc.*, **2002**, 124, 1680-1688.
354. R. K. O'Reilly, V. C. Gibson, A. J. P. White and D. J. Williams, *Polyhedron*, **2004**, 23, 2921-2928.
355. C. S. Campos-Fernandez, B. L. Schottel, H. T. Chifotides, J. K. Bera, J. Bacsa, J. M. Koomen, D. H. Russell and K. R. Dunbar, *J. Am. Chem. Soc.*, **2005**, 127, 12909-12923.
356. H.-J. Kim, W.-C. Zin and M. Lee, *J. Am. Chem. Soc.*, **2004**, 126, 7009-7014.
357. G. T. Spence and P. D. Beer, *Acc. Chem. Res.*, **2013**, 46, 571-586.
358. A. P. S. Pannu, J. R. Stevens and P. G. Plieger, *Inorg. Chem.*, **2013**, 52, 9327-9337.
359. S. Zhou, Z. Zeng, X. Li and Z. Gao, *Zhongguo Yaowu Huaxue Zazhi*, **2001**, 11, 172-173.
360. D. D. Perrin and W. L. F. Armarego, *Purification of Laboratory Chemicals*, Butterworth-Heinemann, Oxford, 3rd edn., 1997.
361. G. M. Sheldrick, *Acta Crystallogr. Sect. A: Found. Crystallogr.*, **2008**, 64, 112-122.
362. O. V. Dolomanov, L. J. Bourhis, R. J. Gildea, J. A. Howard and K. H. Puschmann, *J. Appl. Crystallogr.*, **2009**, 42, 339-341.